Synthesis and Characterization of New Amphiphilic And Chiral Squaraines

Dissertation

Zur
Erlangung des Doktorgrades (Dr. rer. nat.)

der

Mathematisch-Naturwissenschaftlichen Fakultät

der

Rheinischen Friedrich-Wilhelms-Universität Bonn

vorgelegt von

Wing-Si Li

aus
Bonn

Bonn 2025

Angefertigt mit der Genehmigung der Mathematisch-Naturwissenschaftlichen Fakultät der Rheinischen Friedrich-Wilhelms-Universität Bonn

Gutachter/Betreuer: Prof. Dr. Arne Lützen
Gutachter: Prof. Dr. Sigurd Höger
Tag der Promotion: 09.10.2025
Erscheinungsjahr: 2025

Erklärung

Ich versichere, dass ich die vorliegende Arbeit unter Einhaltung der Regeln guter wissenschaftlicher Praxis selbstständig verfasst, keine anderen als die angegebenen Quellen und Hilfsmittel benutzt, sowie die Zitate kenntlich gemacht habe.
Bonn, 2025

_____
Wing-Si Li

Acknowledgements

At this point, I want to thank the many people without whom this work would not have been possible. Thank you so much for your support!

First of all, I would like to sincerely thank Prof. Dr. Arne Lützen, who gave me the opportunity to research this highly interesting interdisciplinary topic under his supervision and to be a part of the research training group 2591 Tide. Thank you for always following my work with great interest and always taking the time for me when I needed your advice. I am also grateful for the scientific freedom you granted me and the trust you have placed in me.

A big thank you also goes to Prof. Dr. Moritz Sokolowski, who was the second member of my thesis advisory committee in the Tide context, my host for a 1-month lab internship and chair of the examination board. Thank you for your support and the encouraging conversations. I appreciated those a lot!

I would also like to thank Prof. Dr. Sigurd Höger for being the second reviewer and Prof. Dr Gerd Bendas as the non-specialist. I would like to thank for them all for the participation in the examination committee.

I am grateful to have been part of Tide and for the opportunities Tide provided. As such I would like to express my countless thanks to all my fellow Tide members who accompanied me on this journey. I thank you for the fruitful discussion during the retreats, the summer school and beyond all the official events. Here I would like the opportunity to thank our coordinators, especially Hanna, who always helped when Tide-related questions arose and provided encouragement whenever needed. A big thank you also goes to the Women @ Science initiative within Tide from all my fellow female PhD-students within Tide to Prof. Dr. Selina Olthof. Thank you for the valuable events and the mutual support throughout. With regards to Tide, I am inexpressible thankful for the opportunity given to go abroad for three months.

For this unforgettable and irreplaceable experience alongside the fruitful results and the warm welcome to his research group, I also want to express my heartfelt thanks to my research residence host Prof. Dr. Luca Beverina at Università degli Studi di Milano-Bicocca, Italy and his research group. Grazie mille for allowing me to be a part of the LASMO family and the constant support even after my return back home. I especially want to thank, Anita, Annapia, Alice, Elena, Erika, Francesca, Gabriel, J (Sara), Lorenzo, Matteo, Mauro, Nicolo, Sara and Valentina for integrating and including me so easily each time. Thank you so much for the amazing time together!

Additionally, I would also like to thank the research group of Prof. Dr. Sokolowski, who hosted me for my 1-month lab exchange. Thank you all for including me so effortlessly and helping me peek into a different aspect of chemistry, gaining insights far from the synthesis laboratory. In this regards I want to especially thank my fellow Tide-member and good friend Anna for her patient and easily understandable explanations alongside endless encouragement and mutual support during our PhDs.

I would like to thank our other cooperation partners within and beyond Tide. Within Tide I want to express my thanks to Otgoo from Prof. Dr. Klaus Meerholz's group, Roland Schäfer from Prof. Dr. Lindfor's group and Kristin Gratzfeld from Prof. Dr. Moritz Sokolowski's group. Beyond Tide I want to thank Prof. Dr*. Roland Resel.*

I would like to thank the teams from the Central Analytics Department of the Chemical Institutes at the University of Bonn, the NMR Spectroscopy, Mass Spectrometry, X-ray Structure Analysis, GCMS, and Elemental Analysis departments for their numerous measurements. I would also like to thank Andreas Schneider from the HPLC pool for the possibility to partake in an HPLC introduction course in the beginning of my PhD, it enhanced my understanding for column chromatographic purification.

I would like to thank all my bachelor's and master's interns Alexander, Daniel, Defne, Emmanuil, Felicitas, Gianluca, Jaeeun, Max, Nour, Sophie, Thomas, Tim and Tobias for their motivated work under my supervision. I would also like to thank Sophie and Alexander for their independent and dedicated work during their bachelor's theses, and Fraz Azarnousha for continuing this exciting research topic.

I would like to thank all former and current members of the Lützen research group, namely Anh Tu, Anne, Ayla, Basti, Clemens, Eric, Fee, Fraz, Hannah, Jan, Lea, Lena, Lukas, Marc, Marvin, and our (former) trainees Elisa and Hanna for the convivial lunches and evening beer seminars, the mutual motivation during everyday lab life, the fun girls' nights out, and the annual boozy cabbage tours and Christmas parties. Special thanks go to Jenny and Marvin, who introduced me to the exciting topic of squaraine synthesis and dye aggregation, as well as to my two lab partners, Anne and Ayla, whose support I could always rely on in my daily lab work.

Finally, I would like to thank my family and friends from the bottom of my heart for their unconditional support, encouragement, and constant support over the years. Thank you for making all this possible, for motivating me, and for always believing in me. A big shout out to Cookie, Cream, Caramel, Bourbon, Bailey, Bacardi and Bean for being the best cheer up I could wish for. After a long day nothing beats snuggling with my pet rats. My biggest thank you is addressed to my unwavering supporter and fiancé Tim, who believed in me no matter what happened, even when I was doubtful and feeling insecure. Thank you for your understanding, love, and unconditional support. Thank you for encouraging, empowering and loving me during this time. Thank you for experiencing and celebrating every high and enduring all the lows of my PhD alongside of me!

Thank you all so much for your support!

Summary

Squaraines are a class of dye molecules obtained through reaction of mostly electron-rich molecules with squaric acid. It is an intriguing class of molecules, which has a wide field of applications and seemingly endless possibilities for future endeavors, especially in the field of optoelectronics. With its tunable properties and the many synthetic routes developed, certain characteristics with regards to the employment in photodiodes were deemed especially desirable. As previous works have beautifully shown the introduction of chirality on to the squaraine framework, which is often described as a quadrupolar D-A-D type rigid-rod –like geometry, is highly fascinating. It was discovered that the inherent central chiral information of the chirality source introduced to the framework was translated to the supramolecular level upon aggregation of the dye, resulting in measurable macroscopic circular dichroism both in colloidal solution and in thin films.

In the presented thesis the synthetic route to a new highly versatile class of squaraine was successfully developed. This class is a hybrid combining chiral information introduced by the naturally occurring amino acid alanine with additional alkyl-chains, which were found to be beneficial for the aggregation behavior of squaraines, but could not be introduced to the previous chiral squaraine class due to the nature of the chirality source. The developed synthetic route allows for various substitution patterns for this new family of chiral squaraines. As a result, it also lays the ground stone for further investigation towards other naturally occurring amino acid based squaraines. These newly obtained compounds were characterized and investigated regarding their (chiro-)optical properties in solution.

Beyond the classical field of application, optoelectronics, another ambitious combination was successfully achieved. Here the goal was the synthesis of a squaraine-based stimuli-responsive designer surfactant that could be used for micellar catalysis. It envisioned the combination of the squaric acid core with different solubilizing groups to tune the final solubility of the then amphiphilic squaraine-based surfactant.

In the presented thesis a new amphiphilic squaraine-based surfactant was synthesized, which not only combined the desired squaric acid core with a pH-indicative functional group as originally desired. Additionally, the assembly of micelles and the disassembly thereof were reliably visualized by a color change. Most importantly a new so far unique feature of the newly synthesized squaraine based surfactant results in an attractive advantage during the post-reaction purification process for the new designer surfactant compared to conventional surfactants for micellar catalysis.

TABLE OF CONTENTS

1 Introduction ... 1

1.1 Applications ... 2

1.1.1 Optoelectronic Devices ... 3

1.2 Types of Squaraines ... 5

1.3 Synthesis ... 7

Symmetric Squaraines ... 8

Asymmetric Squaraines ... 9

2 Task and Objective ... 11

3 Amphiphilic Squaraines ... 13

3.1 Surfactants ... 14

3.1.1 Micelles ... 15

3.1.2 Micellar Catalysis ... 16

3.1.3 Challenges ... 17

3.2 Objective ... 18

3.3 Result and Discussion ... 19

3.3.1 Attempts towards the Synthesis of a First Generation of Amphiphilic Squaraines ... 19

3.3.2 Synthesis of a Second Generation of Amphiphilic Squaraines ... 24

3.3.3 Characterization of the Amphiphilic Character of **20** and its Response to Changes in pH ... 28

3.3.4 Testing of **20** as Surfactant for Micellar Catalysis – Test Reactions ... 34

4 Studies towards the Sublimation of Chiral Squaraines ... 37

4.1 Previous Work on ProSQs and the Added Value of Chirality ... 37

4.2 PyrSQ the Smaller Sibling of ProSQ ... 39

5 L-Alanine-Derived Squaraines ... 49

5.1 Establishing *N*,*O*-Ethylation of l-Alaninol as a Model System ... 49

5.1.1 Exploring Squaraine Synthesis with *N*,*O*-Ethylated L-Alaninol as a Model System ... 57

5.1.2 Modification of the Established Condensation Procedure ... 60

5.2 Expanding the Library of AlaSQs ... 61

5.3 Crystallographic Data of AlaSQs ... 66

5.4 UV-Vis Spectroscopic Characterization of New Squaraines in Solution ... 68

5.4.1 Behavior of the Asymmetric OH Bearing Anilino Squaraine (*S*)-**40a** in Solution ... 68

5.4.2 AlaSQs in Solution ... 71

5.4.3 Poor-Solvent Titration Experiments ... 74

5.5 Further insights in the Behavior of (*S*,*S*)-*N*-C3,*O*-C3-Ala-SQ **23b** ... 76

6 Conclusion and Outlook 81
6.1 Squaric Acid-Based Designer Surfactant for Micellar Catalysis 81
6.2 Sublimation of PyrSQ-C1 83
6.3 A New Class of Chiral SQ –AlaSQ 83
7 Experimental Part 87
7.1 General part 87
7.2 Synthesis of amphiphilic squaraines 89
7.3 Synthesis of amine building blocks 98
7.4 Synthesis of squaraines 122
7.5 Crystallographic Data 136
7.6 UV-Vis- and CD spectroscopic Experiments 143
7.7 HLB Value Calculations of **20** 145
7.8 DLS measurements 146
8 List of Abbreviations 151
9 References 155
Appendix A1
NMR Spectra A2
Mass Spectra A59
Additional Visualization of the Crystal structures A114
UV-Vis Spectra A116

1 INTRODUCTION

Squaraines are a class of dye molecules obtained through reaction of mostly electron-rich molecules with squaric acid. The name is a result of the combination of the terms ***squar***ic acid and bet***aine***,[1] highlighting the namesake and the zwitterionic character of this compound class. First discovered back in 1965 by *Jacobs* and *Treibs*[2] this dye has since received an increasing interest over the last decades (Figure 1).[3]

Figure 1*: Publications mentioning squaraines since 1935 according to Sci-Finder®[3] (Last Checked: 28.02.2025) Blue colored bars show the number of publications since 1985,* [1]*where the name squaraine was first established.*

Most publications mentioning squaraines according to Sci-Finder® were released in 2013 (147 articles). Since then, the number of new publications on squaraines fluctuate around 100 articles, with a slight decrease in number during the Covid-19 pandemic indicating a consistent level of interest.

If the more outdated term “squarylium” is also taken into account, the combined output regarding this class of dye starting from 1965 until presence amounts to 3847 publications according to Sci-Finder® (Figure 2).

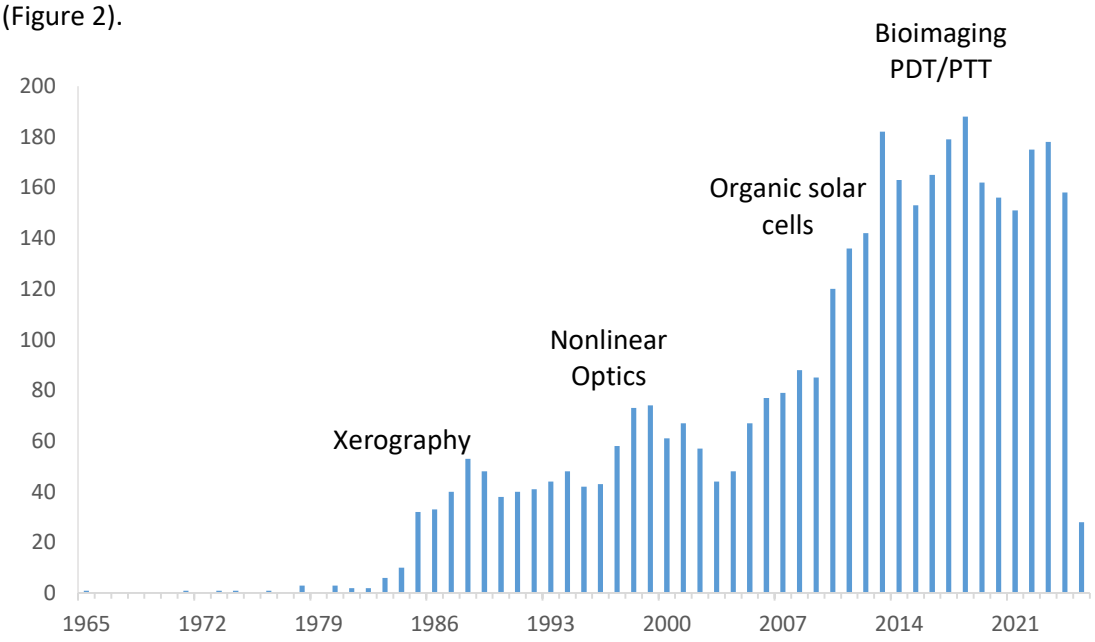

Figure 2*: Publications mentioning the term “squaraine”*[3] *or “squarylium”*[4] *since 1965 according to Sci-Finder® (Last checked: 06.03.2025). Blue colored bars show the number of publications which clearly grows with the different field of applications found for this class of compounds.*

The seemingly staircase like rise in number of publications are most likely due to the discovery of new fields of applications[5] for squaraines with xerography (1980s),[6–9] nonlinear optics (late 1990s),[10–12] organic photovoltaic (late 2000s)[13–21] and bioimaging (2000s)[13,21,22] alongside photodynamic (PDT)[23,24] and photothermal therapy (PTT)[25] as the most impactful interest boosters (Figure 2).

1.1 APPLICATIONS

Upon closer inspection the publications can be neatly mapped out into a so-called knowledge graph (Figure 3) by Sci-Finder®.[26] After roughly sorting the different spots into more biology related aspects (left) and optical aspects (right). The biggest clusters found are medicinal application and fluorescence focused applications of squaraines.

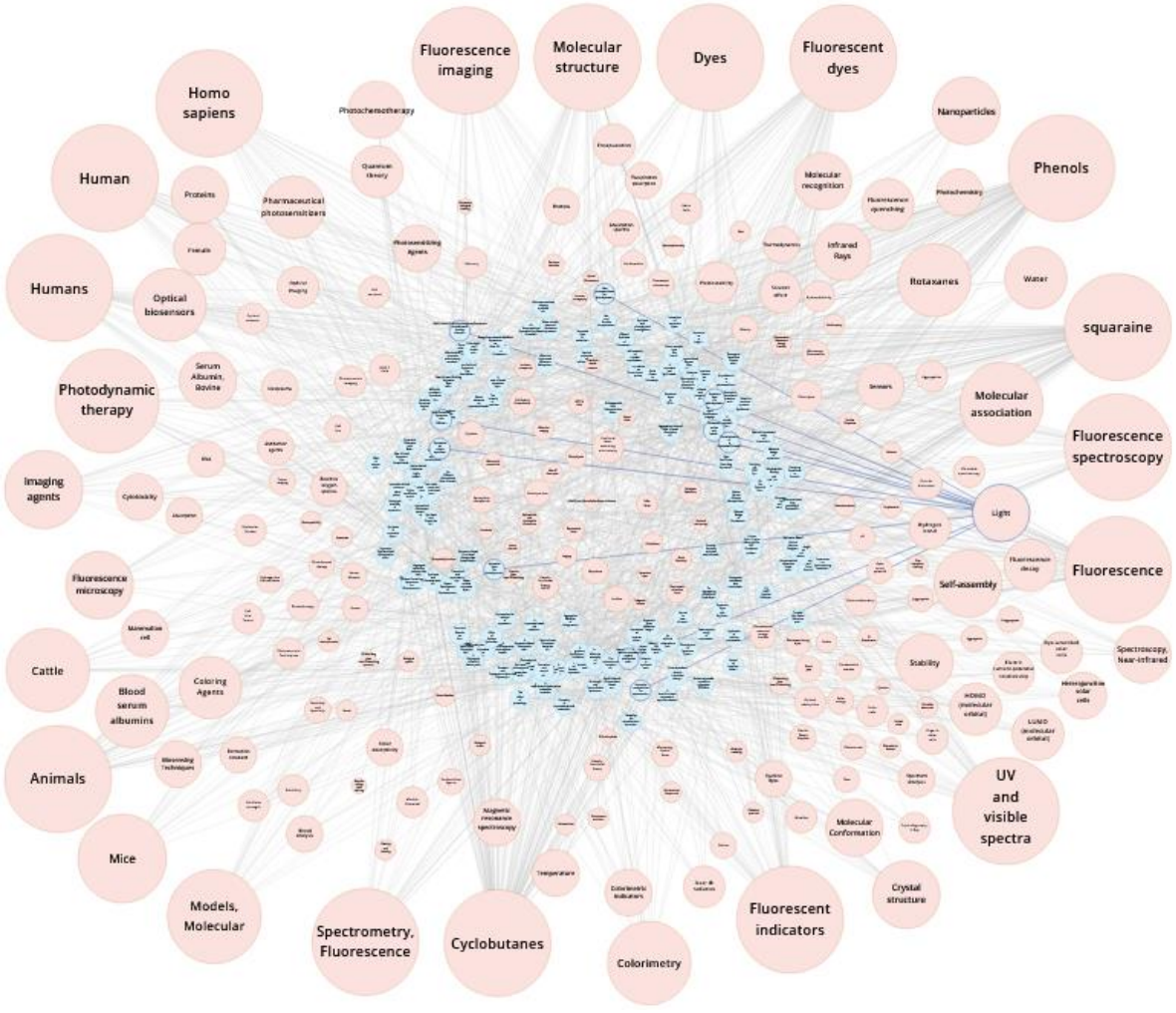

***Figure 3**: Knowledge graph regarding squaraines according to Sci-Finder®.[26] (Last checked and rearranged 28.02.2025) Orange circles show the key words with regards to squaraine mentioned in the respective article cited by Sci-Finder® in blue. The size of the circles correlate to the frequency of certain key words mentioned.*

The low biotoxicity of squaraines and their near-infrared absorption properties combined with the ability to interact with a biological environment such as cells, tissues and organs, resulting in an observable molecular transformation make squaraine attractive and unique materials for biomedicinal applications.[5,21] Here, squaraines can be employed in non-linear optics and as stable near infrared fluorescence absorbers for bioimaging, additionally in photodynamic therapy and its use as organic semiconductor within a photoactive layer for a photoelectrical stimulation of neuronal cells was shown.

Besides the biomedical applications[5,21,25] the other major field of application of squaraines is in organic photovoltaics (OPV) and photodetectors (OPDs).[14–17,19,20,27] As already showcased by the outdated use of squaraines as active material for photoconductive layers in xerographic,[6–8] the ability to generate and transport charges efficiently alongside high molar absorptivity and fluorescence quantum yields makes them attractive for organic solar cells and photodiodes and organic light-emitting diodes (OLEDs).[28–30]

1.1.1 Optoelectronic Devices

With regard to optoelectronic devices the two most relevant examples for squaraines are OPV and OPD, organic photodiodes. In both cases, light is converted into electric current. For photodiodes, which are semiconductor diodes, this conversion happens at a p-n junction between the squaraine usually used as the absorber component and a suitable acceptor material. For solar cells (OPV) a suitable positive bias voltage needs to be applied in order to ensure the function for energy generation. OPD on the other hand are operated in reverse bias by applying a negative voltage or in quasi-short-circuit mode (without an applied voltage). Thus, they act as light sensors or detectors. The generated photocurrent is then linearly dependent on the light intensity. As such, the overarching principle, the ability to convert light into an electric current, is the same for both OPV and OPD, only the mode of operation differs.[5,16,31–33]

Organic photodiodes often feature a typical layered structure (Figure 4) with the respective electrodes on the outset. Sandwiched between these are the respective transport layers, with the electron transport layer (ETL) directly next to the cathode and the hole transport layer (HTL) directly next to the anode. Depending on whether the cathode or the anode form the top layer during the device fabrication these architectures are referred to as normal structure with the cathode at the top or inverted structure when the anode is the top layer. In the middle of the stack is the active layer comprised of the photoactive materials. Here, a mixture of two types of photoactive compounds is present. On the one hand there is the acceptor material and on the other hand there is the donor or absorber material. Donor in this context refers to the ability to donate electrons upon excitation, roughly speaking a p-type semiconductor, whereas acceptor refers to the ability to accept the electron donated by the donor, an n-type semiconductor so to speak. Within the active layer two morphologies are pursued, each having a distinct pros and cons.[31,32,34–37]

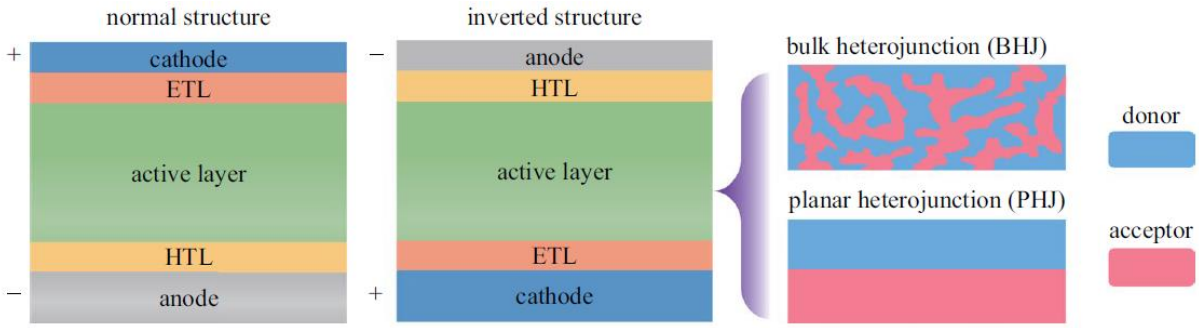

***Figure 4**: Schematic representation of typical organic photodiode architectures. Reprinted with permission from literature.[34]*

The planar heterojunction (PHJ) features the layering of acceptor and donor on top of each other. This results in a clear cut, reproducible and defined topology. Additionally, this type of heterojunction consists of only one interface between donor and acceptor material, which is both an advantage and disadvantage in itself. On the one hand this allows for a simple straightforward fabrication but efficiency is low due to limited exciton diffusion as charge separation of the exciton into electron and hole can only take place at the interface between donor and acceptor material. This means the formed

exciton needs to travel to the donor-acceptor interface. Hence, the generated charge carriers need to travel from this interface to the way to the respective transport layer and ultimately to the corresponding electrode. Thus, the layer thickness of the acceptor layer equals the distance the charge carriers need to travel without recombination along the path.[31,32,34]

Bulk heterojunctions (BHJ) bypass this challenge by its nanostructured interpenetrating network of donor and acceptor material in its blend. This results in a significantly larger interfacial area compared to PHJs, improving the charge separation and efficiency. Additionally, the charge carrier transport is also improved. As of now, BHJ structures have been widely adopted for both OPVs and organic photodiodes. However, reproducibility is a major a challenge as the exact interpenetration and intermixing might vary in each BHJ even if the fabrication parameters remain identical and unchanged. Various solution coating approaches using blended solutions of donor and acceptor have been developed. [31,32,34]

OSCs

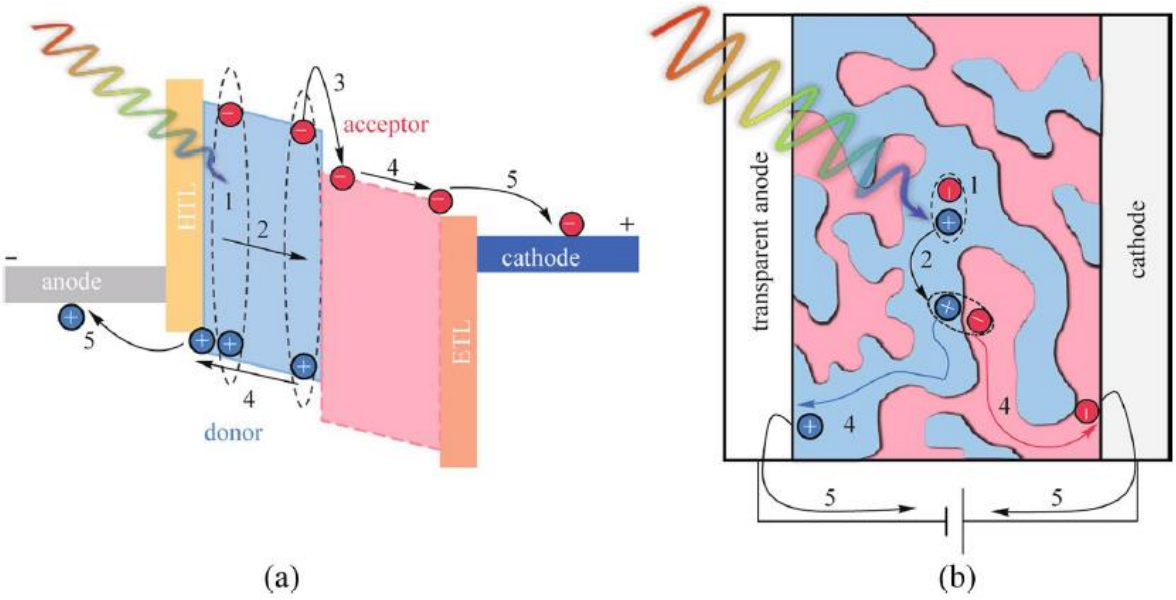

***Figure 5**: Working principles of an organic PHJ photodiode and its BHJ counterpart. Reprinted with permission from literature.[34]*

Fundamentally the working principle of organic photodiodes consists of five key steps (Figure 5): (1) light absorption in the active layer, leading to exciton formation; (2) exciton migration toward the donor-acceptor interface; (3) exciton dissociation into free charge carriers – electrons and holes; (4) transport of charge carriers through the active material towards the hole transport layer (HTL) or the electron transport layer (ETL), respectively; and (5) collection of charges at the electrodes, generating a photocurrent. [31,32,34]

Certain types of squaraines were already successfully implemented in organic photovoltaics and alike. Here, squaraines can be applied either in hybrid and purely organic solar cells of different morphologies, with the BHJ motif as the most common morphology. These BHJ then often feature a blend of squaraines as the donor (electron-donating or p-type) semiconductor and an electron-withdrawing material like fullerenes as the acceptor counterpart. The application of an organic photovoltaic cell with an asymmetric squaraine molecule as an absorber for a dye-sensitized solar cell (DSSC) has demonstrated promising potential of this approach, showing a power conversion efficiency over 8%. [14,16,18,38–41]

1.2 TYPES OF SQUARAINES

Squaraines can roughly be divided into two categories, symmetric ones and asymmetric ones, with more examples for asymmetric ones,[42,43] as significantly more modifications on the squaraine framework are possible. Core-functionalization and side chain modification further expand the family of squaraine dyes, enabling the fine tuning of certain properties for the specific needs of the envisioned applications.

Symmetric squaraines on the other side are often subdivided into two subtypes A and B, referring to the difference of an additional methine-bridge found in type B. Furthermore, both 1,2- and 1,3-substitution, referring to the arrangement of the substituents on the squaric acid core are both known (Scheme 1).[42,43]

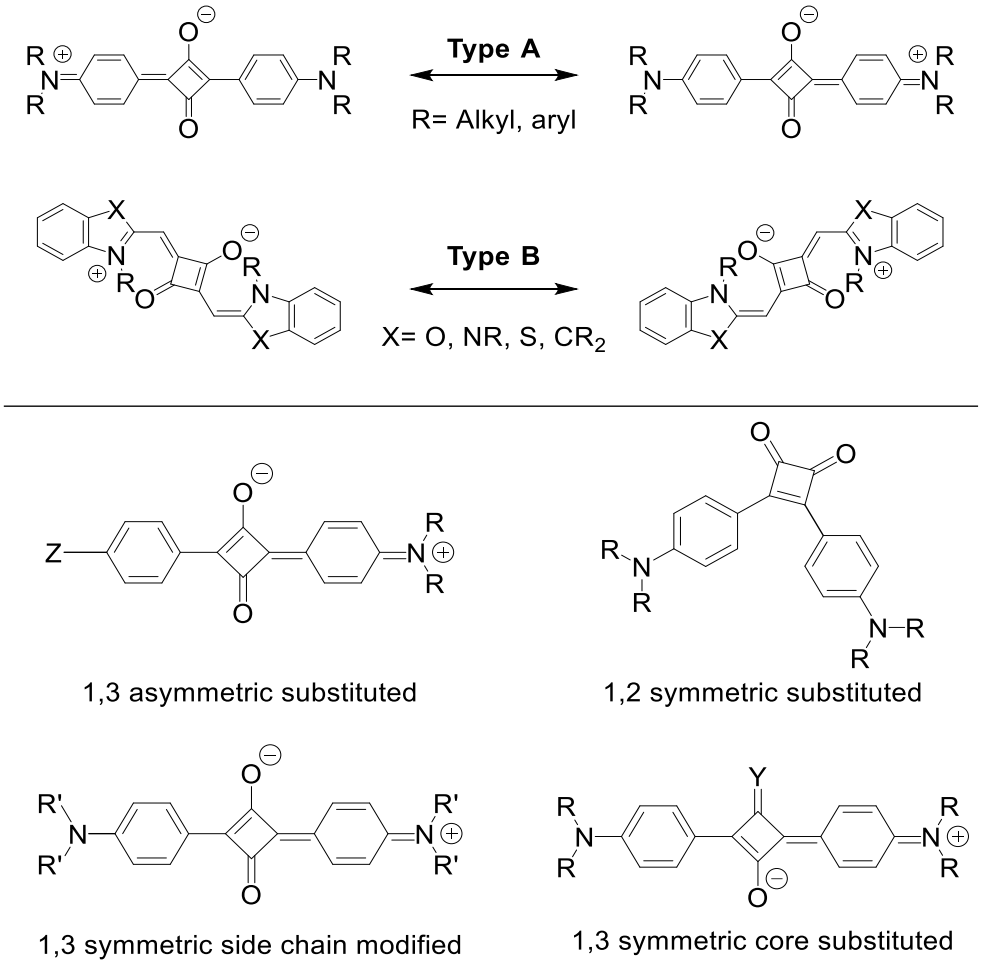

***Scheme 1**: Overview of selected general structures of squaraines, with the two prevalent structure types A and B on the top, which show the additional methine bridge in the type B squaraines, and symmetric representatives of type A squaraines on the bottom to visualize the different substitution patterns.[43]*

A well investigated example of type A symmetric squaraines are the *N*,*N*-dialkylanilino squaraines (*N*-alkyl-SQs).[39,42–46] These are obtained via condensation of an electron-rich aniline with squaric acid. These compounds feature a D-A-D-structure reflecting the quadrupolar nature of the chromophore core.[43] Here, the nitrogen atoms fulfill the role as the donor units and the squarylium core is the acceptor part. Within this subclass the influence of side chains on the nitrogen atoms and the additional hydroxyl-functions on the aromatic ring of the aniline framework were investigated,[31,32,39,44,45,47] and both factors were found to play an important role for the properties of the respective dyes. This is shown in the lowering of the energy level of highest occupied molecular

orbital (HOMO) for the OH-containing anilino squaraine compared to the one without these groups.[39] The squaraines with either two additional OH-functions ($SQ(OH)_2$) or four OH-functions ($SQ(OH)_4$) (Scheme 2) show a different spatial arrangement compared to the SQ without additional OH-groups at the 3 and/or 5 position of the aniline substituent. Coplanarization is the result of intramolecular hydrogen bonds between the carbonyl functions of the cyclobutane core and the additional hydroxyfunctions.[39] This significantly influences the intermolecular interactions as seen in various crystal structures of this class' representatives.[39,48] *N*-alkyl-SQs are mostly investigated regarding their optical properties, their aggregation behavior, and their application in optoelectronics as they typically show sharp absorption between 600-700 nm and high extinction coefficients.[31,32,44,45,48]

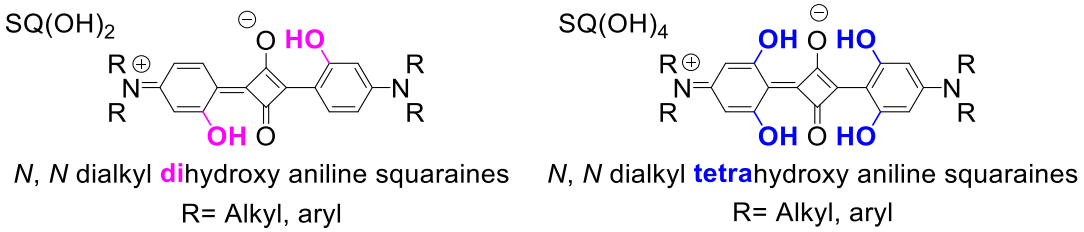

***Scheme 2**: Molecular structures of dihydroxylated (left) and tetrahydroxylated (right) aniline squaraines $SQ(OH)_2$ and $SQ(OH)_4$.*

There are also examples of both symmetric and asymmetric SQ that are used as either photo initiators or co-initiators for polymerization.[49] Here, another case of symmetric SQ is showcased, the direct substitution of a heteroatom on the squaric core. This results in a significantly smaller conjugated π-system as seen in the shift of absorption maxima to 300-500 nm.[49] Thus, these 1,3-bis(arylamino) squaraines are better suited for polymerization reaction in the near UV-range.[49–51] For near-IR polymerization an array of both symmetric and asymmetric 1,2- and 1,3-substituted type B squaraines were published[49,52,53] once again highlighting the versatility and tunability of this dye class (Scheme 3).

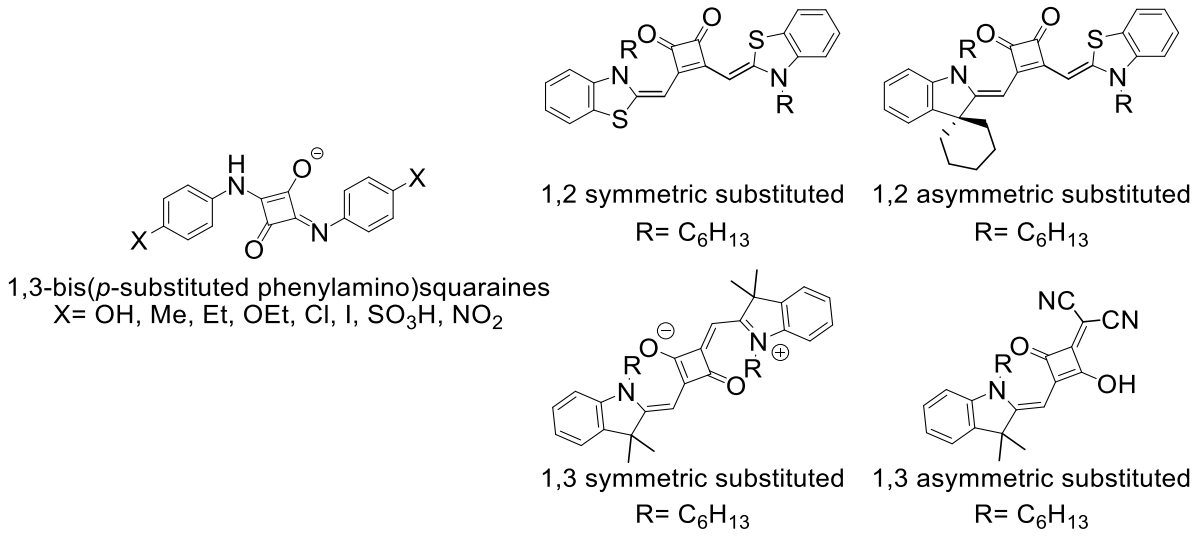

***Scheme 3**: Molecular structures of other core-functionalized types of squaraines that found application in polymerization processes.*

Asymmetric squaraines offer even more structural possibilities and setscrews for modifications. With more modification sites available, vastly different properties can be achieved, which result in an even broader application spectrum. Besides the aforementioned application in optoelectronics, photovoltaic and medicine, ion recognition as well as pH-indication are also possible. Nevertheless, the major direction of research is still focused on the application in either medicine, especially bioimaging as a stable near infrared fluorescence absorber, or in optoelectronics such as photovoltaics

and photodetectors. However, an asymmetric structure also allows for the introduction of both, polar and apolar functional groups, which leads to the synthesis of amphiphilic SQs. These are prominently used in bioimaging application and photothermal therapy due to their excellent biocompatibility and low cytotoxicity.[5,21] Furthermore, they might also be interesting compounds for synthetic approaches like micellar or emulsion catalysis (see also Chapter 3).

Beside the monomeric squaraines, there are also oligo- and polysquaraines.[49,54,55] As their names suggest they contain multiple squaraine units. Again, the most important field of application of these is photovoltaics. Often these polymeric squaraine achieve better results compared to their monodisperse monomeric counterparts, as has been shown in certain BHJ-OSC.[43,55] The major drawback of polymeric compounds, however, is the limited reproducibility, a problem inherent to the fabrication process. Thus, better control over the material for the active photolayer is usually achieved when highly pure monodisperse compounds are used.

As highlighted by the diverse fields of application, squaraine are a versatile class of molecules whose individual final properties highly depend on its structure. Thus, gaining a better impression about structure activity relationships is of utmost interest to be able to tailor these properties. Hence, different synthetic pathways have been evolved to access the different kinds of squaraines.

1.3 SYNTHESIS

Generally speaking, the synthesis of squaraines can be simplified to a twofold substitution at the squaric acid core, mostly resulting in the liberation of smaller compounds while the desired larger framework is obtained. Thus, it is most often referred to as a twofold condensation reaction. Depending on the employed nucleophiles and the source of the squaric acid core, a broad variety of squaraines can be addressed.[5,42,43,56]

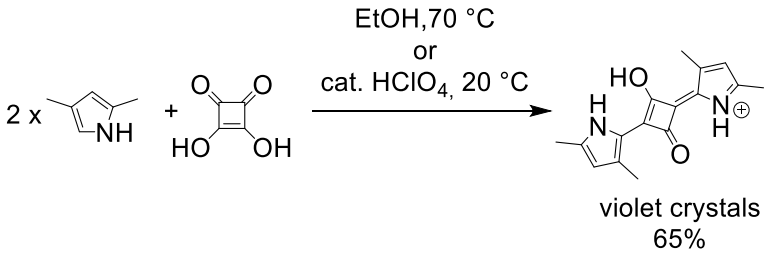

***Scheme 4**: Synthesis of the first squaraine reported by Jacobs and Treibs.[2]*

The original and historic approach by *Jacobs* and *Treibs* from 1965[2] features the direct reaction of an electron-rich aromatic amine with squaric acid (Scheme 4). Since then, different new synthetic approaches were developed in order to make more synthetic targets accessible. Most of them rely on the intermediate removal of water in order to make the condensation reaction irreversible and shifting the equilibrium more towards the desired product. This can either be achieved by usage of desiccants like molecular sieves, drying reagents like ortho-formic ester[57] or the azeotropic removal of water by using high boiling polar solvents such as alcohols like 1-butanol and an aromatic hydrocarbon.[5,32,42,43] Originally, the azeotropic water removal was developed by *Sprenger* and *Ziegenbein*[58] and used a 1/1 mixture of 1-butanol/benzene. Nowadays, benzene is exchanged for the less toxic toluene in this standard synthetic approach for squaraines. In fact, the use of alcohols facilitates the synthesis of the desired squaraine as suggested by the most commonly proposed reaction mechanism (Scheme 5).[5]

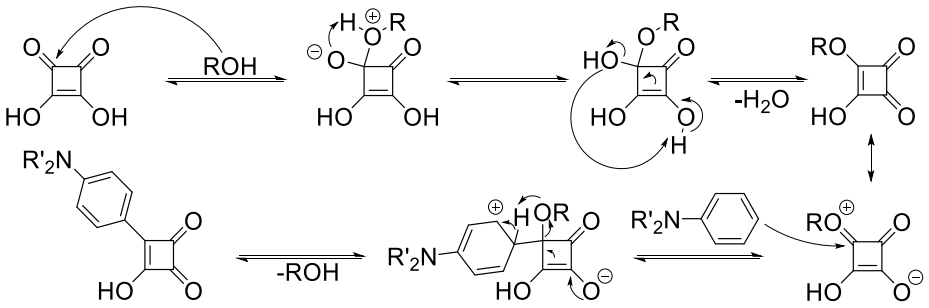

***Scheme 5**: First part of the proposed mechanism for the formation of squaraines in a twofold condensation procedure.[5]*

The alcohol activates the squaric acid for the reaction as it intermediately forms an ester with the acid, diminishing the mesomeric stabilization of the core, and hence, increasing its reactivity towards the attack of the nucleophile, like an electron rich aromatic compound, resulting in the nucleophilic substitution of the previously introduced alkoxy group with the nucleophile.[59] The so formed hemisquaraine can then in turn react with either a second moiety of the same nucleophile or a different second nucleophile giving the desired symmetric or asymmetric squaraine and liberating the second equivalent of water (Scheme 6).[5,31,32,60]

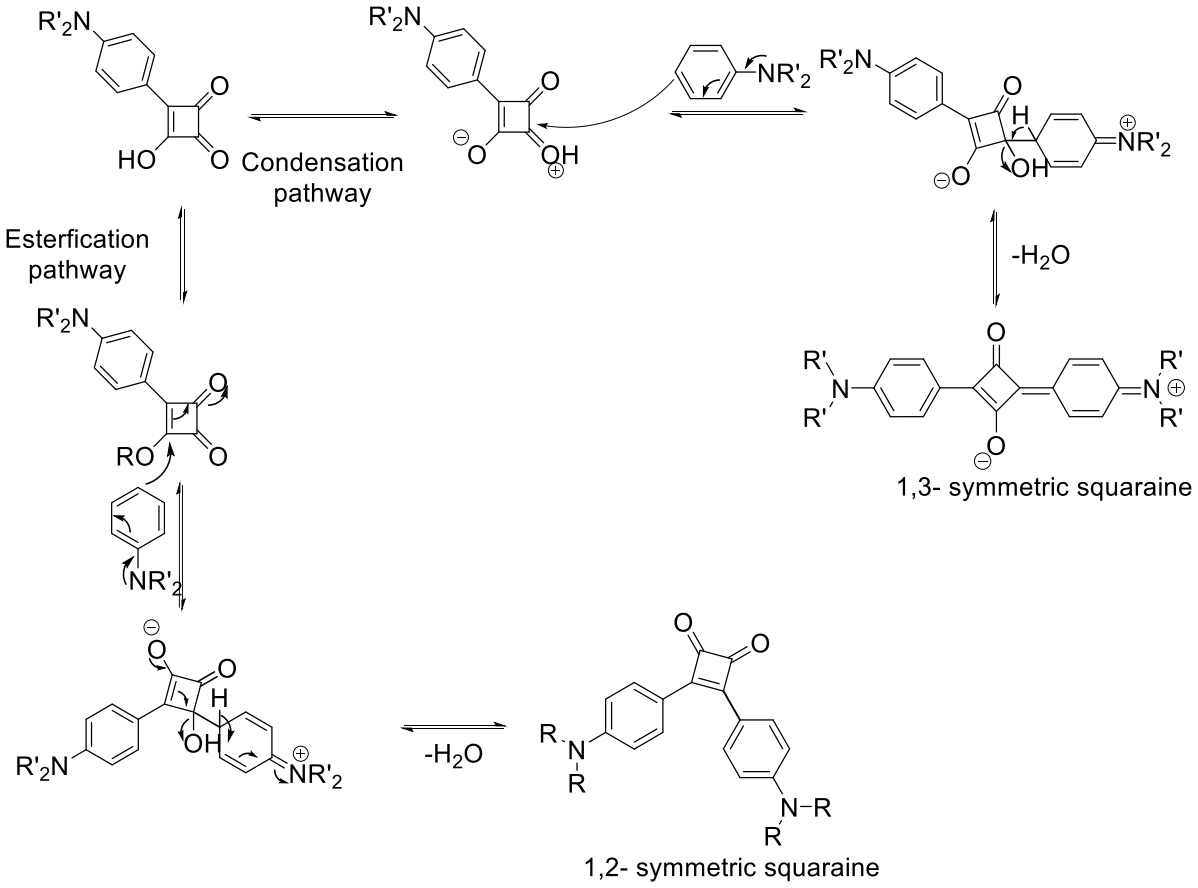

***Scheme 6**: Second part of the proposed mechanism for the formation of squaraines in a twofold condensation procedure showing the two pathways to the regioisomeric 1,2- and 1,3-squaraines.*

Symmetric Squaraines

If a second moiety of the initial nucleophile is used, the resulting squaraine is of symmetric nature with two possible substitution patterns. Depending on the reaction site, which is heavily influenced by the reactivity of the nucleophile, either the 1,2- or the 1,3-substituted symmetric squaraine is obtained.[42] On average, the preferred product is the 1,3-substituted product.[61]

The 3-position of the squaric core of the hemisquaraine is more reactive compared to the 2 position, due to its increased electron density. This allows for a more facile protonation by either an additional squaric acid molecule or by itself, as hemisquaraines are relatively acidic themselves.[42] However, the 1,2-substituted squaraine can be synthesized on purpose, when highly reactive nucleophiles are used and the reaction is performed at significantly elevated temperatures and prolonged reaction times.[43] Elsewise, it is only obtained as a byproduct. Type A squaraines are directly obtained using an electron-rich aromatic compound, often pyrroles, phenols, azulenes or anilines, as nucleophiles.[5] For type B squaraines anhydrobases derived from the *in-situ* deprotonation of a suitable methylazinium precursor (benzothiazolium, indoleninium, pyridinium, quinolinium, etc.) with a base[42,43] are used as nucleophiles.

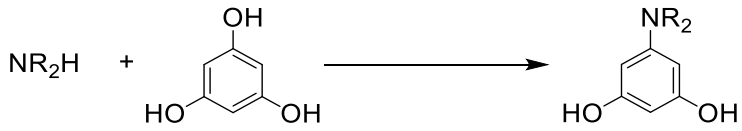

***Scheme 7**: Synthesis of 3,5-hydroxylated anilines from phloroglucinol and secondary amines.*

As for the synthesis of the highly desired *N*,*N*-dialkyl-di- and tetrahydroxy anilino squaraines the nucleophiles in question are *N*,*N*-dialkyl-3-hydroxyaniline and *N*,*N*-dialkyl-3,5-dihydroxyaniline, respectively. These are either accessible via commercially available 3-aminophenol and 3,5-dihydroxyaniline, respectively, or if more elaborated and sophisticated substituents at the nitrogen center are supposed to be established the corresponding aniline building block can be prepared from the condensation of phloroglucinol with a decorated secondary amine (Scheme 7).[45,48,62]

Asymmetric Squaraines

The synthesis of asymmetric squaraines is slightly more complex, as the intermediate isolation of the hemisquaraines is necessary.[63–65]

Similar to the symmetrical squaraines, both 1,2- and 1,3- substitution are possible and the influence of the nucleophile is still determining the regioselectivity of the second substitution. In rare cases, such as certain highly electron-rich quinoline anhydrobase derivates,[42,66] the use of squaric acid in excess during the condensation reaction selectively yields the hemisquaraine. Substitution with an electron-withdrawing substituent on the quinolone ring instead leads to the isolation of the respective symmetrical squaraine.[42,66] A more versatile approach is the use of a squaric acid analogue to introduce the squaric core like its esters or squarylium chloride.[67] Both are commercially available and readily obtainable from squaric acid via esterification with the respective alcohol of transformation towards squarylium chloride using thionyl chloride. As squarylium chloride is more reactive compared to the esters, it is suitable for less reactive substrates (e.g., electron-poor aromatic compounds), making those accessible for the squaraine synthesis, whereas the squaric acid esters are sufficient for electron-rich substrates. In both cases, the isolated hemichloride and hemisquarate can be hydrolyzed both under acidic or basic conditions to the desired hemisquaraine, which in turn is used for the following condensation with the second nucleophile to obtain the asymmetric squaraine.[43] This approach allows for a modular synthetic strategy, giving rise to a highly diverse and broad variety of squaraines.

2 TASK AND OBJECTIVE

As already established squaraines are an intriguing class of molecules, which have a wide field of applications and seemingly endless possibilities for future endeavors, especially in the field of optoelectronics. With its tunable properties and the many synthetic routes developed, certain characteristics with regards to the employment in photodiodes were deemed especially desirable. This is true for both, processibility, i.e., solution processing and chemical vapor deposition, in order to create thin films and specific (chir-)optical properties.

However, squaraines are also promising candidates for new synthetic approaches, e.g., micellar or emulsion catalysis where a combination of amphiphilic properties and switchable optical properties might open up new avenues for these approaches that allow naked eye detection of the state of the additive amphiphile to facilitate the workup of such synthesis, and ultimately the isolation of the desired products.

Hence, the goal of this thesis is to synthesize new (chiral) squaraines to further investigate the structure-activity relations of these compounds in order to gain a deeper insight and understanding of the molecular structure on the materials properties focusing on three different aspects.

- Synthesis of amphiphilic squaraines for an application in micellar or emulsion catalysis (Chapter 3)

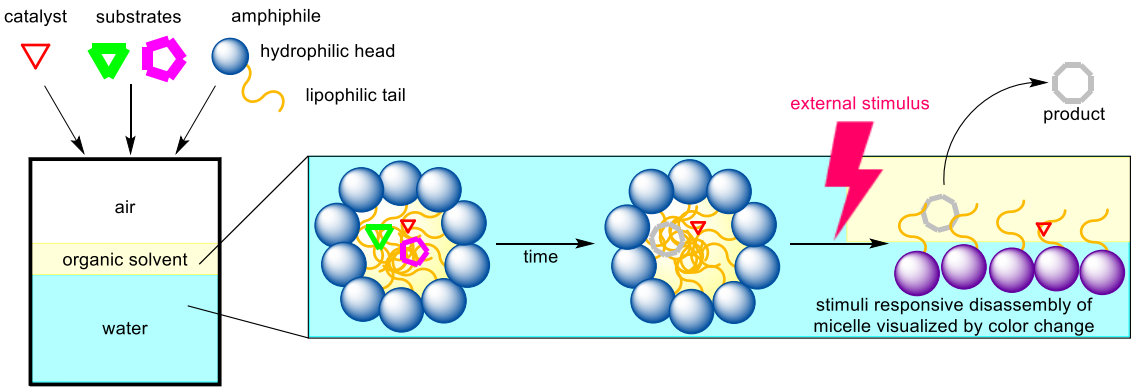

- Synthesis of chiral squaraines and testing of their sublimability (Chapter 4)

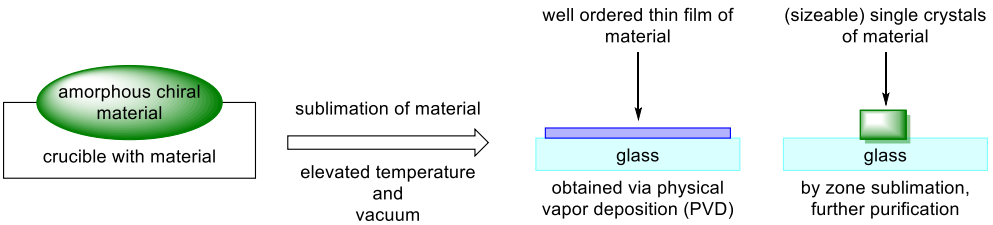

- Synthesis of a new class of chiral squaraines that combines benefits of the aggregation behavior of achiral *N*,*N*-dialkyl anilino squaraines with the chiroptical properties of proline-derived anilino squaraines (Chapter 5)

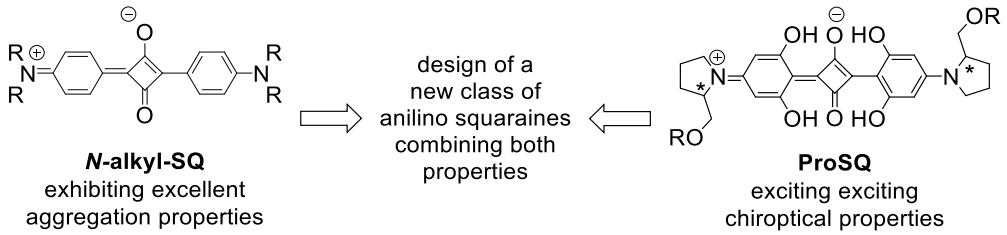

***N*-alkyl-SQ**
exhibiting excellent
aggregation properties

ProSQ
exciting exciting
chiroptical properties

Here, the reoccurring focus was the combination of promising structural motifs, which were tested separately from each other, into hybrids that bridges the respective demands for the envisioned applications.

In the following chapters each of these aspects will be introduced in more detail together with a discussion of the results obtained during this thesis.

3 AMPHIPHILIC SQUARAINES

As of now the majority of amphiphilic squaraines are used for bioimaging application,[21,24] photothermal therapy[21] and as chromophores in solar cells. These mostly highlight the aspects of the low cytotoxicity squaraine exhibits and its NIR-absorbance ability.[5] Thus, the excellent biocompatibility gave rise to multiple patents[68,69] focusing on the high potential regarding the development of more biocompatible amphiphilic squaraines and their use as NIR-fluorescence probes.[5,70–73]

Amphiphilic squaraines have to feature both lipophilic structural motifs and hydrophilic motifs. To achieve this certain functional groups are often introduced into the molecule to increase its hydrophilicity as this characteristic is more challenging to introduce into an organic molecule. The most common motif for introduction of hydrophilicity are glycolic chains.[74–76] Alternatively, the respective squaraine quaternary ammonium bromides were used.[77] The introduction of highly polar functional groups like free hydroxyl groups,[22] amines[77], carboxylic acids[78] and sulfonates[78] are also viable strategies. This often results in asymmetric squaraines. The synthesis of the two precursors which are predominantly polar and apolar, respectively, and the subsequent reactions thereof with squaric acid or its derivatives forming the amphiphilic squaraine is in general more practical and easier to handle than trying to use two amphiphilic precursors forming a symmetric squaraine. Additionally symmetric amphiphilic squaraines would be less suited to form the desire micelles. A further advantage is related to the simplified synthetic pathways towards the precursors with clear solubility preferences, as their reactivity is better defined, the purification is comparably straightforward since extraction with suitable solvents is less complicated and less unpredictable interferences can occur. Additionally, this approach enables a modular synthetic approach, allowing a better control over the amphiphilicity as the respective precursors can be adjusted to fine-tune the resulting amphiphilicity. A possible measure for amphiphilicity that takes the structure of the molecule of choice into account is the *hydrophilic-lipophilic balance* (HLB).[79–83] The other possibilities to evaluate the amphiphilicity of a given compound involve mostly empirical methods, like the measurement of the contact angle of a water droplet on a surface coated with the compound in question.

Hydrophilic-Lipophilic Balance (HLB)

The HLB of an amphiphilic compound refers to the mass ratio and balance between the hydrophilic and lipophilic regions of the molecule. This parameter is among other things used to estimate the amphiphilicity of surfactants. It is given in a dimensionless numeric scale differentiating between neutral lipophilic surfactants (HLB < 10), which favor water-in-oil emulsions; hydrophilic surfactants (HLB > 10), suitable for oil-in-water emulsions; and balanced surfactants with an HLB of 10. Surfactants with charges generally have HLB values exceeding 20. The HLB can be calculate either according to Griffin as shown in equation 1[79,83] or according to Davies (equation 2).[81,84]

$$HBL = \frac{Mass\ of\ Hydrophilic\ Portion}{Total\ Mass\ of\ Molecule} \times 20 \qquad \textbf{(Equation 1)}$$

$$HBL = \Sigma(Hydrophilic\ Group\ Values) - \Sigma(Lipophilic\ Group\ Values) + 7 \qquad \textbf{(Equation 2)}$$

Davies approach as the more recent development attributes so-called group values to functional groups and structural motifs. These are determined according to empirical data and the correlation between functional group contributions to surfactant behavior, such as emulsification tendencies and water/oil solubility with adjustment according to the molecular environment as the group values take the typical behavior of the respective functional group in a specific molecular environment into account.

3.1 SURFACTANTS

An interesting phenomenon observable with amphiphilic molecules is the ability to influence on the surface and interface energy, which results in the reduction of surface and interface tension between two immiscible phases. This is due to the alignment of the surface-active agents (surfactants) according to their preferences, e.g., in case of a water/oil interface the amphiphilic compound will in the way to maximize the attractive interaction. Hence, the lipophilic part of the compound will immerse into the oil phase, whereas the hydrophilic part will interact with the water. This principle also explains the facilitated emulsification, dispersion and foaming in the presence of a surfactant compared to the case without. This can be nicely visualized with the example of immiscible water and oil mixture, that easily separates back into two phases, even after vigorous mixing, compared to homogeneous appearing water and oil mixture like pasteurized milk or mayonnaise.[85]

Historically speaking, the discovery of surfactants dates back to around 2800 BCE in ancient Mesopotamia.[86–88] Traces of soap-like substances created from boiling animal fats with wood ash were recorded on Babylonian clay tablets. Through the course of history and various ancient civilizations this approach was improved upon moving from animal fats to plant-based oils and later large-scale industrial productions.[86–88] With the scale-up of production and the better availability soaps, which once were a luxury product, became wide spread. Alongside the discovery and better understanding of germs around the 19th Century, soaps significantly contributed to disease prevention and overall improved sanitation.[86–89] This nowadays common knowledge still shows its valuable and beneficial influence as most recently experienced during the COVID-19 pandemic, where even a simple act of hand washing was crucial for reducing the infection risk.[88,90,91] This effect still is rooted in the amphiphilicity of soaps. The ability to disrupt microbial structures through interaction of the lipophilic part with lipid membrane of microbes, and thus, the physical removal of pathogens from the skin, especially the hands, by micelle formation, all result in reducing the transmission of infectious diseases.[88,89] Additional benefits resulting from disease prevention is significantly reduced child mortality alongside improved public health and hygiene in general.[88,90,91]

Besides longevity improving benefits of soaps, more recently other fields of application of amphiphilic compounds became popular. On the one hand food additives like emulsifier such as lecithin and polysorbates as well as mono- and diglycerides of fatty acids are widely used to improve texture and prevents ingredient separation of process food to enhance shelf life.[92,93] On the other hand cosmetics also greatly benefit from amphiphilic compounds.[94,95] With the typical characteristics of surfactants, better emulsions like lotion and creams with smoother textures and improved stabilization of the finish product are obtained. Besides the textural improvement, the employed surfactants can also help to deliver active compounds of the cosmetics to achieve an enhanced skin penetration. These desirable impacts overall lead to an almost omnipresent demand for surfactants whenever stabilization and prevention of phase separation of ingredients is sought after.[88,94,95]

Typical everyday examples of surfactant are found in detergents, like surfactants in dishwasher soap, or food. Surfactants can be naturally occurring, like e.g., casein or lecithin. The most prominent examples found in detergents like SLS (sodium lauryl sulfate, also known as SDS sodium dodecyl sulfate) or SLE (sodium laureth sulfate, also known as sodium dodecyl polyoxyethylene sulfate) are commercially available due to large-scale industrial production.[96–98] Both SLS and SLE are representatives of anionic surfactants. Beside these, there are categories of nonionic (e.g., **Koliphor EL**), cationic (e.g., CTAB) and zwitterionic (e.g., CAPB) surfactants (Scheme 8). Beside these widely spread and commercially available surfactants there is also the class of so-called designer surfactants, amphiphilic molecules specifically designed and synthesized to fulfill well defined tasks.

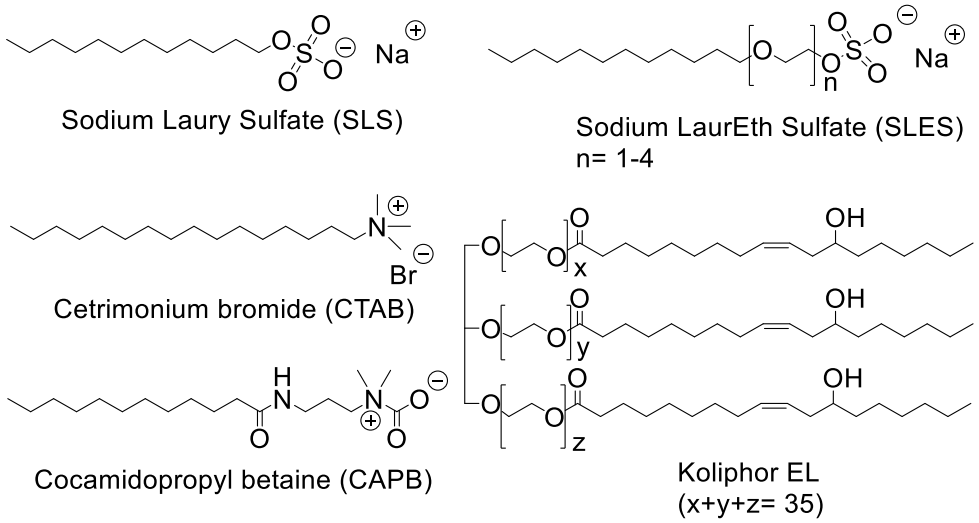

***Scheme 8**: Examples for widespread commercially available surfactants including anionic, cationic, zwitterionic and neutral ones.*

3.1.1 Micelles

When surfactants are added to an immiscible biphasic system, for example water and air, they will localize at the surface of the aqueous phase, with the hydrophilic parts immersed in water and the lipophilic part reaching out into the air until the surface is completely covered by surfactant molecules. Upon further addition of surfactants into a system where the interface is already saturated the additional surfactants will self-aggregate in order to maximize favorable interactions under avoidance and minimization of unfavorable interactions. This phenomenon results in interesting architectures called micelles on a nanometer scale (Figure 6). Micelles are formed when the number of surfactants in an environment surpasses the specific concentration characteristically defined for that surfactant. This concentration is defined as the critical micellar concentration (CMC) and varies from surfactant to surfactant. Ideal micelles are depicted as spheres, where in an aqueous medium the hydrophilic part form the shell facing outwards toward the aqueous surrounding whereas the hydrophobic parts, often shown as lipophilic tails, gather inside the sphere. This results in a non-polar core of the micelle. Realistically speaking the size and shape of the micelle greatly depend on the surfactant employed as the structure and characteristics of it dictate the geometry. Additionally, the concentration of the surfactant in an aqueous system can also cause the shape and size to deviate from the idealized sphere.[85]

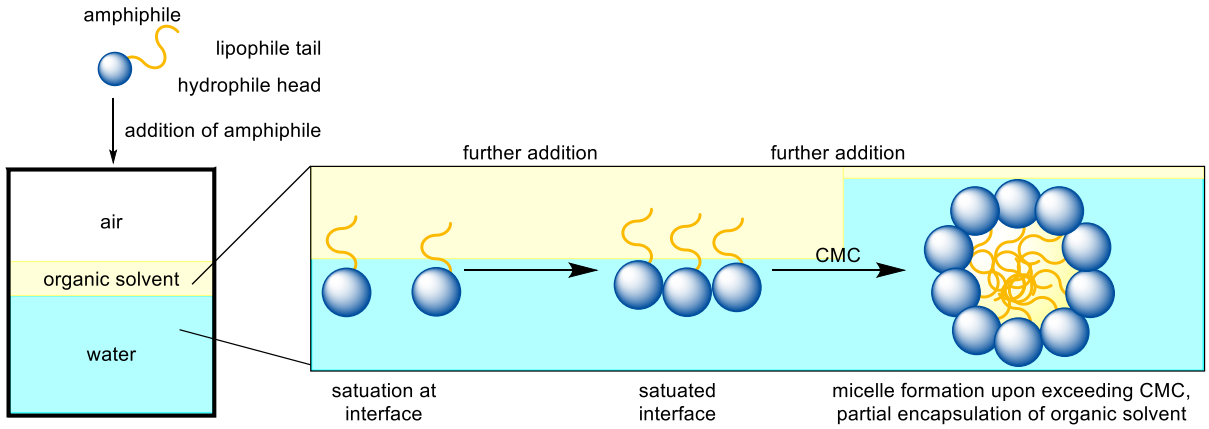

***Figure 6**: Cartoon illustrating the formation of micelles using amphiphilic surfactants. Pale yellow coloring indicates organic solvent; light blue coloring indicates aqueous milieu. Critical micelle concentration is abbreviated as CMC.*

3.1.2 Micellar Catalysis

The term micellar catalysis refers to an upcoming new synthetic approach towards catalysis.[85,99–103] It utilizes surfactants, both industrial grade or highly functionalized designer ones, as additives to introduce a novel reaction environment for a catalytic transformation.[104] Here, most often a solvent mixture of water and an organic solvent is employed.[105] Compared to the traditional and conventional synthetic method, the amount of organic solvent needed for the catalysis is significantly reduce.[106] This is due to the solubilizing effect of the hydrophobic part of the surfactant, forming a hydrophobic cavity within the micelle. As a result, the small amount of the organic solvent and with it the organic molecules are encapsulated in the micelle. Ultimately, this results in an increased effective concentration of substrates within the micelle, often resulting in an accelerated and more efficient reaction. Thus, the micelles can be perceived as a nanoreactor providing a unique environment for chemical reactions. Additional effects of the compartmentalization include the interface between the hydrophobic core and the hydrophilic shell, which can offer a favorable environment for catalytic reactions as in case of transition metal catalyzed reactions, such as the well-known Suzuki-Miyaura reaction.[106–108] The water-soluble transition metal cations tend to co-localize at the hydrophilic shell of the micelles, resulting in closer proximities of substrate and catalyst, which in turn allows for a sizeable reduction of the catalyst loading. Hence, further advantages resulting from the increased effective concentration can be found in the shortened reaction times and lowered reaction temperature.[106,109]

Additional advantages of the encapsulation can be found in the resulting oxygen-free micelle core, leading to the bypassing of the need for an inert anaerobe atmosphere.[106] This can be seen in the possibility to perform Suzuki−Miyaura micellar cross-coupling in water, under ambient conditions referring to room temperature and aerobic atmosphere.[107,109] Moreover, beside the increased effective concentration of the substrates within the micelle, another effect is postulated, which results from the unique reaction environment found in micelles.[99] In some cases, the conventional and traditional synthetic approach and the novel micellar catalysis approach led to different selectivity,[110] and hence, different synthetic products. This can once again be explained by the unique environment within the micelles that can help stabilize reaction intermediates or transition states, which might otherwise be energetically highly unfavorable in bulk solution. Depending on the absence of charges and highly polar functional groups, the non-polar intermediate can be stabilized in the apolar hydrophobic core, whereas polar and charged transition states experience the stabilizing influence in the polar region. As a result, the activation energy of the reaction could be lowered leading to the formation of another product compared to the respective reaction performed in bulk solution.[110,111]

In summary, there are many advantages in favor of micellar catalysis starting from the significantly increased effective concentration of the substrates within the micelle, which leads to shortening of reaction times, lowering of reaction temperatures and reduction of catalyst loading. The compartmentalization furthermore provides an oxygen-free environment within the micelles which allows to bypass tedious degassing of solvents and reaction atmosphere for oxygen sensitive reactions like some cross-coupling reactions. Followed by the reduced amounts of organic solvent needed during the synthesis as micelles enables the reaction to be carried out in water, which in most cases is not a suitable solvent for organic molecules. Last but not least compounds which cannot be obtained from conventional bulk reaction conditions can sometimes be accessed, as the stabilization of intermediates and transition states through the micelle open up new possibilities.[99,100,104,106,107,109–111]

3.1.3 Challenges

Besides the significant improvement of both hygienic standards and life quality provided through the discovery of surfactants, there have been major negative environmental impacts due to industrial production of surfactants frequently making headlines in the news.[112] Especially persistent foam in all sorts of bodies of water pose a threat to biodiversity and human health.[113,114] With the already challenging growing water demands and the currently observable impacts of climate change like drought and heat waves, water scarcity problems become even more severe. Water is an essential resource but its sources are finite. Thus, water pollution is a problem that needs to be addressed urgently. Beside the water scarcity threat, another danger of tenside contaminated water is the toxicity towards aquatic organisms sometimes even with long-term effects. This on the one hand highlight the need for better regulation regarding waste water disposals, especially in both in industrial and emerging countries, as these are often impacted most severely.[97,98,113,115] On the other hand it stresses the challenge of surfactant removal once it leeks into the environment uncontrolled. Thus, as seen in the current trend of research towards biodegradable[116] and more effective tensides in industry,[117,118] the need for more specialized surfactants with improved removal procedure are needed. Ideally, this is accompanied with easy visualization and indication for micelle breakage.

Similar problems are still prevalent when surfactants are used for synthesis. The various applications and the quick rise in significance clearly show how promising micellar catalysis is. Nonetheless, as a rather recent synthetic approach, there are still challenges that need to be addressed. For once, a frequent stated advantage is the reduced amount of organic solvent used during the reaction compared to traditional procedures. What often gets left out is the amount of solvent that is needed to remove the surfactant. Due to its amphiphilic nature, typical extraction protocols for initial product purification straight from the reaction mixture, become more complicated.

Additionally, the control of actual micelle formation is hard. Realistically speaking, the geometric morphology of the surfactants aggregate is widely unidentified.[100,111] Thus, the portrayal as a monodisperse suspension of idealized micelle is drastically simplified. The more probable description is an ensemble of diverse aggregates with varying size and geometric structure forming a colloidal suspension. [111]

Nevertheless, the aforementioned advantages of reduced catalyst loading, reduced reaction time and temperature as well as the inherent oxygen-free reaction milieu still hold true if a suitable surfactant is used as the structure of surfactant drastically influence the reaction outcome. Hence, the choice of surfactant is crucial. Certain parameters need to be reconsidered in order to make an educated decision. For example, reactions that require a more hydrophobic environment may benefit from surfactants with lower HLB values (indicating a greater lipophilic character), while more hydrophilic reactions may require surfactants with higher HLB. Additionally, it was demonstrated that structural similarities between surfactant and reactants are advantageous.[104] This is reasoned to be caused by comparably more favorable intermolecular interactions between surfactant and reactant, which results in a better solubility and preferred accumulation, and thus, a higher effective concentration in close vicinity of the surfactants. [109]

All in all, the great influence of surfactants in general on everyday life and its desirable traits alongside the high potential of micellar catalysis is obvious and clearly justifies the need to search for new and improved surfactants with improved and/or tailored properties. In industry this is mostly focused on finding a more environmentally friendly, biodegradable but still highly functioning surfactant for mass applications. Whereas in academia the research is often times more towards improved functionality regarding synthesis, resulting in highly specified designer surfactants. In both cases ideally some of the presented challenges regarding surfactants are address or taken into account.

3.2 OBJECTIVE

As a collaborative project during the three-month research stay abroad with Prof. Luca Beverina at the University of Milano-Bicocca, Milano, Italy a new amphiphilic squaraine was envisioned. Here, the idea was to connect the properties of squaraines with typical functional groups ensuring amphiphilic properties in order to generate a designer surfactant for an application in micellar catalysis. Additionally, this surfactant should allow for stimulus responses which in turn would result in a disorganization, and hence, a breakage of micelles, allowing for facilitated isolation of the desired product after micellar catalysis and higher recover and recycling rates of the employed surfactant.

With the typical structural elements for squaraines, especially with the work done regarding influences of additional OH-groups at the aniline framework (Scheme 9), the obvious choice for the desired designer surfactant was the introduction of a pH sensitive motif. This would result in a pH dependent response accompanied by a visual color change, allowing for monitoring assembly formation and disorganization of micelles by naked eye.

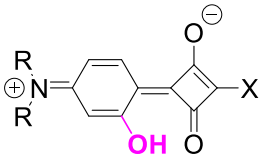

R = alkyl groups (rendering this part lipophilic)
X = second aryl unit furnished with hydrophilic groups

***Scheme 9**: Suggested core structure of the desired asymmetric amphiphilic squaraine designed for a use as a designer surfactant for micellar catalysis. The hydroxyl group (pink) is implemented as an inherent stimuli responsive group that influences the absorption behavior of the squaraine upon its protonation state resulting in a visual signal on the compound's aggregation state.*

Figure 7 is showing the principal idea of using a pH-sensitive squaraine-based designer surfactant in micellar catalysis: At low to medium pH the squaraine has amphiphilic character and forms micelles which can encapsulate the catalyst and the substrates to achieve the desired transformation via micellar catalysis. Upon raising the pH of the solution, the squaraine gets deprotonated, and hence, loses his amphiphilic character becoming more hydrophilic. Thus, the micelles disassemble allowing an easy isolation of the product (and the catalyst). As an additional benefit the dye changes its color upon deprotonation allowing for naked eye detection of the assembly state of the surfactant. Upon acidifying the solution deprotonation is reversed, leading again to a color change and micelle formation.

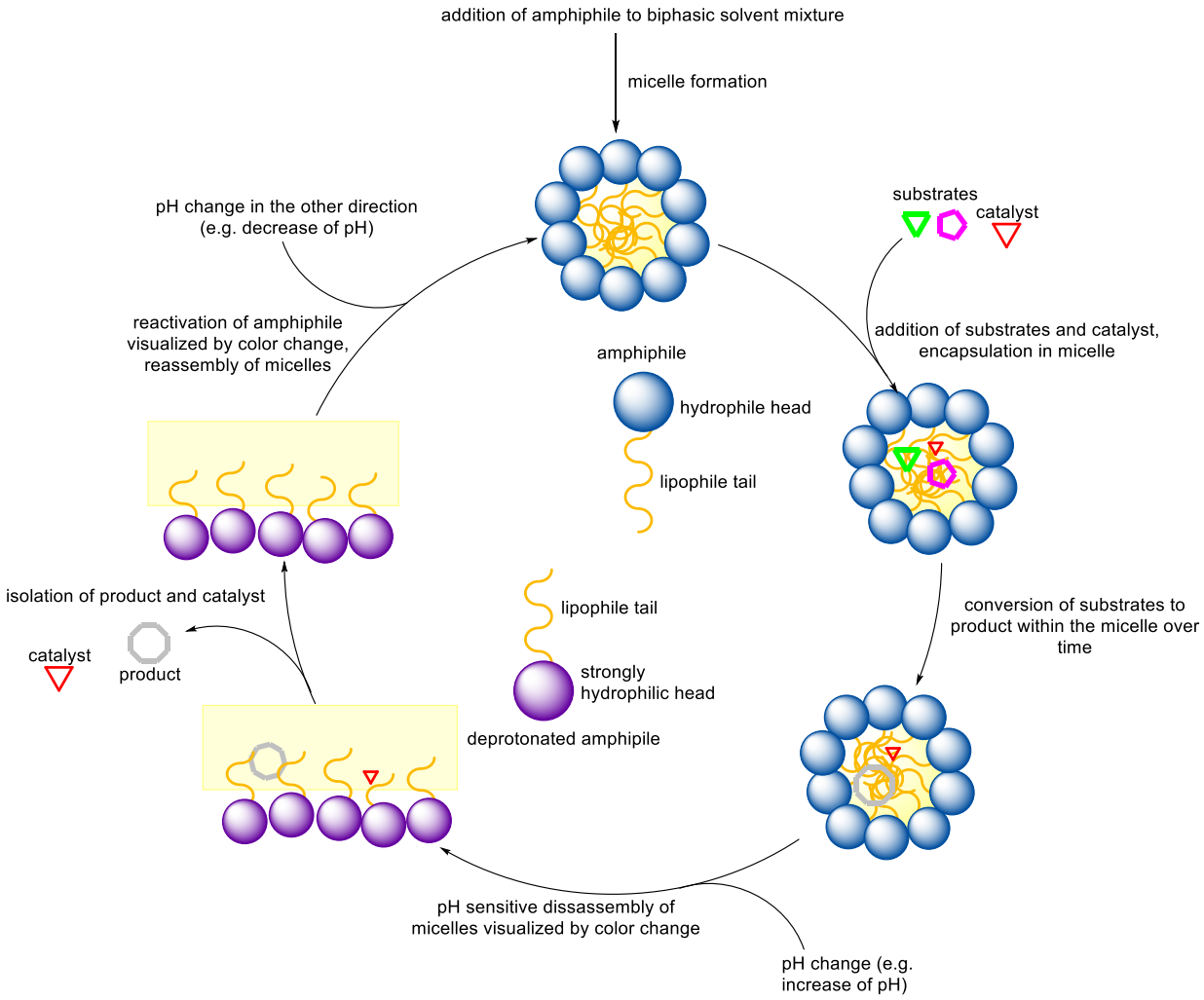

***Figure 7**: Cartoon illustrating the working principle of a pH-sensitive squaraine-based surfactant in micellar catalysis. The biphasic milieu was depicted in a reduced manner omitting the aqueous phase (previously shown as blue surrounding) while as the organic phase is still shown in the pale-yellow coloring seen in the rectangles and within the micelles.*

Thus, the goal of this part of the project was to design and synthesis such a pH-sensitive squaraine-based surfactant and then test it in some model reaction for its applicability in micellar catalysis and compare its performance to established surfactants for this purpose like **Koliphor EL**.[111,119]

3.3 Result and Discussion

3.3.1 Attempts towards the Synthesis of a First Generation of Amphiphilic Squaraines

With parts of the structure of the surfactant (Scheme 9) already being defined as a *N*,*N*-dialkyl 3-hydroxy aniline, a first generation of target structures using succinic acid units as an anchor for the hydrophilic groups as part of X was designed (Scheme 10).

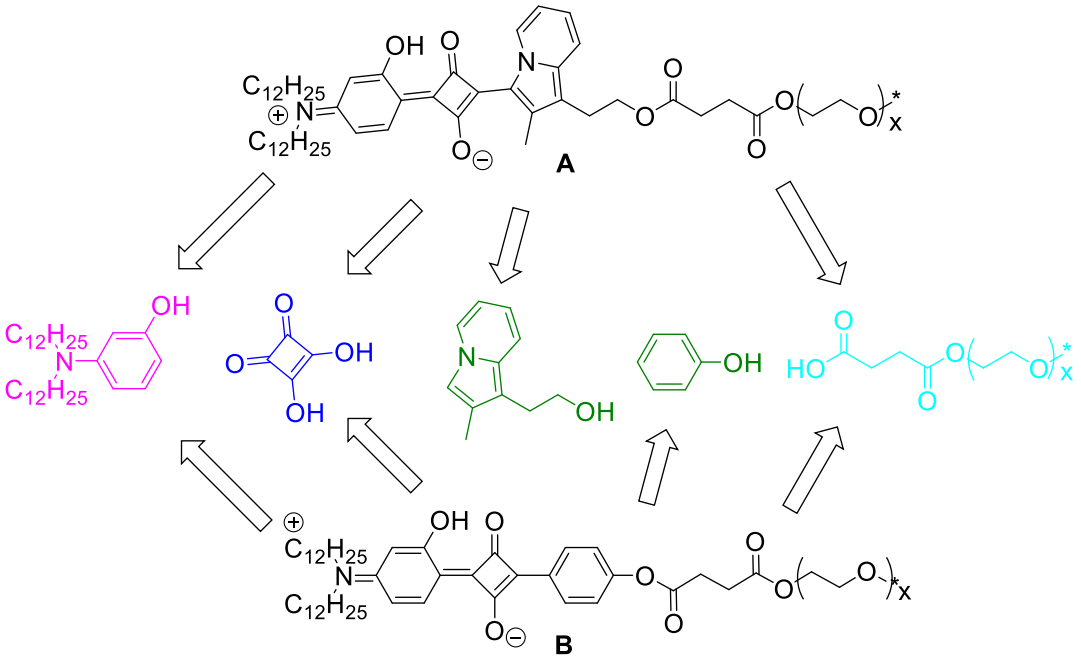

***Scheme 10**: Initial design of pH-sensitive squaraine-based amphiphiles **A** and **B**.*

Here, the dodecyl-groups at the nitrogen provide the lipophilic side of the molecule, whereas the hydrophilicity is introduced by the MPEG-succinic acid ester. As shown in Scheme 10 targets **A** and **B** can be divided into very similar building blocks in a modular approach. Hence, the identical fragments were to be synthesized first, which should then be combined with the respective aryl connector (green) to give either **A** or **B**.

Additionally, this approach takes a vital strategy regarding synthesis of amphiphilic molecules into account: connect the polar and apolar part as late as possible. This strategy delays the significantly more complicated purification of amphiphilic compounds compared to predominantly polar or apolar compounds, respectively. Such a strategy usually results in higher purity and much easier isolation, and hence, increased yields.

Target **A** was pursued first as the aryl connector (green) was already successfully synthesized by *A. Zucchi* from the *Beverina* lab and was kindly made available for this project. Thus, the anilino hemisquarate and its precursors needed to be synthesized first. Double alkylation of 3-aminophenol gave literature known **1** in excellent yield (Scheme 11).

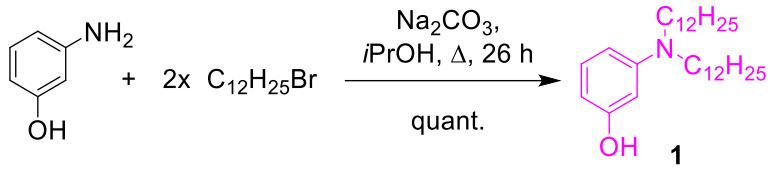

***Scheme 11**: Synthesis of **1**.*

As mentioned before, asymmetric squaraines are more likely obtained when squaric acid derivatives like the corresponding esters or chlorides are used in the condensation reaction instead of the acid itself. Hence, the use of the squarylium chloride (Figure 8) was deemed to be the more promising starting material for the synthesis of the desired hemisquaraine.

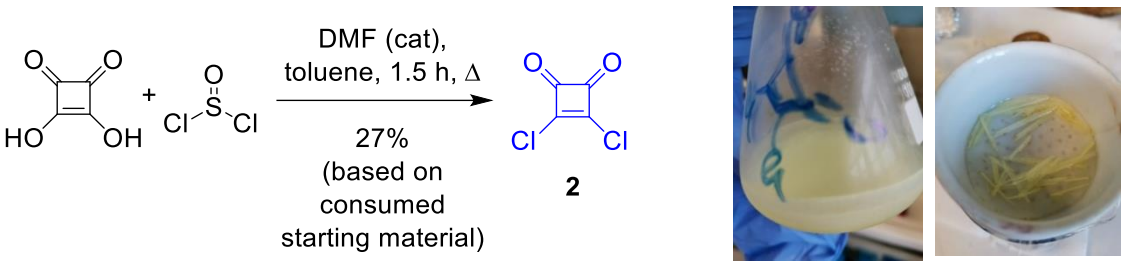

***Figure 8**: Synthesis of **2** (besides the desired squarylium chloride 60% of non-reacted squaric acid were reisolated). Pictures on the right show the isolation of the desired product as large crystals.*

Notably, adapting the purification procedure allowed for an easy collection of **2** as very large and easy to handle light yellow crystals (Figure 8).

With fragment **1** in hand and following the general guidelines for the synthesis of amphiphilic compounds, the next step was the Friedel-Crafts acylation of squarylium chloride and the aryl connector **3** provided from the *Beverina* group. Unfortunately, however, this reaction (Scheme 12) proved to be very inefficient and the amount of potential target hemisquarate **4** was so little that this approach was stopped

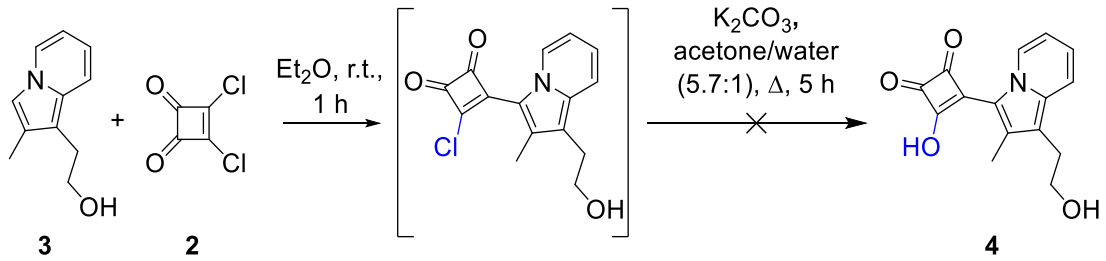

***Scheme 12**: Attempted synthesis of **4**.*

Instead, focus was laid on the synthesis of target compound **B** next. According to the retrosynthesis shown in Scheme 13, here, a phenol was envisioned as the aryl connector (green) which should be esterified with succinic acid anhydride (light blue) whose second carboxylic acid function should be used to install the hydrophilic MPEG chain via a second late-stage esterification.

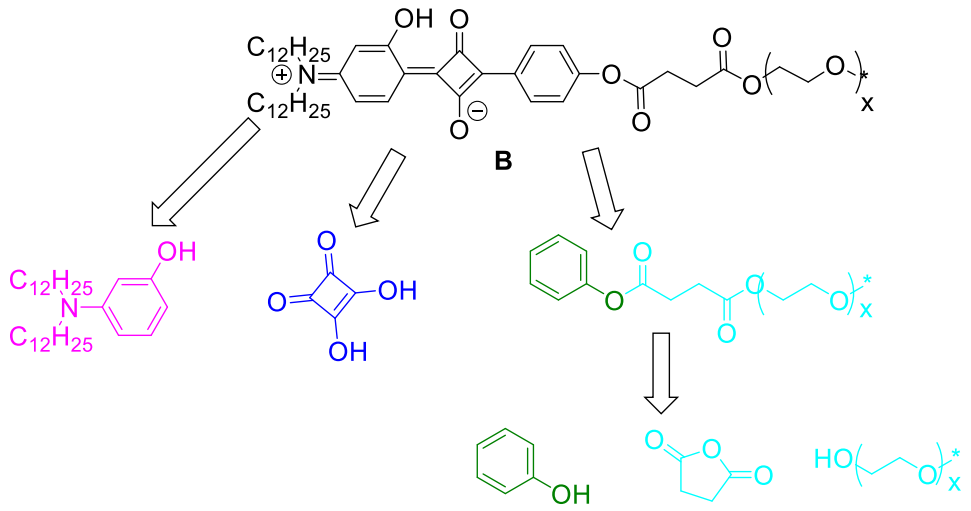

***Scheme 13**: Retrosynthesis of **B**.*

The esterification was tested under three different literature known conditions (Table 1) and it was found that the best yields were obtained for the approach listed as entry 3.

***Table 1**: Synthesis of succinic acid phenyl ester **5**.*

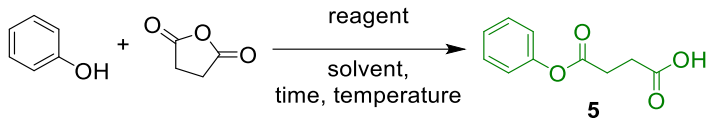

entry	reagent	solvent	time	temperature	w/w	yield
1	Na_2CO_3	water	21 h	0°C → r.t.	-	0%
2	-	-	28 h	130°C	2/1	46%
3	-	-	48 h	130°C	4/1	78%

Due to the tendency of the phenol to sublime and adhere to the flask walls, intermediate repositioning of said materials back into the melt was important for the outcome.

The next step was the second esterification of monoester **5** with MPEG. Here, $MPEG_{750}$ was used (Scheme 14) to give non-symmetric succinic acid ester **6**.

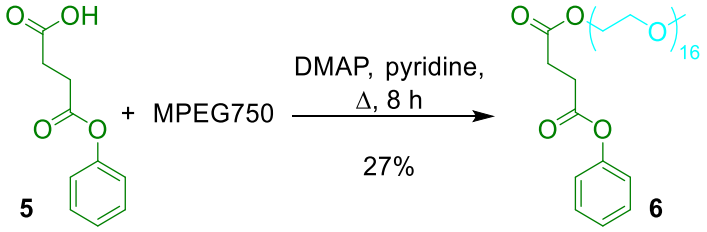

***Scheme 14**: Synthesis of **6**.*

This gave the fully furnished aryl fragment **6** ready to be condensated with squarylium chloride **2** via a Friedel-Crafts alkylation. Unfortunately, however, this transformation could not be achieved using aluminum chloride as the Lewis acid (Scheme 15).

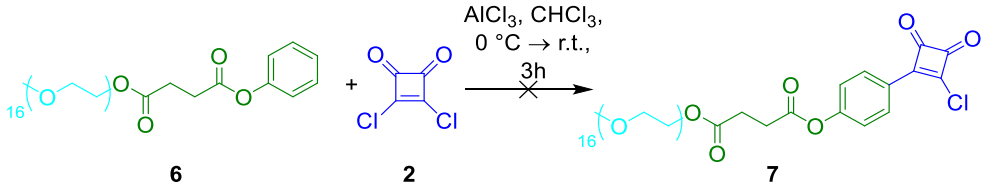

***Scheme 15**: Synthesis of **7**.*

Unfortunately, these conditions led to a random cleavage of the MPEG750 chain resulting in a messy mixture of different compounds. To tackle this problem the order of connecting the two different fragments – the lipophilic and the hydrophilic aryl building block to the squaric core was switched.

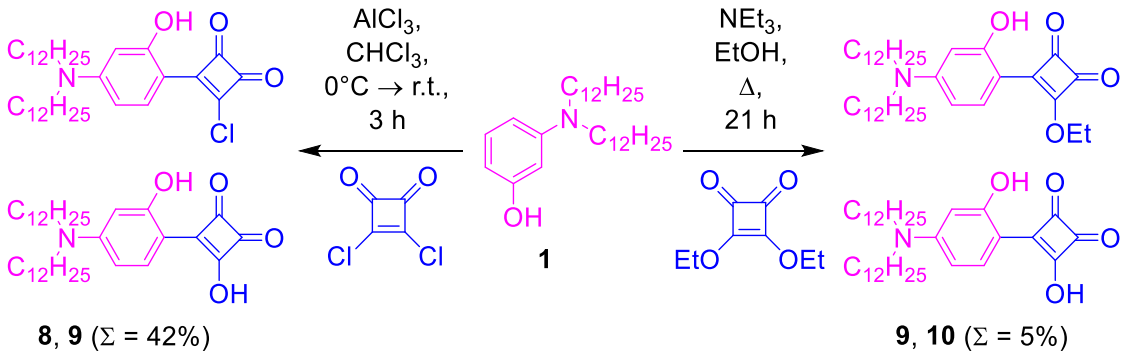

***Scheme 16**: Synthesis of hemisquaraines **8, 9** and **10**.*

In both cases, the desired acyl chloride **8** or monoester **10** was partially hydrolyzed to the corresponding acid **9** during the purification process (Scheme 16). Thus, it was decided to use the crude mixtures directly for the condensation reaction with the phenol building block **6** (Scheme 17). Unfortunately, this attempt resulted in a complicated mixture of different compounds which proved to be extremely difficult to separate (Figure 9).

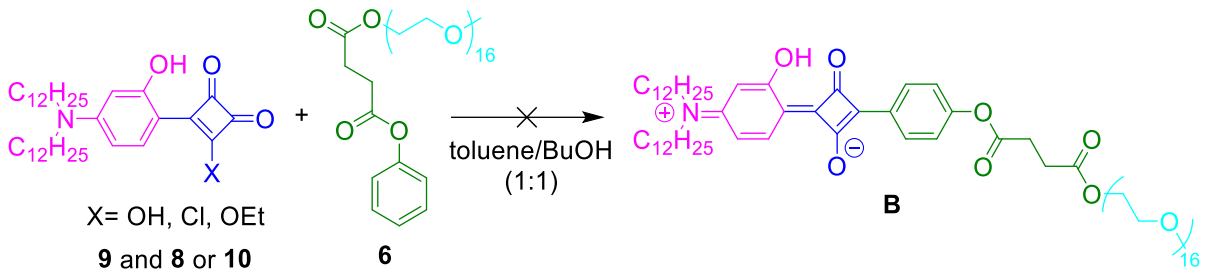

***Scheme 17**: Attempted synthesis of amphiphilic squaraine **B**.*

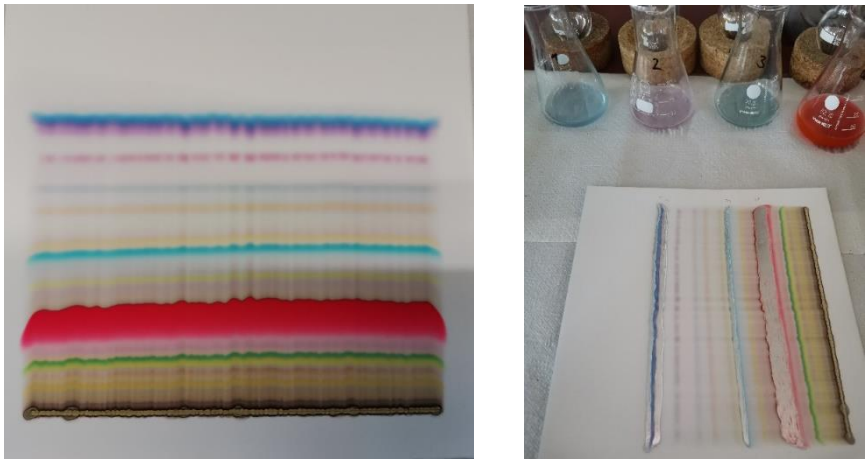

***Figure 9**: Thin layer chromatography of products obtained in the synthesis of amphiphilic squaraine **B** according to the procedure depicted in Scheme 17.*

Since the scale as this point had already dropped to milligram scale, the obtained crude product was purified via preparative thin layer chromatography (Figure 9). Analysis of the most promising bands gave further insights (Table 2).

***Table 2**: Analysis of different fractions obtained from the attempt to prepare amphiphilic squaraine **B**.*

chromatographic band/fraction	color of material	structural assignment
1	blue	symmetric squaraine **11** (see Scheme 18)
2	pink	impurities
3	cyan	unidentifiable
4	red	desired hemisquarate **9**

This suggests that the phenol building block **6** might not be nucleophilic enough to undergo the desired condensation reaction. Possible improvements would be the use of a suitable (Lewis) acid as a catalyst to activate the squaric acid core for the nucleophilic attack of this building block. This still bears the risk of random cleavage of the MPEG chain if an unsuitable acid will to be employed. The reisolated hemisquarate **9** was saved for future endeavors in this direction and the focus was again shifted towards a new generation of amphiphilic squaraines.

To confirm the finding of the symmetric anilino squaraine **11** it was deliberately synthesized using **1** and squaric acid in a 2/1 ratio (Scheme 18).

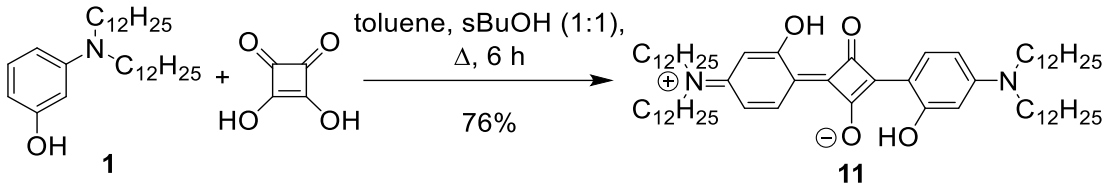

***Scheme 18**: Synthesis of symmetric anilino squaraine **11** to confirm the findings obtained in the attempted synthesis of amphiphilic squaraine B.*

The synthesis proceeds picture perfectly showing the typical color change to a deep blue within minutes (Figure 10). The obtained product was purified using column chromatography, but further purification via recrystallization proved more complicated. The long alkyl chains significantly increased the solubility of the squaraine in the typical recrystallization solvent cyclohexane, which in turn resulted in no crystal growth in this milieu. The other method using a mixture of methanol and dichloromethane mixture also proved unsuccessful as the long alkyl chains led to rapid precipitation of the product as amorphous solids, thus inhibiting formation of well-defined crystals.

***Figure 10**: Photographs taken during the synthesis of anilino squaraine **11**.*

The obtained analytical data of the deliberately synthesized symmetric squaraine **11** match the findings for the blue chromatographic band (Table 2) of preparative thin layer chromatography, thus confirming the finding.

3.3.2 Synthesis of a Second Generation of Amphiphilic Squaraines

After the synthesis of the first generation of targeted amphiphilic squaraine unfortunately failed I went back to the drawing board to design a second generation of new target compounds. The idea was to put a hydrophilic aryl unit on one side and a lipophilic indolylmethine on the other side of the target squaraine in order to facilitate the second condensation step. That led to the new target compound **(E)-AHP12MI-400** (Scheme 19).

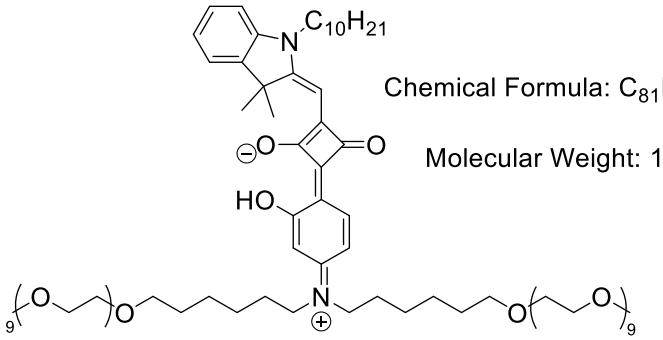

(E)-3-(4-(bis(6-(2-poly(ethylene glycol)methylether)hexyl)**A**mino)-2-**H**ydroxy**P**henyl)-4-((1-**decyl**-3,3-di**M**ethyl**I**ndolin-2-ylidene)methyl) cyclobut-3-ene-1,2-dione

(E)-AHP12MI-400

***Scheme 19**: Amphiphilic squaraine **(E)-AHP12MI-400**.*

The indolenine fragment was synthesized via alkylation of 2,3,3-trimethylindol **12** with decyl iodide. This gave the desired alkylation product **13** in good yields (Scheme 20).

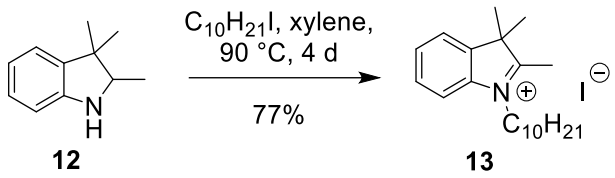

***Scheme 20**: Synthesis of **13**.*

With this in hand the next step was to prepare the respective hemisquaraine. Here, commercially available diethyl squarate **14** was used (Scheme 21).

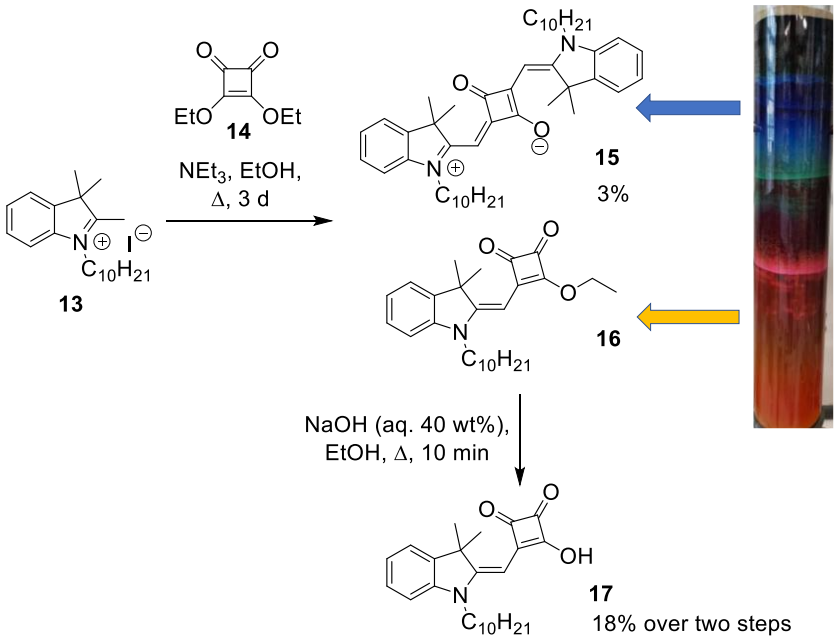

***Scheme 21**: Synthesis of hemisquaraine **17**. As a side product the symmetric squaraine **15** was also obtained.*

It was also possible to isolate the symmetric squaraine **15** as a byproduct of this reaction during the purification via column chromatography (Scheme 21). This intensely blue colored compound was recovered from the column and further purified using recrystallization. The high tendency to crystallize

allowed growing of sizable crystals (Figure 11) that were also suitable to perform single crystal X-ray diffraction analysis to reveal the crystal structure of the compound (see experimental part for details).

The main and originally desired product hemisquaraine ethyl ester **16** was already partially hydrolyzed during the purification. Thus, the isolated compound was subjected to alkaline aqueous conditions to fully hydrolyze to yield the desired hemisquarate **17**.

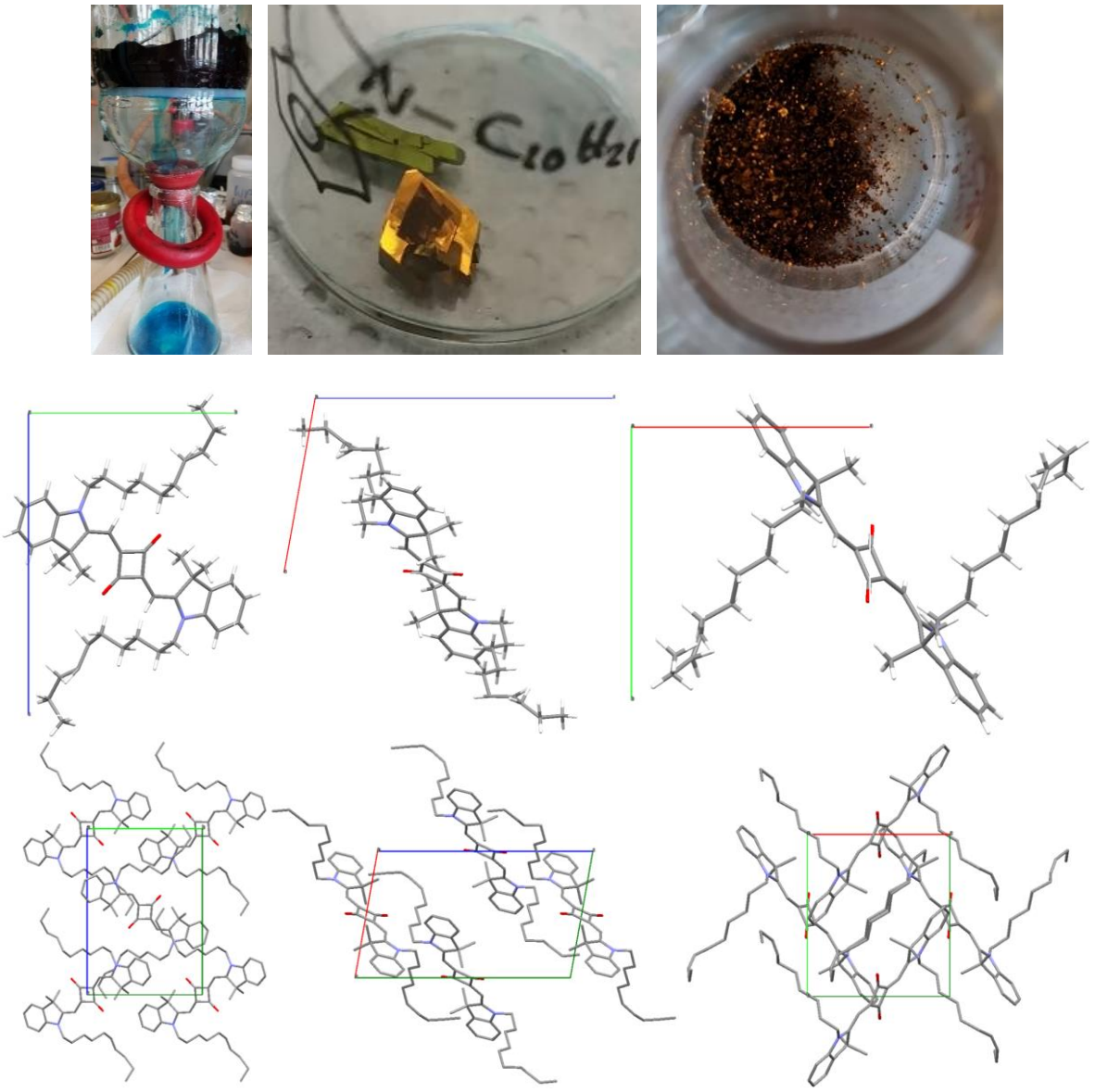

***Figure 11**: Top: photographs taken from crystallization of indolenine squaraine **15**. Middle: its molecular structure as determined by single crystal XRD analysis, visualizing the monoclinic unit cell as individual molecule viewing along the unit cell axis a (middle left), b (middle center) and c (middle right), respectively. Bottom: Visualization of the molecular packing (hydrogen atoms are omitted for clarity) along the unit cell axis a (bottom left), b (bottom center) and c (bottom right). (color code: blue: c-axis, nitrogen atoms, dark green: expansion of the unit cell, green: b-axis, grey: carbon atoms, red: a-axis, oxygen atoms, white: hydrogen atoms).*

Alkylation of the 3-hydroxyaniline was planned in analogy to the successful synthesis of **1** (see Scheme 11) implementing dodecyl groups at the nitrogen. However, in contrast to the first generation amphiphiles this time hydrophilic groups should be introduced here. Therefore, PEG-ylated alkyl bromide **18** provided by *M. Sassi* from the *Beverina* group was chosen as the alkylating agent (Scheme 22). Unfortunately, however, this reaction failed but instead large amounts of the starting material 3-hydroxyaniline were recovered.

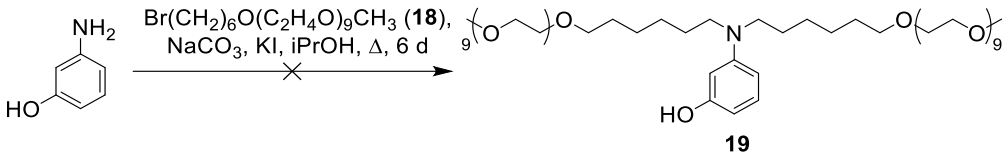

***Scheme 22**: Attempted synthesis of N,N-dialkylated aniline **19**.*

Since 3-hydroxyaniline is reasonably hydrophilic it was decided to use this directly to prepare a variant of the proposed second generation amphiphilic squaraine by directly condensing hemisquaraine **17** with 3-hydroxyaniline in a toluene/BuOH (1:1 v/v) mixture (Scheme 23) giving rise to the desired squaraine **20** in 16% yield.

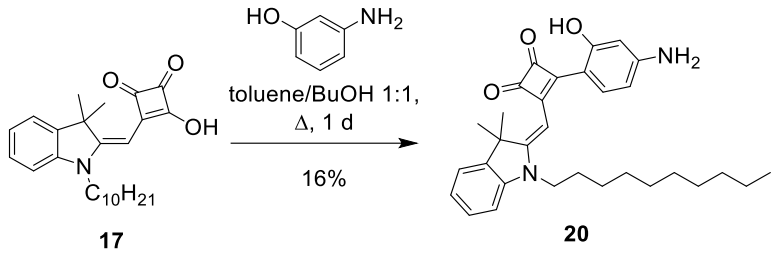

***Scheme 23**: Synthesis of amphiphilic squaraine **20**.*

20 was obtained as a violet solid with fascinating properties (Figure 12). In the solid state it exhibits an intense red fluorescence under UV-light which is quite remarkable as anilino squaraines usually show no fluorescence in the solid state due to aggregation induced quenching of the fluorescence. Unfortunately, it was not possible to determine the crystal structure by XRD analysis even though the compounds appeared crystalline.

***Figure 12**: a) and b) Photographs of amphiphilic squaraine **20** in the solid state under ambient light and c) its fluorescence in the solid state upon irradiation with UV-light. d) and e) Photographs of solutions of **20** in ethyl acetate showing pH-dependent switching of color from red to green upon alkalizing the solution by addition of aqueous KOH (6 N).*

Empirical tests also demonstrated the desired pH-dependent color change of solutions of **20** from dark red to green upon alkalizing it. This finding indicates the envisioned promising features of a pH dependent color change. More detailed investigations are discussed in the following chapter 3.3.3.

The configuration of the double bond was determined by NOESY-NMR as the correlation observed between the vinyl-H atom with the alkyl chain on the amine can only stem from this arrangement. Additional interaction between the methyl groups and the free OH-group suggest a rather collapsed structure (Figure 13) compared to the originally assumed unfolded conformation. All in all, the observed correlation by NOESY-NMR suggest the formation of the 1,2-squaraine, where the phenyl ring of the anilino part is rotated towards the indoline part.

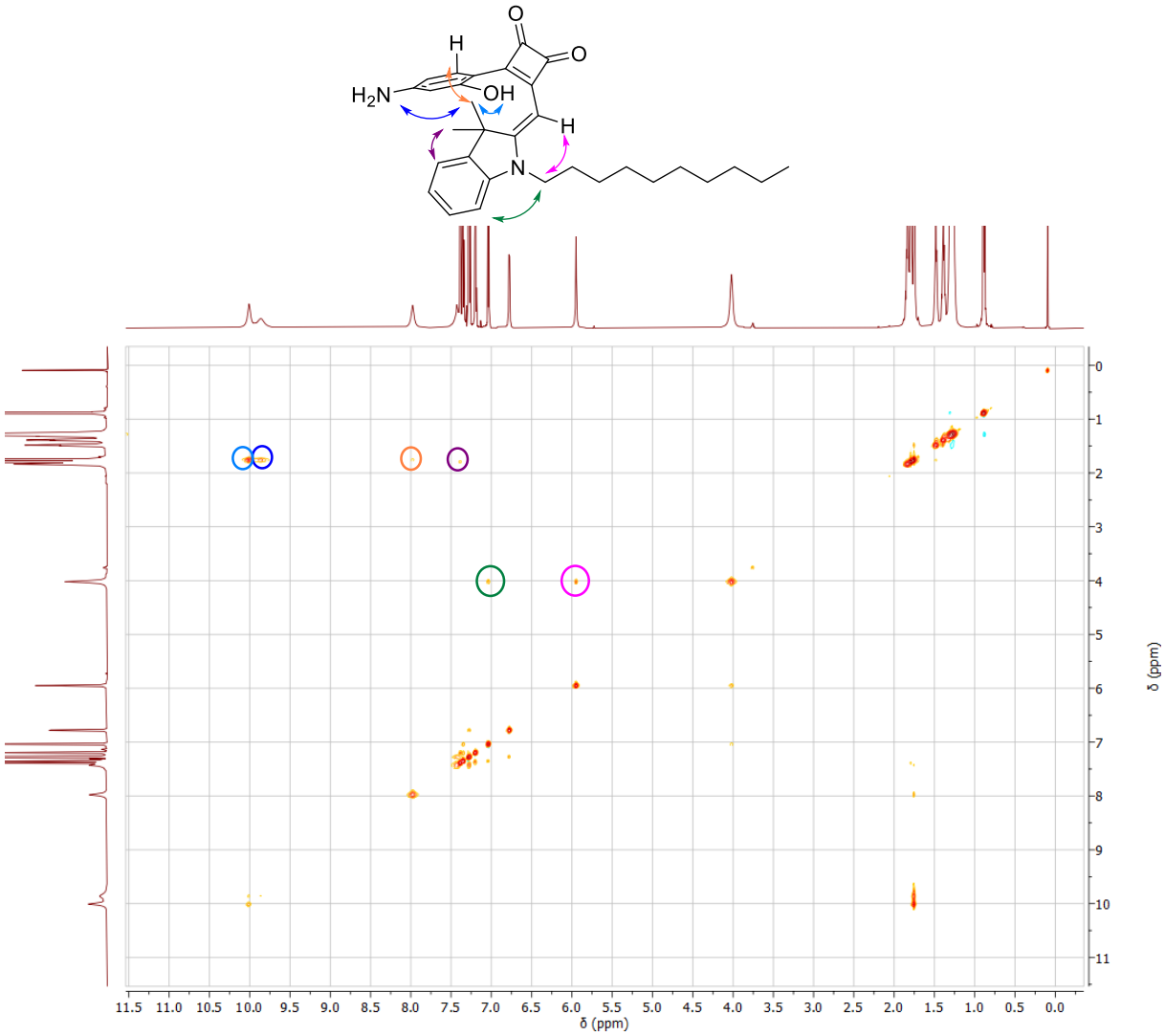

***Figure 13**: 2D-1H-NOESY spectrum (700 MHz, $CDCl_3$, 298 K) of amphiphilic squaraine **20** and its molecular structure showing an assignment of the individual NOESY signals in the spectrum. The circled cross peaks are presented in the same color as the respective correlation between the part within the molecule. These support the proposed and shown constitution, configuration and conformation of the compound.*

3.3.3 Characterization of the Amphiphilic Character of 20 and its Response to Changes in pH

Calculation of HLB Values

Even though the actually obtained squaraine **20** does not contain the originally planned MPEG groups to ensure the hydrophilicity of this part of the molecule, it instead features a terminal amine which is rather polar and can be addressed by acids, thus, tuning the solubility of the compound accordingly. To test whether it works as a surfactant the HLB value of **20** was determined first (see experimental part for details).

According to Griffin[79]: $HLB_{Griffin}$ (**20**) = ($M(NH_2)$ + M(OH) + 2 x M(CO))/ M(**20**) x 20 = 3.7

And according to Davies[81]: HLB_{Davies} (**20**) = 3.0 + 1.9 + 2 x 7.5 – (2 x 2.4 + 15 x 0.475) + 7 = ~15

As previously shown these values result in contradicting results as neutral lipophilic surfactants are known to have HLB < 10 and hydrophilic surfactants HLB > 10. Thus, according to Davies with an HLB value of 15 it should have a more hydrophilic character, meaning a better suitedness for application in a medium with high water contents compared to organic solvents.

However, according to Griffin's method the HLB value of 3.7 would rather suggest a neutral lipophilic compound, indicating that compound **20** is better suited for an application in a water-in-oil emulsion. Thus, favoring a medium with lower water contents compared to the organic solvent. The actually observed solvation behavior of **20** suggests that Griffin's method is more accurate, as the solubility in apolar solvent is significantly better compared to aqueous surroundings.

DLS Experiments

This is also reflected in the observations made during sample preparation for the dynamic light scattering (DLS) experiments which were performed to examine their aggregation behavior and the formation of micelles.

The underlying principle of a DLS experiment is the analysis of the fluctuations in intensity of the scattered light caused by the movement of particles in a solution, which follows Brownian motion. The rate thereof is related to the diffusion coefficient of the particles, which is then used to calculate their hydrodynamic size using the Stokes –Einstein equation[120]:

$$D = \mu * k_b * T = \frac{k_B * T}{6\pi * \eta * r} \qquad \textbf{(Equation 3)}$$

Here, *D* is the diffusion coefficient, μ the mobility defined as the terminal drift velocity resulting from application of a force, k_B the Boltzmann constant and *T* the absolute temperature. This can also be expressed as the ratio between the product of $k_B \cdot T$ divided by $6\pi \cdot \eta \cdot r$ when a spherical geometry is assumed with r as the radius of the sphere and η as the viscosity of the medium. Using this the diffusion coefficient can be converted into the hydrodynamic diameter. This gives the apparent size of the particle including solvation layers. Additionally, DLS also gives insights to the polydispersity index (*PDI*) of the sample, thus, showing how uniform the size of the present aggregates is (where a *PDI* = 1 translates to a monodisperse sample).[120]

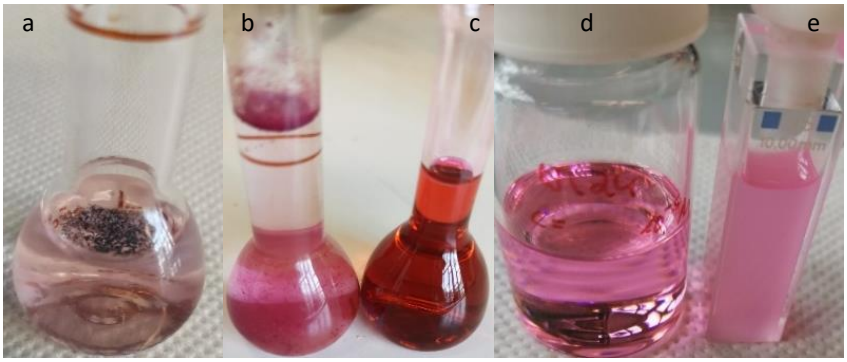

***Figure 14**: Photographs of samples of **20** prepared in different solvent systems to perform the DLS experiments. a) particles of **20** floating atop of water, b) same sample after further dilution, frantic mixing heating to 40°C and exposure to sonification for 15 min while warmed to 40°C, c) sample of **20** dissolved in toluene c= 7.15 x 10^{-4} M, d) further dilution with toluene till c = 7.15 x 10^{-6} M, e) sample of **20** in toluene with a droplet of water for DLS measurements.*

The DLS measurements were performed by *A. Fappani* and *S. Mattiello* in the *Beverina* group, providing insight into the behavior of **20** in different solvent systems: pure water, pure toluene and toluene with a droplet of water (Figure 14). For the sample in water **20** was found to form aggregates with a size of around 200 nm (DLS data say 206 nm, with a polydispersity index of *PDI* = 0.435, meaning a standard

deviation of 136 nm, see Experimental Part for details). No scattering is observed in toluene, implying the formation of a homogeneous solution of non-aggregated **20**. Upon addition of a drop of water to the toluene solution of **20**, an emulsion formed, resulting in the detection of a signal corresponding to particles of several micrometers in size. In fact, the particles present in these emulsion droplets are larger than the upper size limit that can be determined accurately by DLS (≤ 1 µm). These experiments clearly show that **20** can indeed be used as a surfactant.

UV-Vis Spectroscopic Properties in Solution

For the UV-Vis measurements a stock solution of **20** in chloroform was prepared. The compound was weighed in as a solid and then diluted with chloroform aiming for a concentration in the range of $c_{stock\ solution} = 7.15 \times 10^{-4}$ M. The sample for each measurement was prepared using 50 µL of stock solution with 2950 µL of the desired solvent. The obtained sample resulted in a final concentration of $c_{sample} = 11.9$ µM. As already observed during the synthesis of **20** the respective solutions are also intensely colored (Figure 15).

***Figure 15**: Photographs of samples of **20** prepared in different solvent systems to perform the UV-Vis spectroscopic experiments (from left to right, toluene, chloroform, ethyl acetate, diethyl ether, THF, cyclohexane, dichloromethane, ethanol, methanol, acetone, acetonitrile, DMSO, and DMF).*

Already by inspection with the naked eye it became apparent how different the compound behaves in the respective solvents (Figure 15). The majority of the samples show a sharp absorption maximum in the region around 527 nm (Figure 16) which a second shoulder near 500 nm. Exception to this majority are samples in DMF and DMSO. These have an absorption maximum at 440 nm, resulting in the observed yellow color. A significant broad tailing into to the 440 nm region can be seen in the absorption spectra of acetone and acetonitrile. This blue shift of absorption in these solvents comparably good hydrogen-bond accepting solvents according to their Kamlet-Taft polarity β[121–123] ($\beta_{Acetone} = 0.43$, $\beta_{Acetonitrile} = 0.40$, $\beta_{DMF} = 0.69$, $\beta_{DMSO} = 0.76$, β_{MeOH} =0-66) including methanol, hint at the observation of a solvatochromic effect. This might lead to the stabilization of the ground state by intermolecular hydrogen bonds between the solute and the solvent which in turn results in the excitation at a shorter wavelength.

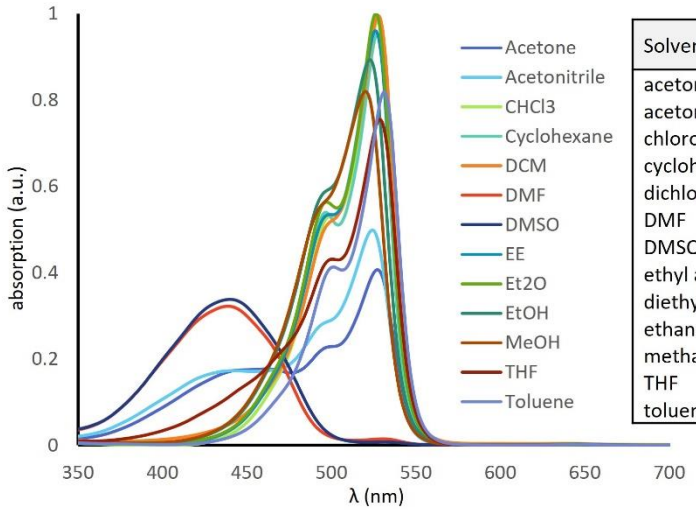

Solvent	λ_{Max}
acetone	528
acetonitrile	524
chloroform	528
cyclohexane	527
dichloromethane	528
DMF	439
DMSO	440
ethyl acetate	526
diethyl ether	527
ethanol	523
methanol	520
THF	529
toluene	532

***Figure 16**: Normalized UV-Vis spectra of **20** in different solvents.*

As shown above dissolving of asymmetric squaraine **20** in organic solvents, even highly polar ones like methanol and ethanol, is no problem. This is in accordance with the determined HLBs, as those suggest a rather lipophilic compound. This can also be seen in the solvation behavior of **20** in mixtures of methanol and water with increasing water amounts (Figure 17).

As seen in praxis up to 50% water in the mixture can be tolerated to still ensure a homogeneous mixture in which **20** is well dissolved. Further increase of the water content led to phase separation and precipitation of **20** aggregates from the mixtures.

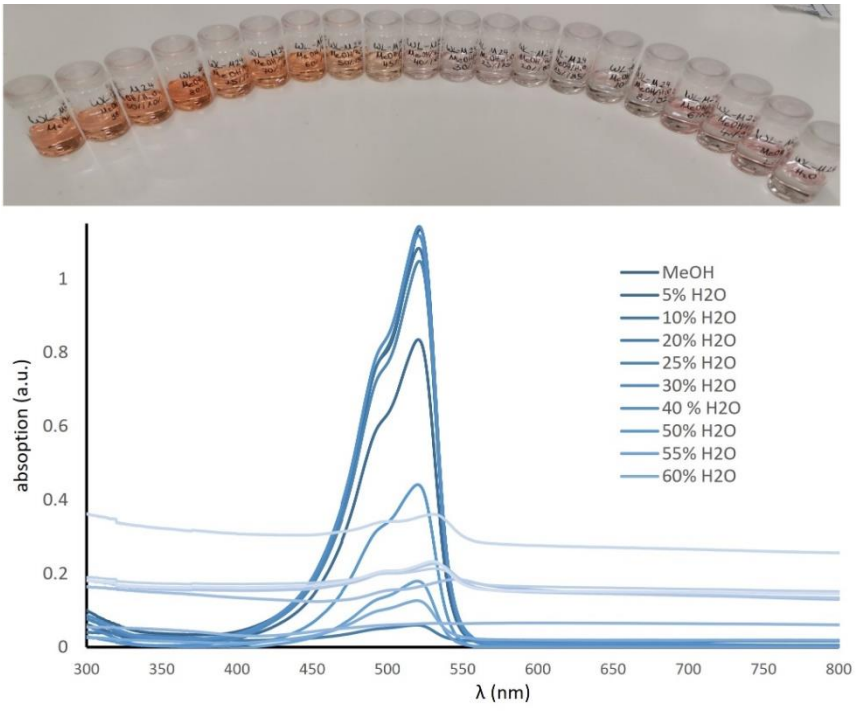

***Figure 17**: Top: Photographs of (colloidal) solutions of **20** in mixtures of methanol and water containing varying amounts of water. Bottom: Normalized UV-Vis spectra of these samples.*

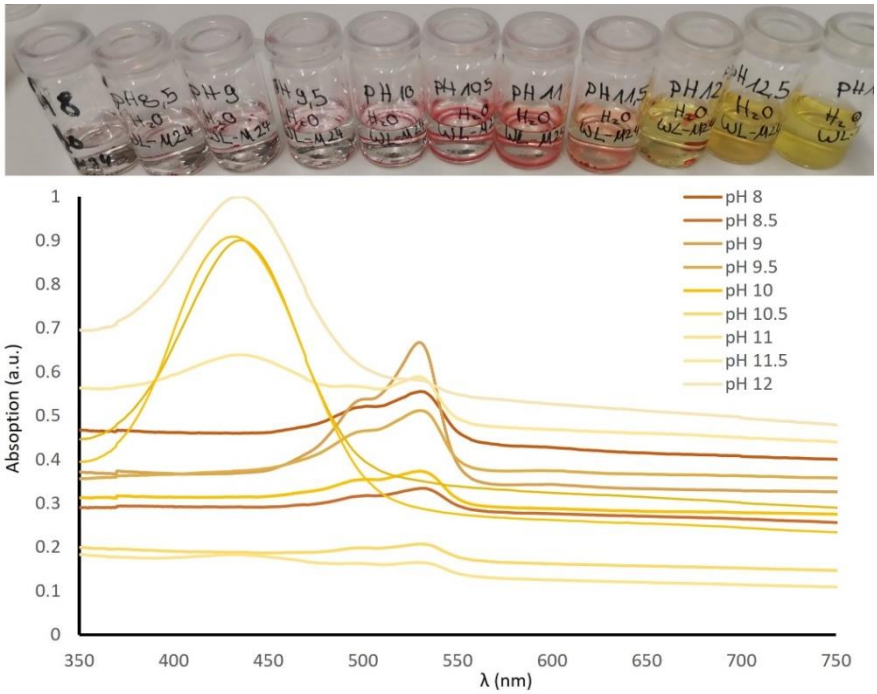

***Figure 18**: Top: Photographs of mixtures of **20** in chloroform and water of adjusted pH value. Bottom: Normalized UV-Vis spectra of these samples.*

Next, the influence of the solutions pH value was examined. Therefore, 50 µL of the chloroform stock solution were mixed with 2950 µL of water with adjusted pH value. Here, an increase in absorbance was observed for samples with pH 11.5 and higher, which could also be seen with the naked eye (Figure 18). Below pH 11.5 almost no absorption can be detected due to phase separation, as **20** was only dissolved in the chloroform of the stock solution. This leads to the orange reddish droplets with in the aqueous sample. The initially immiscible chloroform of the stock solution becomes well-dispersed with no apparent phase separation only at pH above 11.5, hinting at the solubility of deprotonated **20** in both water and chloroform. This further supported the assumption of **20** being a more lipophilic compound, which needed to be taken into account when test reactions for micellar catalysis were chosen.

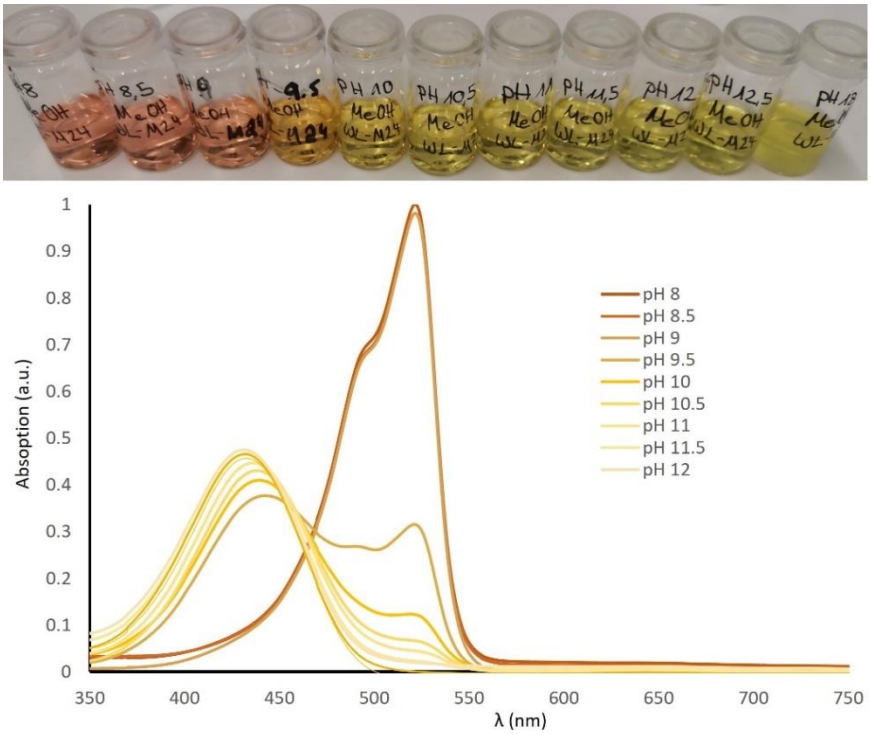

***Figure 19**: Top: Photographs of mixtures of **20** in methanol of adjusted pH value. Bottom: Normalized UV-Vis spectra of these samples.*

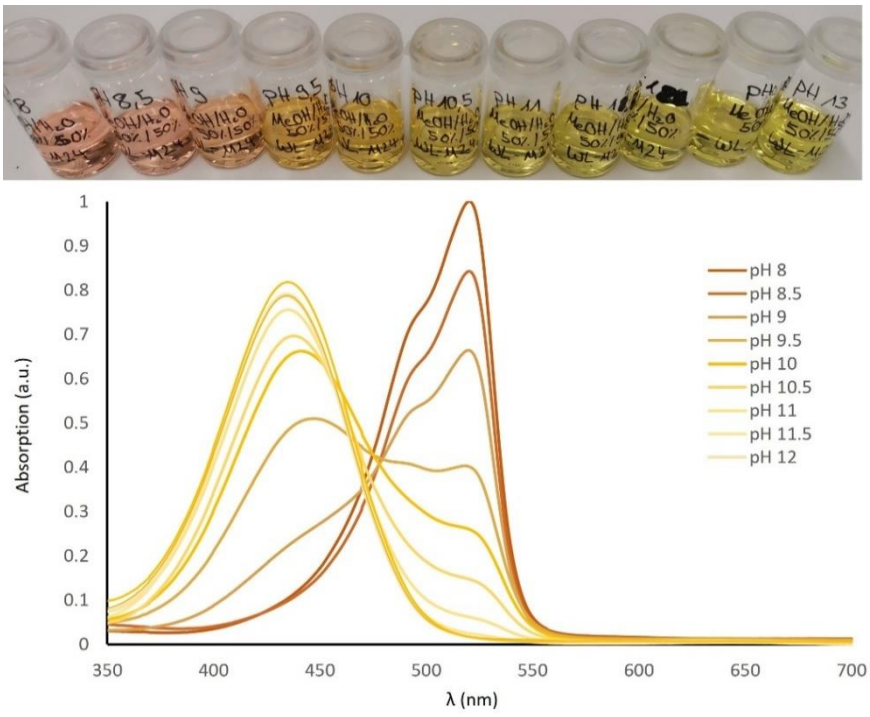

***Figure 20**: Top: Photographs of **20** in 1:1 mixtures of methanol & water of adjusted pH value. Bottom: Normalized UV-Vis spectra of these samples.*

Next, samples in pure methanol were prepared in which **20** is soluble and their pH was adjusted by dissolving the respective amount of NaOH in them. This was possible until we reached a limit at pH > 13 as the solubility limit of NaOH in methanol might become a concern. Beside this the prepared samples (Figure 19) and the measure absorption spectra show an abrupt transition of the absorption maximum from 520 nm at pH = 8 to 433 nm at pH = 12.5. The 50/50 v/v methanol/water sample show the most

gradual and smooth transition between the two aforementioned absorption maxima upon changes in the pH (Figure 20).

All in all, these experiments show that **20** cannot only act as a surfactant but its properties are also pH-sensitive making it water soluble in an alkaline environment. All these make it a promising candidate to be tested as a designer surfactant for the use in micellar or emulsion catalysis.

3.3.4 Testing of 20 as Surfactant for Micellar Catalysis – Test Reactions

In order to test this hypothesis **20** was tested in a first set of Suzuki cross-coupling reactions (Figure 21) and compared to surfactant-free conditions as well as commercially available **Koliphor EL** which has already been proven to be useful for this purpose.[99,110,111] The reactions for each test were performed parallel to each other to ensure the least possible deviation of irreproducible environmental influences (fluctuation of humidity, brightness, ambient temperature and more).

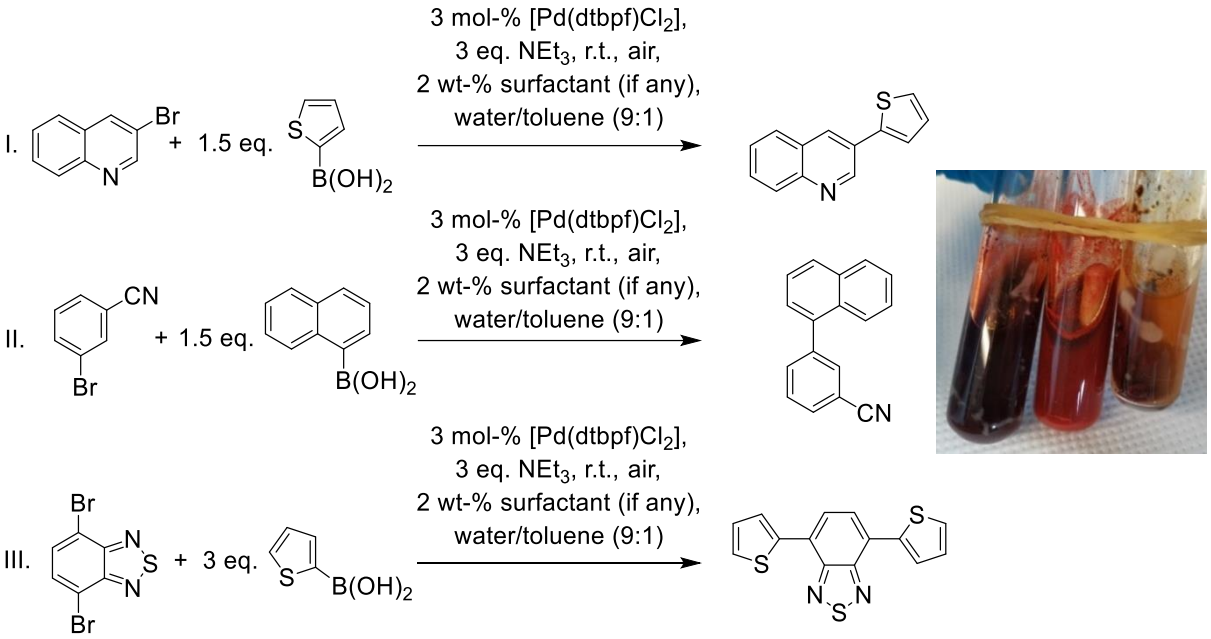

***Figure 21**: Left: Micellar catalytic Suzuki cross-coupling reactions. Right: photographs of the reactions for II, left to right with Koliphore El as surfactant, with **20** as surfactant, surfactant-free conditions.*

For all three test reactions standardized condition were employed meaning ambient temperature and atmosphere, 2 wt-% of surfactant (if used), 0.5 M aryl bromide, 1.5 eq. of boronic acid for each functional group, 3.00 eq. of NEt_3 and 3 mol-% [Pd(dtbpf)Cl_2] as catalyst in a 9/1 v/v water/toluene mixture. The reactions were monitored by GC-MS and full conversion of the reactions was not of central interest.

Test reaction I. ran for 26 h and after 21 h GC-MS still showed significant amounts of start material in case of the surfactant free reaction (36%) or that with **20** as surfactant (42%) while the one using **Koliphor EL** already reached 93% conversion. In case of test reaction II. GC-MS after 4 h showed 81% product alongside with 19% homocoupling product for the surfactant free conditions. For the surfactant containing reactions the amounts of homocoupling byproduct could be reduced to 10% in case of **Koliphor EL** and 15% in case of the new designer surfactant **20**. Test reaction III. gave no further insights as GC-MS after only 3 h already resulted in complete conversion in all three cases with comparable yields in all cases.

When taking the reaction conditions into consideration the most important advantage is the possibility to perform these kinds of cross-coupling reaction under ambient conditions. This includes the omitting

of degassed solvents as well as the exposure to air instead of inert gas atmospheres. Thus, the reduced percentage of homocoupling product in the surfactant containing reaction conditions imply a reaction milieu which is lower in oxygen levels compared to the surfactant-free condition. It is well-known how higher oxygen levels increases the amount of homocoupling during the Suzuki-reaction.[124,125]

From the few test reactions performed, it appears as **20** is performing slightly worse than **Koliphor EL** but shows the same oxygen excluding effect to a certain degree. It is important to keep in mind that a newly synthesized surfactant is compared to a well-established commercially available surfactant that was found to be ideally suited for this type of reaction. Nevertheless, **20** features a major advantage with regard to post reaction work-up with regard to the reisolation of the utilized amphiphilic surfactant molecules.

Gratifyingly, the recovery of **20** turned out to be comparably easy. As previously stated, the addition of a base leads to a well-visible color change from red to green or yellow depending on the dilution (Figure 22).

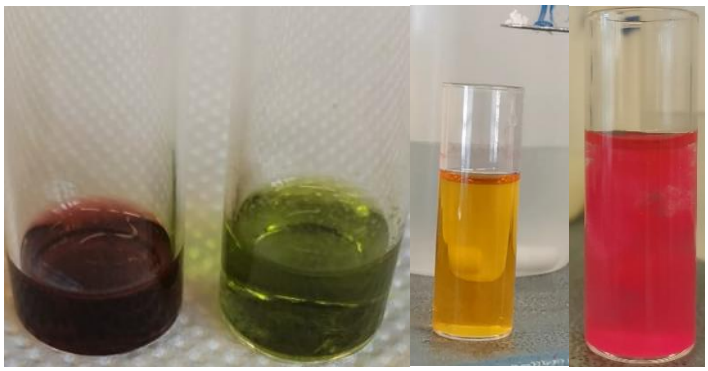

***Figure 22**: Photographs of the reaction mixtures of the micellar catalytic transformations using **20** as a surfactant. Left: Color change of the mixture from red to green/yellow upon increasing the pH by addition of aqueous KOH (6 N); middle: low concentration sample of a sample at high pH; right: the same mixture after addition of zinc(II) chloride showing the formation of a red metal complex.*

This not only indicated the change in pH, but also shows the disassembly of the micellar aggregates.

In addition to achieving the desired and targeted pH-dependent stimuli response, which not only visualized the disassembly of the aggregates but also led to the drastic change in the solvation behavior, as already shown, an even greater success was achieved. This can be seen by the formation of a red metal complex, which can easily be removed by filtration, upon addition of zinc (II) chloride to a solution of **20** at high pH. This complex formation was observed for solutions of **20** in ethyl acetate, toluene, water, methanol and ethanol. Removal by filtration and subsequent washing of said precipitate with suitable solvents allows for efficient isolation of the reaction product and simultaneous purification of the re-isolated surfactant as drying of the remaining solid gives the surfactant as a Zn-complex. Re-protonation liberates the surfactant for further uses with little to no loss in effectiveness. It was found that re-protonation with aqueous citric acid or HCl (1 M) work, extraction with ethyl acetate thereof proved to be most effective for reisolation of **20**. After removal of the solvent reisolated **20** is obtained for further micellar catalysis reaction with little to no loss of effectiveness.

All in all, the research stay abroad in Milan was fruitful. As shown, it was possible to synthesize a designer surfactant that combined the needed amphiphilic nature of a surfactant with the familiar squaric acid core. The final compound **20** significantly differs from the targets proposed in the beginning, as it is less hydrophilic due to the absence of hydrophilicity promoting PEG groups. This reduced hydrophilicity compared to the initial targets might even be a decisive factor that allowed for

the advantageous precipitation of the surfactant **20**-zinc complex. As of now it was concluded that this intriguing behavior of the precipitation of a zinc complex upon addition of $ZnCl_2$ in an alkaline milieu is due to the arrangement of the deprotonated hydroxyl-group and the carbonyl group of the squaric acid core, which apparently forms a perfect chelating template for Zn (II) ions (Figure 23). In this regard additional hydrophilicity by MPEG-chains might interfere with the complex formation.

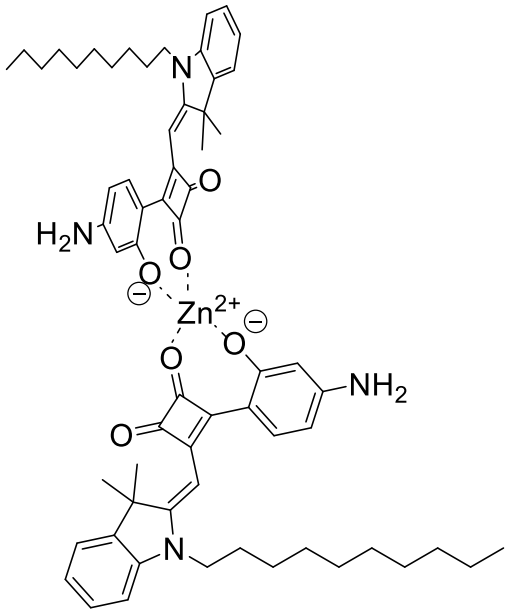

***Figure 23**: Proposed chelatisation of zinc (II) cations by two deprotonated units of **20**, resulting in a tetrahedral coordination of Zn (II).*

Ultimately this feature gives the newly synthesized designer surfactant **20** a significant advantage compared to commercially availyble surfactants such as Kolliphor EL, as the post reaction purification of the cross-coupling product is drastically facilitated and the reisolation of the surfactant is easily possible. Additionally, instead of tedious extraction protocols with complicated phase separation due to the amphiphilic nature of surfactants and thus the difficult removal thereof from the desired product, a simple basification with aqueous base combined with the addition of $ZnCl_2$ as a solid gives rise to the precipitation of the rose-colored surfactant **20**-zinc complex. A sequence of filtration, washing with organic solvent to extract the desired organic cross-coupling product from the filtercake and drying yields the pure surfactant **20**-zinc complex as a solid. Simple dissolving in aqueous acid and extraction thereof with an organic solvent gives pristine surfactant **20** after removal of the solvent with little to no loss in effectiveness, readily employable for further micellar catalytic reaction

In conclusion the obtained squaraine based surfactant **20** shows promising results with regard to the utilization in micellar catalysis, as it exhibits the same oxygen excluding effect as Kolliphor EL. Besides the inherent selling-points of micellar catalysis such as reduced amounts of homocoupling product during the cross-coupling reaction under ambient conditions (ambient air, non-degassed solvents room temperature) an intriguing behavior that is unique for **20** so far, makes further research into squaraine based surfactants even more attractive.

4 STUDIES TOWARDS THE SUBLIMATION OF CHIRAL SQUARAINES

Chirality is defined as "*The geometric property of a rigid object (or spatial arrangement of points or atoms) of being non-superimposable on its mirror image; such an object has no symmetry elements of the second kind […]. If the object is superimposable on its mirror image the object is described as being achiral."* according to IUPAC.[126,127] The most palpable example for chirality is its namesake as the term chirality originates from the ancient Greek word χείρ which translates to hands. With regards to chemistry, chirality is divided into three categories: central, axial and planar chirality.

An important and fascinating observation made with chiral molecules is their ability to interact with polarized light. In case of linear polarized light, the plane of polarization is rotated by a molecule characteristic angle in the one direction by one of the enantiomers, while the other enantiomer rotates the plane of polarization to the same degree in the other direction. This characteristic is known as the specific optical rotation and can be measured by polarimetry. For a racemic mixture where both enantiomers are present in the same amount the resulting optical rotation is zero as the effects of both enantiomers cancel each other out.[128]

Another method, especially well-suited to larger compounds like biomolecules or supramolecular aggregates, is the circular dichroism (CD) spectroscopy. Here the difference of absorption of circular left- or right-handed polarized light by a sample is measured. This difference of absorption results in an elliptically polarized light.

Introduction of chirality into the photoactive layer of both organic photovoltaic and especially organic photodiodes unlocks multiple possibilities for future applications. With regards to detection devices it enables a higher density of transmitted information as it would be possible to differentiate left-handed circular polarized light from right-handed circular polarized light.[129] Other compounds are able to emit circularly polarized light can be used for 3D displays or spin filters employing the so-called CISS effect.[130] Hence, different information could be transmitted from diverse sources and could be detected and processed individually and independent from each other.[129]

4.1 PREVIOUS WORK ON PROSQS AND THE ADDED VALUE OF CHIRALITY

As stated before, symmetric squaraines like *N*,*N*-dialkyl-anilino squaraines (***N*-alkyl-SQs**) are well investigated dyes due to their intriguing properties.[45,131] A special class of squaraines, which is closely related to ***N*-alkyl-SQ**s, takes advantage of the benefits of the additional hydroxyl functions and the found influence of the alkyl groups on the amine, introducing chirality, a new aspect, to squaraine synthesis. The source of chirality was proline, hence, resulting in the so-called proline-derived squaraines (**ProSQ**s), first presented by *S. Hecht et al*.[132] and further investigated by *M. Schulz*,[32,62,133,134] *J. Zablocki*[31,134] and *M. F. Schumacher*[135,136] in our group. This class of squaraines shows fascinating behavior in both colloidal solutions and in solid states like crystals and thin films. Astonishing and impressive CD values were measured for **ProSQ**s,[31,134,136] suggesting the formation of chiral supramolecular aggregates in solution and thin films,[135] resulting from the transferring of the intrinsic central chirality of the proline substituent onto a supramolecular level (Figure 24).

Further investigations have uncovered even more intriguing characteristics of the unusual aggregation behavior and the resulting optical properties.[137] However, a structural model that can explain all of these features is still elusive also because it has not been possible to elucidate a single crystal structure of a **ProSQ** that resembles the behavior of the thin films and the devices studies so far. Another issue

is that processing of **ProSQ**s was usually done using solution-based approaches like spin or drop casting.

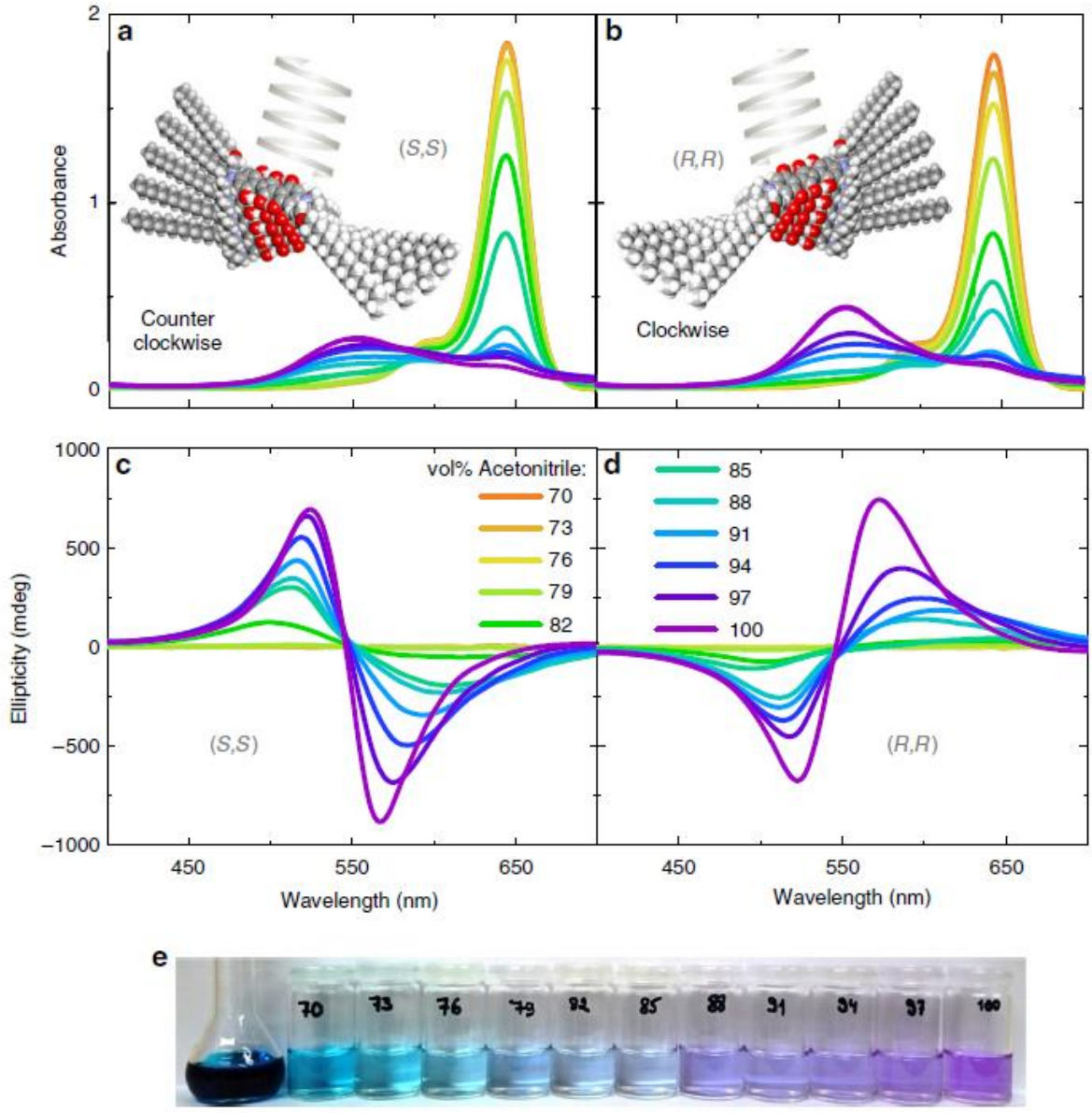

***Figure 24**: Early-stage aggregation experiments of **(S,S)-ProSQ-C16** and **(R,R)-ProSQ-C16** in chloroform/acetonitrile mixtures. a, b show the respective UV-vis spectra and c,d the ellipticity spectra. The concentration is approximately 5.7 µM. The volume fraction of acetonitrile is increased as indicated. The insets in a and b show sketches of the proposed helical aggregation of the molecules, deduced from the line shape of the CD bands. In e a photograph of the stock solution and the respective samples with increasing acetonitrile volume faction from left to right is shown. Reprinted from open access article Schulz, M., Zablocki, J., Abdullaeva, O.S. et al. Giant intrinsic circular dichroism of prolinol-derived squaraine thin films. Nat Commun 9, 2413 (2018).[134] No further permission needed.*

Therefore, two aspects should be examined in this thesis. First, it should be investigated if a similar class of chiral squaraines – an alkylated pyrrolidine-derived anilino squaraine called **PyrSQ** can be sublimed which would allow to apply vapor deposition techniques to prepare high-quality thin films. Second, and even more important a new class of chiral squaraines should be designed that combines both the interesting optical and aggregation properties of ***N*-alkyl-SQ**s with the intriguing chiroptical properties of the **ProSQ**s.

4.2 PyrSQ the Smaller Sibling of ProSQ

As beautifully seen in case of **ProSQ**s inherent chiral information can drastically influence the aggregation behavior of squaraines, and hence, its (chir-)optical properties. The series of different alkyl-chains on the oxygen of prolinol has verified the previous insights regarding the influence of the chain length on the aggregation behavior in poor solvents. Unfortunately, the members of the **ProSQ** family show a rather weak tendency to form high quality single crystals suitable for XRD analysis, so that the bulk structure of these materials in the solid state is still unknown. In addition, it proved to very difficult to sublime these compounds as they were found to easily decompose under these conditions. Sublimation however would be the prerequisite to allow vapor deposition approaches to generate high-quality thin films from these materials. Following up on previous work of *J. Zablocki et al*.[44] to address the latter question, a closely related class of chiral squaraines the **PyrSQ** was chosen that has a rather high tendency to crystallize when carrying short alkyl groups to investigate its sublimation behavior.

Therefore, the synthesis of **(*R*,*R*)-PyrSQ-C1** and its enantiomer **(*S*,*S*)-PyrSQ-C1** was scaled-up and both were synthesized on a gram-scale and semi-gram scale, respectively (Scheme 24).

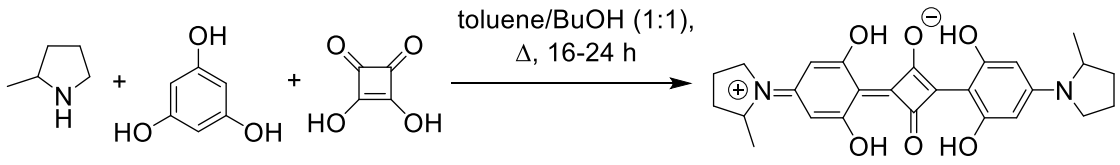

***Scheme 24**: Synthesis of **PyrSQ-C1**.*

These comparably large-scale syntheses proved to be as challenging as originally expected, since the purity of the obtained squaraines was of utmost importance. Following the established purification protocols for squaraines mentioned in the introduction consisting of initial filtration of the precipitated product straight from the reaction mixture, followed by meticulous washing with methanol until the filtrate runs clear. Subsequent Celite® supported column chromatography on silica with dichloromethane as eluent and two- to three-fold recrystallization from methanol/dichloromethane 10-5/1 v/v and cyclohexane/dichloromethane 10-5/1 v/v mixtures the pure products were obtained as crystalline materials (Figure 25).

***Figure 25**: Visualization of the purification steps of **PyrSQ-C1**.*

J. Zablocki obtained two different polymorphs of **(*R*,*R*)-PyrSQ-C1**: The first green-bluish polymorph was found to crystallize in the monoclinic space group *C2* whereas the second one crystalized in the orthorhombic space group $P2_12_12_1$ as golden bricks.[44] The given description perfectly matched the visually observed color and shape of the isolated pure (***S*,*S*)-** and **(*R*,*R*)-PyrSQ-C1** (Figure 25) and comparison by XRD confirmed the known crystal structure of the orthorhombic polymorph (Figure 26).

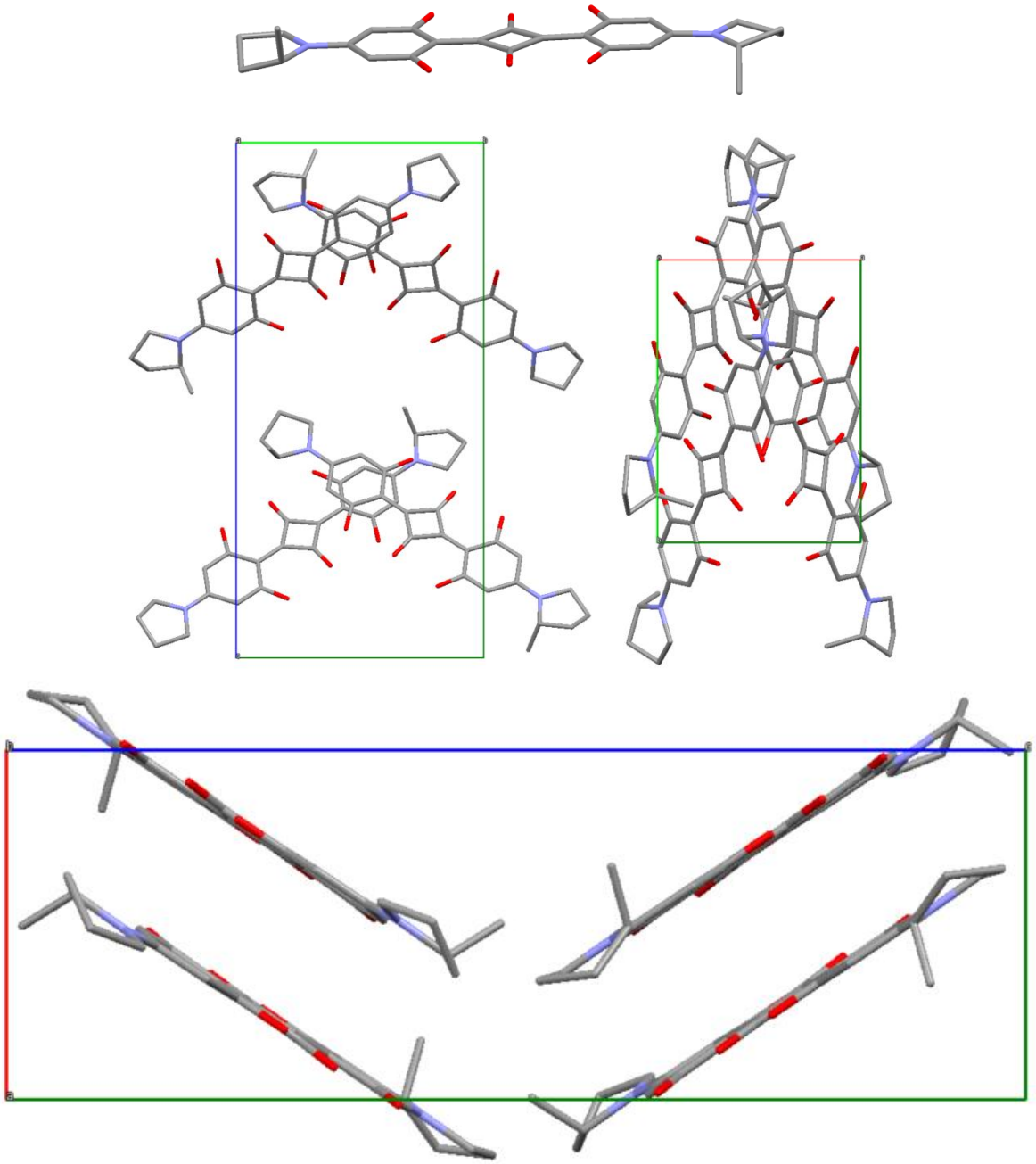

***Figure 26**: Structure of the orthorhombic polymorphs of **(S,S)-PyrSQ-C1** as determined by XRD analysis (hydrogen atoms are omitted for clarity; color code: grey = carbon, re = oxygen, blue = nitrogen). Visualization of the elucidated structure of **(S,S)-PyrSQ-C1** by XRD as an isolated molecule (Top), highlighting constitution and configuration of this enantiomer. Visualization of the molecular packing viewing along the unit cell axis a (middle left), b (bottom) and c (middle right), respectively. (color code: blue: c-axis, nitrogen atoms, dark green: expansion of the unit cell, green: b-axis, grey: carbon atoms, red: a-axis, oxygen atoms).*

The crystal structure is highly dependent on the procedure of how the crystals were grown. As an alternative to the already published vapor diffusion method[31,44] and the aforementioned and shown layer diffusion procedure, an alternative would be sublimation, which is more prominently used for further purification of substances. A favorable side effect of this is the formation of comparably bigger crystals. This is often due to the larger affinity of the sublimed substance to deposit on already formed nuclei of said substance compared to the glass surface of the sublimation chamber.

During a one moth lab internship in the Sokolowski group at the Clausius-Institute of Physical and Theoretical Chemistry, further purification via zone sublimation (Figure 27) alongside the growth of larger crystals were aimed for.

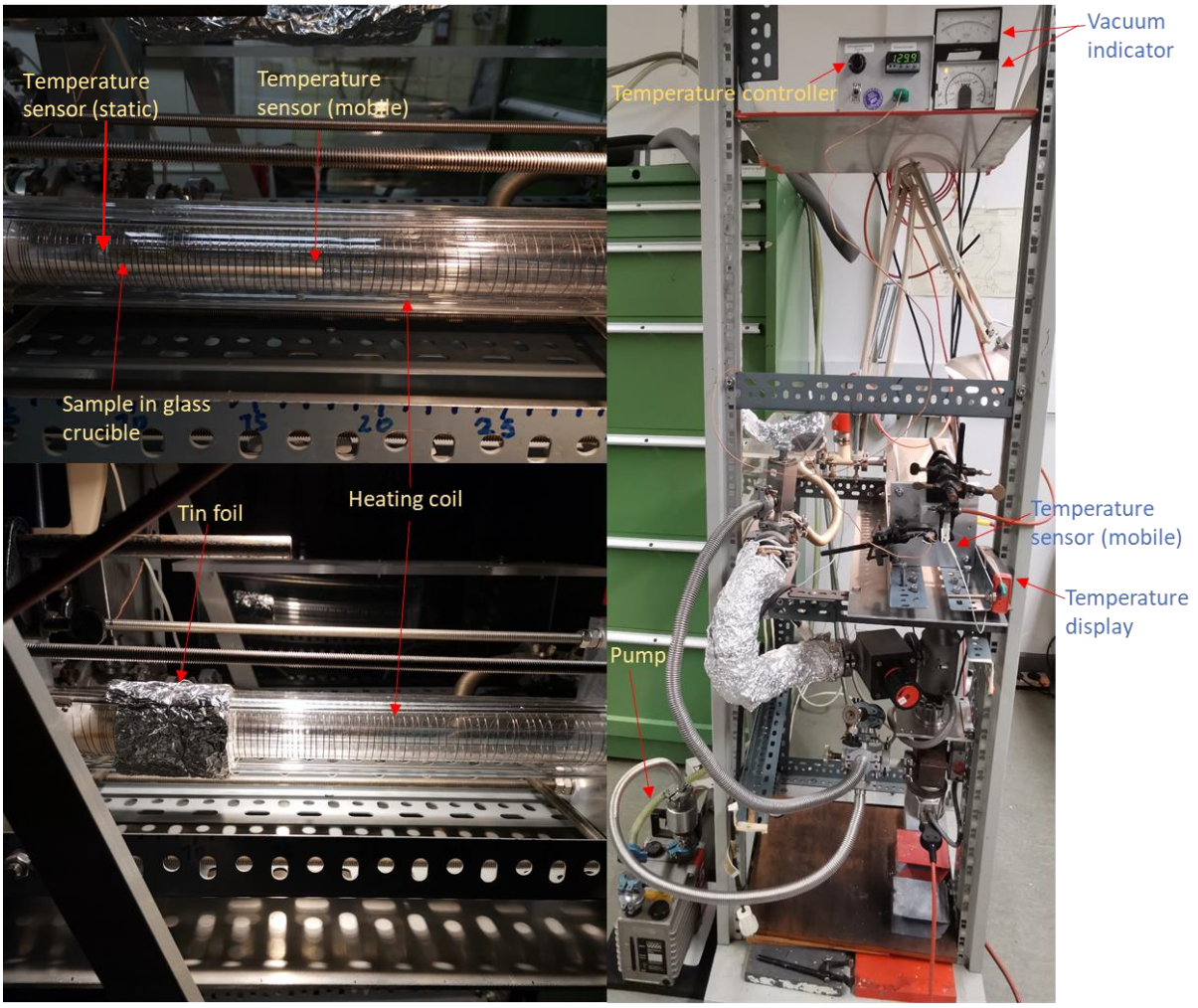

***Figure 27**: Experimental setup for the zone sublimation experiments performed with enantiomerically pure **PyrSQ-C1**.*

In order to ensure the necessary temperature gradient to achieve zone sublimation the heating coil is wrapped in a way where the distance between each winding is slightly increased over the length of the sublimation chamber. As shown in Figure 27 a ruler is mounted on the outside, giving guidance regarding the distance from the heating source (located at 0 cm). The highest temperature is designed to be at the position where the 4 cm long glass crucible filled with the pure (*R*,*R*)-PyrSQ-C1 sample is placed in the sublimation chamber (12 cm). The temperature at the sample was set using a temperature controller that controlled the current passing thought the heating coil. An integrated PID controller in the temperature control unit allowed for a sensitive temperature control. The resulting heating of the coil was checked by the integrated static temperature sensor positioned around the middle of the sample and a second mobile temperature sensor was used to monitor the actual temperature at the predefined distances (Table 3).

***Table 3**: Temperature profile of the zone sublimation experiments with* enantiomerically pure **PyrSQ-C1**.

T_{set} [°C]	6 cm	12 cm	18 cm	24 cm	30 cm	Pressure x 10^{-5} [mbar]
85	96.3	96.9	90.1	82.7	74.2	3.0
90	97.7	101.0	95.4	87.9	78.6	3.0
95	109.9	109.4	101.3	91.9	81.8	1.5
100	110.0	111.0	103.2	94.9	85.4	1.5
105	119.0	120.0	110.6	101.9	90.5	1.5
110	121.6	122.5	116.9	106.4	92.4	1.5
115	125.3	127.1	119.9	109.6	96.3	1.5
120	133.0	135.5	126.0	114.3	101.1	1.5
125	138.9	139.7	129.8	119.0	103.0	1.5
130	143.3	143.7	134.1	121.4	106.3	1.5
135	145.7	146.8	137.4	125.9	110.8	1.5
140	153.1	153.6	142.1	130.9	115.3	1.5
145	157.6	157.9	146.2	133.7	118.8	1.5
150	159.4	161.3	151.1	138.8	123.2	1.5
155	167.2	170.2	159.5	146.6	125.6	1.5
160	171.5	172.2	161.3	146.3	129.6	1.5
165	174.8	178.8	165.4	151.1	134.4	1.5
175	189.7	189.9	172.7	159.8	139.4	1.5
180	195.6	195.7	179.1	166.9	144.3	1.5
185	200.0	200	185.0	170.1	150.2	1.5
190	201	204	187.4	173.6	152.3	1.5
195	207	209	195.3	176.1	150.0	1.5
200	210	210	197.0	181.0	160.1	1.5
205	218	218	204	187.2	163.2	1.5
210	223	223	205	188.4	167.2	1.5
215	231	230	214	198.4	173.3	1.5
220	230	230	216	201	177.1	2.1
225	239	236	223	205	183.5	3.0
230	243	241	225	212	177.1	1.5

The temperature was increased in five-degree steps on the temperature controller. The actual temperature measured within the chamber was around 10 °C higher than the set temperature. The vacuum within the chamber was stable around 1.5 x 10^{-5} mbar. At a T_{set} = 225°C the pressure increased to 3.0 x 10^{-5} mbar. This sudden increase of pressure was interpreted as the beginning of the sublimation process. Thus, the temperature was slightly increased to 230 °C and kept at this temperature for 7 days. Over this period a greenish deposit formed at a distance of 20 cm (20 cm-26 cm, ~207 °C). Additionally, the faint purple discoloration that could be observed at the edge of the glass crucible dispersed over the period. Furthermore, the originally crystalline and highly reflective sample turned dull as it lost its shine, this was accompanied by the color change from golden greenish to a reddish-brown appearance.

In attempt to reignite the sublimation process, the temperature was stepwise elevated further. Additionally, an extra tin foil layer was installed externally around the position where the heating coil is wrapped most tightly to minimalize the cooling of the chamber from air. Over the course of 8 h the temperature was increased to 250 °C in 5 °C steps. This caused the zone of the observed deposition to slowly move from initially 20 cm to 22 cm and a slight visual intensification and color deepening of the greenish blue deposit. After an additional week at this temperature the sublimation was halted and

after steady cooling back to room temperature the sublimation tube was removed and cut into the respective zones (Figure 28).

zone	range	findings
1	0-6 cm	crucible with insoluble residues
2	6-14 m	empty
3	14-22 cm	majority of (*R*,*R*)-**PyrSQ-C1**
4	22-25 cm	(*R*,*R*)-**PyrSQ-C1**
5	25-31 cm	traces of (*R*,*R*)-**PyrSQ-C1**
6	31 cm-End	yellow fragmentation product

***Figure 28**: Result of the zone sublimation experiments performed with enantiomerically pure **PyrSQ-C1**. Photographs of the intact sublimation tube after removal from the equipment (top), the fragmentated sublimation tube after being cut into the respective zones (right), close-up on the crucible containing the pristine **PyrSQ-C1** before the experiment (left middle), close-up of the sample after the experiment, showing a distinct change of color and texture (left bottom).*

Upon closer inspection the desired bigger crystal could not be found and only trace amounts of substrate could actually be sublimed. The majority remained in the crucible and deteriorated.

Additionally, samples of the synthesized and purified products were also provided to collaboration partners within and beyond the research training group 2591 (TIDE). Within TIDE, *O. R. Schäfer* from the Lindfors group, University of Cologne was supplied with **PyrSQ-C1**s for investigations regarding light-matter interactions of these dyes.

Beyond TIDE, a co-operation with *R. Resel* from Graz University of Technology, Austria was established. Here, the thin film preparation of **PyrSQ-C1**s by physical vapor deposition (PVD) techniques was tested. Three set-ups (Table 4 & Figure 29) using different evaporators, evaporating sources and varying distances between source and target, as well as different base pressures were employed.

***Table 4**: Overview of evaporator specifications used in the Resel group for the PVD experiments.*

evaporator	base pressure [mbar]	evaporating source	distance to target
1	1×10^{-5}	W filament with Al insert	10 cm
2	1×10^{-6}	W filament with Al insert	25 cm
3	3×10^{-10}	Kentax 3 cell evaporator with quartz crucible	16 cm

As can be seen by the unique specification of each set-up, the degree of precision is improved from evaporator 1 to 2 and evaporator 3, which allows the most precise control over the filament current. The set-up of evaporator 1 lacks the opportunity for a substrate heating set-up, but features the smallest target to substrate distance with only 10 cm. This set-up is the most rudimental one as it lacks in precise control over the evaporating temperature. Thus, the evaporation rate was unstable. Furthermore, the achievable base pressure is the highest with 10^{-5} mbar compared to the others. Evaporator 2 provides an improved vacuum of 10^{-6} mbar and more precise control over the evaporation rate compared to the former one, but also suffers the longest distance between target and substrate of 25 cm. Further upgrades were possible through the use of an ultrahigh vacuum (UHV) PVD set-up as in the case of evaporator 3 reaching a base pressure of 3×10^{-10} mbar. This unit is fully equipped with the possibility to measure XPS, UPS and LEED, respectively. It features a Kentax three cell evaporator (Figure 29) consisting of three independent evaporating sources and is liquid cooled allowing for the most precise temperature control compared to the other two. With a target to substrate distance of 16 cm it ranks in the middle of the possible distances.

***Figure 29**: Experimental setups used for the PVD experiments performed with **PyrSQ-C1** in the Resel group. a) set up of evaporator 1, b) evaporator 2, c) evaporator 3 (UHV PVD set-up), d) close-up on the evaporation chamber of evaporator 3, e) crucibles for evaporator 3 before (right) and after (left) PVD experiments.*

Samples of both enantiomers with different purity grades were investigated in these PVD experiments (Table 5). In this context purity grades refer to the method of crystallization in order to obtain the material. Purity #1 was obtained from recrystallization of PyrSQ-C1 directly isolated by column chromatographic purification of said crude product in DCM/MeOH 1/2 v/v followed by recrystallization from DCM/cyclohexane 1/2 v/v. Purity #2 was obtained by further concentrating the filtrate from the

recrystallization for purity #1 and chilling thereof to promote further crystal growth. The same was repeated with the supernatant thereof to obtain purity #3. Thus purity #1 is the highest purity grade.

***Table 5**: Overview of the results of the PVD experiments in the Resel group.*

evaporator	sample	substrate	thin film
1	R-chiral purity #2	glass	1 out of 3
2	R-chiral purity #2	glass	---
2	R-chiral purity #3	glass	---
3	R-chiral purity #1	palladium crystal	---
3	R-chiral purity #2	palladium crystal	---
3	S-chiral purity #1	palladium crystal	---

As summarized in Table 5, most of the PVD attempts unfortunately did not resulted in thin films. Only in one case an amorphous thin film was obtained. Post deposition annealing of the probe at 140 °C, 160 °C and 180 °C show no improvement and the film remained amorphous.

Due to the missing temperature control units, it was impossible to monitor the evaporation temperature when evaporator 1 and 2 were used. For evaporator 3 it was noted that once the evaporator reached a temperature of 140 °C an evaporation rate of 0.01 Å/sec, which started to deteriorate with time, was observed. Elevating the temperature further until 210 °C increased the evaporation rate negligibly to 0.02 Å/sec. No evaporation was observed between 210 °C and 240 °C. Surprisingly, further evaporation of the material was observed for the temperature range from 240 °C to 280 °C. Beyond 280 °C no further evaporation was detected.

Nevertheless, an interesting discovery was made during the PVD experiments. Throughout the different set-ups one observation remained constant. In the respective sources for the PVD a brownish black material remained. X-ray photoelectron spectroscopy (XPS) and elemental analysis identified the remains as polymerized squaraine. This finding refutes the initial assumption of deterioration of the substrate during the zone sublimation and indicates that the more probable cause for the low sublimation rate and PVD observed is due to the more favorable polymerization of the **PyrSQ-C1** independent from the purity.

When compared to the previously successfully vapor-deposited squaraines like **SQIB**[20,47,48] and core-functionalized **Se-SQ-C4**[138](Scheme 25) an important structural difference becomes apparent, only **PyrSQ**s have a non-aromatic ring. Accompanied by the so far also unsuccessful PVD attempts for thin film fabrication of **ProSQ**s, who have a closely related underlying substructure, the explanation of a preferred polymerization reaction compared to evaporation under these conditions appear even more reasonable.

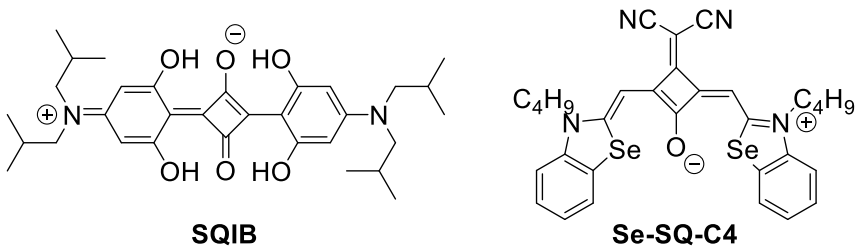

***Scheme 25**: Molecular structure of squaraines **SQIB** and **Se-SQ-C4** which could both be successfully vapor-deposited on solid supports.*

In conclusion, the search for chiral sublimable squaraines has to continue. Fortunately, PVD is not the only possibility to deposit a compound onto the targeted substrate for device fabrication. Alternatives

for thin film fabrication, although less popular due to the inherent challenges of the process, are solvent processing procedures. These envision dissolving of the material in suitable solvents followed by drop or spin casting thereof onto the desired substrates. The biggest concern in this process, even more than in case of PVD, is the purity of the material as every impurity in question falsifies the results and hampers the reproducibility. Additionally, the inherent unevenness of the thin films obtained through drop or spin casting, as the edges ultimately differs in thickness compared to the center of the films.

5 L-ALANINE-DERIVED SQUARAINES

To expand the library of existing chiral squaraines and thereby, combine chirality with the promising solubility and aggregation effects of ***N*-alkyl-SQ**s, a new class of amino acid-based squaraine was envisioned that would furnish the termini of an anilino squaraines with two alkyl groups each. Following in the foot step of the **ProSQ**s the utilization of the abundant, naturally in high enantiomeric purity occurring amino acid L-alanine was chosen as the chiral backbone. As the smallest naturally occurring amino acid the resulting alanine-derived squaraines (**AlaSQ**) can then serve as baseline for comparison with other amino acid-based squaraines in the future. Even though the characteristic residue of alanine is a methyl group, the resulting steric hindrance might give interesting insights for future endeavors. In addition, other than the secondary amine prolinol, primary amine alaninol offers the chance to introduce two alkyl groups – one on the oxygen atom and one on the nitrogen atom – of varying size to elucidate some structure-property relationships.

Employing the established and proven synthetic strategy of doing a condensation of squaric acid, phloroglucinol and a secondary amine of choice, [45,132,139]the synthesis of the new class of **AlaSQ**s appeared to be straightforward (Scheme 26).

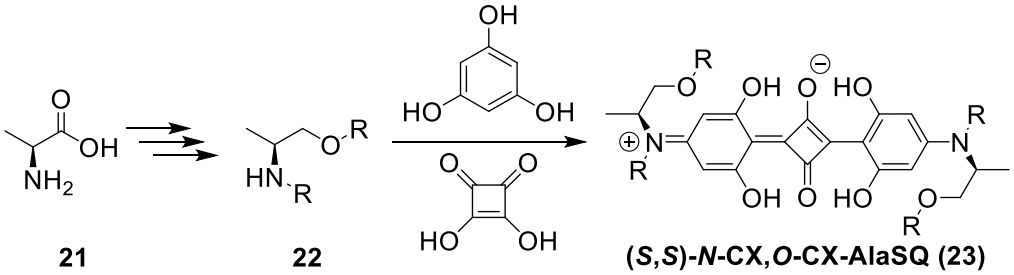

***Scheme 26**: General synthetic strategy to prepare **AlaSQ**s (**23**).*

5.1 ESTABLISHING *N,O*-ETHYLATION OF L-ALANINOL AS A MODEL SYSTEM

Similar to the synthesis of the **ProSQ**s, the commercially available corresponding amino alcohol L-alaninol (**24**) was used instead of the amino acid (**21**) directly. It was then intended to introduce an alkyl chain each on the nitrogen atom and oxygen atom simultaneously. Statistically speaking, the alkylation could result in multiple products (Scheme 27): monoalkylation at oxygen (**25**) *or* nitrogen (**26**), monoalkylation at oxygen *and* nitrogen (**22**), dialkylation of nitrogen (**27**) or even peralkylation of both oxygen and nitrogen (**28**) of alaninol (**24**) and – depending on the conversion – there might even still be some of the starting material left. Thus, a worst-case scenario would result in a mixture of six compounds coexisting in the reaction mixture, which would complicate the separation and purification process significantly. Furthermore, this unfavorable ratio of 1/5 of desired product **22** to undesired byproducts seems highly unsustainable, and thus, less desirable. While two of the byproducts (**25** & **26**) and the starting material (**24**) could still be redeemed, the *N*-dialkylated products **27** and **28** remain inaccessible for the synthesis of **AlaSQ**s as the final condensation step asks for a secondary amine and does not work with a tertiary one.

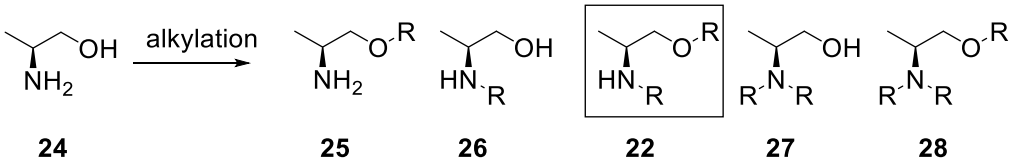

***Scheme 27**: Potential alkylation products **22**, **25**, **26**, **27**, and **28** of alaninol (**24**) (R = alkyl).*

Additionally, this approach would be highly dependent on the alkylation reagent and demands for fine-tuning for each derivative. Thus, it does not promise a robust and versatile synthetic protocol but rather asks for a suitable protecting group strategy to avoid undesired over-alkylation. To test this, it was decided to focus on ethylations first to establish a suitable protecting group strategy as ethyl iodide is a reasonable reactive electrophile that gives rise to more promising products than the even more reactive but also way more toxic methyl iodide although in the end even longer alkyl halides were supposed to be used.

N-Boc-Protection Strategy

The first protecting group explored was the Boc-group as it already proved successful in the synthesis of **ProSQ**s in the past. Introduction of the Boc-group was straightforward giving the desired product in good to excellent yields in a reliable manner (Table 6).

***Table 6**: N-Boc-protection of alaninol.*

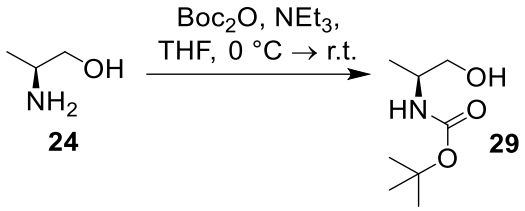

entry	reaction time	atmosphere	yield	scale
1	1.5 h	argon	95%	50 mg
2	1.5 h	argon	85%	1 g
3	2.0 h	argon	96%	2 g
4*	2.0 h	air	81%	1 g
5*	1.5 h	air	79%	1 g

* Result obtained by a bachelor student supervised during his advanced organic chemistry lab course

This highlights the robustness of this protection method, showing consistent and reliable yields even when bypassing inert gas conditions.

With this in hand the next step was to introduce the desired alkyl chains via nucleophilic substitution conditions. Following the successfully established procedure for the synthesis of **ProSQ**s ethyl iodide and sodium hydride were used in DMF. This, however, led to the formation of the *N*-alkylated oxazolidinone **30** instead of the desired product **31** (Scheme 28). This was formed in an intramolecular transesterification due to intramolecular attack of the intermediate alkoxide at the carbamate *C*-atom which is obviously more favorable than the desired intermolecular ether formation upon reaction with the ethyl iodide as an electrophile. A most likely subsequent alkylation at the nitrogen atom then finally led to the observed product **30**.

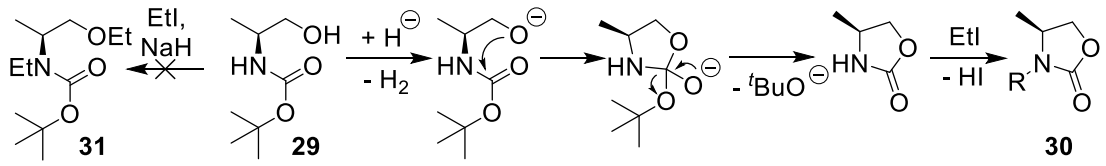

***Scheme 28**: Formation of N-alkylated oxazolidinone **30** upon attempted O-alkylation of N-Boc-protected alaninol **29**.*

According to literature this is an expected outcome for Boc-protected amino alcohol in the presence of strong bases.[140,141] The exception is the special case of prolinol. As a cyclic secondary α-amino alcohol the resulting oxazolidinone would be part of a bicyclic structure experiencing significant ring strain, which in turn outweighs the favorability of an intramolecular reaction. Thus, the intermolecular alkylation via Williamson-ether synthesis for the synthesis of **ProSQ**s does not suffer from oxazolidinone formation when performed at non-elevated temperatures in DMF.[31,32,140]

In principle, oxazolidinone **30** could be reopened to further proceed with this route – even offering the chance to introduce a different alkyl group at the oxygen atom. Multiple different approaches[142] have been established for this, however, testing the one under alkaline aqueous conditions[143] unfortunately did not work to open **30**, and this approach was therefore stopped at this point.

The next idea was to avoid the formation of the oxazolidinone. Therefore, the reaction conditions for the alkylation needed to be adjusted. The first setscrew was finding an alternative base instead of the strong base sodium hydride. Out of the tested inorganic bases potassium carbonate turned out to be the most promising (Table 7).

***Table 7**: Screening of O-alkylation conditions of N-Boc-protected alaninol.*

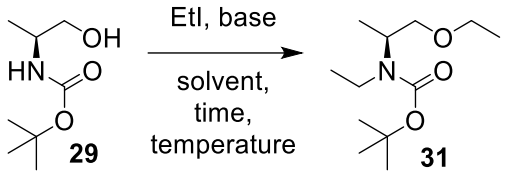

entry	base	eq. of EtI	solvent	reaction time	reaction temperature	NMR-yield	scale
1	Na_2CO_3	9.0	DMF	24 h	0 °C → r.t.	0%#	50 mg
2	K_2CO_3	9.0	DMF	24 h	0 °C → r.t.	25%	50 mg
3	K_3PO_4	9.0	DMF	24 h	0 °C → r.t.	0%§	50 mg
4*	K_2CO_3	9.0	DMF	21 h	0 °C → r.t.	66 %	500 mg
5	K_2CO_3	3.0	DMF	24 h	0 °C → r.t.	26 %	500 mg
6	K_2CO_3	6.0	DMF	48 h	0 °C → r.t.	52 %	500 mg
7	K_2CO_3	6.0	DMF (wet)	48 h	0 °C → r.t.	60 %	50 mg
8	K_2CO_3	9.0	acetone	20 h	0 °C → r.t.	0%#	50 mg
9	K_2CO_3	9.0	DMF	24 h	0 °C → 60 °C	42%	50 mg

* Result obtained by a bachelor student during his/her advanced organic chemistry lab course,
# 100% recovered starting material, § formation of byproduct 30a in 50% yield

After ethylation, the next step was the deprotection of the Boc-group, which is usually achieved by treatment with a strong acid like trifluoroacetic acid (Scheme 29).

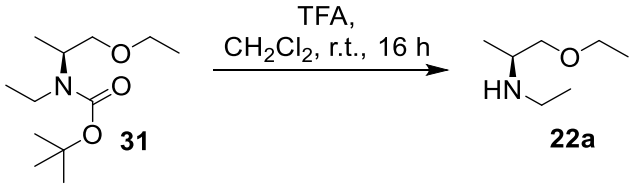

***Scheme 29**: Application of standard conditions to remove the Boc protecting group from **31** to release the desired N,O-dialkylated alaninol **22a**.*

In this case acidic hydrolysis posed a problem due to the high solubility of the obtained product in water, as the introduced ethyl chains cannot outweigh the hydrophilicity of the amine group even after

rendering the pH value to slightly basic conditions. Thus, the desired product remained in the aqueous phase and extraction with dichloromethane or ethyl acetate proved less successful than expected. Due to all these problems, this approach was stopped and a new protection group was tested next.

Phthalimide Protection Strategy

In the search for a suitable alternative for the Boc-group the phthalimide (Pht) group was tested as a protection group next.[144] An added value of this group is that it adds fluorescence upon UV irradiation to the compounds which significantly facilitates the detection of the respective protected compounds compared to the corresponding Boc-protected ones, which in praxis need additional staining reagents such as ninhydrin or potassium permanganate in order to be able to monitor the progress of the reactions or column chromatography via TLC. These experiments were performed in the course of the bachelor thesis of *S. Schimmelpfennig* whom I was supervising to explore the possibilities of the Pht-protecting groups.[145]

Introduction of this protecting group was straight forward (Table 8). Interestingly, the best results were obtained under solvent free neat condition.

***Table 8**: Screening of protection of alaninol (**24**) as phthalimide **32**.*

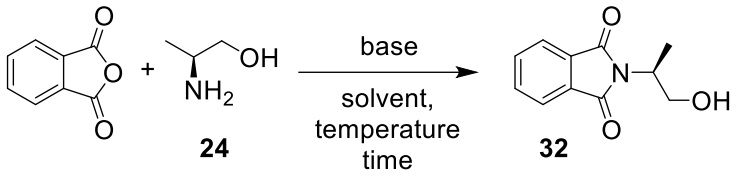

entry	eq. of anhydride	base	eq. of base	solvent	reaction time	temperature	yield	scale
1	1.0	NEt_3	1.0	toluene	21 h	reflux	80%	1 g
2	1.0	NEt_3	0.1	toluene	3 h	reflux	82%	500 mg
3	1.1	-	-	-	16 h	140 °C.	96%	1 g

With **32** in hand the alkylation of the hydroxyl function was performed. Using standard conditions with *in situ* generation of the alkoxide and addition of alkyl iodide only low yields were observed for butyl iodide and octyl iodide. This was also verified when ethyl iodide was used (Table 9).

***Table 9**: Screening of alkylation of phthalimide-protected alaninol **32**.*

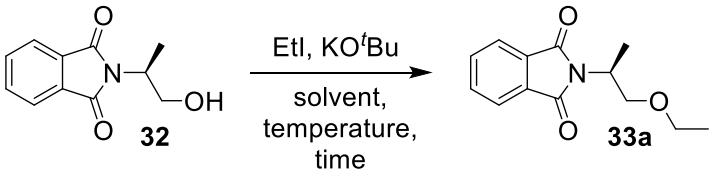

entry	solvent	reaction time	temperature	ratio of product:starting material	scale
1	THF	21 h	r.t.	-	50 mg
2	THF	21 h	60 °C	5/1	50 mg
3	DMF	22 h	r.t.	1.7/1	50 mg
4	DMF	22 h	60 °C	1/1	50 mg

Building on this insight, it was concluded that a reversal of polarity could be more promising. Thus, the hydroxyl function was transformed into a tosylate as a suitable leaving group (Scheme 30).

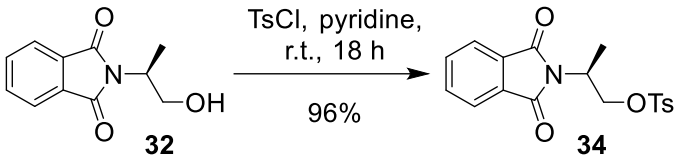

***Scheme 30**: Tosylation of phthalimide-protected alaninol **32**.*

With **34** in hand an S_N2-reaction was tested next to form the desired ether **33a** using ethoxide as the nucleophile (Table 10). Sodium ethoxide was added as a commercially available 21% w/w solution in ethanol no further solvent was necessary.

***Table 10**: Screening of alkylation of tosylated phthalimide-protected alaninol **34**.*

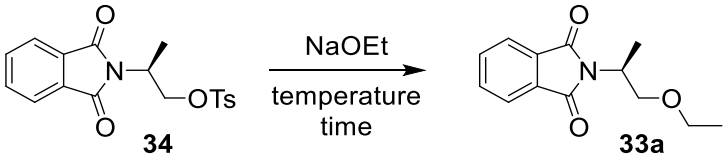

entry	eq. of NaOEt *	cosolvent	concentration [mmol/mL]	temperature	reaction time	yield	scale
1	4.8	-	0.6	r.t.	24 h	39%	100 mg
2	4.8	-	0.6	50 °C	24 h	31%	100 mg
3	5.0	-	0.3	r.t.	2 h	77%	50 mg
4	5.0	-	0.3	50 °C	2 h	59%	50 mg
5	5.0	-	0.3	r.t.	1 h	50%	50 mg
6	5.0	DMF	0.3	r.t.	1 h	60%	50 mg
7	5.0	DMF	0.3	r.t.	4 h	21%	50 mg
8	5.0	-	0.3	r.t.	4 h	34%	50 mg

*NaOEt was added as a 21% w/w solution in ethanol which also provided the solvent for the reactions.

With the successful introduction of the ethyl ether the next step was to remove the Pht-protecting group. This can be done in various ways.[144] The arguably best-known method is the cleavage upon treatment with hydrazine. Thus, this was tested first with a fresh batch of hydrazine monohydrate. Following the literature procedure[145,146] (Scheme 31) and also adapted conditions with varying amount of hydrazine monohydrate (2.5 eq. – 50 eq), increasing reaction time (4 h - 24 h) and reaction temperature (40 °C -60°C), the product was never found in the organic phase but assumingly persisted in the aqueous phase. The described white precipitate was observed, but isolation of the desired product remained tricky when working in aqueous milieus.

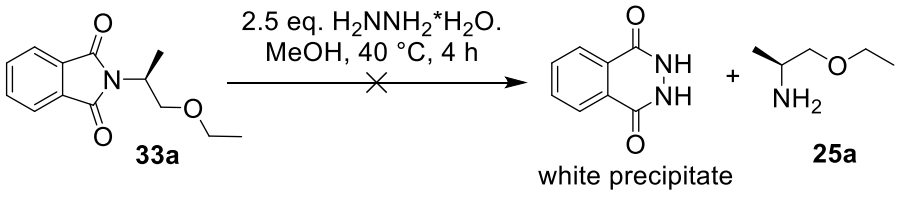

***Scheme 31**: First attempt to remove of phthalimide protecting group from O-alkylated alaninol derivative **33a** via treatment with hydrazine.*

Likewise, the other two prominent deprotecting methods involving either a reductive cleavage with a subsequent acidic work-up in acetic acid or alkaline hydrolysis appeared to run into the same problem of product isolation challenges once the primary amine is exposed to water.

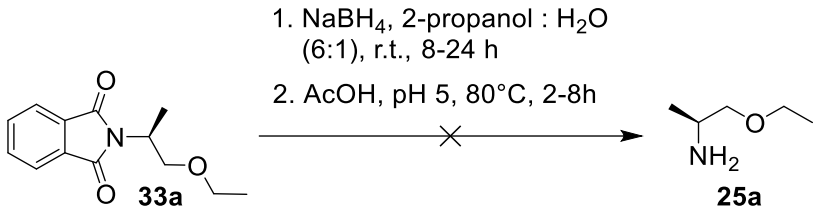

***Scheme 32**: Second attempt to remove the phthalimide protecting group from O-alkylated alaninol derivative **33a** via reduction with sodium borohydride.*

A quick test of a reductive dephthalimidation conditions[147] (Scheme 32) verified the afore suspected complication. In conclusion, this approach appears to be a dead-end as long as ethyl chains are desired as the overall polarity of the compound will prefer polar solvents over apolar ones, with an especially high affinity to water as shown. Thus, further endeavors into alternative deprotection methods were halted.

In the search for a different approach to achieve the desired ether formation a short break from protecting group strategies was taken and direct-conversion approaches were thought of next.

Direct Conversion Approaches

The idea behind this was the direct introduction of suitable functional groups into the alaninol framework ensuring the avoidance of water for once the desired secondary amine is formed. In theory, this would also result in a more atom economic approach.

Inspired by the reduction of esters to the respective ether by Sakai,[148] the direct reduction of amides and esters to secondary amines and ethers, respectively, was envisioned (Scheme 33).

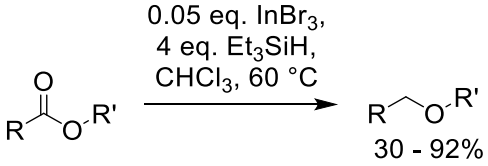

***Scheme 33**: Indium bromide-mediated reduction of esters to ethers according to the procedure developed by N.Sakai and coworkers.*

These conditions were tested successfully on various esters ranging from aliphatic over cyclic to aromatic systems.[148] Even tertiary amides were successfully converted to the corresponding tertiary amines. Even though the original literature states that "*unfortunately, reductive deoxygenation using a secondary amide did not form the desired secondary amine*"[148] two test system were designed (Scheme 34).

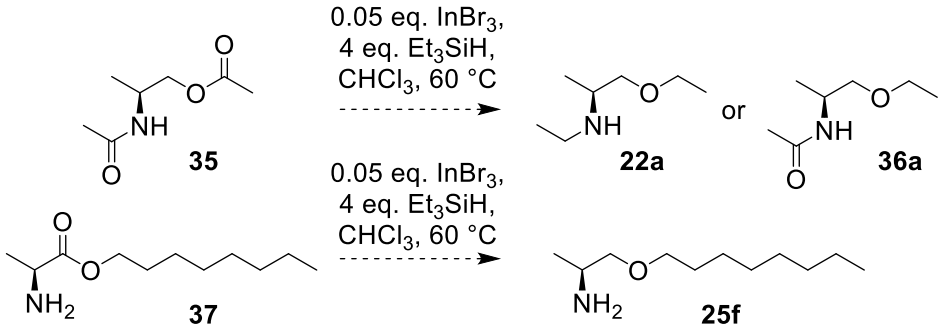

***Scheme 34**: Envisioned test reactions for indium bromide-mediated reduction of N,O-diacylated alaninol derivative **35** and alanine octyl ester **37**.*

The synthesis of the test substrates **35** and **37** were straightforward and yielded the desired compounds in satisfying to good yields, respectively (Schemes 35 & 36).

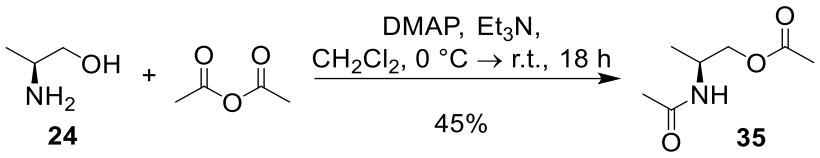

***Scheme 35**: Synthesis of N,O-diacylated alaninol derivative **35**.*

Simultaneous ester and amide formation was achieved using acetic anhydride, triethyl amine and DMAP to give the desired product **35** in 45% yield which is considerably less than reported in the literature (72%)[149]which might be explained by complication during the purification.

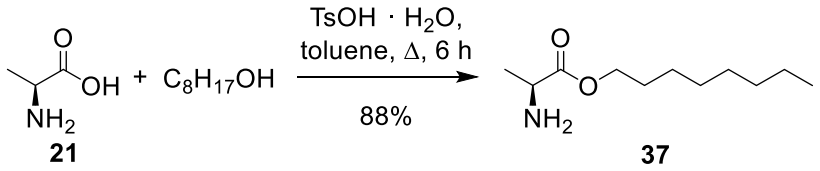

***Scheme 36**: Synthesis of alanine octyl ester **37**.*

The second test substrate **37** was synthesized using a simple esterification of L-alanine (**21**) with 1-octanol. This gave the desired product **37** in good yields, only slightly lower than literature (94%).[150]

Trying the above-mentioned indium bromide mediated reduction with both test substrate **35** and **37** using the literature conditions according to Scheme 34 unfortunately did not work but only allowed to recover parts of the non-converted starting materials for reasons that remain unclear.

A less sophisticated approach but still following the same intention of improved atom economy and overall reduced numbers of steps toward the synthesis of the respective desired secondary amine **22** could be a reductive amination approach via formation of an intermediate imine.[151] However, the close proximity of the hydroxyl group should favor the formation of the corresponding oxazolidine as an *N*,*O*-acetal that should be rather stable against reducing agents (Scheme 37) which is why this idea was not followed any longer.

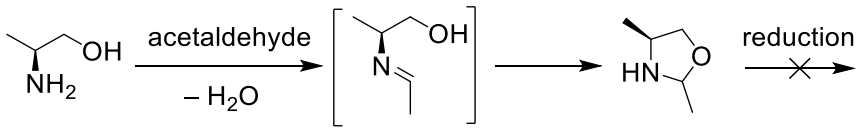

***Scheme 37**: Synthesis of an oxazolidine via condensation of an α-amino alcohol like alaninol with acetaldehyde.*

Benzylic imines (also 2-phenyloxazolidines), however, are much easier to reduce, and hence, reductive amination using benzaldehyde was thought to be a good way to achieve *N*-benzylated alaninol derivatives establishing the benzyl group as a well-known amine protecting group for our purposes.[144]

Benzyl Protecting Strategy

As the above-mentioned direct conversion approaches did not give satisfying results the protection group strategy was revisited. Building on the experience gathered from both the Boc and the Pht protecting group, the most important condition during the deprotection step, where the desired secondary amine **22** would be released, is to avoid a of possible exposure to aqueous basic or acidic work-up strategies. Furthermore, this approach should also offer the added benefits of a UV-active protecting group facilitating monitoring by TLC without the need to additional reagents for

visualization. Therefore, the benzyl protecting group seemed to be a very promising candidate to fulfill all these demands. It ensures UV-detectable reaction control via TLC and can be removed by reductive hydrogenation,[144] which does not require an aqueous work-up. Additionally, the introduction by reductive amination ensures selective *N*-protection and avoids possible overalkylation which usually hampers normal alkylation of primary amines via S_N2 reactions.

Fortunately, the reductive amination proceeded highly efficient yielding the desired product **38** in reliably good to excellent yields even on decagram scale.

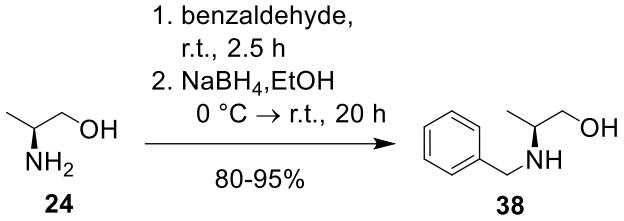

***Scheme 38**: Synthesis of N-benzyl protected alaninol **38**.*

With **38** in hand the next step was the ethylation of the Bn-protected alaninol. Once again Williamson ether synthesis conditions were chosen to simultaneously introduce identical alkyl chains onto both, nitrogen and oxygen (Scheme 39 and also Table 12 in Chapter 5.2).

Deprotection was performed using palladium on charcoal as catalyst in a hydrogen atmosphere (Scheme 39). Depending on the scale, though, larger batch sizes were found to need considerably more time than smaller ones to achieve comparable yields.

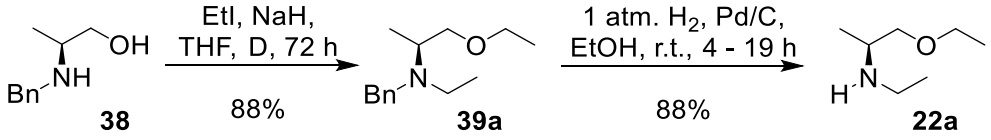

***Scheme 39**: Alkylation of benzyl-protected alaninol **38** and subsequent deprotection of N-benzyl protecting group from dialkylated intermediate **39a** giving rise to alaninol-based secondary amine **22a**.*

It is worth mentioning here, that initial attempts resulted in shockingly low yields, which was once again caused by an unsuitable work-up procedure. The typical removal of the catalyst is done by Celite® supported flash filtration through silica with sufficient eluent volume. In case of the here obtained secondary amine **22a**, the high polarity causes the amine to adhere strongly to the stationary phase. Thus, a disproportionally increasing amount of eluent was needed to flush the product from the stationary phase. The following adaption of the work-up procedure significantly improved the yields: The exchange of the flash column for a two-fold filtration proved most efficient. For the first filtration conventional filter paper was used, which holds back the majority of Pd/C and gives a first filtrate that still contains some of the elusive small particles. Swift rinse of the collected solid residue with sufficient amounts of ethanol ensures the best extraction of the product from the solids. For the second filtration a commercially available syringe filter was used featuring a membrane of 20 µm permeability to also remove the small particles resulting in a clear solution. Removal of the solvent under reduced pressure gave the desired secondary amine. Interestingly, prolonged exposure (t > 30 min) to pressures below 50 mbar led to diminished isolated yields (differences of about 10% same scale, same work-up), suggesting partial evaporation of the product during removal of the solvent.

5.1.1 Exploring Squaraine Synthesis with *N,O*-Ethylated L-Alaninol as a Model System

Exploring the Standard Three Component Condensation Approach

With the desired secondary amine at hand, the one-pot-two-step condensation reaction in a 1/1 mixture of toluene/n-butanol for azeotropic removal of the formed water was performed. This resulted in the desired product alongside two main side products (Scheme 40).

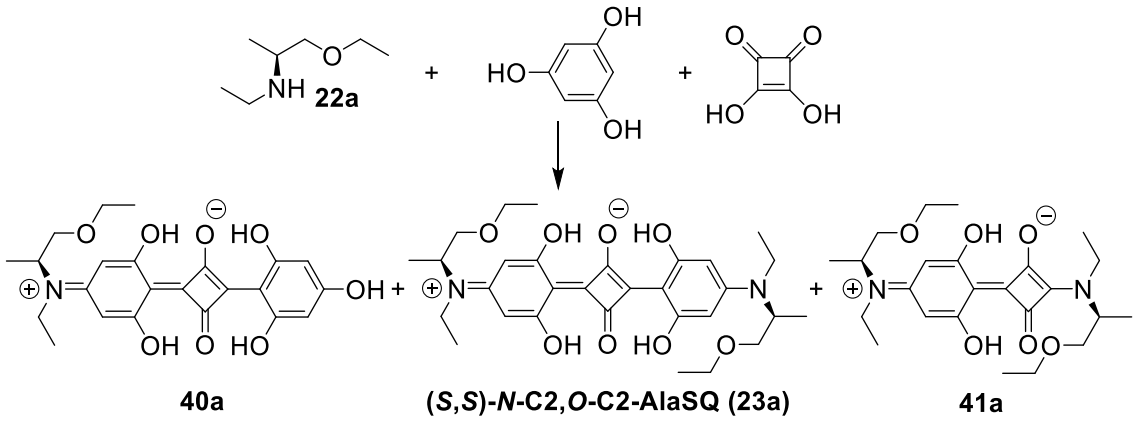

***Scheme 40**: Synthesis of **N-C2,O-C2-AlaSQ** (**23a**) and squaraines **40a** and **41a** as side products of the one-pot-two-step condensation of alaninol derivative **22a**, phloroglucinol and squaric acid.*

The formation of the direct condensation product **41a** of the amine with the squaric acid core is a well-known phenomenon that occurs during the one-pot-two-step condensation of squaraines when the initial condensation between phloroglucinol and the respective secondary amine is insufficient and free amine remains in the reaction mixture.[31] Beside the already expected yellow side product **41a**, an additional dark blue side product was observed which is the corresponding complementary squaraine resulting from the direct condensation of the hemisquaraine with non-converted phloroglucinol. This side product showcases an additional free hydroxyl function instead of the targeted amine function, thus, resulting in the asymmetric squaraine **40a**, which also shows interesting behavior in solution (Chapter 5.4.1).

***Figure 29**: Chromatographic separation and isolation o squaraines **N-C2,O-C2-AlaSQ** (**23a**), **40a** and **41a**.*

As depicted in Figure 29 the separation of these squaraines turned out to be very tedious, and hence, other approaches were considered to access the desired ***N*-C2,*O*-C2-AlaSQ 23a**. In order to avoid the first condensation step of the secondary amine **22a** and phloroglucinol to form the corresponding aniline derivative transition metal-catalyzed reactions seemed to be a promising alternative.

Exploring Buchwald-Hartwig Amination to Access the Alaninol-Derived Dihydroxy Aniline Derivative

A major selling point of the one-pot-two-step condensation sequence is the ability to build an extended π-conjugated system without the need of sophisticated reagents, additives or catalysts. However, as the yields obtained for ***N*-C2,*O*-C2-AlaSQ 23a** were comparably low, even for the standards of squaraine syntheses, which on average range between 10-20%. Thus, an alternative synthetic approach was also tested. Since it was possible to synthesize the secondary amines **22** rather reliably, the idea was to replace the apparently problematic first condensation of amine **22** and phloroglucinol with a transition-metal catalyzed Buchwald-Hartwig amination reaction.[152–154]

In order to avoid the use of the rather volatile *N*,*O*-diethyl-alaninol derivative **22a** in these tests, *N*,*O*-dioctyl- and *N*,*O*-diheptyl-alaninol derivatives **22f** and **22e** (see also Table 12 in section 5.2) were chosen as the secondary amine components and tried to be reacted with 3,5-dihydroxyhalobenzenes.

First and foremost, the standard Buchwald-Hartwig conditions established in our group for similar reactions[155,156] were put to test (Scheme 41).

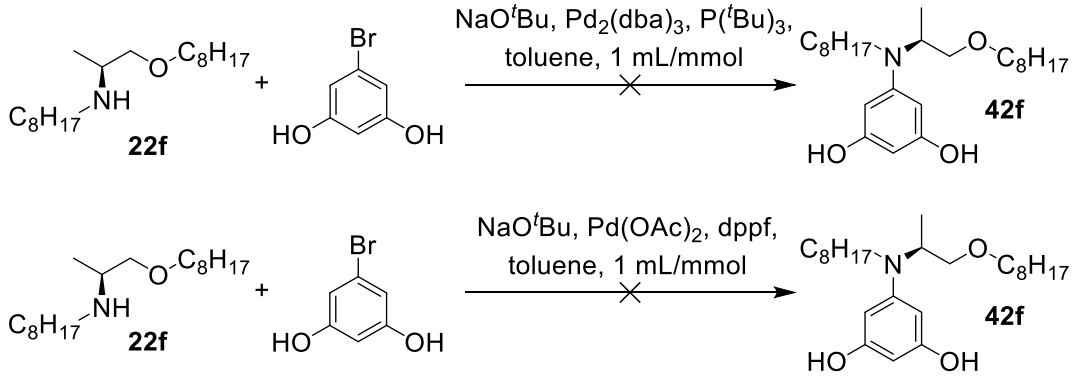

***Scheme 41**: Attempts to synthesize N,O-alkylated alaninol-based aniline **42f** via Buchwald-Hartwig amination.*

Unfortunately, this led to dehalogenation of bromo resorcinol and reisolation of the starting amine material (70%). A potential explanation for this could be that the facile deprotonation of the hydroxy functions might inhibit the desired cross-coupling reaction. Therefore, the hydroxyl groups were protected as benzyl ethers (Scheme 42) next.

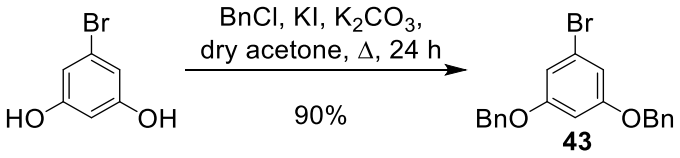

***Scheme 42**: Synthesis of 3,5-dibenzyloxybromobenzene **43**.*

With **43** in hand further attempts to successfully achieve Buchwald-Hartwig amination were made (Scheme 43).

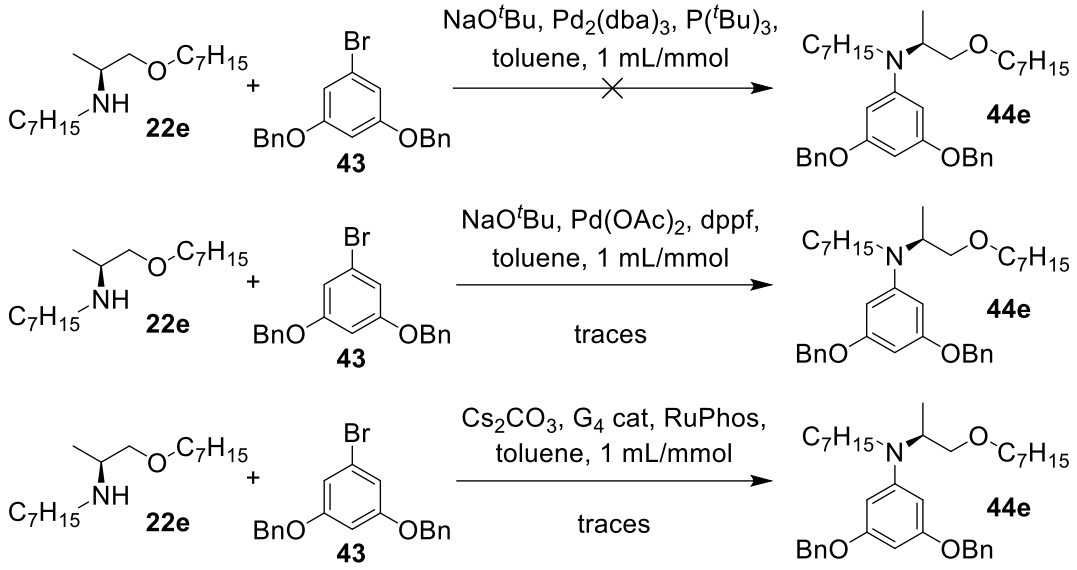

***Scheme 43**: Attempts to synthesize N,O-alkylated alaninol-based aniline **44e** via Buchwald-Hartwig amination.*

Searching the literature revealed that α-branched secondary amines are significantly less nucleophilic than their respective non-branched or cyclic counterparts.[153,157] This is supported by the problems we experienced during the first condensation reactions towards the desired aniline derivative **43** and the squaraines formed thereof. In order to improve the cross-coupling reaction it might be reasonable to exchange the previously tested standard catalysts for highly specialized and more reactive catalysts like a CPhos/JackiePhos hybrid or a RuPhos/JackiePhos hybrid in the future.[153,157,158]

As the short excursion into the realm of transition-metal catalyzed reactions was not successful to access the desired anilines **43**, a point was reached that asked for a strategic decision on how to proceed. Besides trying out further attempts to prepare the **AlaSQ**s **23** an alternative would be to use a constitutional isomer of alaninol - 1-aminopropan-2-ol **45** which is not branched on the α-carbon atom of the amine function, and hence, should show improved nucleophilicity. This would lead to a new class of chiral anilino squaraines **46** shown in Scheme 44.

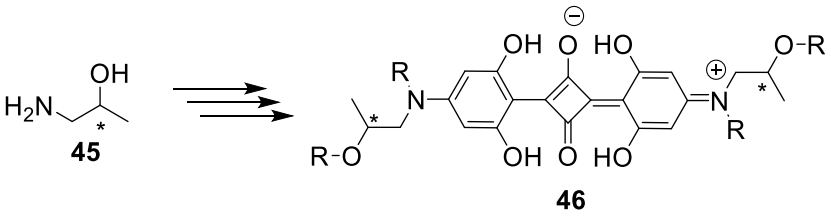

***Scheme 44**: Proposed structure of **AProSQ**s as a new class of chiral aniline squaraines **46** based on 1-aminopropan-2-ol (**45**).*

However, the cyclic prolinol-derived **ProSQ**s and the 2-methylpyrrolidine-based **PyrSQ** clearly show, that it is possible to successfully transform amines substituted at the α-carbon atom next to the amine function into the corresponding anilines and their squaraine derivatives. Thus, it seemed reasonable to stick to the respective alaninol building blocks and explore changes in the original condensation approach, e.g., by splitting the one-pot-two-step condensation approach into two separate steps resulting in the respective aniline in the first step and the desired squaraine only in the second one. Unwilling to abandon the desired AlaSQs the second path towards improving the condensation was chosen.

5.1.2 Modification of the Established Condensation Procedure

For better results during the condensation reaction the reactivity issue had to be addressed. The two principal approaches for improvement would either be to increase the nucleophilicity of the secondary amine or to increase the electrophilicity of phloroglucinol. Possible approaches in this regard would be the introduction of a suitable Lewis acid as a catalyst, which would only coordinate at the carbonyl-oxygen. Brønstedt acids hold the risk of protonation of the secondary amine, and thus, forming an ammonium ion, which prevents the possibility of a nucleophilic attack of the amine. As the increase of electrophilicity of phloroglucinol involves further additives, the option of increasing the nucleophilicity of the secondary amine was investigated first. The nucleophilicity of compounds not only depend on the structure of the compound, which determine the Brønsted basicity, polarizability of the donor atom and steric hindrance[159] but can also be influenced by the solvent due to the solvent effects. Thus, an adaption of the solvent system might be advantageous. An even easier set-screw for the adaptation of the reaction conditions is the increase of the concentration of the amine. As the condensation reaction still follows the principle of SN2 reactions,[159] an increase of amine concentration or even an increase in concentration for the overall reaction mixture by decreasing the employed solvents might lead to an easy and straightforward improvement for the reaction outcome.

Thus, in a first set of experiments, the concentration of the reaction mixture with regard to the amine was increased during the reaction. This and prolonged reaction time were implemented for the next condensation attempts (Table 11).

***Table 11**: Screening of conditions of the one-pot-two-step condensation for the synthesis of **N-C2,O-C2-AlaSQ** (**23a**).*

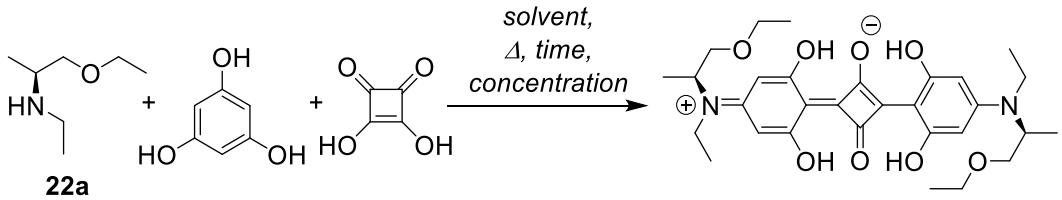

22a (*S*,*S*)-*N*-C2,*O*-C2-AlaSQ (23a)

entry	reaction time [h]	solvent	concentration [M]	scale [mmol]	yield
1	22 h + 24 h	toluene/1-BuOH 1/1	0.06	2.87	0%
2	16 h+ 21 h	toluene /1-BuOH 1/1	0.08	3.34	traces
3#*	5 d + 24 h	toluene /1-BuOH 3/1	0.83	5.22	traces
4+*	24 h +21 h	toluene /1-BuOH 4/1	0.15	0.58	< 2%
5+*	19 h +23 h	toluene /1-BuOH 4/1	0.50	6.58	20%

* Removal of solvent and exchange for toluene/1-BuOH 1/1 after first reaction period. # Intermediate purification and employment of 2.00 eq. of phloroglucinol. + use of 0.75 eq. phloroglucinol and with respective thereof 0.5 eq. squaric acid. Concentration with respect to the amine.

In the first two attempts (Table 11 entries 1 & 2) 0.5 eq. of squaric acid was added directly into the reaction mixture of phloroglucinol and alaninol derivative **22a** after 22 and 16 h, respectively Unfortunately, this proved to be counterproductive as only traces of the desired product were obtained whereas the byproducts 40a and 41awere found.

Obviously, the first condensation step supposed to yield the aniline derivative **42a** seemed to be the problematic step which needed further improvement. In order to improve the solubility of phloroglucinol and also improve the nucleophilicity of the secondary amine **22a** at the same time the polarity of the solvent for the initial step was decreased by increasing the relative content of toluene in the mixture of toluene and 1-butanol first. This allowed to increase the relative amount of phloroglucinol to 2 eq. and in addition the reaction time was extended to 5 days in order to make the formation of the intermediate aniline **42a** more favorable. However, since the second condensation reaction with the squaric acid asks for a more polar solvent mixture and in order to avoid the non-desired side reaction of excess phloroglucinol with squaric acid it seemed reasonable to follow the protocol of *M. Schulz*[32] and remove the initial solvent mixture and the excess phloroglucinol before dissolving the raw intermediate aniline **42a** again in a 1:1 mixture of toluene and 1-butanol together with 0.5 eq. of squaric acid (Table 11 entry 3). Unfortunately, however, the desired squaraine **23a** was only obtained in traces in this attempt.

In parallel experiments towards the synthesis of *N*,*N*-dialkyl-3,5-dihydroxyanilines performed by *M. Schumacher* it was observed that exposure of the intermediate to air during the intermediate isolation process proved to be problematic especially when working on a rather small scale. Therefore, it was decided not to isolate the intermediate anymore but only exchange the solvent mixture before adding the squaric acid and also decrease the relative amount of phloroglucinol to 0.75 eq.. This procedure finally led to the successful isolation of the desired ***N*-C2,*O*-C2-AlaSQ 23a** (Table 11, entries 4 & 5).

5.2 EXPANDING THE LIBRARY OF ALASQS

After establishing a promising synthetic approach towards the model compound ***N*-C2,*O*-C2-AlaSQ 23a**, the next logical step was to expand it to the synthesis of a library of **AlaSQs**. Starting from the already synthesized benzyl protected amine **38**, the introduction of further alkyl chains followed the tested and proven Williamson-ether synthesis like conditions.

Alkylation of N-Benzyl-Protected Alaninol

During the course of the Williamson ether syntheses, it was found that increasing the amount of alkylating agent and base from 1.00 eq-1.50 eq. per functional group to 2.00 eq. gave the most promising results. Additionally, also longer reaction times proved to be favorable for the reaction leading to higher yield of the desired twofold alkylated products **39**. In addition to the twofold alkylated product **39** also monoalkylated products **47** and **48** were also isolated in some cases (Table 12).

The different results can be correlated to the reactivity of the alkylating agent explaining the higher yields of the doubly alkylated products with the more reactive shorter alkyl iodides. With the shortest ethyl chain only the desired double-alkylated product **39a** was found (Table 12, entries 1 & 2). With propyl iodide it is possible to isolate significant amounts of the monoalkylated amine **48** (Table 12, entry 3), whereas even longer alkyl chains predominately give rise to monoalkylated ethers **47**. In line with these findings longer reactions are usually needed for longer alkyl iodides and lower reaction temperatures proved to be better to avoid elimination to the corresponding alkene (Table 12, entry 11). Also, adding the alkylating agent in two portions can be beneficial (Table 12, entries 9 & 10).

***Table 12**: Overview of the alkylations of N-benzyl-protected alaninol **38**.*

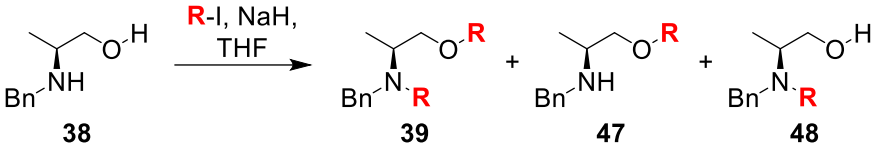

entry	**R**-I	reaction time [h]	temperature [°C]	product (yield)	product (yield)	product (yield)
1	ethyl-I	18	50	**39a** (48%)	-	-
2	ethyl-I	72 h	reflux	**39a** (88%)	-	-
3*	propyl-I	48 h	reflux	**39b** (26%)	-	**48b** (33%)
4*	butyl-I	48 h	reflux	**39c** (34%)	**47c** (40%)	-
5	pentyl-I	20 h	reflux	**39d** (11%)	**47d** (33%)	-
6	pentyl-I	70 h	reflux	**39d** (43%)	n.i.	-
7	heptyl-I	42 h	reflux	**39e** (8%)	**47e** (38%)	-
8*	heptyl-I	14 d	r.t.	**39e** (40%)	n.i.	-
9	octyl-I	2x 24 h	50	**39f** (33%)	**47f** (22%)	-
10	octyl-I	2x 24 h	reflux	**39f** (62%)	**47f** (10%)	-
11	nonyl-	46 h	reflux	**39g** (8%)	**47g** (61%)	-
12	nonyl-I	60-72 h	50-60	**39g** (16-34%)	**47g** (50-54%)	-

*2.40 eq. of base, n.i.= not isolated

The monoalkylated derivatives **47** and **48** offer the possibility to furnish the alaninol derivatives with different alkyl chains allowing to access an even larger variety of chiral secondary amines as building blocks for the synthesis of **AlaSQ**s (Table 13).

***Table 13**: Second alkylation of the previously obtained monoalkylated products **47** and **48**.*

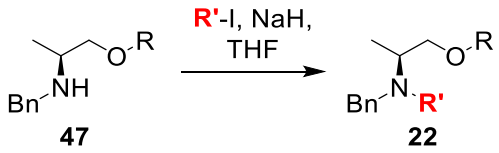

entry	substrate	R	**R'**-I	temperature [°C]	reaction time [h]	product	isolated yield [%]
1	**47c**	butyl	nonyl-I	50	96	**22h**	56
2	**47e**	heptyl	propyl-I	reflux	68	**22i**	60
3	**47g**	nonyl	propyl-I	reflux	63–93	**22j**	55–76
4	**47g**	nonyl	butyl-I	reflux	89	**22k**	66

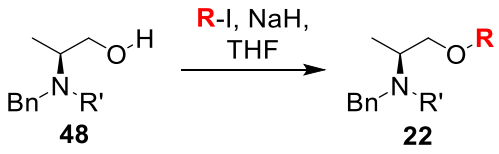

entry	substrate	R'	**R**-I	temperature [°C]	reaction time [h]	product	isolated yield [%]
5	**48b**	propyl	heptyl-I	reflux	72	**22i**	36
6	**48b**	propyl	nonyl-I	reflux	43	**22j**	30

To some extent the results reflect the previously observed preferences of the different alkylating agents for certain alkylation sites and the trends concerning their relative reactivity in terms of

favorable reaction times and temperatures. Thus, *N*-propyl-*O*-nonyl derivative **22j** is rather prepared starting from *O*-nonyl ether **47g** and propyl iodide than from *N*-propyl amine **48b** and nonyl iodide (Table 13, entries 3 & 6), respectively, and a similar trend is observed for the *N*-propyl-*O*-heptyl derivative **22i** (Table 13, entries 2 & 5).

Debenzylation of Alkylated Alaninols

Standard reductive deprotection of *N*-benzyl-protected alaninol derivatives **39a-k** gave the corresponding secondary amines **22a-k** in excellent yields (Table 14). Notably, the procedure can be applied to both large- and small-scale reactions as long as the period of bubbling of hydrogen throughout the reaction mixture and reaction time under static hydrogen atmosphere is adjusted accordingly.

***Table 14**: Debenzylation of N-benzyl-protected **39** to the respective secondary amines **22**.*

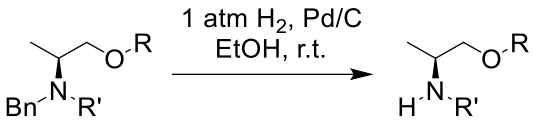

39 **22**

entry	substrate	scale [mmol]	bubbling time	reaction time[h]	product	R	R'	yield [%]
1	**39a**	0.9	2 min	4	**22a**	ethyl	ethyl	88
2	**39b**	16.0	30 min	19	**22b**	propyl	propyl	87
3	**39c**	4.9	10 min	18	**22c**	butyl	butyl	quant.
4	**39d**	7.1	15 min	24	**22d**	pentyl	pentyl	quant.
5	**39e**	2.2	10 min	16	**22e**	heptyl	heptyl	quant.
6	**39f**	7.6	15 min	18	**22f**	octyl	octyl	quant.
7	**39g**	6.1	15 min	19	**22g**	nonyl	nonyl	98
8	**39h**	5.1	10 min	18	**22h**	butyl	nonyl	83
9	**39i**	6.8	15 min	18	**22i**	heptyl	propyl	quant.
10	**39j**	3.7	6 min	20	**22j**	nonyl	propyl	99
11	**39k**	4.6	10 min	21	**22k**	nonyl	butyl	83

Reaction times were adapted according to the scale.

Synthesis of AlaSQs

With the secondary amines **22a-k** in hand the final condensation reactions to prepare the desired **AlaSQ**s **23** were performed building on the experiences made when optimizing the synthesis of **(*S*,*S*)-*N*-C2,*O*-C2-AlaSQ** (**23a**) described in Chapter 5.1.3.

Notably, it proved crucial to separate the two condensations steps which also include a change of the solvent system from a less polar 4:1 mixture of toluene and 1-butanol that ensures better solubility of the phloroglucinol to a more polar 1:1 mixture of toluene and 1-butanol for the second condensation of intermediate aniline **42** with squaric acid.

For syntheses on larger scale (Table 15 entries 2 & 3) it was found to be beneficial to use phloroglucinol in excess (1.5 - 2.0 eq.), prolonged reaction times for the first condensation and to remove excess phloroglucinol and isolation of the intermediate aniline **42** via flash chromatography before subjecting it to the second condensation as the large scale overcompensated for the loss of respective aniline **42** during this procedure (see General Procedure A for the Synthesis of **AlaSQ** in the Experimental Part) due to degradation upon exposure to air.

***Table 15**: Condensation reactions of **22a-k** with phloroglucinol and squaric acid to give the desired **AlaSQs 23**.*

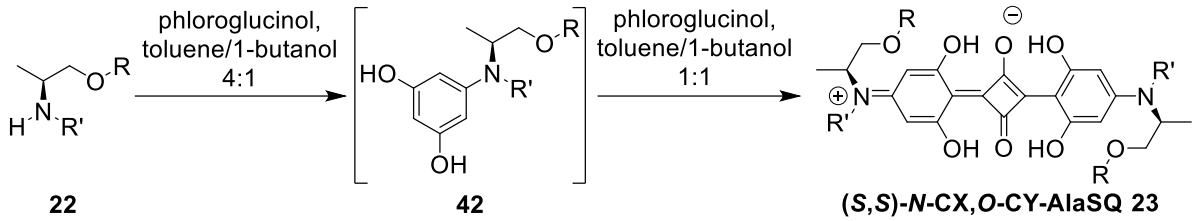

22 **42** **(*S*,*S*)-*N*-CX,*O*-CY-AlaSQ 23**

entry	substrate	R	R'	reaction time [h]	product	yield [%]
1#	**22a**	ethyl	ethyl	19 h+23 h	***N*-C2,*O*-C2-AlaSQ 23a**	20
2*	**22b**	propyl	propyl	5 d + 24 h	***N*-C3,*O*-C3-AlaSQ 23b**	23
3*	**22c**	butyl	butyl	5 d + 24 h	***N*-C4,*O*-C4-AlaSQ 23c**	5
4#	**22d**	pentyl	pentyl	18 h	***N*-C5,*O*-C5-AlaSQ 23d**	0.1
5#	**22e**	heptyl	heptyl	22 h + 22 h	***N*-C7,*O*-C7-AlaSQ 23e**	0.8
6#	**22f**	octyl	octyl	21 h + 22 h	***N*-C8,*O*-C8-AlaSQ 23f**	1
7#	**22g**	nonyl	nonyl	24 h + 24 h	***N*-C9,*O*-C9-AlaSQ 23g**	3
8#	**22h**	butyl	nonyl	24 h + 24 h	***N*-C9,*O*-C4-AlaSQ 23h**	9
9#	**22i**	heptyl	propyl	24 h + 24 h	***N*-C3,*O*-C7-AlaSQ 23i**	4
10#	**22j**	nonyl	propyl	18 h + 22 h	***N*-C3,*O*-C9-AlaSQ 23j**	0.8
11#	**22k**	nonyl	butyl	19 h + 23 h	***N*-C4,*O*-C9-AlaSQ 23k**	1

Removal of solvents after first interval and addition of fresh solvent in a ratio of 1/1 toluene/1-butanol; *Intermediate purification via flash column chromatography

Syntheses on smaller scale significantly suffered from losses of intermediate **42** upon exposure to air during the chromatography. Therefore, it proved to be better to use the secondary amines **22** in excess (1.25 - 1.50 eq.), reduce the reaction time of the first condensation to 16-24 h before removing the 4/1 solvent mixture of toluene and 1-butanol quickly and exchanging it for a 1/1 mixture of toluene and 1-butanol upon addition of squaric acid without isolating the intermediate aniline **42** (see General Procedure B for the Synthesis of **AlaSQ** in the Experimental Part). This gave the desired products **23** in varying yields depending on both scale and substitution of the alaninyl chain (Table 15 Entry 1 & 4-11).

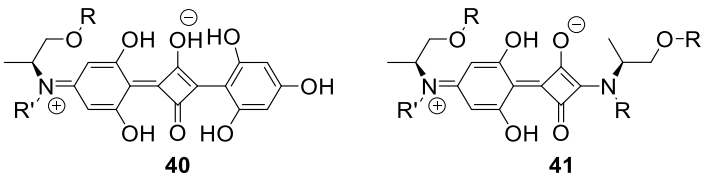

40 **41**

intense dark blue yellow

***Scheme 45**: General structures of asymmetric condensation byproducts **40** and **41** found during the two-step one-pot condensation approach*

The products obtained via following the General Procedure A were significantly easier to purify as the amounts of possible side products (Scheme 45) were considerably reduced due to the isolation of intermediate of aniline **42** and the removal of remaining phloroglucinol and secondary amine **22** via flash chromatography. The major advantage of General Procedure B, however, is the improved applicability for small scale reactions originating from the generally increased concentration during the reaction. Additionally, the impact of diminishing the possible degradation of the intermediate product **42** by largely avoiding its exposition to air was also found to be crucial to achieve a successful formation of the corresponding **AlaSQ**s.

Further purification of the obtained **AlaSQ**s involved a two-fold recrystallization/precipitation first from mixtures of methanol/dichloromethane (between 9:1 and 5:1 v/v depending on the solubility of the respective squaraine). The solids obtained thereof were subjected to a second recrystallization/precipitation from mixtures of cyclohexane/dichloromethane (between 9:1 and 5:1 v/v depending on the solubility of the respective squaraine). Unfortunately, the majority of these processes did not result in high quality single crystalline materials but the respective **AlaSQ**s **23** were received as amorphous solids. Exceptions were **(*S*,*S*)-*N*-C3,*O*-C3-** (**23b**) and **(*S*,*S*)-*N*-C4,*O*-C4-AlaSQ** (**23c**) both carrying rather short alkyl chains which could by investigated by XRD analysis. For the even shorter representative **(*S*,*S*)-*N*-C2,*O*-C2-AlaSQ** (**23a**) the initially obtained crystals were overgrown and have been regrown. Crystals of **(*S*,*S*)-*N*-C2,*O*-C2-AlaSQ** (**23a**) were summitted for XRD measurements, the results are still pending.

5.3 Crystallographic Data of AlaSQs

Single crystals of **(*S*,*S*)-*N*-C3,*O*-C3-AlaSQ** (**23b**) and **(*S*,*S*)-*N*-C4,*O*-C4-AlaSQ** (**23c**) suitable for single crystal structure analysis via X-ray diffraction were directly obtained from the above-mentioned purification process. Single crystals of **23b** and **23c** were analyzed using either a STOE STADIVARI diffractometer measuring at 100 K employing Cu-Kα radiation (λ= 1.54186 Å) or a Bruker D8 Venture diffractometer measuring at 104 K employing Mo-Kα radiation (λ= 0.71073 Å), respectively. The structures were solved with SHELXL-2019/1 and then refined with the SHELXL 2018/3.[160] The single crystal structure data were analyzed with VESTA 3.5.7[161]and are visualized with Mercury 4.2.0.[162]

Figures 30 and 31 show the molecular structures of the two **AlaSQ**s **23b** and **23c**, respectively, alongside the unit cell parameter. The selected crystallographic data are listed in Table 16.

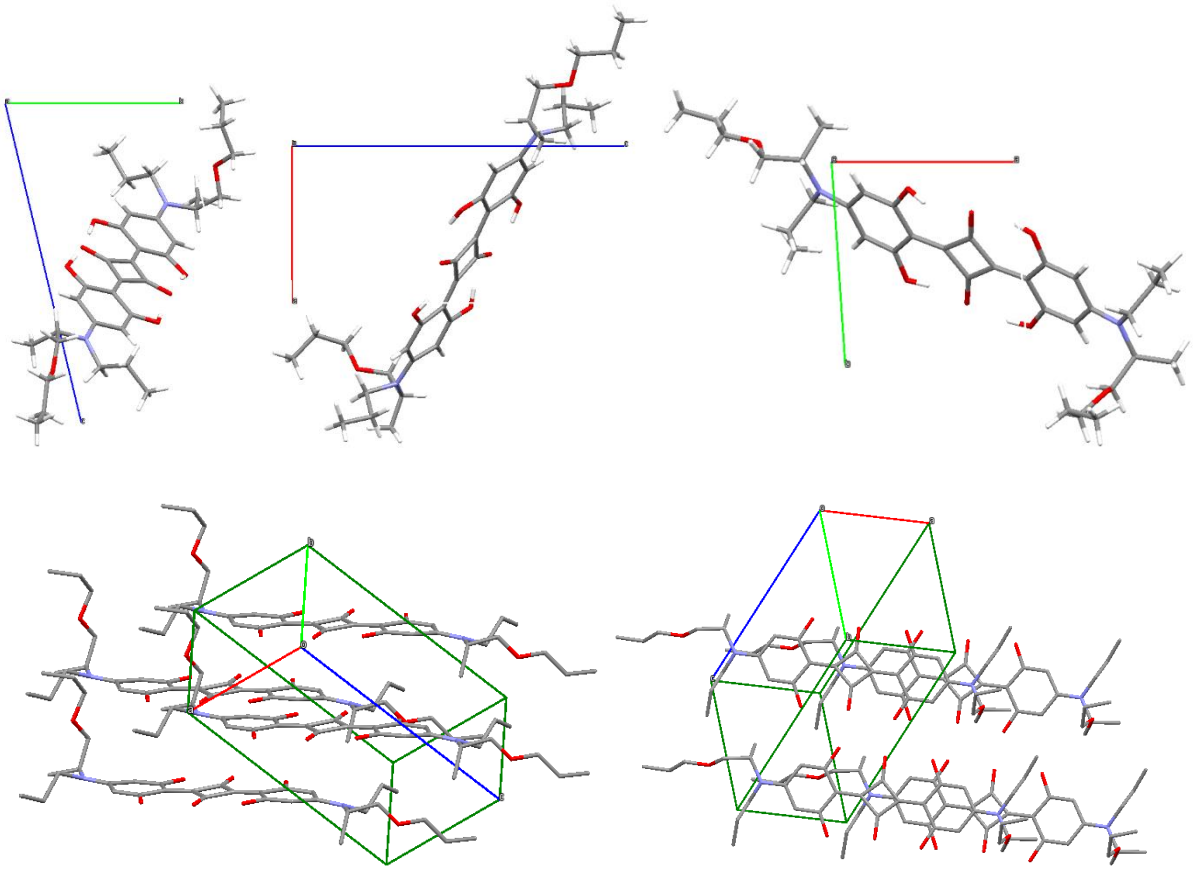

***Figure 30**: Visualization of the molecular structure of **(S,S)-N-C3,O-C3-AlaSQ** (**23b**) in its triclinic unit cell as individual molecule viewing along the unit cell axis a (top left), b (top middle) and c (,top right), respectively. Visualization of the molecular packing (hydrogen atoms are omitted for clarity) highlighting the herring bone structure (bottom left) and the intermolecular π-stacking (bottom right) (color code: blue: c-axis, nitrogen atoms, dark green: expansion of the unit cell, green: b-axis, grey: carbon atoms, red: a-axis, oxygen atoms, white: hydrogen atoms).*

In both molecules the typical herringbone structure is well defined and the intermolecular π-stacking contributes to the overarching order indicating the preferential relative arrangement of the molecules towards each other.

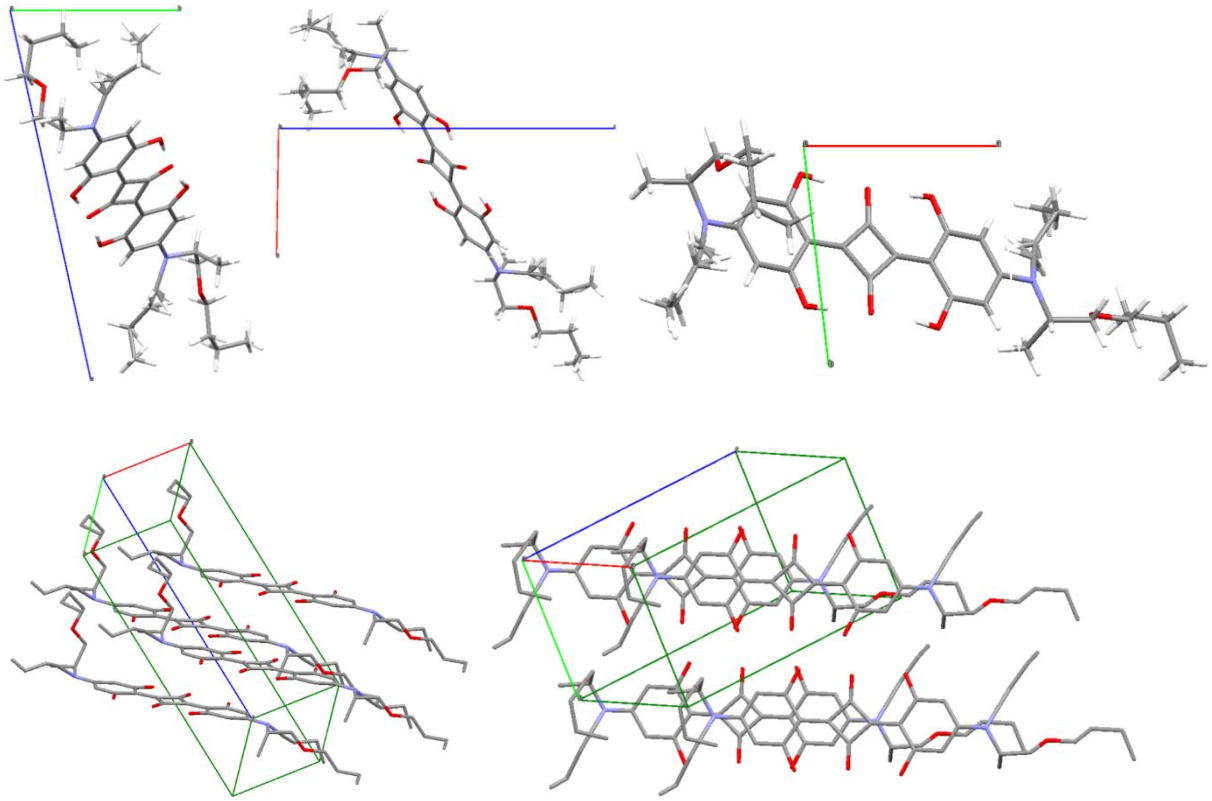

***Figure 31**: Visualization of (S,S)-N-C4,O-C4-AlaSQ (**23c**) in its triclinic unit cell as individual molecule viewing along the unit cell axis a (top left), b (top middle) and c (top right), respectively. Visualization of the molecular packing (hydrogen atoms are omitted for clarity) highlighting the herring bone structure (bottom left) and the intermolecular π-stacking (bottom right) (color code: blue: b-axis, nitrogen atoms, dark green: expansion of the unit cell, green: c-axis, grey: carbon atoms, red: a-axis, oxygen atoms, white: hydrogen atoms).*

***Table 16**: Crystallographic data determined by XRD analysis of single crystals of **(S,S)-N-C3,O-C3-AlaSQ** (**23b**)and **(S,S)-N-C4,O-C4-AlaSQ** (**23c**).*

parameter	***(S,S)-N*-C3,*O*-C3-AlaSQ (23b)**	***(S,S)-N*-C4,*O*-C4-AlaSQ (23c)**
T (K)	100	104
a (Å)	6.9085(7)	6.6722(4)
b (Å)	7.9615(9)	7.8649(5)
c (Å)	14.9878(18)	17.7046(12)
α (deg)	76.545(9)	77.728(2)
β (deg)	88.888(9)	89.535(2)
γ (deg)	85.988(9)	83.543(2)
crystal system	triclinic	triclinic
space group	P1	P1
Z	1	1
crystal habitus	clear bluish green plank	metallic dark green plank

5.4 UV-Vis Spectroscopic Characterization of New Squaraines in Solution

5.4.1 Behavior of the Asymmetric OH Bearing Anilino Squaraine (*S*)-40a in Solution

Sample preparation

For the UV-Vis measurements of solutions of (*S*)-**40a** a stock solution in chloroform was prepared. The compound was weighted in as a solid (2.56 mg) and then diluted with chloroform resulting in a concentration of $c_{stock\ solution}$ = 2.31 x 10^{-4} M. The sample for each measurement was prepared using 50 µL of stock solution with 2950 µL of the desired solvent. The obtained sample resulted in a final concentration of c_{sample} = 3.84 -3.85 µM which was then measured using a Specord 200 spectrometer (Analytic Jena) using 10 mm glass cuvettes (Hellma) and a parallel recording of a spectrum of the pure solvent as a baseline correction.

Data and Results

First, the absorption properties of **40a** were investigated in various solvents (Figure 32).

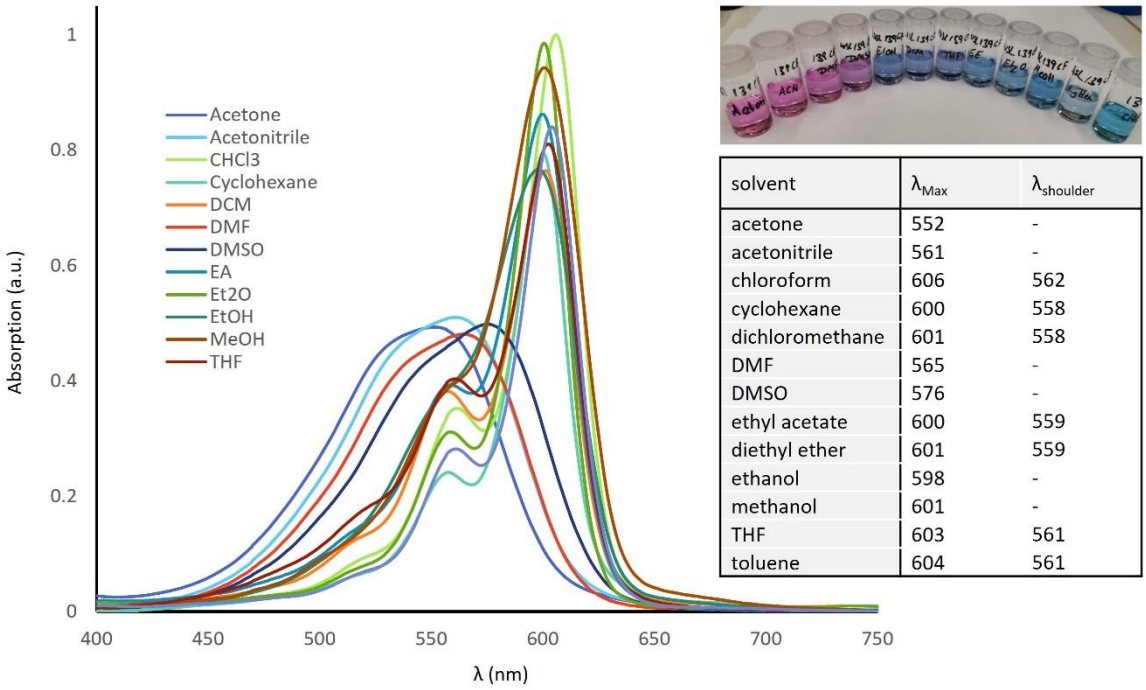

solvent	λ_{Max}	$\lambda_{shoulder}$
acetone	552	-
acetonitrile	561	-
chloroform	606	562
cyclohexane	600	558
dichloromethane	601	558
DMF	565	-
DMSO	576	-
ethyl acetate	600	559
diethyl ether	601	559
ethanol	598	-
methanol	601	-
THF	603	561
toluene	604	561

***Figure 32**: Top right: Photographs of solutions of **40a** in different solvents. Left: UV-Vis spectra of these samples.*

Already with the naked eye it becomes apparent how differently the compound behaves in the respective solvents. The majority of the samples show a sharp absorption maximum in the region around 600 nm (see Table in Figure 32) featuring a second maximum as shoulder near 560 nm. This is most likely the typical vibronic progression which is attributed to the electronic S0→S1 transition along the molecular axis of the squaraine backbone.[134] In general, the absorption region is blue shifted compared to the symmetric ***N*-alkyl-SQ**s and **ProSQ**s, demonstrating the notable influence of the additional free hydroxyl group in place of the respective secondary amine. The second group of solutions in either acetone, acetonitrile, DMF or DMSO features a broad absorption region with its maximum between 552 nm for acetone and 576m for DMSO. These also exhibit a less-well pronounced) shoulder close to the absorption maximum. The notable blue-shift of the absorption

regions in acetone, acetonitrile, DMF and DMSO reminds of the blue shift observed for the formation of aggregates seen in the previous investigations with **ProSQ**s.[31,32]

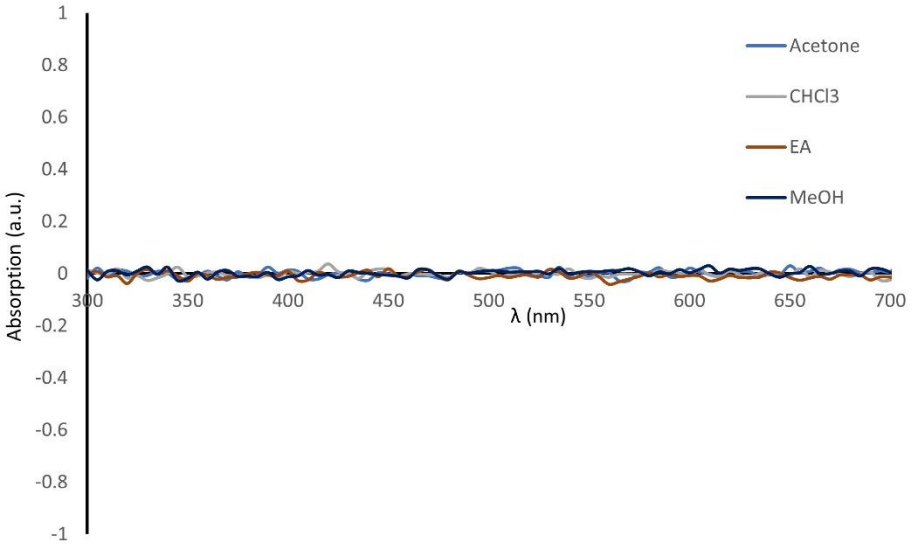

***Figure 33**: CD-spectra of solutions of (S)-**40a** in selected solvents.*

The shift of the absorption of the samples in the latter four solvents seemed too large to just be a result of solvatochromism, and hence, it was hoped that these are caused by the formation of structurally defined aggregates. Due to the chirality of **40a** such aggregates might cause significant CD-effects which is why CD-spectra of the samples in acetone, chloroform, ethyl acetate and methanol as examples for the different kind of solvents were recorded next. Unfortunately, however, none of the samples showed any CD effect suggesting the absence of well-defined chiral aggregates (Figure 33).

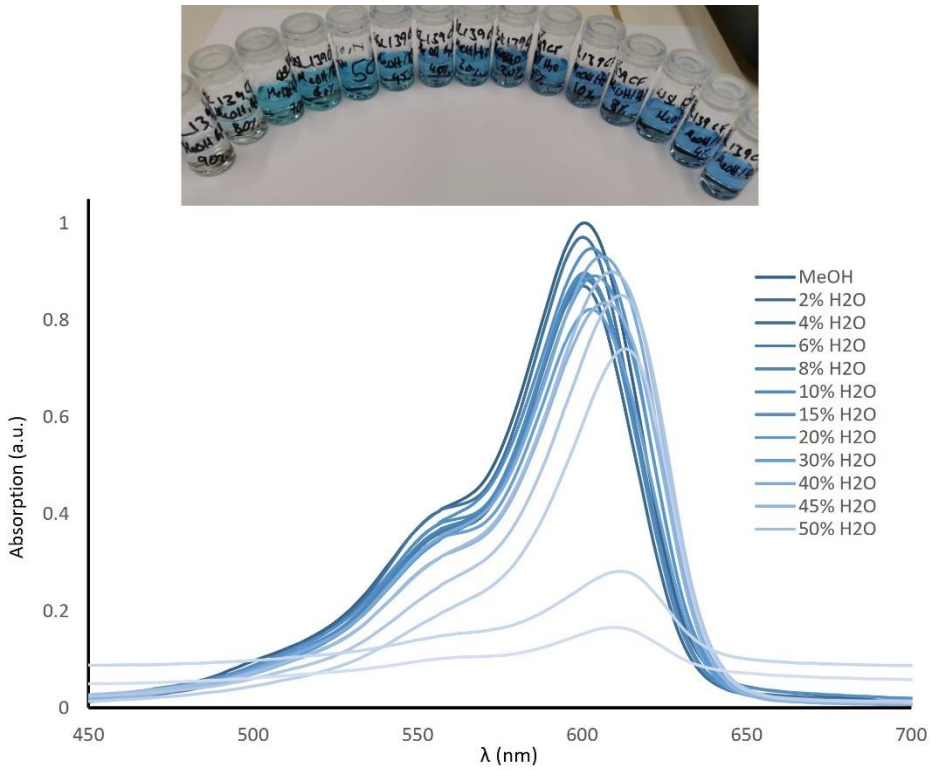

***Figure 34**: UV-Vis spectra of solutions of **40a** in mixtures of methanol and water.*

Another approach to induce aggregation is to perform so-called poor solvent titration where samples containing varying amounts of a bad solvent for the solute are prepared and investigated. Therefore,

mixtures of methanol/water were tested first in this respect (Figure 34). With increasing amount of water, the intensity of the absorption decreased until a content of 80% of water and 20 % of methanol. At this point, apparently the miscibility threshold of the chloroform stock solution with the 2:8 mixture of methanol/water is reached leading to a phase separation, and hence, an abrupt drop in the overall absorption. Unfortunately, again no significant changes in the absorption spectra were observed when increasing the water content as the gradual shift of the absorption maximum from 601 nm in pure methanol to 613 nm in 70% water seems to be a consequence of the change of solvation. Thus, it can be concluded that the asymmetric squaraine **40a** can tolerated high amounts of water and is still soluable and does not aggregate in these mixtures. This implies a significantly higher hydrophilicity compared to the ***N*-alkylSQ**s and **ProSQ**s, most likely originating from the remaining and additional free hydroxy group.

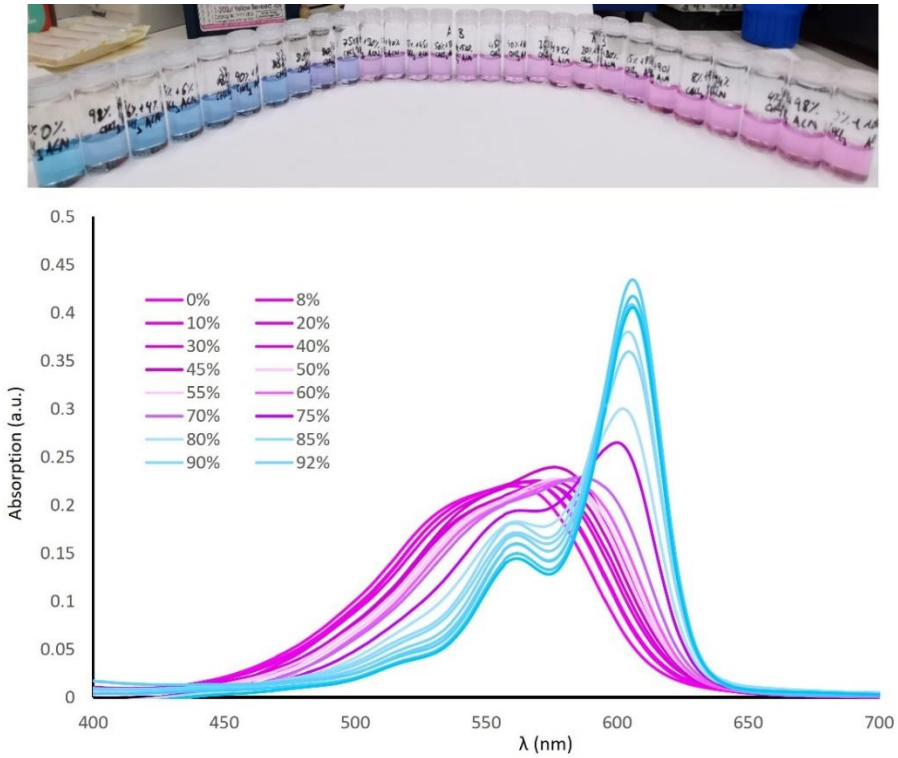

***Figure 35**: UV-Vis spectra of solutions of **40a** in mixtures of acetonitrile and chloroform with the percentages of chloroform.*

Thus, mixtures of acetonitrile and chloroform were tested next (Figure 35) as the absorption behavior in acetonitrile hinted at aggregation occurring in this solvent. However, again no striking changes could be observed but rather a smooth transition from acetonitrile-dominated absorption behavior towards a chloroform-dominated one occurred upon gradually increasing the amount of chloroform with a threshold of ca. 70% chloroform content where the absorption essentially resembles that of samples in pure chloroform. CD spectra which were also recorded of these samples again showed no signals of meaningful intensity which leads to the conclusion that no defined (chiral) aggregates form in these solvent mixtures. A possible explanation might be that the single stereogenic center has only limited influence on the molecules ability to form well-defined aggregates.

Therefore, higher hopes were set in the **AlaSQ**s bearing two stereogenic centers and especially those furnished with longer alkyl chains on the oxygen and/or nitrogen atoms similar to the observations made when investigating the **ProSQ**s.

5.4.2 AlaSQs in Solution

Out of the 11 **AlaSQ**s which could be synthesized during the course of this study the following 9 were explored with regard to their absorption behavior in solution – **(*S*,*S*)-*N*-C2,*O*-C2-AlaSQ**, **(*S*,*S*)-*N*-C3,*O*-C7-AlaSQ**, **(*S*,*S*)-*N*-C3,*O*-C9-AlaSQ**, **(*S*,*S*)-*N*-C4,*O*-C9-AlaSQ**, **(*S*,*S*)-*N*-C5,*O*-C5-AlaSQ**, (*S*,*S*)-*N*-C7,*O*-C7-AlaSQ**, **(*S*,*S*)-*N*-C8,*O*-C8-AlaSQ**, **(*S*,*S*)-*N*-C9,*O*-C4-AlaSQ** and **(*S*,*S*)-*N*-C9,*O*-C9-AlaSQ**. The majority of these UV-Vis experiments including the poor solvent titrations were performed with the help of *F. Azarnousha* from our group.

For the UV-Vis measurements stock solutions of the respective **AlaSQ**s in chloroform were prepared. Therefore, the compounds were weighed in as solids and then diluted with chloroform aiming for a concentration in the range of $c_{stock\ solution}$ = 2.30 – 2.31 x 10^{-4} M. The samples for each measurement were then prepared using 50 µL of the respective stock solution and mixing it with 2950 µL of the desired solvent. Thus, the resulting samples had a final concentration of c_{sample} = 3.84 -3.85 µM. The UV-Vis spectra of these samples were then recorded employing a Specord 200 spectrometer (Analytic Jena) using 10 mm glass cuvettes (Hellma) and a parallel recording of a spectrum of the pure solvent as a baseline correction.

Data and results

Characterization of the absorption behavior of the newly obtained **AlaSQ**s via UV-Vis and in some cases also CD spectroscopy started with exploring the absorption in in various solution (see Appendix), exemplarily shown for **(*S*,*S*)-*N*-C4,*O*-C4-AlaSQ 23c**, **(*S*,*S*)-*N*-C9,*O*-C9-AlaSQ 23g**, **(*S*,*S*)-*N*-C9,*O*-C4-AlaSQ 23h** and **(*S*,*S*)-*N*-C4,*O*-C9-AlaSQ 23k** in Figure 36.

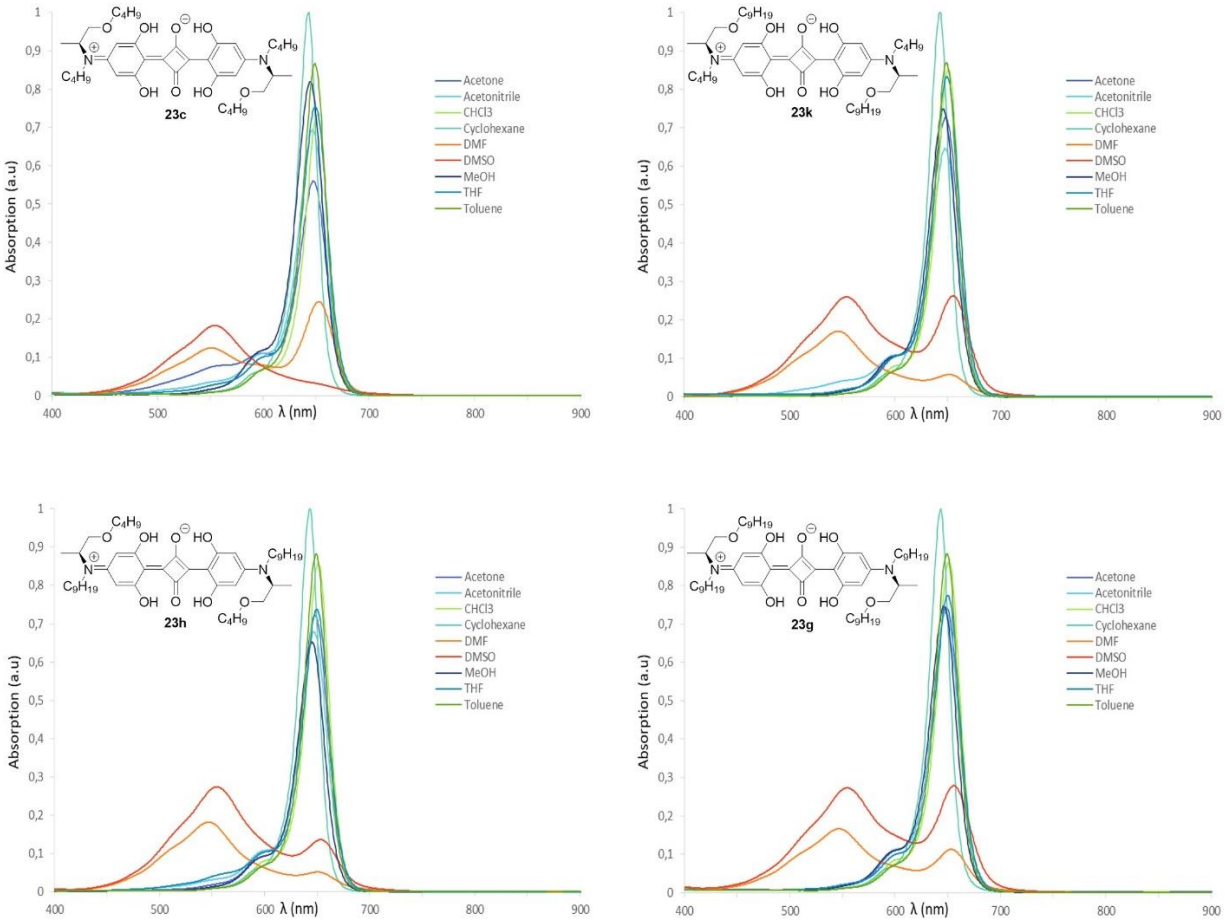

***Figure 36**: Normalized UV-Vis absorption spectra of **23c** (top left), **23k** (top right), **23h** (bottom left) and **23g** (bottom right) in various solvents.*

***Table17**: Absorption maxima (given in nm) of **AlaSQ**s in various solvents.*

AlaSQ	acetone	aceto-nitrile	chloro-form	cyclo-hexane	DMF	DMSO	MeOH	THF	toluene
23a	645	644	648	640	546	553	641	647	647
23b	646	646	650	642	546	554	643	648	648
23c	647	647	651	643	653	554	644	649	649
23d	648	647	651	643	546	554	645	649	649
23e	648	648	651	643	547	555	645	650	649
23f	649	648	651	643	546	554	646	650	649
23g	649	648	651	643	547	656	646	650	649
23h	648	647	651	643	547	555	645	650	649
23i	647	646	650	642	545	554	644	648	648
23j	647	647	650	642	546	554	645	649	648
23k	648	648	651	643	546	655	646	649	649

The most intense absorption for all investigated **AlaSQ**s is found for cyclohexane solutions around 640-643 nm (Figure 36 and Table 17). In general, **AlaSQ**s were found to show sharp absorption maxima in the range of 640 nm - 651 nm in acetone, acetonitrile, chloroform, cyclohexane, methanol, tetrahydrofuran and toluene. Furthermore, a vibronic progression around 590 nm is observed, which originates from the electronic S0→S1 transition along the molecular axis of the squaraine backbone.[134] Additionally, the absorption maxima shift to slightly higher wavelengths with increasing length of the alkyl chain with in the series of symmetric uniformly substituted **AlaSQ 23a**-**23g**, whereas the influence of the position of the longer chain in derivatives with different alkyl chains on the nitrogen and oxygen atoms does not seem to have a major influence, as can be seen in the butyl and nonyl substituted derivatives **(*S*,*S*)-*N*-C9,*O*-C4-AlaSQ 23h** and **(*S*,*S*)-*N*-C4,*O*-C9-AlaSQ 23k** which both show rather similar absorption spectra.

In case of DMF and DMSO, however, a drastic difference is observed as a double hump signature is observed which is similar to the one characteristic for ***N*-alkyl-SQs** in certain solvents. Similarly, the most intense absorption maxima are significantly blue-shifted and broadened, locating them around 545 nm for DMF and 554 nm for DMSO, respectively (Table 17). The reasons for this cannot be elucidated on the base of these data alone but would pose a formidable challenge for future studies including transient spectroscopy and/or sophisticated theoretical modelling.[131,135,137] Also, solvatochromic effects caused by solute-solvent interactions resulting in these hypsochromic shifts cannot be ruled out at this stage.[163,164] In this particular case the decisive characteristic of the solvent is not the absolute polarity of the solvent, as the observed trend of the absorption maxima does neither follow the ordering of the solvents according to their solvent dipolarity (Catalán SdP)[165] nor their Reichardt's ET(30) values[122,163,164] nor their hydrogen bond acceptor ability (β value)[121,123] (Table 18). Instead, it appears to depend on the interplay of these factors in dependence on the particular substitution pattern of the **AlaSQ**. In case of DMF and DMSO the most influential parameter for the observed absorption behavior seem to be the hydrogen bond accepting ability β of the Kamlet-Taft polarity parameter[121,122] and the solvent dipolarity according to Catalán[165]. This can result in the drastically blue-shift of the absorption band as these solvents stabilize the ground state via hydrogen bonding between the hydroxyl-function of the squaraine core, while acting as an H-bond acceptor. This stabilizing effect, albeit in a weaker amount, could also apply for the less pronounced H-bond acceptors acetone, THF and methanol also observed as the tailing of the otherwise sharp absorption band into the region of 500-600 nm is observed, which significantly exceeds the usually observed vibronic progression.

***Table 18**: Overview of selected polarity parameters for the solvents used during the UV-Vis measurements.*

solvent	α	β	π*	Reichardt's ET(30)	(SB)	(SP)	(SdP)	δ
acetone	0.08	0.43	0.71	42.2	0.475	0.651	0.907	19.7
acetonitrile	0.19	0.40	0.75	45.6	0.286	0.645	0.974	24.2
cyclohexane	0.00	0.00	0.00	30.9	0.073	0.683	0.000	16.8
chloroform	0.20	0.10	0.82	39.1	0.071	0.783	0.614	18.9
DMF	0.00	0.69	0.88	43.2	0.613	0.759	0.997	24.0
DMSO	000	0.76	1.00	45.1	0.647	0.830	1.000	26.6
methanol	0.98	0.66	0.60	55.4	0.545	0.608	0.904	29.3
THF	0.00	0.55	0.58	37.4	0.591	0.714	0.634	19.0
toluene	0.00	0.11	0.54	33.9	0.128	0.782	0.284	18.2
water	1.17	0.47	1.09	63.1	0.025	0.681	0.997	47.9

Kamlet-Taft polarity parameter (α, β, π*) where α is the hydrogen bond donating ability, β is for hydrogen bond accepting ability and π* for dipolarity/polarizability.[121] Reichardt's ET(30) refers to the empirical polarity scales established by Reichhardt with Reichhardt's betaine B30 as the reference.[163,164] the Catalán SdP (solvent dipolarity),[165] SP (solvent polarizability), SB (solvent basicity).[165] Values from Ref.[121–123]

Further overarching similarities are seen in the relative shift of absorption maxima depending on the solvent. Excluding the outliers DMF and DMSO, the solvent in which the measured **AlaSQ**s absorbed at the lowest wavelength was cyclohexane, and the solvent for the highest wavelength was chloroform. With cyclohexane as a non-polar, non-hydrogen bond acceptor and (non-hydrogen bond donor solvent it can in this context be considered to be the most innocent solvent as the remaining solvents interact with the solute more closely. Hence, the interaction with solvents like acetone, acetonitrile, chloroform, methanol, THF and toluene lead to a small red-shift in comparison. This suggests a stabilization of the excited states. For toluene this could be the provided by the introduction of π- π-interaction between the squaraine core and the aromatic solvent.

***Table 19**: Wavelength of the secondary absorption peak observed in DMF and DMSO.*

entry	**AlaSQ**	2nd absorption maximum in DMF	2nd absorption maximum in DMSO
1	**23e**	646	650
2	**23f**	650	652
3	**23g**	653	555
4	**23h**	650	653
5	**23k**	652	554

Interestingly, the larger representatives **23e**-**23g** of the uniformly substituted **AlaSQ**s and **23h** and **23k** of the mixed substituted ones exhibit an additional secondary absorption peak in the UV-Vis spectra recorded in DMSO and DMF as already mentioned above (Figure 19). However, further sophisticated experimental and theoretical studies are needed to elucidate the origin of these bands that go beyond the scope of this thesis.

5.4.3 Poor-Solvent Titration Experiments

Following the tested and proven approach of inducing aggregation by increasing the amount of a poor solvent a solvent mixture of a poor solvent with an even worse solvent was needed, as the solubility of the **AlaSQ**s in most solvents proved to much higher than that of the corresponding **ProSQ**s which carry only a single alkyl chain on each terminus. This is also true for acetonitrile in which **AlaSQ** obviously do not aggregate but the corresponding **ProSQ**s do.[62] This rules out the use of an acetonitrile/chloroform system which proved to be suitable to study aggregation of **ProSQ**s with longer chain lengths in such a poor solvent titration experiment. Instead a methanol/water system was chosen similar to the experiments with **ProSQ**s bearing intermediate alkyl chain lengths.[135]

For the Poor-solvent titration experiments the same stock solutions of the respective **AlaSQ** in chloroform ($c_{stock\ solution}$ = 2.30 – 2.31 x 10^{-4} M) as for the UV-Vis measurements in various solvents were used. Hence, also the targeted final concentrations of the samples c_{sample} = 3.84 -3.85 µM were the same. The sample for each measurement was prepared using 50 µL of stock solution and mixing it with 2950 µL of the desired solvent mixture. The obtained samples were then measured using a Specord 200 spectrometer (Analytic Jena) employing 10 mm glass cuvettes (Hellma) and a preceding measurement of the pure solvent as a baseline correction.

Data and Results

After having studied the absorption behavior in different solvents the next task was to examine the early stage aggregation behavior in solution using the established **ProSQ**s[62,132–135] as benchmark for comparison. Figure 37 shows exemplarily the spectra recorded from **AlaSQ**s **23c**, **23g**, **23h** and **23k**.

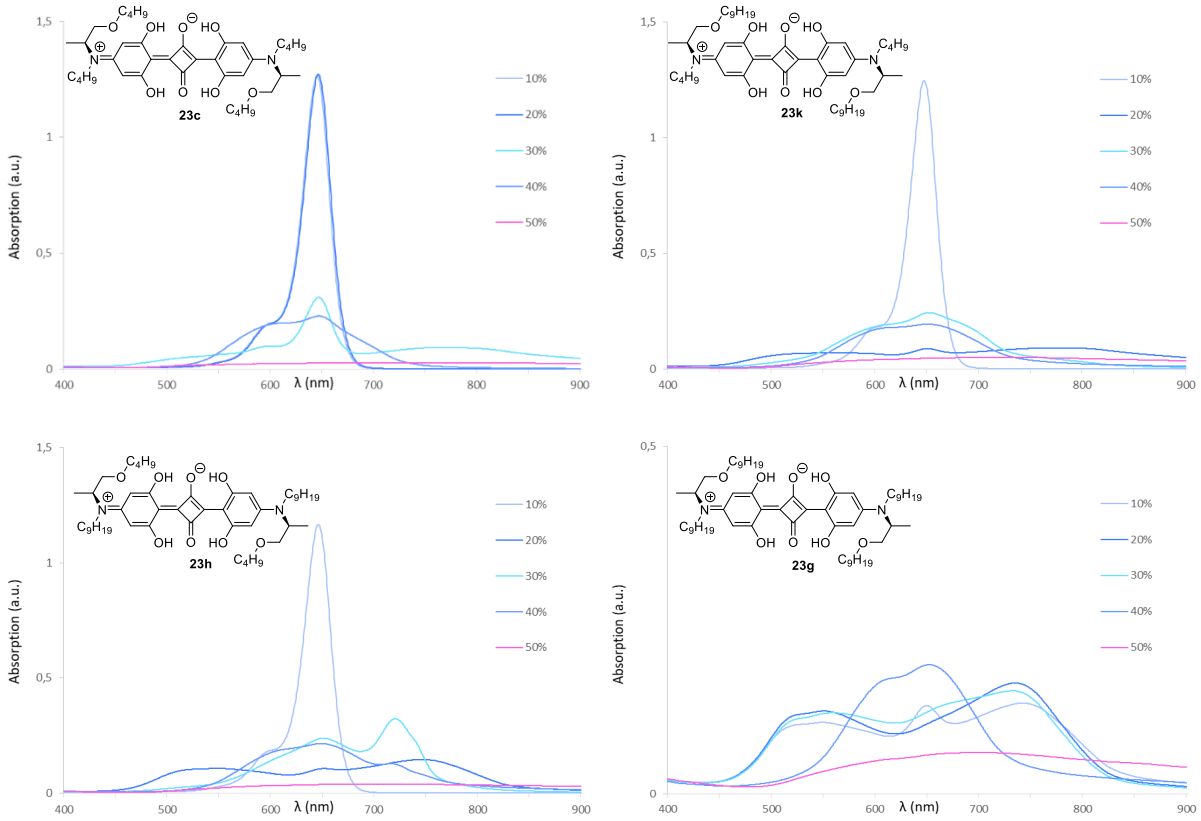

***Figure 37**: Normalized UV-Vis absorption spectra of **23c** (top left), **23k** (top right), **23h** (bottom left) and **23g** (bottom right) in methanol/water mixtures with increasing water percentage.*

Qualitatively, it is apparent, that the addition of increasing amounts of water causes the formation of a colloidal solution. This can be seen in the taking shape of both a red-shifted and a blue-shifted absorbance band with respect to the monomeric band alongside the broadening of the absorption bands from a sharp well-defined peak of the presumably monomeric state into two regions, as similarly observed for the ***N*-alkyl-SQ**s and the **ProSQ**s.[134,135] The hypsochromically shifted band can usually be interpreted as a result of the formation of so-called H-aggregates. [166,167]The bathochromically shifted band, however, is less easy as these could result either from J-aggregates[166–168] which form as an independent second type of aggregate, from structural disorder of a single type of aggregate which contains H- and J-type like relative orientation of the individual chromophores, or additional CT-states which might occur.[39,48,131,135,169–173] This, however asks for additional sophisticated experimental and theoretically studies which go beyond the scope of this thesis. In this respect, also CD spectroscopy might offer additional insight as the occurrence of CD effects of significant intensity clearly indicate order as it results from a transfer of the chiral information from a molecular to a supramolecular and therefore detectable level.[129,173–176] Also, the sign of potential Cotton effects can give insight in the nature and number of aggregates present in the solutions.[131,135,137,173,174] Hence, also these measurements should be addressed in future studies of the **AlaSQ**s which need to be accompanied by corresponding theoretical studies.

Nevertheless, some qualitative conclusions can be drawn from these poor solvent titrations. Most notable is the obvious and expected significant decrease of absorption intensity upon addition of the poor solvent.[[135]] For the **AlaSQ** bearing the longest alkyl chains **23f** and **23g** the addition of 10% water proved already sufficient to induce aggregation. **23a** and **23b** bearing the short ethyl or propyl chains, however, tolerate higher water contents even exceeding the highest tested one of 50% (see Appendix). This was kind of expected as the shorter alkyl chains overall also translate into significantly more polar compounds compared to **23f** and **23g**. However, already with butyl chains like in **23c** signs of aggregation can be observed in the examined range of water content.

Interestingly and counterintuitively, in case of **23f**-**23h** and **23k** a rise in absorption is observed upon further water addition from 20% to 30% and 30% to 40%, respectively. This is accompanied by another shift of the absorption maxima, suggesting the formation of a more complex aggregation behavior compared to the idealized border cases of H- and J-aggregates, which requires further investigation.

5.5 FURTHER INSIGHTS IN THE BEHAVIOR OF (*S*,*S*)-*N*-C3,*O*-C3-ALA-SQ 23B

As **(*S*,*S*)-*N*-C3,*O*-C3-AlaSQ 23b** could be prepared in considerably large quantities this compound was studied in further detail. This started with studying the absorption behavior in even more solvents to elucidate solvatochromic effects or even aggregation-induced effects (Figure 38).

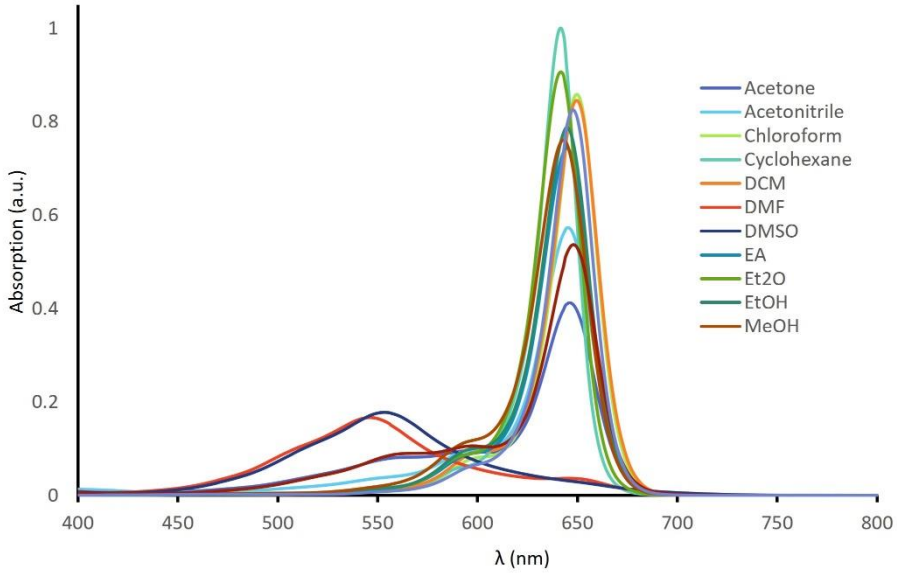

***Figure 38**: UV-Vis absorption spectra of **23b** in different solvents.*

The additional solvents investigated here, were ethyl acetate, diethyl ether and ethanol (Table 20). These solvents were chosen with certain expectation in mind. Ethyl acetate was chosen as a comparison to acetone. It still contains a carbonyl group to act as an H-bond acceptor, but the mesomeric contribution of the ester function combined with the steric demand of the ethyl chain seems to reduce the stabilizing effect compared to acetone. This can be seen in the less pronounced tailing into the range of shorter wavelengths and the more intense absorption in the 650 nm range.

***Table 20**: Overview of selected polarity parameter for the solvents used during the UV-Vis measurements of **AlaSQ 23b**.*

solvent	α	β	π*	Reichardt's ET(30)	(SB)	(SP)	(SdP)	δ
acetone	0.08	0.43	0.71	42.2	0.475	0.651	0.907	19.7
cyclohexane	0.00	0.00	0.00	30.9	0.073	0.683	0.000	16.8
ethyl acetate	0.00	0.45	0.55	38.1	0.542	0.656	0.603	18.4
diethyl ether	0.00	0.47	0.27	34.5	0.562	0.617	0.385	15.4
ethanol	0.98	0.75	0.600	51.9	0.658	0.633	0.783	26.0
methanol	0.98	0.66	0.60	55.4	0.545	0.608	0.904	29.3
THF	0.00	0.55	0.58	37.4	0.591	0.714	0.634	19.0

Kamlet-Taft polarity parameter (α, β, π*) where α is the hydrogen bond donating ability, β is for hydrogen bond accepting ability and π* for dipolarity/polarizability.[121] Reichardt's ET(30) refers to the empirical polarity scales established by Reichhardt with Reichhardt's betaine B30 as the reference.[163] the Catalán SdP (solvent dipolarity), SP (solvent polarizability), SB (solvent basicity).[165] Values from Ref.[121–123]

Diethyl ether was chosen for comparison with THF. Both are molecules of comparable molecular weight and similar functional groups. The main difference here is the 5-membered ring structure of THF compared to the open chain structure seen in diethyl ether. This drastically influences their behavior. The sample in THF shows closer resemblance to the one in acetone, especially with regard to the pronounced tailing into the lower wavelength region, whereas the diethyl ether sample shows

more similarities to the absorption observed in cyclohexane. This difference is probably mostly due to the less directed dipole moment of diethyl ether compared to THF and the additional shielding due to steric demand of the ethyl groups. This demand is less in THF due to the ring structure, which fixates the alkyl groups in one direction, giving a comparable more directed dipole moment.

Last but not least ethanol was chosen as comparison to methanol, diethyl ether and ethyl acetate. Here, the difference between all samples is rather negligible as the absorption maxima all appeared at almost the same wavelengths – λ_{Max}(EtOH) = 645 nm, λ_{Max}(Et_2O) = 642 nm, λ_{Max}(EtOAc) = 645 nm and λ_{Max}(MeOH) = 643 nm.

To investigate whether the transition of the absorption behavior of **23b** in solvent mixtures with drastically different characteristics happen gradually featuring a smooth transition or abruptly, two additional solvent system beyond the already presented methanol/water system were tested. In addition, CD spectroscopic experiments were also performed with the samples of the poor solvent titration experiments (Figures 39 & 40). The first solvent system explored was the DMSO/chloroform mixtures (Figure 39). Here, a drastic change from the DMSO dominated spectra to the absorption behavior typical for chloroform was observed when the content of chloroform exceeded 10%.

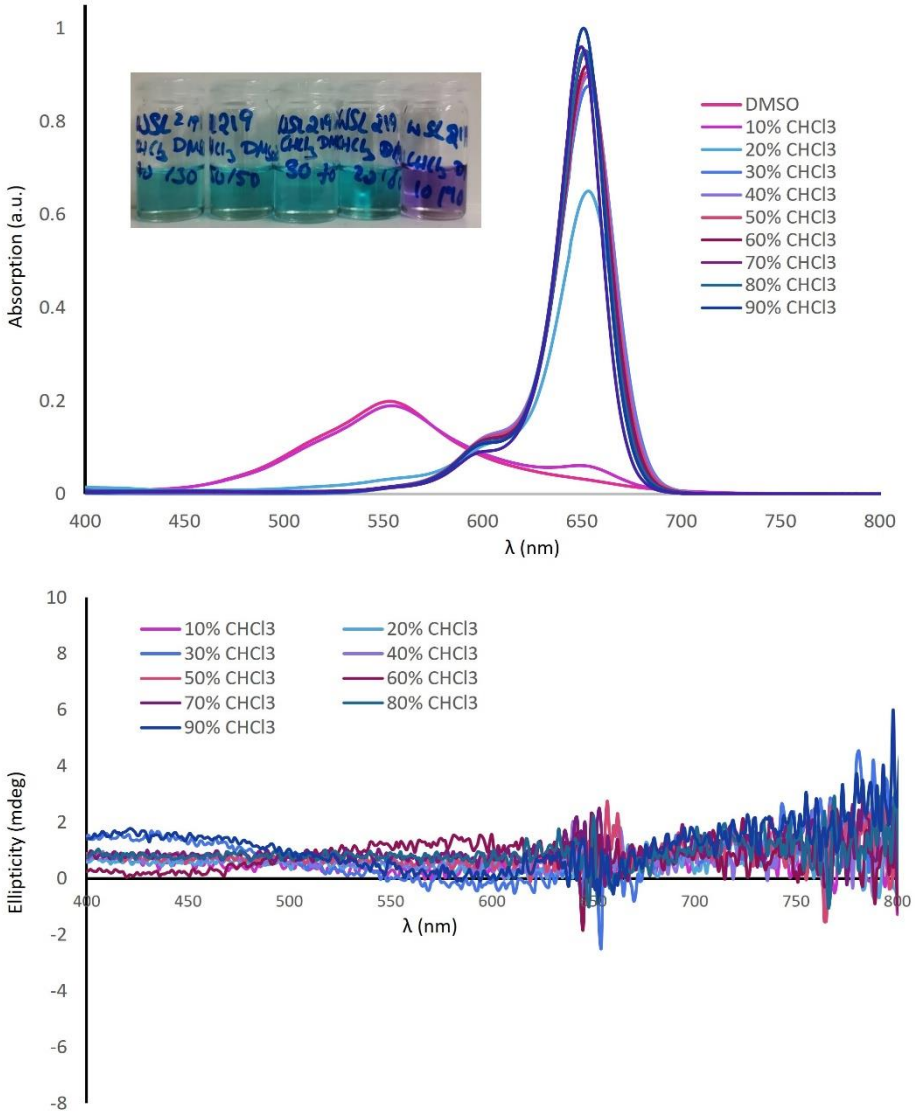

***Figure 39**: Photographs of samples of **(S,S)-23b** in DMSO containing different amounts of chloroform and the UV-Vis absorption spectra as well as CD-spectra of these samples.*

Unfortunately, though aggregation of **AlaSQ 23b** seems to occur, the CD spectra clearly hint that these should not be stereochemically well defined leading to significant CD effects. This statement also holds true for the other explored solvent mixtures of DMSO/water and methanol/water with increasing contents of water (Figure 40) as essentially no CD signals are observed (max. intensity less than 10 mdeg) which is orders of magnitude less than it was observed for the **ProSQ**s (Figure 41).[135]

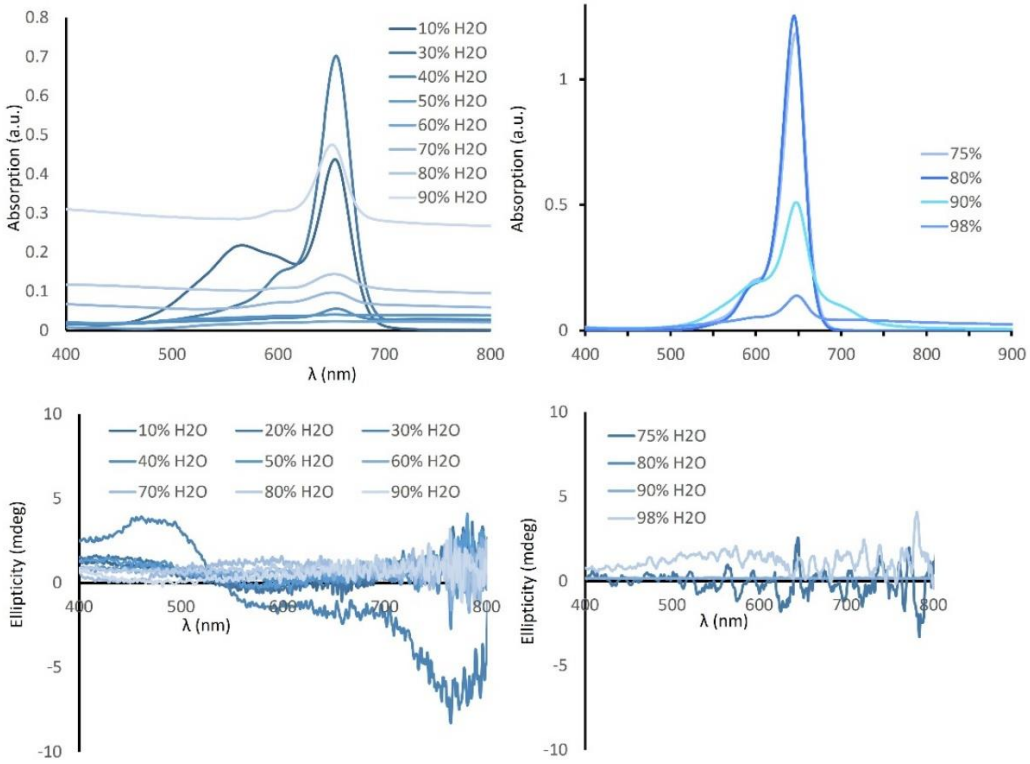

***Figure 40**: UV-Vis absorption and CD spectra of **AlaSQ (S,S)-23b** in mixtures of DMSO and water (left) and methanol and water (right) containing increasing amounts of H_2O.*

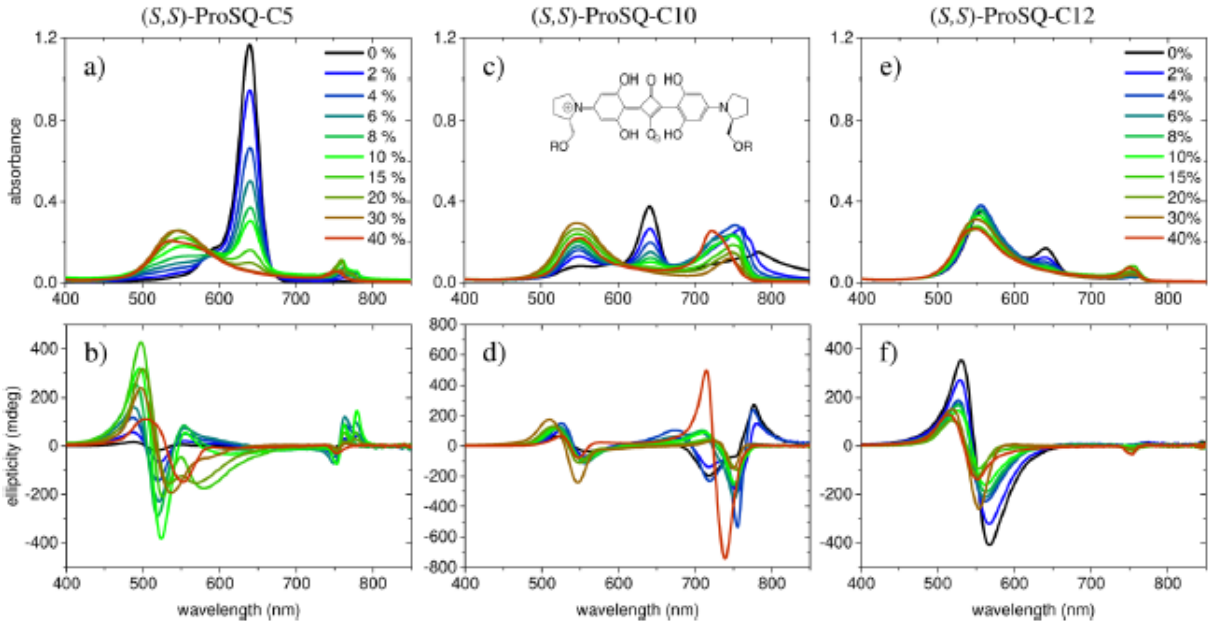

***Figure 41**: UV-Vis absorption (top row) and CD spectra (bottom row) of selected (S,S)-**ProSQ** derivatives with varying alkyl chain length (a & b C5, c & d C10, and e & f C12) in mixtures of methanol and water with increasing content of water. Reprinted with permission from source [135]*

Even though the results of the aggregation behavior of **AlaSQ 23b** in solution were somewhat disappointing in comparison to the ones found for the corresponding **ProSQ**s the experiments in solution are only tests for the ultimately envisioned experiments and potential applications in thin films. Thankfully, it was possible to investigate the properties of **AlaSQ 23c** in solution-processed thin films within the network of the DFG-funded research training group 2591 (TIDE) framework with the help of *O. Erdene-Ochir* from the Meerholz group at the University of Cologne.

Figure 42 shows a first set of solution-processed thin films of **AlaSQ 23b**. To obtain these a stock solution of **23b** was prepared in chloroform (6 mg/mL). This solution was spin casted on float glass (25 x 25 mm^2). After the drop of the **AlaSQ** solution was put on glass substrate it was allowed to dwell for 3 seconds. The spin coating speed was set to 2000 rpm for 60 seconds. The obtained thin-films were post annealed at different set temperatures for 1 h each. Upon post-preparation annealing the look of the sample visually changed.[177] This is most pronounced for the difference between the sample prepared at room temperature and the one which was annealed at 80 °C. Another stark change was observed for the 160°C sample when dewetting seemed to occur. This assumption was corroborated by the respective solid-state UV-Vis absorption experiments.

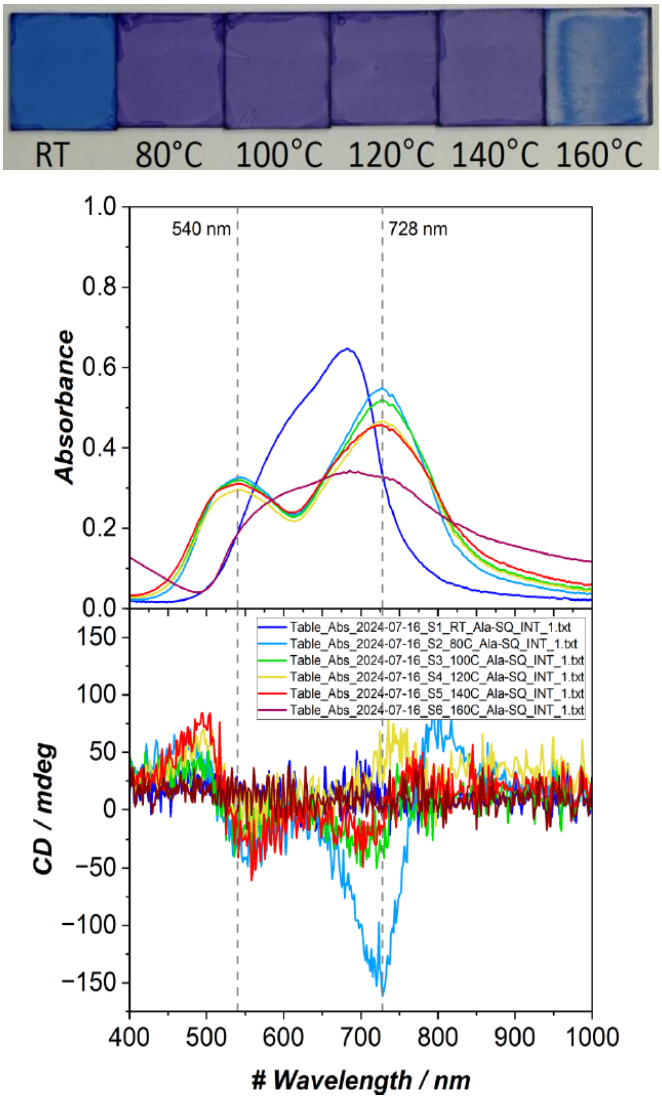

***Figure 42**: Photographs of solution-processed thin films of **AlaSQ (S,S)-23b** after post-preparation thermal annealing at different temperatures (top) and solid-state UV-Vis absorption (middle) and CD spectra (bottom) thereof.*

As can be seen in the spectra depicted in Figure 42 the broad absorbance with a maximum around 670 nm signal of the sample prepared at room temperature develops into two distinct broad humps with the respective absorption maxima of 540 nm for the blue-shifted signal and 728 nm for the red-shifted signal upon annealing at elevated temperatures. This is accompanied by the observed zero crossing seen in the respective CD measurement in close proximity of said wavelengths. This enforces the theory of a complex and intriguing aggregate formation, which cannot be explained by Kasha's theory[166,167,170] with referring to H- and J- aggregates alone.

In the close-up direct comparison between the sample prepared at room temperature with the one annealed at 80 °C, where the red-shifted signal and more importantly the CD signal is most prominent, the change in absorption behavior is most visible and obvious (Figure 43).

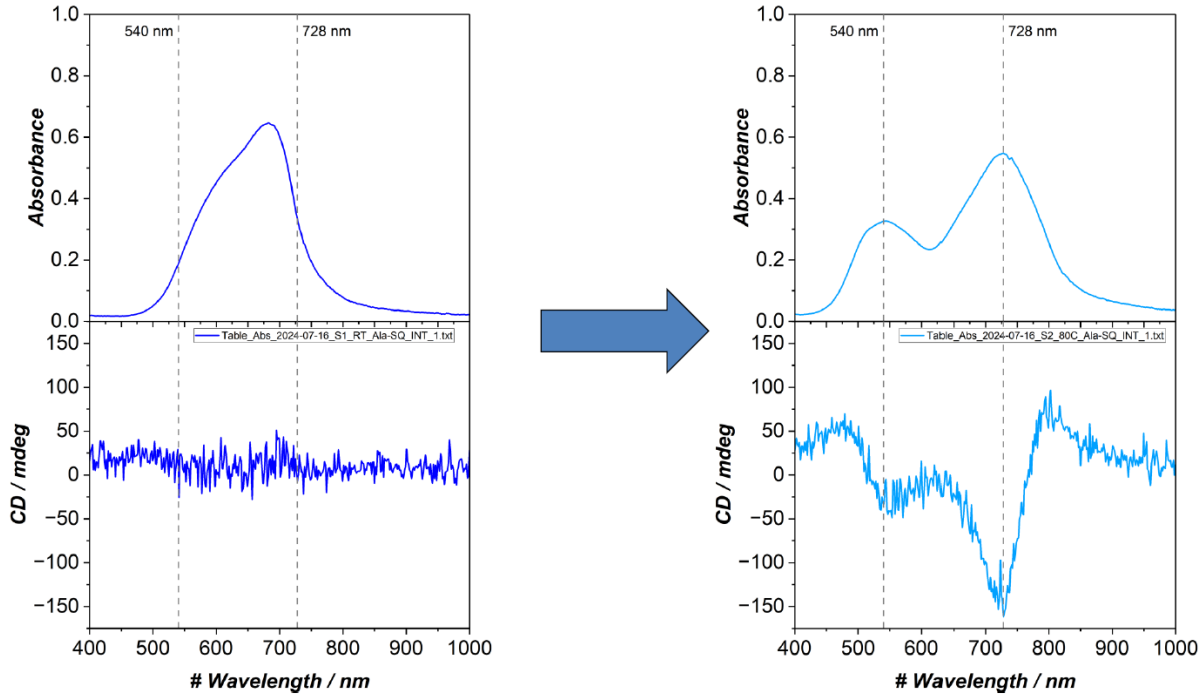

***Figure 43**: Comparison of UV-Vis absorption (top row) and CD spectra (bottom row) of thin film samples of **AlaSQ (S,S)-23b** prepared at room temperature (left) and annealed at 80 °C (right).*

When compared to the giant intrinsic CD observed for thin films of **ProSQ-C16**[134] the values obtained for **AlaSQ 23b** might look small. However, it should be noted that the values for the samples of **ProSQ-C3** bearing similar short alkyl chains were found to be in the same ball park. Hence, these results are very promising and make the synthesis of **AlaSQ**s with longer alkyl chains a worthwhile endeavor to test them also with regard to their chiral aggregation behavior in thin films and their application in optoelectronic devices employing their chiroptical properties.

6 CONCLUSION AND OUTLOOK

The aim of this mainly synthetically oriented thesis was to prepare squaraine dyes and investigate their properties to answer three main questions:

- Can amphiphilic squaraines act as stimuli responsive designer surfactants for an application in micellar or emulsion catalysis?
- Can chiral squaraines be sublimed to form ordered thin films or even crystalline material?
- Can a new class of chiral squaraines be designed and synthesized that combines beneficial structural features of achiral *N*,*N*-dialkyl anilino squaraines with the chiral properties of proline-derived anilino squaraines in order to combine the superb aggregation behavior of the achiral material with the outstanding chiroptical properties of the latter one?

6.1 SQUARIC ACID-BASED DESIGNER SURFACTANT FOR MICELLAR CATALYSIS

In the search for new applications for squaraine dyes the synthesis of amphiphilic derivatives was targeted in collaboration with the group of *Luca Beverina* to apply them in micellar catalysis. Therefore, a new squaraine-based designer surfactant was synthesized whose color proved to be pH sensitive, and hence, inherently stimuli responsive. Albeit the final product's molecular structure differs drastically from the initially designed target structures, the asymmetric amphiphilic squaraine **20** (Scheme 46) was obtained and characterized with regard to their ability to form micelles and emulsions.

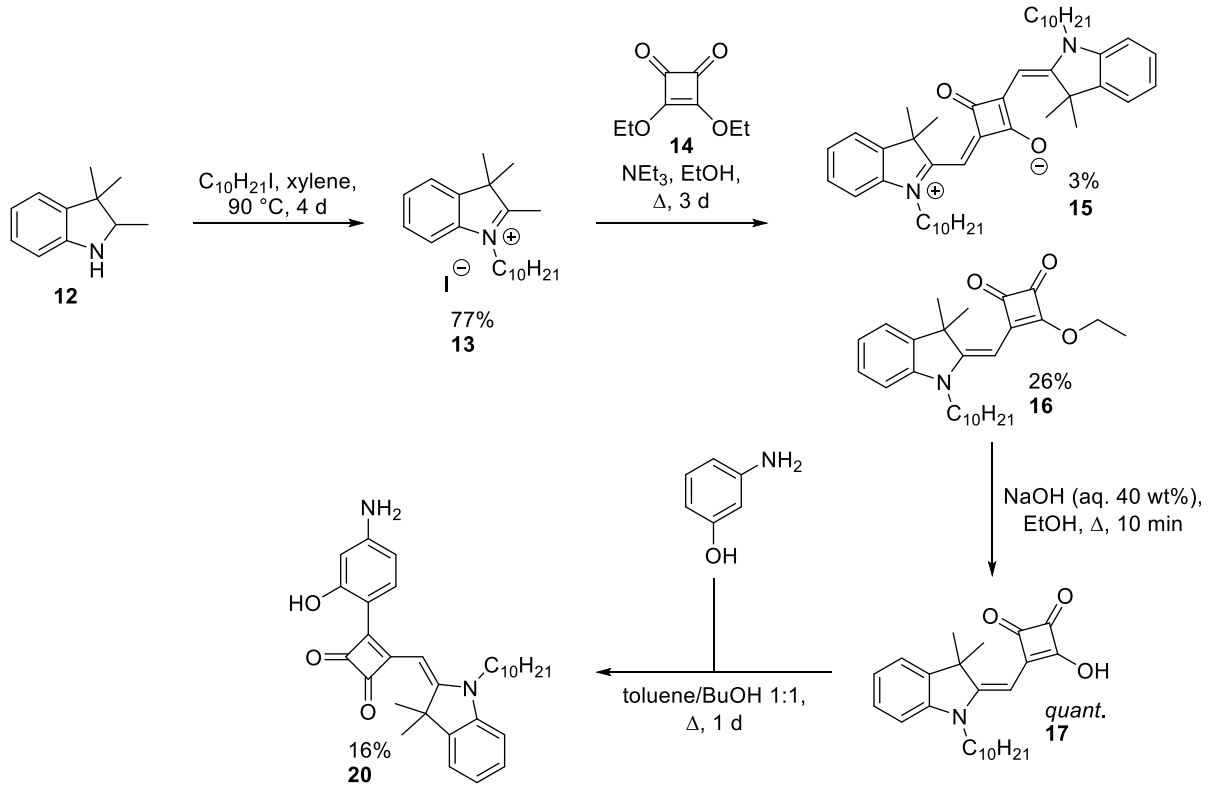

***Scheme 46**: Overview of synthetic route of **20**.*

Compound **20** was tested in Suzuki cross-coupling reactions with regard to its applicability as a designer surfactant in micellar catalysis. During these Suzuki-reactions **20** was compared to, commercially

available **Koliphor EL** as a well-established surfactant for micellar catalysis and surfactant-free conditions. Although the new surfactant performed not as good as **Koliphor EL** it was found to be better than surfactant free conditions. However, the envisioned unique selling point (Figure 44) with stimuli response and facilitated reisolation of the surfactant was hugely successful and provides a clear advantage compared to **Koliphor EL**. Amphiphile **20** does not only work as a pH indicator as an increase of pH results in a color change from deep red to green/yellow depending on the concentration of the dye. More important for its use in micellar catalysis, this color change also indicates the disassembly of the micelle. Furthermore, addition of $ZnCl_2$ leads to the precipitation of a rose-colored solid, which can be removed by filtration. Simple dissolving in aqueous acid followed by extraction with organic solvents such as ethyl acetate and subsequent removal thereof allows for reisolation of amphiphile **20** as a solid for employment in further micellar catalysis. All in all, this sequence allows for an efficient and easy isolation of the reaction product and simultaneous purification of the re-isolated surfactant.

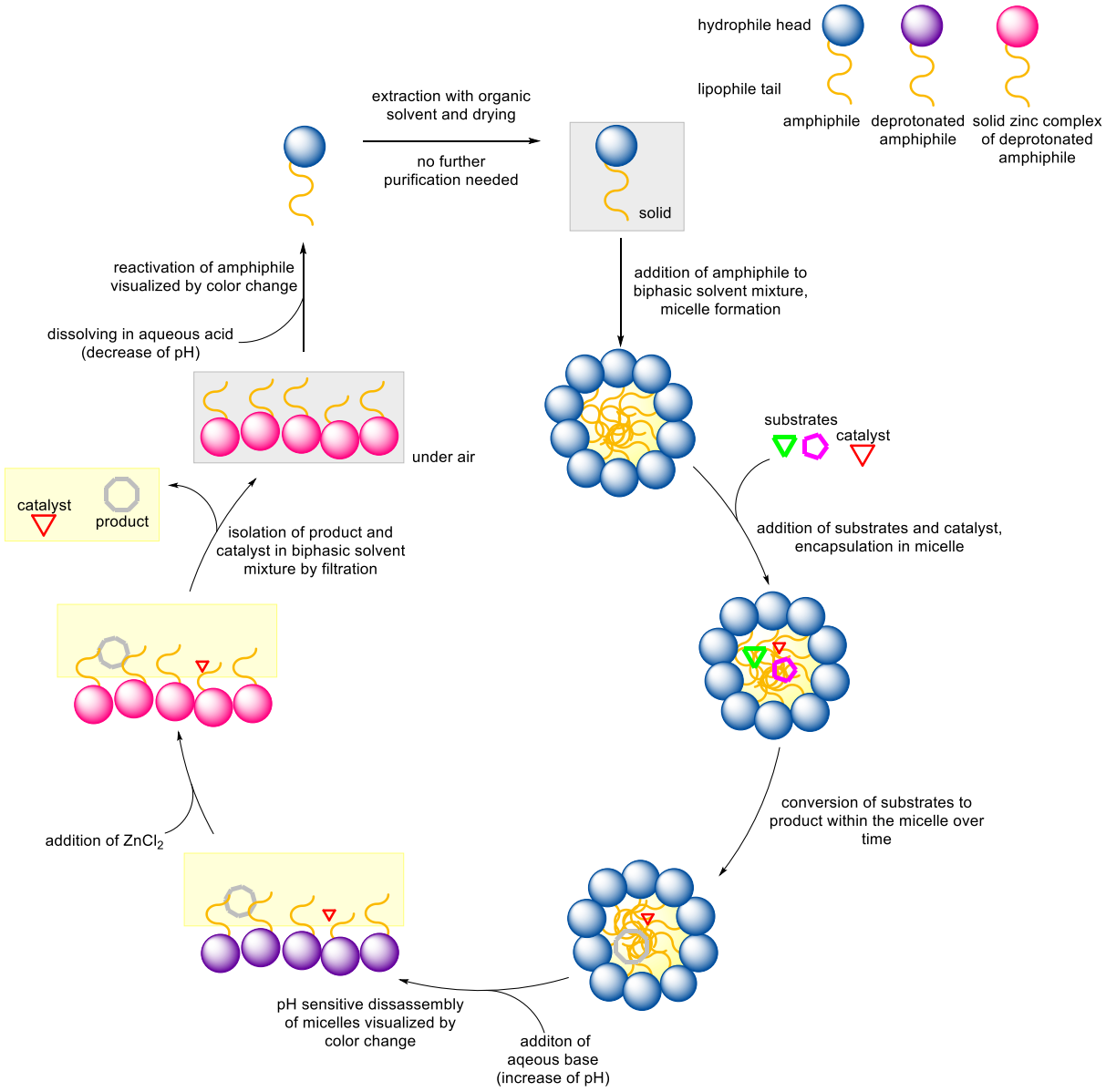

***Figure 44**: Cartoon illustrating the working principle of the pH-sensitive squaraine-based surfactant **20** in micellar catalysis. The biphasic milieu was depicted in a reduced manner omitting the aqueous phase (previously shown as blue surrounding) while as the organic phase is still shown in the pale-yellow coloring seen in the rectangles and within the micelles. Additionally, air is shown as a grey background.*

This provides proof of the principal feasibility of this approach, which now needs to be optimized in further work and extended to other transformations.

6.2 SUBLIMATION OF PYRSQ-C1

Chiral squaraines proved to have interesting chiroptical properties that even led to their applications in optoelectronic devices. A drawback of these materials, however, is that thin films could usually only be obtained by applying solution-processing techniques. As vapor deposition approaches usually result in higher quality thin films testing of the sublimation behavior of chiral squaraines was needed.

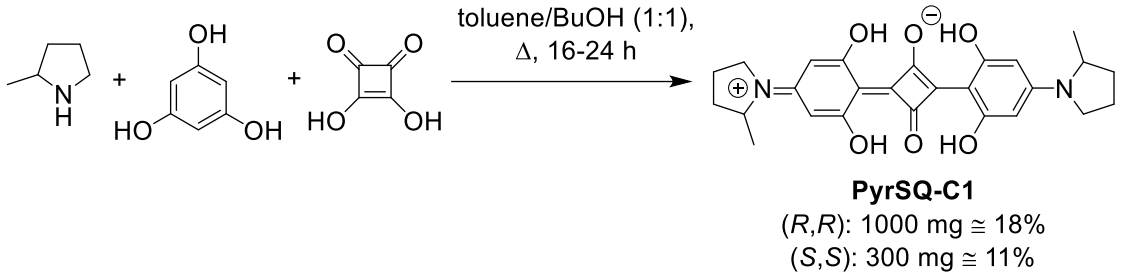

***Scheme 47**: Molecular structure of chiral squaraine **PyrSQ-C1**.*

To address this previously prepared **PyrSQ-C1** (Scheme 47) was chosen as a chiral test squaraine as it is known to readily crystallize from solutions in two defined polymorphs depending on the crystal growth conditions. Therefore, both enantiomer of PyrSQ-C1 were successfully synthesized in 300 mg (*S*,*S*-enantiomer) and 1.00 g (*R*,*R*-enantiomer) scale, respectively. The compounds were provided to collaborators within and beyond the network of the DFG-funded research training group 2591 – TIDE. Through, these studies provided new insight in the behavior of this class of compounds efficient sublimation turned out to be very problematic. During the physical vapor deposition (PVD) attempts for thin film fabrication instead of obtaining said thin films another observation was made which matches with an observation during the unsuccessful zone sublimation attempts aiming at the growth of larger crystals. The visually deteriorated sample was proven to be polymerized squaraine which is assumed to happen due to a thermally induced radical ring opening of the 5-membered ring under the high vacuum conditions at elevated temperatures. This might also explain the so far largely unsuccessful PVD of **ProSQ**s, which also features a non-aromatic 5-membered ring of similar structure.

Therefore, it seems to be more promising to improve thin film qualities of these compounds by optimizing solution-processing approaches in the future especially since drop- and spin-casting have already proven to be suitable to obtain good quality thin films and single crystals from **PyrSQ-C1**.[44]

6.3 A NEW CLASS OF CHIRAL SQ –ALASQ

Besides the two aspects described above the main aim of this thesis was to design a new class of chiral squaraines that combines structural features of both achiral ***N*-alkyl-SQ**s and chiral **ProSQ**s. This was achieved with the successful synthesis and characterization of the new class of alanine-based **AlaSQ**s (Scheme 48) which not only bears a stereogenic center on each terminus of the anilino squaraine skeleton but also two alkyl chains.

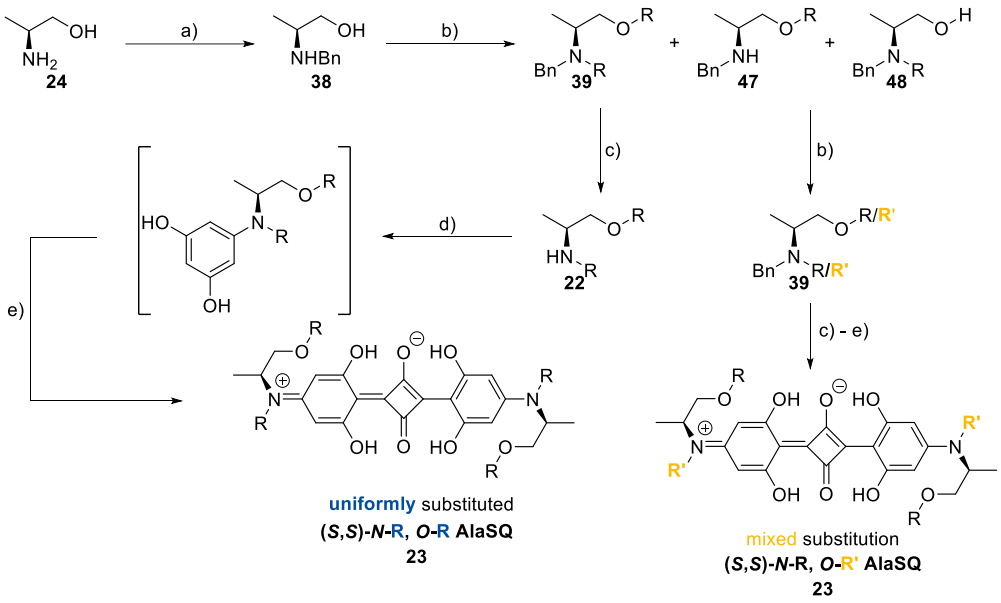

***Scheme 48**: Overview of reaction sequence with the respective reaction condition: a) benzaldehyde, r.t., 2.5 h; $NaBH_4$, 0 °C → r.t., EtOH, b) NaH, R-I/R'-I, r.t. → Δ, THF, c) H_2, Pd/C (10 mmol-%), r.t., EtOH, d) phloroglucinol, reflux, toluene/n-butanol 4/1, e) squaric acid, reflux, toluene/n-butanol 1/1, 24 h.*

During the course of the synthesis a certain preference for first alkylation in the sequence of the twofold Williamson ether synthesis of benzyl-protected alaninol was observed. This resulted in the possibility to synthesize uniformly substituted (R = R') but also mixed substituted derivatives (R ≠ R').

In total 11 different members of the **AlaSQ**s were successfully prepared, allowing preliminary investigations on the **AlaSQ**s' aggregation behavior by poor solvent titrations. Here, the expected high dependency on the chain lengths of the decorating *n*-alkyl groups was verified. Long chains facilitate aggregation whereas those with short chains are – as expected – less prone to aggregation in solution. In general, however, the tendency to form well-defined chiral aggregates in solution is less strong than for the previously tested ProSQs. Nevertheless, preliminary studies together *O. Erdene-Ochir* (Meerholz group, University of Cologne) with within the TIDE network of thin film samples prepared from **(*S*,*S*)-*N*-C3,*O*-C3-AlaSQ 23b** via solution processing and thermal annealing gave promising results that chiral order can be achieved that might lead to a potential application in photodetectors for circularly polarized light.

In the future, these studies should be intensified and extended to other members of the AlaSQ family and supplemented by transient spectroscopic investigations, which need to be accompanied by theoretical studies.

In summary, the foundation for further investigations of the **AlaSQ**s was laid. Building on the newly established synthetic route considering the regioselectivity of the respective alkyl iodide in the alkylation reactions, it is now possible to synthesize a variety of new uniformly and differently substituted **AlaSQ**. It should be noted, though, that further optimization of the synthesis of some of the AlaSQs is necessary to allow access to sufficient amounts of the materials for further investigations. Also, further expanding the library of chiral squaraines should be addressed, especially focusing on the longer alkyl chains like decyl, dodecyl and hexadecyl chains which proved to be beneficial or even responsible to achieve some of the most attractive and spectacular properties observed for ***N*-alkyl-SQ**s and **ProSQ**s. With these the comparison of the effect of the long chain compared to a shorter chain on the other heteroatom on the aggregate formation, and thus, establishing of structure-activity relationships should be facilitated. In theory, this should give insights on the importance of the position

of said substituents, hopefully elucidating the hierarchy of impact between the *N*-substituent and the *O*-substituent.

Besides expanding the family of the **AlaSQ**s the established synthetic route might also be applied to synthesize other classes of chiral squaraines. Here, the closely related **AProSQ**s derived from 1-aminopropan-2-ol come to mind (Figure 45). In theory, the synthesis of these should be less challenging than the one of the **AlaSQ**s and comparison them could shed light on the influence of the relative proximity of the stereogenic centers to the chromophore backbone, as these are one position further away in **AproSQ**s than in **AlaSQ**s.

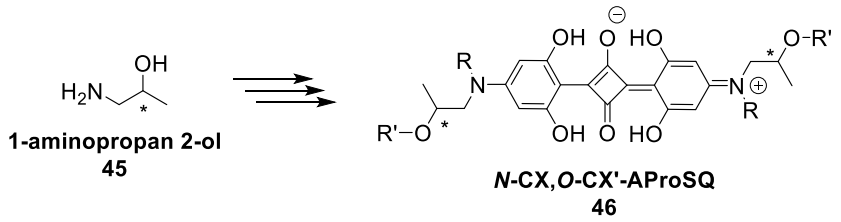

***Figure 45**: Molecular structure of **AproSQs** as a potential new class of chiral squaraines.*

Additionally, the synthetic procedure developed for the **AlaSQ**s could also be transferred to other naturally occurring amino acid or their respective amino alcohols. This would unlock an almost unlimited variety of chiral squaraines and the influence of each natural amino acid's specific characteristic substituent could be investigated. Here, the amino acids with hydrophobic purely hydrocarbon side chains such as valine, (iso-)leucine and phenylalanine seem to be the logical next candidates.

7 EXPERIMENTAL PART

7.1 GENERAL PART

Chemicals

As staring material, L-alaninol **24** ((*S*)-2-aminopropan-1-ol) was purchased from BLDPharm Germany in >98 % purity and ee >98% and used as received. All other chemicals were purchased from standard suppliers and used without further purification. Solvents were purified with standard methods and, if necessary, dried according to literature procedures and stored under argon atmosphere over 4 Å molecular sieves. Reactions under inert gas conditions were performed under dry argon or dry nitrogen atmosphere with dry solvents in flame-dried glassware using Schlenk techniques. Room temperature refers to a temperature range between 20-28°C. The following compounds were synthesized according to literature: **29**,[178] **32**,[145] **33a**,[145] **34**,[145] **35**[149] and **37**.[150]

NMR spectroscopy

^{1}H and ^{13}C NMR spectra were recorded at 298 K at 700 MHz and 176 MHz or 500 MHz and 126 MHz or 400 MHz and 100 MHz, respectively. ^{1}H NMR chemical shifts are reported on the δ scale (ppm) relative to tetramethyl silane. The residual non-deuterated solvent signal was used as the internal standard. ^{13}C NMR chemical shifts are given in δ values (ppm) relative to tetramethyl silane and referenced to the deuterated solvent as the internal standard.

NMR samples measured during the research stay in Milan were recorded with an AVANCE III HD 400 MHz (Bruker) at 400 MHz. Due to measurement time restrictions only ^{1}H NMR spectra were recorded. In many cases the compound was totally consumed in the multi-step synthesis, and hence, could not be brought to Bonn for further characterization.

The following abbreviations or combination thereof were used throughout: s = singlet, d = doublet, t= triplet, q = quartet, m= multiplet, br. = broad. Coupling constants through n bonds (^{n}J) are given in Hertz [Hz].

Coloum chromatography

Column chromatographic separations were carried out on silica gel 60 (40–63 µm) from *Merck* in glass columns of different diameters and suitable eluents.

Thin layer chromatography (TLC)

TLC were performed for reaction control, tracking of progress during column chromatographic purification and purification of certain reactions with crude product amounts below 20 mg when applicable. Silica gel-coated aluminum plates from *Merck* (0.2 mm with fluorescent indicator) were used as the stationary phase. The substance spots were detected using UV light at wavelengths λ = 254 nm and λ = 366 nm. Non-UV-active substances were stained by oxidation with an aqueous potassium permanganate solution. Alternatively for amines the staining was done using an ethanolic ninhydrin solution.

DLS measurements

DLS measurements were performed on a Zetasizer Nano-S manufactured by Malvern Panalytical at University of Milano-Bicocca, Department of material science, Milan, Italy. The data was analyzed using the instrument specific software and exported. These exported correlograms were fitted to autocorrelation functions via cumulative method over two measurements.

Mass spectrometry

Electrospray ionization (ESI) mass spectra were taken on an Orbitrap XL (Thermo Fisher Scientific). Atmospheric pressure chemical ionization (APCI) mass spectra were taken on an Orbitrap XL (Thermo Fisher Scientific). Electron ionization (EI) spectra were measured on a MAT 95 XL sector field instrument from Thermo Finnigan.

Elemental analysis

Elemental analysis was performed on a Vario EL (Heraeus). All compounds were measured at least two times.

7.2 SYNTHESIS OF AMPHIPHILIC SQUARAINES

Synthesis of N,N-didodecyl 3-hydroxy aniline (1)

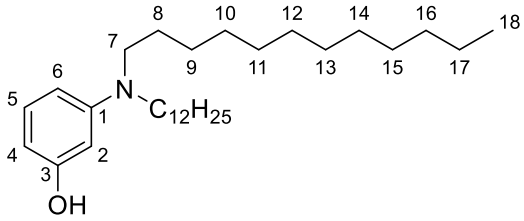

The compound was prepared adapting a protocol developed in the Beverina group.[179]

3-Aminophenol (5.00 g, 1.00 eq., 45.82 mmol), Na_2CO_3 (10.20 g, 2.10 eq., 96.22 mmol) and dodecyl bromide (46 mL, 4.20 eq, 192.55 mmol) were suspended in *i*-PrOH (50 mL) and refluxed for 26 h. After GC-MS a TLC monitoring revealed complete consumption of the starting material the mixture was filtered and CH_2Cl_2 was added to the filtrate, which caused further precipitation. A second filtration was done and the solvent was removed under reduced pressure. The remaining purple oil was further subjected to vacuum distillation to remove the excess dodecyl bromide (T = 110°C, p = 0.042 mbar). The product was obtained as a purple oil (20.42 g, 45.82 mmol, quant.)

Yield: quant.

Molecular weight: $C_{30}H_{55}NO$, 445.776 g/mol

^{1}H-NMR: (700 MHz, acetone-d_6, 298 K) δ [ppm] = 6.93 (t, 1 H, H-5, $^3J_{5,6;4}$= 8.0 Hz), 6.20-6.14 (m, 2 H, H-2, H-4), 6.10-6.06 (m, 1 H, H-6), 3.25 (t, 4 H, H-7, $^3J_{7,8}$= 7.6 Hz, 1.57 (t, 4 H, H-8, $^3J_{8,7}$= 7.5 Hz), 1.35-1.24 (m, 36 H, H-9 – H-17), 0.88 (t, 6 H, H-18, $^3J_{18,17}$= 7.0 Hz).

^{13}C-NMR: (176 MHz, acetone-d_6, 298 K) δ [ppm] = 159.3 (C-3), 150.6 (C-1), 130.5 (C-5), 104.5 (C-4), 103.5 (C-6), 99.8 (C-2), 51.7 (C-7), 32.6 (C-16), 30.4[#] (C-10, C-11, C-12, C-13, C-14, C-15), 28.1 (C-8), 27.8 (C-9), 23.3 (C-17), 14.4 (C-18).

[#]unambiguous assignment not possible.

MS: (EI, acetone-d_6, M = $C_{30}H_{55}NO$) *m/z* = 445.3 $[M]^{\bullet+}$, 290.2 $[M\text{-}C_{11}H_{23}]^{\bullet+}$.

EI HRMS: calculated for $[C_{30}H_{55}NO]^{\bullet+}$: *m/z* = 445.4284, found: *m/z* = 445.4282.

Attempted Synthesis of N,N-PEGylated 3-hydroxy aniline 19

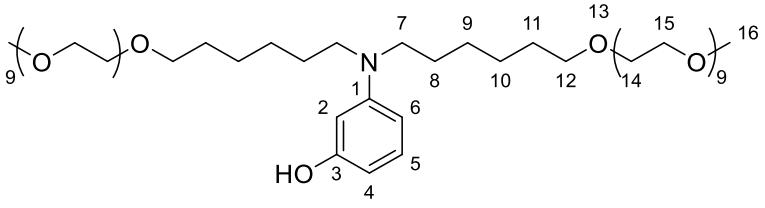

The synthesis was attempted adapting a protocol developed in the Beverina group.[179]

3-Aminophenol (581 mg, 1.00 eq., 5.32 mmol), Na_2CO_3 (1.19 g, 2.10 eq., 11.17 mmol) and $(CH_2)_6O(C_2H_4O)_9CH_3Br$ **18** (6.00 g, 2.00 eq, 10.64 mmol) were suspended in *i*-PrOH (5 mL) and refluxed for 64 h. As TLC monitoring still revealed the presence of staring material, KI (44 mg, 0.05 eq., 0.27 mmol) was added. The mixture was refluxed for additional 64 h. Afterwards, the mixture was

cooled and the solvent was removed. The residue was dissolved in water (20 mL). After tedious extraction with ethyl acetate (3 x 20 mL) and CH_2Cl_2 (3 x 20 mL), the organic phases were combined and the solvents were removed. The remaining aqueous phase was also concentrated under reduced pressure. The respective residues were dissolved in water (70 mL), slightly acidified with NH_4Cl (400 mg) until pH = 7. However, unfortunately, the desired product **19** could not be identified in one of these.

Synthesis of squarylium dichloride (2)

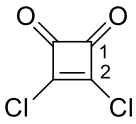

The synthetic protocol was adapted from the literature[180] and a protocol developed in the Beverina group.[179]

The reaction was performed under a nitrogen atmosphere. Squaric acid (4.90 g, 1.00 eq., 43.84 mmol) was dissolved in toluene (10 mL). Freshly distilled thionyl chloride (6.4 mL, 2.00 eq., 87.67 mmol) and catalytic amounts of DMF (200 µL) was added. The reaction was refluxed for 1.5 h. The heat was removed and the mixture was stirred at r.t. for additional 19 h. Filtration over tinted glass, followed by washing of the precipitate with toluene allowed reisolation of parts of the starting material (2.9 g). The solvent of the filtrate was removed under reduced pressure giving a yellow residue. To this residue heptane (10 mL) was added and the mixture was heated to 60 °C and agitated using a sonificator. Decantation of the light-yellow solution and cooling of this allowed isolation of the desired product **2** as yellow crystalline needles (700 mg, 4.63 mmol, 26% based on reacted starting material).

Yield: 26%

Molecular weight: $C_4O_2Cl_2$, 150.942 g/mol

^{1}H-NMR: (700 MHz, $CDCl_3$, 298 K) δ [ppm] = no signals

^{13}C-NMR: (176 MHz, $CDCl_3$, 298 K) δ [ppm] = 189.6 (C-1), 188.3 (C-2).

[#]unambiguous assignment not possible.

MS: (EI, M = $C_4O_2Cl_2$) *m/z* = 149.9 $[M]^{\bullet+}$.

EI HRMS: calculated for $[C_4O_2Cl_2]^{\bullet+}$: *m/z* = 149.9275, found: *m/z* = 149.9270.

The analytical data are in accordance with those published in the literature.[180]

Synthesis of hemisquarate 4

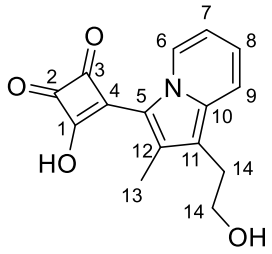

The compound was prepared adapting a protocol developed in the Beverina group.[179]

The reaction was performed under a nitrogen atmosphere. 2-Methyl-1-indolizineethanol (116 mg, 1.00 eq., 0.66 mmol) synthesized and provided by *A. Zucchi* was dissolved in Et_2O (2 mL), squarylium dichloride (100 mg, 1.00 eq., 0.66 mmol) was added. The resulting deep red solution alongside a brown precipitate was kept at r.t. for 1 h. After TLC control revealed complete consumption of the starting material the solvent was removed under reduced pressure. The residue was dissolved acetone (25 mL) and K_2CO_3 (828 mg, 9.08 eq., 5.99 mmol) in water (4.4 mL) was added. The mixture was heated to reflux for 5 h. Afterwards the mixture was further diluted with water (10 mL) and the majority of the acetone was removed under reduced pressure. The resulting residue was treated with aq. HCl (1.5 mL conc. HCl in 36.3 mL water) and then extracted using Et_2O (3x70 mL) and ethyl acetate (2 x 70 mL). The combined organic phases were dried with $MgSO_4$ and the solvent was removed. Purification by column chromatography gave the desired product **4** as red oil (30 mg, 0.11 mmol, 17%).

Yield: 17%

Molecular weight: $C_{12}H_{13}NO_4$, 271.272 g/mol

^{1}H-NMR: (500 MHz, $CDCl_3$, 298 K) δ [ppm] = 7.82 (d, 1 H, H-6, $^3J_{6,7}$= 7.0 Hz), 7.57 (dt, 1 H, H-9, $^3J_{9,8}$= 8.8 Hz, $^4J_{9,7}$= 1.2 Hz), 7.10-7.01 (m, 1 H, H-8), 6.57 (td, 1 H, H-7, $^3J_{7,6}$= 6.8 Hz, $^4J_{7,9}$= 1.3 Hz), 3.67 (t, 2 H, H-15, $^3J_{15,14}$= 7.1 Hz), 2.99-2.94 (m, 2 H, H-14), 2.11 (s, 3 H, H-13).

Synthesis of 1-Phenyl butanedioate (5)

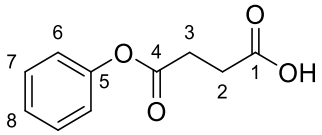

The compound was prepared adapting a protocol developed in the Beverina group.[179]

Phenol (503 mg, 1.00 eq., 5.34 mmol) and succinic anhydride (2.01 g, 3.75 eq., 20.04 mmol) were combined in a reaction tube. The temperature was increased until both reagents were completely molten (130°C) and the mixture was kept at this temperature for 48 h. After cooling to r.t. the mixture was suspended in toluene and filtered. Removal of the solvent under reduced pressure gave the crude product as a white solid (973 mg), according to NMR the ratio of product and remaining succinic anhydride amounted to 1:0.3825, resulting in an overall yield of the desired product **5** of 78% (812 mg, 4.19 mmol). The compound was used as is for the next reaction.

Yield: 78%

Molecular weight: $C_{10}H_{10}O_4$, 194.1860 g/mol

^{1}H-NMR: (700 MHz, $CDCl_3$, 298 K) δ [ppm] = 7.42-7.33 (m, 2 H, H-7), 7.25-7.21 (m, 1 H, H-8), 7.13-7.05 (m, 1 H, H-6), 2.90 (ddd, 2 H, H-2, $^{3}J_{2,3}$= 7.3 Hz, $^{4}J_{7,9}$= 1.3 Hz), 2.81 (ddd, 2 H, H-3, $^{3}J_{3,2}$= 7.3 Hz, $^{4}J_{7,9}$= 1.3 Hz).

^{13}C-NMR: (176 MHz, $CDCl_3$, 298 K) δ [ppm] = 173.6 (C-1), 171.7 (C-4), 152.1 (C-5), 130.3 (C-7), 126.5 (C-8), 122.6 (C-6), 29.9 (C-2), 29.4 (C-3).

Synthesis of PEG-ylated 1-Phenyl butanedioate (6)

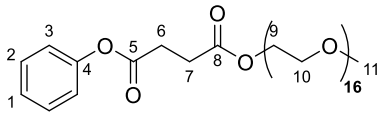

The synthetic protocol was adapted from the literature.[181]

The reaction was performed under a nitrogen atmosphere. 1-Phenylbutanedioate (970 mg, 1.00 eq., 5.00 mmol), MPEG 750 (3.75 g, 1.00 eq., 5.00 mmol) and DMAP (61 mg, 0.10 eq., 0.50 mmol) were dissolved in pyridine (25 mL). The mixture was refluxed for 4 h. Afterwards the mixture was cooled with an ice bath. The ice-cooled mixture was acidified using aq. HCl (1.5 N, 70 mL). CH_2Cl_2 (2 x 50 mL, 2 x 30 mL) was used for extraction and the combined organic phases were washed with brine (100 mL) and dried with $MgSO_4$. The solvent was removed under reduced pressure and the crude product **6** (4.7 g) was obtained as a yellow oil with traces of pyridinium chloride and significant amount of unreacted starting material (MPEG). The compound was used as is for the coupling reaction.

Molecular weight: $C_{43}H_{76}O_{20}$, 913.0610 g/mol

^{f1}H-NMR: (400 MHz, DMSO-d_6, 298 K) δ [ppm]: 9.32 (s, 1 H, H-1), 7.21-7.08 (m, 2 H, H-3), 6.79-6.71 (m, 2 H; H-2), 3.62-3.56 (m, 2 H, H-7), 3.56-3.45 (m, 64 H, H-9, H-10) .3.45-3.39 (m, 2 H, H-6), 3.24 (s, 3 H, H-11).

Synthesis of hemisquarates 8 and 9

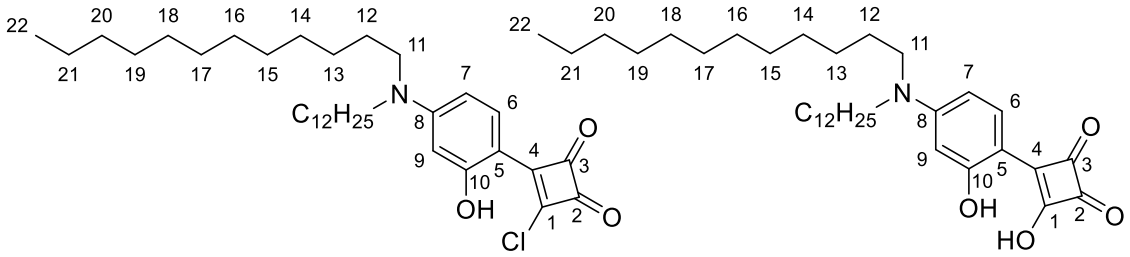

The synthetic protocol was adapted from the literature.[182]

The reaction was performed under a nitrogen atmosphere. A solution of *N*,*N*-didodecyl 3-hydroxy aniline **1** (500 mg, 1.00 eq., 1.12 mmol) and squarylium dichloride **2** (169 mg, 1.00 eq., 1.12 mmol) in dry CH_2Cl_2 (10 mL) was added to an ice-cooled solution of $AlCl_3$ (150 mg, 1.00 eq., 1.12 mmol) in CH_2Cl_2 (10 mL). The mixture was kept at 50 °C for 3 h. The red colored mixture was directly poured into crushed ice and extracted with CH_2Cl_2 (4 x 5 mL). The combined organic extracts were dried with Na_2SO_4 and the solvent was removed. Column chromatography on silica gel (2:1 CH_2Cl_2/cyclohexane) yielded the desired product **8** alongside the hydrolyzed product **9** as an orange to red oil (276 mg, 0.49 mmol, 42%).

Yield: 42%

Analytical data of **9**

Molecular weight: $C_{34}H_{55}NO_4$, 541.817 g/mol

^{1}H-NMR: (500 MHz, $CDCl_3$, 298 K) δ [ppm] = 10.34 (s, 1 H, C-10-OH), 7.59 (d, 1 H, H-6, $^3J_{6,7}$= 9.3 Hz), 6.25 (dd, 1 H, H-7, $^3J_{7,6}$= 9.3 Hz, $^4J_{7,9}$= 2.6 Hz), 6.18 (d, 1 H, H-9, $^2J_{9,7}$= 2.5 Hz), 3.37-3.29 (m, 4 H, H-11), 1.68-1.59 (m, 4 H, H-12), 1.36-1.20 (m, 36 H, H-13 – H-21), 0.88 (t, 6 H, H-22, $^3J_{22,21}$= 6.9 Hz).

^{13}C-NMR: (126 MHz, $CDCl_3$, 298 K) δ [ppm] = 191.4 (C-2), 176.7$^{\#}$ (C-1, C-3), 162.7 (C-10), 154.6 (C-8), 130.6 (C-6), 105.5 (C-7), 105.2 (C-5), 99.7 (C-9), 51.4 (C-11), 32.1 (C-20), 29.8$^{\#}$ (C-13 – C-18), 29.7$^{\#}$ (C-13 – C-18), 29-6$^{\#}$ (C-13 – C-18), 29.5$^{\#}$ (C-13 – C-18), 27.7 (C-20), 27.2 (C-19), 22.8 (C-21), 14.3 (C-22).

$^{\#}$unambiguous assignment not possible.

MS (8): (APCI, dichloromethane, M = $C_{34}H_{55}NO_4$) *m/z* = 560.385$[M+H^+]^+$.

ESI HRMS(8): calculated for $[C_{34}H_{56}NO]^{\bullet+}$: *m/z* = 560.3865 , found: *m/z* = 560.3850.

MS(9): (APCI, dichloromethane, M = $C_{34}H_{55}NO_4$) *m/z* = 542.422 $[M+H^+]^+$.

APCI HRMS(9): calculated for $[C_{34}H_{56}NO]^{\bullet+}$: *m/z* = 542.4204 , found: *m/z* = 542.4214

Synthesis of symmetric squaraine (11)

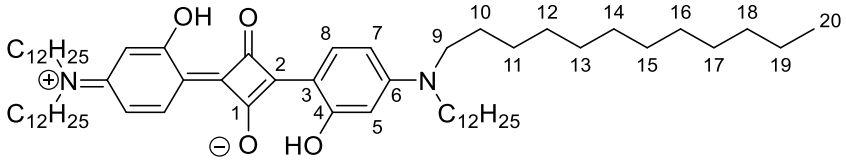

The compound was prepared adapting a protocol developed in the Beverina group.[179]

N,N-didodecyl 3-hydroxy aniline (**1**) (781 mg, 1.75 mmol, 1 eq.) and squaric acid (100 mg, 0.88 mmol, 0.5 eq.) were dissolved in a mixture of toluene/2-BuOH 1/1 v/v (9 mL). The mixture was refluxed under N2-atmosphere for 4 h. During this period the originally purple mixture turned deep blue within 10 minutes. The desired product readily participated from the mixture upon cooling. Filtration and subsequent purification by column chromatography (Si2O, DCM) gave desired product as green solid with a metallic sheen (576 mg, 0.66 mmol, 75%). Further purification by crystallization did not result in single crystal growth and was thus deemed unfeasible.

Yield: 75%

Molecular weight: $C_{64}H_{108}N_2O_4$, 969.5780 g/mol

^{1}H-NMR: (500 MHz, $CDCl_3$, 298 K) δ [ppm] = 12.00 (s, 2 H, OH), 7.82 (d, 2 H, H-8, $^3J_{8,7}$= 9.2 Hz), 6.36 (dd, 2 H, H-7, $^3J_{7,8}$= 9.2 Hz, $^4J_{7,5}$= 2.4 Hz), 6.10 (d, 2 H, H-5, $^4J_{5,7}$ = 2.4 Hz), 3.42-3.34 (m, 8 H, H-9), 1.70-1.58 (0, 8 H, H-10), 1.31-1.22 (m, 72 H, H-11 – H-19), 0.90-0-85 (m, 12 H, H-20).

^{13}C-NMR: (126 MHz, acetone-d_6, 298 K) δ [ppm] = 132.7 (C-8), 52.9 (C-9), 32.1 (C-18), 29.8$^{\#}$ (C-12, C-13, C-14, C-15, C-16, C-17), 29.7$^{\#}$ (C-12, C-13, C-14, C-15, C-16, C-17), 29.5$^{\#}$ (C-12, C-13, C-14, C-15, C-16, C-17), 27.5 (C-10), 27.1 (C-11), 22.8 (C-19), 14.3 (C-20).

$^{\#}$unambiguous assignment not possible.

^{13}C-NMR Signals for C-1 – C-7 not found, concentration of probe was probably too low.

MS: (ESI (+), dichloromethane, M = **:** $C_{64}H_{108}N_2O_4$) *m/z* = 614.623 $[M\text{-}C_{24}H_{49}O^-]^+$.

ESI (+) HRMS: calculated for $[C_{64}H_{109}N_2O_4]^+$: *m/z* = 969.8387 , found: *m/z* = 969.8386.

Synthesis of indole derivative (13)

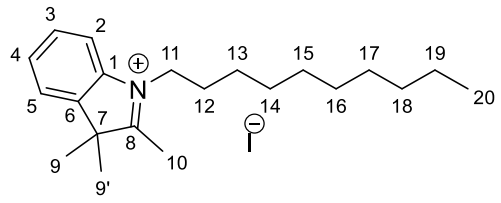

The compound was prepared adapting a protocol developed in the Beverina group.[179]

The reaction was performed under a nitrogen atmosphere. A solution of 2,3,3-trimethylindol **12** (5.18 g, 1.00 eq., 32.55 mmol) and decyl iodide (9.5 mL, 1.44 eq., 46.78 mmol) in xylene (10 mL) was kept at 90 °C for 16 h. The red solution gradually turned purple and more viscous over time. Addition of Et_2O prompted precipitation of an off-white solid. Decanting the solvent and subsequent washing of the remaining precipitate with heptane (15 mL) and Et_2O, followed by drying of the solid under reduced pressure gave the desired product **13** as an orange to red oil (11.48 g, 25.20 mmol, 82%).

Yield: 82%

Molecular weight: $C_{21}H_{34}IN$, 300.5095 g/mol

^{1}H-NMR: (700 MHz, acetone-d_6, 298 K) δ [ppm] = 8.10-8.06 (m, 1 H, H-2), 7.90-7.88 (m, 1 H, H-5), 7.68 (dd, 2 H, H-3, H-4) 5.62 (s, 3 H, H-10), 4.71 (t, 2 H, H-11, $^3J_{11,12}$= 7.9 Hz), 2.09-2.06 (m, 2 H, H-13), 1.71 (s, 6 H, H-9, H-9'), 1.61-1.54 (m, 2 H, H-12), 1.44-1.36 (m, 2 H, H-19), 1.35-1.22 (m, 10 H, H-14 – H-18), 0.86 (t, 3 H, H-20, $^3J_{20,21}$= 7.1 Hz).

^{13}C-NMR: (176 MHz, acetone-d_6, 298 K) δ [ppm] = 197.5 (C-8), 143.2 (C-6), 142.4 (C-1), 130.7 (C-4), 130.1 (C-3), 124.5 (C-5), 116.6 (C-2), 55.9 (C-10), 55.0 (C-7), 49.6 (C-11), 32.6 (C-18), 30.3 (C-14), 29.9* # (C-15 – C-17), 28.6 (C-13), 27.3 (C-12), 23.3 (C-19) 22.8 (C-9, C-9'), 14.3 (C-20).

#unambiguous assignment not possible.

MS: (ESI (+), dichloromethane, M = $C_{21}H_{34}IN$) *m/z* = 300.267 $[M\text{-}I^-]^+$.

ESI (+) HRMS: calculated for $[C_{21}H_{34}N]^+$: m/z = 300.2686, found: *m/z* = 300.2675.

Synthesis of Hemisquarate 17

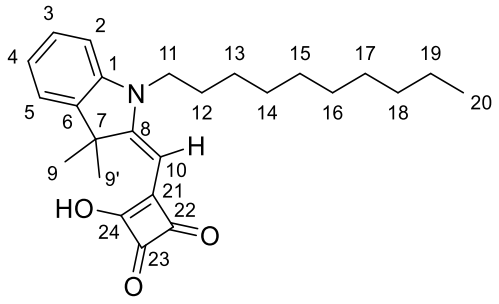

The synthetic protocol was adapted from the literature.[183]

Indole derivative **13** (5.00 g, 1.00 eq, 16.64 mmol) and diethyl squarate **14** (1.76 g, 0.65 eq., 10.98 mmol) were dissolved in EtOH (22 mL). The mixture was heated to reflux for 1 h before NEt_3 was added dropwise. Afterwards the mixture was refluxed for 3 h. The resulting dispersion of a green solution alongside of yellow solids was concentrated by removal of the solvent under reduced pressure. The residue was diluted with ethyl acetate (40 mL) and washed with water (3 x 20 mL). The organic phase was dried with $MgSO_4$ and the solvent was removed. The resulting crude product was then further purified via column chromatography on silica gel (heptane/ethyl acetate 8/2 → 1/1) to give the desired hydrolyzation product hemisquarate **17** alongside with its corresponding ethyl squarate **16**. Additionally symmetrical squaraine **15** was recovered from the column as a bronze colored solid (500 mg, 0.74 mmol, 3%).

To also convert the ethyl ester **16** into the desired hemisquarate the mixture was subjected to further hydrolyzation. The obtained mixture was dissolved in EtOH (11.5 mL) and heated to reflux. Then aq. NaOH (40% w/w, 0.7 mL) was added dropwise. After 10 min the hot reaction mixture was poured into EtOH/H_2O (2/11 v/v, 29 mL) under vigorous stirring. Concentrated aq. HCl (1.9 mL) was added, turning the mixture opaque and resulting in precipitation of a beige solid alongside a yellow solution and a brown oil on top. The precipitate was collected by filtration, washed with water and dried in a vacuum oven to give the desired product **17** as a brick colored solid (734 mg, 1.86 mmol, 17%).

Yield: 17%

Molecular weight: $C_{25}H_{33}NO_3$, 395.5430 g/mol

^{1}H-NMR: (700 MHz, acetone-d_6, 298 K) δ [ppm] = 7.41 (d, 1 H, H-5, $^3J_{5,4}$= 7.3 Hz), 7.29 (t, 1 H, H-3, , $^3J_{3,4}$= 7.7 Hz), 7.11 (d, 1 H, H-2, $^3J_{2,3}$= 7.7 Hz), 7.07 (d, 1 H, H-4, $^3J_{4,5}$= 7.4 Hz), 5.64 (s, 1 H, H-10), 3.97 (t, 2 H, H-11, $^3J_{11,12}$= 7.6 Hz), 1.83-1.76 (m, 4 H, H-12), 1.65 (s, 6 H, H-9, H-9'), 1.52-1.45 (m, 2 H, H-13), 1.43-1.38 (m, 2 H, H-14), 1.35-1.22 (m, 10 H, H-15 – H-19), 0.88 (t, 3 H, H-20, $^3J_{20,21}$= 7.0 Hz).

^{13}C-NMR: (176 MHz, acetone-d_6, 298 K) δ [ppm] = 192.1 (C-23), 189.9 (C-22, C-24), 174.7 (C-21), 167.8 (C-8), 144.0 (C-1), 141.5 (C-6), 128.7 (C-3), 123.0 (C-4), 122.7 (C-5), 109.4 (C-2), 81.9 (C-10), 43.3 (C-11), 48.3 (C-7), 32.6 (C-18), 30.6 (C-14), 29.9* # (C-15 – C-17), 27.5 (C-9), 27.4 (C-13), 27.0 (C-12), 23.3 (C-19), 14.4 (C-20).

#unambiguous assignment not possible.

MS: (ESI (-), dichloromethane, M = $C_{25}H_{33}NO_3$) *m/z* = 394.239 $[M\text{-}H^+]^-$.

ESI (-) HRMS: calculated for $[C_{25}H_{32}NO_3]^-$: *m/z* = 394.2388, found: *m/z* = 394.2388.

Synthesis of indoline squaraine 15

Isolated during synthesis of **16**.

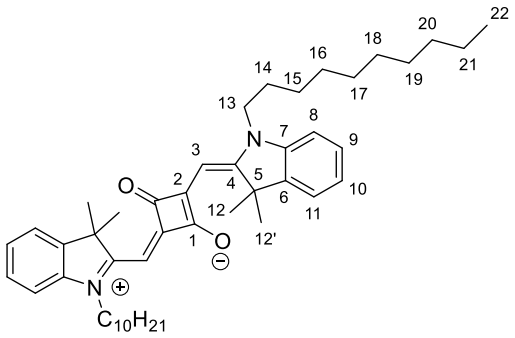

Yield: 3%

Molecular weight: $C_{46}H_{64}N_2O_2$, 677.030 g/mol

^{71}H-NMR: (700 MHz, $CDCl_3$, 298 K) δ [ppm] = 7.35 (dd, 2 H, H-11, $^3J_{11,10}$= 7.5 Hz, $^4J_{11,9}$= 1.2 Hz), 7.30 (td, 1 H, H-9, $^3J_{9,10}$= $^3J_{9,8}$= 7.5 Hz, $^4J_{9,11}$= 1.2 Hz), 7.14 (td, 1 H, H-10, $^3J_{10,9}$= $^3J_{10,11}$= 7.5 Hz, $^4J_{10,8}$= 0.9), 6.97 (d, 1 H, H-8, $^3J_{8,9}$= 7.9 Hz), 5.96 (s, 2 H, H-3), 4.07-3.84 (m, 4 H, H-13), 1.83-1.75 (m, 16 H, H-12, H-12', H-14), 1.47-1.39 (m, 4 H, H-15), 1.38-1.31 (m, 4 H, H-16), 1.32-1.20 (m, 20 H, H-17 – H-21), 0.87 (t, 6 H, H-22, $^3J_{22,21}$= 7.1 Hz).

^{13}C-NMR: (176 MHz $CDCl_3$, 298 K) δ [ppm] = 182.6 (C-1), 179.7 (C-2), 170.2 (C-4), 142.7 (C-7), 142.4 (C-6), 127.9 (C-9), 123.8 (C-10), 122.4 (C-11), 109.5 (C-8), 86.7 (C-3), 49.4 (C-5), 43.9 (C-13), 32.0 (C-20), 29.6 [#] (C-17 – C-19), 29.5(C-16), 29.4[#] (C-17 – C-19), 27.3 (C-15), 27.2 (C-12, C-12', C-14), 22.9 (C-21), 14.3 (C-22).

[#]unambiguous assignment not possible.

MS: (ESI (+), dichloromethane, M = $C_{46}H_{64}N_2O_2$) *m/z* = 709.494 $[M+Na^+]^+$, *m/z* = 677.503 $[M+H^+]^+$.

ESI (+) HRMS: calculated for $[C_{46}H_{65}N_2O_2]^+$: *m/z* = 677.5041, found: *m/z* = 677.5031.

Synthesis of amphiphilic squaraine 20

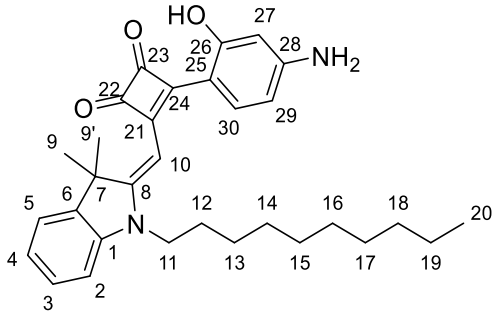

1 (100 mg, 1.00 eq, 0.91 mmol) and **17** (360 mg, 1.00 eq., 0.91 mmol) were dissolved in a mixture of toluene/1-BuOH 1/1 v/v (20 mL). The mixture was heated to reflux for 1 d. Upon heating the brown mixture turned intensely red. Afterwards water (2 x 5 mL) was added and the solvents were removed under reduced pressure. The resulting crude product was then further purified via column chromatography on silica gel (ethyl acetate). This gave the desired product **20** as an orange oil. Recrystallization from EtOH gave **20** as a purple crystalline solid that shows red fluorescence (220 mg, 0.15 mmol, 50%).

Yield: 50%

Molecular weight: $C_{31}H_{38}N_2O_3$, 486.6560 g/mol

^{1}H-NMR: (700 MHz, $CDCl_3$, 298 K) δ [ppm] = 10.01 (s, 1 H, OH), 9.86 (s, 1 H, NH2), 7.98 (s, 1 H, H-27), 7.39 (dd, 1 H, H-5, $^3J_{5,4}$= 7.4 Hz, $^4J_{5,3}$= 1.1 Hz), 7.35 (td, 1 H, H-3, $^3J_{3,2}$= 7.7 Hz, $^4J_{3,5}$= 1.2 Hz), 7.27 (d, 1 H, H-30, $^3J_{30,29}$= 8.0 Hz), 7.20 (td, 1 H, H-4, $^3J_{4,5}$= 7.4 Hz, $^4J_{4,2}$= 0.9 Hz), 7.04 (d, 1 H, H-2, $^3J_{2,3}$= 7.9 Hz), 6.78 (dd, 1 H, H-29, $^3J_{29,30}$= 7.9 Hz, $^4J_{29,27}$= 2.2 Hz), 5.95 (s, 1 H, H-10), 4.02 (s, 2 H, H-11), 1.83 (dt, 2 H, H-12, $^3J_{12,11}$= 7.8 Hz),1.79 (s, 3 H, H-9/H-9'), 1.75, (s, 3 H; H-9/H-9'), 1.53-1.44 (m, 2 H, H-13), 1.43-1.35 (m, 2 H, H-14), 1.35-1.19 (m, 10 H, H-15 – H-19), 0.89 (t, 3 H, H-20, $^3J_{20,21}$= 7.1 Hz).

^{13}C-NMR: (176 MHz, $CDCl_3$, 298 K) δ [ppm] = 178.6 (C-22/C-23), 173.6 (C-22/C-23), 171.4 (C-8), 158.1 (C-26), 142.5 (C-1), 142.0 (C-6), 138.8 (C-28), 130.5 (C-30), 124.1 (C-4), 122.4 (C-5), 112.9 (C-29), 111.4 (C-25), 109.8 (C-2), 107.6 (C-27), 85.9 (C-10), 49.4 (C-7), 44.0 (C-11), 32.0 (C-18), 29.7 (C-14), 29.5* # (C-15 – C-17), 27.3 (C-13), 27.2 (C-9/C-9'), 27.1 (C-9/C-9', C-12), 22.8 (C-19), 14.3 (C-20).

#unambiguous assignment not possible.

MS: (EI, M = $C_{31}H_{38}N_2O_3$) *m/z* = 486.2 $[M]^{\bullet+}$.

EI HRMS: calculated for $[C_{31}H_{38}N_2O_3]$: *m/z* = 486.2882, found: *m/z* = 486.287

7.3 SYNTHESIS OF AMINE BUILDING BLOCKS

Synthesis of 31a

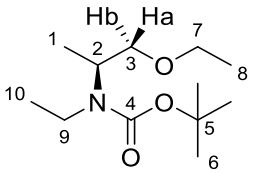

The synthetic protocol was adapted from the literature.[184]

A solution of Boc-alaninol **29** (500 mg, 2.85 mmol,1.00 eq) dissolved in dry DMF (7 mL) was added to an ice-cooled suspension of anhydrous K_2CO_3 (1.65 g, 11.97 mmol, 4.20 eq.) in dry DMF (7 mL) at 0°C. This mixture is kept at that temperature for 30 min before the ethyl iodide (0.7 mL, 8.55 mmol, 3.00 eq.) was added. The mixture was allowed to warm to r.t. and kept at this temperature for 16-24 h. Afterwards, water (5 mL) and NH_4Cl (sat. aq., 5 mL)) are added. Ethyl acetate (5x 5 mL) was used for extraction and the resulting combined organic phase was dried over $MgSO_4$ before removal of the solvent. The crude product was obtained as a pale-yellow oil (0.45 g, 1.89 mmol, 66%*). It was used as if for the next reactions.

Yield: 66%* under assumption of pure product

Molecular weight: $C_{12}H_{25}NO_3$, 231.3360 g/mol

^{1}H-NMR: (500 MHz, $CDCl_3$, 298 K) δ [ppm] = 4.21 (4 H, H-7, H-9, q, $^3J_{7,8} = {}^3J_{9,10}$ = 7.1 Hz), 3.77 (1 H, H-2, ddq, $^3J_{2,1}$ = 6.7 Hz, $^3J_{2,3b}$ = 6.3 Hz, $^3J_{2,3a}$ = 3.4 Hz), 3.65 (1 H, H-3a, dd, $^2J_{3a,3b}$ = 10.9 Hz, $^3J_{3a,2}$ = 3.7 Hz), 3.51 (1 H, H-3b, dd, $^2J_{3b,3a}$ = 10.9 Hz, $^3J_{3b,2}$ = 6.3 Hz), 1.45 (9 H, H-6, s), 1.32 (6 H, H-8, H-10, t, $^3J_{8,7} = {}^3J_{10,9}$ = 7.1 Hz), 1.15 (3 H, H-1, d, $^3J_{5,4}$ = 6.8 Hz).
^{13}C-NMR: (126 MHz, $CDCl_{3z}$, 298 K) δ [ppm] =156.5 (C-4), 79.9 (C-5), 67.8 (C-3), 64.4 (C-7, C-9), 48.9 (C-2), 28.5 (C-6), 17.5 (C-8, C-10), 14.4 (C-1).

MS (ESI (+), Dichloromethane, M = $C_{25}H_{33}NO_3$) m/z = 270.132 $[M+K^+]^+$.

Synthesis of oxazolidinone byproduct 30
Isolated during the synthesis of **31a** when a strong base like NaH is used.

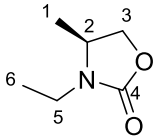

Yield: 50%

Molecular weight: $C_6H_{12}NO_3$, 129.159 0g/mol

^{1}H-NMR: (500 MHz, Acetone-d_6, 298 K) δ [ppm] = 4.37 (t, 1 H, H-3a, $^3J_{3a,2}$= 8.3 Hz), 3.96 (m, 1 H, H-2), 3.76 (dd, 1 H, H-3b, $^3J_{3b,2}$= 7.0 Hz), 3.41-3.31 (m, 2 H, H-5a), 3.16-3.06 (m, 1 H, H-5b), 1.25 (d, 3 H, H-1, $^3J_{1,2}$= 6.1 Hz), 1.09 (t, 3 H, H-6, $^3J_{6,5}$= 7.2 Hz).

^{13}C-NMR: (146 MHz, Acetone-d_6, 298 K) δ [ppm] = 162.8 (C-4), 69.4 (C-3), 51.2 (C-2), 36.8 (C-5), 28.2 (C-1), 12.9 (C-6).

MS (ESI (+), Dichloromethane, M = $C_6H_{11}NO_2$) m/z = 130.086 $[M+H^+]^+$.

Synthesis of 43

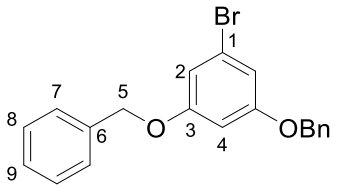

The synthetic protocol was adapted from the literature.[185]

Benzyl chloride (140 µL, 1.01 mmol, 2. 00eq.) was added dropwise to a suspension of bromo resorcinol (100 mg, 0.5 mmol, 1.00 eq), KI (42 mg, 0.25 mmol, 0.50 eq.) and anhydrous K_2CO_3 (280 mg, 2.02 mmol, 4.00 eq.) in dry acetone (5 mL). This mixture was kept refluxed under argon atmosphere for 16 h. Afterwards, the mixture was directly poured into water (20 mL). This was then extracted with DCM (4x 20 mL). The resulting combined organic phase was dried over Na_2SO_4 before removal of the solvent. The product was obtained as a pale-yellow oil (168 mg, 0.45 mmol, 90%).

Yield: 90%

Molecular weight: $C_{20}H_{17}BrO_2$, 369.2580 g/mol

^{1}H-NMR: (500 MHz, acetone-d_6, 298 K) δ [ppm] = 7.49-7.46 (m, 4H, H-8), 7.42-7.38 (m, 4 H, H-7), 7.37-7.31 (m, 2 H, H-9), 6.81 (d, 2 H, H-2, $^4J_{2,4}$ = 2.2 Hz), 6.68 (t, 1 H, H-4, $^4J_{4,2}$ = 2.2 Hz), 5.13 (s, 4 H, H-5).

Synthesis of 44e

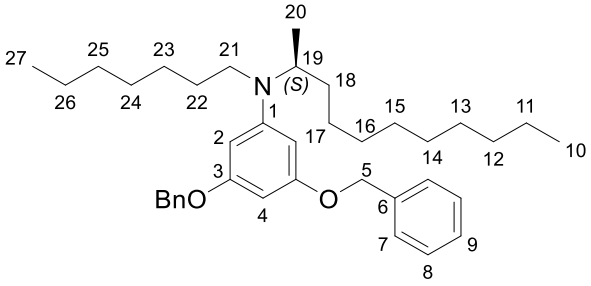

The synthetic protocol was adapted from the literature.[158]

Reaction was performed under Schlenk-conditions.

RuPhos precatalyst (0.4 mg, 0.01 mmol, 0.5 mol%), RuPhos (0.5 mg, 0.01 mmol, 0.5 mol%), 1.0 mmol (if solid) **43** (57 mg, 0.15 mmol, 1.00 eq.) and secondary amine **22e** (50 mg, 0.18 mmol, 1.20 eq.) and Cs_2CO_3 (72 mg, 0.18 mmol, 1.20 eq.) were dissolved in tert-buthanol (1 mL). The reaction mixture was heated to 85 ºC and the reaction mixture was stirred vigorously for 16 h under argon athmosphere. The reaction mixture was then cooled to room temperature, diluted with ethyl acetate (1 mL), washed with water (3 mL), dried over Na_2SO_4, concentrated in vacuo. Traces of the product were found in both NMR and MS.

Molecular weight: $C_{37}H_{53}NO_3$, 559.8350g/mol

^{1}H-NMR: (400 MHz, $CDCl_3$, 298 K) δ [ppm] = 7.51-7.45 (m, 4 H, Benzyl-H), 7.42-7.33 (m, 6 H, Benzyl-H), 6.81 (s, 2 H, H-2), 6.68 (s, 1 H, H-4), 5.13 (s, 4 H, H-5), 3.44-3.35, 3.27-3.21, 2.84-2.75, 2.63-2.51, 1.60-1.48, 1.47-1.40, 1.37-1.25, 0.93 (d, 3 H, H-20) 0.89-0.85 (m, 6 H, H-10, H-27)

MS (ESI (+), Dichloromethane, M = $C_{37}H_{53}NO_3$) m/z = 560.410 $[M+H^+]^+$, 272.294 $[M-C_{20}H_{16}O_2+H^+]^+$.

ESI HRMS: calculated for $[C_{37}H_{54}NO_3^+]^+$: *m/z* = 560.4098, found: *m/z* = 560.4098.

Synthesis of N-Benzyl-L-alaninol (38):

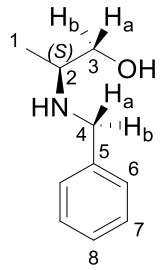

The synthetic protocol was adapted from the literature.[186]

L-Alaninol **24** (10.00 g, 133.14 mmol, 1.00 eq.) was dissolved in dry ethanol (100 mL) and benzaldehyde (13.6 mL, 133.14 mmol, 1.00 eq.) was added dropwise. The reaction was stirred at r.t. for 2.5 h and cooled to 0 °C before sodium borohydride was added portion wise over a period of 15 min. The reaction mixture was allowed to warm to r.t. and was stirred at this temperature for 20 h. After TLC-control indicated complete conversion of the start material, the reaction mixture was cooled with an ice-bath before water (20 mL) and CH_2Cl_2 (20 mL) were added. The suspension was stirred for additional 3 h at r.t. and filtered afterwards. The collected precipitate was washed with additional CH_2Cl_2 (3 x 50 mL) and the volume of the combined filtrates was reduced to 50 mL under reduced pressure. The resulting solution was diluted with water (20 mL), extracted with CH_2Cl_2 (4 x 20 mL) and dried with Na_2SO_4. The solvent was removed under reduced pressure and the product **38** was obtained as a colorless oil that solidified within 4 h at r.t (17.6 g, 106.51 mmol, 80% — 22.0 g, 133.14 mmol, quant.).

Yield: 80%—quant.

Molecular weight: $C_{10}H_{15}NO$, 165.236 g/mol

^{1}H-NMR: (500 MHz, acetone-d_6, 298 K) δ [ppm] = 7.36 (d, 2 H, H-6, H-6‘,$^3J_{6(6'),7(7')}$= 6.8 Hz), 7.29 (dd, 2 H, H-7, H-7‘, $^3J_{7(7'),8}$= 8.5 Hz, $^3J_{6(6'),7(7')}$= 6.8 Hz), 7.21 (t, 1 H, H-8, $^3J_{7(7'),8}$= 7.3 Hz), 3.85 (d, 1 H, H-4a, $^2J_{4a,4b}$= 13.3 Hz), 3.73 (d, 1 H, H-4b, $^2J_{4b,4a}$= 13.3 Hz), 3.48 (dd, 1 H, H-3a, $^2J_{3a,3b}$= 10.4 Hz, $^3J_{3a,2}$= 4.7 Hz), 3.32 (dd, 1 H, H-3b, $^2J_{3b,3a}$= 10.3 Hz, $^3J_{3b,2}$= 6.8 Hz), 2.74 (qd, 1 H, H-2, $^3J_{2,1}$= 6.5 Hz, $^3J_{2,3a}$= 4.7 Hz), 1.02 (d, 3 H, H-1, $^3J_{1,2}$= 6.4 Hz).

^{13}C-NMR: (126 MHz, chloroform-d_1, 298 K) δ [ppm] = 142.6 (C-5), 129.1 (C-7, C-7‘), 128.9 (C-6, C-6‘), 127.5 (C8), 66.8 (C-3), 55.1 (C-2), 51.9 (C-4), 17.6 (C-1).

MS: (ESI(+), dichloromethane, M = $C_{10}H_{15}NO$) *m/z* = 166.123 $[M+H]^+$, 91.055 $[C_7H_7^{+\bullet}]^+$

ESI HRMS: $[M+H]^+ = C_{10}H_{16}NO^+$, calculated for $[C_{10}H_{16}NO]^+$: *m/z* = 166.1227, found: *m/z* = 166.1226.

The NMR-measurements were performed in another solvent compared to the literature.[186]

General procedure for the Synthesis of N-benzyl-N-alkyl-L-alaninyl alkyl ethers 39

N-benzyl-L-alaninol **38** (1.00 eq.) is dissolved in abs. THF (2.5 mL/mmol) and added to an ice-cooled suspension of sodium hydride (1.20-2.00 eq/functional group., 60 wt-% in mineral oil) in abs THF under argon atmosphere dropwise. The reaction mixture is slowly warmed to r.t. and further stirred at this temperature for 45 min–1 h. Afterwards the appropriate alkyl iodide (1.20-2.00 eq/functional group.) is added dropwise. The resulting suspension is refluxed until TLC monitoring revealed complete consumption of the starting material. Then the reaction is cooled with an ice-bath before water is added. The organic solvent is removed under reduced pressure and the residue is taken up in water and extracted with CH_2Cl_2 (4 x 2.5 mL/mmol). The combined organic phases are washed with brine and dried with Na_2SO_4. The solvent is removed under reduced pressure and the crude product is purified by column chromatography on silica gel (eluent cyclohexane/ethyl acetate in different mixtures). The *N*-benzyl-*N*-alkyl-L-alaninyl ethers **39** are obtained as colorless oils. As a major byproduct the monoalkylated *N*-benzyl-L-alaninyl ethers 47 and in one case also *N*-benzyl,*N*-propyl-L-alaninol **48b** can also be obtained as a byproduct. These can in turn be used to synthesis the non-uniform *N*-benzyl-*N*-alkyl-L-alaninyl ethers where a different alkyl chain is introduced to the nitrogen in a follow-up alkylation.

Synthesis of N-benzyl-N-ethyl-L-alaninyl ethyl ether (39a)

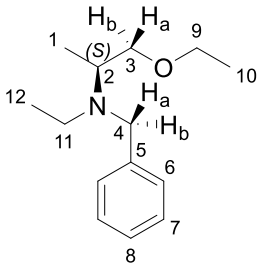

The synthesis was performed according to the general procedure for the synthesis of *N*-benzyl-*N*-alkyl-L-alaninyl alkyl ethers **39** using *N*-benzyl-L-alaninol **38** (2.00 g, 1.00 eq, 12.10 mmol), NaH (60 wt-% in mineral oil, 1.94 g, 4.00 eq, 48.45 mmol) and ethyl iodide (3.9 mL, 4.01 eq., 48.51 mmol) in THF (30 mL) and was refluxed for 72 h. Purification via column chromatography on silica gel (eluent cyclohexane/ethyl acetate 2:1 (v:v) gave the desired product **39a** as a colorless oil (2.36 g, 10,65 mmol, 88 %).

Yield: 88%.

Molecular weight: $C_{14}H_{23}NO$, 221,344 g/mol

^{1}H-NMR: (500 MHz, acetone-d_6, 298 K) δ [ppm] = 7.37 (ddt, 2 H, H-6, H-6‘,$^3J_{6(6'),7(7')}$= 6.8 Hz), 7.30-7.25 (m, 2 H, H-7, H-7’), 7.21-7.19 (m, 1 H, H-8), 3.72 (d, 1 H, H-4a, $^2J_{4a,4b}$= 14.4 Hz), 3.59 (d, 1 H, H-4b, $^2J_{4b,4a}$= 14.4 Hz), 3.52 (dd, 1 H, H-3a, $^2J_{3a,3b}$= 9.4 Hz, $^3J_{3a,2}$= 5.5 Hz),3.42 (qd, 2 H, H-9, $^3J_{9,10}$= 7.0 Hz) 3.31 (dd, 1 H, H-3b, $^2J_{3b,3a}$= 9.4 Hz, $^3J_{3b,2}$= 6.9 Hz), 2.99 (pd, 1 H, H-2, $^3J_{2,1}$= 6.7 Hz, $^3J_{2,3a}$= 5.5 Hz), 2.54 (qq, 2 H, H-11, $^3J_{11,12}$= 7.1 Hz), 1.12 (t, 3 H, H-10, $^3J_{10,9}$= 7.0 Hz), 1.03 (d, 3 H, H-1, $^3J_{1,2}$= 6.7 Hz), 0.98 (t, 3 H, H-12, $^3J_{12,11}$= 7.1 Hz).

^{13}C-NMR: (126 MHz, acetone-d_6, 298 K) δ [ppm] = 142.6 (C-5), 129.1 (C-6, C-6‘), 128.8 (C-7, C-7‘), 127.2 (C8), 74.2 (C-3), 66.7 (C-9), 54.9 (C-4), 54.6 (C-2), 44.9(C-11), 15.6 (C-10), 14.7 (C-12), 13.1 (C-1).

MS: (ESI(+), dichloromethane, M = $C_{14}H_{23}NO$) *m/z* = 222.185 $[M+H]^+$.

ESI HRMS: calculated for $[C_{14}H_{24}NO]^+$: *m/z* = 222.1852, found: *m/z* = 222.1850.

Synthesis of N-benzyl-N-propyl-L-alaninyl propyl ether (39b)

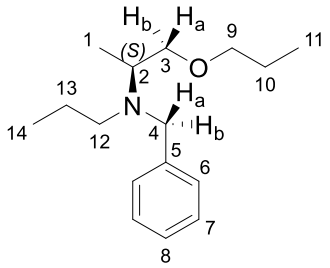

The synthesis was performed according to the general procedure for the synthesis of *N*-benzyl-*N*-alkyl-L-alaninyl alkyl ethers **39** using *N*-benzyl-L-alaninol **38** (2.00 g, 1.00 eq, 12.10 mmol), NaH (60 wt-% in mineral oil, 1.16 g, 2.40 eq, 29.07 mmol) and *n*-propyl iodide (4.7 mL, 4.01 eq., 48.51 mmol) in THF (30 mL) and was refluxed for 48 h. Purification via column chromatography on silica gel (eluent cyclohexane/ethyl acetate 4:1 (v:v) gave the desired product **39b** as a colorless oil (785 mg, 3.15 mmol, 26%).

Additionally, the monoalkylated amine **48b** was isolated (839 mg, 4.04 mmol, 33%) as a colorless oil.

Yield 5b: 26%.

Molecular weight: $C_{16}H_{27}NO$, 249.398g/mol

^{1}H-NMR: (700 MHz, acetone-d_6, 298 K) δ [ppm] = 7.39-7.36 (m, 2 H, H-6, H-6‘,$^3J_{6(6'),7(7')}$= 6.8 Hz), 7.30-7.25 (m, 2 H, H-7, H-7’), 7.21-7.19 (m, 1 H, H-8), 3.73 (d, 1 H, H-4a, $^2J_{4a,4b}$= 14.3 Hz), 3.60 (d, 1 H, H-4b, $^2J_{4b,4a}$= 14.3 Hz), 3.52 (dd, 1 H, H-3a, $^2J_{3a,3b}$= 9.4 Hz, $^3J_{3a,2}$= 5.7 Hz),3.32 (dddd, 3 H, H-3b, H 9, $^2J_{3b,3a}$= 9.4 Hz, $^3J_{3b,2}$= 6.2 Hz), 2.97 (pd, 1 H, H-2, $^3J_{2,1}$= 6.7 Hz, $^3J_{2,3a}$= 5.7 Hz), 2.52-2.44 (m, 2 H, H-12), 1.54 (dtd, 2 H, H-10, $^3J_{10,9}$= 6.4 Hz, $^3J_{12,11}$= 7.1 Hz), 1.41 (h, 2 H, H-13, $^3J_{13,12}$= 7.4 Hz, $^3J_{13,14}$= 7.4 Hz), 1.03 (d, 3 H, H-1, $^3J_{1,2}$= 6.7 Hz), 0.90 (t, 3 H, H-11, $^3J_{11,10}$= 7.4 Hz), 0.80 (t, 3 H, H-1,4 $^3J_{14,13}$= 7.4 Hz).

^{13}C-NMR: (176 MHz, acetone-d_6, 298 K) δ [ppm] = 142.7(C-5), 129.2 (C-6, C-6‘), 128.8 (C-7, C-7‘), 127.3 (C8), 74.4 (C-3), 73.3 (C-9),55.6 (C-4), 54.7 (C-2), 52.9 (C-12), 23.8(C-10), 22.6 (C-13), 13.0 (C-1), 12.0 (C-14), 11.0 (C-11).

MS: (ESI(+), dichloromethane, M = $C_{16}H_{27}NO$) *m/z* = 250.216 $[M+H]^+$.

ESI HRMS: calculated for $[C_{16}H_{27}NO]^+$: *m/z* = 250.2165, found: *m/z* = 250.2158.

Synthesis of N-benzyl-N-propyl-L-alaninyl amine (48b)

Isolated during the synthesis of **39b**.

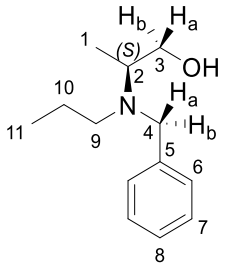

Yield: 33%

Molecular weight: $C_{13}H_{21}NO$, 207.317g/mol

^{1}H-NMR: (500 MHz, acetone-d_6, 298 K) δ [ppm] = 7.37-7.33 (m, 2 H, H-6, H-6‘), 7.32-7.28 (m, 2 H, H-7, H-7’), 7.24-7.20 (m, 1 H, H-8), 3.79 (d, 1 H, H-4a, $^{2}J_{4a,4b}$= 13.0 Hz), 3.49-3.42 (m, 2 H, H-3a, H-4b), 3.31 (m, 1 H, H-3b), 2.90 (dddd, 1 H, H-2, $^{3}J_{2,1}$= 6.7 Hz, $^{3}J_{2,3a}$= 5.7 Hz), 2.43 (m, 2 H, H-9), 1.55-1.36 (m, 2 H, H-10), 0.96 (d, 3 H, H-1, $^{3}J_{1,2}$= 6.7 Hz), 0.83 (t, 3 H, H-11, $^{3}J_{11,10}$= 7.4 Hz).

^{13}C-NMR: (126 MHz, acetone-d_6, 298 K) δ [ppm] = 141.7(C-5), 129.5 (C-6, C-6‘), 129.0 (C-7, C-7‘), 127.5 (C-8), 64.0 (C-3), 56.5 (C-2), 54.6 (C-4), 51.8 (C-9), 22.4(C-10), 12.0 (C-11), 10.1 (C-1).

MS: (ESI(+), dichloromethane, M = $C_{13}H_{21}NO$) *m/z* = 208.169 $[M+H]^+$.

ESI HRMS: calculated for $[C_{13}H_{21}NO]^+$: *m/z* = 208.1696, found: *m/z* = 208.1690.

Synthesis of N-benzyl-N-butyl-L-alaninyl butyl ether (5c)

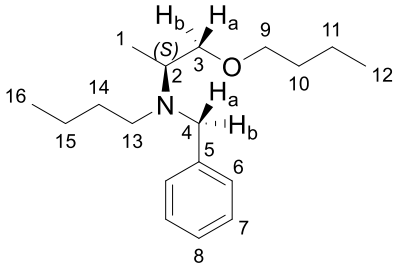

The synthesis was performed according to the general procedure for the synthesis of *N*-benzyl-*N*-alkyl-L-alaninyl alkyl ethers **39** using *N*-benzyl-L-alaninol **38** (10.00 g, 1.00 eq, 60.45 mmol), NaH (5.90 g, 2.40 eq, 145.08 mmol) and *n*-butyl iodide (27.5 mL, 4.00 eq., 241.81 mmol) in THF (150 mL) and was refluxed for 72 h. Purification via column chromatography on silica gel (eluent cyclohexane/ethyl acetate 4:1 (v:v) gave the desired product **39c** as a colorless oil (5.69 g, 20.52 mmol, 34%). Additionally, the monoalkylated ether **47c** was isolated (5.37 g, 24.28 mmol, 40%) as a colorless oil.

Yield: 34%

Molecular weight: $C_{17}H_{29}NO$, 277.452 g/mol

^{1}H-NMR: (500 MHz, acetone-d_6, 298 K) δ [ppm] = 7.37 (dtt, 2 H, H-6, H-6‘,$^{3}J_{6(6'),7(7')}$= 7.3 Hz), 7.30-7.25 (m, 2 H, H-7, H-7’), 7.21-7.17 (m, 1 H, H-8), 3.72 (d, 1 H, H-4a, $^{2}J_{4a,4b}$= 14.3 Hz), 3.59 (d, 1 H, H-4b, $^{2}J_{4b,4a}$= 14.3 Hz), 3.52 (dd, 1 H, H-3a, $^{2}J_{3a,3b}$= 9.4 Hz, $^{3}J_{3a,2}$= 5.7 Hz), 3.37 (td, 2H. H-9, J=6.4Hz, J=1.4 Hz), 3.32 (dd, 1 H, H-3b, $^{2}J_{3b,3a}$= 9.4 Hz, $^{3}J_{3b,2}$= 6.7 Hz), 2.96 (pd, 1 H, H-2, $^{3}J_{2,1}$= $^{3}J_{2,3b}$= 6.7 Hz, $^{3}J_{2,3a}$= 5.7 Hz), 2.57-2.44 (m, 2 H, H-13), 1.54-1.47 (m, 2 H, H-10), 1.43-1.34 (m, 4 H, H-11, H-14), 1.33-1.24 (m, 2 H, H-15), 1.02 (d, 3 H, H-1, $^{3}J_{1,2}$= 6.7 Hz), 0.90 (t, 3 H, H-12, $^{3}J_{12,11}$= 7.4 Hz), 0.82 (t, 3 H, H-16, $^{3}J_{16,15}$= 7.3 Hz).

^{13}C-NMR: (126 MHz, acetone-d_6, 298 K) δ [ppm] = 142.6 (C-5), 129.2 (C-6, C-6‘), 128.8 (C-7, C-7‘), 127.2 (C8), 74.2 (C-3), 71.3 (C-9), 55.5 (C-4), 54.5 (C-2), 50.5 (C-13), 32.8 (C-10), 31.8 (C-14), 20.9 (C-15), 20.1 (C-11), 14.3 (C-12), 14.2 (C-16), 12.9 (C-1).

MS: (ESI(+), dichloromethane, M = $C_{18}H_{31}NO$) *m/z* = 278.248 $[M+H]^+$.

ESI HRMS: calculated for $[C_{18}H_{31}NO]^+$: *m/z* = 278.2478, found: *m/z* = 278.2478.

Synthesis of N-benzyl-L-alaninyl butyl ether (47c)

Isolated during the synthesis of **39c**.

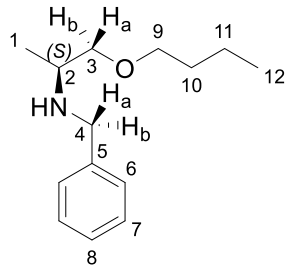

Yield : 40%

Molecular weight: $C_{14}H_{23}NO$, 207.317g/mol

^{1}H-NMR: (400 MHz, acetone-d_6, 298 K) δ [ppm] = 7.37-7.33 (m, 2 H, H-6, H-6‘), 7.32-7.26 (m, 2 H, H-7, H-7’), 7.23-7.18 (m, 1 H, H-8) 3.85 (d, 1 H, H-4a, $^2J_{4a,4b}$= 13.4 Hz), 3.74 (d, 1 H, H-4b, $^2J_{4b,4a}$= 13.4 Hz), 3.46-3.35 (m, 2 H, H-9), 3.30 (dd, 2 H, H-3a, H-3b, $^3J_{2,3a}$= 5.9 Hz), 2.93-2.84 (m, 1 H, H-2), 1.55-1.45 (m, 2 H, H-10),1.40-1.32 (m, 2 H, H-10), 1.01 (d, 3 H, H-1, $^3J_{1,2}$= 6.4 Hz), 0.89 (t, 3 H, H-12, $^3J_{12,11}$= 7.4 Hz).

^{13}C-NMR: (100 MHz, acetone-d_6, 298 K) δ [ppm] = 142.3(C-5), 129.0 (C-7, C-7‘), 128.9 (C-6, C-6‘), 127.4 (C-8), 76.0 (C-3), 71.3 (C-9), 52.7 (C-2), 51.7 (C-4), 32.6 (C-10), 20.0 (C-11), 17.7 (C-1), 14.2 (C-12).

MS: (ESI(+), dichloromethane, M = $C_{14}H_{23}NO$) *m/z* = 222.185 $[M+H]^+$.

ESI HRMS: calculated for $[C_{14}H_{23}NO]^+$: *m/z* = 222.1852, found: *m/z* = 222.1846.

Synthesis of N-benzyl-N-pentyl-L-alaninyl pentyl ether (39d)

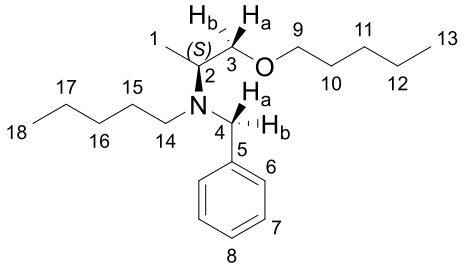

The synthesis was performed according to the general procedure for the synthesis of *N*-benzyl-*N*-alkyl-L-alaninyl alkyl ethers **39** using *N*-benzyl-L-alaninol **38** (1.00 g, 1.00 eq, 6,05 mmol), NaH (970 mg, 4.00 eq, 24.22 mmol) and *n*-pentyl iodide (3.17 mL, 4.00 eq., 24.21 mmol) in THF (75 mL) and was refluxed for 70 h. Purification via column chromatography on silica gel (eluent cyclohexane/ethyl acetate 4:1 (v:v) gave the desired product **39d** as a colorless oil (795 mg, 2.60 mmol, 43%).

Yield: 43%.

Molecular weight: $C_{20}H_{35}NO$, 305.506 g/mol

^{1}H-NMR: (500 MHz, acetone-d_6, 298 K) δ [ppm] = 7.40-7.34 (m, 2 H, H-6), 7.32-7.24 (m, 2 H, H-7, H-7’), 7.22-7.15 (m, 1 H, H-8), 3.73 (d, 1 H, H-4a, $^2J_{4a,4b}$= 14.3 Hz), 3.59 (d, 1 H, H-4b, $^2J_{4b,4a}$= 14.3 Hz), 3.52 (dd, 1 H, H-3a, $^2J_{3a,3b}$= 9.4 Hz, $^3J_{3a,2}$= 5.8 Hz),3.37 (td, 2 H, H-9, $^3J_{9,10}$= 6.5 Hz, $^3J_{9,10}$= 1.0 Hz) 3.31 (dd, 1 H, H-

3b, $^{2}J_{3b,3a}$= 9.4 Hz, $^{3}J_{3b,2}$= 6.6 Hz), 2.99 (pd, 1 H, H-2, $^{3}J_{2,1}$= 6.6 Hz, $^{3}J_{2,3b}$= 6.6 Hz), 2.57-2.43 (m, 2 H, H-14), 1.60-1.48 (m, 2 H, H-10), 1.45-1.36 (m, 2 H, H-15), 1.37-1.31 (m, 4 H, H-11, H-12), 1.31-1.19 (m, 4 H, H-16, H-17), 1.02 (d, 3 H, H-1, $^{3}J_{1,2}$= 6.7 Hz), 0.82 (t, 3 H, H-16, $^{3}J_{16,15}$= 7.3 Hz), 0.89 (m, 3 H, H-13), 0.85 (m, 3 H, H-18).

^{13}C-NMR: (126 MHz, acetone-d_6, 298 K) δ [ppm] = 142.6 (C-5), 129.2 (C-6, C-6‘), 128.8 (C-7, C-7‘), 127.2 (C-8), 74.2 (C-3), 71.4 (C-9), 55.4 (C-4), 54.5 (C-2), 50.8 (C-14), 30.3* (C-10), 30.2* (C-15), 29.3* (C-11, C-16), 23.2 (C-12, C-17), 14.4 (C-13, C-18), 12.9 (C-1).

*Signals partially covered by signal of residual non deuterated solvent.

MS: (ESI(+), dichloromethane, M = $C_{20}H_{35}NO$) *m/z* = 306.278 $[M+H]^+$.

ESI HRMS: calculated for $[C_{20}H_{36}NO]^+$: *m/z* = 306.2791, found: *m/z* = 306.2785

Synthesis of N-benzyl -L-alaninyl pentyl ether (47d)

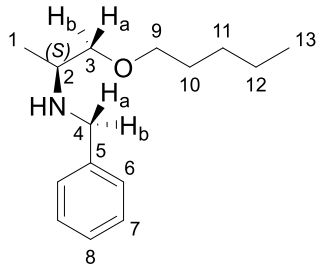

The synthesis was performed according to the general procedure for the synthesis of *N*-benzyl-*N*-alkyl-L-alaninyl alkyl ethers **39** using *N*-benzyl-L-alaninol **38** (5.00 g, 1.00 eq, 30.26 mmol), NaH (4.84 g, 4.00 eq, 121.04 mmol) and *n*-pentyl iodide (9.0 mL, 2.27 eq., 68.71 mmol) in THF (75 mL) and was refluxed for 70 h. Purification via column chromatography on silica gel (eluent cyclohexane/ethyl acetate 4:1 (v:v) gave the desired product **47d** as a colorless oil (3.82 g,16.24 mmol, 54%).

Yield: 54%.

Molecular weight: $C_{15}H_{25}NO$, 235.371 g/mol

^{1}H-NMR: (700 MHz, acetone-d_6, 298 K) δ [ppm] = 7.37-7.33 (m, 2H, H-6, H-6’), 7.33-7.26 (m, 2 H, H-7, H-7’), 7.22-7.18 (m, 1 H, H-8), 3.85 (d, 1 H, H-4a, $^{2}J_{4a,4b}$= 13.4 Hz), 3.74 (d, 1 H, H-4b, $^{2}J_{4b,4a}$= 13.4 Hz), 3.43-3.35 (m, 2 H, H-9), 3.33-3.27 (m, 2 H, H-3a, H-3b), 2.87 (pd, 1 H, H-2, $^{3}J_{2,1}$= 6.4), 1.56-1.51 (m, 2 H, H-10), 1.32 (h, 4 H, H-11, H-12), 1.01 (d, 3 H, H-1, $^{3}J_{1,2}$= 6.4 Hz), 0.91-0.86 (m, 3 H, H-15).

^{13}C-NMR: (176 MHz, chloroform-d_1, 298 K) δ [ppm] = 142.6 (C-5), 129.0 (C-7, C-7‘), 128.8 (C-6, C-6‘), 127.4 (C-8), 76.1 (C-3), 71.6 (C-9), 52.8 (C-2), 51.9 (C-4), 30.2* (C-10), 29.2* (C-11), 23.3 (C-12), 17.8 (C-1), 14.3 (C-13).

*Signals partially covered by signal of residual non deuterated solvent.

APCI: (ESI(+), dichloromethane, M = $C_{15}H_{25}NO$) *m/z* = 236.201 $[M+H]^+$.

ESI HRMS: calculated for $[C_{15}H_{26}NO]^+$: *m/z* = 236.2009, found: *m/z* = 236.2010.

Synthesis of N-benzyl-N-heptyl-L-alaninyl heptyl ether (39e)

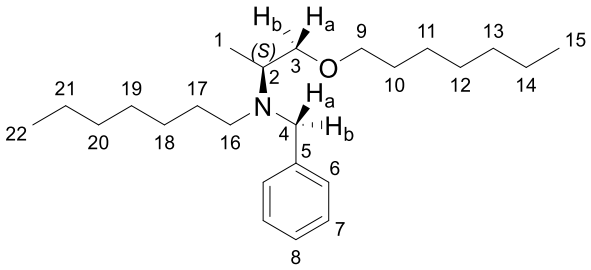

The synthesis was performed according to the general procedure for the synthesis of *N*-benzyl-*N*-alkyl-L-alaninyl alkyl ethers **39** using *N*-benzyl-L-alaninol **38** (5.00 g, 1.00 eq, 30.23 mmol), NaH (60 wt% in mineral oil, 1.74 mg, 2.40 eq, 72.55 mmol) and *n*-heptyl iodide (20.9 mL, 4.00 eq., 120.90 mmol) in THF (75 mL) and was stirred at r.t. for 14 d. Purification via column chromatography on silica gel (eluent cyclohexane/ethyl acetate 9:1 (v:v) gave the desired product **39e** as a colorless oil (4.31 mg, 12.00 mmol, 40%). Additionally, the monoalkylated ether **47e** was isolated (4.15 g, 11.49 mmol, 38%) as a colorless oil.

Yield: 40%.

Molecular weight: $C_{24}H_{43}NO$, 361,614 g/mol

^{1}H-NMR: (500 MHz, acetone-d_6, 298 K) δ [ppm] = 7.39-7.35 (m, 2H, H-6, H-6'), 7.30-7.25 (m, 2 H, H-7, H-7'), 7.21-7.19 (m, 1 H, H-8), 3.73 (d, 1 H, H-4a, $^2J_{4a,4b}$= 14.3 Hz), 3.58 (d, 1 H, H-4b, $^2J_{4b,4a}$= 14.3 Hz), 3.52 (dd, 1 H, H-3a, $^2J_{3a,3b}$= 9.4 Hz, $^3J_{3a,2}$= 5.8 Hz),3.37 (t, 2 H, H-9, $^3J_{9,10}$= 6.4 Hz) 3.32 (dd, 1 H, H-3b, $^2J_{3b,3a}$= 9.4 Hz, $^3J_{3b,2}$= 6.5 Hz), 3.02-2.93 (m, 1 H, H-2), 2.57-2.44 (m, 2 H, H-16), 1.58-1.49 (m, 2 H, H-10) 1.45-1.17 (m, 18 H, H-11, H-12, H-13, H-14, H-17, H-18, H-19, H-20, H-21), 1.02 (d, 3 H, H-1, $^3J_{1,2}$= 6.7 Hz), 0.87 (dt, 6 H, H-15, H-22, $^3J_{15,14}$= $^3J_{22,11}$= 7.0 Hz).

^{13}C-NMR: (126 MHz, chloroform-d_1, 298 K) δ [ppm] = 142.6 (C-5), 129.2 (C-6, C-6'), 128.8 (C-7, C-7'), 127.2 (C-8), 74.4 (C-3), 71.6 (C-9), 55.5 (C-4), 54.4 (C-2), 50.8 (C-16), 32.7 (C-13), 32.6 (C-20), 30.6 (C-10), 30.0 (C-12, C-17), 29.8* (C-19), 29.4* (C-17), 27.9 (C-11), 27.0 (C-18), 23.3 (C-14, C-21), 14.4 (C15, C-22), 12.9 (C-1).

*Signals partially covered by signal of residual non deuterated solvent.

MS: (ESI(+), dichloromethane, M = $C_{24}H_{43}NO$) *m/z* = 362.342 $[M+H]^+$.

ESI HRMS: calculated for $[C_{24}H_{44}NO]^+$: *m/z* = 362.3417, found: *m/z* = 362.3420.

Synthesis of N-benzyl -L-alaninyl heptyl ether (47e)

Isolated during the synthesis of **39e**.

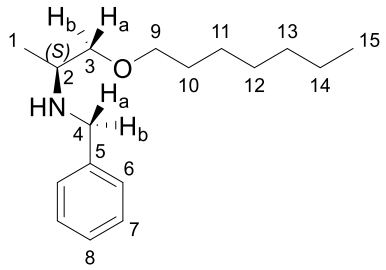

Yield: 38%.

Molecular weight: $C_{17}H_{29}NO$, 263.425 g/mol

^{1}H-NMR: (500 MHz, acetone-d_6, 298 K) δ [ppm] = 7.37-7.33 (m, 2H, H-6, H-6'), 7.33-7.26 (m, 2 H, H-7, H-7'), 7.24-7.19 (m, 1 H, H-8), 3.85 (d, 1 H, H-4a, $^2J_{4a,4b}$= 13.3 Hz), 3.74 (d, 1 H, H-4b, $^2J_{4b,4a}$= 13.3 Hz), 3.44-3.35 (m, 2 H, H-9), 3.34-3.26 (m, 2 H, H-3a, H-3b), 2.86 (pd, 1 H, H-2, $^3J_{2,1}$= 6.4), 1.57-1.48 (m, 2 H, H-10), 1.38-1.22 (m, 6 H, H-11, H-12, H-13, H-14), 1.01 (d, 3 H, H-1, $^3J_{1,2}$= 6.4 Hz), 0.91-0.84 (m, 3 H, H-15).

^{13}C-NMR: (126 MHz, chloroform-d_1, 298 K) δ [ppm] = 142.5 (C-5), 129.0 (C-7, C-7'), 128.8 (C-6, C-6'), 127.3 (C-8), 76.1 (C-3), 71.6 (C-9), 52.8 (C-2), 51.8 (C-4), 32.6 (C-13), 30.6* (C-10), 29.8* (C-12), 27.6 (C-11), 23.3 (C-14), 17.8 (C-1), 14.3 (C15).

*Signals partially covered by signal of residual non deuterated solvent.

MS: (ESI(+), dichloromethane, M = $C_{17}H_{29}NO$) *m/z* = 264.232 $[M+H]^+$.

ESI HRMS: calculated for $[C_{17}H_{30}NO]^+$: *m/z* = 264.2322, found: *m/z* = 264.2315.

Synthesis of N-benzyl-N-octyl-L-alaninyl octyl ether (39f)

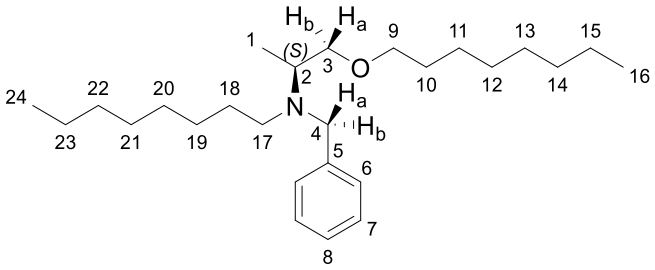

The synthesis was performed according to the general procedure for the synthesis of *N*-benzyl-*N*-alkyl-L-alaninyl alkyl ethers **39** using *N*-benzyl-L-alaninol **38** (2.00 g, 1.00 eq, 12.10 mmol), NaH (1.94 g, 4.00 eq, 48.45 mmol) and *n*-octyl iodide (8.4 mL, 4.01 eq., 48.51 mmol) in THF (30 mL) and was refluxed for 2 x 24 h. Purification via column chromatography on silica gel (eluent cyclohexane/ethyl acetate 4:1 (v/v) gave the desired product **39f** as a colorless oil (2.97 g,7.50 mmol, 62%). Additionally, the monoalkylated ether **47f** was isolated (471 mg, 1.21 mmol, 10%) as a colorless oil.

Yield: 62%.

Molecular weight: $C_{26}H_{47}NO$, 389.668 g/mol

^{1}H-NMR: (500 MHz, acetone-d_6, 298 K) δ [ppm] = 7.40-7.35 (m, 2 H, H-6, H6'), 7.30-7.24 (m, 2 H, H-7, H-7'), 7.21-7.16 (m, 1 H, H-8), 3.75-3.56 (m, 2 H, H-4a, H-4b), 3.52 (dd, 1 H, H-3a, $^{2}J_{3a,3b}$= 9.4 Hz, $^{3}J_{3a,2}$= 5.9 Hz),3.37 (t, 2 H, H-9, $^{3}J_{9,10}$= 6.4 Hz) 3.32 (dd, 1 H, H-3b, $^{2}J_{3b,3a}$= 9.4 Hz, $^{3}J_{3b,2}$= 6.5 Hz), 2.98 (td, 1 H, H-2, $^{3}J_{2,1}$= 6.7 Hz, $^{3}J_{2,3a}$= 6.0 Hz), 2.56-2.44 (m, 2 H, H-17), 1.58-1.49 (m, 2 H, H-10), 1.45-1.16 (m, 22 H, H-11, H-12, H-13, H-14, H-15, H-18, H-19, H-20, H-21, H-22, H-23), 1.02 (d, 3 H, H-1, $^{3}J_{1,2}$= 6.8 Hz), 0.92-0.82 (m, 6 H, H-16, H-24).

^{13}C-NMR: (126 MHz, acetone-d_6, 298 K) δ [ppm] = 142.6 (C-5), 129.2 (C-6, C-6'), 128.8 (C-7, C-7'), 127.2 (C-8), 74.4 (C-3), 71.6 (C-9), 55.5 (C-4), 54.6 (C-2), 50.8 (C-17), 32.6 (C-14), 32.5 (C-22), 30.6 (C-10), 30.0* (C-12, C-13, C-20, C-21), 29.4* (C-18), 27.9 (C-11), 27.1 (C-19), 23.3 (C-15, C-23), 14.4 (C-16, C-24), 12.9 (C-1).

*Signals partially covered by signal of residual non deuterated solvent.

MS: (ESI(+), dichloromethane, M = $C_{26}H_{47}NO$) *m/z* = 390.372 $[M+H]^+$.

ESI HRMS: calculated for $[C_{26}H_{48}NO]^+$: *m/z* = 390.3730, found: *m/z* = 390.3726.

Synthesis of N-benzyl -L-alaninyl octyl ether (47f)

Isolated during the synthesis of **39f**.

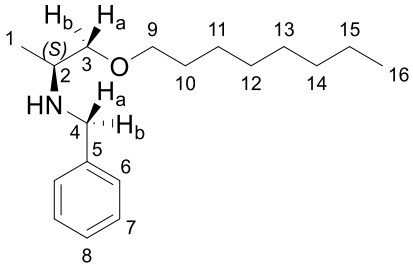

Yield: 10%.

Molecular weight: $C_{18}H_{31}NO$, 277.452 g/mol

^{1}H-NMR: (500 MHz, acetone-d_6, 298 K) δ [ppm] = 7.37-7.33 (m, 2H, H-6, H-6'), 7.33-7.26 (m, 2 H, H-7, H-7'), 7.24-7.19 (m, 1 H, H-8), 3.85 (d, 1 H, H-4a, $^{2}J_{4a,4b}$= 13.3 Hz), 3.74 (d, 1 H, H-4b, $^{2}J_{4b,4a}$= 13.3 Hz), 3.44-3.35 (m, 2 H, H-9), 3.34-3.26 (m, 2 H, H-3a, H-3b), 2.86 (pd, 1 H, H-2, $^{3}J_{2,1}$= 6.4), 1.57-1.48 (m, 2 H, H-10), 1.38-1.22 (m, 6 H, H-11, H-12, H-13, H-14), 1.01 (d, 3 H, H-1, $^{3}J_{1,2}$= 6.4 Hz), 0.91-0.84 (m, 3 H, H-15).

^{13}C-NMR: (126 MHz, chloroform-d_1, 298 K) δ [ppm] = 142.5 (C-5), 129.0 (C-7, C-7'), 128.8 (C-6, C-6'), 127.3 (C-8), 76.1 (C-3), 71.6 (C-9), 52.8 (C-2), 51.8 (C-4), 32.6 (C-14), 30.6* (C-10), 29.8* (C-12), 27.6 (C-11), 23.3 (C-15), 17.8 (C-1), 14.3 (C-16).

*Signals partially covered by signal of residual non deuterated solvent.

MS: (ESI(+), dichloromethane, M = $C_{14}H_{23}NO$) *m/z* = 278.248 $[M+H]^+$.

ESI HRMS: calculated for $[C_{14}H_{23}NO]^+$: *m/z* = 278.2478, found: *m/z* = 278.2481.

Synthesis of N-benzyl-N-nonyl-L-alaninyl nonyl ether (39g)

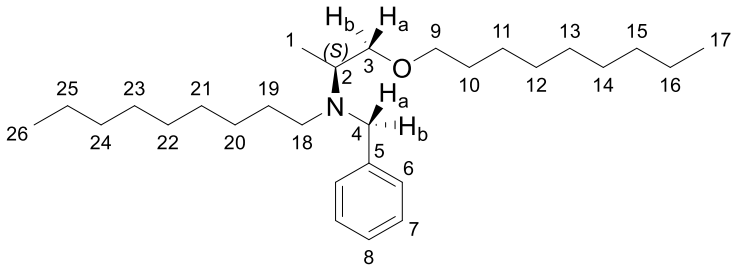

The synthesis was performed according to the general procedure for the synthesis of *N*-benzyl-*N*-alkyl-L-alaninyl alkyl ethers **39** using *N*-benzyl-L-alaninol **38** (1.00 g, 1.00 eq, 6.05 mmol), NaH (60 wt% in mineral oil, 440 mg, 1.80 eq, 10.89 mmol) and *n*-nonyl iodide (3.6 mL, 3.00 eq., 18.16 mmol) in THF (15 mL) and was heated to 60°C for 72 h. Purification via column chromatography on silica gel (eluent cyclohexane/ethyl acetate 19:1 (v:v) gave the desired product **39g** as a colorless oil (872 mg, 2.09 mmol, 34%). Additionally, the monoalkylated ether **47g** was isolated (952 mg, 3.27 mmol, 54%) as a colorless oil.

Yield: 34%.

Molecular weight: $C_{28}H_{51}NO$, 417,722 g/mol

H-NMR: (700 MHz, acetone-d_6, 298 K) δ [ppm] = 7.39-7.35 (m, 2 H, H-6, H6'), 7.27 (t, 2 H, H-7, H-7', $^3J_{7(7'),6(6')}=^3J_{7(7'),8}$= 7.6 Hz), 7.21-7.17 (m, 1 H, H-8), 3.73 (d, 1 H, H-4a, $^2J_{4a,4b}$= 14.3 Hz), 3.59 (d, 1 H, H-4b, $^2J_{4b,4a}$= 14.3 Hz), 3.52 (dd, 1 H, H-3a, $^2J_{3a,3b}$= 9.4 Hz, $^3J_{3a,2}$= 5.9 Hz), 3.38 (t, 2 H, H-9, $^3J_{9,10}$= 6.4 Hz) 3.32 (dd, 1 H, H-3b, $^2J_{3b,3a}$= 9.4 Hz, $^3J_{3b,2}$= 6.4 Hz), 2.98 (h, 1 H, H-2, $^3J_{2,1}$= 6.6 Hz), 2.56-2.46 (m, 2 H, H-18), 1.57-1.51 (m, 2 H, H-10), 1.46-1.35 (m, 2 H, H-19), 1.34-1.18 (m, 24 H, H-11, H-12, H-13, H-14, H-15, H-16, H-20, H-21, H-22, H-23, H-24, H-25), 1.02 (d, 3 H, H-1, $^3J_{1,2}$= 6.7 Hz), 0.88 (td, 6 H, H-17, H-26).

^{13}C-NMR: (176 MHz, acetone-d_6, 298 K) δ [ppm] = 142.7(C-5), 129.3 (C-6, C-6'), 128.8 (C-7, C-7'), 127.3 (C-8), 74.4 (C-3), 71.6 (C-9), 55.5 (C-4), 54.6 (C-2), 50.8 (C-18), 32.7 (C-15, C-24), 30.7, 30.6 (C-10), 30.4*# (C-12/C-13/ C-14/ C-21/ C-22/ C-23), 2x 30.3(C-12/C-13/ C-14/ C-21/ C-22/ C-23), 30.2*# (C-12/C-13/ C-14/ C-21/ C-22/ C-23), 29.8* (C-19), 27.9 (C-11), 27.1 (C-20), 23.4 (C-16, C-25), 14.4 (C-17, C-26), 12.9 (C-1).

*Signals partially covered by signal of residual non deuterated solvent. #unambiguous assignment not possible.

MS: (ESI(+), dichloromethane, M = $C_{28}H_{51}NO$) *m*/z = 418.404 $[M+H]^+$.

ESI HRMS: calculated for $[C_{28}H_{52}NO]^+$: *m/z* = 418.4043, found: *m/z* = 418.4038.

Synthesis of N-benzyl -L-alaninyl nonyl ether (47g)

Isolated during the synthesis of **39g**.

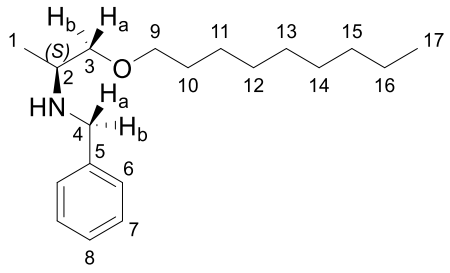

Yield: 54%.

Molecular weight: $C_{19}H_{33}NO$, 219,479 g/mol

^{1}H-NMR: (500 MHz, acetone-d_6, 298 K) δ [ppm] = 7.37-7.33 (m, 2H, H-6, H-6'), 7.32-7.27 (m, 2 H, H-7, H-7'), 7.23-7.19 (m, 1 H, H-8), 3.86 (d, 1 H, H-4a, $^2J_{4a,4b}$= 13.3 Hz), 3.74 (d, 1 H, H-4b, $^2J_{4b,4a}$= 13.3 Hz), 3.44-3.35 (m, 2 H, H-9), 3.34-3.26 (m, 2 H, H-3a, H-3b), 2.86 (pd, 1 H, H-2, $^3J_{2,1}$= 6.4), 1.57-1.48 (m, 2 H, H-10), 1.38-1.22 (m, 6 H, H-11, H-12, H-13, H-14), 1.01 (d, 3 H, H-1, $^3J_{1,2}$= 6.4 Hz), 0.91-0.84 (m, 3 H, H-15).

^{13}C-NMR: (126 MHz, chloroform-d_1, 298 K) δ [ppm] = 142.2 (C-5), 129.0 (C-7, C-7'), 128.9 (C-6, C-6'), 127.4 (C-8), 75.6 (C-3), 71.6 (C-9), 52.7 (C-2), 51.7 (C-4), 32.6 (C-13), 30.5* (C-10), 30.4*$^{\#}$ (C-13/ C-14), 29.8* (C-12), 27.0 (C-11), 23.3 (C-16), 17.6 (C-1), 14.3 (C-17).

*Signals partially covered by signal of residual non deuterated solvent. $^{\#}$unambiguous assignment not possible.

MS: (ESI(+), dichloromethane, M = $C_{19}H_{33}NO$) *m/z* = 292.262 $[M+H]^+$.

ESI HRMS: calculated for $[C_{19}H_{34}NO]^+$: *m/z* = 292.2635, found: *m/z* = 292.2638.

Synthesis of N-benzyl-N-nonyl-L-alaninyl butyl ether (39h)

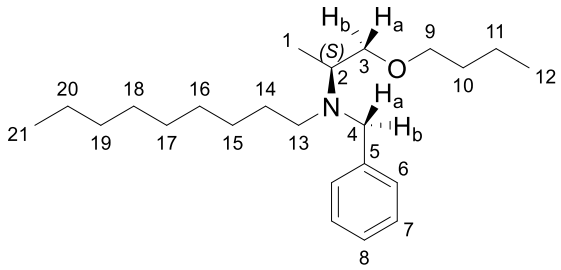

The synthesis was performed according to the general procedure for the synthesis of *N*-benzyl-*N*-alkyl-L-alaninyl alkyl ethers **39** using *N*-benzyl-L-alaninyl butyl ether (**47c**) (2.00 g, 1.00 eq, 9.04 mmol), NaH (723 mg, 2.00 eq, 18.08 mmol) and *n*-nonyl iodide (2.7 mL, 1.50 eq., 13.55 mmol) in THF (30 mL) and was refluxed for 96 h. Purification via column chromatography on silica gel (eluent cyclohexane/ethyl acetate 19:1 (v:v) gave the desired product **39h** as a colorless oil (1.77 g, 5.10 mmol, 56%).

Yield: 56%.

Molecular weight: $C_{23}H_{41}NO$, 347.587 g/mol

^{1}H-NMR: (500 MHz, acetone-d_6, 298 K) δ [ppm] = 7.40-7.35 (m, 2 H, H-6, H-6‘), 7.31-7.25 (m, 2 H, H-7, H-7’),7.19 (t, 1 H, H-8, $^{3}J_{8,7(7')}$= 7.3 Hz), 3.72 (d, 1 H, H-4a, $^{2}J_{4a,4b}$= 14.3 Hz), 3.58 (d, 1 H, H-4b, $^{2}J_{4b,4a}$= 14.3 Hz), 3.52 (dd, 1 H, H-3a, $^{2}J_{3a,3b}$= 9.4 Hz, $^{3}J_{3a,2}$= 5.8 Hz),3.43-3.34 (m, 2 H, H-9) 3.31 (dd, 1 H, H-3b, $^{2}J_{3b,3a}$= 9.4 Hz, $^{3}J_{3b,2}$= 6.6 Hz), 2.97 (pd, 1 H, H-2, $^{3}J_{2,1}$= 6.7 Hz, $^{3}J_{2,3a}$= 5.8 Hz), 2.56-2.44 (m, 2 H, H-13), 1.56-1.45 (m, 2H, H-10), 1.42-1.27 (m, 16 H, H-11, H-14, H-15 H-16, H-17, H-18 H-19, H-20), 1.02 (d, 3 H, H-1, $^{3}J_{1,2}$= 6.7 Hz), 0.89 (m, 6 H, H-12, H-21).

^{13}C-NMR: (126 MHz, chloroform-d_1, 298 K) δ [ppm] = 142.7(C-5), 129.3 (C-6, C-6‘), 128.8 (C-7, C-7‘), 127.3 (C-8), 74.5 (C-3), 71.3 (C-9), 55.5 (C-4), 54.7 (C-2), 50.8 (C-13), 32.8 (C-19), 32.7 (C-10), 30.3*$^{\#}$ (C-16, C-17, C-18), 29.8* (C-14), 27.9 (C-15), 23.4 (C-20), 14.4$^{\#}$ (C-12, C-21), 14.2$^{\#}$ (C-12, C-21), 12.9 (C-1).

*Signals partially covered by signal of residual non deuterated solvent. $^{\#}$unambiguous assignment not possible.

MS: (ESI(+), dichloromethane, M = $C_{23}H_{41}NO$) *m/z* = 348.326 $[M+H]^+$.

ESI HRMS: calculated for $[C_{23}H_{42}NO]^+$: *m/z* = 348.3261, found: *m/z* = 348.3258.

Synthesis of N-benzyl-N-propyl-L-alaninyl heptyl ether (39i)

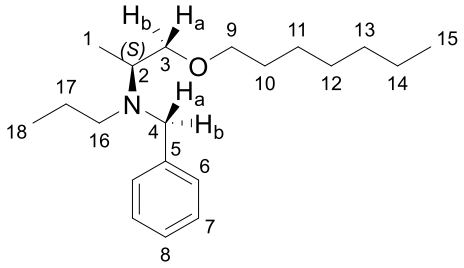

The synthesis was performed according to the general procedure for the synthesis of *N*-benzyl-*N*-alkyl-L-alaninyl alkyl ethers **39** using *N*-benzyl-L-alaninyl heptyl ether (**47e**) (3.01 g, 1.00 eq, 11.42 mmol), NaH (685 g, 1.50 eq, 17.13 mmol) and *n*-propyl iodide (1.7 mL, 1.50 eq., 17.13 mmol) in THF (29 mL) and was refluxed for 72 h. Purification via column chromatography on silica gel (eluent cyclohexane/ethyl acetate 19:1 (v:v) gave the desired product **39i** as a colorless oil (2.08 g, 6.80 mmol, 60%).

Yield: 60%.

Molecular weight: $C_{20}H_{35}NO$, 305.506 g/mol

^{1}H-NMR: (500 MHz, acetone-d_6, 298 K) δ [ppm] = 7.37 (d, 2 H, H-6, H-6‘,$^{3}J_{6(6'),7(7')}$= 7.5 Hz), 7.27 (t, 2 H, H-7, H-7’, $^{3}J_{7(7'),6(6')}$=$^{3}J_{7(7'),8}$= 7.6 Hz), 7.19 (t, 1 H, H-8, $^{3}J_{8,7(7')}$= 7.3 Hz), 3.73 (d, 1 H, H-4a, $^{2}J_{4a,4b}$= 14.3 Hz), 3.59 (d, 1 H, H-4b, $^{2}J_{4b,4a}$= 14.3 Hz), 3.51 (dd, 1 H, H-3a, $^{2}J_{3a,3b}$= 9.4 Hz, $^{3}J_{3a,2}$= 5.8 Hz), 3.37 (td, 2 H, H-9, $^{3}J_{9,10}$= 6.4 Hz), 3.31 (dd, 1 H, H-3b, $^{2}J_{3b,3a}$= 9.4 Hz, $^{3}J_{3b,2}$= 6.6 Hz), 3.01-2.92 (m, 1 H, H-2), 2.47 (td, 2 H, H-16, $^{3}J_{16,17}$= 6.9 Hz), 1.53 (tt, 2H, H-10), 1.46-1.37 (m, 2 H, H-17), 1.37-1.23 (m, 8 H, H-11, H-12, H-13, H-14), 1.03 (d, 3 H, H-1, $^{3}J_{1,2}$= 6.7 Hz), 0.88 (m, 3 H, H-15, $^{3}J_{15,14}$= 6.9 Hz), 0.83 (t, 3 H, H-18, $^{3}J_{18,17}$= 7.4 Hz).

^{13}C-NMR: (126 MHz, chloroform-d_1, 298 K) δ [ppm] = 142.6(C-5), 129.1 (C-6, C-6‘), 128.8 (C-7, C-7‘), 127.2 (C-8), 74.4 (C-3), 71.6 (C-9), 55.6 (C-4), 54.5 (C-2), 52.7 (C-16), 32.7 (C-13), 30.6* (C-10), 30.4* (C-12), 27.90 (C-11), 23.3 (C-14), 22.6 (C-17), 14.3 (C-15), 13.0 (C-1), 12.1 (C-18).

*Signals partially covered by signal of residual non deuterated solvent.

MS: (APCI, dichloromethane, M = $C_{20}H_{35}NO$) *m/z* = 306.279 $[M+H]^+$.

APCI HRMS: calculated for $[C_{20}H_{36}NO]^+$: *m/z* = 306.2791, found: *m/z* = 306.2791.

Synthesis of N-benzyl-N-propyl-L-alaninyl nonyl ether (39j)

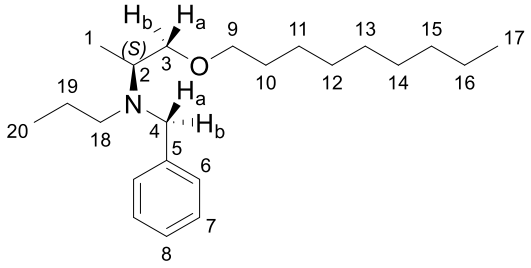

The synthesis was performed according to the general procedure for the synthesis of *N*-benzyl-*N*-alkyl-L-alaninyl alkyl ethers **39** using *N*-benzyl-*N*-propyl-L-alaninyl amine (**48b**) (3.00 g, 1.00 eq, 14.48 mmol), NaH (60 wt%, 700 mg, 1.20 eq, 17.5 mmol) and *n*-nonyl iodide (5.7 mL, 2.00 eq., 28.96 mmol) in THF (45 mL) and was refluxed for 45 h. Purification via column chromatography on silica gel (eluent cyclohexane/ethyl acetate 2:1 (v:v) gave the desired product **39j** as a colorless oil (1.47 g, 3.51 mmol, 30%).

Yield: 30%.

Molecular weight: $C_{22}H_{39}NO$, 333.560 g/mol

^{1}H-NMR: (700 MHz, acetone-d_6, 298 K) δ [ppm] = 7.39-7.36 (m, 2 H, H-6, H-6‘,), 7.28 (t, 2 H, H-7, H-7’, $^3J_{7(7'),6(6')}$=$^3J_{8,7(7')}$= 7.6 Hz), 7.21-7.17 (m, 1 H, H-8), 3.73 (d, 1 H, H-4a, $^2J_{4a,4b}$= 14.3 Hz), 3.60 (d, 1 H, H-4b, $^2J_{4b,4a}$= 14.3 Hz), 3.52 (dd, 1 H, H-3a, $^2J_{3a,3b}$= 9.4 Hz, $^3J_{3a,2}$= 5.8 Hz), 3.37 (td, 2 H, H-9, $^3J_{9,10}$= 6.4 Hz), 3.31 (dd, 1 H, H-3b, $^2J_{3b,3a}$= 9.4 Hz, $^3J_{3b,2}$= 6.6 Hz), 2.96 (h, 1 H, H-2, $^3J_{2,1}$= $^3J_{2,3}$= 6.6 Hz), 2.47 (td, 2 H, H-18, $^3J_{18,19}$= 6.9 Hz), 1.53 (dq, 2H, H-10, $^3J_{10,9}$= 6.5 Hz), 1.44-1.39 (m, 2 H, H-19), 1.39-1.33 (m, 2 H, H-11), 1.32-1.24 (m, 10 H,H-12, H-13, H-14, H-15, H-16), 1.03 (d, 3 H, H-1, $^3J_{1,2}$= 6.7 Hz), 0.88 (t, 3 H, H-17, $^3J_{17,16}$= 7.0 Hz), 0.83 (t, 3 H, H-20, $^3J_{20,19}$= 7.4 Hz).

^{13}C-NMR: (176 MHz, chloroform-d_1, 298 K) δ [ppm] = 142.6(C-5), 129.2 (C-6, C-6‘), 128.8 (C-7, C-7‘), 127.3 (C-8), 74.4 (C-3), 71.6 (C-9), 55.5 (C-4), 54.6 (C-2), 52.8 (C-18), 32.7 (C-15), 30.6* (C-10), 30.4* (C-12), 30.2*$^{\#}$ (C-13/ C-14/C-15), 27.0 (C-11), 23.3 (C-16), 22.6 (C-19), 14.4 (C-17), 13.0 (C-1), 12.0 (C-20).

*Signals partially covered by signal of residual non deuterated solvent. $^{\#}$unambiguous assignment not possible.

MS (APCI, dichloromethane, M = $C_{22}H_{39}NO$) *m/z* = 334.311 $[M+H]^+$.

APCI HRMS: calculated for $[C_{22}H_{40}NO]^+$: *m/z* = 334.3104, found: *m/z* = 334.3109.

Synthesis of N-benzyl-N-butyl-L-alaninyl nonyl ether (39k)

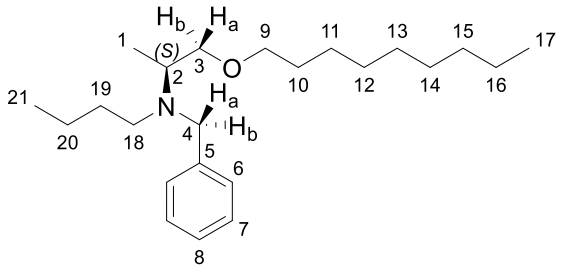

The synthesis was performed according to the general procedure for the synthesis of *N*-benzyl-*N*-alkyl-L-alaninyl alkyl ethers **39** using *N*-benzyl-L-alaninyl nonyl ether **47g** (2.00 g, 1.00 eq, 6.86 mmol), NaH (60 wt%, 550 mg, 2.00 eq, 13.72 mmol) and *n*-butyl iodide (1.6 mL, 2.00 eq., 13.72 mmol) in THF (45 mL) and was refluxed for 45 h. Purification via column chromatography on silica gel (eluent cyclohexane/ethyl acetate 19:1 (v:v) gave the desired product **39k** as a colorless oil (1.58 g, 4.55 mmol, 66%).

Yield: 66%.

Molecular weight: $C_{23}H_{41}NO$, 347.587 g/mol

^{1}H-NMR: (700 MHz, acetone-d_6, 298 K) δ [ppm] = 7.38-7.36 (m, 2 H, H-6, H-6‘), 7.27 (dd, 2 H, H-7, H-7’, $^3J_{7(7'),6(6')}$= 6.9 Hz), 7.21-7.16 (m, 1 H, H-8), 3.73 (d, 1 H, H-4a, $^2J_{4a,4b}$= 14.3 Hz), 3.60 (d, 1 H, H-4b, $^2J_{4b,4a}$= 14.3 Hz), 3.52 (dd, 1 H, H-3a, $^2J_{3a,3b}$= 9.5 Hz, $^3J_{3a,2}$= 5.8 Hz),3.37 (t, 2 H, H-9, $^3J_{9,10}$= 6.4 Hz) 3.32 (dd, 1 H, H-3b, $^2J_{3b,3a}$= 9.4 Hz, $^3J_{3b,2}$= 6.5 Hz), 2.97 (pd, 1 H, H-2, $^3J_{2,1}$= 6.8 Hz, $^3J_{2,3a}$= 5.9 Hz), 2.57-2.46 (m, 2 H, H-18), 1.57-1.51 (m, 2H, H-10), 1.44-1.34 (m, 4 H, H-19, H-11), 1.34-1.25 (m, 12 H,H-12, H-13, H-14, H-15, H-16, H-20), 1.02 (d, 3 H, H-1, $^3J_{1,2}$= 6.7 Hz), 0.88 (t, 3 H, H-17, $^3J_{17,16}$= 7.0 Hz), 0.83 (t, 3 H, H-21, $^3J_{21,20}$= 7.4 Hz

^{13}C-NMR: (176 MHz, chloroform-d_1, 298 K) δ [ppm] = 142.7(C-5), 129.2 (C-6, C-6‘), 128.8 (C-7, C-7‘), 127.3 (C-8), 74.4 (C-3), 71.6 (C-9), 55.5 (C-4), 54.6 (C-2), 50.6 (C-18), 32.7 (C-15), 31.7 (C-19), 30.6* (C-10), 30.4* (C-12), 30.2*$^{\#}$ (C-13/ C-14/C-15), 27.6 (C-11), 23.3 (C-16), 21.0 (C-20), 14.4 (C-17), 14.3 (C-21), 13.0 (C-1).

*Signals partially covered by signal of residual non deuterated solvent. $^{\#}$unambiguous assignment not possible.

MS: (APCI, dichloromethane, M = $C_{23}H_{41}NO$) *m/z* = 348.325 $[M+H]^+$.

APCI HRMS: calculated for $[C_{24}H_{42}NO]^+$: *m/z* = 348.3261, found: *m/z* = 348.3260.

General procedure for the Synthesis of O-alkyl-L-alaninyl N-alkyl amines 22

The corresponding *N*-benzyl-*N*-alkyl-L-alaninyl ethers **39** (1.00 eq.) and palladium on charcoal (10 wt-%, 0.10 eq.) are placed in a flame-dried flask and suspended in abs. ethanol (9 mL/mmol). The atmosphere inside of the flask is exchanged for hydrogen by degassing the mixture by 5 evacuation cycles under vigorous stirring and repressurizing with hydrogen. During the reaction hydrogen is bubbled through the suspension continually for 2-30 min, afterwards the apparatus is closed and the reaction mixture is kept under static hydrogen atmosphere for the indicated periods of time. After complete conversion of the starting material, the catalyst is removed by two-fold filtration, first over filter paper to remove the major part and afterwards through a syringe filter (0.2 µm). The remaining precipitate is washed with ethanol and the solvent of the filtrate is removed under reduced pressure. The product **22** is obtained as a colorless oil.

The obtained products are used in the subsequent synthetic steps on the way to the desired squaraine without further purification

Synthesis of O-ethyl-L-alaninyl N-ethyl amine (22a)

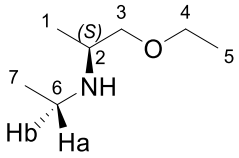

The synthesis was performed according to the general procedure for the synthesis of *O*-alkyl-L-alaninyl *N*-alkyl amine using *N*-benzyl-*N*-ethyl-L-alaninyl ethyl ether (**39a**) (200 mg, 1.00 eq, 0.90 mmol) as starting material with palladium on charcoal (10 wt-%, 96.2 mg, 0.10 eq.) in ethanol (8.4 mL). This mixture was stirred under hydrogen atmosphere for 4 h was and the desired product **22a** was obtained as a colorless oil (104 mg, 0.79 mmol, 88%).

Yield: 88%.

Molecular weight: $C_7H_{17}NO$, 131.219 g/mol

^{1}H-NMR: (500 MHz, acetone-d_6, 298 K) δ [ppm] 3.48-3.39 (m, 2 H, H-4), 3.26-3.18 (m, 2 H, H-3), 2.78 (pd, 1 H, H-2, $^3J_{2,1}$= 6.4 Hz, $^3J_{2,3a}$= 5.2 Hz),2.64 (dq, 1 H, H-6a, $^2J_{6a,6b}$= 11.1 Hz, $^3J_{6a,7}$= 7.2 Hz), 2.54 (dq, dq, 1 H, H-6b, $^2J_{6b,6a}$= 11.1 Hz, $^3J_{6b,7}$= 7.1Hz), 1.12 (t, 3 H, H-5, $^3J_{5,4}$= 7.0 Hz), 1.02 (d, 3 H, H-7, $^3J_{7,6}$= 7.1 Hz), 0.94 (t, 3 H, H-1, $^3J_{1,12}$= 6.4 Hz).

^{13}C-NMR: (126 MHz, acetone-d_6, 298 K) δ [ppm] = 76.0 (C-3), 66.7 (C-4), 53.5 (C-2), 42.2(C-6), 17.9 (C-1), 16.0 (C-7), 15.5 (C-5).

MS: (ESI(+), dichloromethane, M = $C_7H_{17}NO$) *m/z* = 132.138 $[M+H]^+$.

ESI HRMS: calculated for $[C_7H_{18}NO]^+$: *m/z* = 132.1383, found: *m/z* = 132.1380.

Synthesis of O-propyl-L-alaninyl N-propyl amine (22b)

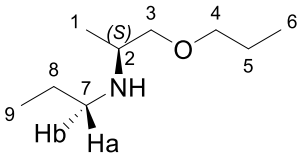

The synthesis was performed according to the general procedure for the synthesis of *O*-alkyl-L-alaninyl *N*-alkyl amine using *N*-benzyl-*N*-propyl-L-alaninyl propyl ether (**39b**) (4.00 g, 16.04 mmol, 1.00 eq.) as starting material with palladium on charcoal (10 wt-%, 1.71 g, 0.10 eq.) in ethanol (150 mL). This mixture was stirred under hydrogen atmosphere for 19 h was and the desired product **22b** was obtained as a colorless oil (2.22 g, 13.95 mmol, 87%).

Yield: 87 %

Molecular weight: $C_9H_{21}NO$, 159.273 g/mol

^{1}H-NMR: (500 MHz, acetone-d_6, 298 K) δ [ppm] = 3.41-3.29 (m, 2 H, H-4), 3.28-3.20 (m, 2 H, H-3), 2.79 (pd, 1 H, H-2, $^3J_{2,1}$= 6.4 Hz, $^3J_{2,3a}$= 5.1 Hz), 2.58 (ddd, 1 H, H-7a, $^2J_{7a,7b}$= 11.1 Hz, $^3J_{7a,8}$= 7.2 Hz, $^3J_{7a,NH}$= 6.8 Hz), 2.52-2.46 (m, 1 H, H-6b), 1.58-1.50 (m, 2 H, H-5), 1.48-1.40 (m, 2 H, H-8), 0.95 (d, 3 H, H-1, $^3J_{1,2}$= 6.4 Hz), 0.89 (dt, 6 H, H-6, H-9, $^3J_{6,5}$= $^3J_{9,8}$= 7.4 Hz).

^{13}C-NMR: (126 MHz, acetone-d_6, 298 K) δ [ppm] = 76.0 (C-3), 73.2 (C-4), 53.4 (C-2), 49.8(C-7), 24.2 (C-8), 22.6 (C-5), 17.8 (C-1), 12.1 (C-9), 10.9 (C-6).

MS: (ESI(+), dichloromethane, M = $C_9H_{21}NO$) *m/z* = 160.169 $[M+H]^+$.

ESI HRMS: calculated for $[C_9H_{22}NO]^+$: *m/z* = 160.1696, found: *m/z* = 160.1693.

Synthesis of O-butyl-L-alaninyl N-butyl amine (22c)

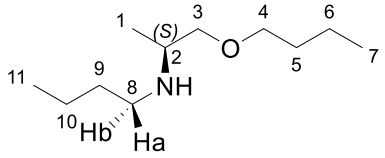

The synthesis was performed according to the general procedure for the synthesis of *O*-alkyl-L-alaninyl *N*-alkyl amine using *N*-benzyl-*N*-butyl-L-alaninyl butyl ether (**39c**) (1.37 g, 1.00 eq, 4.93 mmol) as starting material with palladium on charcoal (10 wt-%, 524 mg, 0.10 eq.) in ethanol (45 mL). This mixture was stirred under hydrogen atmosphere for 18 h was and the desired product **22c** was obtained as a colorless oil (920 mg, 4.93 mmol, quant.).

Yield: quant%.

Molecular weight: $C_{11}H_{25}NO$, 187.327 g/mol

^{1}H-NMR: (500 MHz, acetone-d_6, 298 K) δ [ppm] = 3.40 (qt, 2 H, H-4, $^3J_{4,5}$= 6.4 Hz), 3.29-3.19 (m, 2 H, H-3), 2.78 (pd, 1 H, H-2, $^3J_{2,1}$= 6.4 Hz, $^3J_{2,3a}$= 5.0 Hz), 2.62 (dt, 1 H, H-8a, $^2J_{8a,8b}$= 11.1 Hz, $^3J_{8a,9}$= 7.0 Hz), 2.52 (dt, 1 H, H-8b, $^2J_{8b,8a}$= 11.1 Hz, $^3J_{8b,9}$= 6.7 Hz), 1.57-1.47 (m, 2 H, H-5), 1.46-1.29 (m, 6 H, H-6, H-9, H-10), 0.94 (d, 3 H, H-1, $^3J_{1,2}$= 6.4 Hz), 0.90 (dt, 6 H, H-7, H-11, $^3J_{7,6}$= $^3J_{11,10}$= 7.3 Hz).

^{13}C-NMR: (126 MHz, acetone-d_6, 298 K) δ [ppm] = 76.2 (C-3), 71.2 (C-4), 53.6 (C-2), 47.6 (C-8), 33.5 (C-9), 32.6 (C-5), 21.1 (C-10), 20.1 (C-6), 17.8 (C-1), 14.3 (C-11), 14.2 (C-7).

MS: (ESI(+), dichloromethane, M = $C_{11}H_{25}NO$) *m/z* = 188.200 $[M+H]^+$.

ESI HRMS: calculated for $[C_{11}H_{26}NO]^+$: *m/z* = 188.2009, found: *m/z* = 188.2005.

Synthesis of O-propyl-L-alaninyl N-propyl amine (22d)

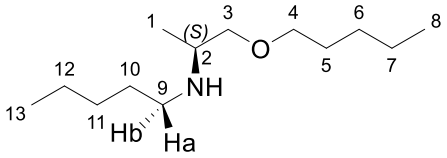

The synthesis was performed according to the general synthetic procedures of *O*-alkyl-L-alaninyl *N*-alkyl amine using *N*-benzyl-*N*-propyl-L-alaninyl propyl ether (**39d**) (2.17 g, 1.00 eq, 7.10 mmol) as starting material with palladium on charcoal (10 wt-%, 757 mg, 0.10 eq.) in ethanol (66 mL). This mixture was stirred under hydrogen atmosphere for 24 h was and the desired product **22d** was obtained as a colorless oil (1.53 g, 7.10 mmol, quant.).

Yield: quant.

Molecular weight: $C_{13}H_{29}NO$, 215.381 g/mol

^{1}H-NMR: (500 MHz, acetone-d_6, 298 K) δ [ppm] = 3.46-3.36 (m, 2 H, H-4), 3.29-3.21 (m, 2 H, H-3), 2.80 (m, 1 H, H-2), 2.68-2.59 (m, 1 H, H-9a), 2.58-2.49 (m, 1 H, H-9b), 1.61-1.50 (m, 2 H, H-5), 1.40-1.42 (m, 2 H, H-10), 1.40-1.27 (m, 8 H, H-6, H-7, H-11, H-12), 0.96 (d, 3 H, H-1, $^3J_{1,2}$= 6.3 Hz), 0.90-0.85 (m, 6 H, H-8, H-13).

^{13}C-NMR: (126 MHz, acetone-d_6, 298 K) δ [ppm] = 76.2 (C-3), 71.5 (C-4), 53.6 (C-2), 48.0 (C-9), 31.4 (C-10), 30.4* (C-5), 30.2*(C-11), 29.2 (C-6), 23.3 (C-7, C-12), 17.9 (C-1), 14.4 (C-7, C-11).

*Signals partially covered by signal of residual non deuterated solvent.

MS: (ESI(+), dichloromethane, M = $C_{13}H_{29}NO$) *m/z* =216.232 $[M+H]^+$.

ESI HRMS: calculated for $[C_{13}H_{29}NO]^+$: *m/z* = 216.2322, found: *m/z* = 216.2314.

Synthesis of O-heptyl-L-alaninyl N-heptyl amine (22e)

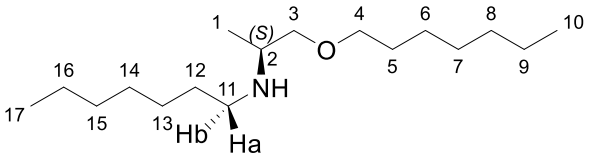

The synthesis was performed according to the general procedure for the synthesis of *O*-alkyl-L-alaninyl *N*-alkyl amine using *N*-benzyl-*N*-heptyl-L-alaninyl heptyl ether (**39e**) (791 mg, 1.00 eq, 2.19 mmol) as starting material with palladium on charcoal (10 wt-%, 233 mg, 0.10 eq.) in ethanol (20 mL). This mixture was stirred under hydrogen atmosphere for 16 h was and the desired product **22e** was obtained as a colorless oil (593 mg, 2.19 mmol, quant.).

Yield: quant.

Molecular weight: $C_{17}H_{37}NO$, 271.489 g/mol

^{1}H-NMR: (500 MHz, acetone-d_6, 298 K) δ [ppm] = 3.44-3.34 (m, 2 H, H-4), 3.31-3.20 (m, 2 H, H-3), 2.80 (m, 1 H, H-2), 2.63 (dt, 1 H, H-11a, $^{2}J_{11a,11b}$= 11.1 Hz, $^{3}J_{11a,12}$= 7.0 Hz), 2.53 (dt, 1 H, H-11b, $^{2}J_{11b,11a}$= 11.1 Hz, $^{3}J_{11b,12}$= 6.9 Hz), 1.58-1.50 (m, 2 H, H-5), 1.48-1.40 (m, 2 H, H-12), 1.39-1.22 (m, 16 H, H-6, H-7, H-8, H-9, H-13, H-14, H-15, H-16), 0.95 (d, 3 H, H-1, $^{3}J_{1,2}$= 6.4 Hz), 0.90-0.85 (m, 6 H, H-10, H-17).

^{13}C-NMR: (126 MHz, acetone-d_6, 298 K) δ [ppm] = 76.1 (C-3), 71.5 (C-4), 53.6 (C-2), 47.9 (C-11), 32.6 (C-8, C-15), 31.3 (C-12), 30.5* (C-5), 29.8* (C-7, C-14), 28.1 (C-13), 27.0 (C-6), 23.3 (C-9, C-16), 17.8 (C-1), 14.4 (C-10, C-17).

*Signals partially covered by signal of residual non deuterated solvent.

MS: (ESI(+), dichloromethane, M = $C_{17}H_{37}NO$) *m/z* = 272.294 $[M+H]^+$.

ESI HRMS: calculated for $[C_{17}H_{38}NO]^+$: *m/z* = 272.2950, found: *m/z* = 272.2948.

Synthesis of O-octyl-L-alaninyl N-octyl amine (22f)

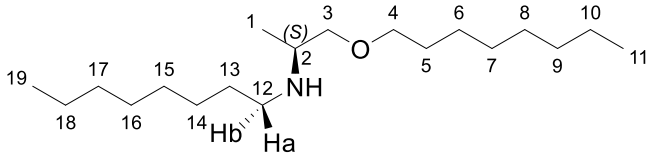

The synthesis was performed according to the general procedure for the synthesis of *O*-alkyl-L-alaninyl *N*-alkyl amine using *N*-benzyl-*N*-octyl-L-alaninyl octyl ether (**39f**) (2.97 g, 1.00 eq, 7.62 mmol) as starting material with palladium on charcoal (10 wt-%, 811 mg, 0.10 eq.) in ethanol (71 mL). This mixture was stirred under hydrogen atmosphere for 18 h was and the desired product **22f** was obtained as a colorless oil (2.28 g, 7.62 mmol, quant.).

Yield: quant.

Molecular weight: $C_{19}H_{41}NO$, 299.543 g/mol

^{1}H-NMR: (500 MHz, acetone-d_6, 298 K) δ [ppm] = 3.44-3.34 (m, 2 H, H-4), 3.28-3.19 (m, 2 H, H-3), 2.78 (pd, 1 H, H-2, $^{3}J_{2,1}$= 6.4 Hz, $^{3}J_{2,3a}$= 4.8 Hz), 2.62 (dt, 1 H, H-12a, $^{2}J_{12a,12b}$= 11.1 Hz, $^{3}J_{12a,13}$= 7.0 Hz), 2.52 (dt, 1 H, H-12b, $^{2}J_{12b,12a}$= 11.1 Hz, $^{3}J_{12b,13}$= 6.9 Hz), 1.57-1.50 (m, 2 H, H-5), 1.47-1.39 (m, 2 H, H-13), 1.39-1.22 (m, 20 H, H-6, H-7, H-8, H-9, H-10, H-14, H-15, H-16, H-17, H-18), 0.94 (d, 3 H, H-1, $^{3}J_{1,2}$= 6.4 Hz), 0.91-0.84 (m, 6 H, H-11, H-19).

^{13}C-NMR: (126 MHz, acetone-d_6, 298 K) δ [ppm] = 76.2 (C-3), 71.5 (C-4), 53.5 (C-2), 48.0 (C-12), 32.6 (C-8, C-16), 31.3 (C-13), 30.5* (C-5), 30.0*$^{\#}$ (C-7, C-15, C-17), 28.1$^{\#}$ (C-9, C-14), 27.0 (C-6), 23.3 (C-10, C-18), 17.8 (C-1), 14.4 (C-11, C-19).

*Signals partially covered by signal of residual non deuterated solvent. $^{\#}$unambiguous assignment not possible.

MS: (ESI(+), dichloromethane, M = $C_{19}H_{41}NO$) *m/z* = 300.325 $[M+H]^+$.

ESI HRMS: calculated for $[C_{19}H4_2NO]^+$: *m/z* = 300.3261, found: *m/z* = 300.3257.

Synthesis of O-nonyl-L-alaninyl N-nonyl amine (22g)

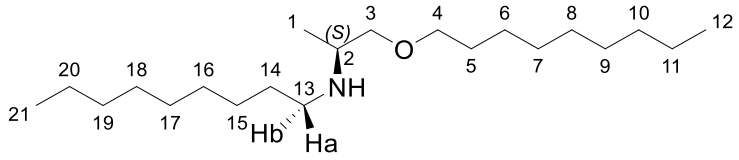

The synthesis was performed according to the general procedure for the synthesis of *O*-alkyl-L-alaninyl *N*-alkyl amine using *N*-benzyl-*N*-nonyl-L-alaninyl nonyl ether (**39g**) (2.55 g, 1.00 eq, 6.10 mmol) as starting material with palladium on charcoal (10 wt-%, 650 mg, 0.10 eq.) in ethanol (57 mL). This mixture was stirred under hydrogen atmosphere for 19 h was and the desired product **22g** was obtained as a colorless oil (1.96 g, 5.98 mmol, 98%).

Yield: 98%.

Molecular weight: $C_{21}H_{45}NO$, 327.597 g/mol

^{1}H-NMR: (500 MHz, acetone-d_6, 298 K) δ [ppm] = 3.46-3.34 (m, 2 H, H-4), 3.29-3.18 (m, 2 H, H-3), 2.79 (pd, 1 H, H-2, $^3J_{2,1}$= 6.6 Hz, $^3J_{2,3a}$= 5.0 Hz), 2.62 (dt, 1 H, H-13a, $^2J_{13a,13b}$= 11.1 Hz, $^3J_{13a,14}$= 7.0 Hz), 2.52 (dt, 1 H, H-13b, $^2J_{13b,13a}$= 11.1 Hz, $^3J_{13b,14}$= 6.9 Hz), 1.58-1.49 (m, 2 H, H-5), 1.48-1.40 (m, 2 H, H-14), 1.40-1.22 (m, 24 H, H-6, H-7, H-8, H-9, H-10, H-11, H-15, H-16, H-17, H-18, H-19, H-20), 0.94 (d, 3 H, H-1, $^3J_{1,2}$= 6.9 Hz), 0.92-0.85 (m, 6 H, H-12, H-21).

^{13}C-NMR: (126 MHz, acetone-d_6, 298 K) δ [ppm] = 76.2 (C-3), 71.5 (C-4), 53.5 (C-2), 48.0 (C-13), 32.7 (C-10, C-19), 31.4 (C-14), 30.5* (C-5), 30.0*# (C-7, C-8, C-9,C-17, C-18), 28.1(C-15), 27.0 (C-6, C-16), 23.3 (C-11, C-20), 17.9 (C-1), 14.4 (C-12, C-21).

*Signals partially covered by signal of residual non deuterated solvent. #unambiguous assignment not possible.

MS: (ESI(+), Dichloromethane, M = $C_{21}H_{45}NO$) *m/z* = 328.357 $[M+H]^+$.

ESI HRMS: calculated for $[C_{21}H_{46}NO]^+$: *m/z* = 328.3574, found: *m/z* = 328.3569.

Synthesis of O-butyl-L-alaninyl N-nonyl amine (22h)

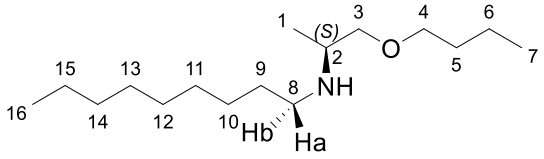

The synthesis was performed according to the general procedure for the synthesis of *O*-alkyl-L-alaninyl *N*-alkyl amine using *N*-benzyl-*N*-nonyl-L-alaninyl butyl ether (**39h**) (1.76 g, 1.00 eq, 5.06 mmol) as starting material with palladium on charcoal (10 wt-%, 539 mg, 0.10 eq.) in ethanol (47 mL). This mixture was stirred under hydrogen atmosphere for 18 h was and the desired product **22h** was obtained as a colorless oil (1.08 g, 4.19 mmol, 83%).

Yield: 83%.

Molecular weight: $C_{16}H_{35}NO$, 257.462 g/mol

^{1}H-NMR: (500 MHz, acetone-d_6, 298 K) δ [ppm] = 3.45-3.33 (m, 2 H, H-4), 3.29-3.20 (m, 2 H, H-3), 2.79 (td, 1 H, H-2, $^3J_{2,1}$= 6.6 Hz, $^3J_{2,NH}$= 5.3 Hz), 2.63 (dt, 1 H, H-8a, $^2J_{8a,8b}$= 11.1 Hz, $^3J_{8a,9}$= 7.0 Hz), 2.57-2.49

(m, 1 H, H-8b), 1.56-1.48 (m, 2 H, H-5), 1.46-1.40 (m, 2 H, H-9), 1.39-1.24 (m, 14 H, H-6, H-10, H-11, H-12, H-13, H-14, H-15), 0.95 (d, 3 H, H-1, $^{3}J_{1,2}$= 6.4 Hz), 0.94-0.86 (m, 6 H, H-7, H-16).

^{13}C-NMR: (126 MHz, acetone-d_6, 298 K) δ [ppm] = 76.2 (C-3), 71.3 (C-4), 53.6 (C-2), 48.0 (C-8), 32.7 (C-14), 31.3 (C-9), 30.5* (C-5), 30.3*# (C-11, C-13), 28.1 (C-10), 27.0 (C-12), 23.3 (C-15), 20.1 (C-6), 17.9 (C-1), 14.4 (C-16), 14.2 (C-7).

*Signals partially covered by signal of residual non deuterated solvent. #unambiguous assignment not possible.

MS: (ESI(+), dichloromethane, M = $C_{16}H_{35}NO$) *m/z* = 258.281 $[M+H]^+$.

ESI HRMS: calculated for $[C_{16}H_{36}NO]^+$: *m/z* = 258.2791, found: *m/z* = 258.2796.

Synthesis of O-heptyl-L-alaninyl N-propyl amine (22i)

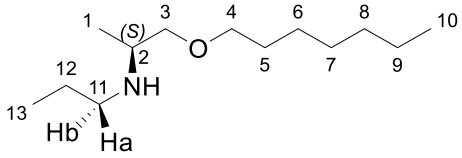

The synthesis was performed according to the general procedure for the synthesis of *O*-alkyl-L-alaninyl *N*-alkyl amine using *N*-benzyl-*N*-propyl-L-alaninyl heptyl ether (**39i**) (2.08 g, 1.00 eq, 6.80 mmol) as starting material with palladium on charcoal (10 wt-%, 724 mg, 0.10 eq.) in ethanol (63 mL). This mixture was stirred under hydrogen atmosphere for 18 h was and the desired product **22i** was obtained as a colorless oil (1.46 g, 6.80 mmol, quant.).

Yield: quant.

Molecular weight: $C_{13}H_{29}NO$, 215.381 g/mol

^{1}H-NMR: (500 MHz, acetone-d_6, 298 K) δ [ppm] = 3.44-3.34 (m, 2 H, H-4), 3.27-3.19 (m, 2 H, H-3), 2.83-2.73 (m, 1 H, H-2), 2.58 (ddd, 1 H, H-11a, $^{2}J_{11a,11b}$= 11.1 Hz, $^{4}J_{11a,13}$= 7.5 Hz, $^{3}J_{11a,NH}$= 6.7 Hz), 2.49 (ddd, 1 H, H-11b, $^{2}J_{11b,11a}$= 11.1 Hz, $^{4}J_{11b,13}$= 7.2 Hz, $^{3}J_{11b,NH}$= 6.6 Hz), 1.57-1.49 (m, 2 H, H-5), 1.48-1.39 (m, 2 H, H-12), 1.39-1.24 (m, 8 H, H-6, H-7, H-8, H-9), 0.94 (d, 3 H, H-1, $^{3}J_{1,2}$= 6.3 Hz), 0.92-0.85 (td, 6 H, H-10, H-13, $^{4}J_{11b,13}$= 7.2 Hz, $^{3}J_{13,12}$ =5.5 Hz).

^{13}C-NMR: (126 MHz, acetone-d_6, 298 K) δ [ppm] = 76.2 (C-3), 71.5 (C-4), 53.5 (C-2), 50.0 (C-11), 32.6 (C-8), 30.5* (C-5), 30.3* (C-7), 26.9(C-6), 24.4 (C-12), 23.3 (C-9), 17.9 (C-1), 14.4 (C-10), 12.1 (C-13).

*Signals partially covered by signal of residual non deuterated solvent.

MS: (ESI(+), dichloromethane, M = $C_{13}H_{29}NO$) *m/z* = 216.231 $[M+H]^+$.

ESI HRMS: calculated for $[C_{13}H_{30}NO]^+$: *m/z* = 216.2322, found: *m/z* = 216.2320.

Synthesis of O-nonyl-L-alaninyl N-propyl amine (22j)

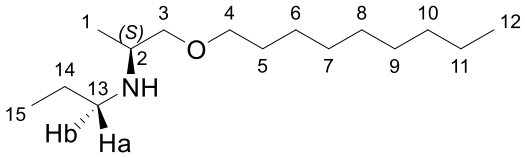

The synthesis was performed according to the general procedure for the synthesis of *O*-alkyl-L-alaninyl *N*-alkyl amine using *N*-benzyl-*N*-propyl-L-alaninyl nonyl ether (**39j**) (1.22 g, 1.00 eq, 3.65 mmol) as starting material with palladium on charcoal (10 wt-%, 388 mg, 0.10 eq.) in ethanol (32 mL). This mixture was stirred under hydrogen atmosphere for 20 h was and the desired product **22j** was obtained as a colorless oil (881 mg, 3.62 mmol, 99%).

Yield: 99%.

Molecular weight: $C_{15}H_{33}NO$, 243,435 g/mol

^{1}H-NMR: (500 MHz, acetone-d_6, 298 K) δ [ppm] = 3.46-3.34 (m, 2 H, H-4), 3.28-3.19 (m, 2 H, H-3), 2.83-2.73 (m, 1 H, H-2), 2.63-2.55 (m, 1 H, H-13a), 2.52-2.45 (m, 1 H, H-13b), 1.54 (tt, 2 H, H-5, $^3J_{5,6}$ =7.6 Hz, $^3J_{5,4}$ =6.2 Hz), 1.48-1.39 (m, 2 H, H-14), 1.38-1.22 (m, 12 H, H-6, H-7, H-8, H-9, H-10, H-11), 0.95 (d, 3 H, H-1, $^3J_{1,2}$= 6.4 Hz), 0.92-0.856(m, 6 H, H-12, H-15).

^{13}C-NMR: (126 MHz, acetone-d_6, 298 K) δ [ppm] = 76.2 (C-3), 71.5 (C-4), 53.5 (C-2), 49.9 (C-11), 32.6 (C-10), 30.5* (C-5), 30.3* (C-7, C-8, C-9), 27.0 (C-6), 24.4 (C-14), 23.3 (C-11), 17.9 (C-1), 14.4 (C-12), 12.1 (C-15).

*Signals partially covered by signal of residual non deuterated solvent.

MS: (ESI(+), dichloromethane, M $C_{15}H_{33}NO$) *m/z* = 244.263 $[M+H]^+$.

ESI HRMS: calculated for $[C_{15}H_{34}NO]^+$: *m/z* = 244.2635, found: *m/z* = 244.2629.

Synthesis of O-nonyl-L-alaninyl N-butyl amine (22k)

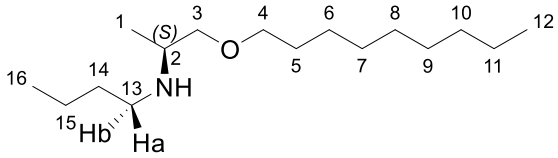

The synthesis was performed according to the general procedure for the synthesis of *O*-alkyl-L-alaninyl *N*-alkyl amine using *N*-benzyl-*N*-butyl-L-alaninyl nonyl ether (**39k**) (1.58 g, 1.00 eq, 4.55 mmol) as starting material with palladium on charcoal (10 wt-%, 484 mg, 0.10 eq.) in ethanol (42 mL). This mixture was stirred under hydrogen atmosphere for 21 h was and the desired product **22k** was obtained as a colorless oil (974 mg, 3.78 mmol, 83%).

Yield: 83%.

Molecular weight: $C_{16}H_{35}NO$, 257.462 g/mol

^{1}H-NMR: (500 MHz, acetone-d_6, 298 K) δ [ppm] = 3.45-3.34 (m, 2 H, H-4), 3.28-3.17 (m, 2 H, H-3), 2.83-2.74 (m, 1 H, H-2), 2.65-2.58 (m, 1 H, H-13a), 2.52-2.48 (m, 1 H, H-13b), 1.53 (tt, 2 H, H-5, , $^3J_{5,4}$= 6.2 Hz, $^3J_{5,6}$= 7.6 Hz), 1.44-1.26 (m, 16 H, H-6, H-7, H-8, H-9, H-10, H-11, H-14, H-15), 0.94 (d, 3 H, H-1, $^3J_{1,2}$= 6.3 Hz), 0.92-0.85 (m, 6 H, H-12, H-16).

^{13}C-NMR: (126 MHz, acetone-d_6, 298 K) δ [ppm] = 76.2 (C-3), 71.5 (C-4), 53.6 (C-2), 47.7 (C-13), 33.6 (C-14), 32.6 (C-10), 30.5* (C-5), 30.3*$^{\#}$ (C-7, C-8, C-9), 27.0(C-6), 23.3 (C-11), 21.1 (C-15), 17.9 (C-1), 14.4 (C-12, C-16).

*Signals partially covered by signal of residual non deuterated solvent. $^{\#}$unambiguous assignment not possible.

MS: (APCI, dichloromethane, M = $C_{16}H_{35}NO$) *m/z* = 258.278 $[M+H]^+$.

APCI HRMS: calculated for $[C_{16}H_{36}NO]^+$: *m/z* = 258.2791, found: *m/z* = 258.2787.

7.4 SYNTHESIS OF SQUARAINES

General Procedure A:

The synthetic protocol was adapted from the literature.[32]

A round-bottom flask, equipped with a reflux condenser, is charged with the corresponding *O*-alkyl-L-alaninyl *N*-alkyl amine (1.00 eq.) and phloroglucinol (1.50 – 2.00 eq.). The reactants are suspended in a mixture of toluene/1-butanol 1:1 (v/v, 10 mL/mmol) followed by degassing the mixture by 5 evacuation cycles under vigorous stirring and repressurizing with argon. The reaction mixture is refluxed under argon atmosphere for 5-7 d. The solvent is removed under reduced pressure and the residue is purified by flash column chromatography on silica gel (eluent cyclohexane/acetone 2:1 (v:v)) to remove the excess of phloroglucinol. The obtained amount of the reddish-brown raw product is used as the basis to calculate the needed amounts of squaric acid (0.50 eq. based on obtained raw product). The raw product and the needed amounts of squaric acid (0.50 eq. based on obtained raw product) are put in around-bottom flask, equipped with a Dean-Stark apparatus and reflux condenser and dissolved in a mixture of toluene/1-butanol 1:1 (v/v, 10 mL/mmol). This is followed by degassing the mixture by 5 evacuation cycles under vigorous stirring and repressurizing with argon. The reaction mixture is refluxed under argon atmosphere for 16 hours. With the beginning of boiling, a sudden color change from yellow/slightly reddish over green to dark blue can be observed. After cooling the reaction mixture to r.t. the solvent is removed and the crude product is purified by column chromatography on silica gel (eluent DCM). The obtained deep blue solid is further purified by recrystallization from dichloromethane/methanol 1:2 (v/v) for PrySQ-C1s and between 1:9 and 1:5 v/v for AlaSQs depending on the solubility and dichloromethane/cyclohexane 1:2 (v/v) for PrySQ-C1s and between 1:9 and 1:5 v/v for AlaSQs depending on the solubility. The precipitated solid is each time filtered off and washed several times with methanol. After drying under vacuum overnight, the squaraine dye is obtained as an intensively colored solid

General Procedure B:

The synthetic protocol was adapted from the literature.[31,45]

A round-bottom flask, equipped with a reflux condenser, is charged with the corresponding *O*-alkyl-L-alaninyl *N*-alkyl amine (1.20-1.50 eq.) and phloroglucinol (1.00 eq.). The reactants are suspended in a mixture of toluene/1-butanol 4:1 (v/v, 10 mL/mmol) followed by degassing the mixture by 5 evacuation cycles under vigorous stirring and repressurizing with argon. The reaction mixture is refluxed under argon atmosphere for 24 h. The solvent is removed and the residue is directly subjected to the second condensation with squaric acid (0.50 eq. based on utilized amounts of phloroglucinol) in a fresh mixture of toluene/1-butanol 1:1 (v/v, 10 mL/mmol) followed by degassing of the mixture by 5 evacuation cycles under vigorous stirring and repressurizing with argon. The reaction mixture is refluxed under argon atmosphere for 16 hours. After cooling the reaction mixture to r.t. the solvent is removed and the crude product is purified by column chromatography on silica gel (eluent DCM). The obtained deep blue solid is further purified by recrystallization from dichloromethane/methanol between 1:9 and 1:5 v/v and dichloromethane/cyclohexane between 1:9 and 1:5 v/v for AlaSQs depending on the solubility The precipitated solid is each time filtered off and washed several times with methanol. After drying under vacuum overnight, the squaraine dye is obtained as an intensively colored solid.

Synthesis of (S,S)-N-C2,O-C2-AlaSQ (23a)

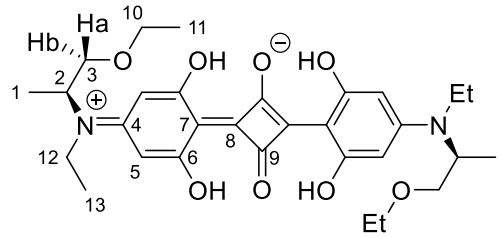

The synthesis was performed according to the general procedure B for the synthesis of squaraines using phloroglucinol (622 mg, 4.93 mmol, 1.00 eq), and *O*-ethyl-L-alaninyl *N*-ethyl amine (**22a**) (863 mg, 1.33 eq, 6.58 mmol) in 4/1 toluene/1-BuOH (13 mL) for the first condensation under reflux over 19 h. Squaric acid (281 mg, 2.47 mmol, 0.50 eq. with regard to phloroglucinol) was added afterwards and the solvent mixture was exchanged for 1/1 toluene/1-BuOH (10 mL), The mixture was refluxed for 23 h. After purification the desired product **23a** was obtained as a yellow-greenish solid (267 mg, 0.48 mmol, 20%).

Yield: 20%.

Molecular weight: $C_{30}H_{40}N_2O_8$, 556.656 g/mol

^{1}H-NMR: (700 MHz, $CDCl_3$, 298 K) δ [ppm] = 10.94 (s, 4 H, OH), 5.92 (s, 4 H, H-5), 4.22 (h, 2 H, H-2, $^3J_{2,1}$= 6.6 Hz), 3.54 (dd, 2 H, H-3a, $^2J_{3a,3b}$= 10.1 Hz, $^3J_{3a,2}$= 6.2 Hz), 3.50-3.42 (m, 10 H, H-3b, H-10, H-12), 1.29 (d, 6 H, H-1, $^3J_{1,2}$= 6.8 Hz), 1.25 (t, 6 H; H-13, $^3J_{13,12}$= 7.1 Hz), 1.17 (t, 6 H, H-11, $^3J_{11,10}$= 7.0 Hz). **^{13}C-NMR:** (176 MHz, $CDCl_3$, 298 K) δ [ppm] = 181.5 (C-9), 163.0 (C-6), 161.7 (C-8), 158.6 (C-4), 103.0 (C-7), 94.6 (C-5), 72.2 (C-3), 66.9 (C-10), 53.9 (C-2), 40.1 (C-12), 15.9 (C-1), 15.2 (C-11), 14.8 (C-13).

MS: (ESI(+), dichloromethane, M = $C_{30}H_{40}N_2O_8$) *m/z* = 557.285 $[M+H]^+$.

ESI HRMS: calculated for $[C_{30}H_{41}N_2O_8]^+$: *m/z* = 557.2857, found: *m/z* = 557.2850, calculated for $[C_{30}H_{40}N_2O_8]^{\bullet+}$:*m/z* = 556.2779, found: *m/z* = 556.2782.

Synthesis of (S,S)-N-C3,O-C3-AlaSQ (23b)

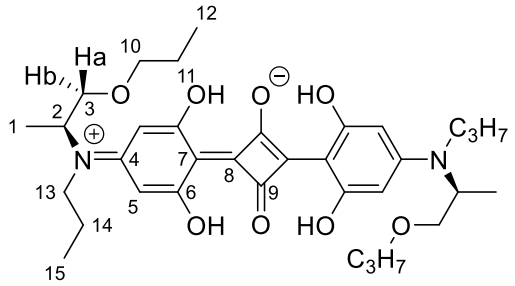

The synthesis was performed according to the general procedure A for the synthesis of squaraines using phloroglucinol (3.03 g, 24.00 mmol, 1.50 eq), and *O*-propyl-L-alaninyl *N*-propyl amine (**22b**) (2.55 g, 16.00 mmol, 1.00 eq) in 1/1 toluene/1-BuOH (160 mL) for the first condensation under reflux over 5 d. Squaric acid (117.32 mg, 1.03 mmol, 0.50 eq. with respect to the amount of isolated intermediate) was added afterwards and the solvent mixture was exchanged for 1/1 toluene/1-BuOH (21 mL), the mixture was refluxed for 24 h. After purification the desired product **23b** was obtained as a green solid (148 mg, 0.24 mmol, 23%).

Yield: 23%.

Molecular weight: $C_{34}H_{48}N_2O_8$, 612.764 g/mol

^{1}H-NMR: (700 MHz, $CDCl_3$, 298 K) δ [ppm] = 10.94 (s, 4 H, OH), 5.87 (s, 4 H, H-5), 4.21 (h, 2 H, H-2, $^3J_{2,1}$= 6.6 Hz), 3.51 (dd, 2 H, H-3a, $^2J_{3a,3b}$= 10.1 Hz, $^3J_{3a,2}$= 6.4 Hz), 3.43 (dd, 2 H, H-3b, $^2J_{3b,3a}$= 10.1 Hz, $^3J_{3b,2}$= 5.5 Hz), 3.41-3.32 (m, 4 H, H-10), 3.29-3.22 (m, 4 H, H-13), 1.71-1.60 (m, 4 H, H-14), 1.59-1.53 (m, 4 H, H-11), 1.28 (d, 6 H, H-1, $^3J_{1,2}$= 6.8 Hz), 0.94 (t, 6 H; H-15, $^3J_{15,14}$= 7.4 Hz), 0.89 (t, 6 H, H-12, $^3J_{12,11}$= 7.4 Hz).
^{13}C-NMR: (176 MHz, $CDCl_3$, 298 K) δ [ppm] = 181.4 (C-9), 162.8 (C-6), 161.5 (C-8), 158.9 (C-4), 102.6 (C-7), 94.3 (C-5), 73.1 (C-10), 72.3 (C-3), 53.6 (C-2), 47.3 (C-13), 22.9 (C-11), 22.5 (C-14), 15.8 (C-1), 11.3 (C-15), 10.6 (C-12).

MS: (ESI(+), dichloromethane, M = $C_{34}H_{48}N_2O_8$) *m/z* =651.304 $[M+K^+]^+$, 160.169 $[M+C_{25}H_{27}NO_7+H^+]^+$,

ESI HRMS: calculated for $[[C_{34}H_{48}N_2O_8K]^+$: *m/z* = 651.3042, found: *m/z* = 651.3038, calculated for $[C_{34}H_{48}N_2O_8Na]^+$: *m/z* = 635.3303, found: *m/z* = 635.3300.

Elemental analysis: calculated for $C_{34}H_{48}N_2O_8$: C: 66.64 H: 7.90 N: 4.57; found: C: 66.64 H: 7.91 N: 4.60.

Synthesis of (S,S)-N-C4,O-C4-AlaSQ (23c)

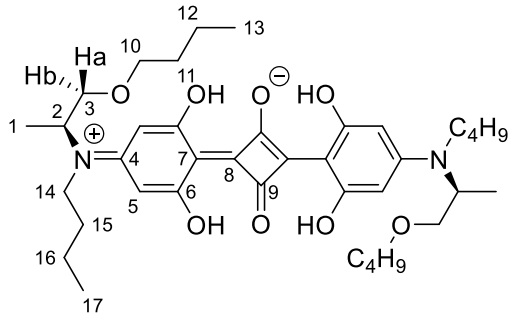

The synthesis was performed according to the general procedure A for the synthesis of squaraines using phloroglucinol (2.73 g, 21.62 mmol, 2.00 eq), and *O*-butyl-L-alaninyl *N*-butyl amine (**22c**) (2.03 g, 10.81 mmol, 1.00 eq) in 1/1 toluene/1-BuOH (108 mL) for the first condensation under reflux over 5 d. Squaric acid (154.44 mg, 1.69 mmol, 0.50 eq. with respect to the amount of isolated intermediate) was added afterwards and the solvent mixture was exchanged for 1/1 toluene/1-BuOH (21 mL)), the mixture was refluxed for 24 h. After purification the desired product **23c** was obtained as a green solid (60 mg, 89.7 µmol, 5%).

Yield: 5%.

Molecular weight: $C_{38}H_{56}N_2O_8$, 668.872 g/mol

^{1}H-NMR: (500 MHz, $CDCl_3$, 298 K) δ [ppm] = 10.94 (s, 4 H, OH), 5.89 (s, 4 H, H-5), 4.21 (p, 2 H, H-2, $^3J_{2,1}$= 6.2 Hz), 3.56-3.49 (m, 2 H, H-3a), 3.47-3.37 (m, 6 H, H-3b,H-10), 3.32-3.29 (m, 4 H, H-14), 1.70-1.59 (m, 4 H, H-11), 1.58-1.49 (m, 4 H, H-15), 1.40-1.31 (m, 8 H, H-12, H-16), 1.28 (d, 6 H, H-1, $^3J_{1,2}$= 6.5 Hz), 0.99-0.96 (m, 6 H, H-17), 0.93-0.88 (m, 6 H, H-13). **^{13}C-NMR:** (126 MHz, $CDCl_3$, 298 K) δ [ppm] = 181.5 (C-9), 162.9 (C-6), 161.7 (C-8), 159.0 (C-4), 102.8 (C-7), 94.5 (C-5), 72.6 (C-3), 71.4 (C-10), 53.9 (C-2), 45.7 (C-13), 31.8 (C-15), 31.5 (C-11), 20.5 (C-16), 19.5 (C-12), 15.9 (C-1), 14.0 (C-13), 13.9 (C-14).

MS: (ESI(+), dichloromethane, M = $C_{38}H_{56}N_2O_8$) *m/z* =669.410 $[M+H]^+$.

ESI HRMS: calculated for $[C_{38}H_{57}N_2O_8]^+$: *m/z* = 669.4109, found: *m/z* = 669.4102.

Synthesis of (S,S)-N-C5, O-C5-AlaSQ (23d)

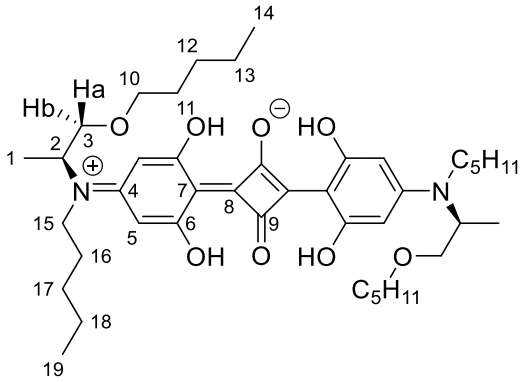

The synthesis was performed according to the general procedure B for the synthesis of squaraines using phloroglucinol (672 mg, 5.33 mmol, 1.00 eq), and *O*-pentyl-L-alaninyl *N*-pentyl amine (**22d**) (1.53 g, 1.33 eq, 7.10 mmol) in 4/1 toluene/1-BuOH (15 mL) for the first condensation under reflux over 18 h Squaric acid (304 mg, 2.66 mmol, 0.50 eq. with regard to phloroglucinol) was added afterwards and the solvent mixture was exchanged for 1/1 toluene/1-BuOH (11 mL), The mixture was refluxed for 22 h. After purification the desired product **23d** was obtained as a green solid (2 mg, 6 µmol, 0.1%).

Yield: 0.1%.

Molecular weight: $C_{42}H_{64}N_2O_8$, 724.980 g/mol

^{1}H-NMR: (700 MHz, $CDCl_3$, 298 K) δ [ppm] = 10.94 (s, 4 H, OH), 5.89 (s, 4 H, H-5), 4.21 (q, 2 H, H-2, $^3J_{2,1}$= 6.5 Hz), 3.51 (dd, 2 H, H-3a, $^2J_{3a,3b}$= 10.1 Hz, $^3J_{3a,2}$= 6.4 Hz), 3.43 (dd, 2 H, H-3b, $^2J_{3b,3a}$= 10.1 Hz, $^3J_{3b,2}$= 5.5 Hz), 3.39 (td, 4 H, H-10, $^3J_{10,11}$= 6.5 Hz), 3.29 (t, 4 H, H-15, $^3J_{15,16}$= 8.4 Hz), 1.68-1.58 (m, 4 H, H-16), 1.57-1.50 (m, 4 H, H-11), 1.40-1.34 (m, 4 H, H-18), 1.33-1.24 (m, 26 H, H-1, H-12, H-13, H-16, H-17), 0.93 (t, 6 H, H-19, $^3J_{19,18}$= 7.2 Hz), 0.88 (t, 6 H, H-14, $^3J_{14,13}$= 6.9 Hz). **^{13}C-NMR:** (176 MHz, $CDCl_3$, 298 K) δ [ppm] = 181.5 (C-9), 162.9 (C-6), 161.6 (C-8), 94.6 (C-5), 72.5 (C-3), 71.5 (C-10), 29.4 (C-11), 29.3 (C-12/C-17), 29.1 (C-16), 28.5 (C-12/C-17), 15.9 (C-1), 14.2 (C-13, C-19).

Signals for C-2, C-4, C-7 and C-15 not resolved.

MS: (ESI(+), dichloromethane, M = $C_{42}H_{64}N_2O_8$) *m/z* =759.436 $[M+ Cl^+]^+$,725.436 $[M+H]^+$.

ESI HRMS: calculated for $[C_{42}H_{65}N_2O_8]$+: *m/z* = 725.4735, found: *m/z* = 725.4737.

Synthesis of (S,S)-N-C7,O-C7-AlaSQ (23e)

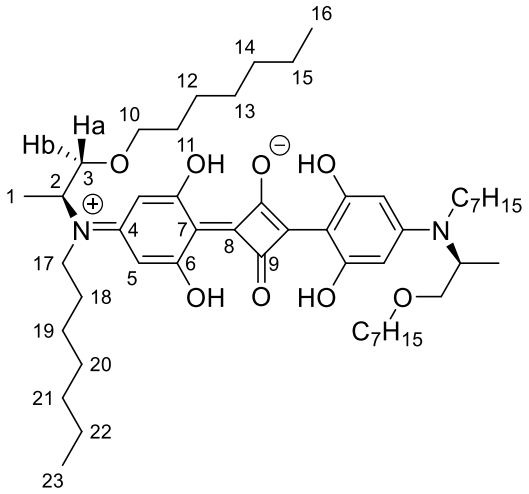

The synthesis was performed according to the general procedure B for the synthesis of squaraines using phloroglucinol (235 mg, 1.86 mmol, 1.00 eq), and *O*-heptyl-L-alaninyl *N*-heptyl amine (**22e**) (674 mg, 1.33 eq, 2.48 mmol) in 4/1 toluene/1-BuOH (6 mL) for the first condensation under reflux over 22 h. Squaric acid (106 mg, 0.93 mmol, 0.50 eq. with regard to phloroglucinol) was added afterwards and the solvent mixture was exchanged for 1/1 toluene/1-BuOH (5 mL). The mixture was refluxed for 22 h. After purification the desired product **23e** was obtained as a green solid (6 mg, 15 µmol, 0.8%).

Yield: 0.8%.

Molecular weight: $C_{50}H_{80}N_2O_8$, 837.196 g/mol

^{1}H-NMR: (500 MHz, $CDCl_3$, 298 K) δ [ppm] = 10.94 (s, 4 H, OH), 5.88 (s, 4 H, H-5), 4.21 (h, 2 H, H-2, $^3J_{2,1}$= 6.6 Hz), 3.51 (dd, 2 H, H-3a, $^2J_{3a,3b}$= 10.1 Hz, $^3J_{3a,2}$= 6.4 Hz), 3.43 (dd, 2 H, H-3b, $^2J_{3b,3a}$= 10.1 Hz, $^3J_{3b,2}$= 5.4 Hz), 3.39 (q, 4 H, H-10, $^3J_{10,11}$= 6.5 Hz), 3.29 (t, 4 H, H-17, $^3J_{17,18}$= 8.4 Hz), 1.68-1.57 (m, 4 H, H-18), 1.55-1.50 (m, 4 H, H-11), 1.36-1.21 (m, 38 H, H-1, H-12, H-13, H-14, H-15, H-19, H-20, H-21, H-22), 0.90 (t, 6 H, H-23, $^3J_{23,22}$= 7.0 Hz), 0.87 (t, 6 H, H-16, $^3J_{16,15}$= 7.0 Hz). **^{13}C-NMR:** (126 MHz, $CDCl_3$, 298 K) δ [ppm] = 181.5 (C-9), 162.9 (C-6), 161.5 (C-8), 158.9 (C-4), 102.9 (C-7), 94.6 (C-5), 72.5 (C-3), 71.7 (C-10), 53.9 (C-2), 45.9 (C-17), 32.0 (C-14, C-21), 29.8 (C-11), 29.4$^{\#}$ (C-13/C-18), 29.3$^{\#}$ (C-12/C-18), 29.1 (C-20), 27.3 (C-19), 26.2 (C-12), 22.7 (C-15, C-22), 15.9 (C-1), 14.2 (C-16, C-23).

$^{\#}$unambiguous assignment not possible.

MS: (ESI(+), dichloromethane, M = $C_{50}H_{80}N_2O_8$) *m/z* =871.560 $[M+ Cl^+]^+$, 272.295 $[M\text{-}C_{33}H_{44}NO_7+H]^+$.

ESI HRMS: calculated for $[C_{50}H_{81}N_2O_8]^+$: *m/z* = 837.5987, found: *m/z* = 837.5985.

Synthesis of (S,S)-N-C8,O-C8-AlaSQ (23f)

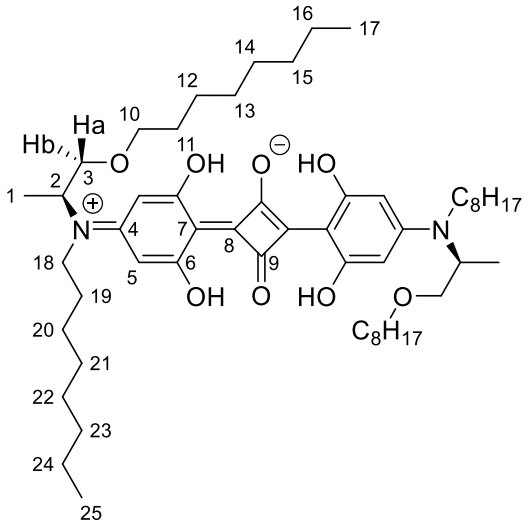

The synthesis was performed according to the general procedure B for the synthesis of squaraines using phloroglucinol (720 mg, 5.72 mmol, 1.00 eq), and *O*-octyl-L-alaninyl *N*-octyl amine (**22f**) (2.28 g, 1.00 eq, 7.62 mmol) in 4/1 toluene/1-BuOH (20 mL) for the first condensation under reflux over 21 h. Squaric acid (326 mg, 2.86 mmol, 0.50 eq. with regard to phloroglucinol) was added afterwards and the solvent mixture was exchanged for 1/1 toluene/1-BuOH (12 mL). The mixture was refluxed for 22 h. After purification the desired product **23f** was obtained as a green solid (22 mg, 55 µmol, 1%).

Yield: 1%.

Molecular weight: $C_{54}H_{88}N_2O_8$, 892.304 g/mol

^{1}H-NMR: (700 MHz, $CDCl_3$, 298 K) δ [ppm] = 10.94 (s, 4 H, OH), 5.88 (s, 4 H, H-5), 4.21 (q, 2 H, H-2, $^3J_{2,1}$= 6.4 Hz), 3.50 (dd, 2 H, H-3a, $^2J_{3a,3b}$= 10.1 Hz, $^3J_{3a,2}$= 6.5 Hz), 3.43 (dd, 2 H, H-3b, $^2J_{3b,3a}$= 10.1 Hz, $^3J_{3b,2}$= 5.5 Hz), 3.41-3.37 (m, 4 H, H-10), 3.29 (t, 4 H, H-18, $^3J_{18,19}$= 8.4 Hz) 1.68-1.60 (m, 4 H, H-19), 1.54-1.48 (m, 4 H, H-11), 1.38-1.18 (m, 46 H,H-1, H-12, H-13, H-14, H-15, H-16, H-20, H-21, H-22, H-23, H-24), 0.92-0.84 (m, 12 H, H-17, H-25). **^{13}C-NMR:** (176 MHz, $CDCl_3$, 298 K) δ [ppm] = 181.5 (C-9), 162.9 (C-6), 161.5 (C-8), 159.0 (C-4), 102.8 (C-7), 94.5 (C-5), 72.5 (C-3), 71.7 (C-10), 32.0 (C-15, C-23), 30.2 (C-14, C-22), 29.9 (C-20), 29,8 (C-11), 29.6 (C-13), 29.4 (C-19), 27.3 (C-21), 26.3 (C-12), 22.8 (C-16, C-24), 15.9 (C-1), 14.2 (C-17, C-25).

Signals for C-2 and C-18 not resolved.

MS: (ESI(+), dichloromethane, M = $C_{54}H_{88}N_2O_8$) *m/z* =893.659 $[M+H]^+$, 300.326 $[M-C_{35}H_{48}NO_7+H]^+$.

ESI HRMS: calculated for $[C_{54}H_{89}N_2O_8]^+$: *m/z* = 893.6613, found: *m/z* = 892.6592.

Synthesis of (S,S)-N-C9,O-C9-AlaSQ (23g)

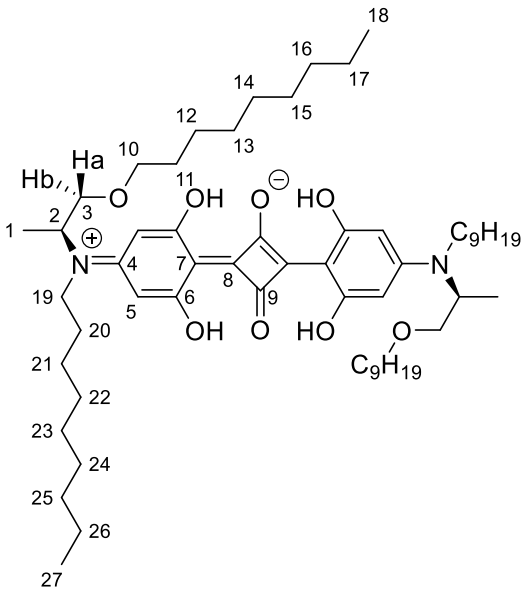

The synthesis was performed according to the general procedure B for the synthesis of squaraines using phloroglucinol (577 mg, 4.58 mmol, 1.00 eq.), and *O*-nonyl-L-alaninyl *N*-nonyl amine (**22g**) (1.97 g, 1.33 eq., 6.10 mmol) in 4/1 toluene/1-BuOH (12 mL) for the first condensation under reflux over 24 h. Squaric acid (261 mg, 2.29 mmol, 0.50 eq. with regard to phloroglucinol) was added afterwards and the solvent mixture was exchanged for 1/1 toluene/1-BuOH (9 mL), The mixture was refluxed for 24 h. After purification the desired product **23g** was obtained as a green solid (69 mg, 72 µmol, 3%).

Yield: 3%.

Molecular weight: $C_{58}H_{94}N_2O_8$, 947.396 g/mol

^{1}H-NMR: (700 MHz, $CDCl_3$, 298 K) δ [ppm] = 10.94 (s, 4 H, OH), 5.89 (s, 4 H, H-5), 4.20 (h, 2 H, H-2, $^3J_{2,1}$= 6.6 Hz), 3.51 (dd, 2 H, H-3a, $^2J_{3a,3b}$= 10.1 Hz, $^3J_{3a,2}$= 6.5 Hz), 3.43 (dd, 2 H, H-3b, $^2J_{3b,3a}$= 10.1 Hz, $^3J_{3b,2}$= 5.4 Hz), 3.41-3.36 (m, 4 H, H-10), 3.29 (t, 4 H, H-14, $^3J_{14,15}$= 8.4 Hz), 1.68-1.56 (m, 4 H, H-11), 1.56-1.49 (m, 4 H, H-20), 1.36-1.19 (m, 54 H, H-1, H-12, H-13, H-14, H-15, H-16, H-17, H-21, H-22, H-23, H-24, H-25, H-26), 0.90-0.88 (m, 6 H, H-18/H-26), 0.88-0.86 (m, 6 H, H-18/H-26). **^{13}C-NMR:** (176 MHz, $CDCl_3$, 298 K) δ [ppm] = 181.6 (C-9), 162.9 (C-6), 161.6 (C-8), 158.9 (C-4), 103.0 (C-7), 94.7 (C-5), 72.5 (C-3), 71.7 (C-10), 54.0 (C-2), 45.9 (C-13), 32.1 (C-25), 32.0 (C-16), 29.8# (C-13/C14/C-15/C-21/C-22/C-23/C-24), 29.7 (C-20), 29.6# (C-13/C14/C-15/C-21/C-22/C-23/C-24), 2x 29.5# (C-13/C14/C-15/C-21/C-22/C-23/C-24), 29.4 (C-11), 27.3# (C-12/C-21), 26.3# (C-12/C-21), 22.8 (C-17,C-26), 15.9 (C-1), 14.2 (C-18, C-27).

#unambiguous assignment not possible.

MS: (ESI(+), dichloromethane, M = $C_{58}H_{96}N_2O_8$) *m/z* =949.723 $[M+H]^+$, 328.357 $[M-C_{37}H_{50}NO_7+H]^+$.

ESI HRMS: calculated for $[C_{58}H_{97}N_2O_8]^+$: *m/z* = 949.7239, found: *m/z* = 949.7228.

Synthesis of (S,S)-N-C9,O-C4-AlaSQ (23h)

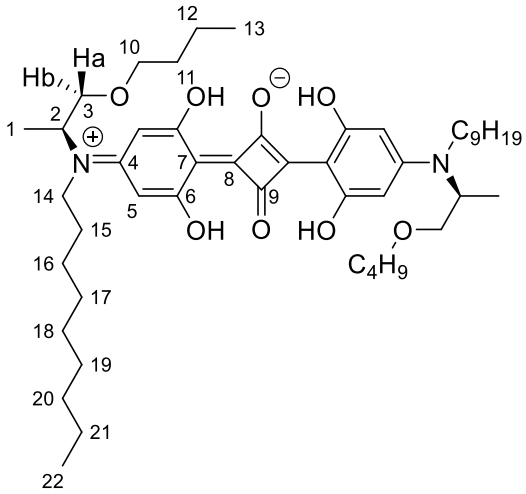

The synthesis was performed according to the general procedure B for the synthesis of squaraines using phloroglucinol (393 mg, 3.12 mmol, 1.00 eq), and *O*-nonyl-L-alaninyl *N*-butyl amine (**22h**) (1.07 g, 4.16 mmol, 1.33 eq.) in 4/1 toluene/1-BuOH (8 mL) for the first condensation under reflux over 24 h. Squaric acid (178 mg, 1.56 mmol, 0.50 eq. with regard to phloroglucinol) was added afterwards and the solvent mixture was exchanged for 1/1 toluene/1-BuOH (6 mL), The mixture was refluxed for 24 h. After purification the desired product **23h** was obtained as a green solid (140 mg, 0.38 mmol, 9%).

Yield: 9%.

Molecular weight: $C_{48}H_{76}N_2O_8$, 809.142 g/mol

^{1}H-NMR: (700 MHz, $CDCl_3$, 298 K) δ [ppm] = 10.94 (s, 4 H, OH), 5.89 (s, 4 H, H-5), 4.20 (q, 2 H, H-2, $^3J_{2,1}$= 6.4 Hz), 3.52 (dd, 2 H, H-3a, $^2J_{3a,3b}$= 10.2 Hz, $^3J_{3a,2}$= 6.3 Hz), 3.43 (dd, 2 H, H-3b, $^2J_{3b,3a}$= 10.2 Hz, $^3J_{3b,2}$= 5.3 Hz), 3.40 (td, 4 H, H-10, $^3J_{10,11}$= 6.5 Hz, $^4J_{10,12}$= 4.8 Hz), 3.29 (t, 4 H, H-14, $^3J_{14,15}$= 8.4 Hz), 1.68-1.59 (m, 4 H, H-11), 1.57-1.46 (m, 4 H, H-15), 1.38-1.18 (m, 34 H, H-1, H-12, H-16, H-17, H-18, H-19, H-20, H-21), 0.91-0.88 (m, 12 H, H-13,H-22). **^{13}C-NMR:** (176 MHz, $CDCl_3$, 298 K) δ [ppm] = 181.6 (C-9), 162.9 (C-6), 161.6 (C-8), 158.8 (C-4), 102.8 (C-7), 94.7 (C-5), 72.5 (C-3), 71.4 (C-10), 53.9 (C-2), 45.8 (C-13), 32.0 (C-20), 31.9 (C-15), 29.7$^{\#}$ (C-17/C-18/C-19), 2x 29.6$^{\#}$ (C-17/C-18/C-19), 29.4 (C-11), 27.3 (C-16), 22.8 (C-21), 19.5 (C-12), 15.9 (C-1), 14.2 (C-22), 14.0 (C-13).

$^{\#}$unambiguous assignment not possible.

MS: (ESI(+), dichloromethane, M = $C_{48}H_{76}N_2O_8$) *m/z* =809.567 $[M+H]^+$, 258.279 $[M\text{-}C_{37}H_{50}NO_7+H]^+$,

ESI HRMS: calculated for $[C_{48}H_{77}N_2O_8]^+$: *m/z* = 809.5674, found: *m/*z = 809.5666.

Synthesis of (S,S)-N-C3,O-C7-AlaSQ (23i)

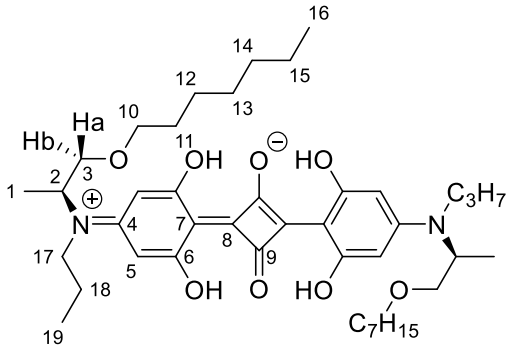

The synthesis was performed according to the general procedure B for the synthesis of squaraines using phloroglucinol (643 mg, 5.10 mmol, 1.00 eq), and *O*-heptyl-L-alaninyl *N*-propyl amine (**22i**) (1.46 g, 1.33 eq, 6.80 mmol) in 4/1 toluene/1-BuOH (14 mL) for the first condensation under reflux over 24 h. Squaric acid (291 mg, 2.55 mmol, 0.50 eq. with regard to phloroglucinol) was added afterwards and the solvent mixture was exchanged for 1/1 toluene/1-BuOH (10 mL), The mixture was refluxed for 24 h.. After purification the desired product **23i** was obtained as a green solid (69 mg, 95 µmmol, 4%).

Yield: 4%.

Molecular weight: $C_{42}H_{64}N_2O_8$, 724.980 g/mol

^{1}H-NMR: (700 MHz, $CDCl_3$, 298 K) δ [ppm] = 10.94 (s, 4 H, OH), 5.89 (s, 4 H, H-5), 4.21 (h, 2 H, H-2, $^3J_{2,1}$= 6.6 Hz), 3.51 (dd, 2 H, H-3a, $^2J_{3a,3b}$= 10.1 Hz, $^3J_{3a,2}$= 6.4 Hz), 3.43 (dd, 2 H, H-3b, $^2J_{3b,3a}$= 10.1 Hz, $^3J_{3b,2}$= 5.4 Hz), 3.39 (td, 4 H, H-10, $^3J_{10,11}$= 6.5 Hz, $^4J_{10,12}$= 4.0 Hz), 3.26 (t, 4 H, H-14, $^3J_{14,15}$= 8.4 Hz), 1.72-1.61 (m, 4 H, H-18), 1.58-1.48 (m, 4 H, H-11), 1.34-1.21 (m, 14 H, H-1, H-12, H-13, H-14, H-15), 0.95 (t, 6 H, H-19, $^3J_{19,18}$= 7.4 Hz), 0.88 (t, 6 H, H-16, $^3J_{16,15}$= 7.0 Hz). **^{13}C-NMR:** (176 MHz, $CDCl_3$, 298 K) δ [ppm] = 181.5 (C-9), 162.9 (C-6), 161.7 (C-8), 159.0 (C-4), 102.9 (C-7), 94.6 (C-5), 72.5 (C-3), 71.7 (C-10), 53.9 (C-2), 47.6 (C-13), 32.0 (C-14), 29.8 (C-11), 29.2 (C-13), 26.2 (C-12), 22.8 (C-15), 22.6 (C-18), 15.9 (C-1), 14.2 (C-16), 11.5 (C-19).

[#]unambiguous assignment not possible.

MS: (ESI(+), dichloromethane, M = $C_{42}H_{64}N_2O_8$) *m/z* =1472.928 $[2M+Na]^+$,759.436 $[M+Cl^+]^+$, 747.457 $[M+Na]^+$, 725.474 $[M+H^+]^+$, 216.232 $[M-C_{29}H_{36}NO_7+H]^+$,

ESI HRMS: calculated for $[C_{42}H_{65}N_2O_8]^+$: *m/z* = 725.4735, found: *m/z* = 725.438.

Synthesis of (S,S)-N-C3,O-C9-AlaSQ (23j)

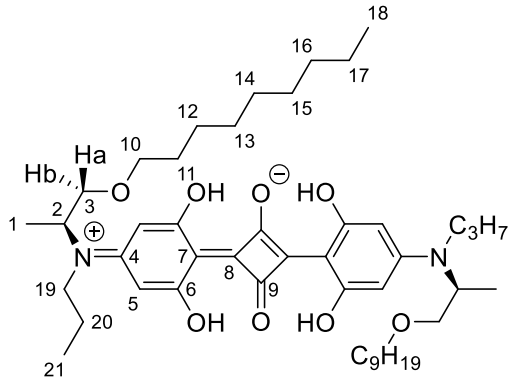

The synthesis was performed according to the general procedure B for the synthesis of squaraines using phloroglucinol (381 mg, 3.02 mmol, 1.00 eq), and *O*-nonyl-L-alaninyl *N*-propyl amine (**22j**) (979 mg, 1.33 eq, 4.02 mmol) in 4/1 toluene/1-BuOH (8 mL) for the first condensation under reflux over 18 h Squaric acid (172 mg, 1.51 mmol, 0.50 eq. with regard to phloroglucinol) was added afterwards and the solvent mixture was exchanged for 1/1 toluene/1-BuOH (6 mL), The mixture was refluxed for 22 h. After purification the desired product **23j** was obtained as a green solid (9 mg, 12 µmol, 0.8%).

Yield: 0.8%.

Molecular weight: $C_{46}H_{72}N_2O_8$, 781.088 g/mol

^{1}H-NMR: (700 MHz, $CDCl_3$, 298 K) δ [ppm] = 10.94 (s, 4 H, OH), 5.89 (s, 4 H, H-5), 4.21 (h, 2 H, H-2, $^3J_{2,1}$= 6.5 Hz), 3.51 (dd, 2 H, H-3a, $^2J_{3a,3b}$= 10.1 Hz, $^3J_{3a,2}$= 6.4 Hz), 3.43 (dd, 2 H, H-3b, $^2J_{3b,3a}$= 10.1 Hz, $^3J_{3b,2}$= 5.4 Hz), 3.39 (td, 4 H, H-10, $^3J_{10,11}$= 6.6 Hz, $^4J_{10,12}$= 4.2 Hz), 3.26 (t, 4 H, H-19, $^3J_{19,20}$= 8.4 Hz), 1.72-1.60 (m, 4 H, H-20), 1.59-1.49 (m, 4 H, H-11), 1.35-1.21 (m, 30 H, H-1, H-12, H-13, H-14, H-15, H-16, H-17), 0.95 (t, 6 H, H-21, $^3J_{21,20}$= 7.4 Hz), 0.90-084 (m, 6 H, H-18). **^{13}C-NMR:** (176 MHz, $CDCl_3$, 298 K) δ [ppm] = 181.5 (C-9), 162.9 (C-6), 161.7 (C-8), 159.0 (C-4), 102.9 (C-7), 94.6 (C-5), 72.5 (C-3), 71.7 (C-10), 53.9 (C-2), 47.4 (C-19), 32.0 (C-16), 29.8 (C-11), 29.7$^{\#}$ (C-13/C-14/C-15), 29.6$^{\#}$ (C-13/C-14/C-15), 29.4$^{\#}$ (C-13/C-14/C-15), 26.3 (C-12), 22.8 (C-17), 22.6 (C-20), 15.9 (C-1), 14.2 (C-18), 11.5 (C-21).

$^{\#}$unambiguous assignment not possible.

MS: (ESI(+), dichloromethane, M = $C_{46}H_{72}N_2O_8$) *m/z* = 781.536 $[M+H]^+$.

ESI HRMS: calculated for $[C_{46}H_{73}N_2O_8]^+$: *m/z* = 781.5361, found: *m/z* = 781.5356.

Synthesis of (S,S)-N-C4,O-C9-AlaSQ (23k)

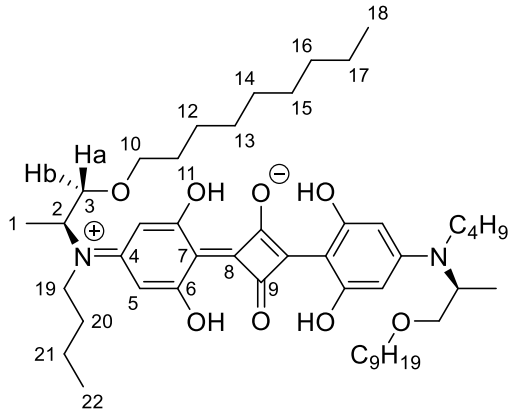

The synthesis was performed according to the general procedure B for the synthesis of squaraines using phloroglucinol (358 mg, 2.48 mmol, 1.00 eq), and *O*-nonyl-L-alaninyl *N*-butyl amine (**22k**) (974 mg, 1.33 eq, 3.78 mmol) in 4/1 toluene/1-BuOH (9 mL) for the first condensation under reflux over 19 h. Squaric acid (161 mg, 1.42 mmol, 0.50 eq. with regard to phloroglucinol) was added afterwards and the solvent mixture was exchanged for 1/1 toluene/1-BuOH (6 mL), The mixture was refluxed for 23 h. After purification the desired product **23k** was obtained as a green solid (14 mg, 17 µmol, 1 %).

Yield: 1%.

Molecular weight: $C_{48}H_{76}N_2O_8$, 809.142 g/mol

^{1}H-NMR: (700 MHz, $CDCl_3$, 298 K) δ [ppm] = 10.94 (s, 4 H, OH), 5.88 (s, 4 H, H-5), 4.21 (h, 2 H, H-2, $^3J_{2,1}$= 6.6 Hz), 3.51 (dd, 2 H, H-3a, $^2J_{3a,3b}$= 10.1 Hz, $^3J_{3a,2}$= 6.5 Hz), 3.43 (dd, 2 H, H-3b, $^2J_{3b,3a}$= 10.1 Hz, $^3J_{3b,2}$= 5.5 Hz), 3.41-3.35 (m, 4 H, H-10), 3.30 (t, 4 H, H-19, $^3J_{19,20}$= 8.4 Hz), 1.68-1.55 (m, 4 H, H-20), 1.55-1.48 (m, 4 H, H-11), 1.37 (h, 4 H, H-21, $^3J_{21,22}$= 7.4 Hz) 1.32-1.21 (m, 30 H, H-1, H-12, H-13, H-14, H-15, H-16, H-17), 0.97 (t, 6 H, H-22, $^3J_{22,21}$= 7.4 Hz), 0.89-0.86 (m, 6 H, H-18). **^{13}C-NMR:** (176 MHz, $CDCl_3$, 298 K) δ [ppm] = 181.5 (C-9), 162.9 (C-6), 161.6 (C-8), 159.0 (C-4), 102.8 (C-7), 94.5 (C-5), 72.5 (C-3), 71.4 (C-10), 53.9 (C-2), 45.6 (C-13), 32.1 (C-16), 31.5 (C-20), 29.8# (C-11/C-13/C-14/C-15), 29.7 (C-11/C-13/C-14/C-15), 29.6# (C-11/C-13/C-14/C-15), 29.4# (C-11/C-13/C-14/C-15), 26.3 (C-12), 22.7 (C-27), 20.5 (C-21), 15.9 (C-1), 14.2 (C-18), 13.9 (C-22).

#unambiguous assignment not possible.

MS: (ESI(+), dichloromethane, M = $C_{48}H_{76}N_2O_8$) m/z = 809.567 $[M+H]^+$, 258.279 $[M-C_{37}H_{50}NO_7+H]^+$.

ESI HRMS: calculated for $[C_{48}H_{77}N_2O_8]^+$: *m/z* = 809.5674, found: *m/z* = 809.5661.

Synthesis of (R,R)-PyrSQ-C1

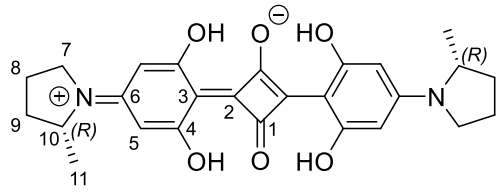

The synthesis was performed adapting the literature procedure.[44]

The synthesis was performed according to the literature protocol[44] using (*R*)-2-methylpyrrolidin (1.00 g, 11.74 mmol, 1.00 eq), and phloroglucinol (1.48 g, 1.00 eq, 11.74 mmol) in 1/1 toluene/1-BuOH (120 mL) for the first condensation under reflux over 24 h. Afterwards squaric acid (172 mg, 1.51 mmol, 0.50 eq. with regard to phloroglucinol) was added and the mixture was refluxed for 24 h. After purification the desired product **(*R*,*R*)-PyrSQ-C1** was obtained as a green solid (1.00 g, 2.15 mmol, 18%).

Yield: 18%.

Molecular weight: $C_{26}H_{28}N_2O_8$, 464.518 g/mol

^{1}H-NMR: (400 MHz, $CDCl_3$, 298 K) δ [ppm] = 11.02 (s, 4 H), 5.74 (s, 4 H), 4.11–4.05 (m, 2 H), 3.56 (dd, 2 H), 3.38 (dt, 2 H), 2.17–2.00 (m, 6 H), 1.84–1.74 (m, 2 H), 1.23 (d, 6 H)

MS: (ESI(+), dichloromethane, M = $C_{26}H_{28}N_2O_8$) *m/z* = 465.202 $[M+H]^+$.

ESI HRMS: calculated for $[C_{26}H_{29}N_2O_8]^+$: *m/z* = 465.2020, found: *m/z* = 465.2012.

The analytical data are in accordance with the ones published in the literature.[44]

Synthesis of (S,S)-PyrSQ-C1

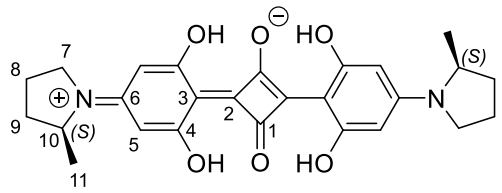

The synthesis was performed adapting the literature procedure.[44]

The synthesis was performed according to the general procedure A for the synthesis of squaraines using (*S*)-2-methylpyrrolidin (508 mg, 5.97 mmol, 1.00 eq), and phloroglucinol (753 mg, 1.00 eq, 5.97 mmol) in 1/1 toluene/1-BuOH (60 mL) for the first condensation under reflux over 19 h Squaric acid (204 mg, 2.98 mmol, 0.50 eq. with regard to phloroglucinol) was added and the mixture was refluxed for 24 h. After purification the desired product **(*S*,*S*)-PyrSQ-C1** was obtained as a green solid (300 mg, 0.65 mmol, 11%).

Yield: 11%.

Molecular weight: $C_{26}H_{28}N_2O_8$, 464.518 g/mol

^{1}H-NMR: (700 MHz, $CDCl_3$, 298 K) δ [ppm] = 11.02 (s, 4 H, OH), 5.74 (s, 4 H, H-5), 4.11–4.05 (m, 2 H, H-10), 3.56 (dd, 2 H, H-7a), 3.38 (dt, 2 H, H-7b), 2.17–2.00 (m, 6 H, H-8, H-9a), 1.84–1.74 (m, 2 H, H-9b), 1.23 (d, 6 H, H-11, $^3J_{11,10}$= 6.4 Hz)

^{13}C-NMR: (176 MHz, $CDCl_3$, 298 K) δ [ppm] = 181.5 (C-1), 162.8 (-4), 161.4 (C-2), 156.3 (C-5), 102.7 (C-3), 94.6 (C-5), 55.1 (C-10), 48.6 (C-7), 32.5 (C-9), 22.8 (C-8), 19.6 (C-11).

MS: (ESI(+), dichloromethane, M = $C_{26}H_{28}N_2O_8$) *m/z* = 465.202 $[M+H]^+$.

ESI HRMS: calculated for $[C_{26}H_{29}N_2O_8]^+$: *m/z* = 465.2020, found: *m/z* = 465.2016.

The analytical data are in accordance with the ones of the enantiomer published in the literature.[44]

7.5 CRYSTALLOGRAPHIC DATA

Single crystals of **15**, **(*S*,*S*)-PyrSQ-C1**, **(*S*,*S*)-*N*-C3,*O*-C3-AlaSQ** (**23b**) and **(*S*,*S*)-*N*-C4,*O*-C4-AlaSQ** (**23c**) suitable for single crystal structure analysis via X-ray diffraction were directly obtained from the above-mentioned purification process. Single crystals of **15**, **(*S*,*S*)-PyrSQ-C1**, **23b** and **23c** were analyzed using either a STOE STADIVARI diffractometer measuring at 100 K employing Cu-Kα radiation (λ= 1.54186 Å) or a Bruker D8 Venture diffractometer measuring at 104 K employing Mo-Kα radiation (λ= 0.71073 Å), respectively. The structures were solved with SHELXL-2019/1 and then refined with the SHELXL 2018/3.[160] The single crystal structure data were analyzed with VESTA 3.5.7[161] and are visualized with Mercury 4.2.0.[162]

For **15** the crystal dimensions of the metallic brownish blue plank measured to 0.18 mm × 0.11 mm× 0.03 mm, an empirical formula of $C_{46}H_{64}N_2O_2$ and weight of 676.99 amu. The space group is determined to be $P2_1/n$ with a = 17.4752(17) Å, b = 9.3823(7) Å, c = 11.9430(12Å, α = 90°, β = 90.108(8)°, γ = 90°, Z = 2, resulting in a volume V = 1958.1(3) Å^3 and density ρ = 1.148 g/cm^3. The absorption coefficient μ =0.52 mm^{-1}, F (000) = 740, Θ range for data collection 5.351to 70.87°, index ranges-21 ≤ h ≤ 14, -9 ≤ k ≤ 11, -11 ≤ l ≤ 14, 20809 reflection were collected (3734 independent reflections R_{int} = 0.0677, observed reflection (I > 2 (I)), completeness to theta = 70.72826° 99.8%, absorption correct by multi-scans. Maximum transmission was 0.9249 and minimum transmission was 0.2499, final *R* indices (I>=2σ (I)) R_1 = 0.0635, wR_2 = 0.1593, R includes (all data) R_1 = 0.0972, wR_2 = 0.1842. Goodness-of-fit on F^2 = 1.078 for 3734 data 43 restraints and 257 parameter, largest diff peak/hole 0.40 eÅ^{-3} and -0.22 e Å^{-3}.

For **(*S*,*S*)-PyrSQ-C1** the crystal dimensions of the metallic plank measured to 0.45 mm × 0.08 mm × 0.07 mm, an empirical formula of $C_{26}H_{28}N_2O_8$ and weight of 464.50 amu. The space group is determined to be $P2_12_12_1$ with a = 8.1189(7)) Å, b = 11.3303(6) Å, c = 23.7029(14) Å, α = 90°, β = 90°, γ = 90°, Z = 4, resulting in a volume V = 2180.4(3) Å^3 and density ρ = 1.415 g/cm^3. The absorption coefficient μ =0.83 mm^{-1}, F (000) = 984, Θ range for data collection 5.401° to 70.357°, index -21 ≤ h ≤ 14, -9 ≤ k ≤ 11, -11 ≤ l ≤ 14, 20809 reflection were collected (3734 independent reflections R_{int} = 0.0677, observed reflection (I > 2 (I)), completeness to theta = 70.216286° 99.8%, absorption correct by multi-scans. Maximum transmission was 0.7800and minimum transmission was 0.6828, final *R* indices (I>=2σ (I)) R_1 = 0.0384, wR_2 = 0.1018, R includes (all data) R_1 = 0.0403, wR_2 = 0.1035. Goodness-of-fit on F^2 = 1.050 for 4142 data 0 restraints and 313 parameter, largest diff peak/hole 0.58 eÅ^{-3} and -0.25 e Å^{-3}.

For **23b** the crystal dimensions of the clear bluish green plank measured to 0.4 mm × 0.2 mm × 0.02 mm, an empirical formula of $C_{34}H_{48}N_2O_8$ and weight of 612.74 amu. The space group is determined to be P1 with a = 6.9085(7) Å, b = 7.9615(9) Å, c = 14.9878(18) Å, α = 76.545(9)°, β = 88.888(9)°, γ = 85.988(9)°, Z = 1, resulting in a volume V = 799.76(16) Å^3 and density ρ = 1.272 g/cm^3. The absorption coefficient μ =0.74 mm^{-1}, F (000) = 330, Θ range for data collection 5.747 to 67.725°, index ranges -6 ≤ h ≤ 8, -7 ≤ k ≤ 9, -17 ≤ l ≤ 17, 25921 reflection were collected (3681 independent reflections R_{int} = 0.1296, observed reflection (I > 2 (I)), completeness to theta = 67.31865° 99.4%, absorption correct by multi-scans. Maximum transmission was 0.8948 and minimum transmission was 0.4690, final *R* indices (I>=2σ (I)) R_1 = 0.1082, wR_2 = 0.2697, R includes (all data) R_1 = 0.1396, wR_2 = 0.3069. Goodness-of-fit on F^2 = 1.217 for 3681 data 483 restraints and 407 parameter, largest diff peak/hole 0.90 eÅ^{-3} and -0.73 e Å^{-3}.

For **23c** the crystal dimensions of the metallic dark green plank measured to 0.5 mm × 0.21 mm × 0.08 mm, an empirical formula of $C_{38}H_{56}N_2O_8$ and weight of 668.84 amu. The space group is determined to be P1 with a = 6. 6722(4) Å, b = 7.8649(5) Å, c = 17.7046(12) Å, α = 77.728(2)°,

β = 89.535(2)°, γ = 83.543(2)°, Z = 1, resulting in a volume V = 901.96(10) Å^3 and density ρ = 1.231 g/cm^3. The absorption coefficient μ =0.085 mm^{-1}, F (000) = 362, Θ range for data collection 2.355° to 27.997°, index ranges -8 ≤ h ≤ 8, -10 ≤ k ≤ 10, -23 ≤ l ≤ 23, 50084 reflection were collected (8708 independent reflections R_{int} = 0.0391, observed reflection (I > 2 (I)), completeness to theta = 27.941006° 99.8%, absorption correct by multi-scans. Maximum transmission was 0.7463 and minimum transmission was 0.6870, final *R* indices (I>=2σ (I)) R_1 = 0.0439, wR_2 = 0.1125, R includes (all data) R_1 = 0.0514, wR_2 = 0.1181. Goodness-of-fit on F^2 = 1.052 for 8708 data 189 restraints and 519 parameter, largest diff peak/hole 0.29 eÅ^{-3} and -0.37 e Å^{-3}.

***Table 21**: Crystallographic data of **15**. Visualization of the single molecule viewing along the unit cell axis a (left), b (middle) and c (right), respectively. (color code: blue: c-axis, nitrogen atoms, dark green: expansion of the unit cell, green: b-axis, grey: carbon atoms, red: a-axis, oxygen atoms).*

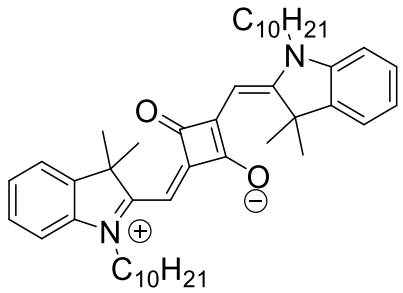

15

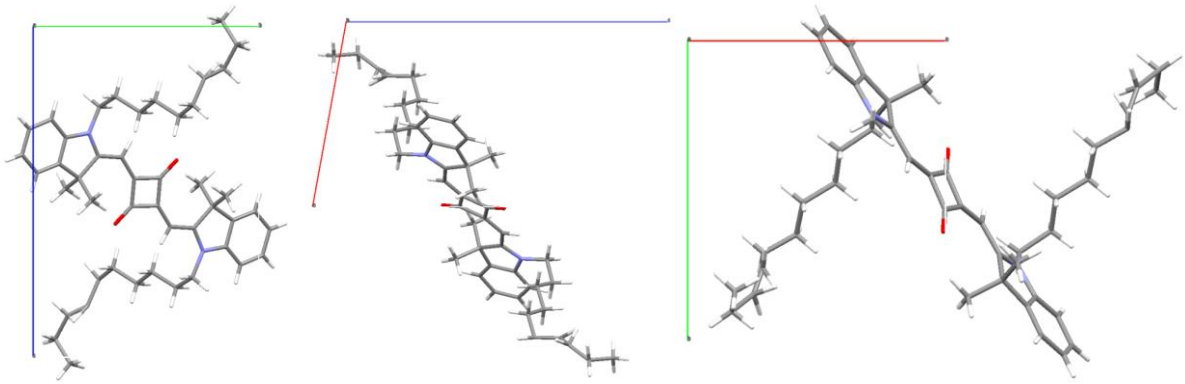

Identification code	GLUE264, WL-M-21_blue // GXray7745_3d
Crystal Habitus	metallic brownish blue plank
Device Type	STOE STADIVARI
Empirical formula	$C_{46}H_{64}N_2O_2$
Moiety formula	C46 H64 N2 O2
Formula weight	676.99
Temperature/K	100
Crystal system	monoclinic
Space group	$P2_1/n$
a/Å	17.4752(17)
b/Å	9.3823(7)
c/Å	11.9430(12)
α/°	90

β/°	90.108(8)
γ/°	90
Volume/Å^3	1958.1(3)
Z	2
ρ_{calc}g/cm^3	1.148
μ/mm^{-1}	0.52
F(000)	740.0
Crystal size/mm^3	0.18 × 0.11 × 0.03
Absorption correction	multi-scan
Tmin; Tmax	0.2499; 0.9249
Radiation	Cu Kα (λ = 1.54186)
2Θ range for data collection/°	10.702 to 141.74°
Completeness to theta	0.998
Index ranges	-21 ≤ h ≤ 14, -9 ≤ k ≤ 11, -11 ≤ l ≤ 14
Reflections collected	20809
Independent reflections	3734 [R_{int} = 0.0677, R_{sigma} = 0.0360]
Data/restraints/parameters	3734/43/257
Goodness-of-fit on F^2	1.078
Final R indexes [I>=2σ (I)]	R_1 = 0.0635, wR_2 = 0.1593
Final R indexes [all data]	R_1 = 0.0972, wR_2 = 0.1842
Largest diff. peak/hole / e Å^{-3}	0.40/-0.22

***Table 22**: Crystallographic data of (S,S)-PyrSQ-C1. Visualization of the single molecule viewing along the unit cell axis a (top middle), b (bottom) and c (top right), respectively. (color code: blue: c-axis, nitrogen atoms, dark green: expansion of the unit cell, green: b-axis, grey: carbon atoms, red: a-axis, oxygen atoms).*

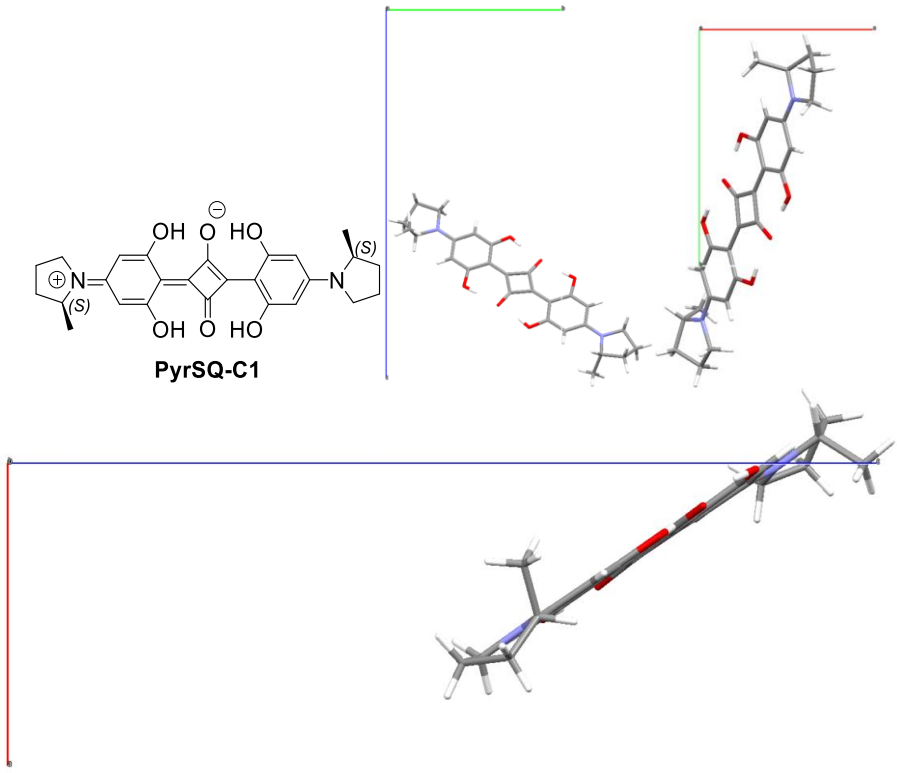

Identification code	GLUE274, WSL-148 // GXray8805_3dn
Crystal Habitus	metallic plank
Device Type	STOE STADIVARI
Empirical formula	$C_{26}H_{28}N_2O_6$
Moiety formula	C26 H28 N2 O6
Formula weight	464.50
Temperature/K	100
Crystal system	orthorhombic
Space group	$P2_12_12_1$
a/Å	8.1189(7)
b/Å	11.3303(6)
c/Å	23.7029(14)
α/°	90
β/°	90
γ/°	90
Volume/Å^3	2180.4(3)
Z	4
ρ_{calc}g/cm^3	1.415
μ/mm^{-1}	0.830
F(000)	984.0
Crystal size/mm^3	0.45 × 0.08 × 0.07
Absorption correction	multi-scan
Tmin; Tmax	0.6828; 0.7800
Radiation	Cu Kα (λ = 1.54186)
2Θ range for data collection/°	10.802 to 140.714°
Completeness to theta	0.999
Index ranges	-9 ≤ h ≤ 9, -6 ≤ k ≤ 13, -28 ≤ l ≤ 27
Reflections collected	53647
Independent reflections	4142 [R_{int} = 0.0305, R_{sigma} = 0.0126]
Data/restraints/parameters	4142/0/313
Goodness-of-fit on F^2	1.050
Final R indexes [I>=2σ (I)]	R_1 = 0.0384, wR_2 = 0.1018
Final R indexes [all data]	R_1 = 0.0403, wR_2 = 0.1035
Largest diff. peak/hole / e Å^{-3}	0.58/-0.25
Flack parameter	0.06(6)

***Table 23**: Crystallographic data of N-C3,O-C3-AlaSQ (**23b**). Visualization of the single molecule viewing along the unit cell axis a (left), b (middle) and c (right), respectively. (color code: blue: c-axis, nitrogen atoms, dark green: expansion of the unit cell, green: b-axis, grey: carbon atoms, red: a-axis, oxygen atoms).*

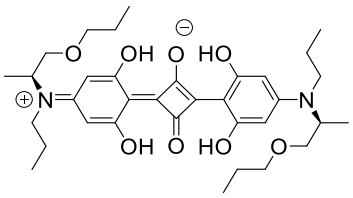

(*S*,*S*)-*N*-C3,*O*-C3-AlaSQ 23b

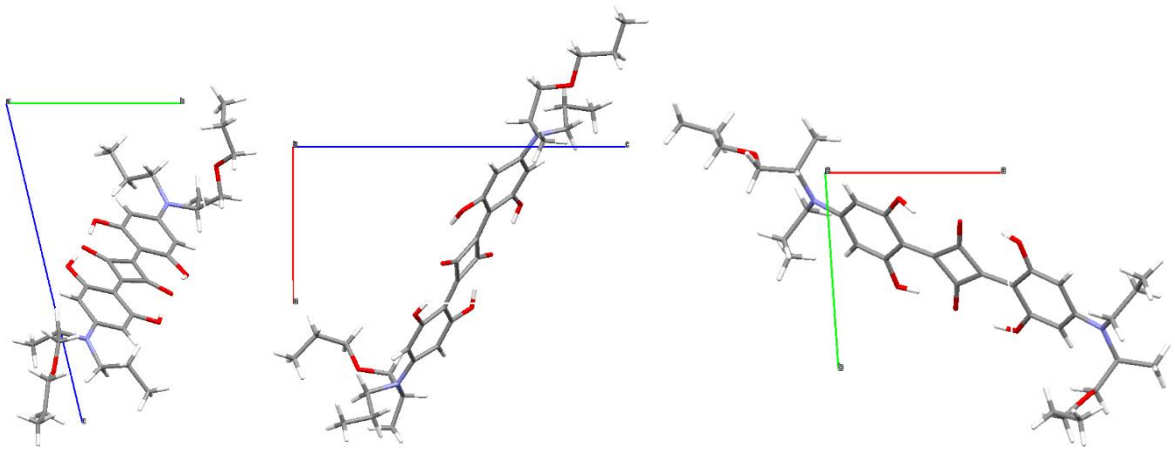

Identification code	GLUE271, WSL216neu // GXraymo_8339f
Crystal Habitus	metallic dark green plank
Device Type	Bruker D8 Venture
Empirical formula	$C_{38}H_{56}N_2O_8$
Moiety formula	C38 H56 N2 O8
Formula weight	668.84
Temperature/K	104.00
Crystal system	triclinic
Space group	P1
a/Å	6.6722(4)
b/Å	7.8649(5)
c/Å	17.7046(12)
α/°	77.728(2)
β/°	89.535(2)
γ/°	83.543(2)
Volume/Å^3	901.96(10)
Z	1
ρ_{calc}g/cm^3	1.231
μ/mm^{-1}	0.085
F(000)	362.0
Crystal size/mm^3	0.5 × 0.21 × 0.08
Absorption correction	multi-scan
Tmin; Tmax	0.6870; 0.7463

Radiation	MoKα (λ = 0.71073)
2Θ range for data collection/°	4.71 to 55.994°
Completeness to theta	0.998
Index ranges	-8 ≤ h ≤ 8, -10 ≤ k ≤ 10, -23 ≤ l ≤ 23
Reflections collected	50084
Independent reflections	8708 [R_{int} = 0.0391, R_{sigma} = 0.0294]
Data/restraints/parameters	8708/189/519
Goodness-of-fit on F^2	1.052
Final R indexes [I>=2σ (I)]	R_1 = 0.0439, wR_2 = 0.1125
Final R indexes [all data]	R_1 = 0.0514, wR_2 = 0.1181
Largest diff. peak/hole / e $Å^{-3}$	0.29/-0.37
Flack parameter	0.3(3)

***Table 24**: Crystallographic data of N-C4,O-C4-AlaSQ (**23c**). Visualization of the single molecule viewing along the unit cell axis a (left), b (middle) and c (right), respectively. (color code: blue: c-axis, nitrogen atoms, dark green: expansion of the unit cell, green: b-axis, grey: carbon atoms, red: a-axis, oxygen atoms).*

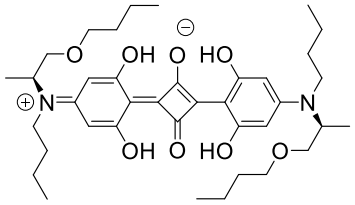

(*S*,*S*)-*N*-C4,*O*-C4-AlaSQ 23c

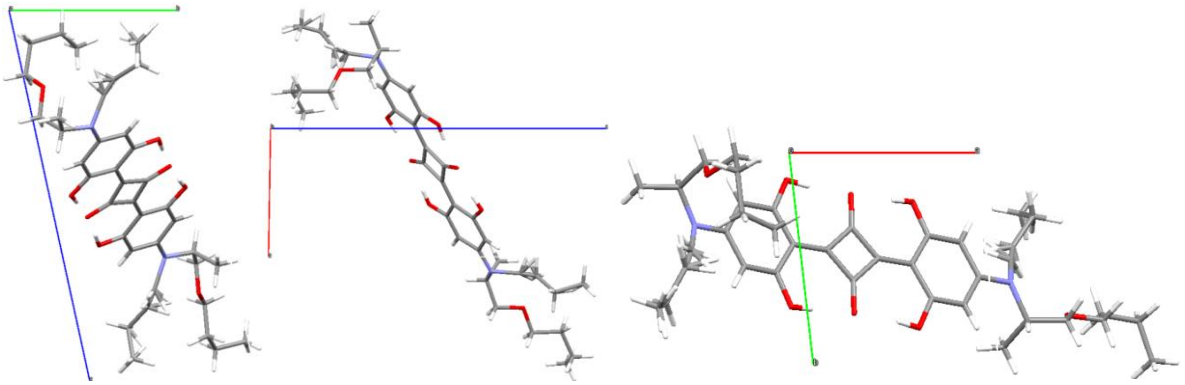

Identification code	GLUE266, WSL-219 // GXray8047_3d
Crystal Habitus	clear bluish green plank
Device Type	STOE STADIVARI
Empirical formula	$C_{34}H_{48}N_2O_8$
Moiety formula	C34 H48 N2 O8
Formula weight	612.74
Temperature/K	100
Crystal system	triclinic
Space group	P1
a/Å	6.9085(7)
b/Å	7.9615(9)

c/Å	14.9878(18)
α/°	76.545(9)
β/°	88.888(9)
γ/°	85.988(9)
Volume/Å^3	799.76(16)
Z	1
ρ_{calc}g/cm^3	1.272
μ/mm^{-1}	0.74
F(000)	330.0
Crystal size/mm^3	0.4 × 0.2 × 0.02
Absorption correction	multi-scan
Tmin; Tmax	0.4690; 0.8948
Radiation	Cu Kα (λ = 1.54186)
2Θ range for data collection/°	11.454 to 135.45°
Completeness to theta	0.994
Index ranges	-6 ≤ h ≤ 8, -7 ≤ k ≤ 9, -17 ≤ l ≤ 17
Reflections collected	25921
Independent reflections	3681 [R_{int} = 0.1296, R_{sigma} = 0.0755]
Data/restraints/parameters	3681/483/407
Goodness-of-fit on F^2	1.217
Final R indexes [I>=2σ (I)]	R_1 = 0.1082, wR_2 = 0.2697
Final R indexes [all data]	R_1 = 0.1396, wR_2 = 0.3069
Largest diff. peak/hole / e Å^{-3}	0.90/-0.73
Flack parameter	0.3(6)

7.6 UV-Vis- and CD spectroscopic Experiments

UV/Vis absorption spectra of diluted samples were measured using a Specord 200 spectrometer from Analytik Jena. Standard measurements were carried out in Hellma quartz cuvettes with a 1 cm path length, except for one case where a 1 mm cuvette was used. The spectra were recorded with a step size of 0.5 nm, a scan speed of 5.0 nm per second, and a bandwidth of 1 nm. A parallel recording of a spectrum of the pure solvent served as a baseline correction.

Sample preparation

For the UV-Vis-measurement in different solvents and solvent mixtures, a stock solution of the respective **AlaSQ** was prepared in chloroform (stabilized with ethanol VWR). The amount of the **AlaSQ** and the final concentrations of both the respective stock solutions and the samples can be found in Table 25. The stock solution was prepared a day before the recording of the spectra and stored in the dark at 19 °C. The solvents and solvent mixture for the experiments were also stored at the same temperature. For the recording of the spectra 50 µL of stock solution were mixed with 2950 µL of the desired solvent/ solvent mixture and transferred into a 10 mm glass cuvette with a final concentrations c_{sample} as given in the Table 21. Experiments were performed immediately after sample preparation and baseline correction was performed using the pristine pure solvent or solvent mixture, respectively, at the same conditions.

***Table 25**: amount (m_{AlaSQ}), added chloroform volume ($V_{solvent}$) and resulting concentration ($c_{stock\ solution}$) of the stock solutions of the respective AlaSQs. c_{sample} refers to the final concentration of the measured sample obtained by diluting 50 µL stock solution with 2950 µL of the desired solvent or solvent mixture.*

AlaSQ	m_{AlaSQ} [mg]	$V_{solvent}$ [mL]	$c_{stock\ solution}$ [10^{-4} M]	c_{sample} [µM]
***N*-C2,*O*-C2-AlaSQ (23a)**	3.21	25	2.31	3.84
***N*-C3,*O*-C3-AlaSQ (23b)**	3.53	25	2.30	3.84
***N*-C4,*O*-C4-AlaSQ (23c)**	3.86	25	2.31	3.85
***N*-C8,*O*-C8-AlaSQ (23f)**	5.15	25	2.31	3.84
***N*-C9,*O*-C9-AlaSQ (23g)**	5.48	25	2.31	3.85
***N*-C9,*O*-C4-AlaSQ (23h)**	4.67	25	2.31	3.85
***N*-C3,*O*-C7-AlaSQ (23i)**	4.18	25	2.31	3.84
***N*-C3,*O*-C9-AlaSQ (23j)**	4.50	25	2.30	3.84
***N*-C4,*O*-C9-AlaSQ (23k)**	4.67	25	2.31	3.85

For the samples of **(*S*,*S*)-*N*-C5,*O*-C5-AlaSQ** (**23d**) and **(*S*,*S*)-*N*-C7,*O*-C7-AlaSQ (23e**) another approach had to be taken. Here, the available amount of the material was the limiting factor, and hence, the volume had to be adjusted to result in a comparable range. As weighing errors for small quantities have a greater impact on the result than for large quantities, this approach gave a less reliable stock solution, making the determination of the extinction coefficient of these two compounds more error-prone.

***Table 26**: Detailed information about the preparation of the dilution series for the determination of extinction coefficient ε.*

sample	V_{SQ} [µL]	from	V_{CHCl3} [µL]	V_{total} [µL]	DF
1	132	stock solution	11868	12000	0.011
2	2400	sample 1	600	3000	0.800
3	1800	sample 1	1200	3000	0.600
4	1200	sample 1	1800	3000	0.400
5	600	sample 1	2400	3000	0.200
6	60	sample 1	2940	3000	0.020

Extinction coefficient Determination

In order to determine the extinction coefficient ε, a series of diluted squaraine solutions with known concentration were prepared (Table 26). These six samples for each **AlaSQ** were measured and the absorbance of each sample at the absorption maximum was correlated to the known concentration of the sample. This gave a linear dependence as seen from the Lambert-Beer-law[120]:

$$A = \varepsilon * c * d$$

with *A* as the absorbance of the compound at a specific wave length, *c* as the concentration and *d* as the distance (here, 1 cm for the width of the cuvette). From the slope of the regression line the extinction coefficient ε was determined as exemplary shown for ***N*-C2,*O*-C2-AlaSQ** (**23a**) (Figure 49).

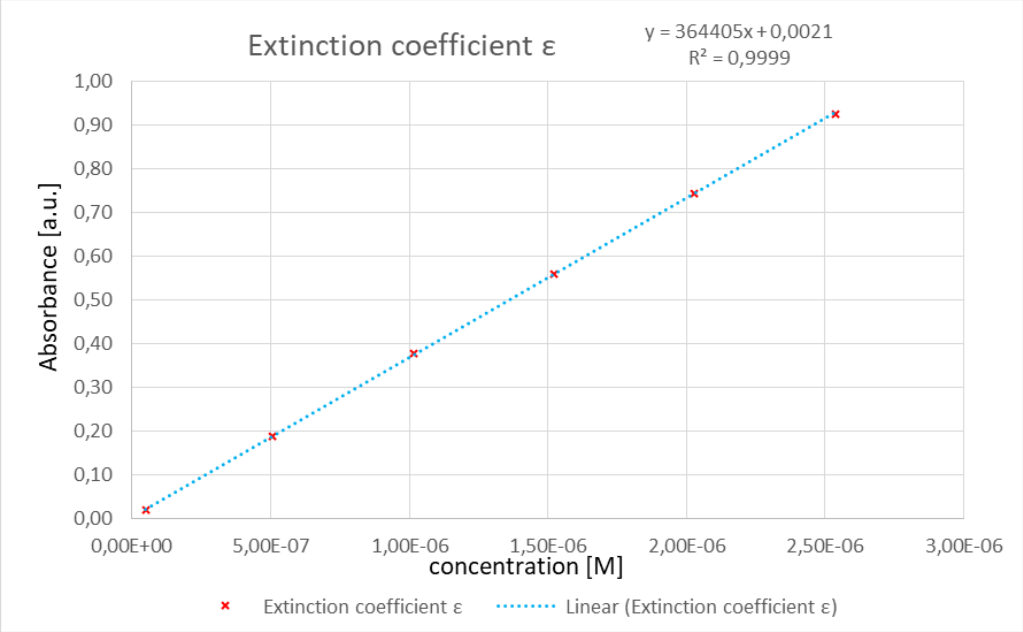

***Figure 49**: Measured absorbance vs. concentration at the absorption maxima of 647.5 nm (red crosses). The extinction coefficient could be calculated to ε = 364405 $M^{-1}cm^{-1}$ for **N-C2,O-C2-AlaSQ** (**23a**).*

The same procedure was applied for the remaining **AlaSQ** where possible. This gave the following extinction coefficients as seen in Table 26.

***Table 26**: Overview of extinction coefficients of the respective AlaSQs in chloroform and the respective wave length for maximum absorption.*

AlaSQ	λ_{max} [nm]	ε [$M^{-1}cm^{-1}$]
***N*-C2,*O*-C2-AlaSQ** (**23a**)	647.5	364000
***N*-C3,*O*-C3-AlaSQ** (**23b**)	649.5	360000
***N*-C4,*O*-C4-AlaSQ** (**23c**)	650.5	352000
***N*-C5,*O*-C5-AlaSQ** (**23d**)	651	n.d.
***N*-C7,*O*-C7-AlaSQ** (**23d**)	651	n.d.
***N*-C8,*O*-C8-AlaSQ** (**23f**)	651	360000
***N*-C9,*O*-C9-AlaSQ** (**23g**)	651	360000
***N*-C9,*O*-C4-AlaSQ** (**23h**)	650.5	374000
***N*-C3,*O*-C7-AlaSQ** (**23i**)	649.5	373000
***N*-C3,*O*-C9-AlaSQ** (**23j**)	650	405000
***N*-C4,*O*-C9-AlaSQ** (**23k**)	650.5	373000

Circular Dichroism (CD) Spectroscopy of Dilute Solutions

The samples were previously used for UV-Vis measurements directly subjected to CD measurements. CD spectra of diluted samples were obtained using a Jasco J-810 spectrometer. Standard measurements were conducted in Hellma quartz cuvettes with a 1 cm path length. Baseline corrections were omitted. Spectra were typically recorded with a 1 nm step size, a scanning speed of 200 nm per minute, and a spectral bandwidth of 1 nm.

7.7 HLB VALUE CALCULATIONS OF 20

For the determination of the HLB according to Griffin[79,80] the molecular mass of functional groups which contribute to the hydrophilicity of 20 were summed up and divided by the total molecular mass of **20**. The result thereof is multiplied by 20. For simplicity reasons all molecular mass values were rounded to no decimal place. The functional groups in questions are the amine (M_{NH2}=16 u), the hydroxyl-group (M_{OH}=17 u) and two times the carbonyl groups (M_{CO}=28 u). The total molecular weight of **20** was rounded to 487 u. Thus according to Griffin the HLB value of 20 is:

$$HLB_{Griffin}(\mathbf{20}) = \frac{Mass\ of\ Hydrophilic\ Portion}{Total\ Mass\ of\ Molecule} \times 20$$
$$= \frac{(\mathrm{M(NH_2)\ +\ M(OH)\ +\ 2\,x\,M(CO)})}{\mathrm{M}(\mathbf{20})} \times 20 = \frac{16\ +17\ +\ 2\,\mathrm{x}\,28}{487} \times 20 = 3.7$$

This would indicate an apolar neutral lipophilic surfactant. This HLB value means that compound **20** is better suited for an application in a water-in-oil emulsion. Thus, favoring a medium with lower water contents compared to the organic solvent.

For the determination of the HLB according to Davies[81] the characteristic group values of each functional group need to be taken into account.

HLB-Incrementable

Hydrophilic functional group	Group value according to Davies[81,187]	Lipophilic functional groups	Group value according to Davies[81,187]
-OH	1.9	phenyl	2.4
$-NH_2$	3.0	CH_2 (alkyl chain)	0.475
$-(CH_2-CH_2-O)-$	0.33	indole	~2
CO	~ 7.5		

The HLB is obtained as the sum of the group values of the hydrophilic components minus the sum of the lipophilic functional groups and increased by seven:

$$HLB_{Davies}(\mathbf{20}) = \Sigma(Hydrophilic\ Group\ Values) - \Sigma(Lipophilic\ Group\ Values) + 7$$
$$= 3.0 + 1.9 + 2\mathrm{x}\ 7.5 - (2 + 15\mathrm{x}\ 0.475 + 2) + 7 = 15.375$$

This HLB value would indicate a hydrophilic surfactant, meaning a better suitedness for application in a medium with high water contents compared to organic solvents.

The HLB values drastically differ depending on the method used for calculation. This is mostly due to the empirical nature of the group values shown in the incrementable used for the calculation according to Davies.

7.8 DLS MEASUREMENTS

DLS measurements were performed on a Zetasizer Nano-S manufactured by Malvern Panalytical at University of Milano-Bicocca, Department of material science, Milan, Italy. The data was analyzed using the instrument specific software, directly yielding the dimension of the aggregates. Exported correlograms were fitted to autocorrelation functions via cumulative method over two measurements.

Sample Details

Sample Name:	WL-24_water avg
SOP Name:	mansettings.nano
General Notes:	Average result created from record number(s): 1 2 3 4 5

File Name:	Wing Si.dts	**Dispersant Name:**	Water
Record Number:	15	**Dispersant RI:**	1,330
Material RI:	1,59	**Viscosity (cP):**	0,8872
Material Absorbtion:	0,010	**Measurement Date and Time:**	venerdì 28 marzo 2025 0...

System

Temperature (°C):	25,0	**Duration Used (s):**	140
Count Rate (kcps):	54,4	**Measurement Position (mm):**	4,65
Cell Description:	Disposable sizing cuvette	**Attenuator:**	9

Results

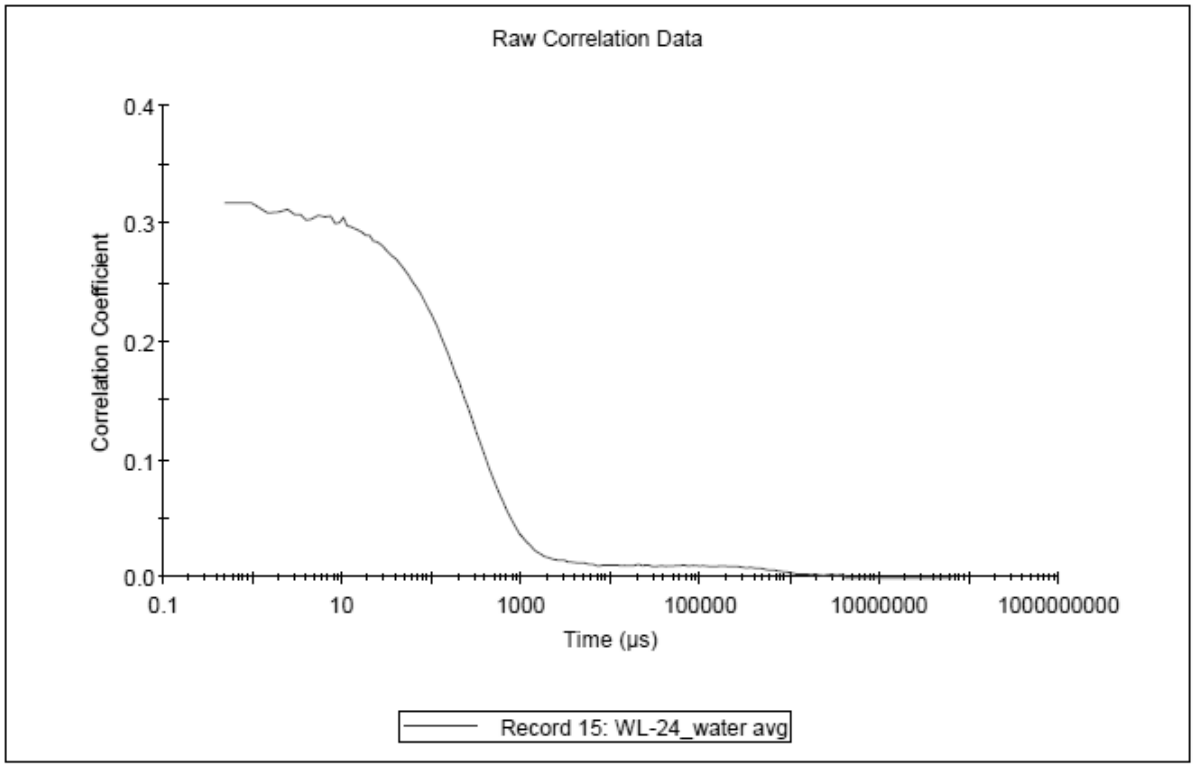

***Figure 50**: Raw correlation data for DLS measurement of 20 in pure water directly obtained from the measuring device and the device internal analysis software.*

Sample Details

Sample Name: WL-24_water avg
SOP Name: mansettings.nano
General Notes: Average result created from record number(s): 1 2 3 4 5

File Name:	Wing Si.dts	**Dispersant Name:**	Water
Record Number:	15	**Dispersant RI:**	1,330
Material RI:	1,59	**Viscosity (cP):**	0,8872
Material Absorbtion:	0,010	**Measurement Date:**	venerdì 28 marzo 2025...

System

Temperature (°C):	25,0	**Duration Used (s):**	140
Count Rate (kcps):	54,4	**Measurement Position (mm):**	4,65
Derived Count Rate (kcps):	450,4	**Attenuator:**	9
Cell Description:	Disposable sizing cuvette		

Results

Cumulants Fit Error: 0,00241

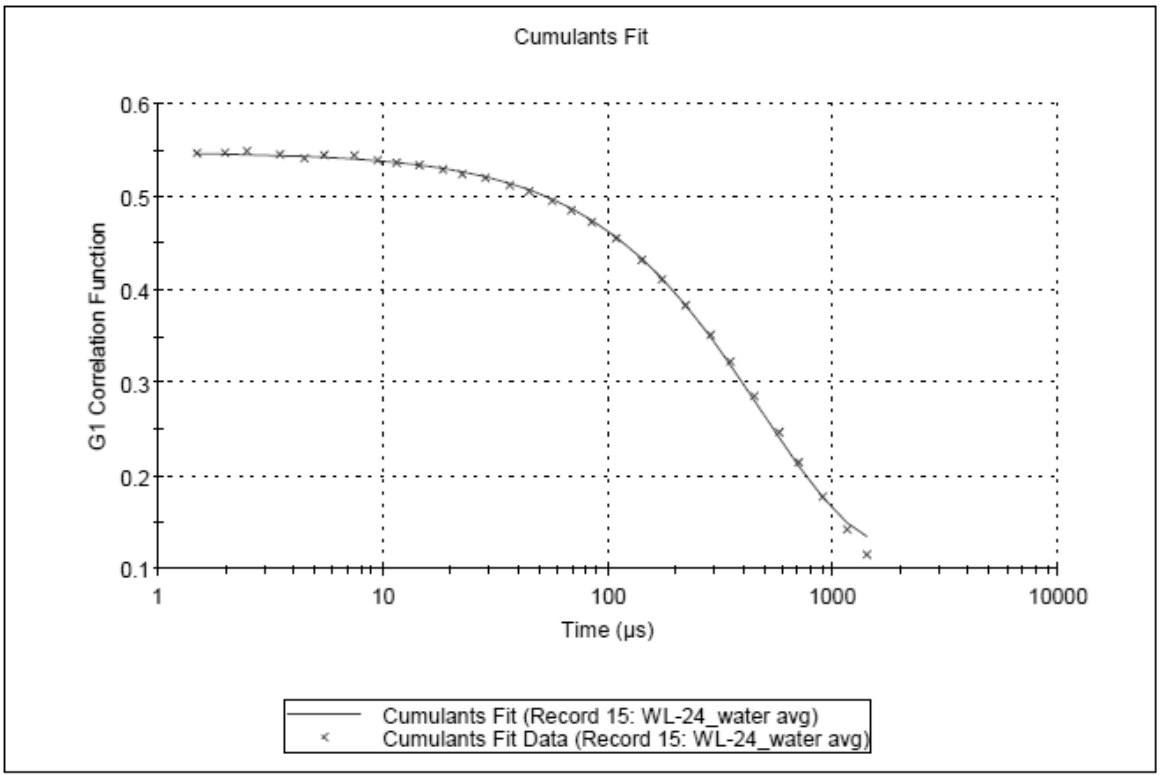

***Figure 51**: Fitted correlation data for DLS measurement of **20** in pure water directly obtained from the measuring device and the device internal analysis software.*

Sample Details

Sample Name: WL-24_toluene_10^-6 avg

SOP Name: mansettings.nano

General Notes: Average result created from record number(s): 7 8 9

File Name:	Wing Si.dts	**Dispersant Name:**	Toluene
Record Number:	16	**Dispersant RI:**	1,496
Material RI:	1,59	**Viscosity (cP):**	0,5564
Material Absorbtion:	0,010	**Measurement Date and Time:**	venerdì 28 marzo 2025 0...

System

Temperature (°C):	25,0	**Duration Used (s):**	10
Count Rate (kcps):	136,2	**Measurement Position (mm):**	4,20
Cell Description:	Low volume glass cuve...	**Attenuator:**	8

Results

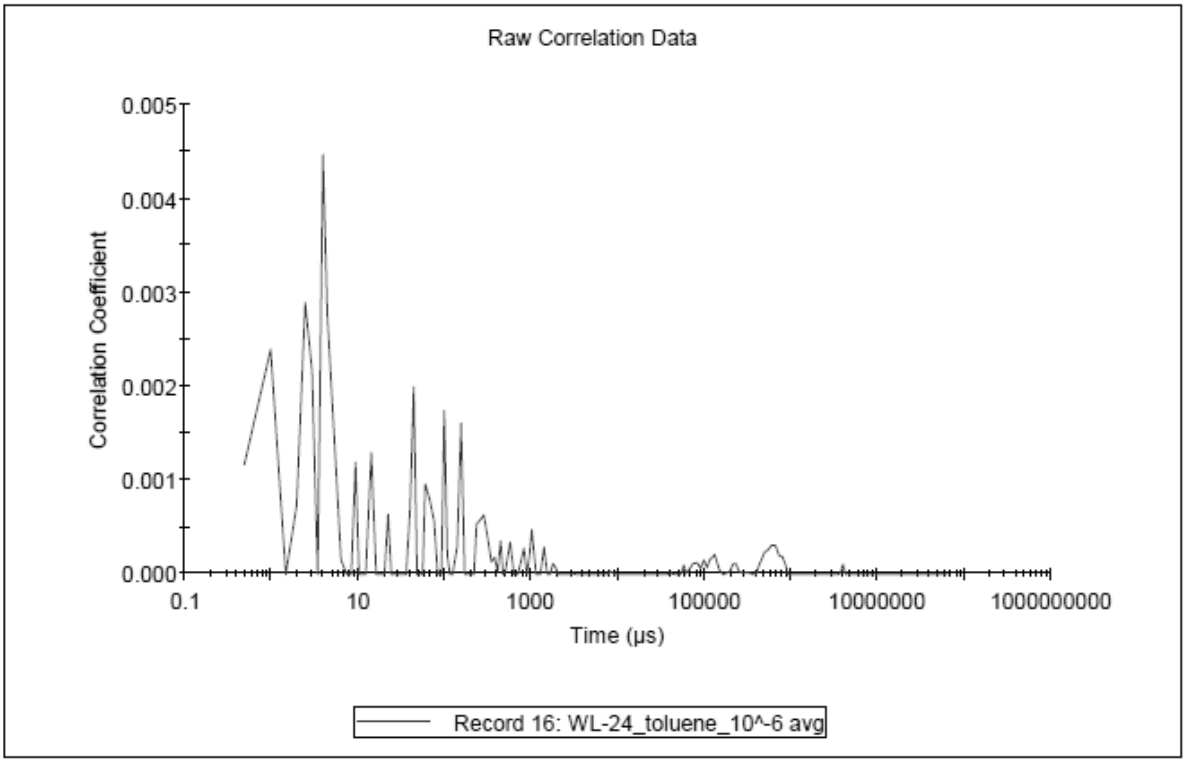

***Figure 52**: Raw correlation data for DLS measurement of **20** in pure toluene directly obtained from the measuring device and the device internal analysis software.*

Sample Details

Sample Name: WL-24_toluene+1drop_H2O_10^-6_2 av

SOP Name: mansettings.nano

General Notes: Average result created from record number(s): 11 12 13

File Name:	Wing Si.dts	**Dispersant Name:**	Toluene
Record Number:	14	**Dispersant RI:**	1,496
Material RI:	1,59	**Viscosity (cP):**	0,5564
Material Absorbtion:	0,010	**Measurement Date and Time:**	martedì 25 luglio 2023 1...

System

Temperature (°C):	25,0	**Duration Used (s):**	60
Count Rate (kcps):	268,5	**Measurement Position (mm):**	0,85
Cell Description:	Low volume glass cuve...	**Attenuator:**	5

Results

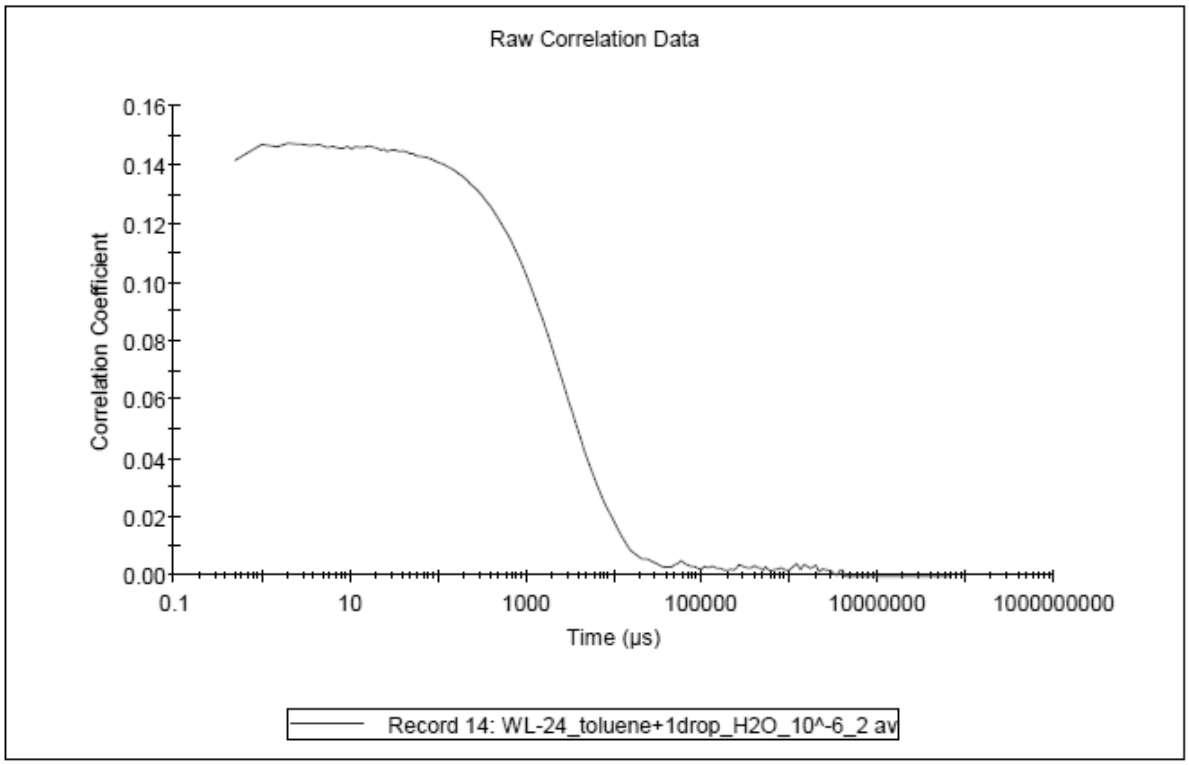

***Figure 53**: Raw correlation data for DLS measurement of **20** in toluene with a drop of water directly obtained from the measuring device and the device internal analysis software.*

Sample Details

Sample Name: WL-24_toluene+1drop_H2O_10^-6_2 av
SOP Name: mansettings.nano
General Notes: Average result created from record number(s): 11 12 13

File Name:	Wing Si.dts	**Dispersant Name:**	Toluene
Record Number:	14	**Dispersant RI:**	1,496
Material RI:	1,59	**Viscosity (cP):**	0,5564
Material Absorbtion:	0,010	**Measurement Date:**	martedì 25 luglio 2023 ...

System

Temperature (°C):	25,0	**Duration Used (s):**	60
Count Rate (kcps):	268,5	**Measurement Position (mm):**	0,85
Derived Count Rate (kcps):	171661,2	**Attenuator:**	5
Cell Description:	Low volume glass cuvette (45µL)		

Results

Cumulants Fit Error: 0,00104

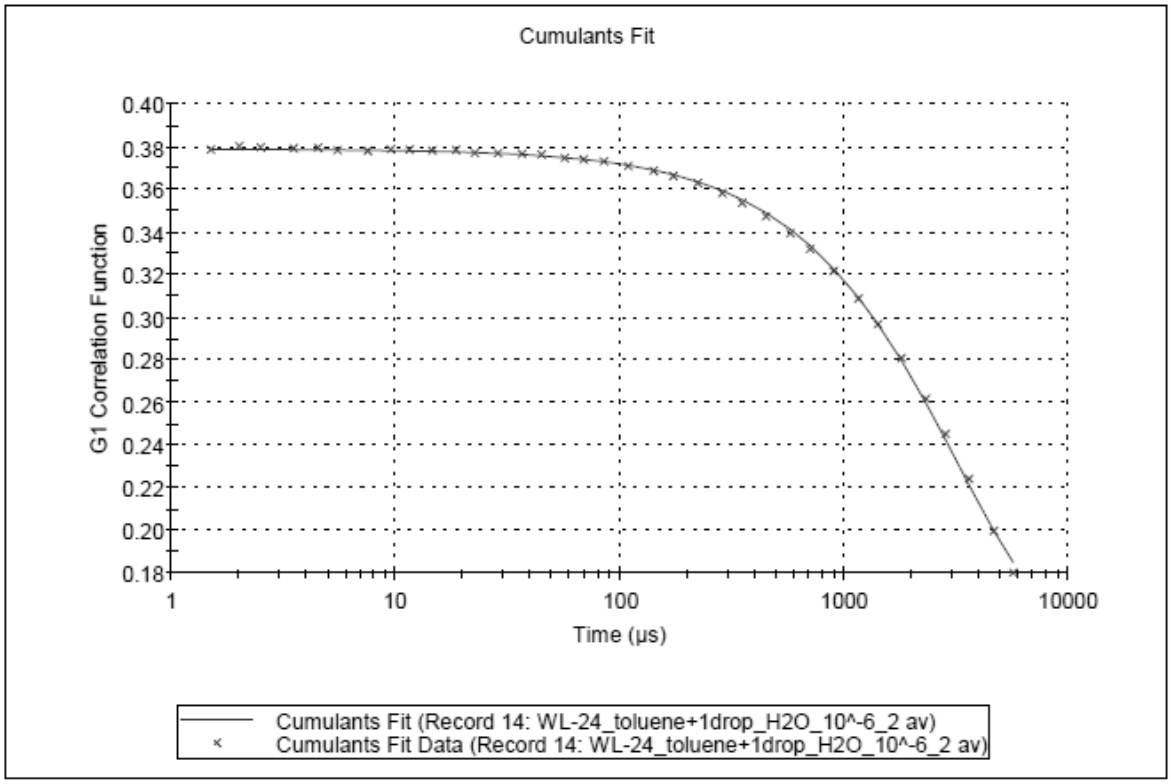

***Figure 54**: Fitted correlation data for DLS measurement of **20** in in toluene with a drop of water directly obtained from the measuring device and the device internal analysis software.*

From the recorded correlograms it becomes apparent, that **20** is completely dissolved in toluene and does not form aggregates. Upon addition of a drop of water aggregates are formed, which are larger in size compared to the aggregates in pure water. This can be seen in the slower movement of the particles reflected higher values for the time scale.

8 LIST OF ABBREVIATIONS

°C	Degrees Celsius
^{1}H-NMR	Proton NMR
^{13}C-NMR	Carbon-NMR
2D	Two dimensional
3D	Three dimensional
A	Acceptor
Å	Ångstöm = 10^{-10} m
AcOH	Acetic acid
AlaSQ	Alanine-derived squaraine
$AlCl_3$	Aluminiumtrichloride
APCI	Atmospheric-pressure chemical ionization
AProSQ	1-Aminopropan-2-ol based squaraine
Aq.	aqueous
atm.	Atmosphere = 1.01325 bar
β	Kamlet-Taft polarity parameter
bar	Unit for pressure
BCE	Before the Common Era
BHJ	Bulk heterojunction
BnCl	Benzylchloride
Boc	tert-butoxycarbonyl
Bu	Butyl
CAPB	Cocamdopropyl betaine
calcd.	Calculated
cat.	Catalyst/catalytic
CD	Circular dichroism
$CDCl_3$	Deuterated chloroform
CH	Cyclohexane
$CHCl_3$	chloroform
CH_2Cl_2	See DCM
CISS	Chirality-induced spin selectivity
CMC	Critical micellar concentration
CPhos	2-Dicyclohexylphosphino-2',6'-bis(N,N-dimethylamino)biphenyl
Cs_2CO_3	Cesium carbonate
CT	Charge transfer
CTAB	Certrimonium bromide
D	Donor
D	Diffusion coefficient
Δ	Elevated temperatures
δ	Chemical shift
DCM	Dichloromethane
DLS	Dynamic light scattering
DMAP	4-Dimethylaminopyridine
DMF	Dimethylformamide
DMSO	Dimethyl sulfoxide
dppf	1,1′-Bis(diphenylphosphino)ferrocene
DSSC	Dye-sensitized solar cell
EA	Ethyl acetate
EE	*Essigsäureethylester* (dt.) = Ethyl acetate
e.g.	*exempli gratia* (Lat.) = for example
EI	Electron ionization
ESI	Electrospray ionization
Et	Ethyl

et al.	*et alii* (lat.) = „and others”
EtI	Ethyliodide
ETL	Electron transport layer
Et_2O	Diethyl ether
EtOH	Ethanol
Et_3SiH	Triethylsilane
eq.	Equivalents
G4 cat	fourth generation Buchwald(G4) precatalysts
GC	Gas chromatography
HCl	Hydrochloric acid
HLB	Hydrophilic-lipophilic balance
$H_2NNH_2*H_2O$	hydrazine monohydrate
HOMO	Highest occupied molecular orbital
HPLC	High pressure liquid chromatography
HRMS	High resolution mass spectrometry
HTL	Hole transport layer
i.e.	*id est* (lat.) = that is
$InBr_3$	Indiumtribromide
iPr	Isopropyl
IR	Infrared
IUPAC	International Union of Pure and Applied Chemistry
JackiePhos	Bis-(3,5-bis-(trifluormethyl)-phenyl)-(2′,4′,6′- triisopropyl-3,6-dimethoxybiphenyl-2-yl)-phosphin
k_b	Boltzmann constante
K_2CO_3	Potassium carbonate
KI	Potassium idodie
KOH	Potassium hydroxide
KOtBu	Potassium tert-butoxide
L	liter
λ	Wave length
LA	Lewis acid
LEED	Low-energy electron diffraction
M	Molecular weight
M	Molar= mol/L
µ	Micro (10^{-6})
µ	Mobility here terminal drift velocity
Me	Methyl
MeCN	Acetonitrile
MeOH	Methanol
mmol	millimol
Mol-%	Mol percentage
MPEG	Methoxy polyethylene glycol, suffix indicate mean molecular weight of the polymer
$MgSO_4$	Magnesium sulfate
MS	Mass spectroscopy
η	viscosity of the medium
$NaBH_4$	Sodiumborohydride
Na_2CO_3	Sodium carbonate
NaH	Sodium hydride
Na_2SO_4	Sodium sulfate
NaOH	Sodium hydroxide
NaO^tBu	Sodium tert-butoxide
NEt_3	Triethylamine
NH_4Cl	Ammonium chloride
NIR	Near infrared

nm	nanometer
NMR	Nuclear magnetic resonance (spectroscopy)
NOESY	Nuclear overhauser enhancement and exchange spectroscopy
OLED	Organic light-emitting diodes
OPD	Organic photodetectors
OPV	Organic photovoltaic
OSC	Organic solar cell
PDI	Polydispersity index
$Pd_2(dba)_3$	Tris(dibenzylideneacetone)dipalladium(0)
$Pd(dtbpf)Cl_2$	1,1′-Bis(di-tert-butylphosphino)ferrocen]dichlorpalladium(II)
$Pd(OAc)_2$	Palladium diacetate
pH	*potentia hydrogenii* (lat.) refers to the acidity of an aqueous probe
Ph	Phenyl
PHJ	Planar heterojunction
Pht	Phthalimide
ProSQ	Proline-derived squaraine
$P(^tBu)_3$	Tri-tert-butylphosphin
PVD	Physical vapor deposition
PyrSQ	2-methylpyrrolidin-based squaraine
Quant.	quantitative
R	(organic) Residue
r	radius
R-I	Alkyl-iodide
r.t.	Room temperature
RuPhos	2-Dicyclohexylphosphino-2′,6′-diisopropoxybiphenyl
SAR	Structure-activity relationship
Sat.	saturated
SDS	Sodium dodecyl sulfate
sec	second
SiO_2	Silicate gel
SLE	Sodium laureth sulfate
SLS	Sodium lauryl sulfate
S_N2	Nucleophilic substitution of second reaction order
SQ	squaraine
$SQ(OH)_2$	*N*, *N* dialkyl dihydroxy aniline squaraines
$SQ(OH)_4$	*N*, *N* tetraalkyl dihydroxy aniline squaraines
T	Temperature
TIDE	research training group 2591
TFA(A)	Trifluoro acetic acid (anhydride)
THF	Tetrahydrofuran
TLC	Thin layer chromatography
TsCl	p-Toluenesulfonyl chloride
UHV	Ultra high vacuum
UPS	Ultraviolet photoelectron spectroscopy
UV	ultraviolett
Vis	Visual light
v/v	Volume per volume
wt%	Weight per weight
w/w	Weight concentration
XPS	X-ray photoelectron spectroscopy
XRD	X-ray diffraction
$ZnCl_2$	Zinc chloride

9 REFERENCES

[1] A. H. Schmidt, *Synthesis* **1980**, *1980*, 961.
[2] A. Treibs, K. Jacob, *Angew. Chem. Int. Ed. Engl.* **1965**, *4*, 694.
[3] *Scifinder*, https://scifinder-n.cas.org/search/reference/681b4a9bf2d8b109e3f3a128/1.
[4] *Scifinder_Squarylium*, https://scifinder-n.cas.org/search/reference/681b4badf2d8b109e3f3bdf1/1.
[5] K. Ilina, W. M. MacCuaig, M. Laramie, J. N. Jeouty, L. R. McNally, M. Henary, *Bioconjugate chemistry* **2020**, *31*, 194.
[6] K.-Y. Law, S. Kaplan, R. K. Crandall, *Dyes Pigm.* **1988**, *9*, 187.
[7] K.-Y. Law, F. Bailey, *Dyes Pigm.* **1988**, *9*, 85.
[8] Brain Halton **2008**.
[9] Nano-Science and Technology Institute, *Nanotechnology 2013: bio sensors, instruments, medical, environment and energy*, CRC Press; NSTI Nano Science and Technology Inst, Boca Raton, Fla., Danville, Calif. **2013**.
[10] S. Sreejith, P. Carol, P. Chithra, A. Ajayaghosh, *J. Mater. Chem.* **2008**, *18*, 264.
[11] F. Meyers, C.-T. Chen, S. R. Marder, J.-L. Brédas, F. Meyers, *Chem. - Eur. J.* **1997**, *3*, 530.
[12] C.-T. Chen, S. R. Marder, L.-T. Cheng, *J. Am. Chem. Soc.* **1994**, *116*, 3117.
[13] J. He, Y. J. Jo, X. Sun, W. Qiao, J. Ok, T. Kim, Z. Li, *Adv. Funct. Mater.* **2021**, *31*.
[14] Y. Chen, W. Zhu, J. Wu, Y. Huang, A. Facchetti, T. J. Marks, *Org. Photonics Photovolt.* **2019**, *6*, 1.
[15] S. Brück, C. Krause, R. Turrisi, L. Beverina, S. Wilken, W. Saak, A. Lützen, H. Borchert, M. Schiek, J. Parisi, *Phys. Chem. Chem. Phys.* **2014**, *16*, 1067.
[16] G. Chen, H. Sasabe, T. Igarashi, Z. Hong, J. Kido, *J. Mater. Chem. A* **2015**, *3*, 14517.
[17] G. Wei, X. Xiao, S. Wang, J. D. Zimmerman, K. Sun, V. V. Diev, M. E. Thompson, S. R. Forrest, *Nano Lett.* **2011**, *11*, 4261.
[18] G. Chen, H. Sasabe, W. Lu, X.-F. Wang, J. Kido, Z. Hong, Y. Yang, *J. Mater. Chem. C* **2013**, *1*, 6547.
[19] J.-Q. Jiang, C.-L. Sun, Z.-F. Shi, H.-L. Zhang, *RSC Adv.* **2014**, *4*, 32987.
[20] S. Wang, E. I. Mayo, M. D. Perez, L. Griffe, G. Wei, P. I. Djurovich, S. R. Forrest, M. E. Thompson, *Appl. Phys. Lett.* **2009**, *94*.
[21] S. K. Mavileti, G. Bila, V. Utka, E. Bila, T. Kato, R. Bilyy, S. S. Pandey, *ACS applied bio materials* **2024**, *7*, 416.
[22] W. Qiao, Z. Li, *Symmetry* **2022**, *14*, 966.
[23] D. Gayathri Devi, T. R. Cibin, D. Ramaiah, A. Abraham, *J. Photochem. Photobiol., B* **2008**, *92*, 153.
[24] H. Luo, S. Gao, *Journal of Controlled Release* **2023**, *362*, 425.
[25] P. Sun, Q. Wu, X. Sun, H. Miao, W. Deng, W. Zhang, Q. Fan, W. Huang, *Chem. Commun. (Cambridge, U. K.)* **2018**, *54*, 13395.
[26] *Scifinder_knowledge graph* **2025**, https://scifinder-n.cas.org/knowledgeGraph/67c1dd00141e447e85fd8a49.
[27] J. H. Kim, T. Schembri, D. Bialas, M. Stolte, F. Würthner, *Advanced materials (Deerfield Beach, Fla.)* **2022**, *34*, e2104678.
[28] K. Strassel, A. Kaiser, S. Jenatsch, A. C. Véron, S. B. Anantharaman, E. Hack, M. Diethelm, F. Nüesch, R. Aderne, C. Legnani, S. Yakunin, M. Cremona, R. Hany, *ACS applied materials & interfaces* **2018**, *10*, 11063.
[29] A. Zampetti, A. Minotto, F. Cacialli, *Adv. Funct. Mater.* **2019**, *29*.
[30] B. Stender, S. F. Völker, C. Lambert, J. Pflaum, *Advanced materials (Deerfield Beach, Fla.)* **2013**, *25*, 2943.
[31] Jennifer Zablocki, *Synthese, Eigenschaften und Anwendung symmetrischer Anilinosquaraine als Komponente in Photodioden*, Bonn **2022**.

[32] Matthias Peter Schulz, *Synthese, Eigenschaften und Anwendung von Squarainen als Komponente in Photodiode*, Bonn **2018**.
[33] M. Jørgensen, K. Norrman, S. A. Gevorgyan, T. Tromholt, B. Andreasen, F. C. Krebs, *Advanced materials (Deerfield Beach, Fla.)* **2012**, *24*, 580.
[34] T. Shan, X. Hou, X. Yin, X. Guo, *Front. Optoelectron.* **2022**, *15*, 49.
[35] L.-M. Chen, Z. Xu, Z. Hong, Y. Yang, *J. Mater. Chem.* **2010**, *20*, 2575.
[36] B. Walker, H. Choi, J. Y. Kim, *Current Applied Physics* **2017**, *17*, 370.
[37] E. L. Ratcliff, B. Zacher, N. R. Armstrong, *J. Phys. Chem. Lett.* **2011**, *2*, 1337.
[38] G. Chen, Z. Ling, B. Wei, J. Zhang, Z. Hong, H. Sasabe, J. Kido, *Front. Chem.* **2018**, *6*, 412.
[39] G. Chen, H. Sasabe, Y. Sasaki, H. Katagiri, X.-F. Wang, T. Sano, Z. Hong, Y. Yang, J. Kido, *Chem. Mater.* **2014**, *26*, 1356.
[40] L. Beverina, R. Ruffo, M. M. Salamone, E. Ronchi, M. Binda, D. Natali, M. Sampietro, *J. Mater. Chem.* **2012**, *22*, 6704.
[41] F. Silvestri, M. D. Irwin, L. Beverina, A. Facchetti, G. A. Pagani, T. J. Marks, *J. Am. Chem. Soc.* **2008**, *130*, 17640.
[42] L. Beverina, P. Salice, *Eur. J. Org. Chem.* **2010**, *2010*, 1207.
[43] L. Beverina, M. Sassi, *Synlett* **2014**, *25*, 477.
[44] J. Zablocki, O. Arteaga, F. Balzer, D. Hertel, J. J. Holstein, G. Clever, J. Anhäuser, R. Puttreddy, K. Rissanen, K. Meerholz, A. Lützen, M. Schiek, *Chirality* **2020**, *32*, 619.
[45] J. Zablocki, M. Schulz, G. Schnakenburg, L. Beverina, P. Warzanowski, A. Revelli, M. Grüninger, F. Balzer, K. Meerholz, A. Lützen, M. Schiek, *J. Phys. Chem. C* **2020**, *124*, 22721.
[46] T. Liu, X. Liu, W. Wang, Z. Luo, M. Liu, S. Zou, C. Sissa, A. Painelli, Y. Zhang, M. Vengris, M. V. Bondar, D. J. Hagan, E. W. van Stryland, Y. Fang, K. D. Belfield, *J. Phys. Chem. C* **2018**, *122*, 3994.
[47] M. Tian, M. Furuki, I. Iwasa, Y. Sato, L. S. Pu, S. Tatsuura, *J. Phys. Chem. B* **2002**, *106*, 4370.
[48] F. Balzer, N. J. Hestand, J. Zablocki, G. Schnakenburg, A. Lützen, M. Schiek, *J. Phys. Chem. C* **2022**, *126*, 13802.
[49] N. Giacoletto, M. Ibrahim-Ouali, F. Dumur, *Eur. Polym. J.* **2021**, *150*, 110427.
[50] J. Kabatc, K. Kostrzewska, K. Jurek, *RSC Adv.* **2016**, *6*, 74715.
[51] K. Kostrzewska, J. Ortyl, R. Dobosz, J. Kabatc, *Polym. Chem.* **2017**, *8*, 3464.
[52] A. Bonardi, F. Bonardi, G. Noirbent, F. Dumur, C. Dietlin, D. Gigmes, J.-P. Fouassier, J. Lalevée, *Polym. Chem.* **2019**, *10*, 6505.
[53] V. Launay, A. Caron, G. Noirbent, D. Gigmes, F. Dumur, J. Lalevée, *Adv. Funct. Mater.* **2021**, *31*.
[54] A. Ajayaghosh, *Chem. Soc. Rev.* **2003**, *32*, 181.
[55] S. F. Völker, S. Uemura, M. Limpinsel, M. Mingebach, C. Deibel, V. Dyakonov, C. Lambert, *Macromol. Chem. Phys.* **2010**, *211*, 1098.
[56] G. Xia, H. Wang, *J. Photochem. Photobiol., C* **2017**, *31*, 84.
[57] K. Law, *Dyes Pigm.* **1992**, *20*, 25.
[58] H.-E. Sprenger, W. Ziegenbein, *Angew. Chem. Int. Ed. Engl.* **1966**, *5*, 894.
[59] K.-Y. Law, F. C. Bailey, *Can. J. Chem.* **1986**, *64*, 2267.
[60] C. W. Dirk, W. C. Herndon, F. Cervantes-Lee, H. Selnau, S. Martinez, P. Kalamegham, A. Tan, G. Campos, M. Velez, *J. Am. Chem. Soc.* **1995**, *117*, 2214.
[61] E. Ronchi, R. Ruffo, S. Rizzato, A. Albinati, L. Beverina, G. A. Pagani, *Org. Lett.* **2011**, *13*, 3166.
[62] M. Schulz, M. Mack, O. Kolloge, A. Lützen, M. Schiek, *Phys. Chem. Chem. Phys.* **2017**, *19*, 6996.
[63] K. M. Shafeekh, S. Das, C. Sissa, A. Painelli, *J. Phys. Chem. B* **2013**, *117*, 8536.
[64] Maximilian Hubert Schreck, *Synthesis and Photophysics of Linear and Star-Shaped Oligomers of Squaraine Dyes*, Würzburg **2018**.
[65] K.-Y. Law, F. C. Bailey, *Can. J. Chem.* **1993**, *71*, 494.
[66] K. Jyothish, K. T. Arun, D. Ramaiah, *Org. Lett.* **2004**, *6*, 3965.

[67] D. Keil, H. Hartmann, *Dyes Pigm.* **2001**, *49*, 161.
[68] Yin, Meizhen., Ji, Chendong., Shen, Jie., Yang, Zheng., *Amphiphilic indole squarylium cyanine dye and application thereof in long-acting marking of lysosome* **2016**, https://eureka.patsnap.com/patent-CN105238093A.
[69] Ramaiah Danaboyina, Thazhathveetil Arun Kalliat, Kuthanapillil Jyothish, *Amphiphilic Squaraine dyes, Process for Preparation therof and use thereof: Application* **2009**, https://patents.justia.com/patent/20090068113.
[70] K. Yang, Y. Yang, L. Si, W. Guo, G. Zhang, G. Xia, H. Wang, *Sens. Actuators, B* **2025**, *430*, 137383.
[71] S. Sreejith, J. Joseph, M. Lin, N. V. Menon, P. Borah, H. J. Ng, Y. X. Loong, Y. Kang, S. W.-K. Yu, Y. Zhao, *ACS nano* **2015**, *9*, 5695.
[72] Y. Xu, A. Malkovskiy, Q. Wang, Y. Pang, *Org. Biomol. Chem.* **2011**, *9*, 2878.
[73] H.-Y. Ahn, S. Yao, X. Wang, K. D. Belfield, *ACS applied materials & interfaces* **2012**, *4*, 2847.
[74] V. Grande, F. Doria, M. Freccero, F. Würthner, *Angewandte Chemie (International ed. in English)* **2017**, *56*, 7520.
[75] J. V. Ros-Lis, B. García, D. Jiménez, R. Martínez-Máñez, F. Sancenón, J. Soto, F. Gonzalvo, M. C. Valldecabres, *J. Am. Chem. Soc.* **2004**, *126*, 4064.
[76] A. K. Singh, J. Nithyanandhan, *ACS Appl. Energy Mater.* **2021**, *4*, 13932.
[77] H. Chen, M. S. Farahat, K.-Y. Law, D. G. Whitten, *J. Am. Chem. Soc.* **1996**, *118*, 2584.
[78] L. I. Markova, E. A. Terpetschnig, L. D. Patsenker, *Dyes Pigm.* **2013**, *99*, 561.
[79] W. C. Griffin, *J. Cosmet. Sci.* **1949**.
[80] W. C. Griffin, *Calculation of HBL values of Non-ionic Surfactants*, New York City **1954**.
[81] J.T. Davies, *A Quantitative Kinetic Theory of Emulsion Type. I. Physical Chemistry of the Emulsifying Agent* **1957**.
[82] Ricardo C. PASQUALI Natalia SACCO, Carlos BREGNI, *Lat. Am. J. Pharm.* **2009**.
[83] ALFA Chemistry, *HLB Value and Calculation* **2025**, https://surfactant.alfa-chemistry.com/hlb-value-and-calculation.html.
[84] M. Nollet, H. Boulghobra, E. Calligaro, J.-D. Rodier, *Int. J. Cosmet. Sci.* **2019**, *41*, 99.
[85] M. J. Rosen, J. T. Kunjappu, *Surfactants and interfacial phenomena*, Wiley, Hoboken, N.J **2012**.
[86] V. Sakkaravarthi, *CSDM* **2022**, *2*, 133.
[87] F. W. Gibbs, *Ann. Sci.* **1939**, *4*, 169.
[88] J. F. Nova, S. Z. Smrity, M. Hasan, M. Tariquzzaman, M. A. A. Hossain, M. T. Islam, M. R. Islam, S. Akter, M. S. Rahi, M. T. R. Joy, Z. Kowser, *Heliyon* **2025**, *11*, e41614.
[89] M. Burton, E. Cobb, P. Donachie, G. Judah, V. Curtis, W.-P. Schmidt, *Int. J. Environ. Res. Public Health* **2011**, *8*, 97.
[90] World Health Organization, *Advice for the public: Coronavirus disease (COVID-19)*, https://www.who.int/emergencies/diseases/novel-coronavirus-2019/advice-for-public.
[91] M. Chopin-Doroteo, E. Krötzsch, *Journal of cosmetic dermatology* **2023**, *22*, 347.
[92] A. Henao-Ardila, M. X. Quintanilla-Carvajal, F. L. Moreno, *Heliyon* **2024**, *10*, e32150.
[93] A. P. Gama, Y.-C. Hung, K. Adhikari, *Foods* **2019**, *8*.
[94] N. Cortes, I. A. Alves, D. M. Aragón, *ACS omega* **2024**, *9*, 48884.
[95] F. Calvo, J. M. Gómez, O. Alvarez, L. Ricardez-Sandoval, *Chem. Eng. Res. Des.* **2022**, *186*, 407.
[96] GlobalNewswire, *Sodium Lauryl Sulfate (SLS) Business Research Report 2024: Market to Reach $919.9 Million by 2030 - Focus on Developing Low-Dose, High-Efficacy SLS Formulations Creates New Opportunities* **2024**, https://www.globenewswire.com/news-release/2024/10/09/2960284/28124/en/Sodium-Lauryl-Sulfate-SLS-Business-Research-Report-2024-Market-to-Reach-919-9-Million-by-2030-Focus-on-Developing-Low-Dose-High-Efficacy-SLS-Formulations-Creates-New-Opportunities.html.

[97] Intratec, *Sodium Lauryl Sulfate Production: Report SLS E11A Cost Analysis* **2020**, https://cdn.intratec.us/docs/reports/previews/sls-e11a-b.pdf.
[98] Intratec, *Sodium Lauryl Ether Sulfate Production: Report SLES E11A Cost Analysis* **2021**, https://cdn.intratec.us/docs/reports/previews/sles-e11a-b.pdf.
[99] M. Sassi, S. Mattiello, L. Beverina, *Eur. J. Org. Chem.* **2020**, *2020*, 3942.
[100] T. N. Ansari, G. Xu, A. Preston, P. Gao, *Org. Process Res. Dev.* **2024**, *28*, 816.
[101] E. Borrego, A. Caballero, P. J. Pérez, *Organometallics* **2022**, *41*, 3084.
[102] G. La Sorella, G. Strukul, A. Scarso, *Green Chem.* **2015**, *17*, 644.
[103] T. Shen, S. Zhou, J. Ruan, X. Chen, X. Liu, X. Ge, C. Qian, *Advances in colloid and interface science* **2021**, *287*, 102299.
[104] C. Ceriani, F. Pallini, L. Mezzomo, M. Sassi, S. Mattiello, L. Beverina, *J. Organomet. Chem.* **2022**, *962*, 122267.
[105] C. M. Gabriel, N. R. Lee, F. Bigorne, P. Klumphu, M. Parmentier, F. Gallou, B. H. Lipshutz, *Org. Lett.* **2017**, *19*, 194.
[106] A. Sanzone, S. Mattiello, G. M. Garavaglia, A. M. Calascibetta, C. Ceriani, M. Sassi, L. Beverina, *Green Chem.* **2019**, *21*, 4400.
[107] S. Mattiello, M. Rooney, A. Sanzone, P. Brazzo, M. Sassi, L. Beverina, *Org. Lett.* **2017**, *19*, 654.
[108] B. H. Lipshutz, A. R. Abela, *Org. Lett.* **2008**, *10*, 5329.
[109] M. Rooney, S. Mattiello, R. Stara, A. Sanzone, P. Brazzo, M. Sassi, L. Beverina, *Dyes Pigm.* **2018**, *149*, 893.
[110] S. Mattiello, E. Ghiglietti, A. Zucchi, L. Beverina, *Curr. Opin. Colloid Interface Sci.* **2023**, *64*, 101681.
[111] A. Ranaudo, C. Greco, G. Moro, A. Zucchi, S. Mattiello, L. Beverina, U. Cosentino, *J. Phys. Chem. B* **2022**, *126*, 9408.
[112] N-TV, *Giftiger Schaum verätzt Teile von Kolumbiens Hauptstadt: Reinigungsmittelabfälle im Fluss* **2022**, https://www.n-tv.de/mediathek/videos/panorama/Giftiger-Schaum-veraetzt-Teile-von-Kolumbiens-Hauptstadt-article23298162.html.
[113] A. R. Nogueira, M. G. C. Da Popi, C. C. S. Moore, L. Kulay, *J. Cleaner Prod.* **2019**, *240*, 118203.
[114] J. R. G. Asio, J. S. Garcia, C. Antonatos, J. B. Sevilla-Nastor, L. C. Trinidad, *Emerging Contaminants* **2023**, *9*, 100205.
[115] researchnester, *Sodium Lauryl Sulfate Market* **2024**, https://www.researchnester.com/reports/sodium-lauryl-sulfate-market/5242.
[116] J. R. A. Kincaid, M. J. Wong, N. Akporji, F. Gallou, D. M. Fialho, B. H. Lipshutz, *J. Am. Chem. Soc.* **2023**, *145*, 4266.
[117] C. Bauer, *Nachhaltige Hygiene* **2020**, https://elements.evonik.com/de/articles/2-2020/nachhaltige-hygiene.html.
[118] Evonik, *Evonik treibt Übergang zu nachhaltigen Biotensiden mit neuer Anlage in der Slowakei voran* **2024**.
[119] BASF Pharma, *Kolliphor® EL: A non-ionic surfactant for various pharmaceutical applications*, https://pharma.basf.com/products/kolliphor-el.
[120] P. W. Atkins, J. de Paula, J. J. Keeler, *Atkins' physical chemistry*, Oxford University Press, Oxford **2023**.
[121] M. J. Kamlet, R. W. Taft, *J. Am. Chem. Soc.* **1976**, *98*, 377.
[122] S. Spange, N. Weiß, *Chemphyschem* **2023**, *24*, e202200780.
[123] S. Spange, N. Weiß, C. H. Schmidt, K. Schreiter, *Chemistry Methods* **2021**, *1*, 42.
[124] C. Adamo, C. Amatore, I. Ciofini, A. Jutand, H. Lakmini, *J. Am. Chem. Soc.* **2006**, *128*, 6829.
[125] W. D. Miller, A. H. Fray, J. T. Quatroche, C. D. Sturgill, *Org. Process Res. Dev.* **2007**, *11*, 359.

[126] V. Gold (Ed.), *The IUPAC Compendium of Chemical Terminology*, International Union of Pure and Applied Chemistry (IUPAC), Research Triangle Park, NC **2019**.
[127] IUPAC, in *The IUPAC Compendium of Chemical Terminology* (Ed.: V. Gold), International Union of Pure and Applied Chemistry (IUPAC). Research Triangle Park, NC **2019**.
[128] IUPAC, in *The IUPAC Compendium of Chemical Terminology* (Ed.: V. Gold), International Union of Pure and Applied Chemistry (IUPAC). Research Triangle Park, NC **2019**.
[129] J. R. Brandt, F. Salerno, M. J. Fuchter, *Nat. Rev. Chem.* **2017**, *1*.
[130] B. P. Bloom, Y. Paltiel, R. Naaman, D. H. Waldeck, *Chem. Rev.* **2024**, *124*, 1950.
[131] R. Bernhardt, M. Manrho, J. Zablocki, L. Rieland, A. Lützen, M. Schiek, K. Meerholz, J. Zhu, T. L. C. Jansen, J. Knoester, P. H. M. van Loosdrecht, *J. Am. Chem. Soc.* **2022**, *144*, 19372.
[132] R. S. Stoll, N. Severin, J. P. Rabe, S. Hecht, *Adv. Mater.* **2006**, *18*, 1271.
[133] M. Schulz, F. Balzer, D. Scheunemann, O. Arteaga, A. Lützen, S. C. J. Meskers, M. Schiek, *Adv. Funct. Mater.* **2019**, *29*.
[134] M. Schulz, J. Zablocki, O. S. Abdullaeva, S. Brück, F. Balzer, A. Lützen, O. Arteaga, M. Schiek, *Nat. Commun.* **2018**, *9*, 2413.
[135] D. Giavazzi, M. F. Schumacher, L. Grisanti, M. Anzola, F. Di Maiolo, J. Zablocki, A. Lützen, M. Schiek, A. Painelli, *J. Mater. Chem. C* **2023**, *11*, 8307.
[136] Marvin F. Schumacher, *Proline- and Indolenine-derived Chiral Squaraines _ Synthesis and Characeristics*, Bonn **2021**.
[137] Robin Bernhardt, *Dynamic, Excitonic and Structural Properties of Squaraine-based Molecular Aggregates*, Köln **2024**.
[138] M. Gsänger, E. Kirchner, M. Stolte, C. Burschka, V. Stepanenko, J. Pflaum, F. Würthner, *J. Am. Chem. Soc.* **2014**, *136*, 2351.
[139] F. Balzer, M. F. Schumacher, S. Mattiello, M. Schulz, J. Zablocki, M. Schmidtmann, K. Meerholz, N. Serdar Sariciftci, L. Beverina, A. Lützen, M. Schiek, *Isr. J. Chem.* **2022**, *62*.
[140] T. Jia, *Lett. Org. Chem.* **2012**, *9*, 325.
[141] C. Agami, F. Couty, L. Hamon, O. Venier, *Tetrahedron Lett.* **1993**, *34*, 4509.
[142] F. Sun, E. V. van der Eycken, H. Feng, *Adv. Synth. Catal.* **2021**, *363*, 5168.
[143] K. C. Nicolaou, P. S. Baran, Y.-L. Zhong, S. Barluenga, K. W. Hunt, R. Kranich, J. A. Vega, *J. Am. Chem. Soc.* **2002**, *124*, 2233.
[144] P. G. M. Wuts, T. W. Greene, *Greene's protective groups in organic synthesis*, Wiley, Hoboken **2007**.
[145] S. V. Schimmelpfennig, *Beiträge zur Synthese von neuen chiralen Squarainen au der Basis von L-Alnanin*, Bonn **2021**.
[146] D. A. Coate, R. Gilmour, Martin, Jose, Alfredo, Martine de la Nava, Eva, Maria, *OXAZOLO [5, 4 -B] PYRIDIN- 5 -YL COMPOUNDS AND THEIR USE FOR THE TREATMENT OF CANCER*.
[147] J. O. Osby, M. G. Martin, B. Ganem, *Tetrahedron Lett.* **1984**, *25*, 2093.
[148] N. Sakai, T. Moriya, K. Fujii, T. Konakahara, *Synthesis* **2008**, *2008*, 3533.
[149] H. Liu, Y.-L. Zhu, Z. Li, *Nat. Commun.* **2019**, *10*, 3881.
[150] Z. Chen, N. D. Urban, Y. Gao, W. Zhang, J. Deng, J. Zhu, X. C. Zeng, B. Gong, *Org. Lett.* **2011**, *13*, 4008.
[151] T. T. Wager, R. Y. Chandrasekaran, T. W. Butler, *MORPHOLINE D3 DOPAMINE ANTAGONISTS* **2008**.
[152] J.-F. Marcoux, S. Wagaw, S. L. Buchwald, *J. Org. Chem.* **1997**, *62*, 1568.
[153] B. T. Ingoglia, C. C. Wagen, S. L. Buchwald, *Tetrahedron* **2019**, *75*, 4199.
[154] P. A. Forero-Cortés, A. M. Haydl, *Org. Process Res. Dev.* **2019**, *23*, 1478.
[155] M. Subat, B. König, *Synthesis* **2001**, *2001*, 1818.

[156] S. Wang, L. Hall, V. V. Diev, R. Haiges, G. Wei, X. Xiao, P. I. Djurovich, S. R. Forrest, M. E. Thompson, *Chem. Mater.* **2011**, *23*, 4789.
[157] N. H. Park, E. V. Vinogradova, D. S. Surry, S. L. Buchwald, *Angewandte Chemie (International ed. in English)* **2015**, *54*, 8259.
[158] D. Maiti, B. P. Fors, J. L. Henderson, Y. Nakamura, S. L. Buchwald, *Chem. Sci.* **2011**, *2*, 57.
[159] G. Ferrer-Sueta, in *Redox Chemistry and Biology of Thiols*, Elsevier **2022**, p. 19.
[160] G. M. Sheldrick, *Acta crystallographica. Section C, Structural chemistry* **2015**, *71*, 3.
[161] K. Momma, F. Izumi, *J. Appl. Crystallogr.* **2011**, *44*, 1272.
[162] C. F. Macrae, I. Sovago, S. J. Cottrell, P. T. A. Galek, P. McCabe, E. Pidcock, M. Platings, G. P. Shields, J. S. Stevens, M. Towler, P. A. Wood, *J. Appl. Crystallogr.* **2020**, *53*, 226.
[163] C. Reichardt, *Chem. Rev.* **1994**, *94*, 2319.
[164] C. Reichardt, *Solvents and solvent effects in organic chemistry*, Wiley-VCH, Weinheim **2003**.
[165] J. Catalán, *J. Phys. Chem. B* **2009**, *113*, 5951.
[166] M. Kasha, H. R. Rawls, M. Ashraf El-Bayoumi, *Pure Appl. Chem.* **1965**, *11*, 371.
[167] M. Kasha, *Radiat. Res.* **1963**, *20*, 55.
[168] E. E. JELLEY, *Nature* **1936**, *138*, 1009.
[169] D. Timmer, F. Zheng, M. Gittinger, T. Quenzel, D. C. Lünemann, K. Winte, Y. Zhang, M. E. Madjet, J. Zablocki, A. Lützen, J.-H. Zhong, A. de Sio, T. Frauenheim, S. Tretiak, C. Lienau, *J. Am. Chem. Soc.* **2022**, *144*, 19150.
[170] N. J. Hestand, F. C. Spano, *Chem. Rev.* **2018**, *118*, 7069.
[171] A. Eisfeld, J. S. Briggs, *Chem. Phys.* **2006**, *324*, 376.
[172] A. S. Davydov, *Sov. Phys. Usp.* **1964**, *7*, 145.
[173] R. Bernhardt, L. Rieland, T. Wang, M. F. Schumacher, A. Lützen, M. Schiek, P. H. M. van Loosdrecht, *Aggregate* **2025**, *6*.
[174] N. Berova, L. Di Bari, G. Pescitelli, *Chem. Soc. Rev.* **2007**, *36*, 914.
[175] A. T. Rösch, Q. Zhu, J. Robben, F. Tassinari, S. C. J. Meskers, R. Naaman, A. R. A. Palmans, E. W. Meijer, *Chem. - Eur. J.* **2021**, *27*, 298.
[176] J. Selby, M. Holzapfel, B. K. Lombe, D. Schmidt, A.-M. Krause, F. Würthner, G. Bringmann, C. Lambert, *J. Org. Chem.* **2020**, *85*, 12227.
[177] A. M. Hassanien, A. Darwish, A. M. Kamal, M. Al-Gawati, T. A. Hamdalla, *Opt. Mater.* **2023**, *142*, 114033.
[178] J. F. Bower, P. Szeto, T. Gallagher, *Org. Lett.* **2007**, *9*, 3283.
[179] Luca Beverina, *Synthetic procedures*.
[180] G. Garbay, T. Tailliez, E. Pavlopoulou, J. Oriou, M. Bezirdjoglou, G. Hadziioannou, E. Cloutet, C. Brochon, *Polym. Chem.* **2018**, *9*, 1288.
[181] R. Moser, S. Ghorai, B. H. Lipshutz, *J. Org. Chem.* **2012**, *77*, 3143.
[182] J. Wu, C. Si, Y. Chen, L. Yang, B. Hu, G. Chen, Z. Lu, Y. Huang, *Chem. - Eur. J.* **2018**, *24*, 3234.
[183] S. Kuster, T. Geiger, *Dyes Pigm.* **2012**, *95*, 657.
[184] R. Rengasamy, M. J. Curtis-Long, W. D. Seo, S. H. Jeong, I.-Y. Jeong, K. H. Park, *J. Org. Chem.* **2008**, *73*, 2898.
[185] Wing-Si Li, *Contributions to the Total Synthesis of Epicoccolide B*, Bonn **2021**.
[186] J. P. Powers, *ARYLSULFONIC ACID SALTS OF PYRIMIDINE-BASED ANTIVIRAL AGENTS* **2001**.
[187] A. Saupe, *Angew. Chem.* **1965**, *77*, 276.

APPENDIX

Contents:

1. NMR Spectra A2
2. Mass Spectra A58
3. Additional Visualization of the Crystal structures A113
4. UV-Vis Spectra A115

NMR SPECTRA

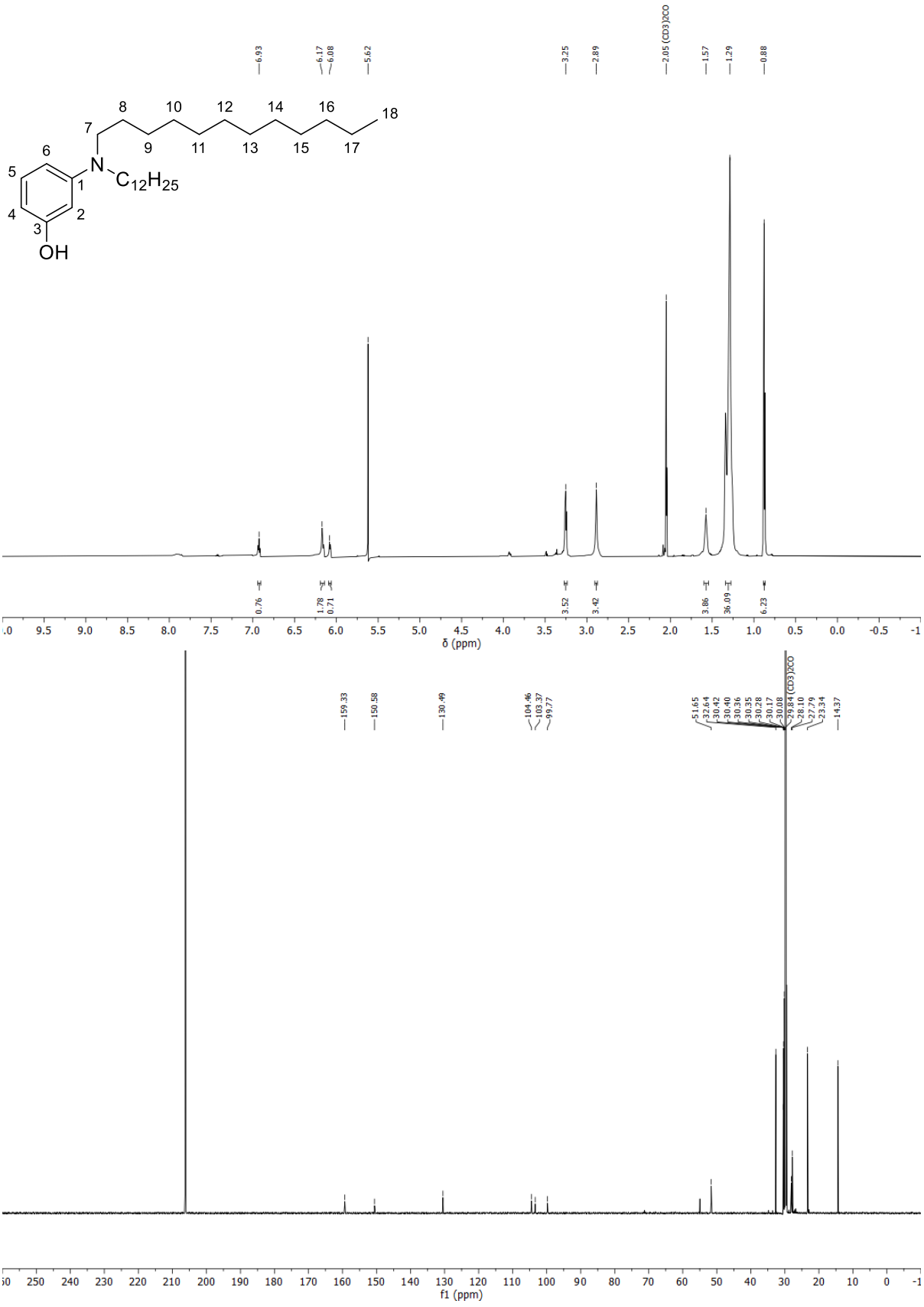

***Figure A1**:[1]H- (top, 700 MHz) and [13]C-NMR (bottom, 176 MHz) spectra of N,N-didodecyl 3-hydroxy aniline (**1**), acetone-d_6, 298 K.*

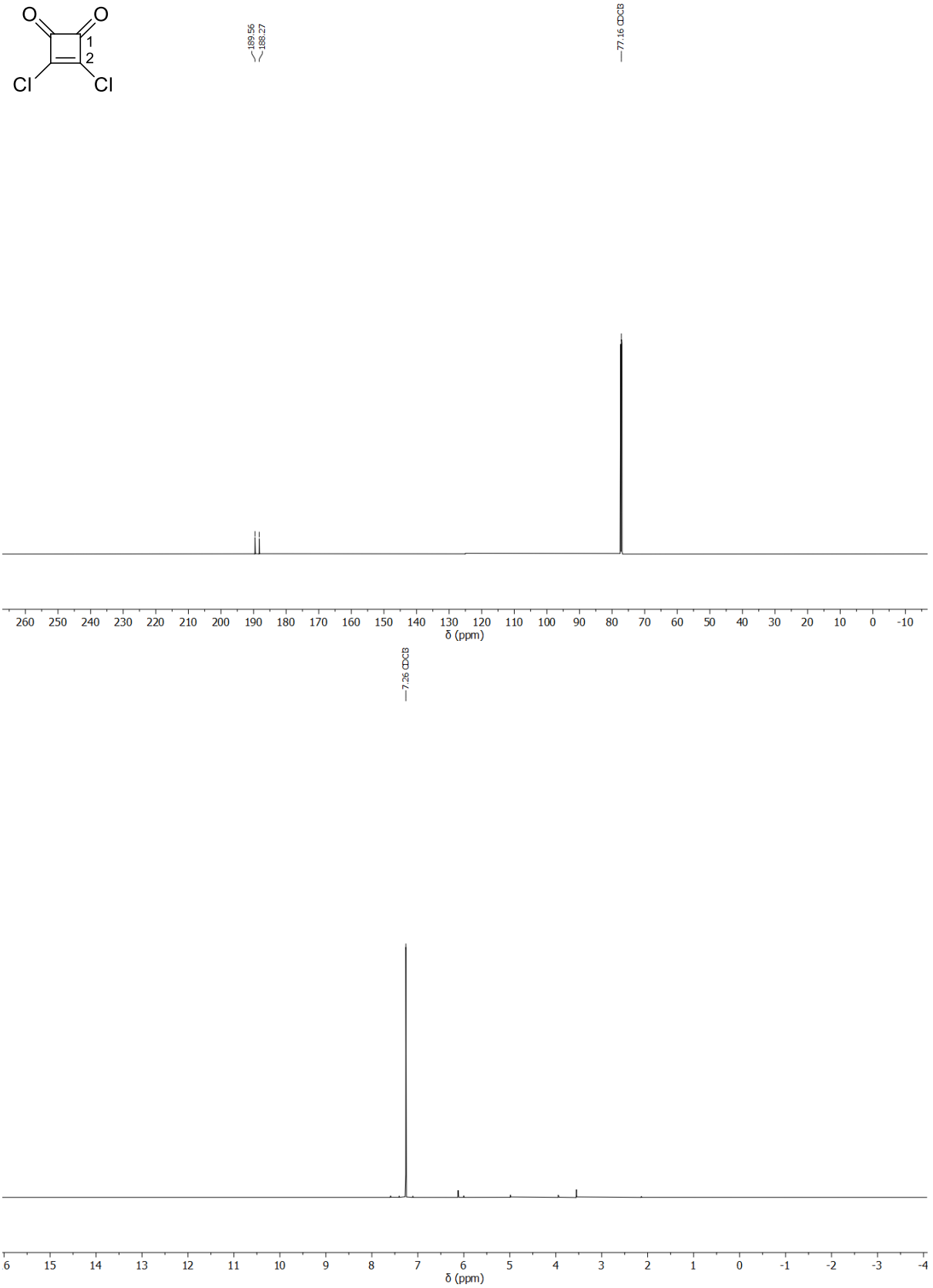

***Figure A2**: ^{1}H- (top, 700 MHz) and ^{13}C-NMR (bottom, 176 MHz) spectra of squarylium dichloride (**2**); $CDCl_3$, 298 K.*

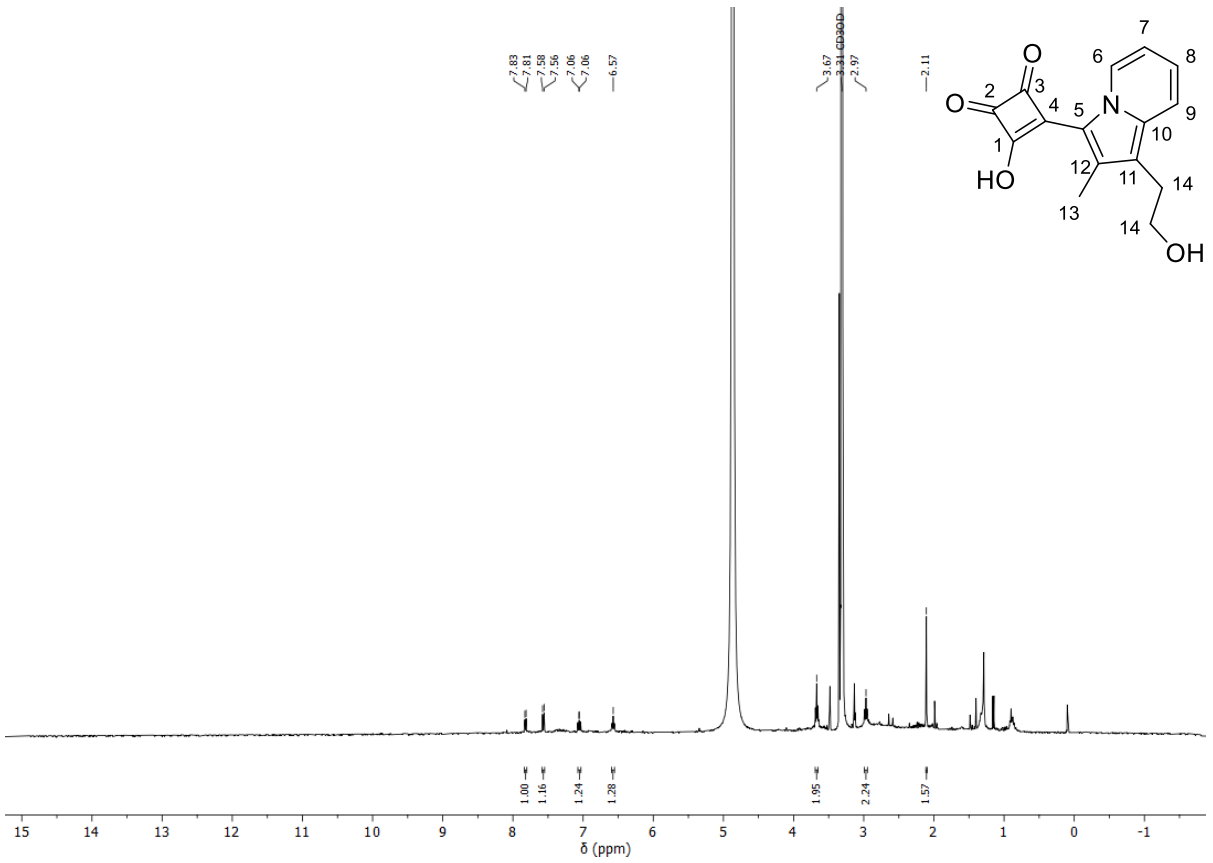

***Figure A3**: [1]H- (top, 500 MHz) of hemisquarate (**4**); $CDCl_3$, 298 K.*

1-phenyl butanedioate (5)

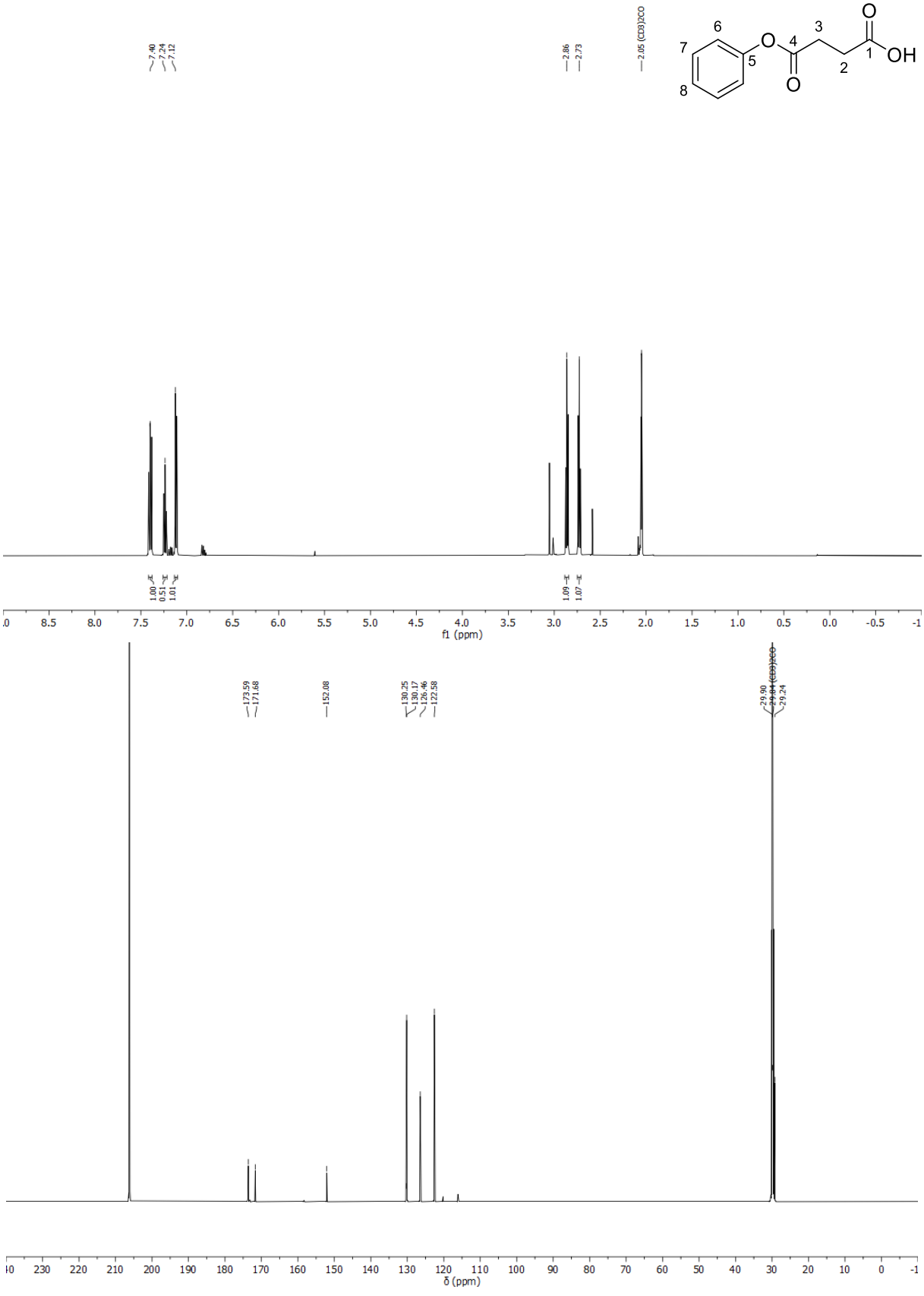

***Figure A4**: ^{1}H- (top, 700 MHz) and ^{13}C-NMR (bottom, 176 MHz) spectra of 1-phenyl butanedioate (**5**); $CDCl_3$, 298 K.*

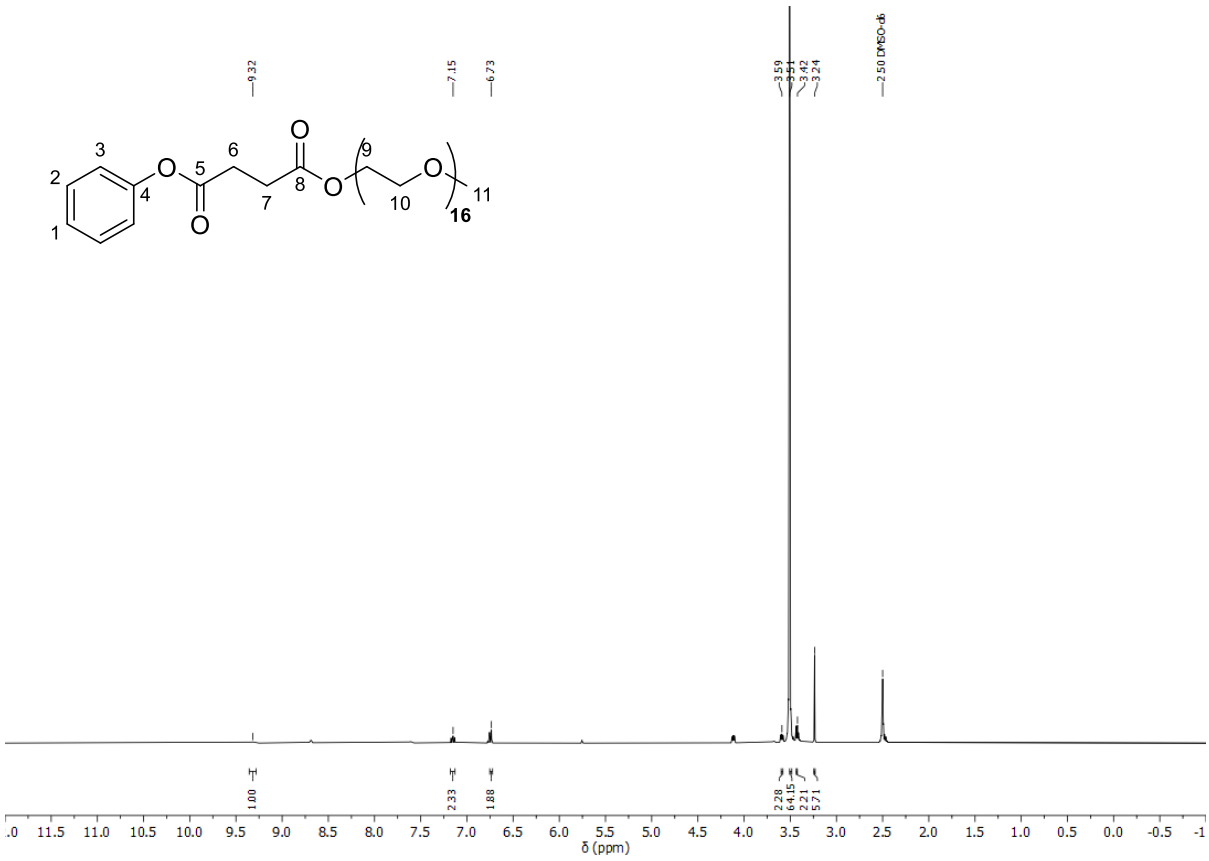

***Figure A5**: [1]H- (top, 400 MHz) of PEG-ylated 1-Phenyl butanedioate (**6**); DMSO-d6, 298 K.*

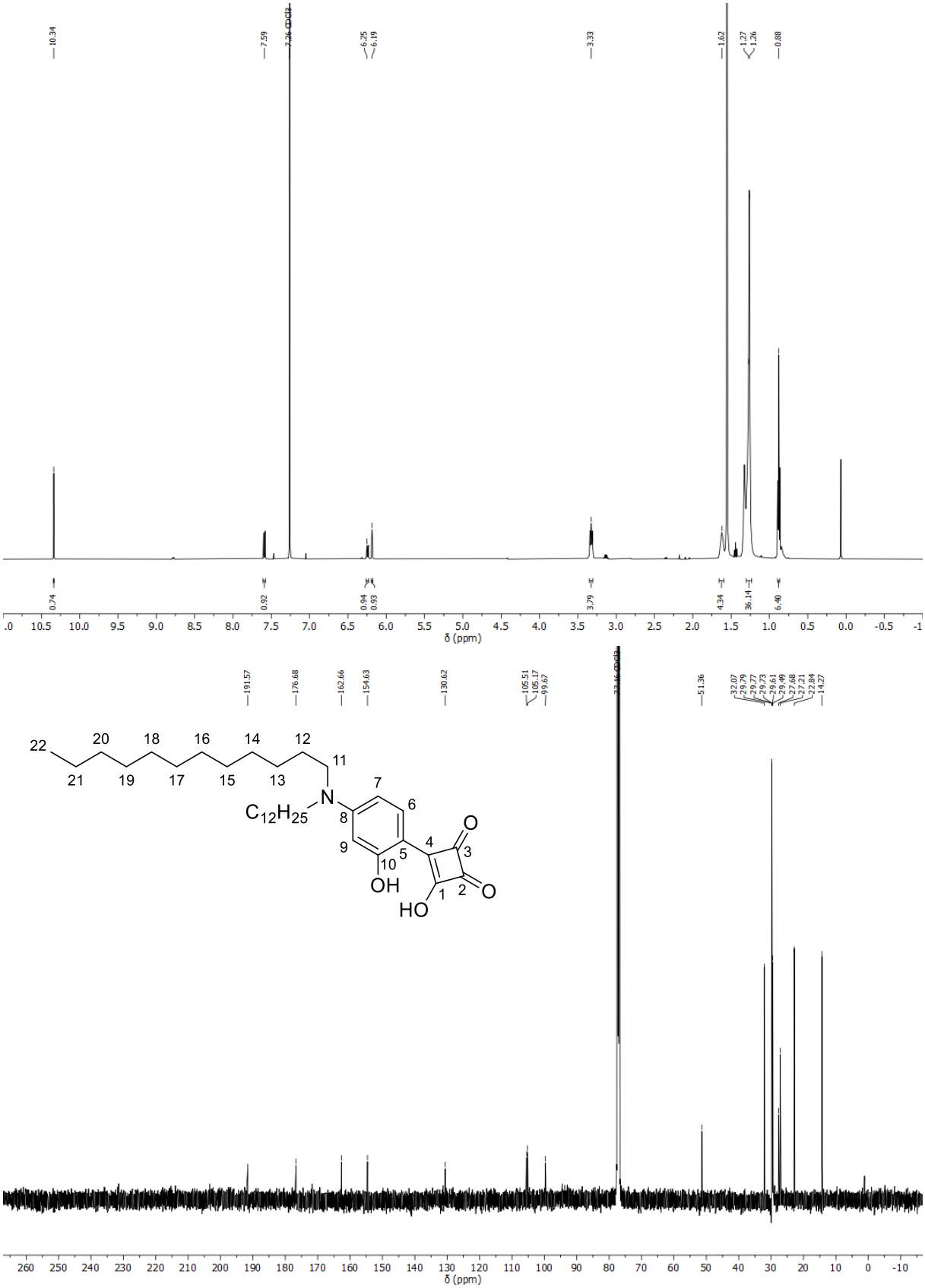

***Figure A6**: ^{1}H- (top, 500 MHz) and ^{13}C-NMR (bottom, 126 MHz) spectra of hemisquarate (**9**); $CDCl_3$, 298 K.*

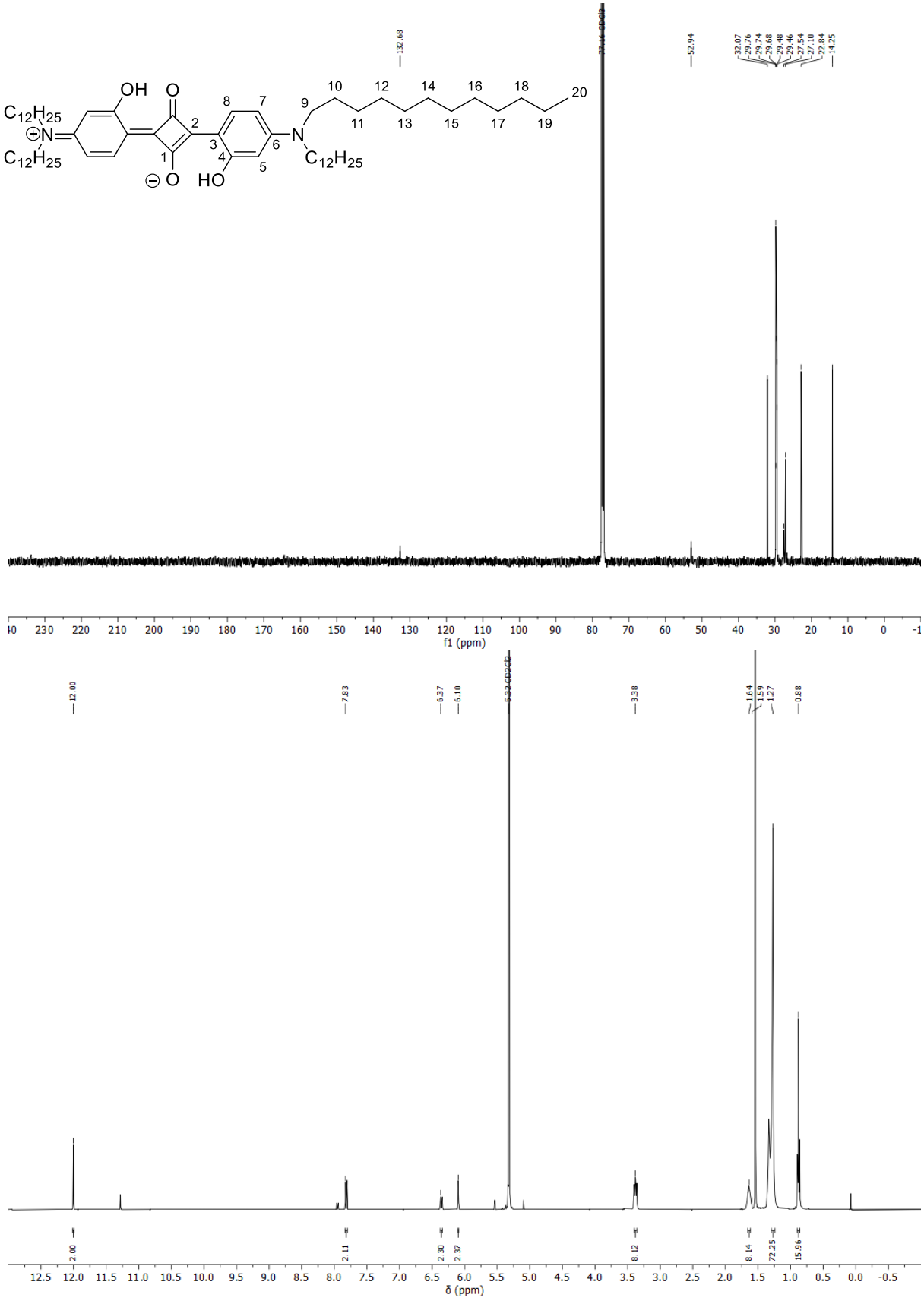

***Figure A7**: ^{1}H- (top, 500 MHz) and ^{13}C-NMR (bottom, 126 MHz) spectra of symmetric squaraine (**11**), $CDCl_3$, 298 K.*

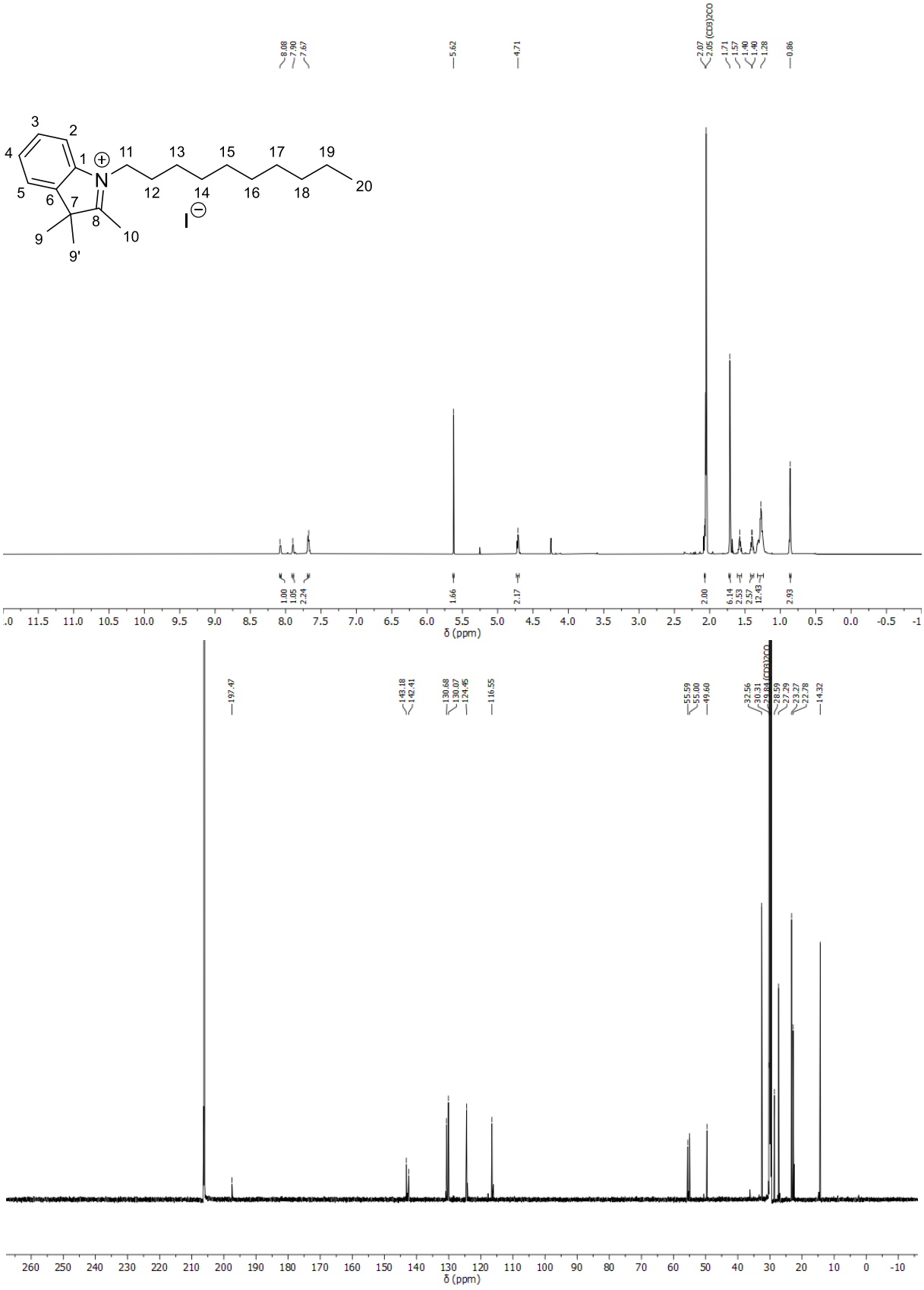

***Figure A8**: ^{1}H- (top, 700 MHz) and ^{13}C-NMR (bottom, 176 MHz) spectra of indole derivative (13), acetone-d_6, 298 K.*

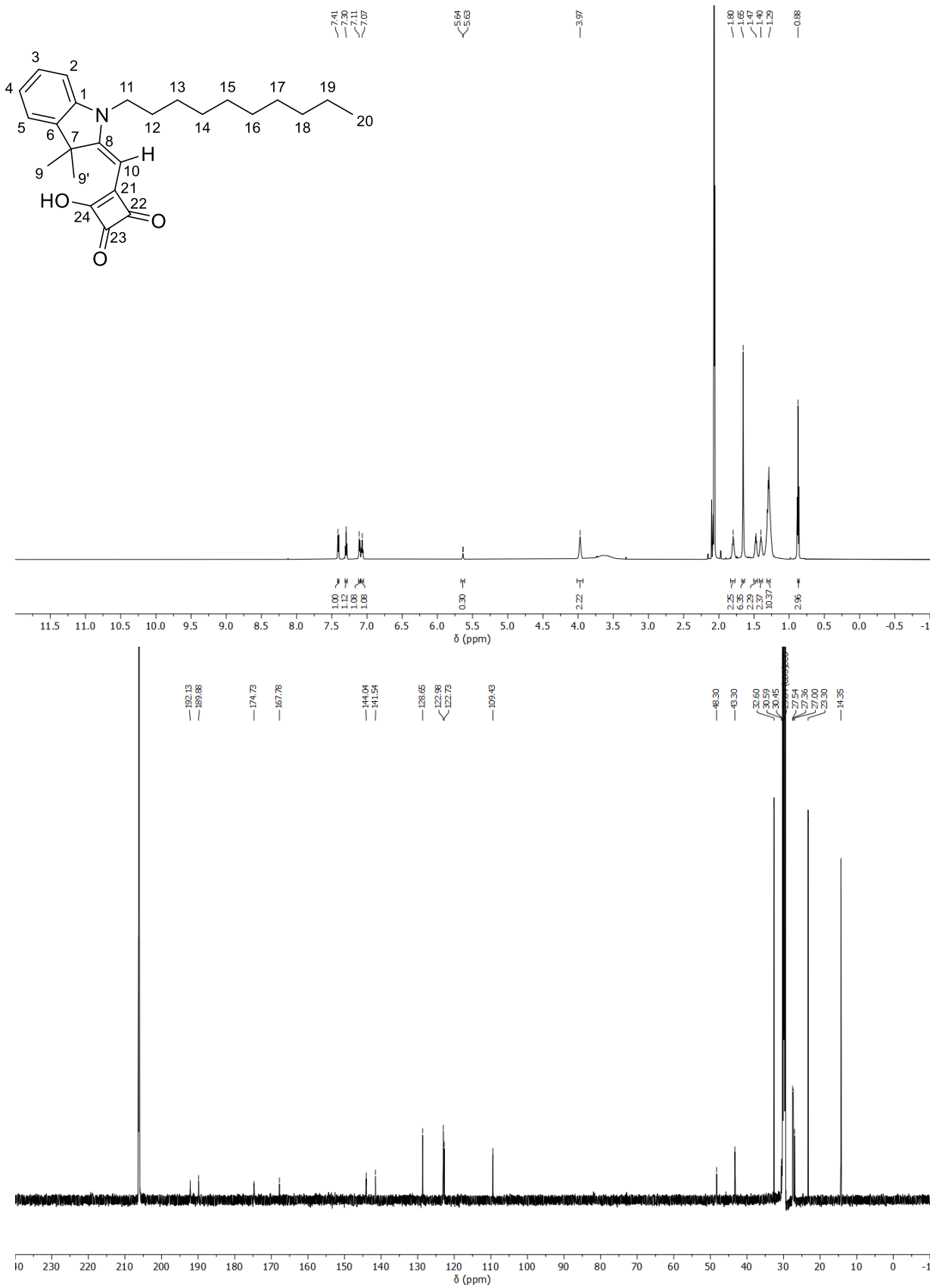

***Figure A9**: [1]H- (top, 700 MHz) and [13]C-NMR (bottom, 176 MHz) spectra of hemisquarate (17), acetone-d_6, 298 K.*

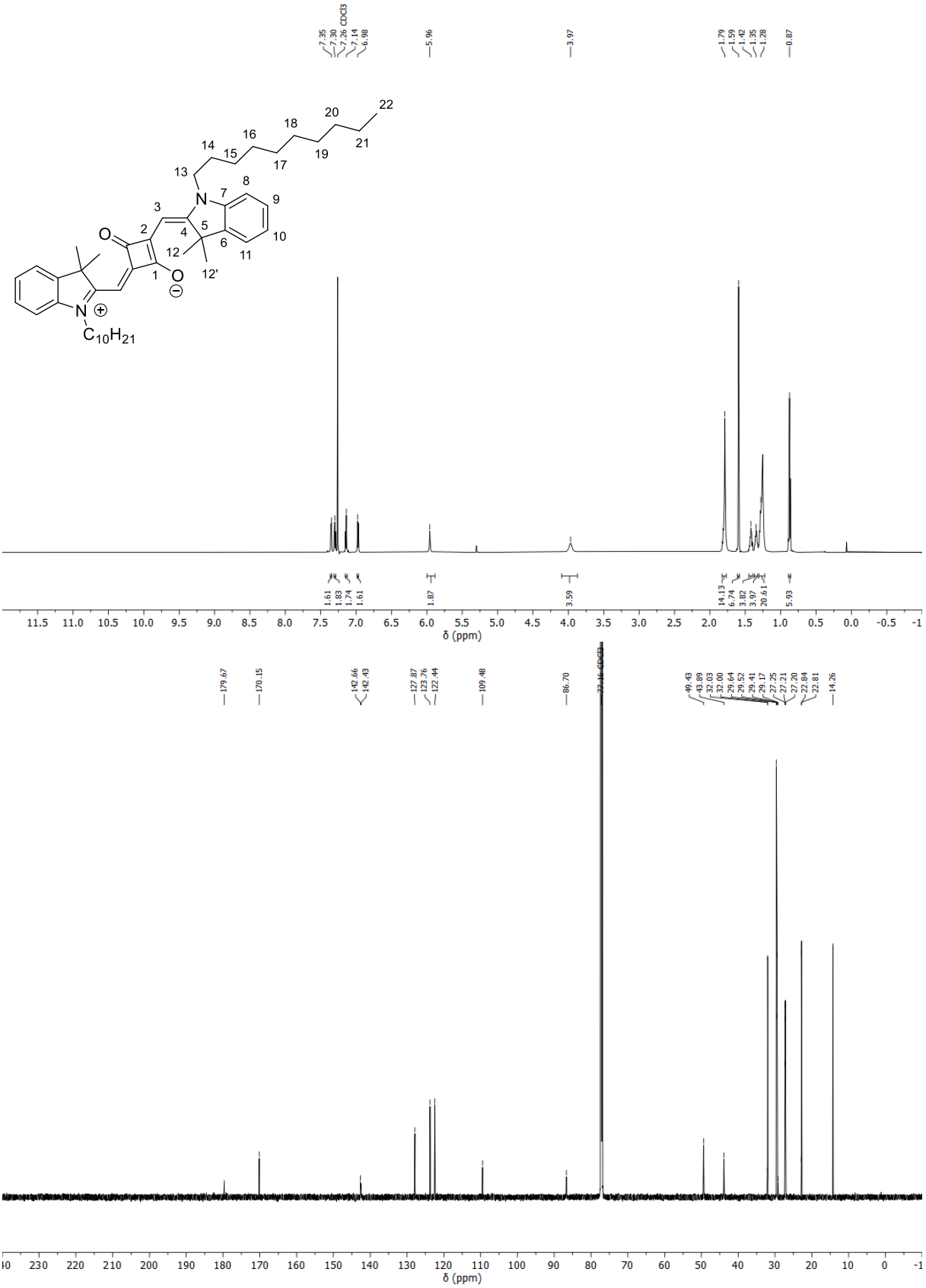

***Figure A10**: [1]H- (top, 700 MHz) and [13]C-NMR (bottom, 176 MHz) spectra indolenine squaraine , $CDCl_3$, 298 K.*

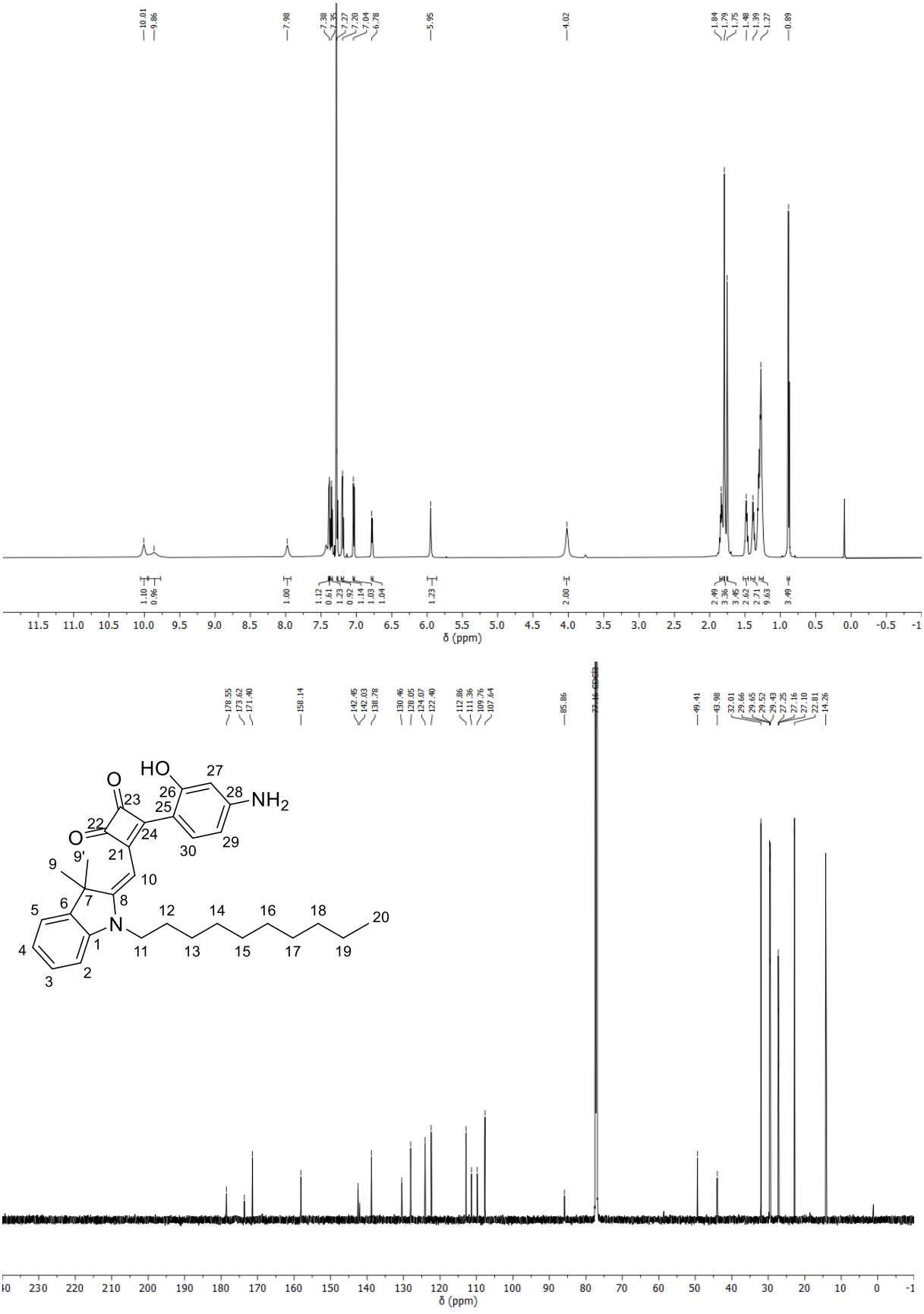

***Figure A11**: ^{1}H- (top, 700 MHz) and ^{13}C-NMR (bottom, 176 MHz) spectra amphiphilic squaraine (**20**), $CDCl_3$, 298 K.*

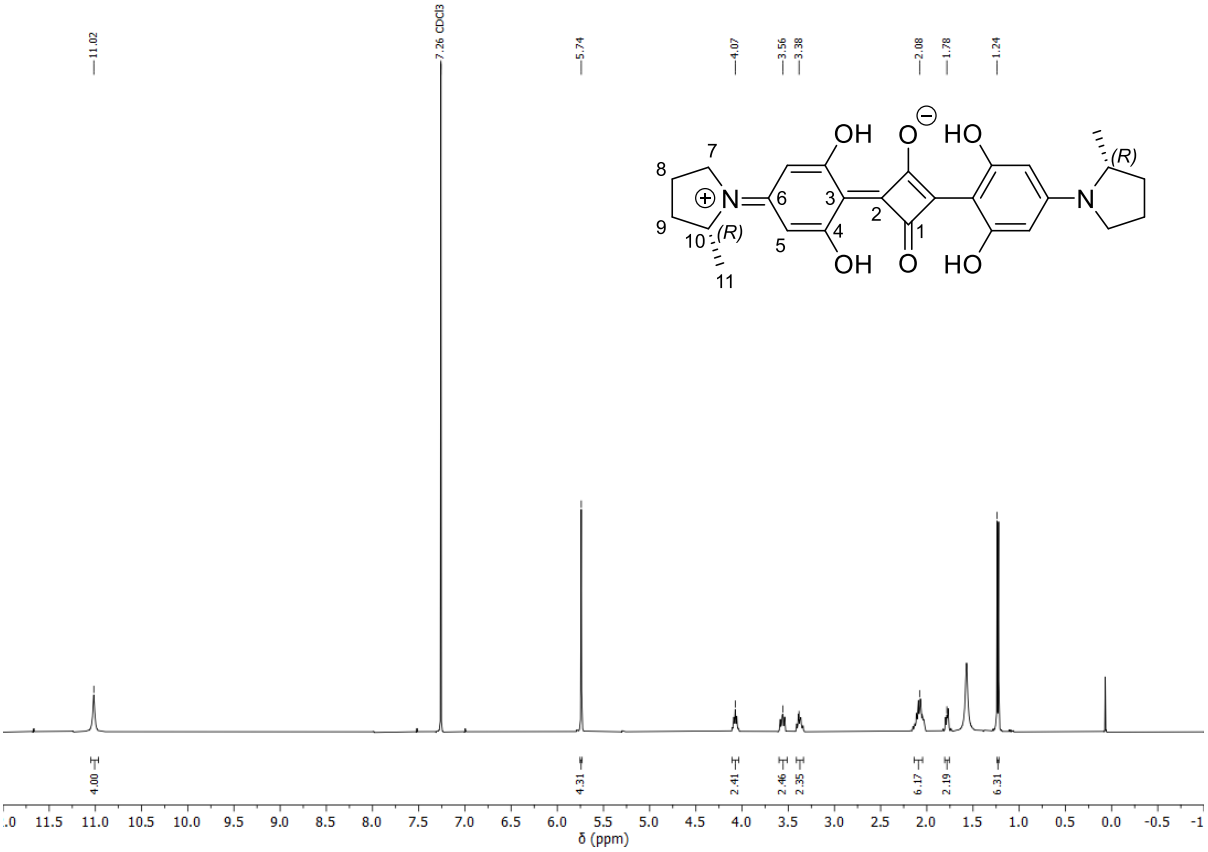

***Figure A12**: ^{1}H- (top, 400 MHz) spectra of literature known (R,R)-PyrSQ-C1, $CDCl_3$, 298 K.*

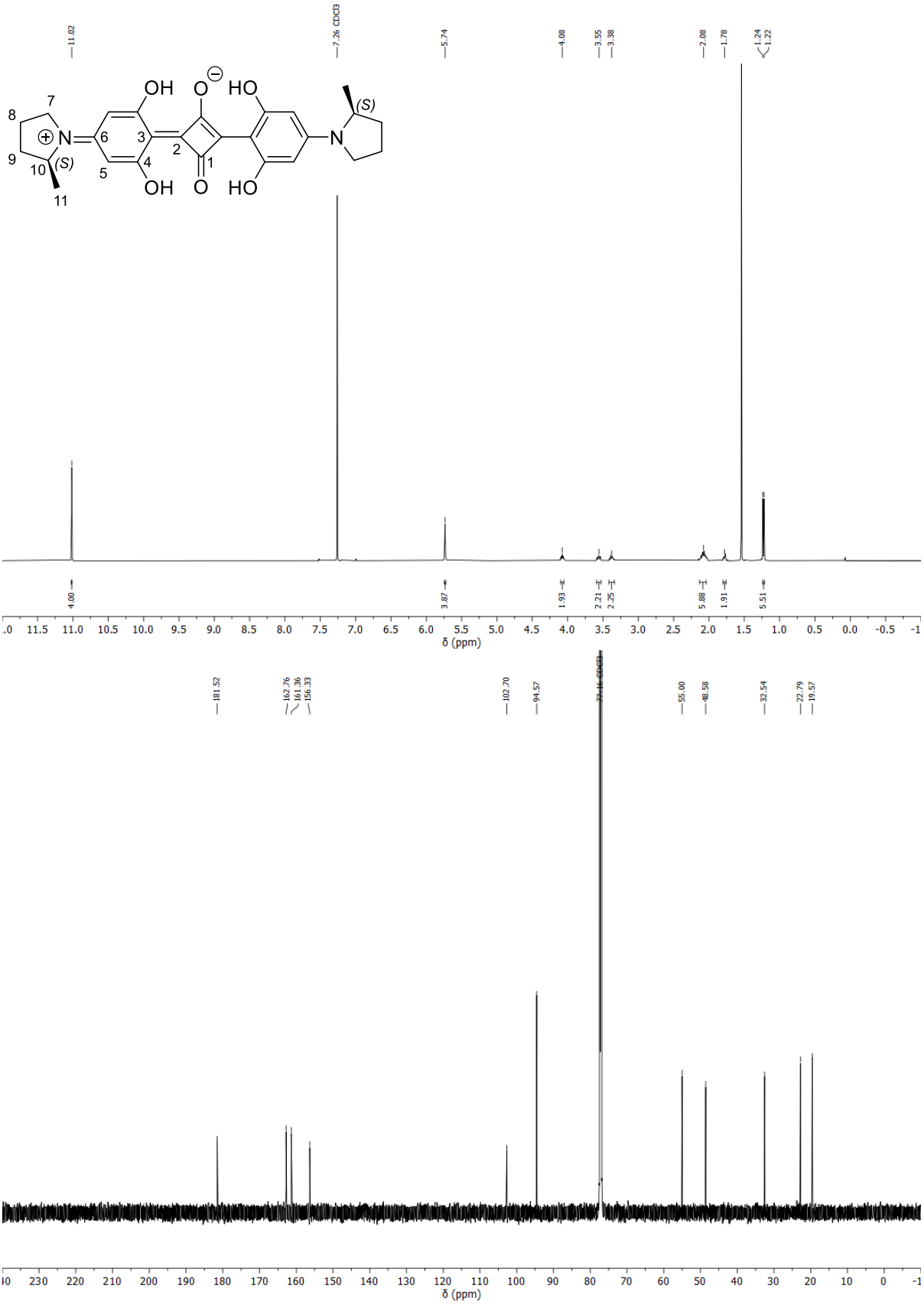

***Figure A13**: ^{1}H- (top, 700 MHz) and ^{13}C-NMR (bottom, 176 MHz) spectra (S,S)-PyrSQ-C1, $CDCl_3$, 298 K.*

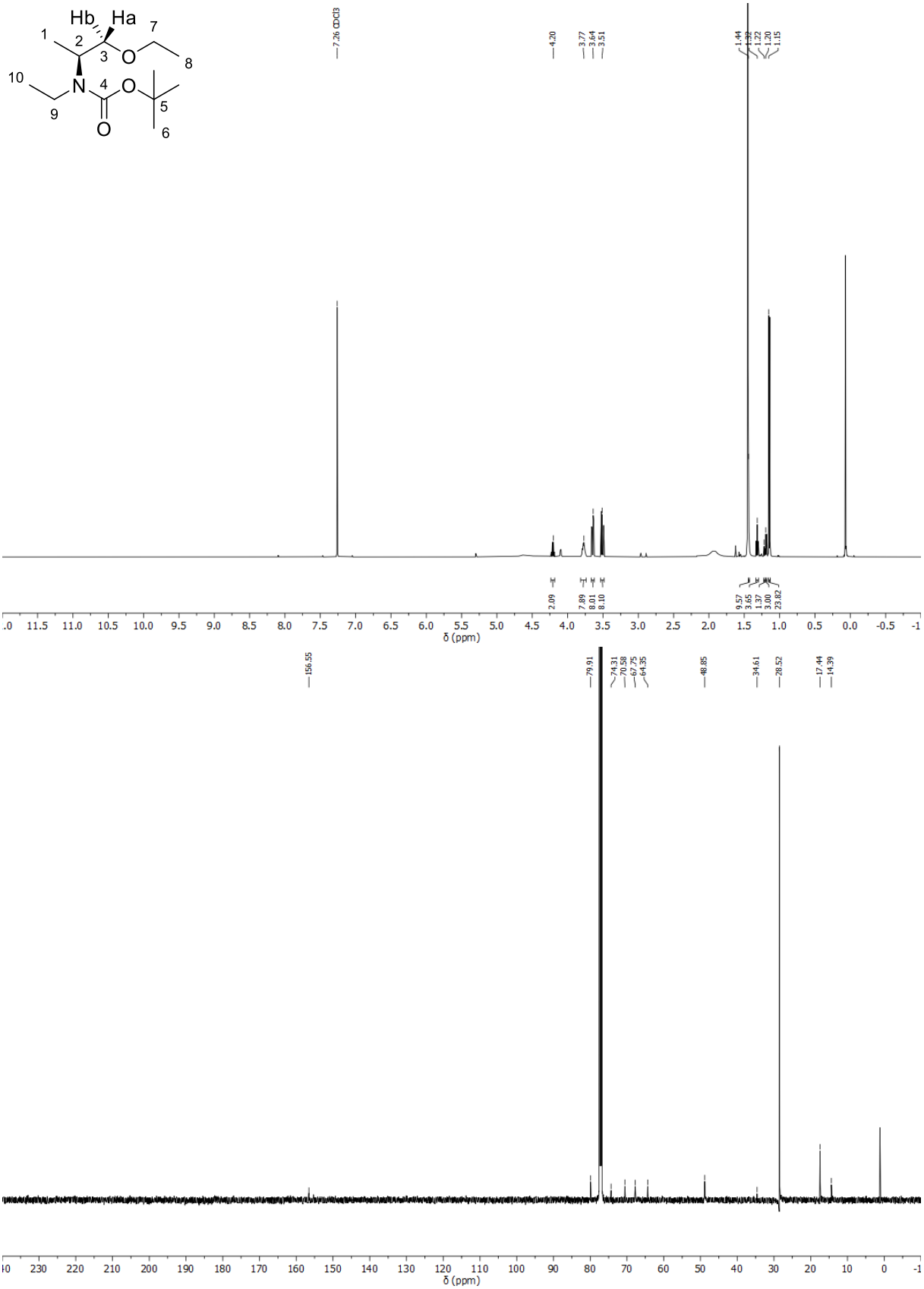

***Figure A14**: ^{1}H- (top, 500 MHz) and ^{13}C-NMR (bottom, 126 MHz) spectra **31a**, $CDCl_3$, 298 K.*

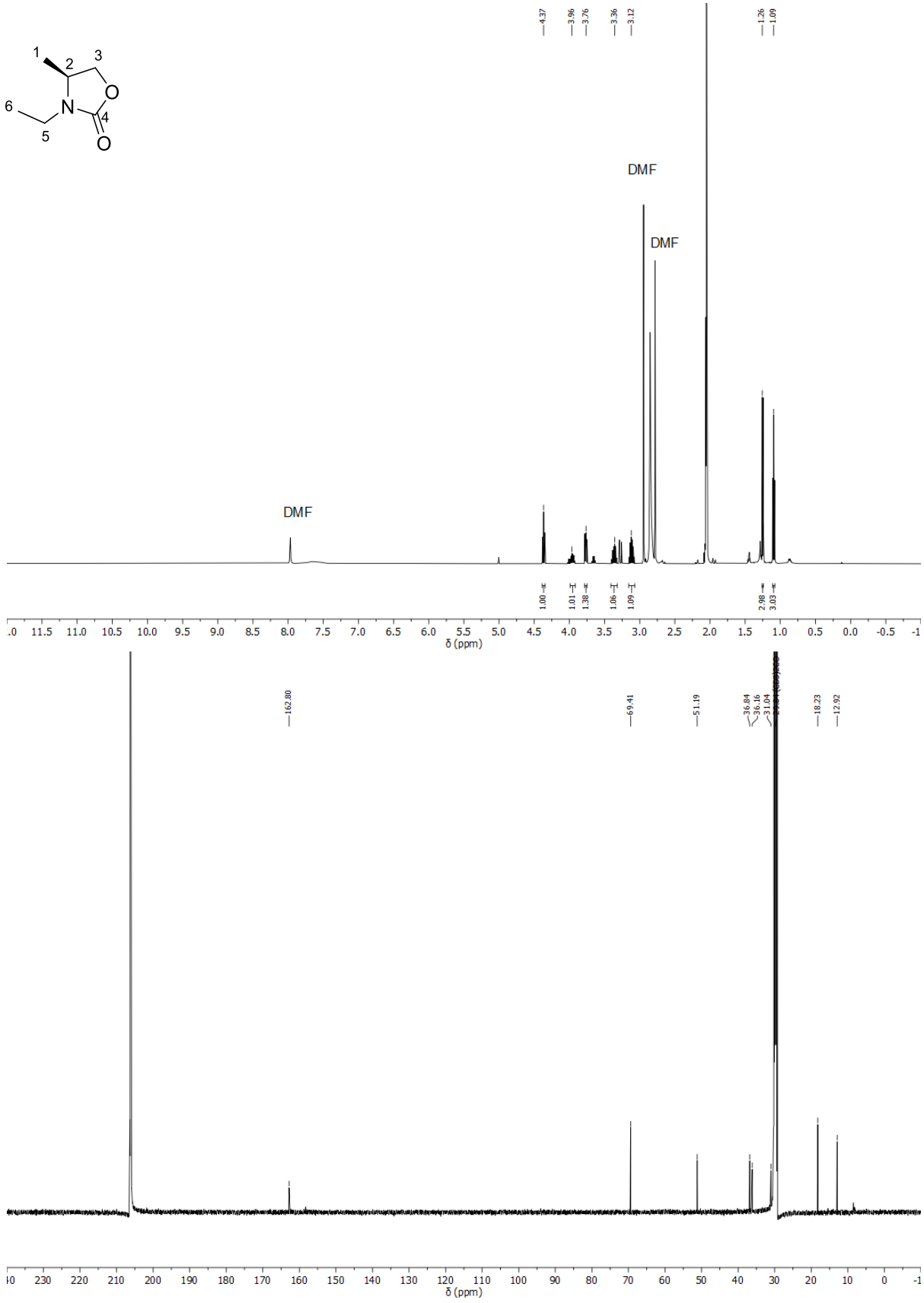

***Figure A15**: ^{1}H- (top, 500 MHz) and ^{13}C-NMR (bottom, 126 MHz) spectra oxazolidinone byproduct **30**, $CDCl_3$, 298 K.*

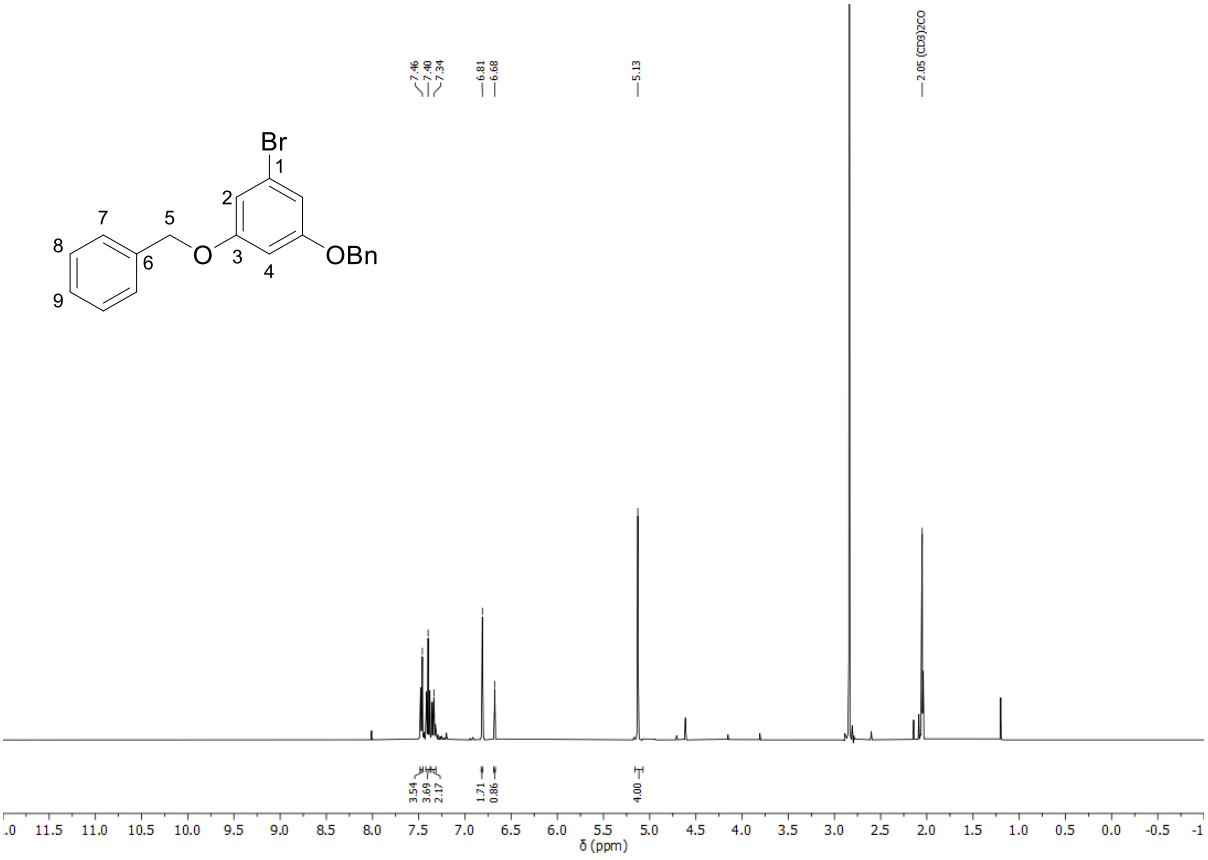

***Figure A16**: ^{1}H- (top, 500 MHz) spectra of **43**, acetone-d_6, 298 K.*

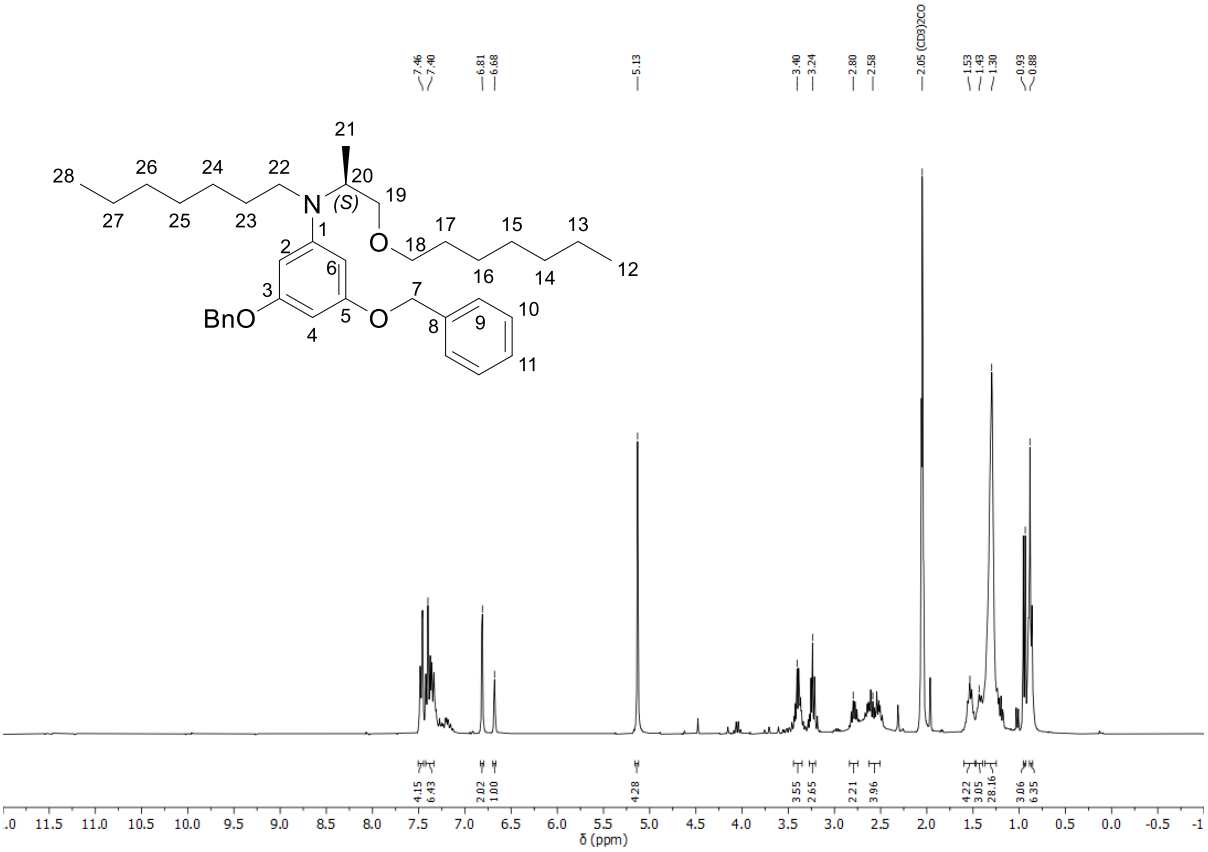

***Figure A17**: ^{1}H- (top, 400 MHz) spectra of **44e**, $CDCl_3$, 298 K.*

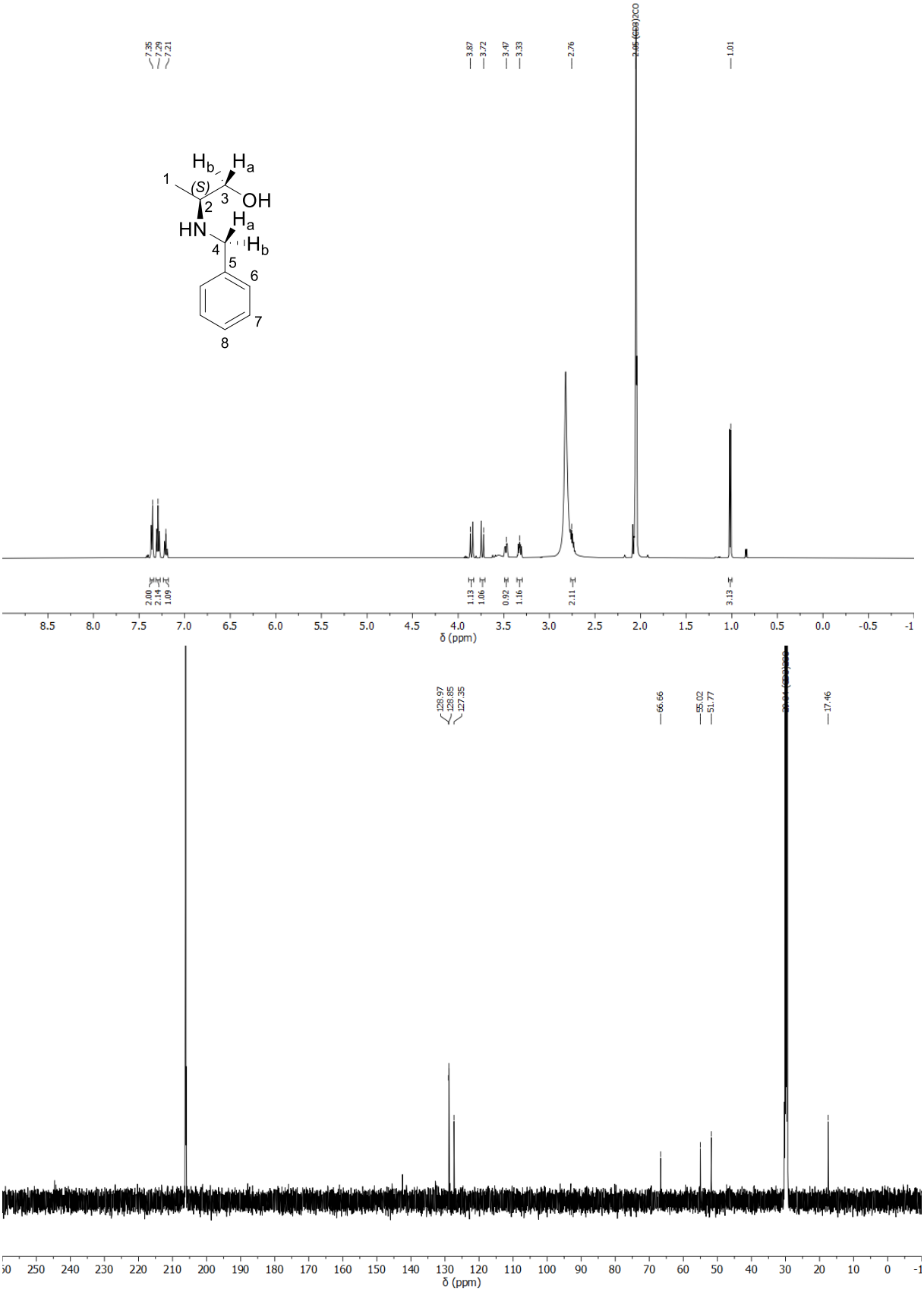

***Figure A18**: ^{1}H- (top, 500 MHz) and ^{13}C-NMR (bottom, 126 MHz) spectra of N-benzyl -L-alaninol (**38**); acetone-d_6, 298 K.*

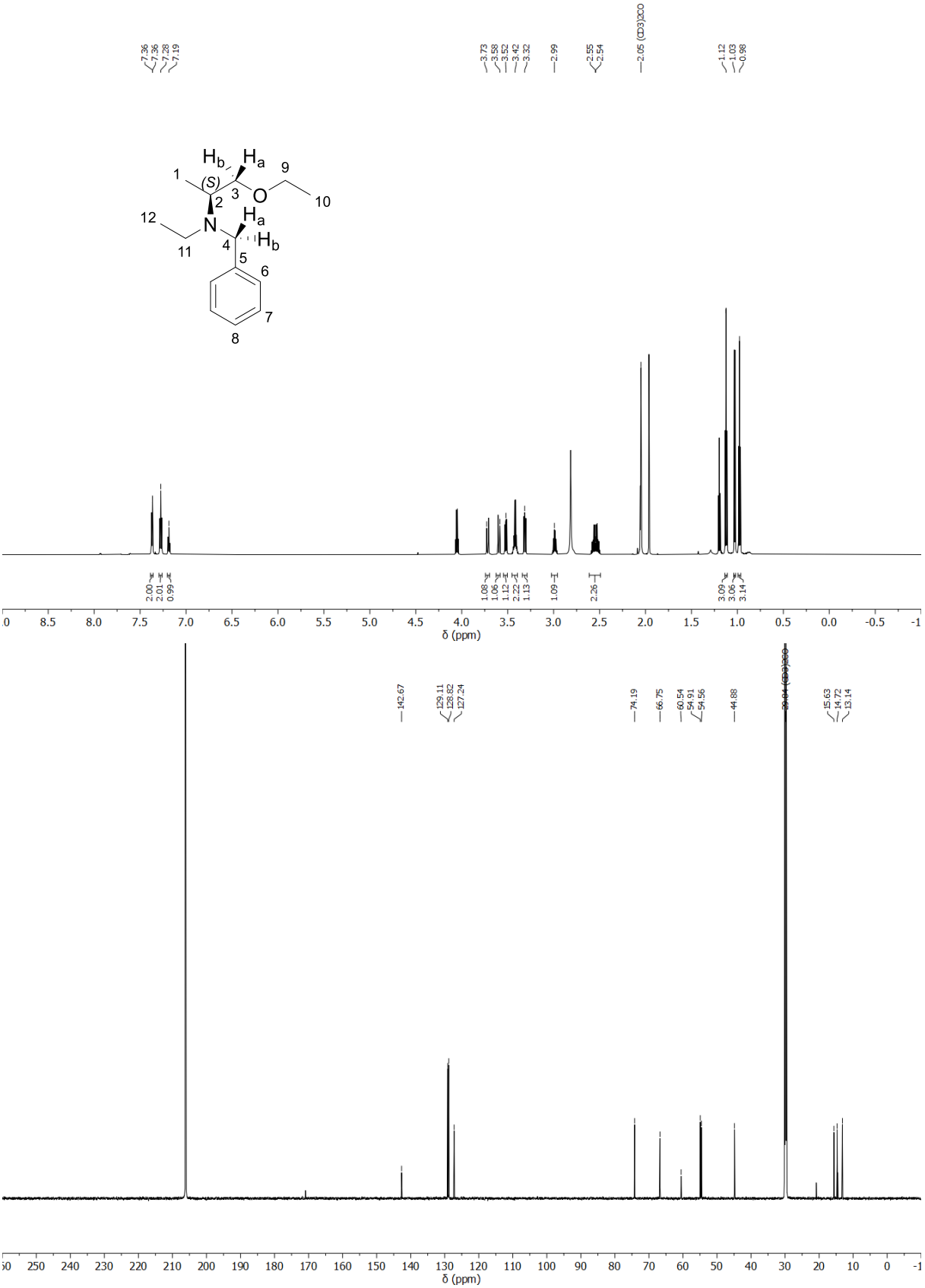

***Figure A19**: ^{1}H- (top, 500 MHz) and ^{13}C-NMR (bottom, 126 MHz) spectra of N-benzyl-N-ethyl-L-alaninyl ethyl ether (**39a**); acetone-d_6, 298 K.*

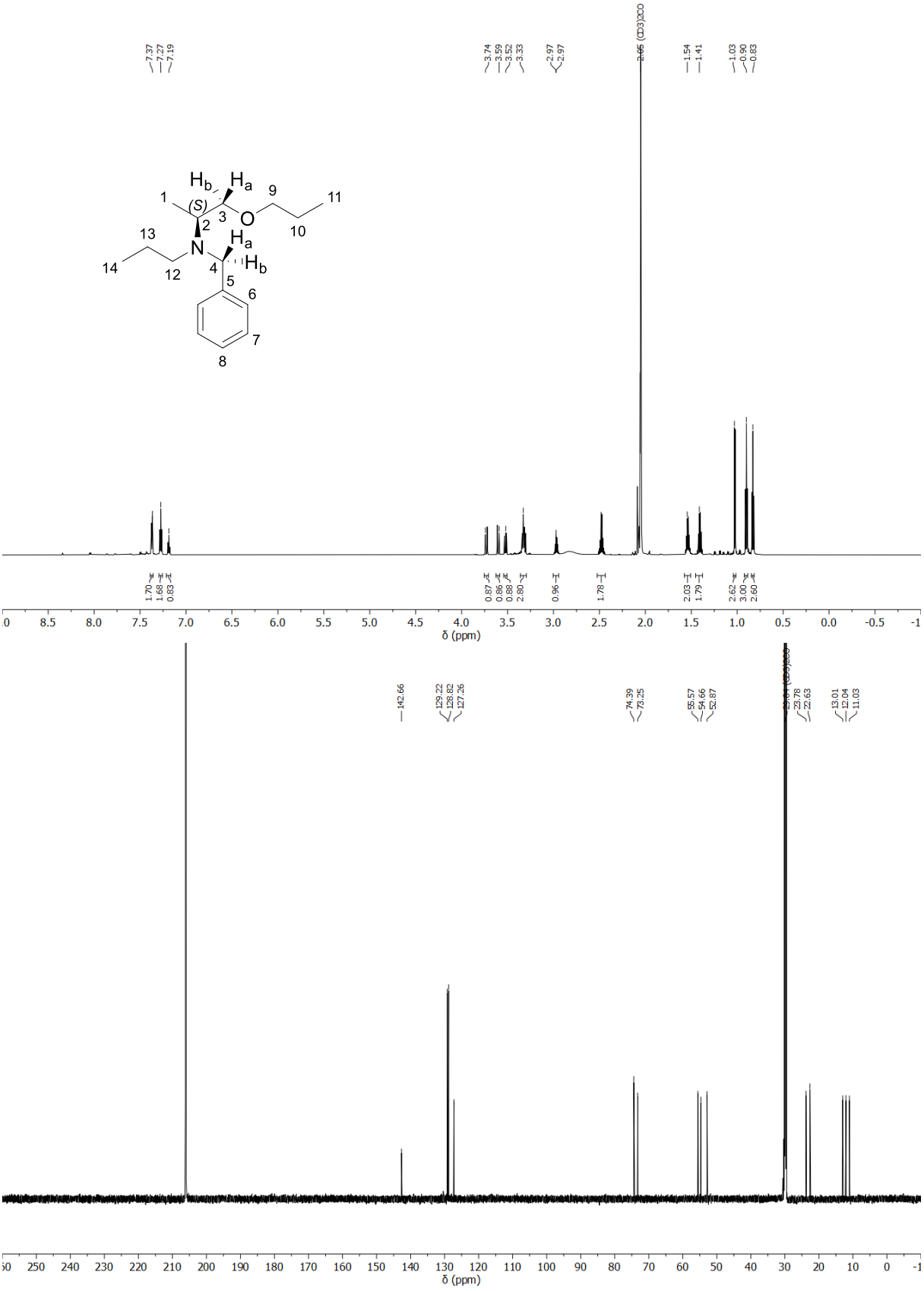

***Figure A20**: [1]H- (top, 700 MHz) and [13]C-NMR (bottom, 176 MHz) spectra of N-benzyl-N-propyl-L-alaninyl propyl ether (**39b**); acetone-d_6, 298 K.*

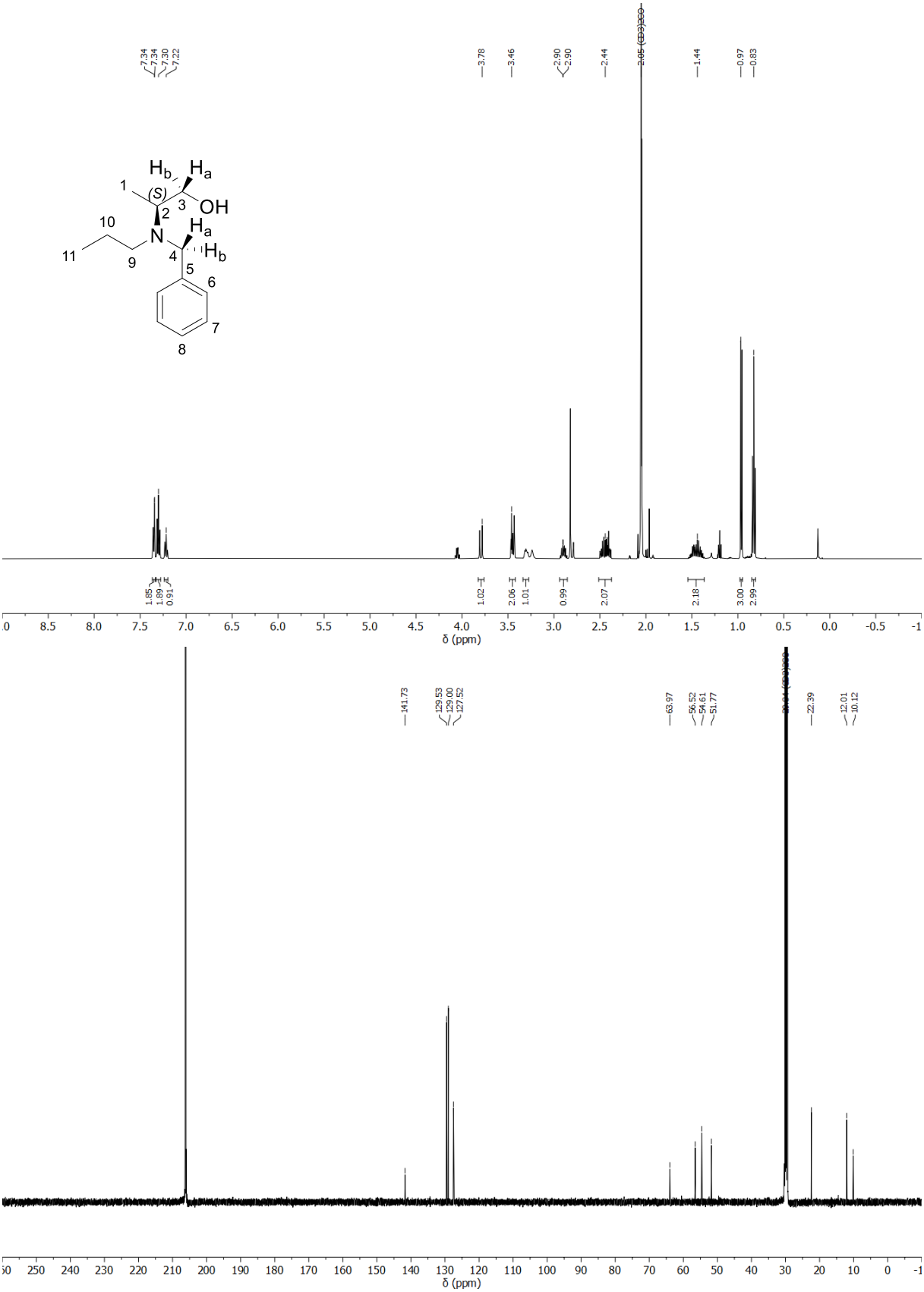

***Figure A21**: ^{1}H- (top, 500 MHz) and ^{13}C-NMR (bottom, 126 MHz) spectra of N-benzyl-N-propyl-L-alaninol (**48b**); acetone-d_6, 298 K.*

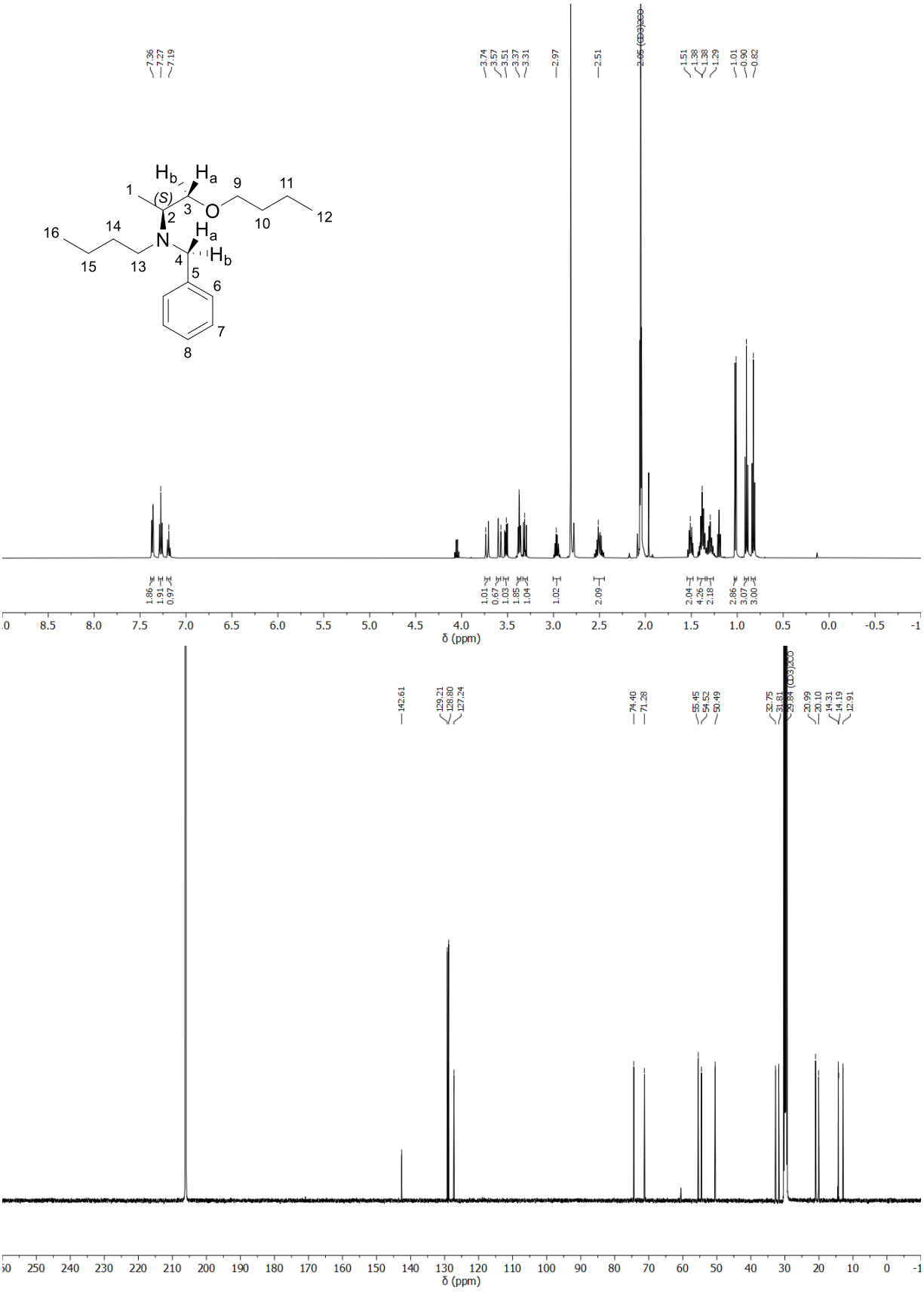

***Figure A22**: [1]H- (top, 500 MHz) and [13]C-NMR (bottom, 126 MHz) spectra of N-benzyl-N-butyl-L-alaninyl butyl ether (**39c**); acetone-d_6, 298 K.*

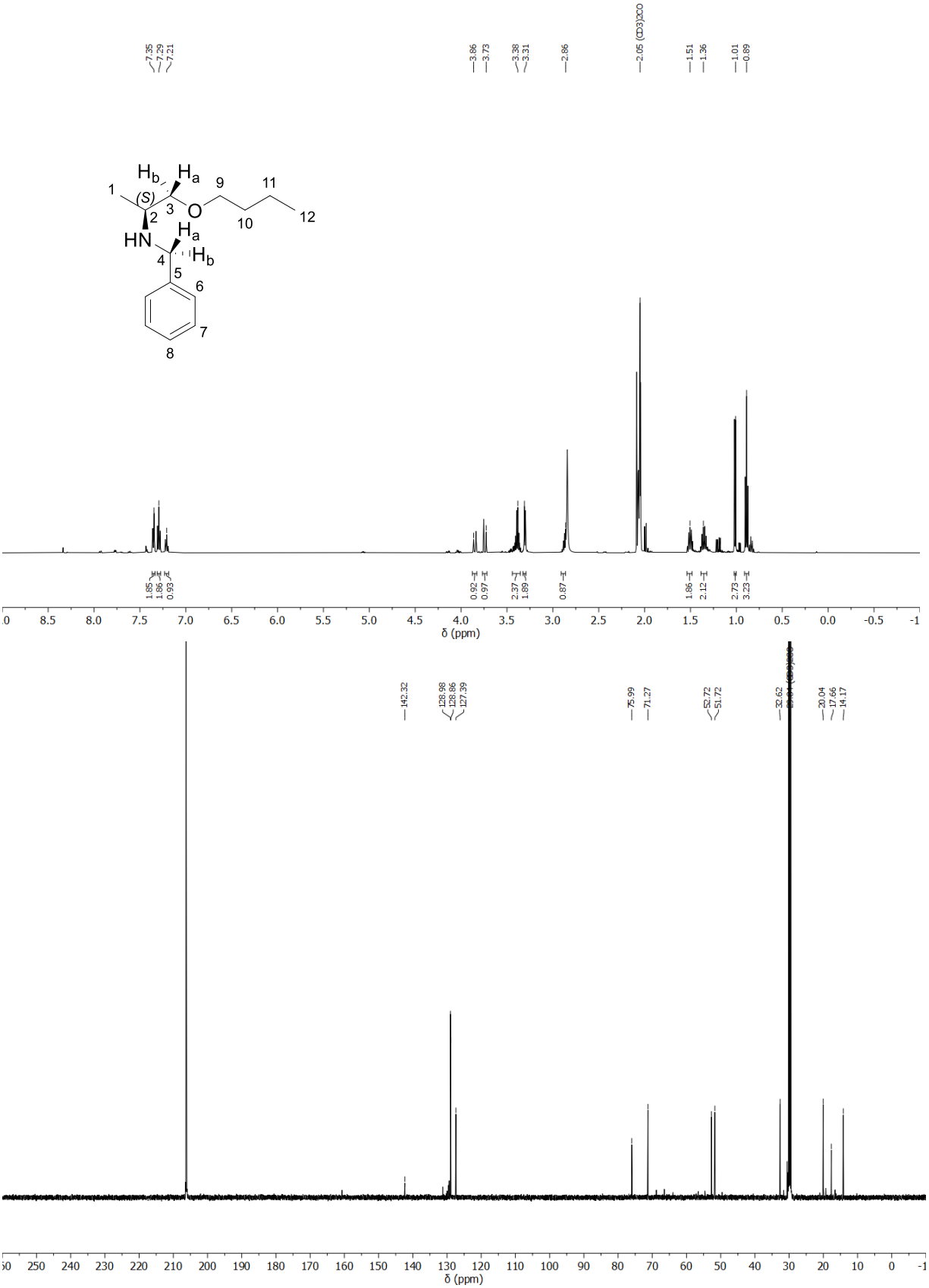

Figure A23: *^{1}H- (top, 500 MHz) and ^{13}C-NMR (bottom, 126 MHz) spectra of N-benzyl-L-alaninyl butyl ether (**47c**); acetone-d_6, 298 K.*

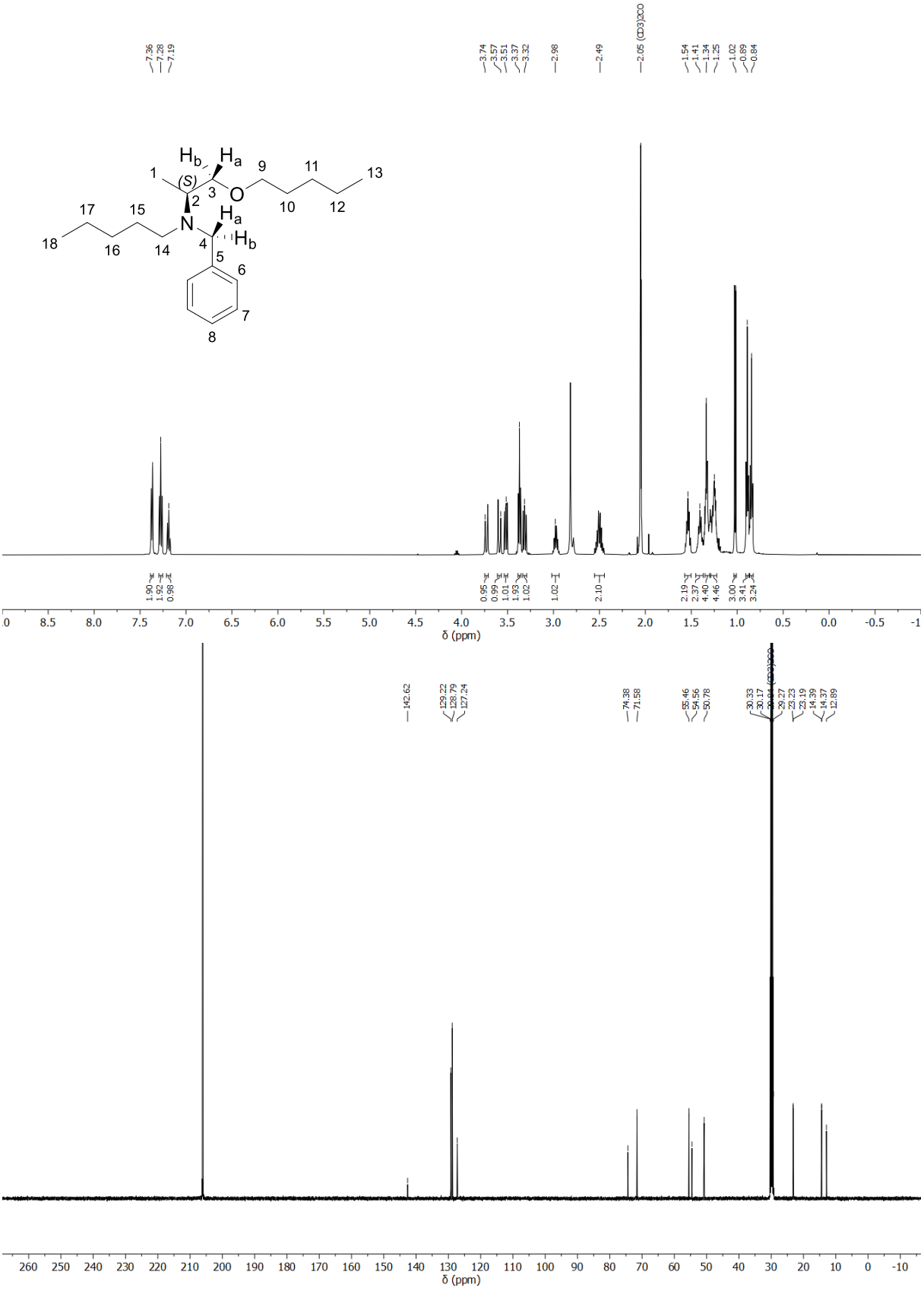

Figure A24: *^{1}H- (top, 500 MHz) and ^{13}C-NMR (bottom, 126 MHz) spectra of N-benzyl-N-pentyl-L-alaninyl pentyl ether (**39d**); acetone-d_6, 298 K.*

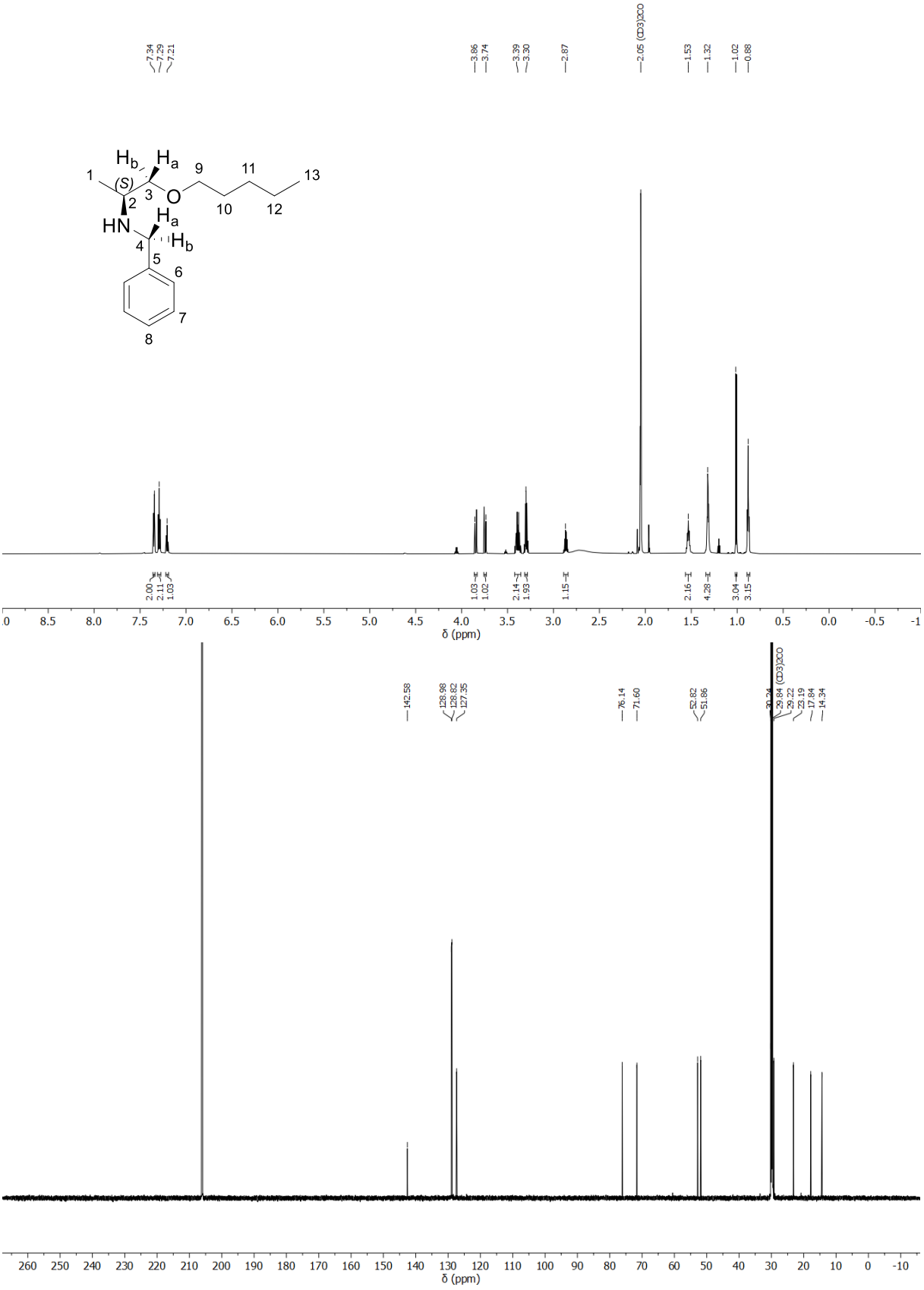

***Figure A25**: [1]H- (top, 700 MHz) and [13]C-NMR (bottom, 176 MHz) spectra of N-benzyl-L-alaninyl pentyl ether (**47d**); acetone-d_6, 298 K.*

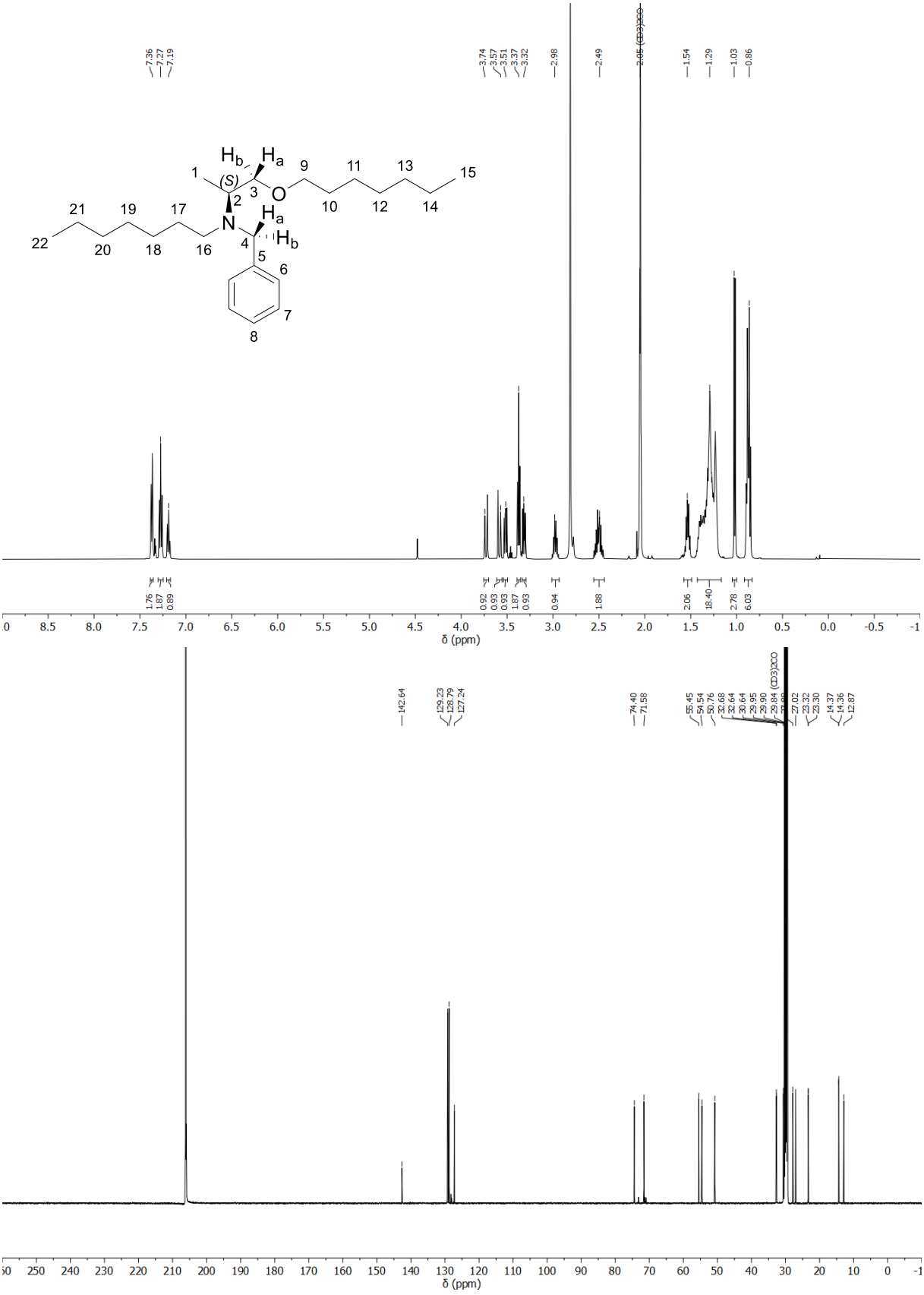

***Figure A26**: [1]H- (top, 500 MHz) and [13]C-NMR (bottom, 126 MHz) spectra of N-benzyl-N-heptyl-L-alaninyl heptyl ether (**39e**); acetone-d_6, 298 K.*

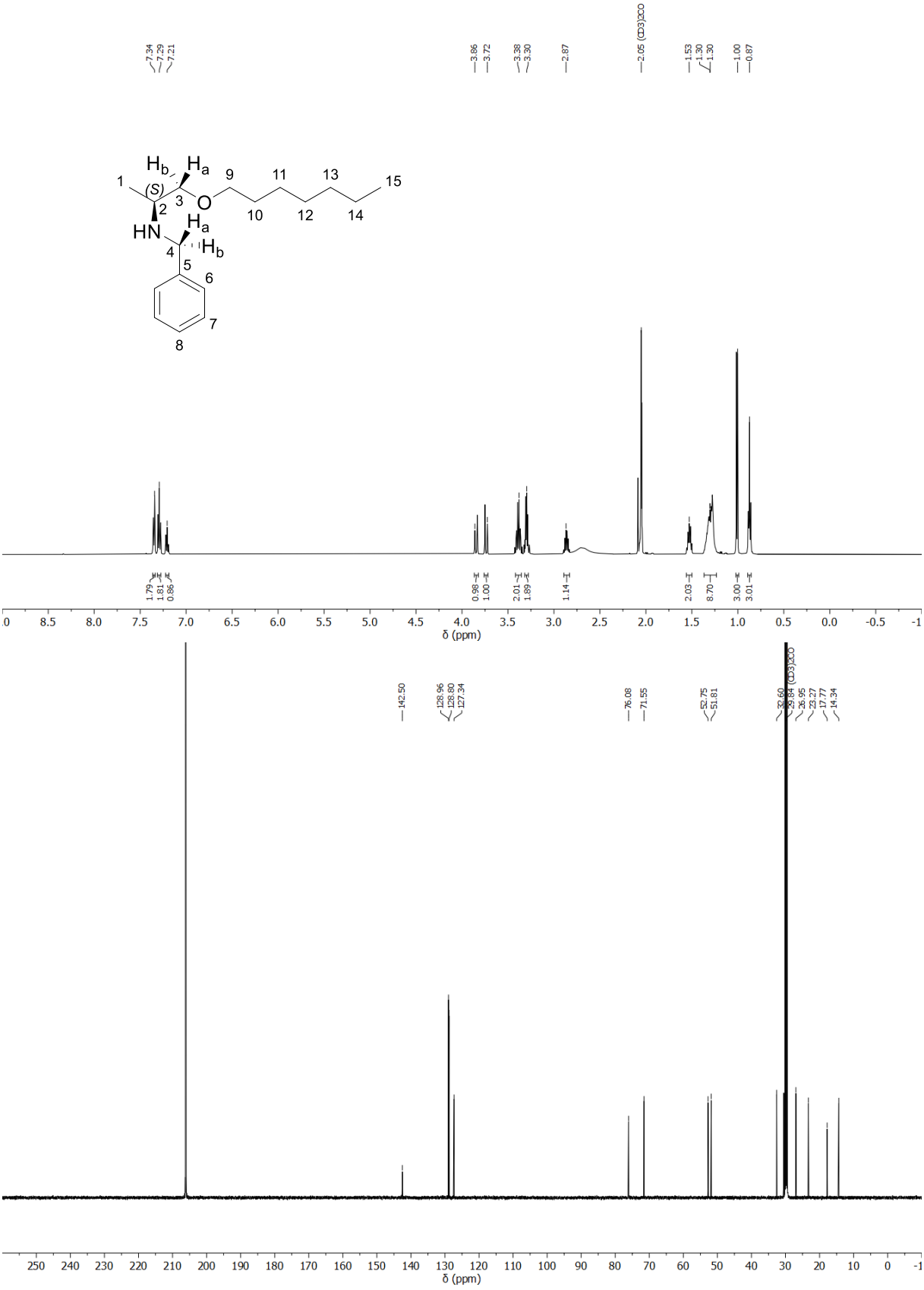

***Figure A27**: [1]H- (top, 500 MHz) and [13]C-NMR (bottom, 126 MHz) spectra of N-benzyl-L-alaninyl heptyl ether (**47e**); acetone-d_6, 298 K.*

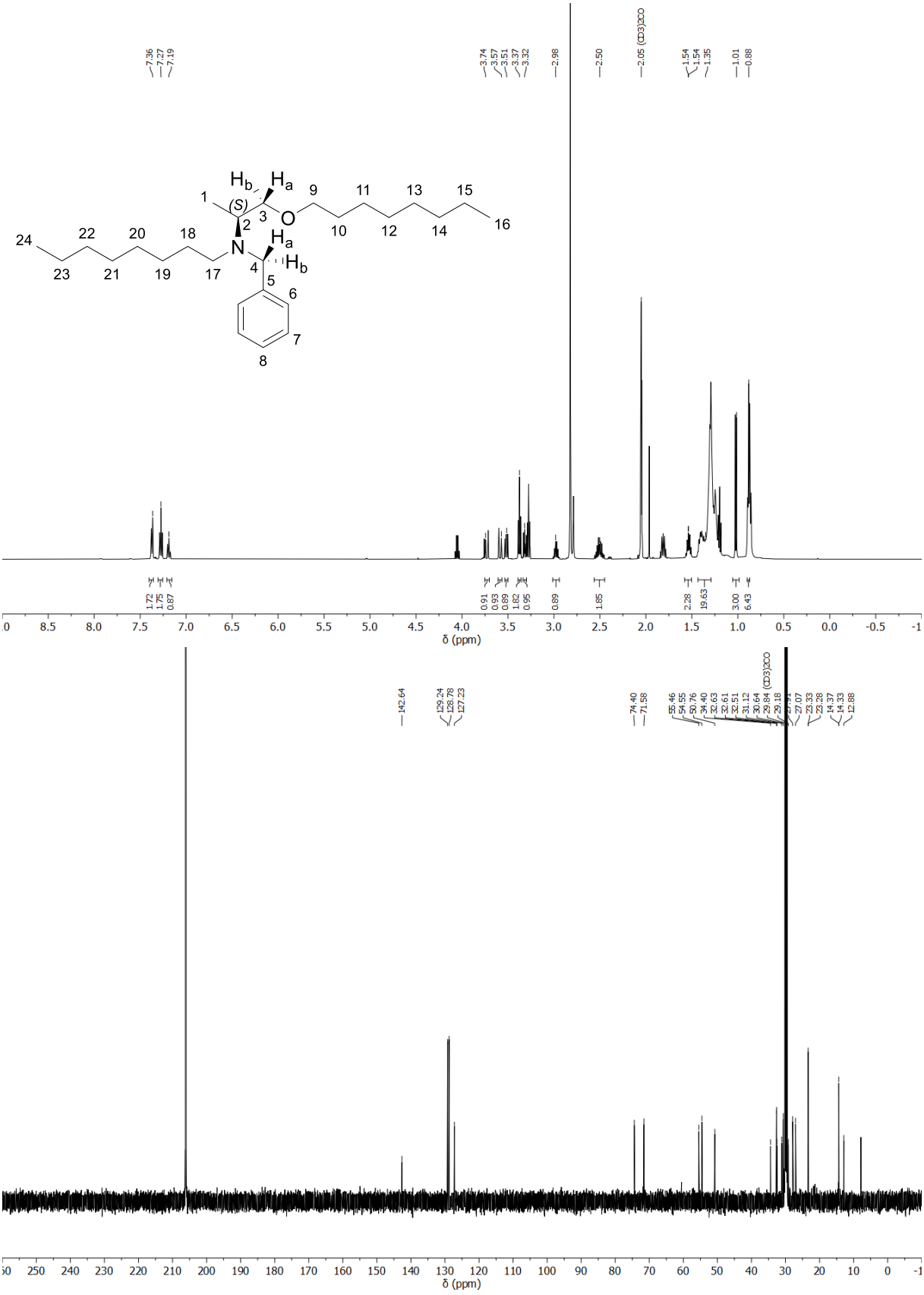

***Figure A28**: [1]H- (top, 500 MHz) and [13]C-NMR (bottom, 126 MHz) spectra of N-benzyl-N-octyl-L-alaninyl octyl ether (**39f**); acetone-d_6, 298 K.*

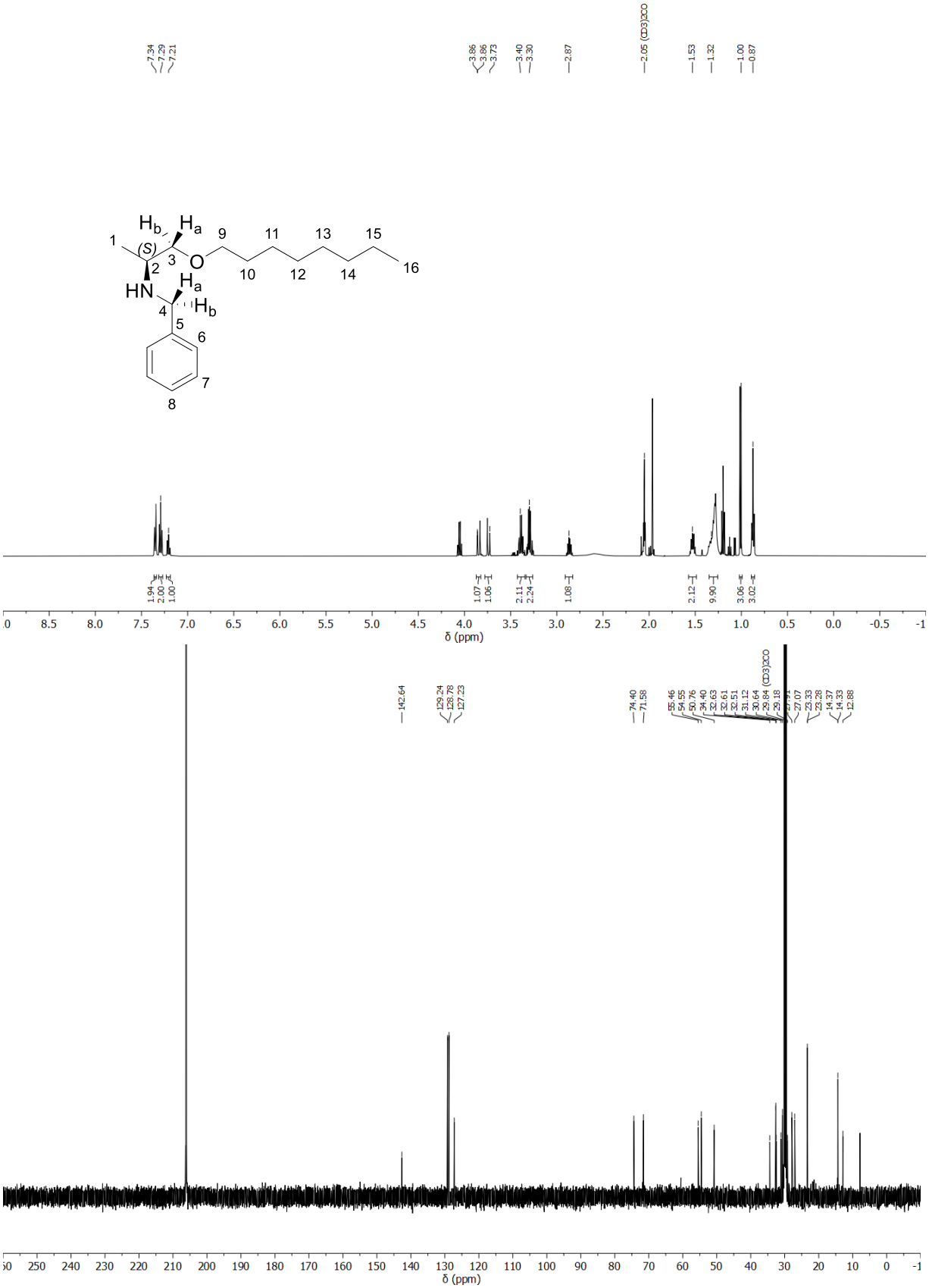

***Figure A 29**: [1]H- (top, 500 MHz) and [13]C-NMR (bottom, 126 MHz) spectra of N-benzyl-L-alaninyl octyl ether (**47f**); acetone-d_6, 298 K.*

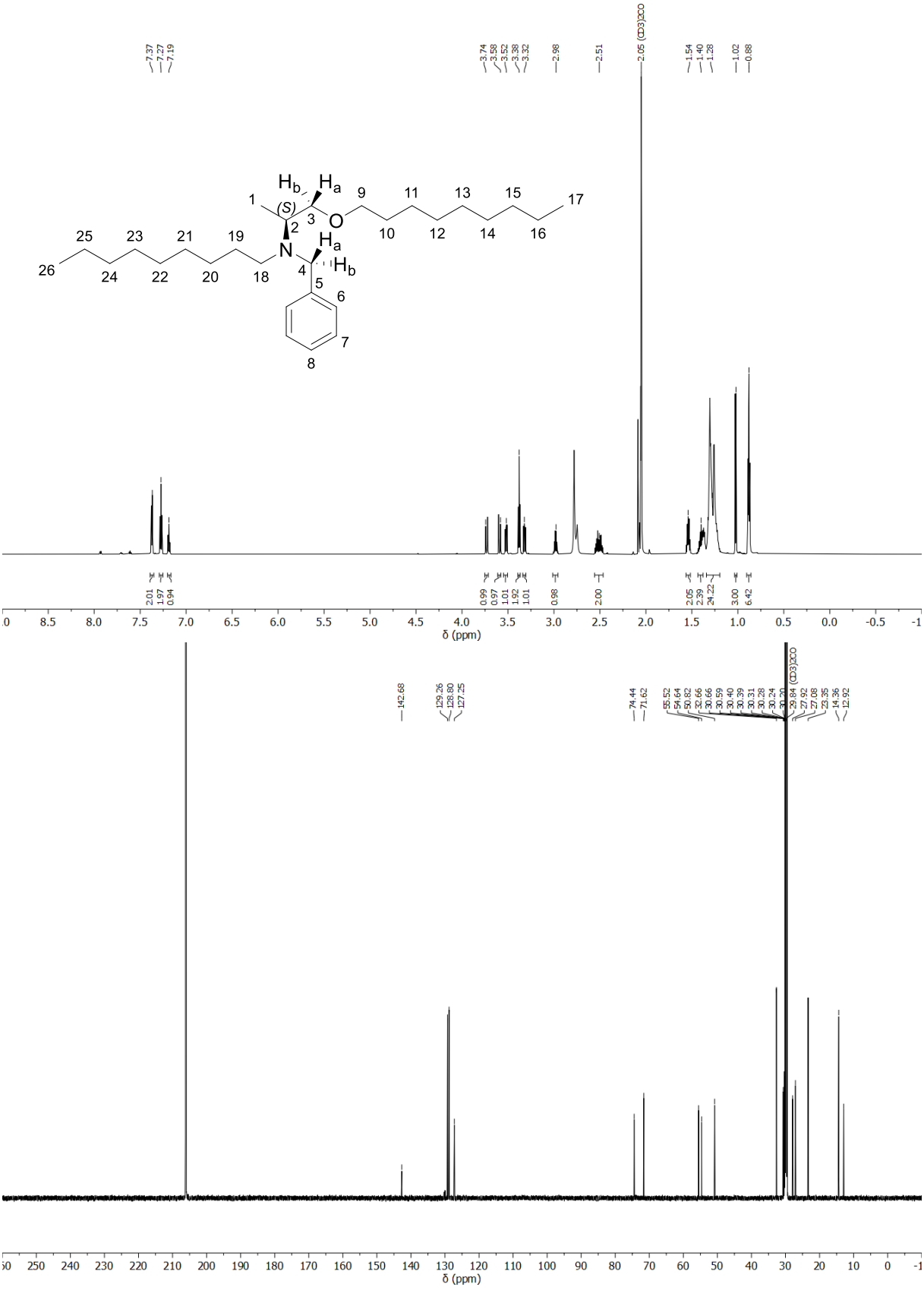

***Figure A30**: [1]H- (top, 700 MHz) and [13]C-NMR (bottom, 176 MHz) spectra of N-benzyl-N-nonyl-L-alaninyl nonyl ether (**39g**); acetone-d_6, 298 K.*

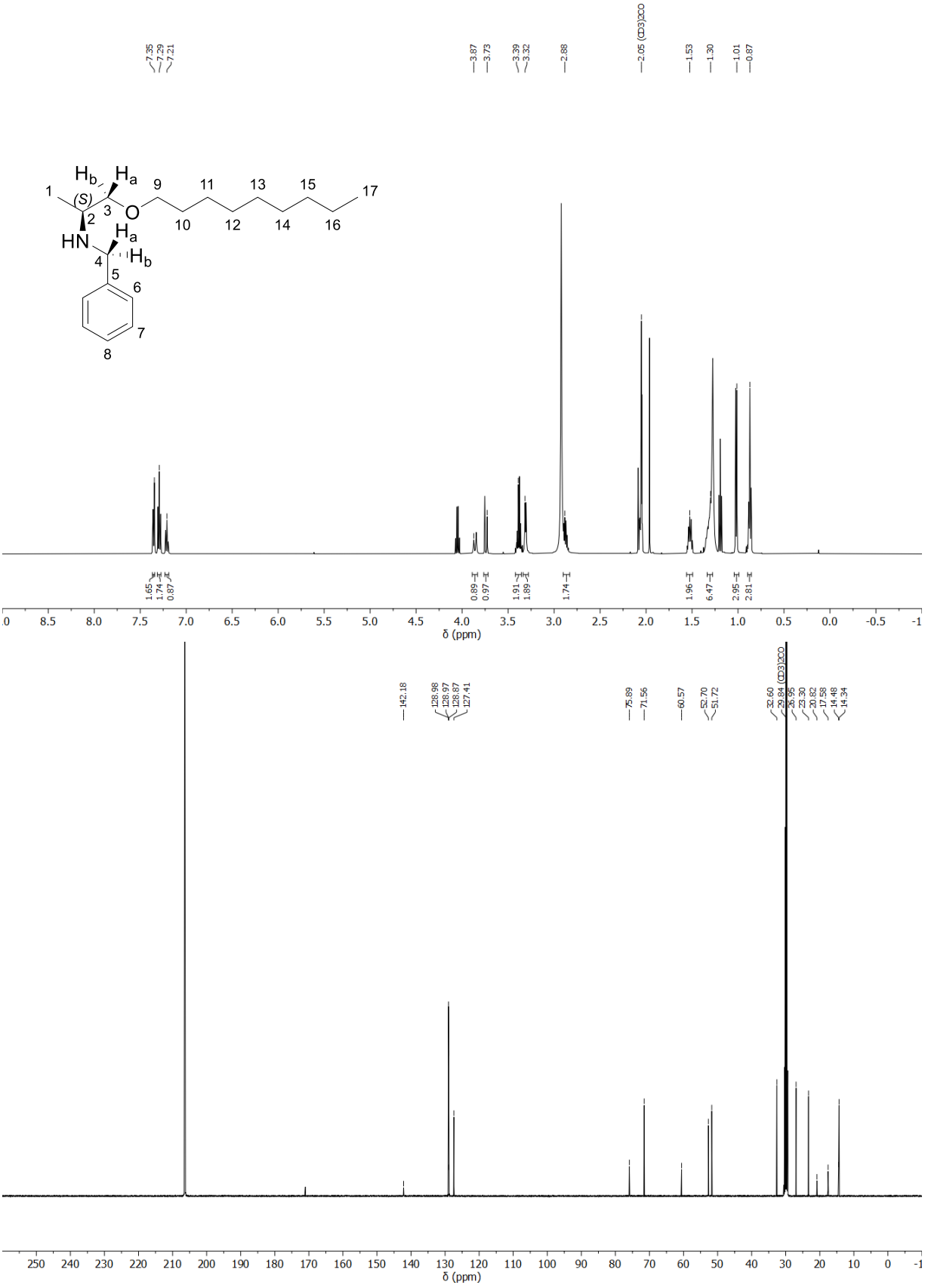

***Figure A31**: ^{1}H- (top, 500 MHz) and ^{13}C-NMR (bottom, 126 MHz) spectra of N-benzyl-L-alaninyl nonyl ether (**47g**); acetone-d_6, 298 K.*

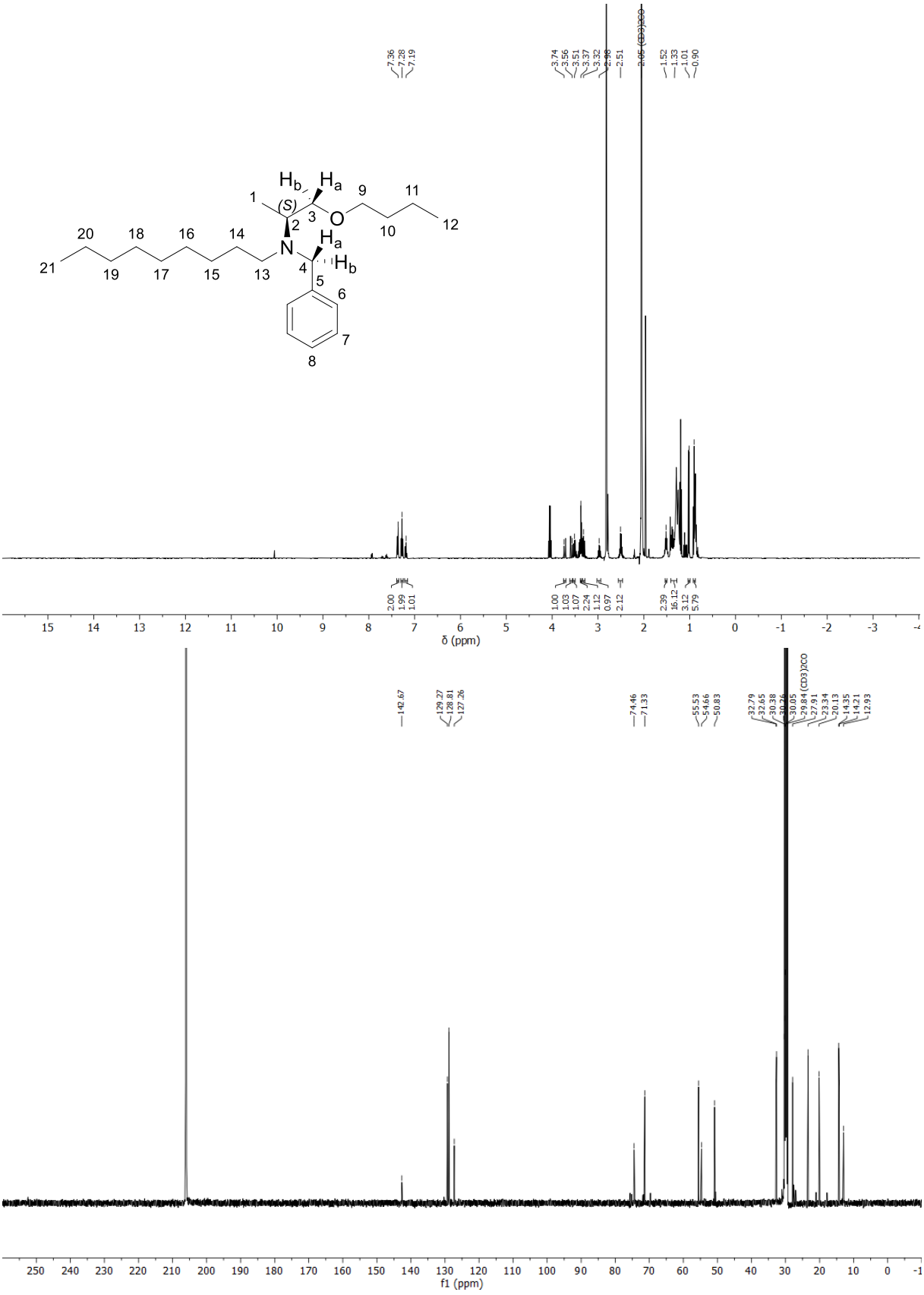

***Figure A32**: ^{1}H- (top, 500 MHz) and ^{13}C-NMR (bottom, 126 MHz) spectra of N-benzyl-N-nonyl-L-alaninyl butyl ether (**39h**); acetone-d_6, 298 K.*

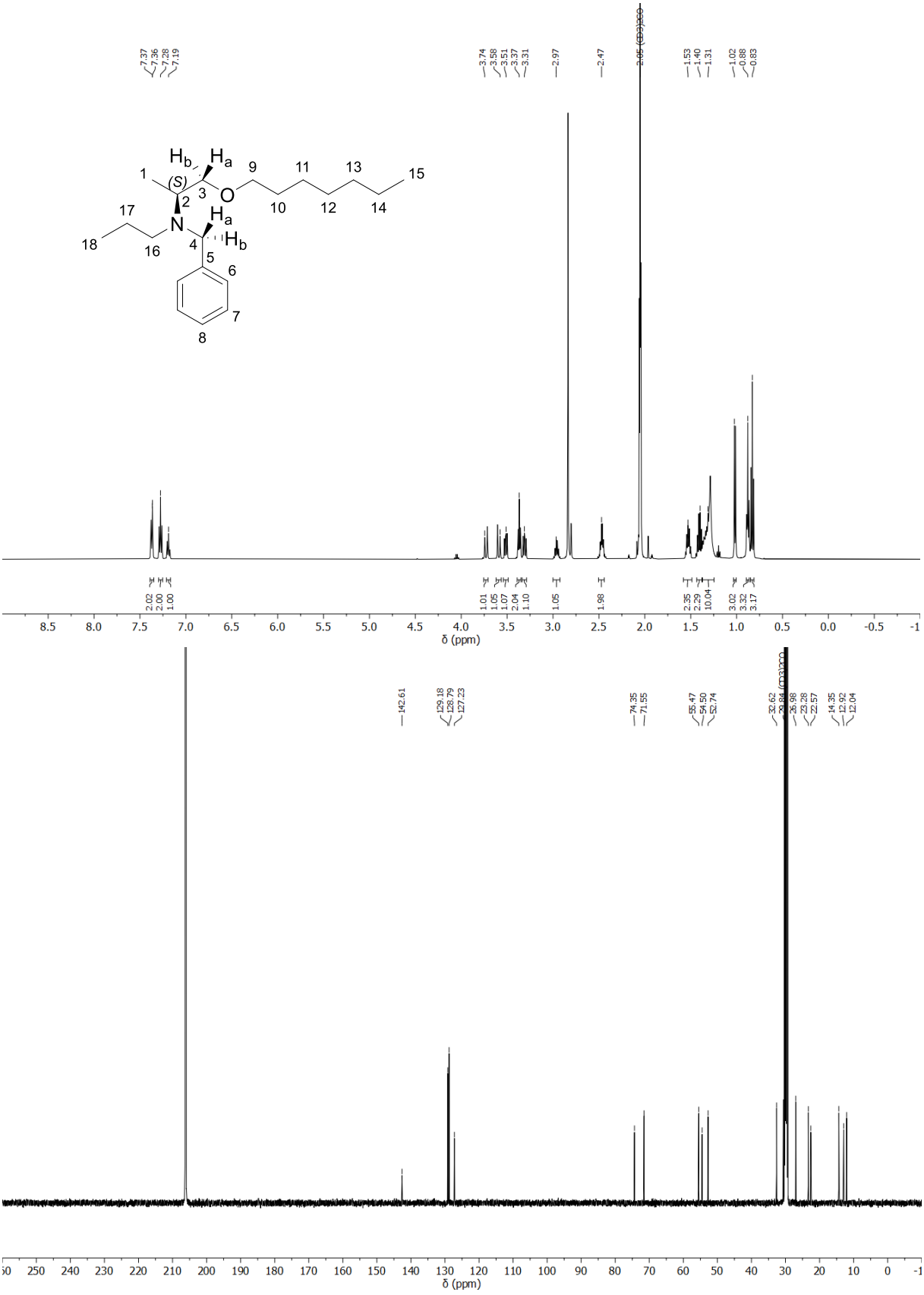

***Figure A33**: ^{1}H- (top, 500 MHz) and ^{13}C-NMR (bottom, 126 MHz) spectra of N-benzyl-N-propyl-L-alaninyl heptyl ether (**39i**); acetone-d_6, 298 K.*

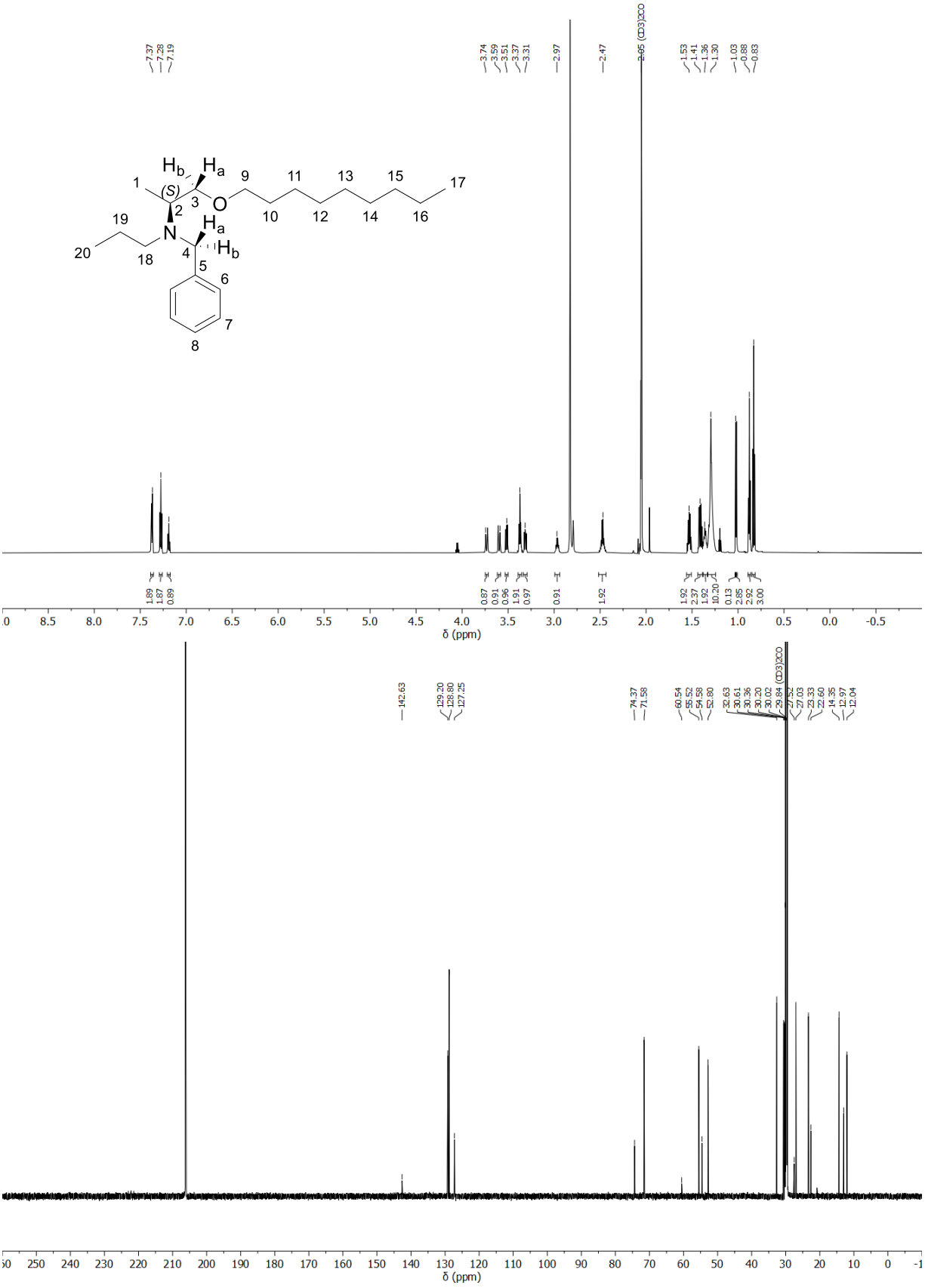

***Figure A 34**: [1]H- (top, 700 MHz) and [13]C-NMR (bottom, 176 MHz) spectra of N-benzyl-N-propyl-L-alaninyl nonyl ether (**39j**); acetone-d_6, 298 K.*

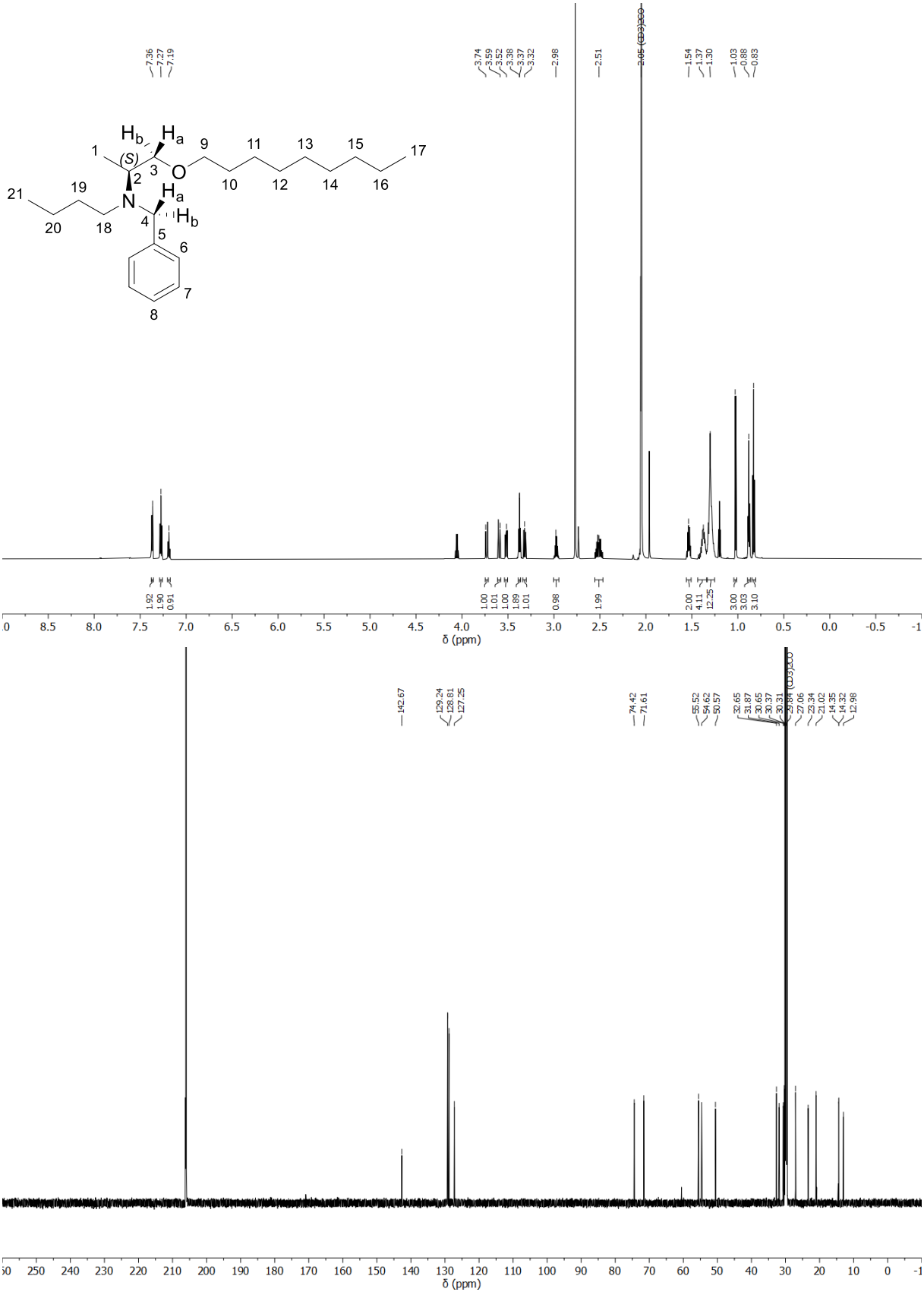

***Figure A35**: ^{1}H- (top, 700 MHz) and ^{13}C-NMR (bottom, 176 MHz) spectra of N-benzyl-N-butyl-L-alaninyl nonyl ether (**39k**); acetone-d_6, 298 K.*

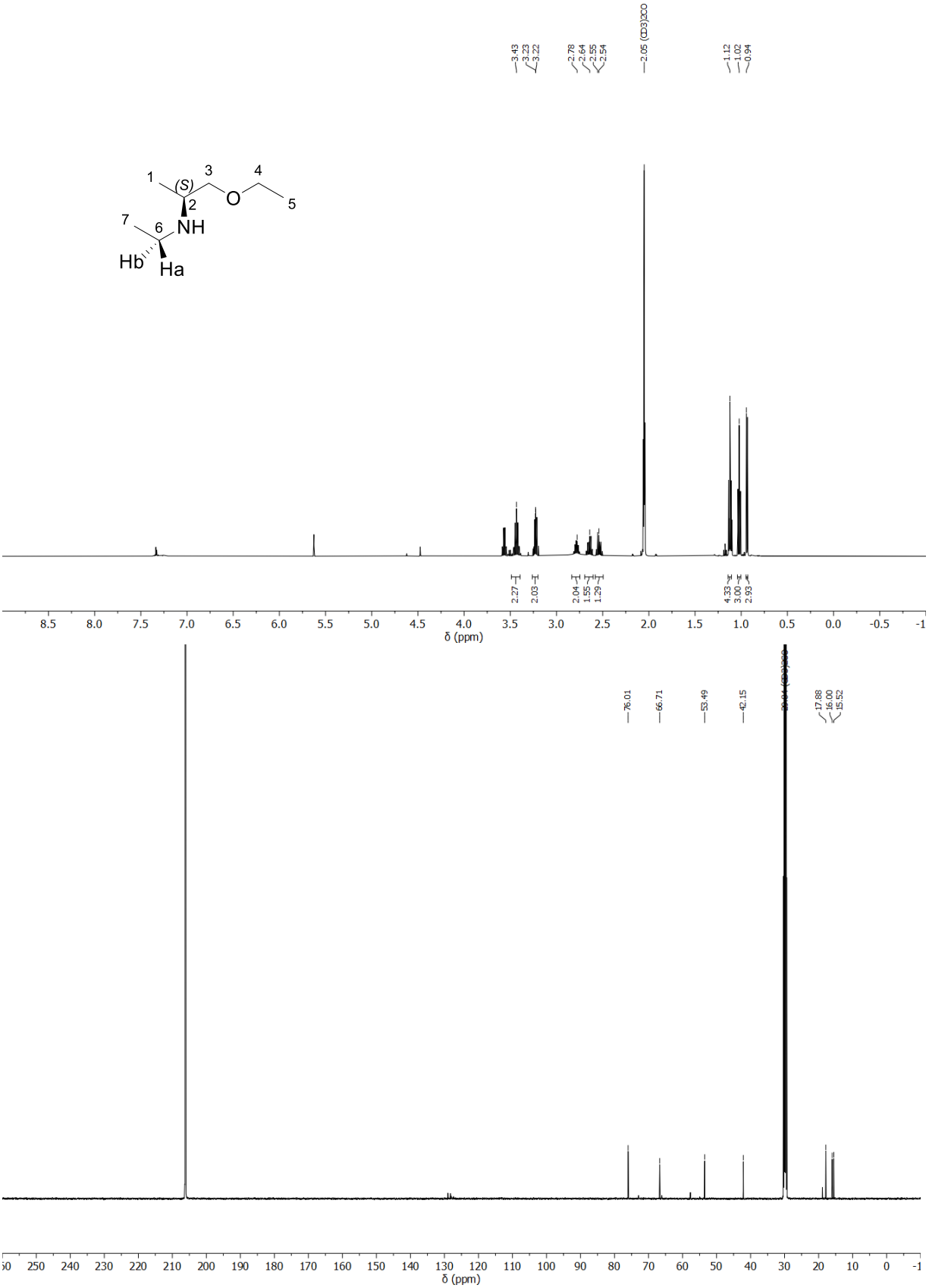

***Figure A36**: [1]H- (top, 500 MHz) and [13]C-NMR (bottom, 126 MHz) spectra of O-ethyl-L-alaninyl N-ethyl amine (**22a**); acetone-d_6, 298 K.*

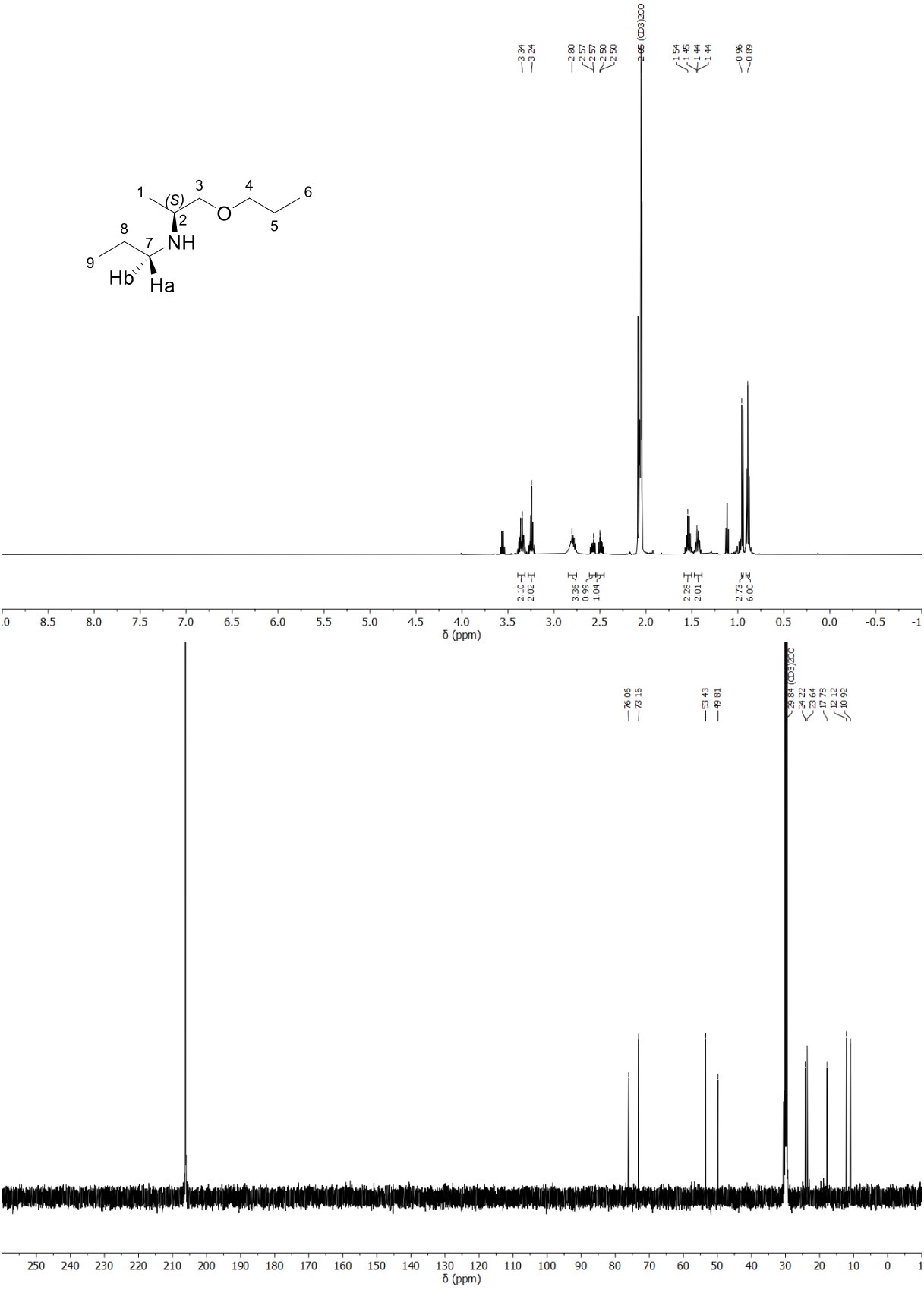

***Figure A37**: ^{1}H- (top, 500 MHz) and ^{13}C-NMR (bottom, 126 MHz) spectra of O-propyl-L-alaninyl N-propyl amine (**22b**); acetone-d_6, 298 K.*

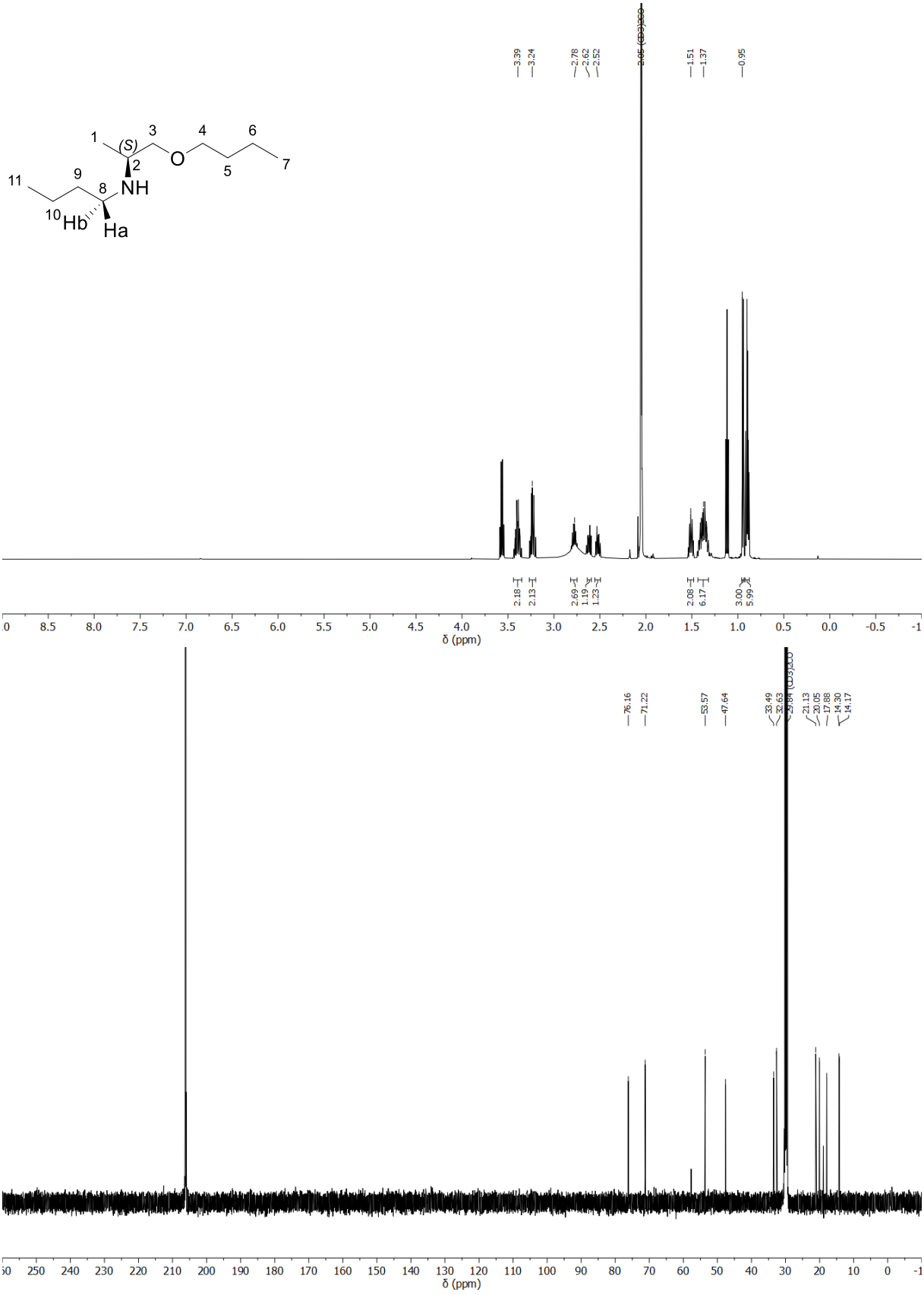

***Figure A38**: ^{1}H- (top, 500 MHz) and ^{13}C-NMR (bottom, 126 MHz) spectra of O-butyl-L-alaninyl N-butyl amine (**22c**); acetone-d_6, 298 K.*

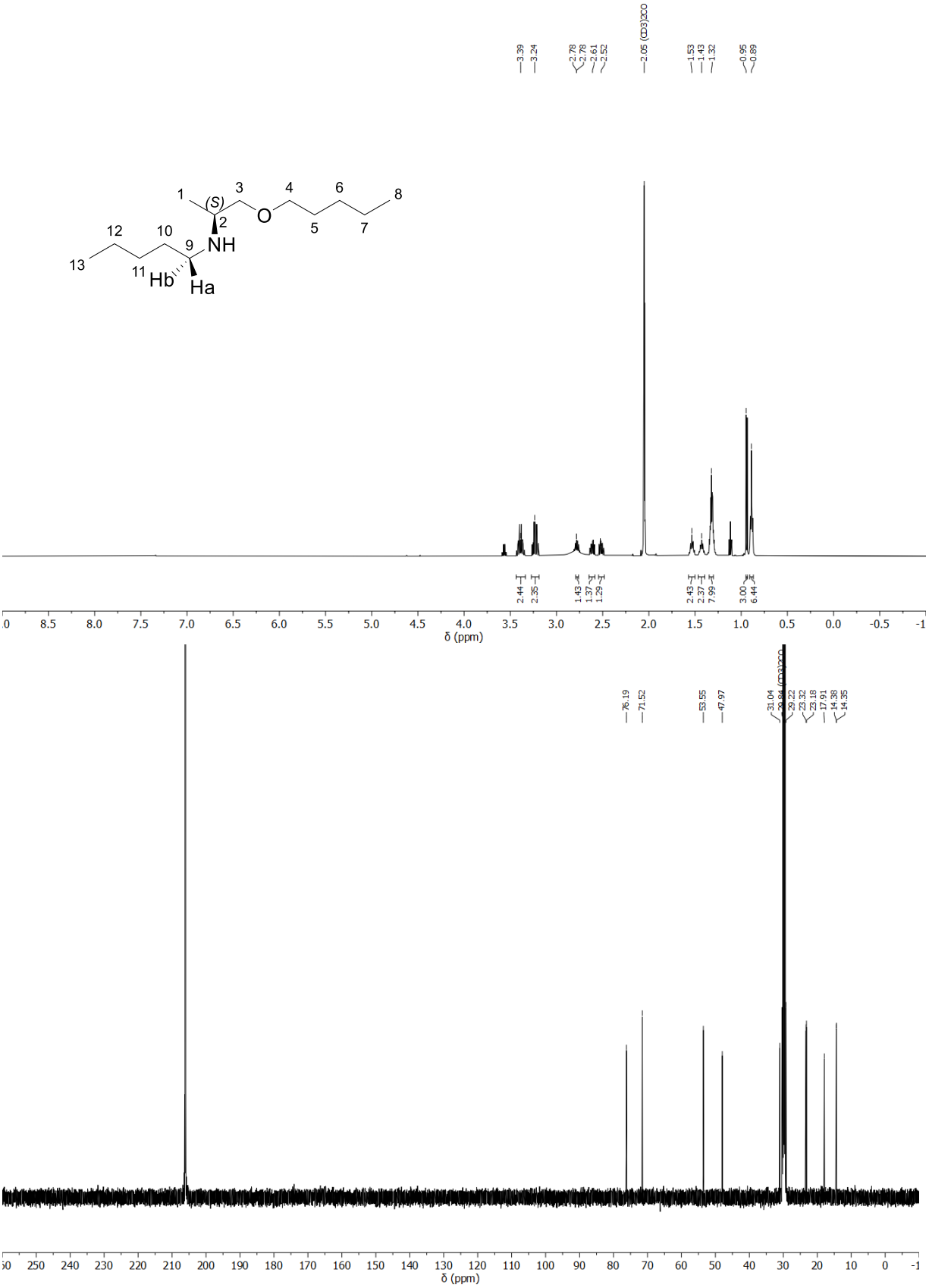

***Figure A 39**: ^{1}H- (top, 500 MHz) and ^{13}C-NMR (bottom, 126 MHz) spectra of O-pentyl-L-alaninyl N-pentyl amine (**22d**); acetone-d_6, 298 K.*

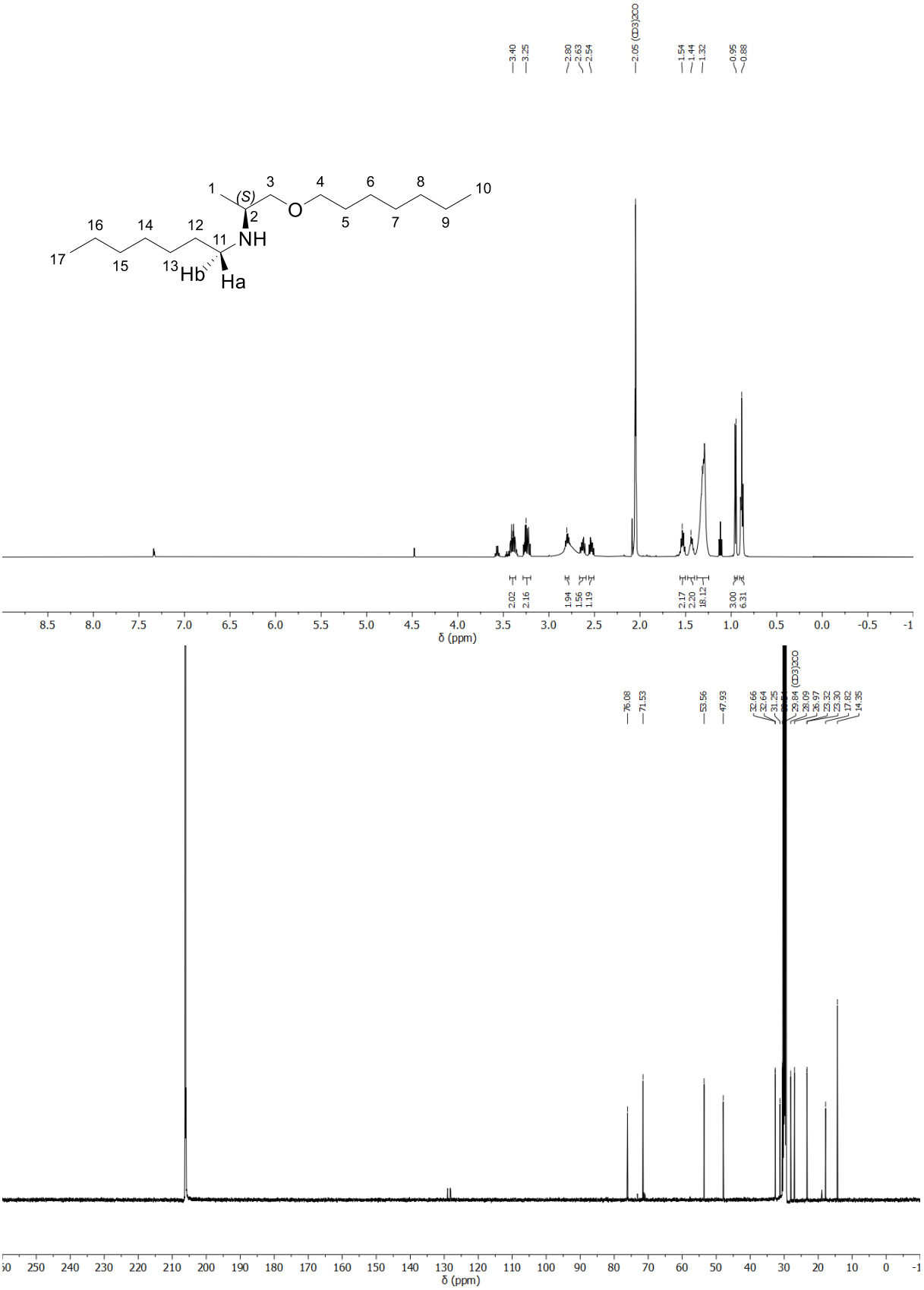

***Figure A40**: ^{1}H- (top, 500 MHz) and ^{13}C-NMR (bottom, 126 MHz) spectra of O-heptyl-L-alaninyl N-heptyl amine (**22e**); acetone-d_6, 298 K.*

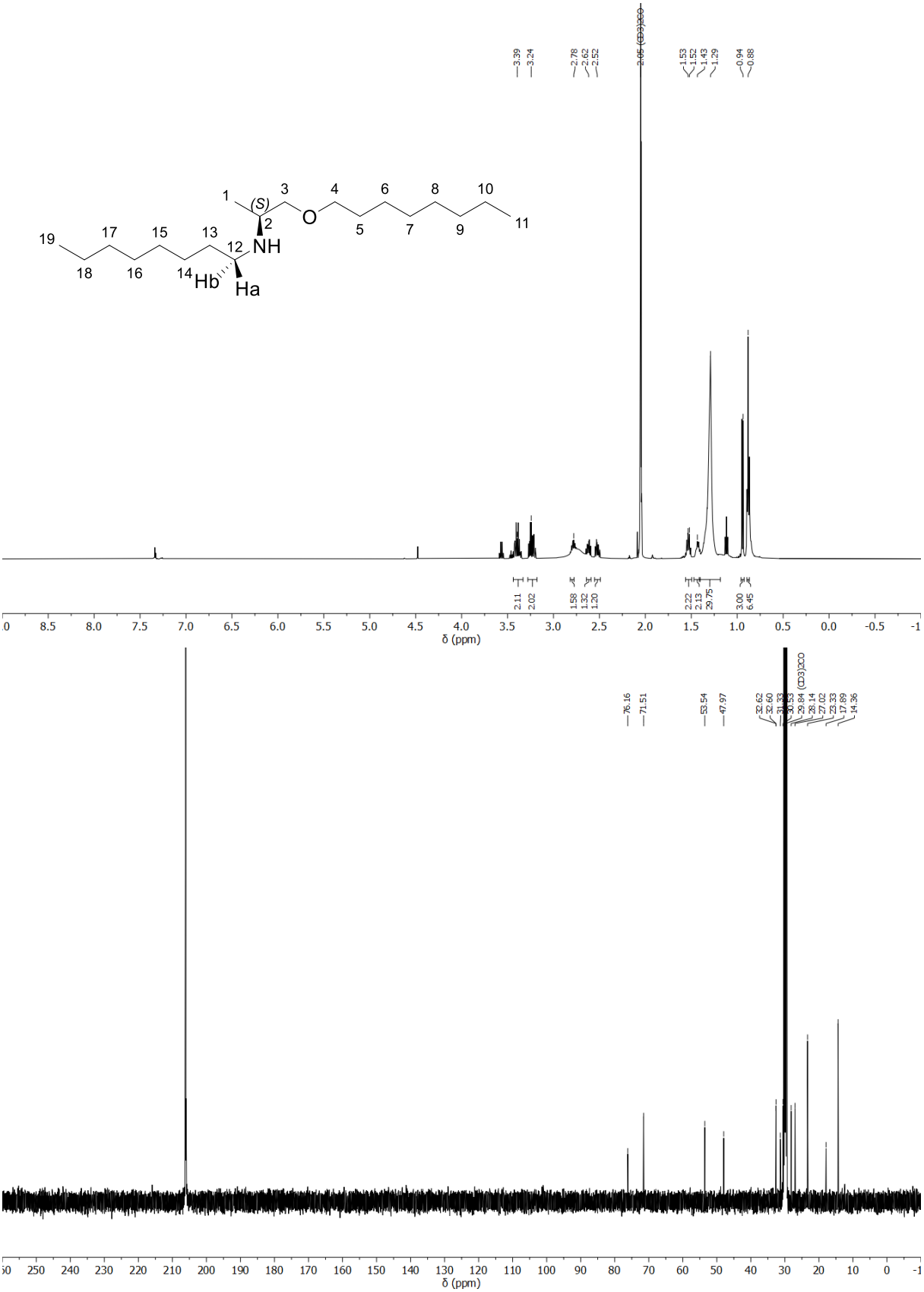

***Figure A41**: ^{1}H- (top, 500 MHz) and ^{13}C-NMR (bottom, 126 MHz) spectra of O-octyl-L-alaninyl N-octyl amine (**22f**); acetone-d_6, 298 K.*

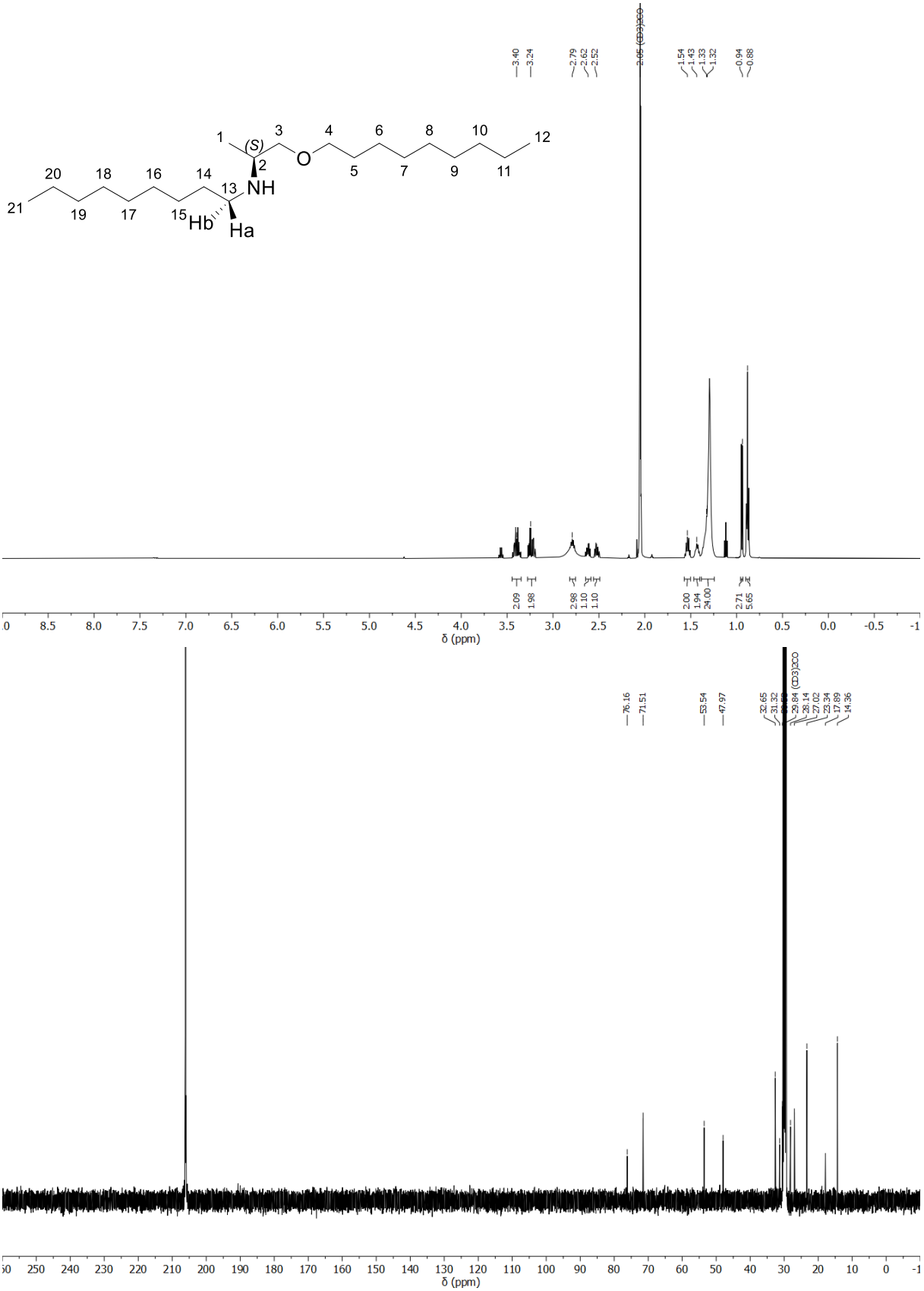

***Figure A42**: [1]H- (top, 500 MHz) and [13]C-NMR (bottom, 126 MHz) spectra of O-nonyl-L-alaninyl N-nonyl amine (**22g**); acetone-d_6, 298 K.*

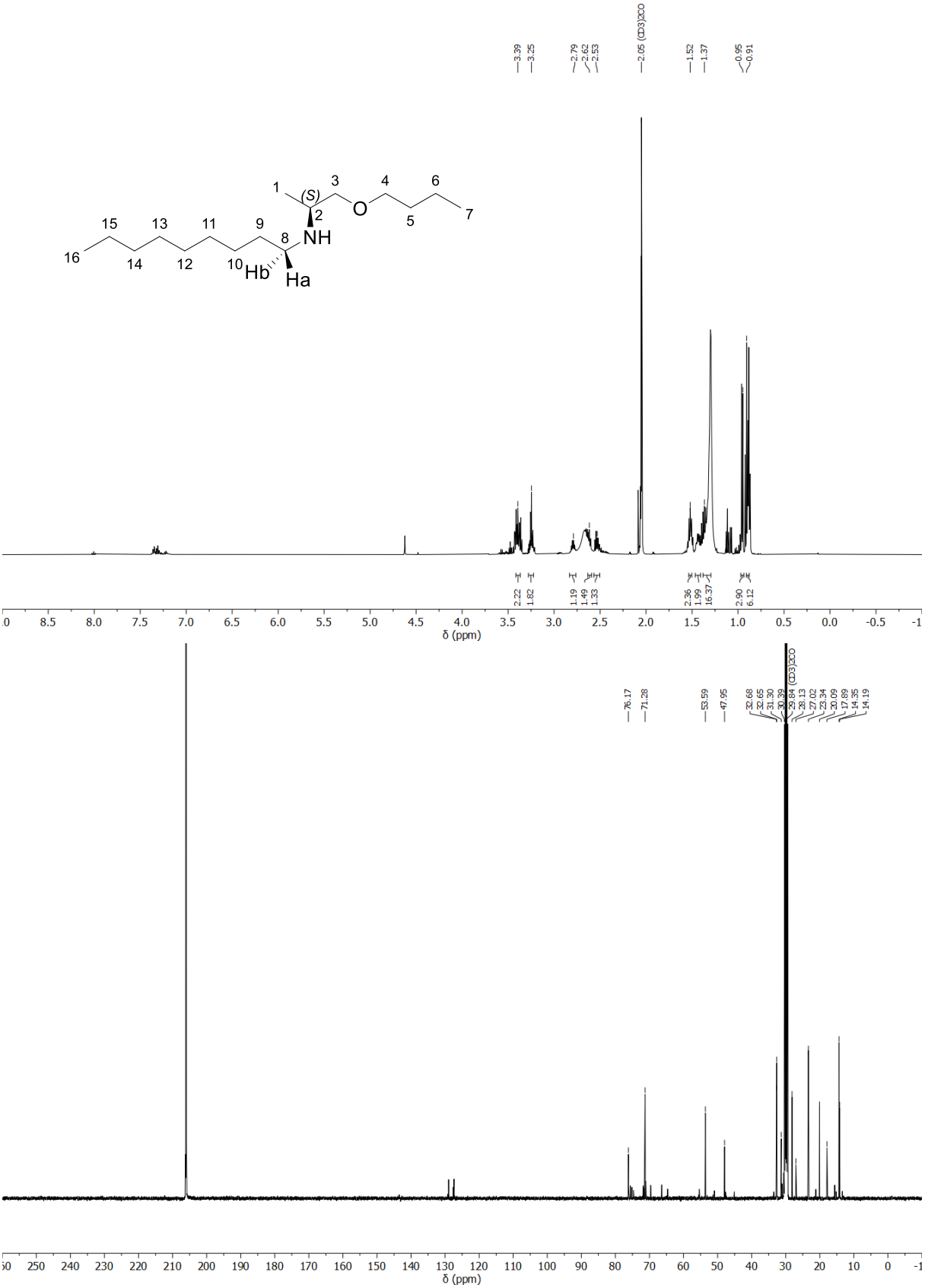

***Figure A43**: [1]H- (top, 500 MHz) and [13]C-NMR (bottom, 126 MHz) spectra of O-butyl-L-alaninyl N-nonyl amine (**22h**); acetone-d_6, 298 K.*

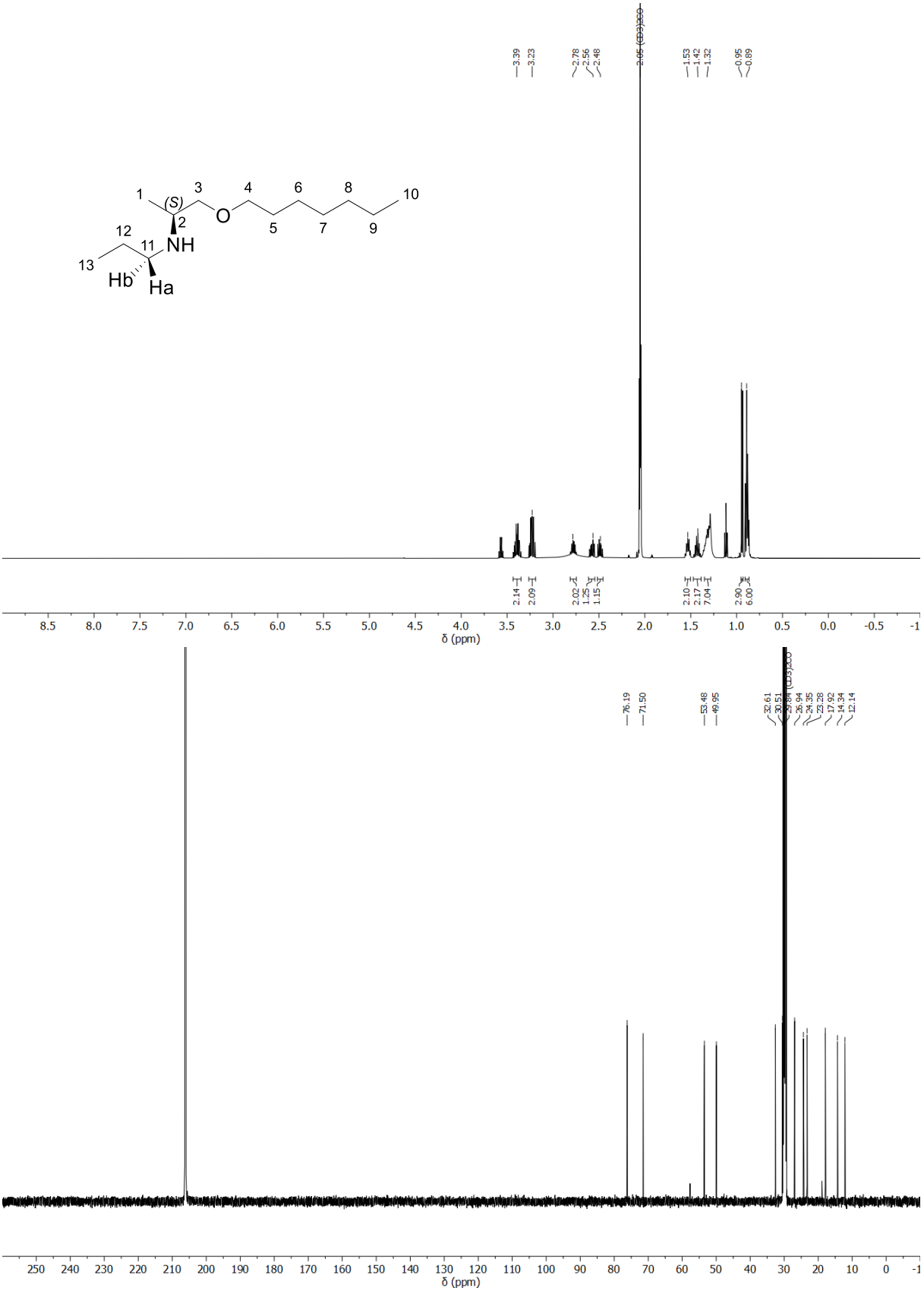

***Figure A44**: [1]H- (top, 500 MHz) and [13]C-NMR (bottom, 126 MHz) spectra of O-heptyl-L-alaninyl N-propyl amine (**22i**); acetone-d_6, 298 K.*

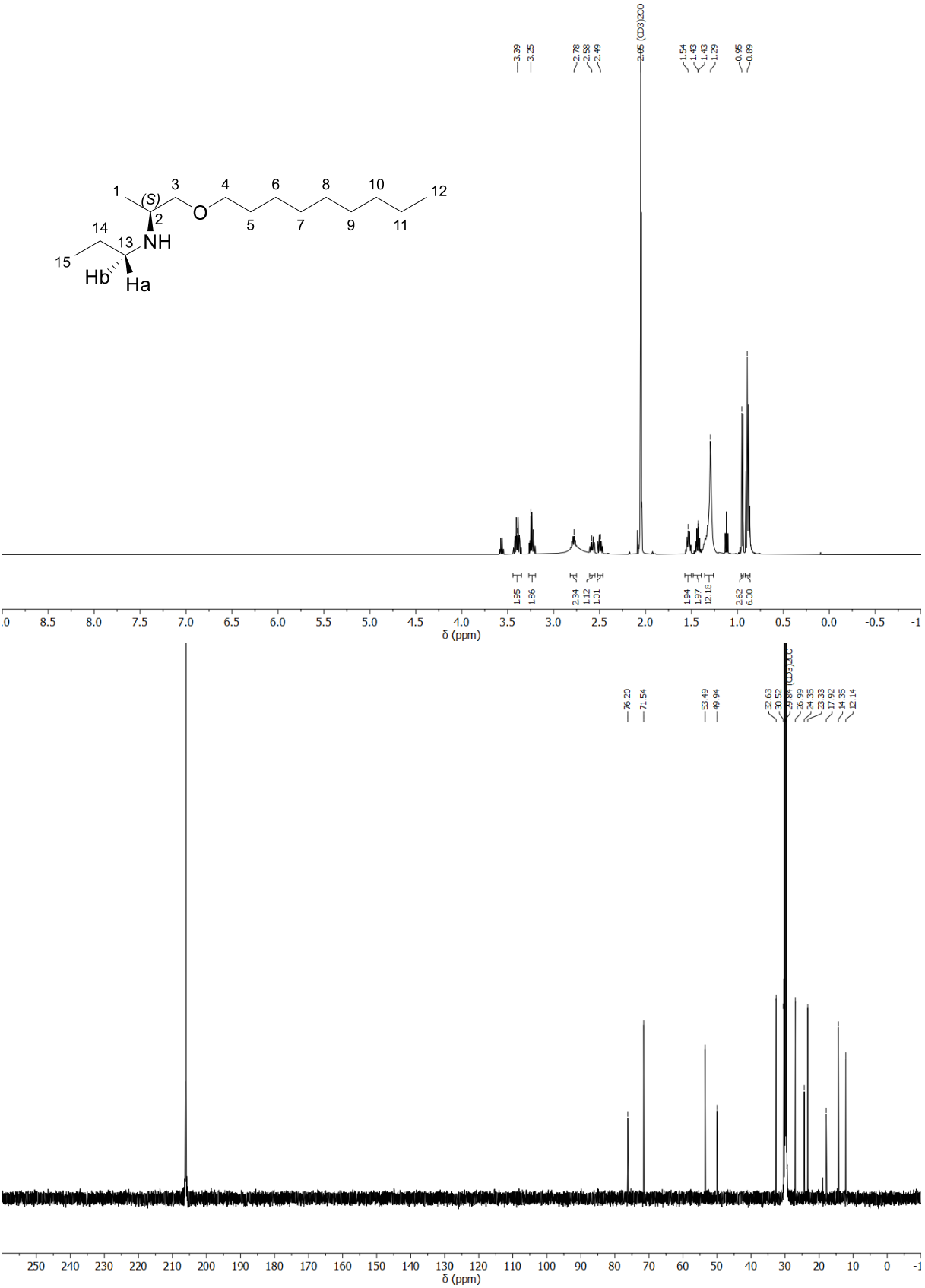

***Figure A45**: [1]H- (top, 500 MHz) and [13]C-NMR (bottom, 126 MHz) spectra of O-nonyl-L-alaninyl N-propyl amine (**22j**); acetone-d_6, 298 K.*

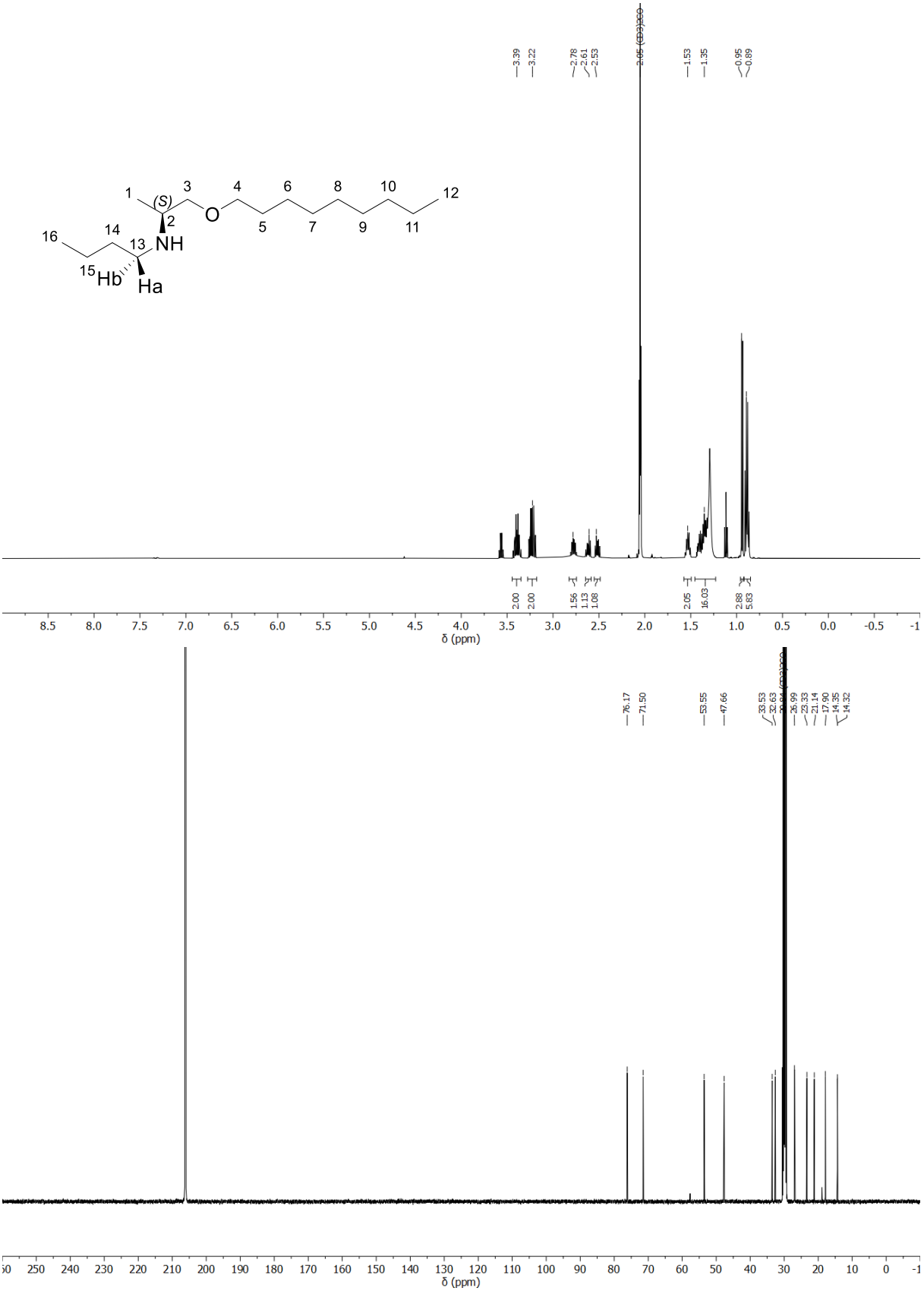

***Figure A46**: [1]H- (top, 500 MHz) and [13]C-NMR (bottom, 126 MHz) spectra of O-nonyl-L-alaninyl N-butyl amine (**22k**); acetone-d_6, 298 K.*

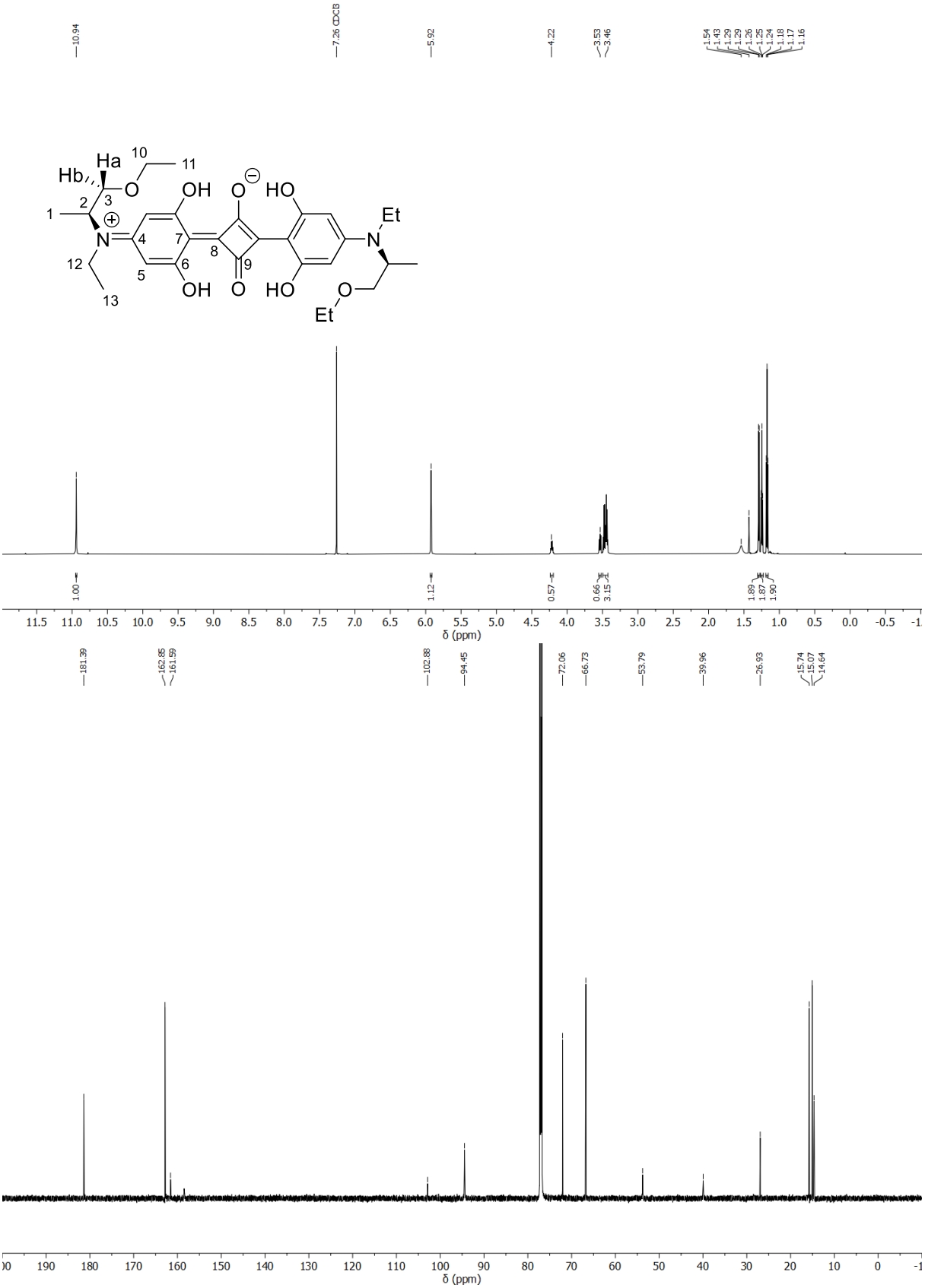

***Figure A47**: ^{1}H- (top, 700 MHz) and ^{13}C-NMR (bottom, 176 MHz) spectra of **(S,S)-N-C2,O-C2-AlaSQ** (**23a**); $CDCl_3$, 298 K.*

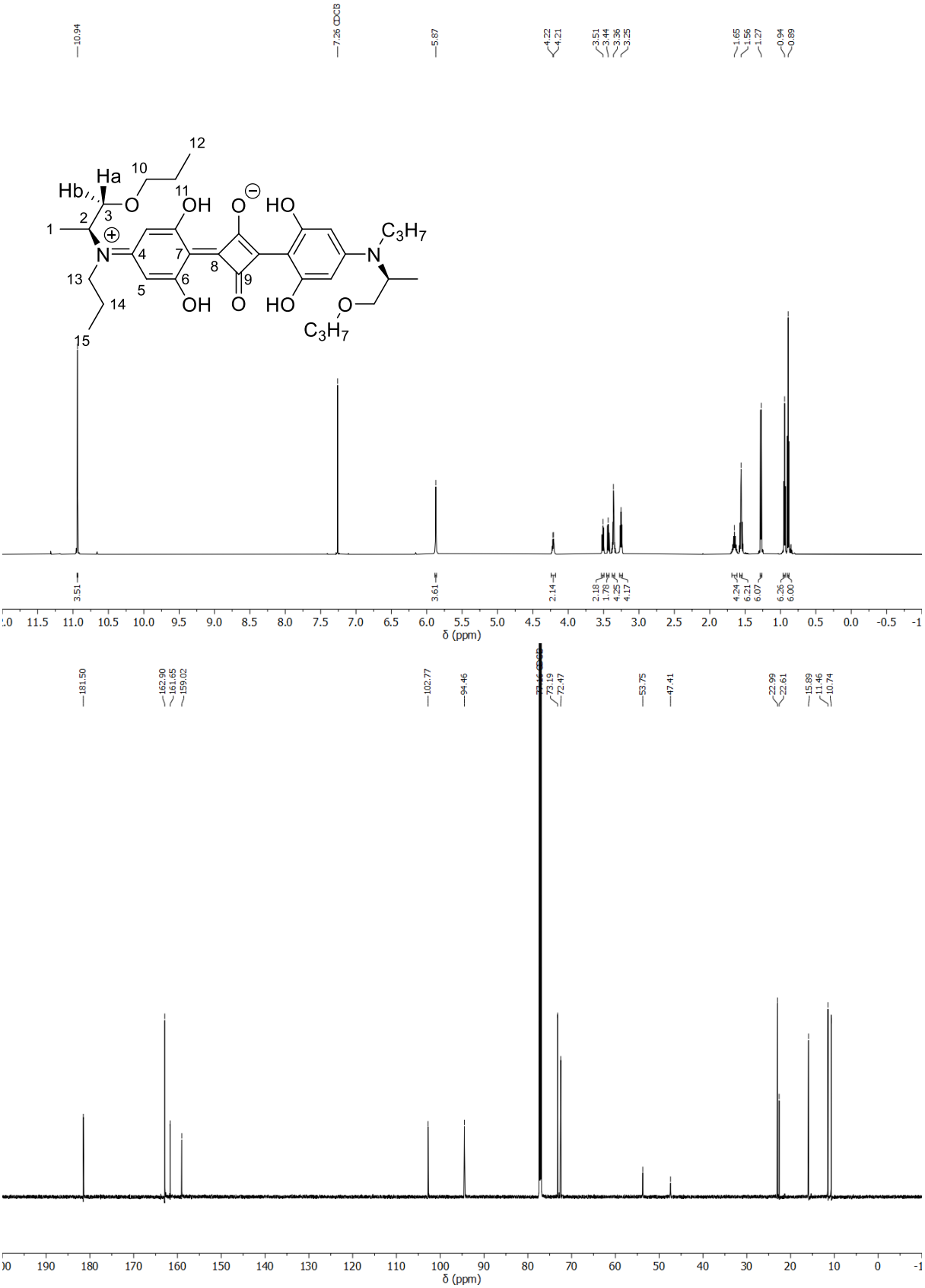

***Figure A48**: [1]H- (top, 700 MHz) and [13]C-NMR (bottom, 176 MHz) spectra of **(S,S)-N-C3,O-C3-AlaSQ** (**23b**); $CDCl_3$, 298 K.*

***Figure A49**: ^{1}H- (top, 500 MHz) and ^{13}C-NMR (bottom, 126 MHz) spectra of **(S,S)-N-C4,O-C4-AlaSQ** (**23c**); $CDCl_3$, 298 K.*

***Figure A50**: ^{1}H- (top, 700 MHz) and ^{13}C-NMR (bottom, 176 MHz) spectra of **(S,S)-N-C5,O-C5-AlaSQ** (**23d**); $CDCl_3$, 298 K.*

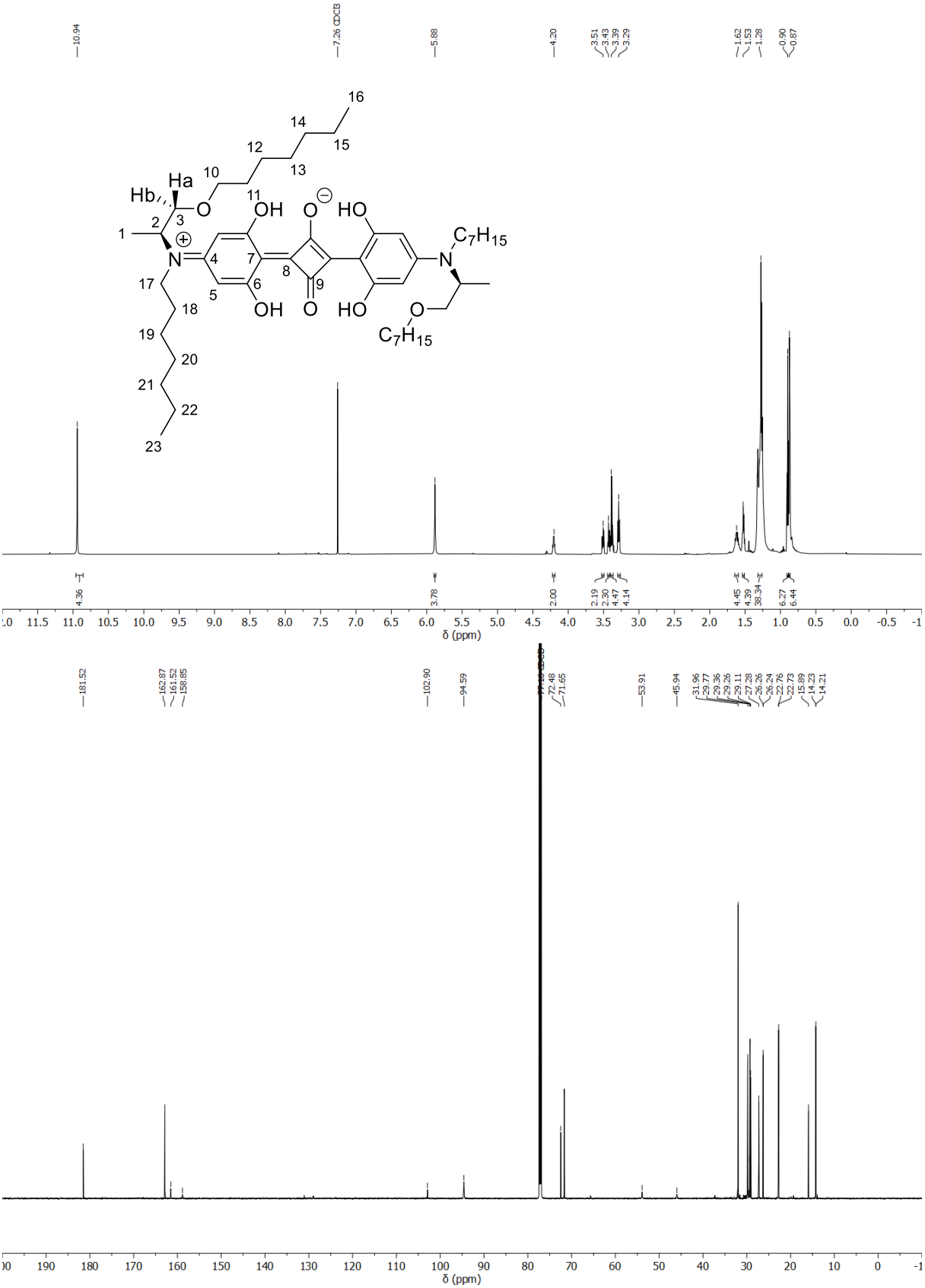

***Figure A51**: ^{1}H- (top, 700 MHz) and ^{13}C-NMR (bottom, 176 MHz) spectra of **(S,S)-N-C7,O-C7-AlaSQ** (**23e**); $CDCl_3$, 298 K.*

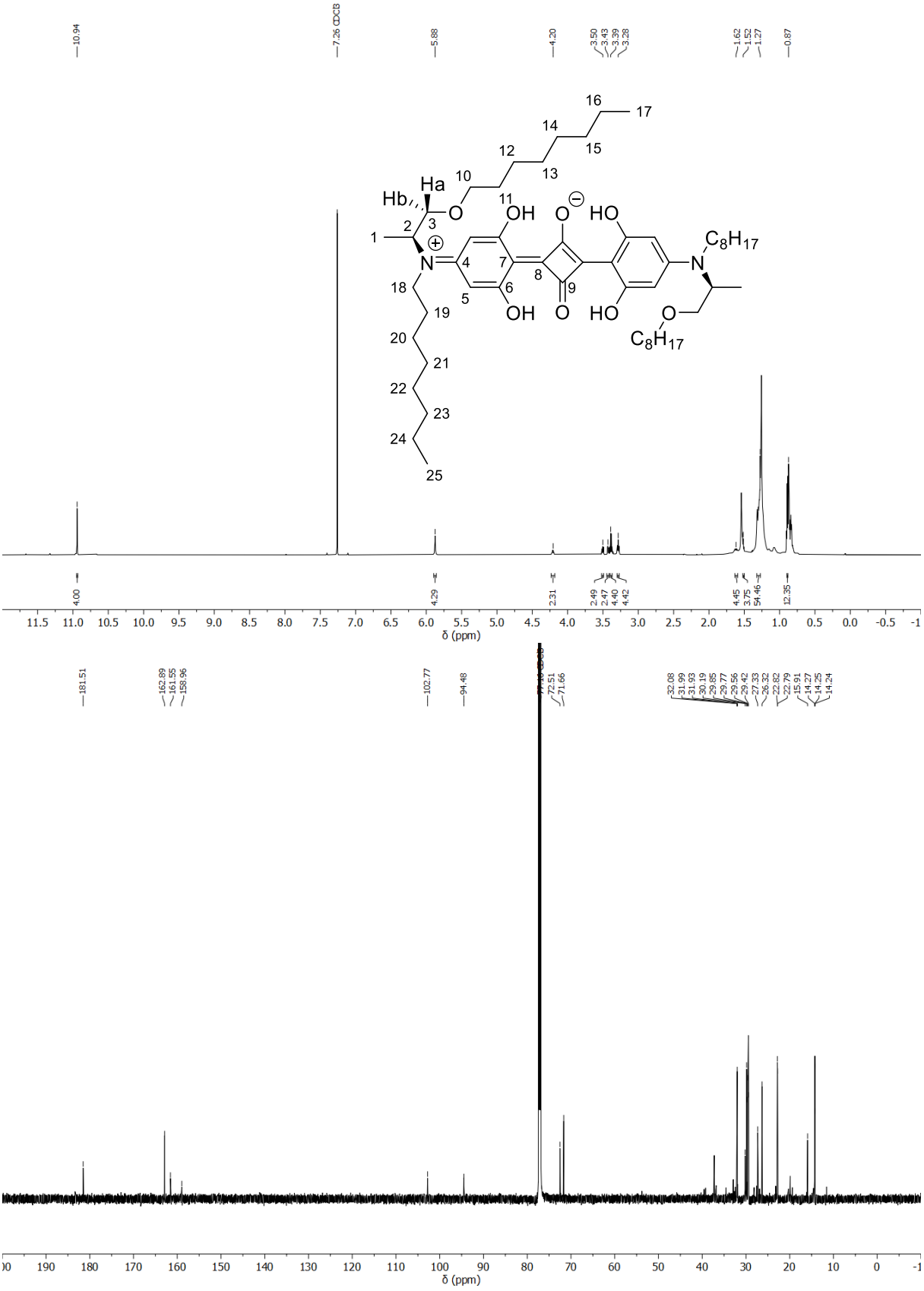

***Figure A52**: ^{1}H- (top, 700 MHz) and ^{13}C-NMR (bottom, 176 MHz) spectra of **(S,S)-N-C8,O-C8-AlaSQ (23f)**; $CDCl_3$, 298 K.*

***Figure A53**: ^{1}H- (top, 700 MHz) and ^{13}C-NMR (bottom, 176 MHz) spectra of **(S,S)-N-C9,O-C9-AlaSQ** (**23g**); $CDCl_3$, 298 K.*

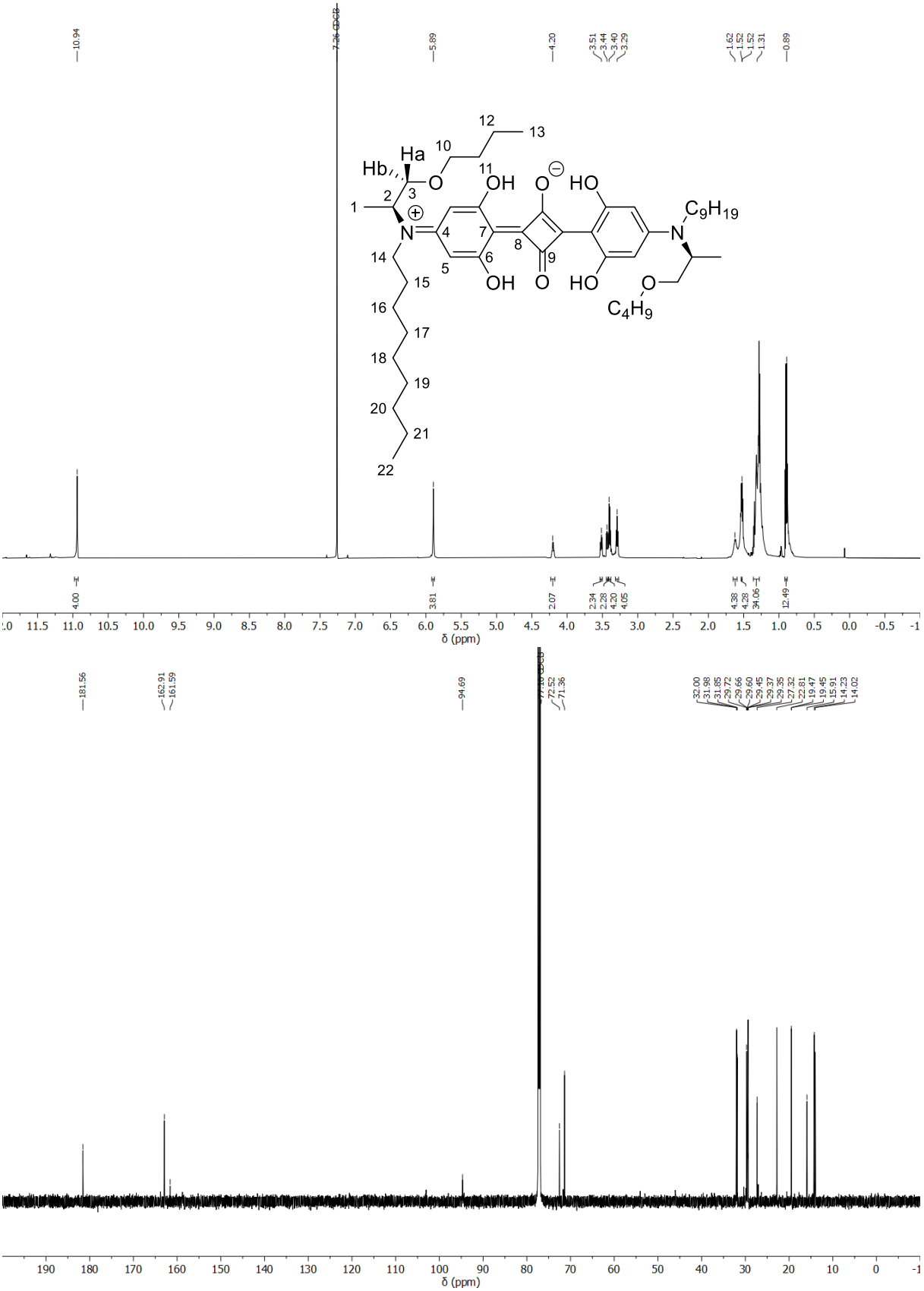

***Figure A54**: ^{1}H- (top, 700 MHz) and ^{13}C-NMR (bottom, 176 MHz) spectra of **(S,S)-N-C9,O-C4-AlaSQ** (**23h**); $CDCl_3$, 298 K.*

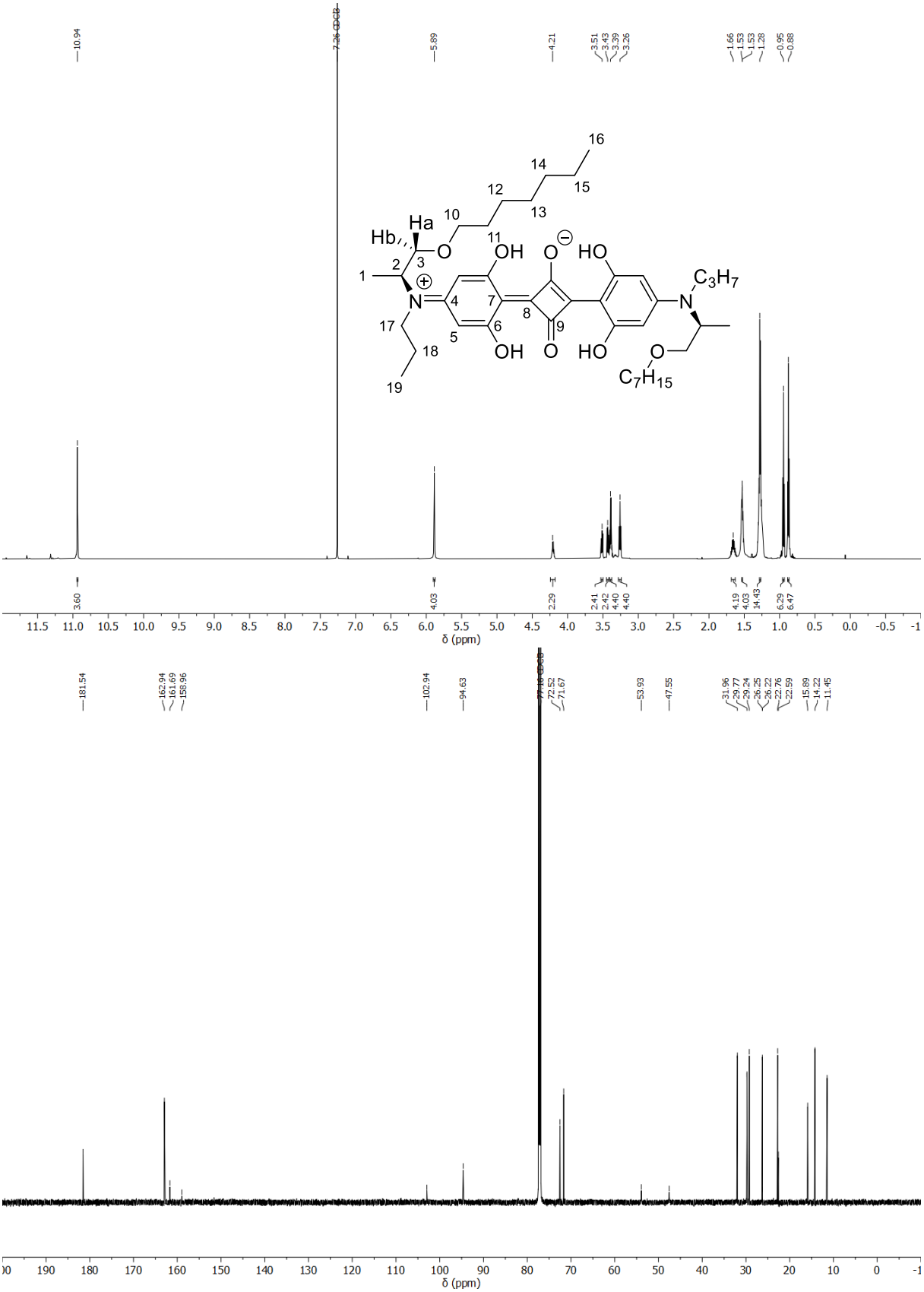

***Figure A55**: ^{1}H- (top, 700 MHz) and ^{13}C-NMR (bottom, 176 MHz) spectra of **(S,S)-N-C3,O-C7-AlaSQ (23i)**; $CDCl_3$, 298 K.*

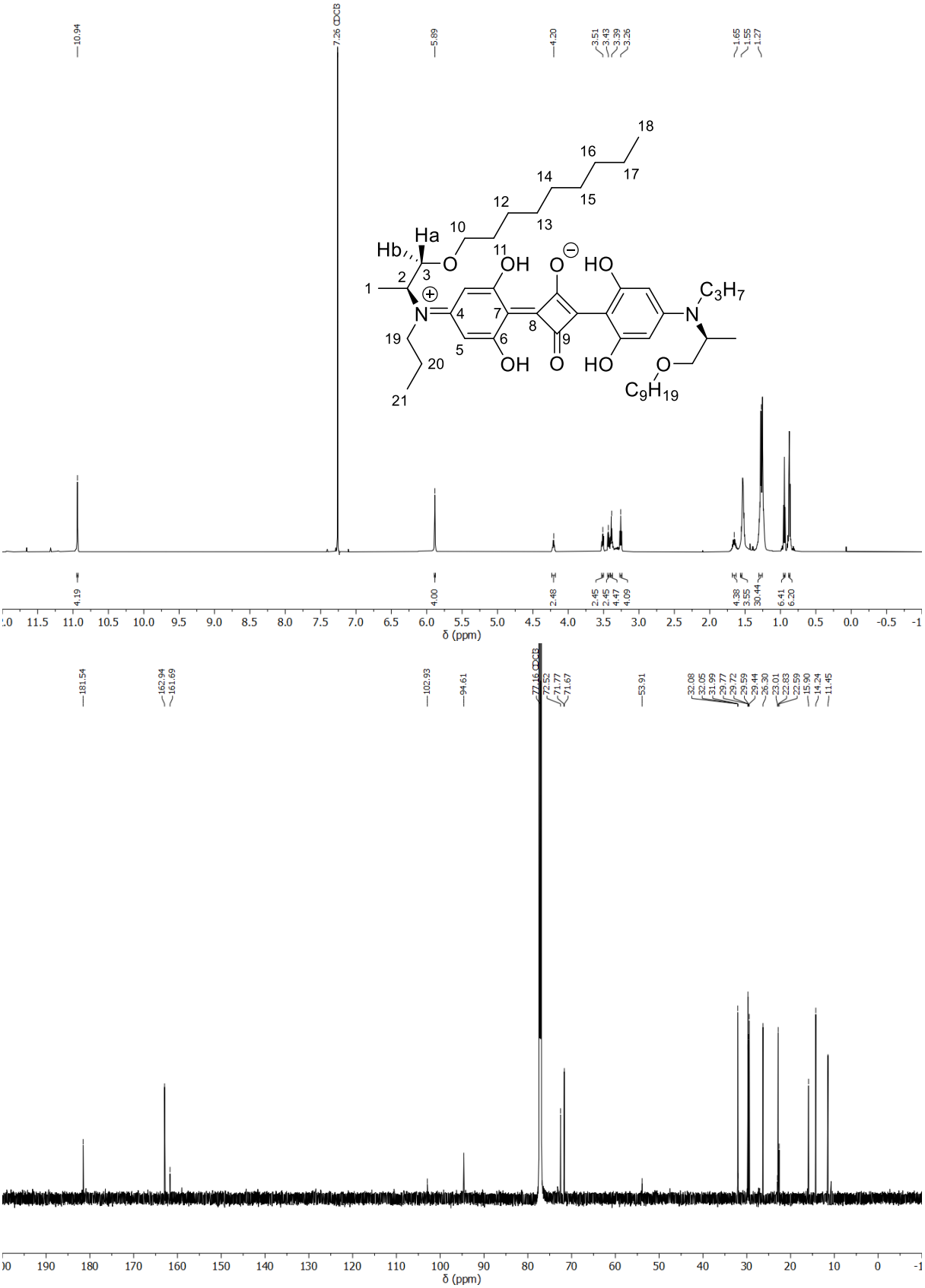

***Figure A56**: ^{1}H- (top, 700 MHz) and ^{13}C-NMR (bottom, 176 MHz) spectra of **(S,S)-N-C3,O-C9-AlaSQ (23j)**; $CDCl_3$, 298 K.*

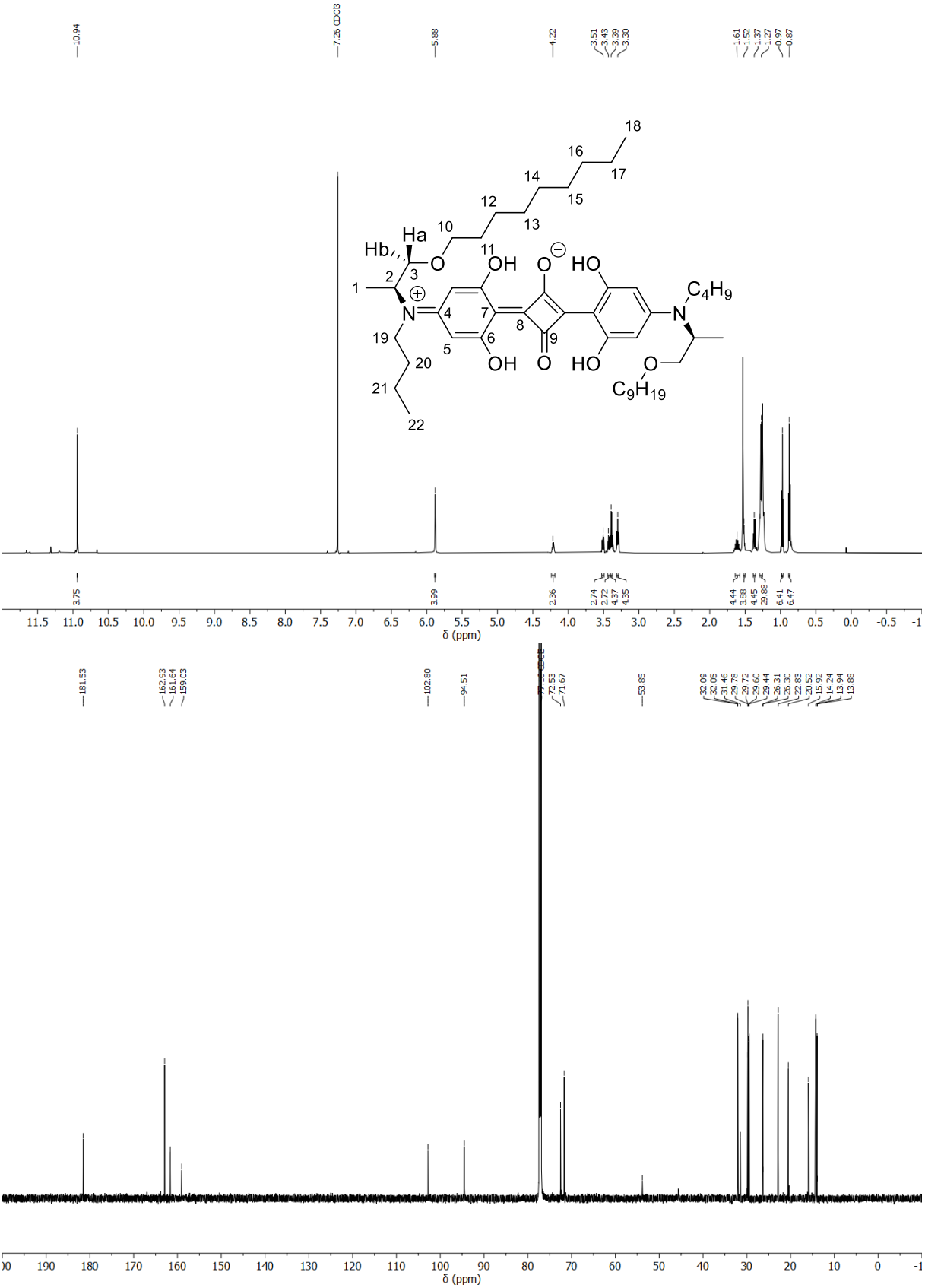

***Figure A57**: ^{1}H- (top, 700 MHz) and ^{13}C-NMR (bottom, 176 MHz) spectra of **(S,S)-N-C4,O-C9-AlaSQ** (**23k**); $CDCl_3$, 298 K.*

MASS SPECTRA

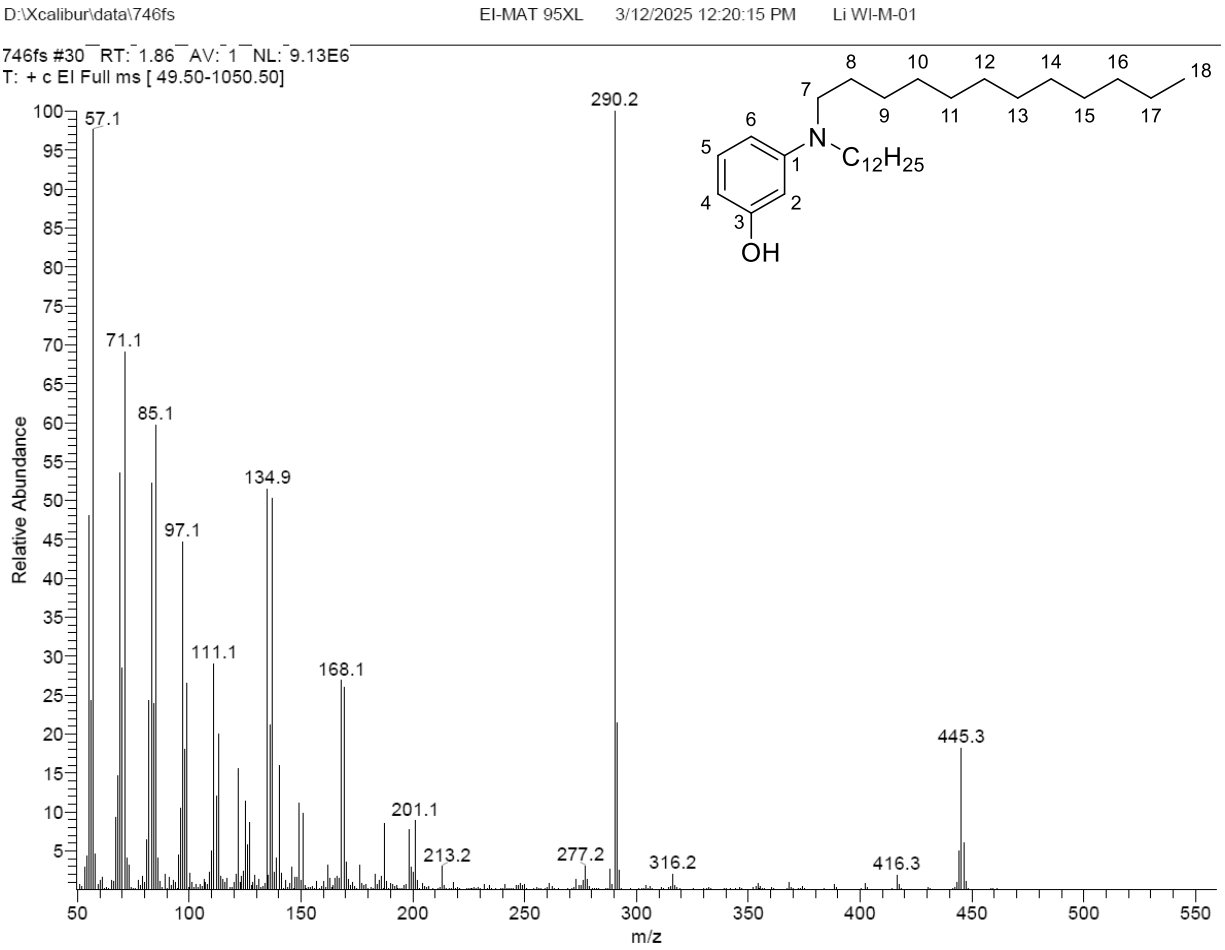

Figure A58: *EI Mass spectra of N,N-didodecyl 3-hydroxy aniline (**1**).*

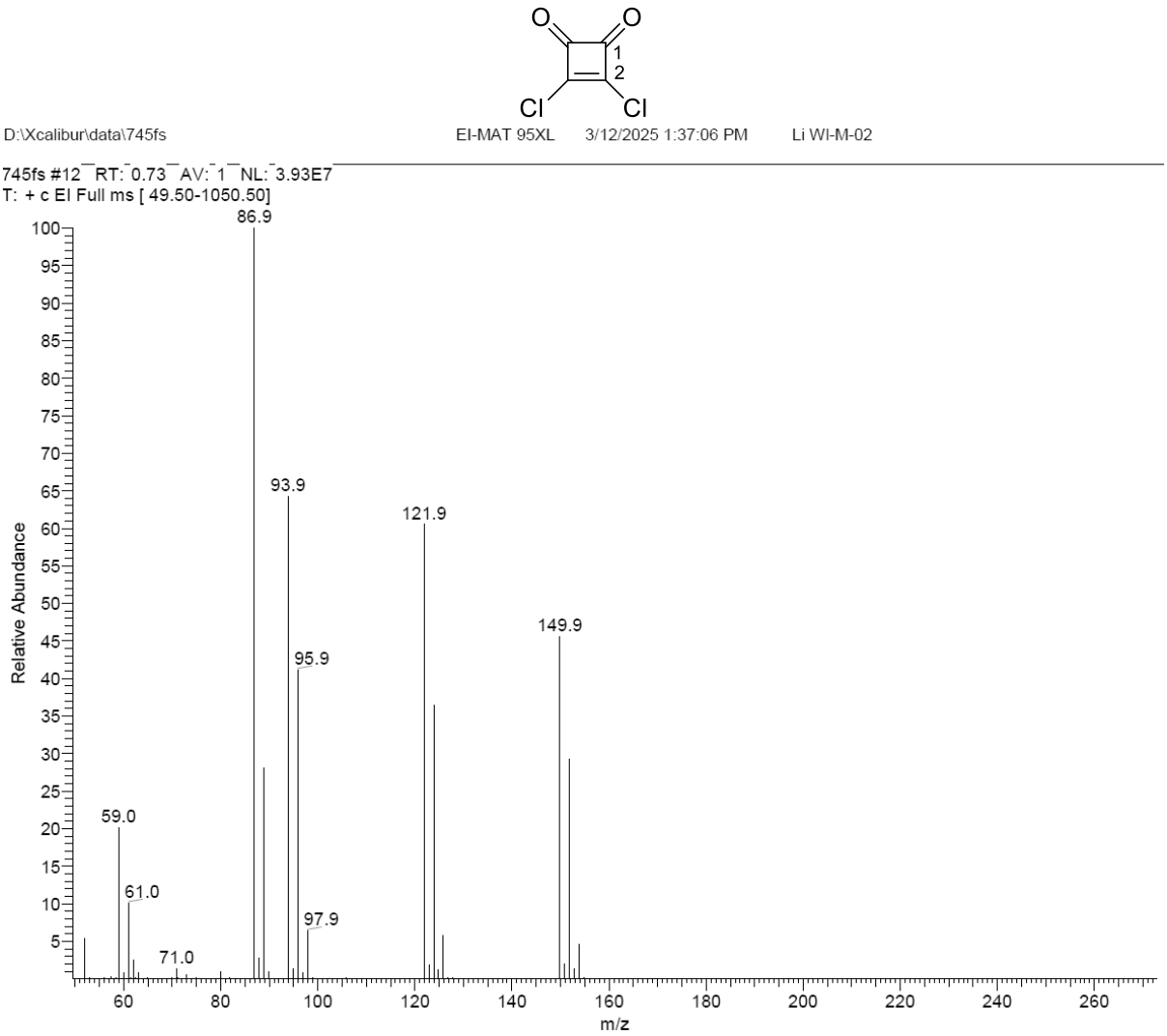

Figure A59: *EI Mass spectra of squarylium dichloride (**2**).*

*hemisquarate **4***

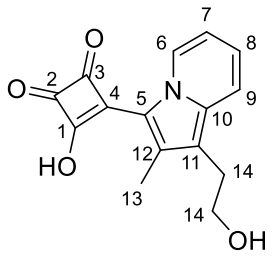

Was used up during research stay in Milan, no mass was measured.

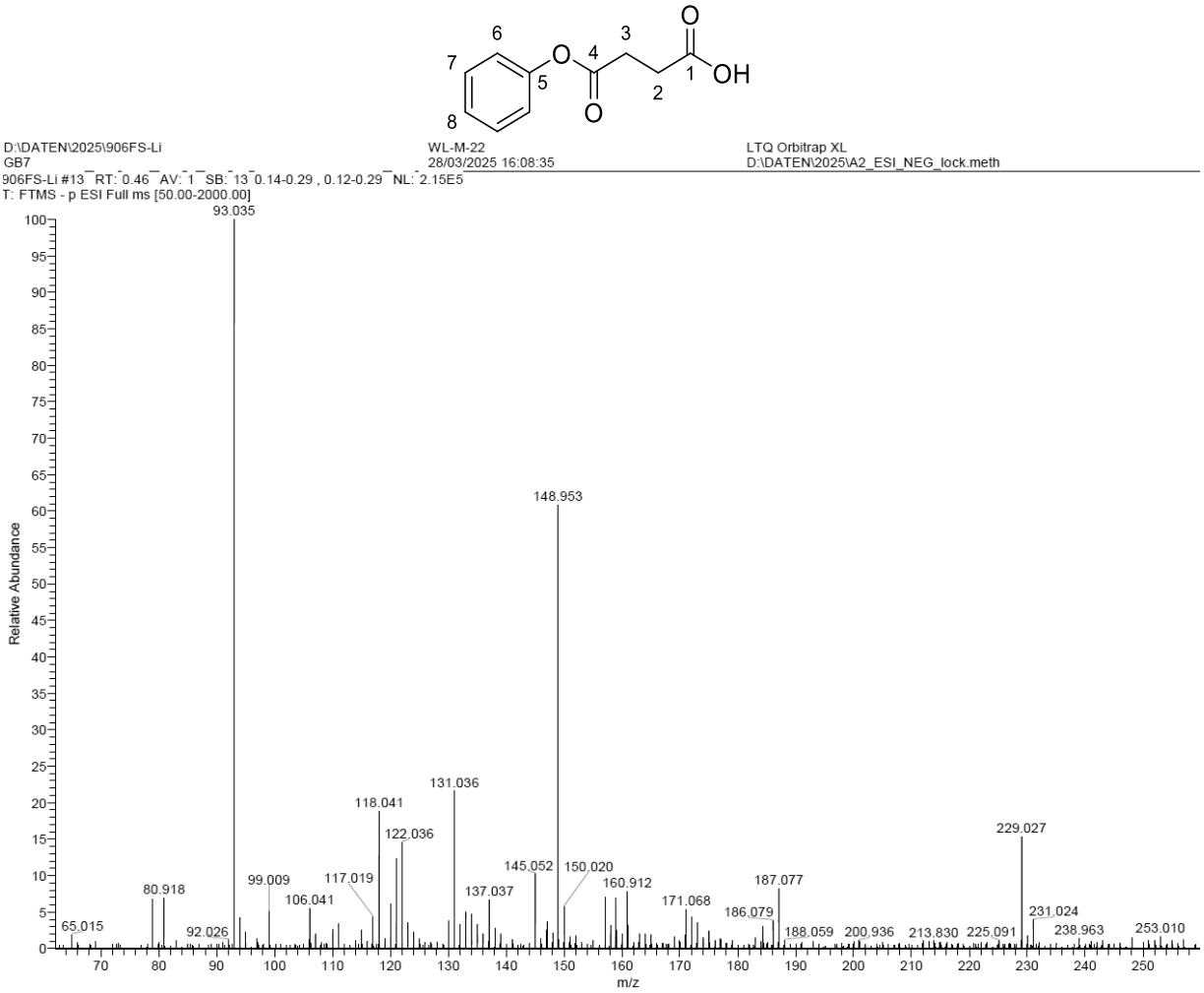

***Figure A60**: ESI(-) Mass spectra of 1-phenyl butanedioate (**5**).*

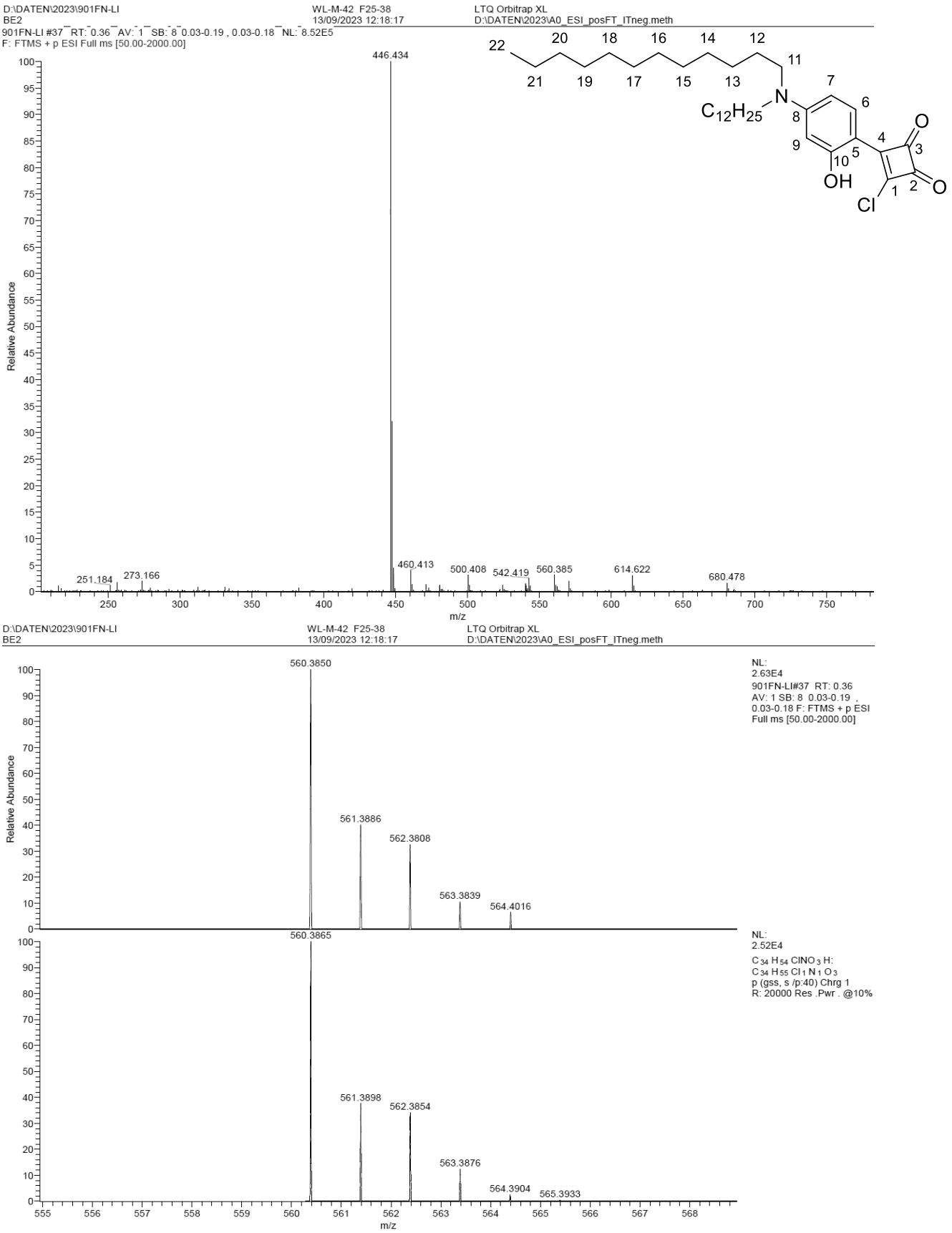

Figure A61: *ESI(+) Mass spectra of hemisquarates* ***8****.*

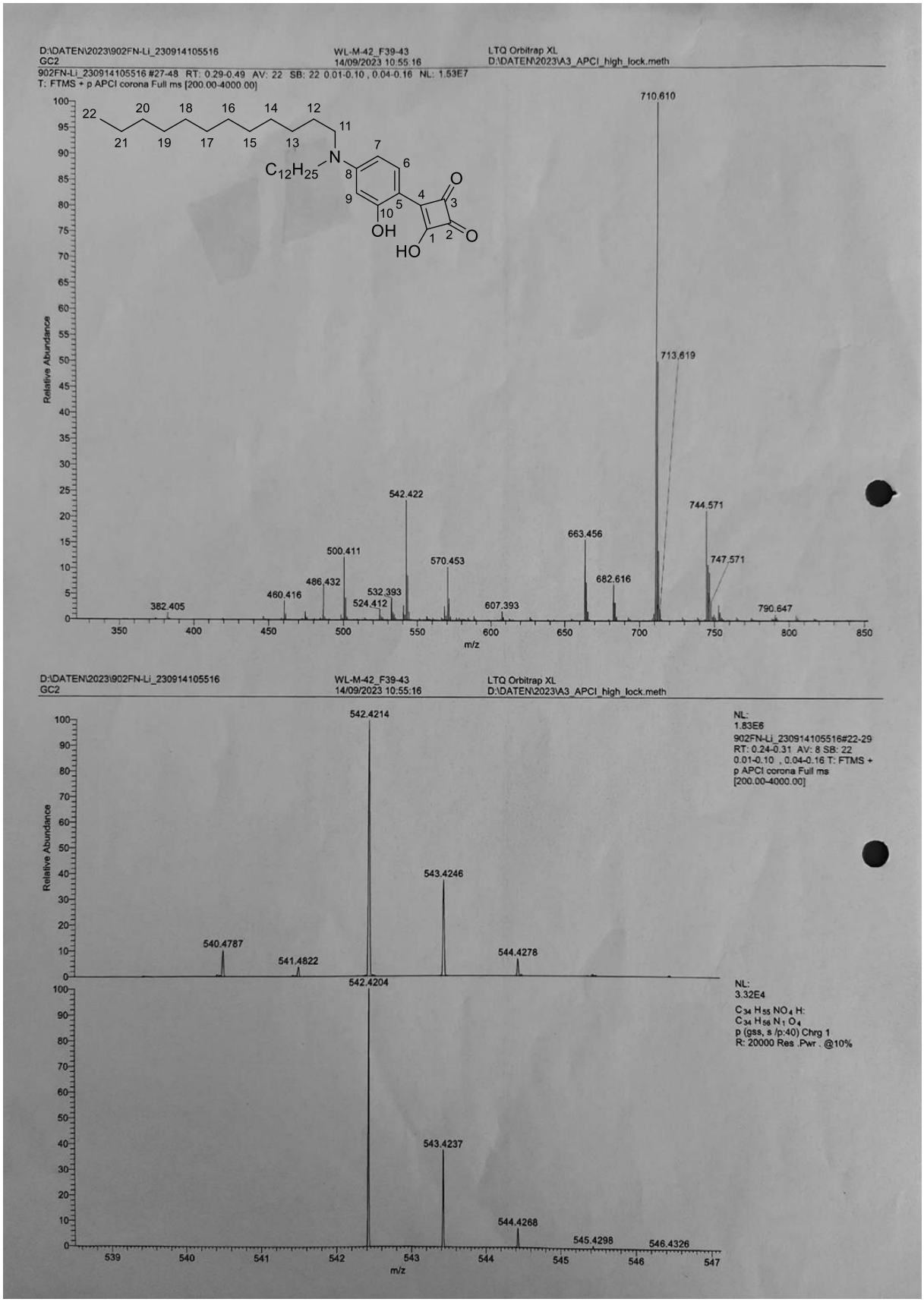

***Figure A62**: APCI Mass spectra of hemisquarates **9**.*

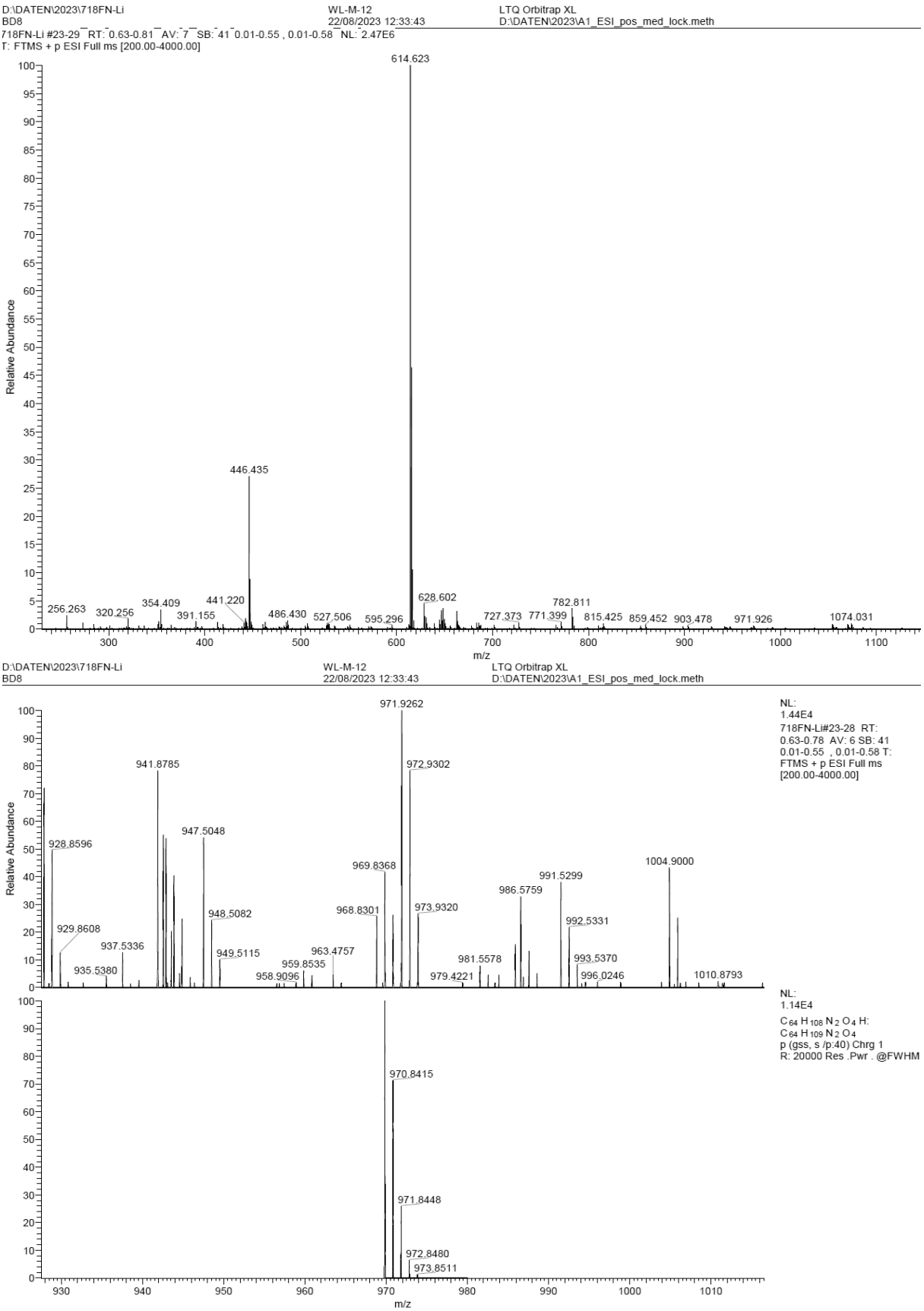

***Figure A63**:ESI (+) Mass spectra od symmetric squaraine (**11**).*

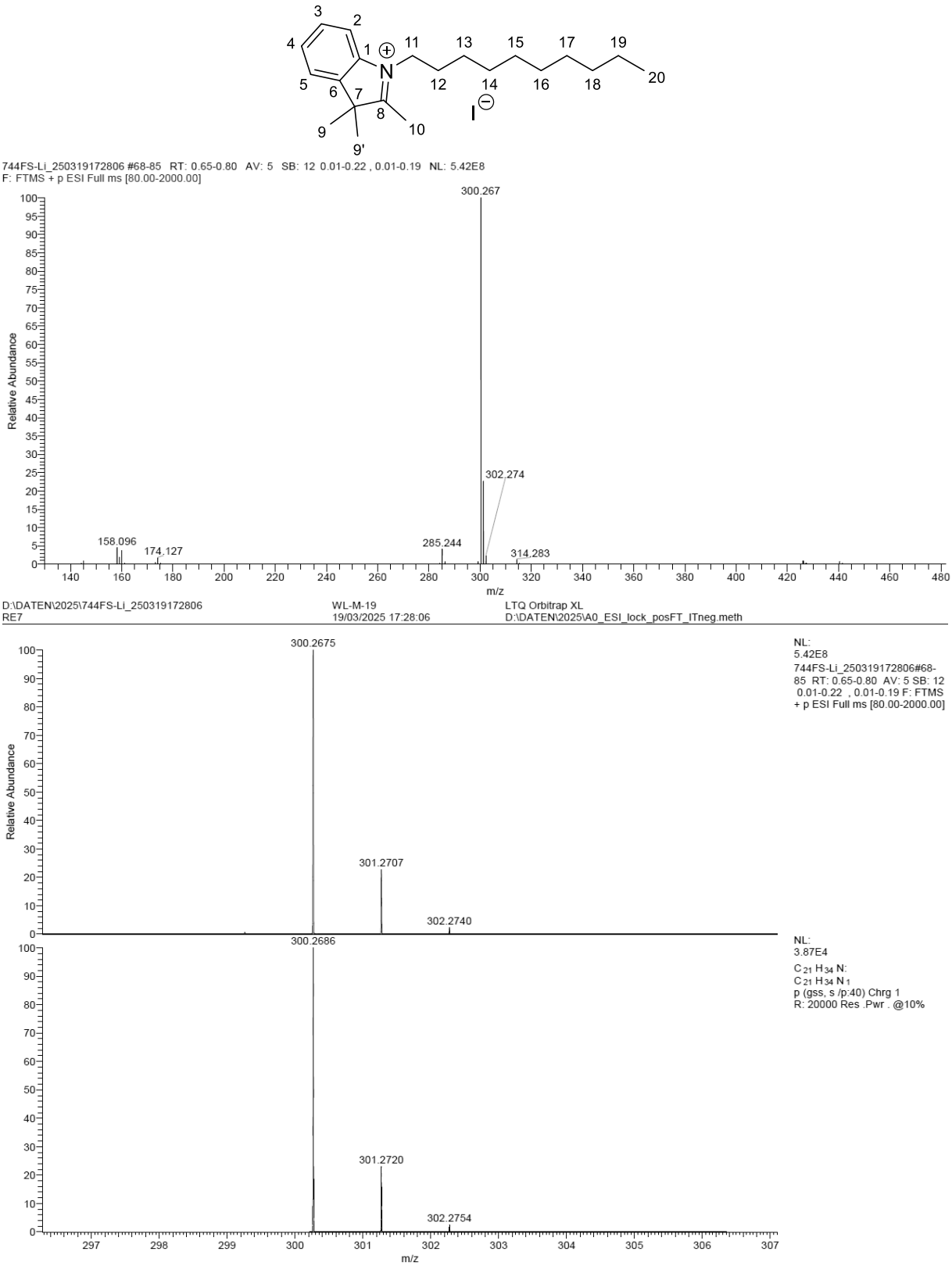

***Figure A 64**: ESI(+) Mass spectra of indole derivative (**13**).*

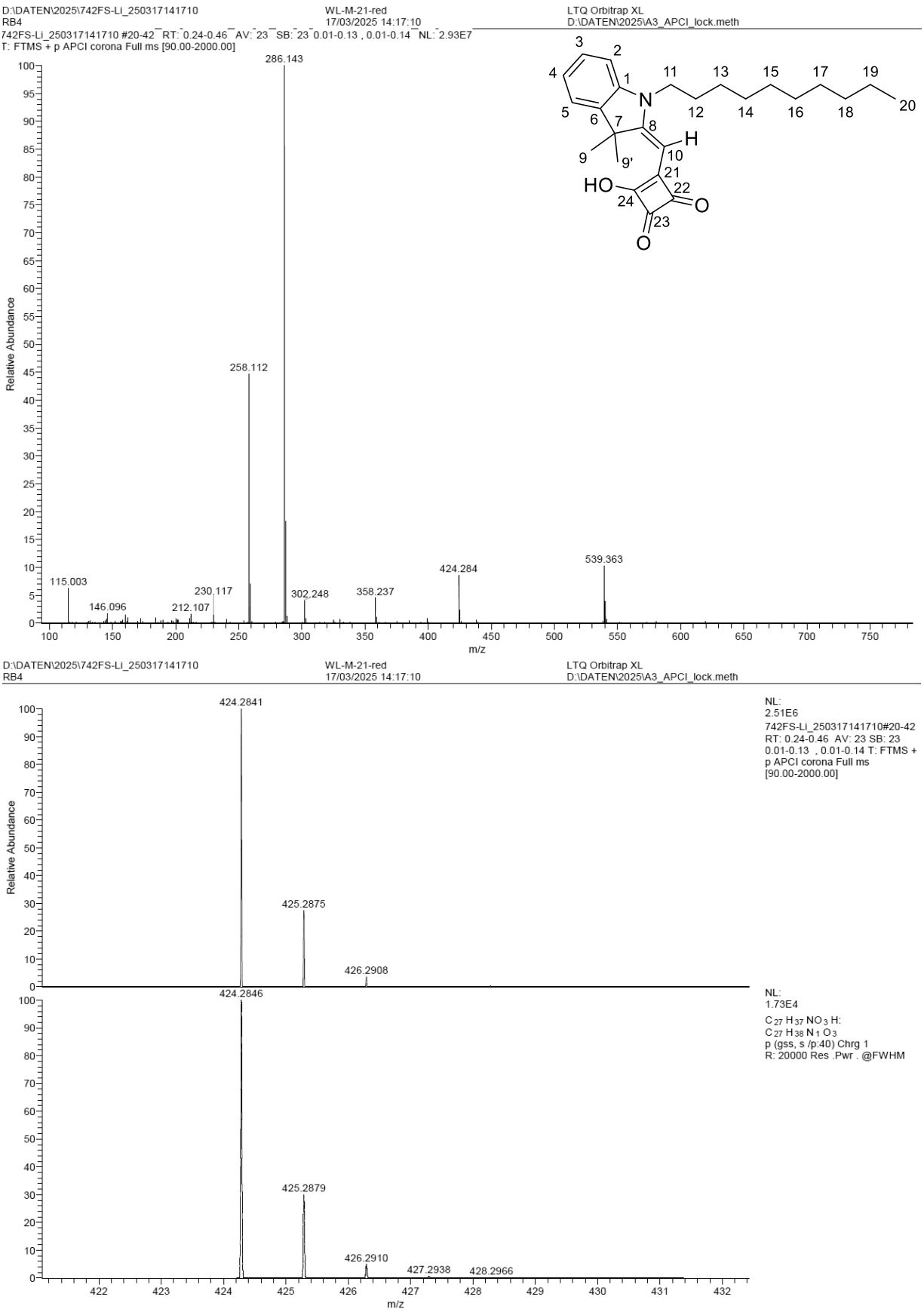

***Figure A65**: ESI(+) Mass spectra of indole derivative (**13**).*

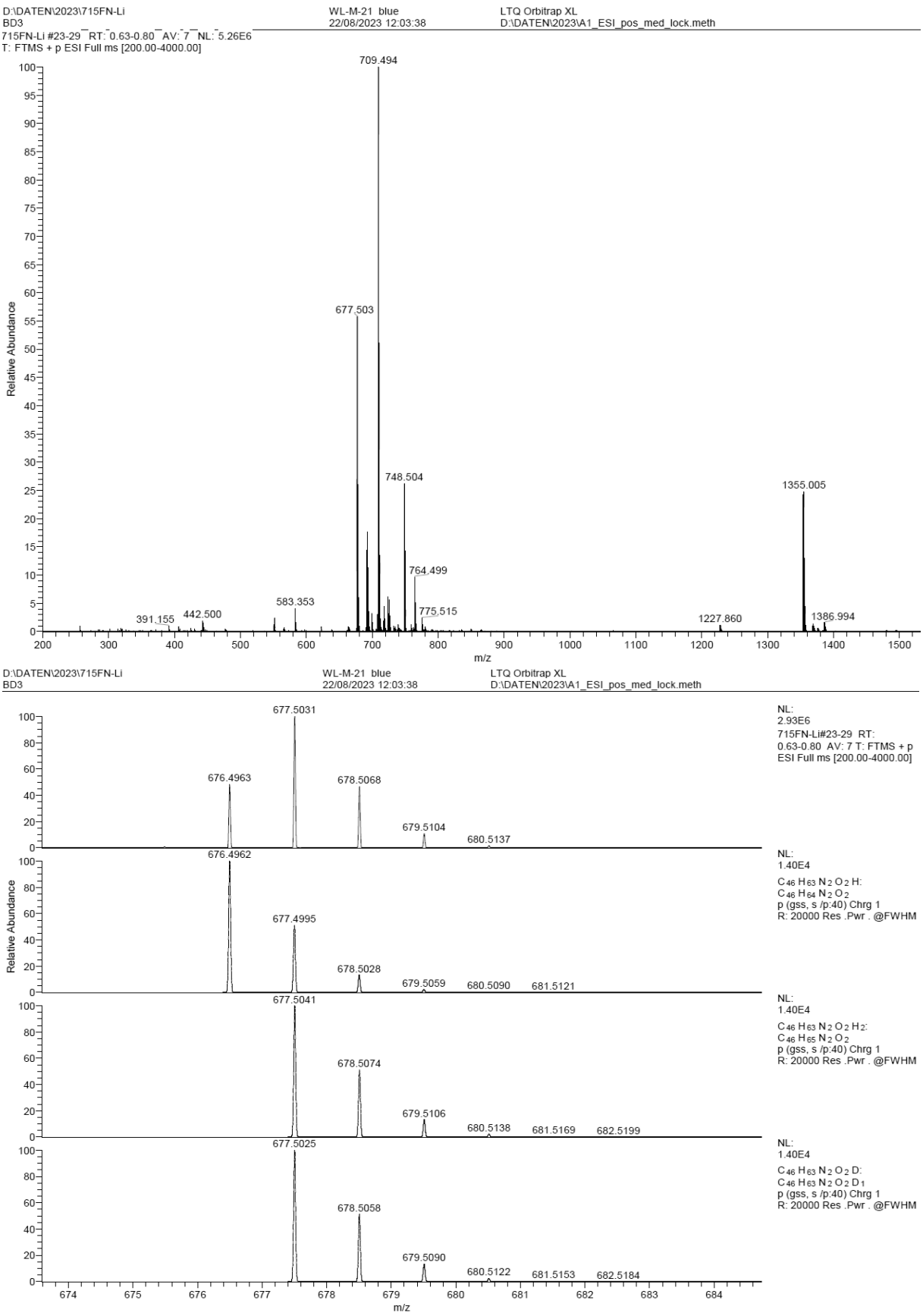

***Figure A66**: ESI(+) Mass spectra of symmetric indoline squaraine (**15**).*

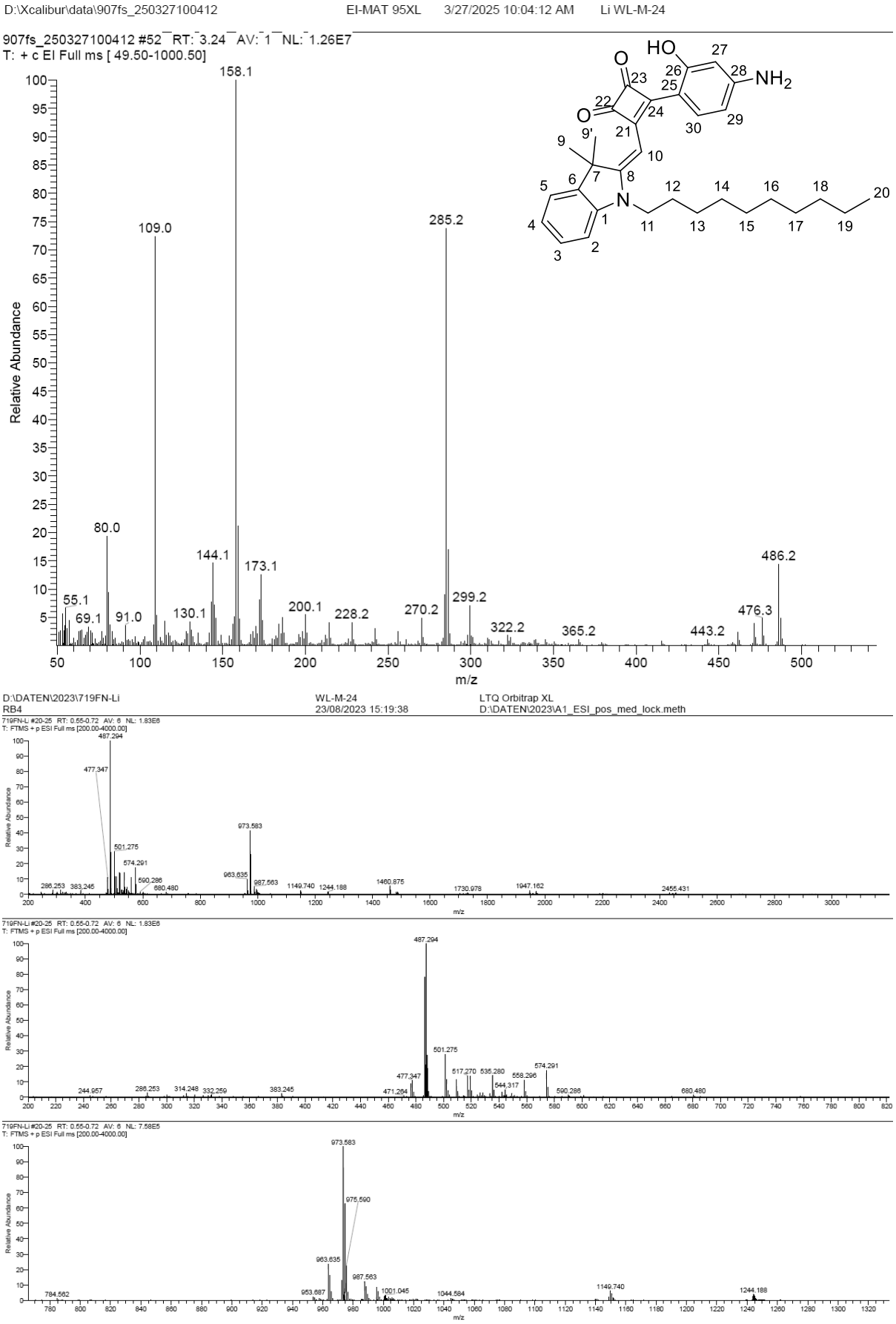

Figure A67: ESI(+) Mass spectra of amphiphilic squaraine **20**.

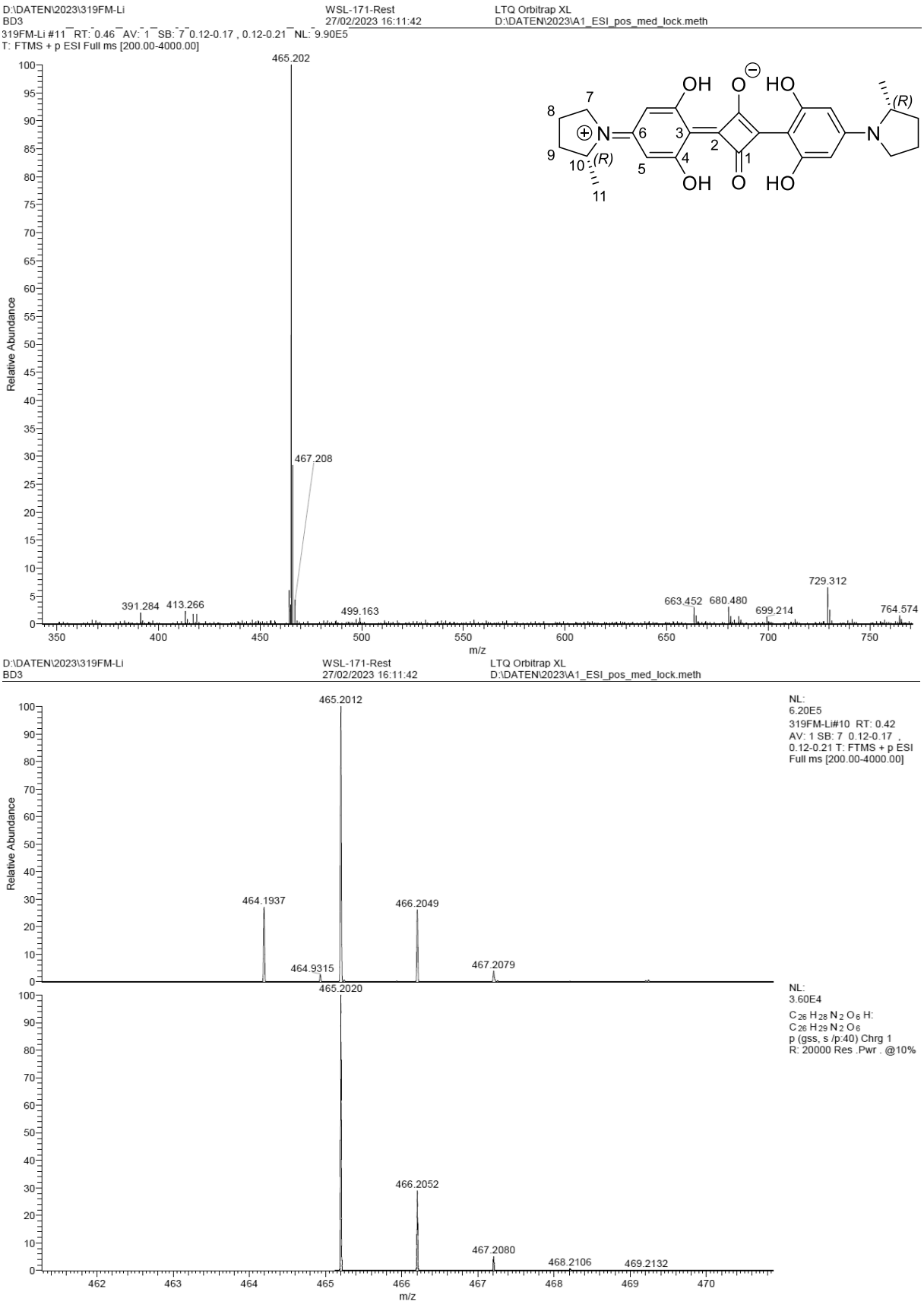

***Figure A68**: ESI(+) Mass spectra of* **(R,R)** ***PyrSQ-C1**.*

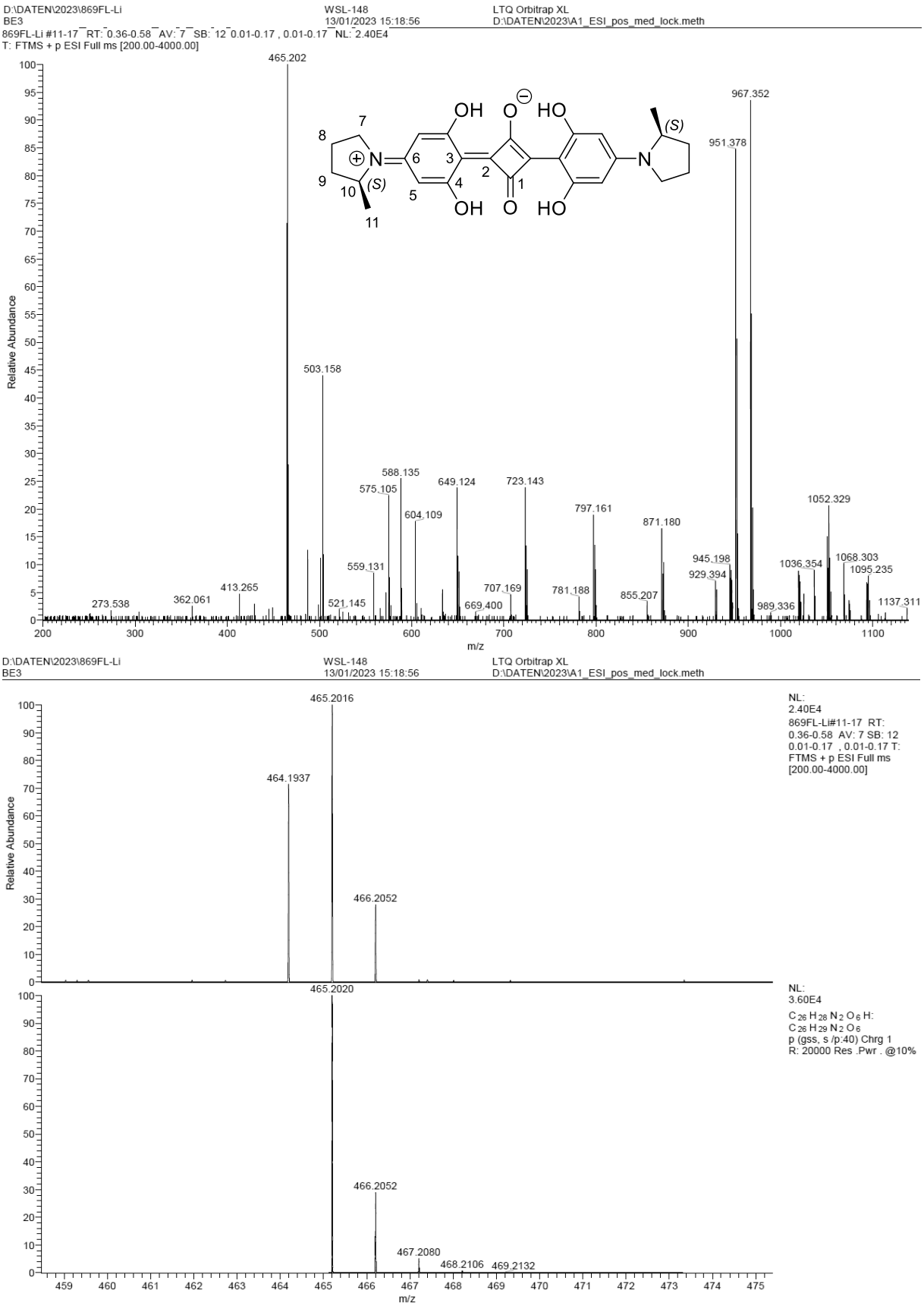

***Figure A69**: ESI(+) Mass spectra of **(S,S) PyrSQ-C1**.*

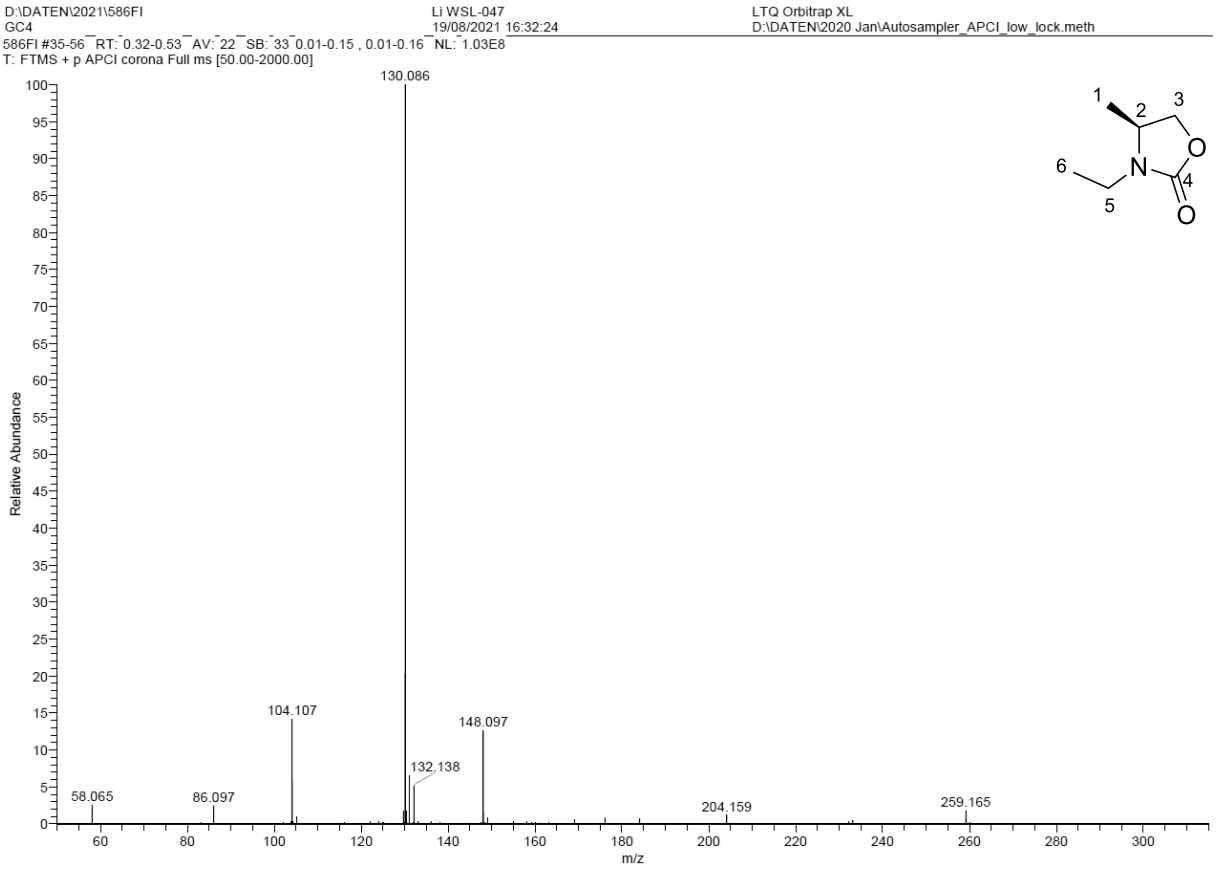

***Figure A70**: APCI Mass spectra of oxazolidinone byproduct **30**.*

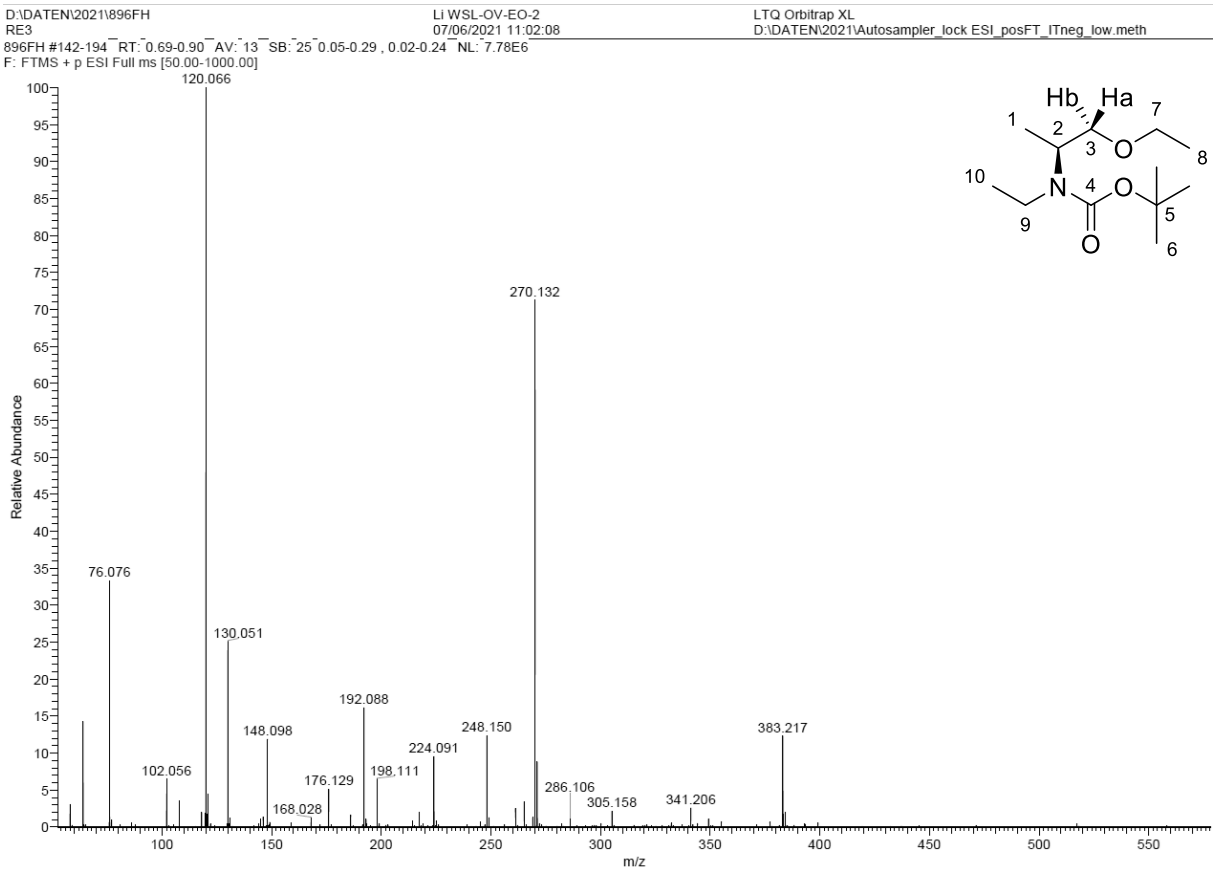

***Figure A71**: APCI Mass spectra of **31a**.*

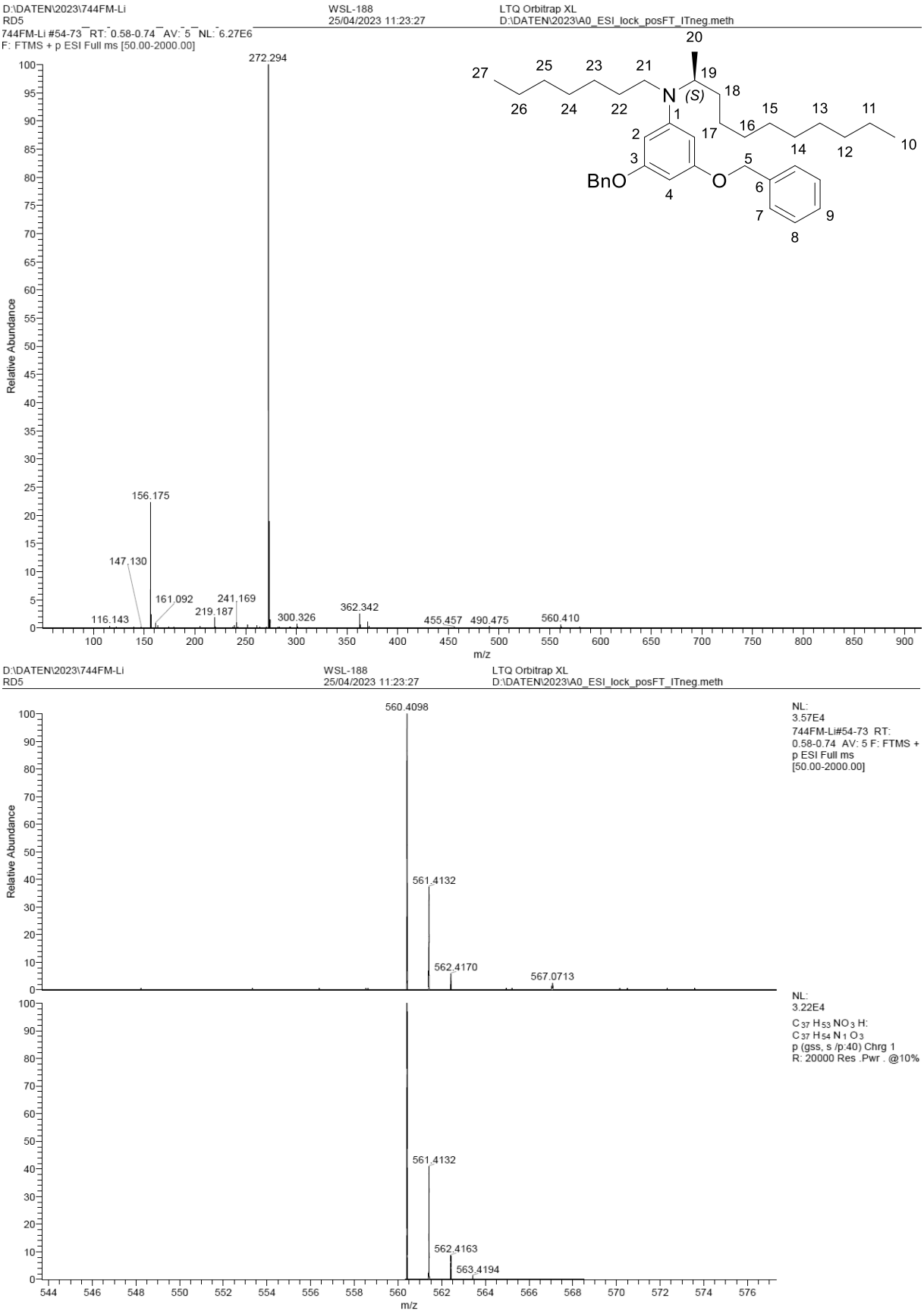

***Figure A72**: ESI (+) Mass spectra of oxazolidinone byproduct **44e**.*

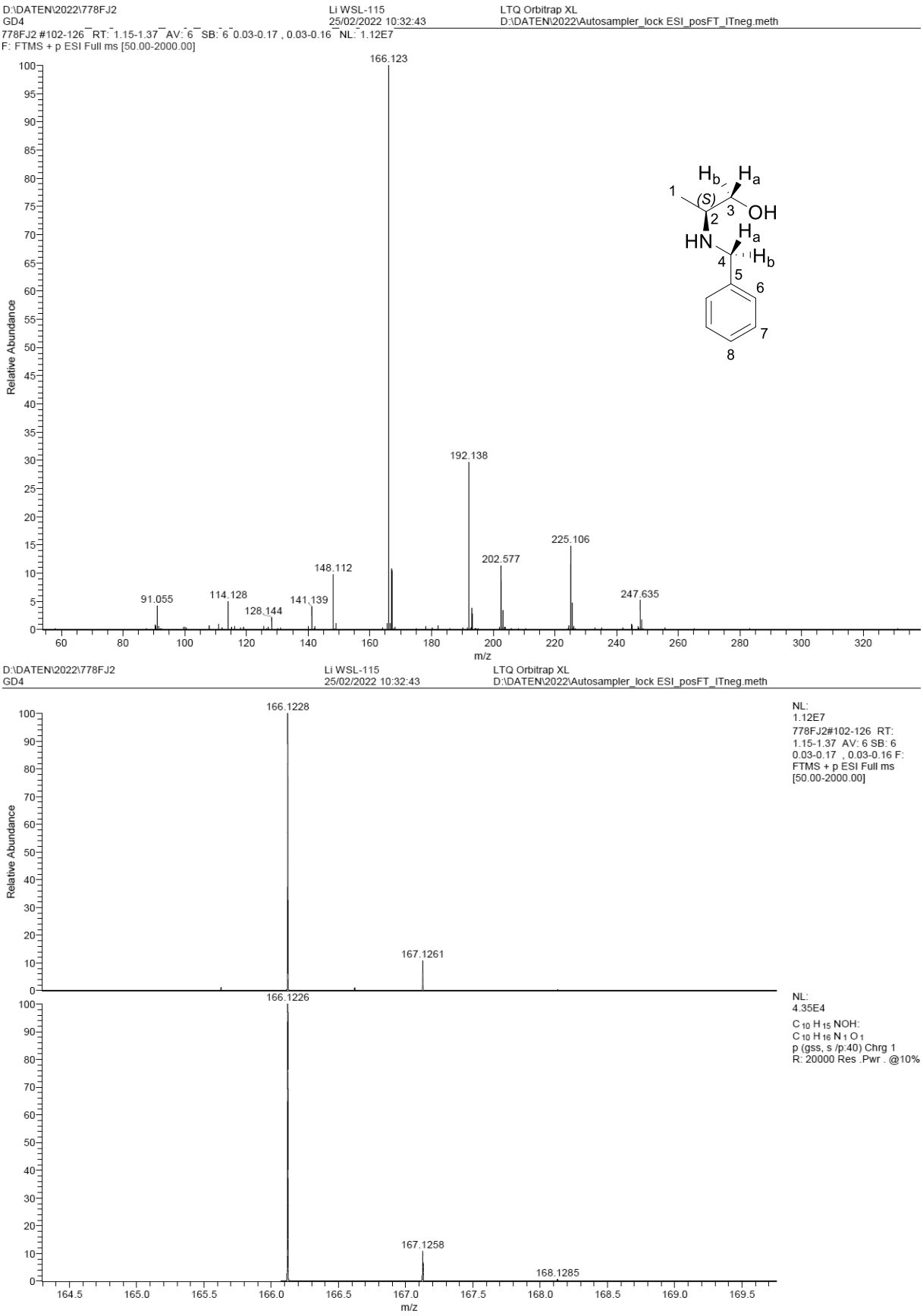

***Figure A73**: ESI(+) Mass spectra of N-benzyl-L-alaninol (**38**):*

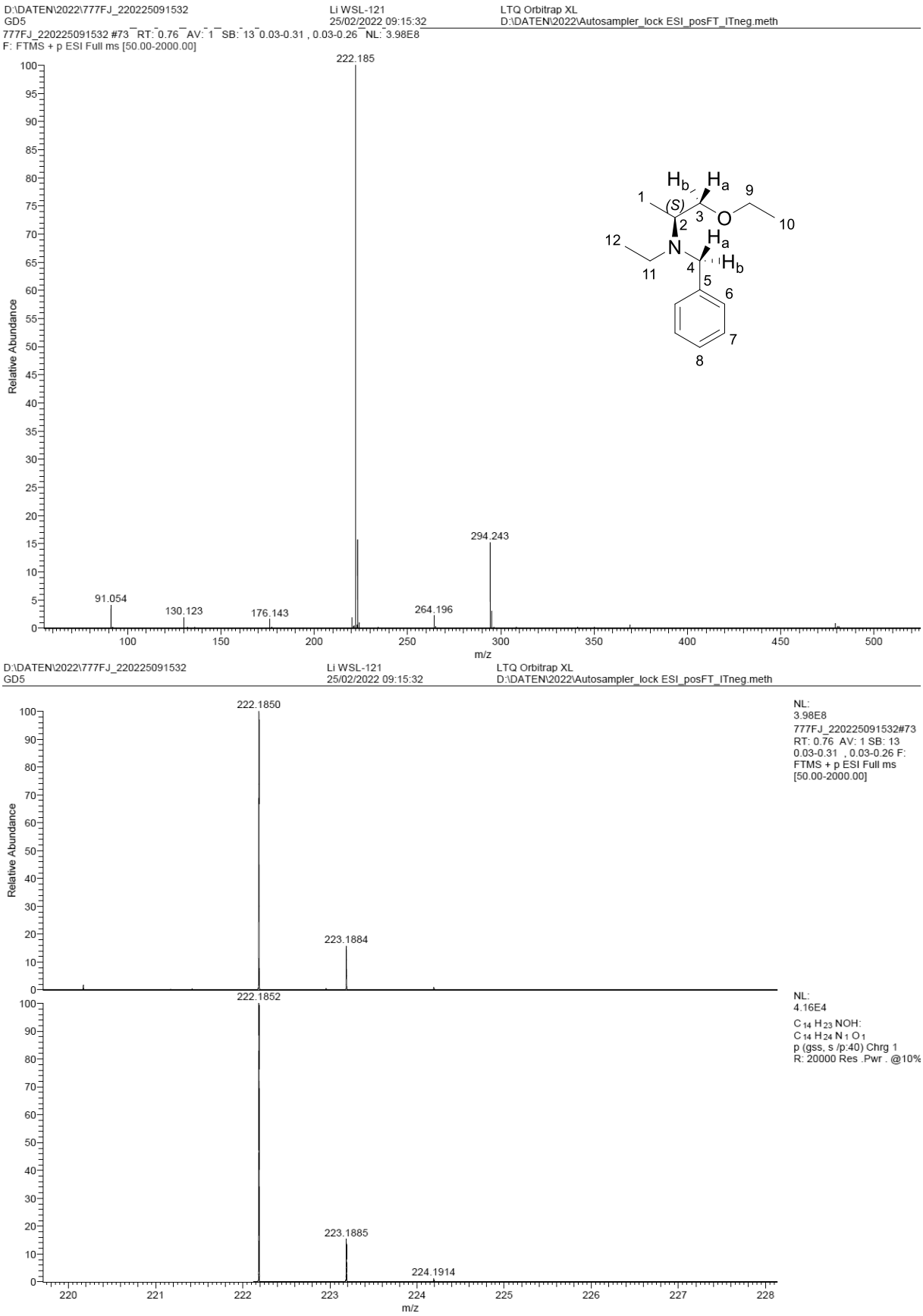

***Figure A74**: ESI(+) Mass spectra of N-benzyl-N-ethyl-L-alaninyl ethyl ether (**39a**).*

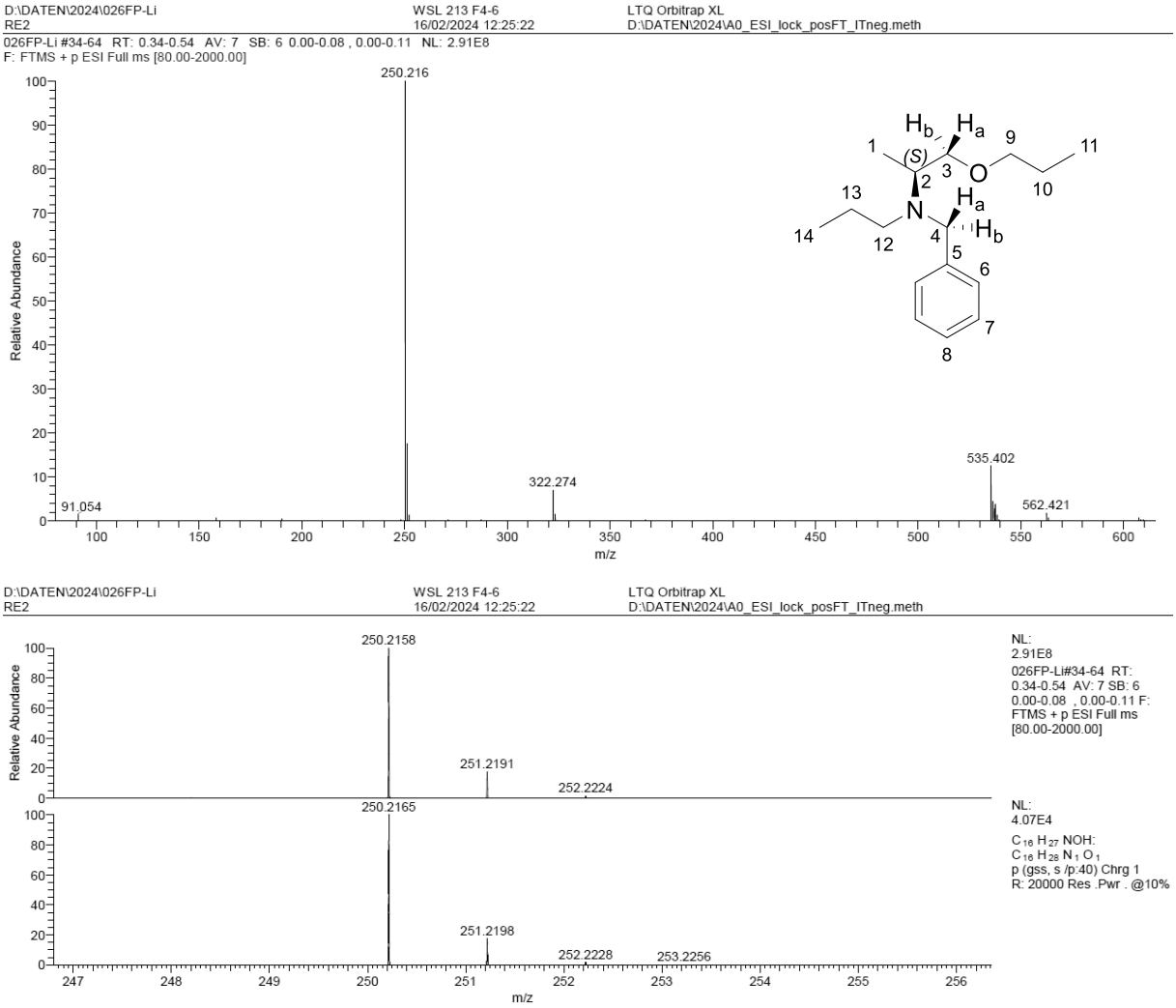

***Figure A75**: ESI(+) Mass spectra of N-benzyl-N-propyl-L-alaninyl propyl ether (**39b**).*

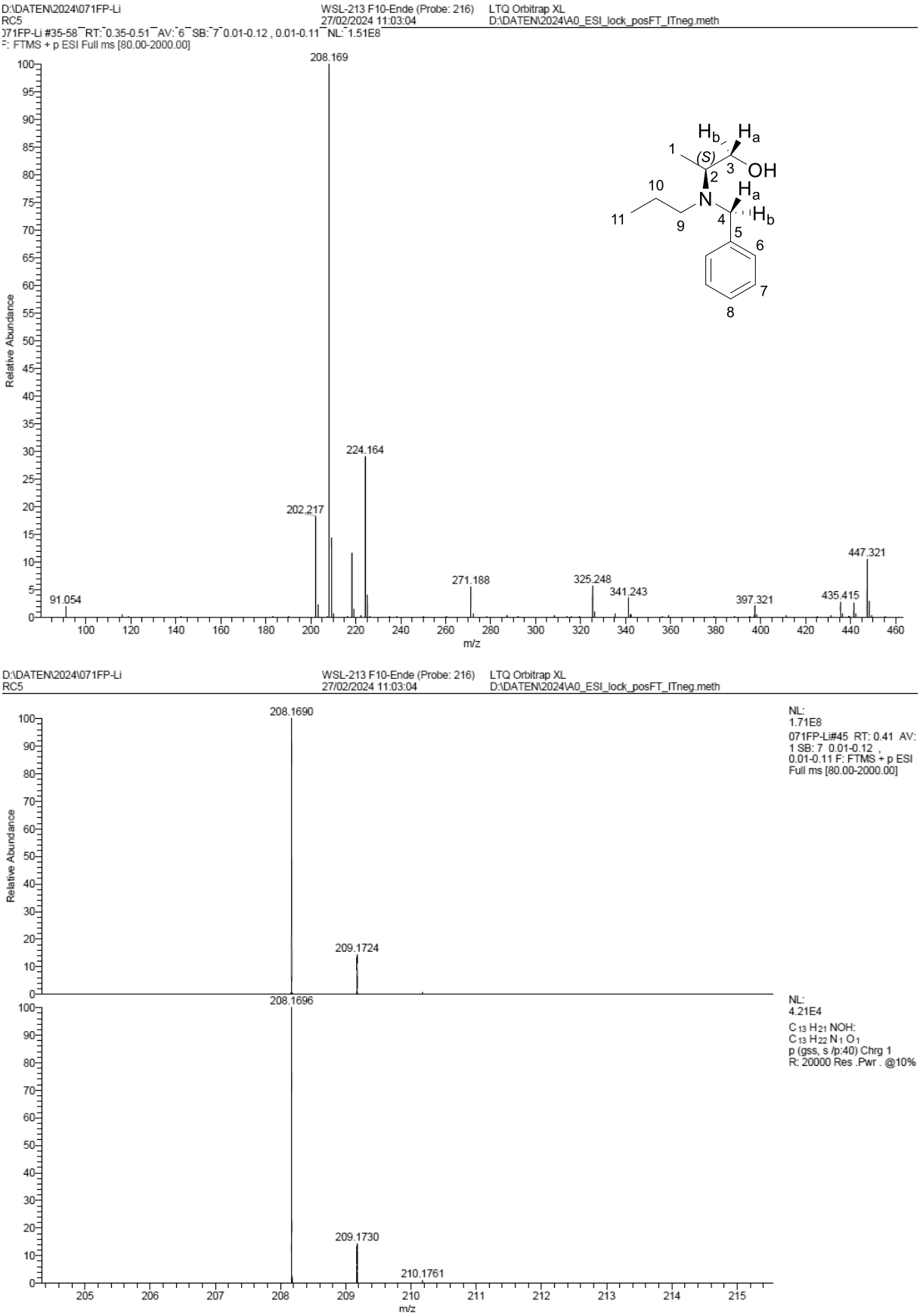

***Figure A76**: ESI(+) Mass spectra of N-benzyl-N-propyl-* L*-alaninyl amine (**48b**).*

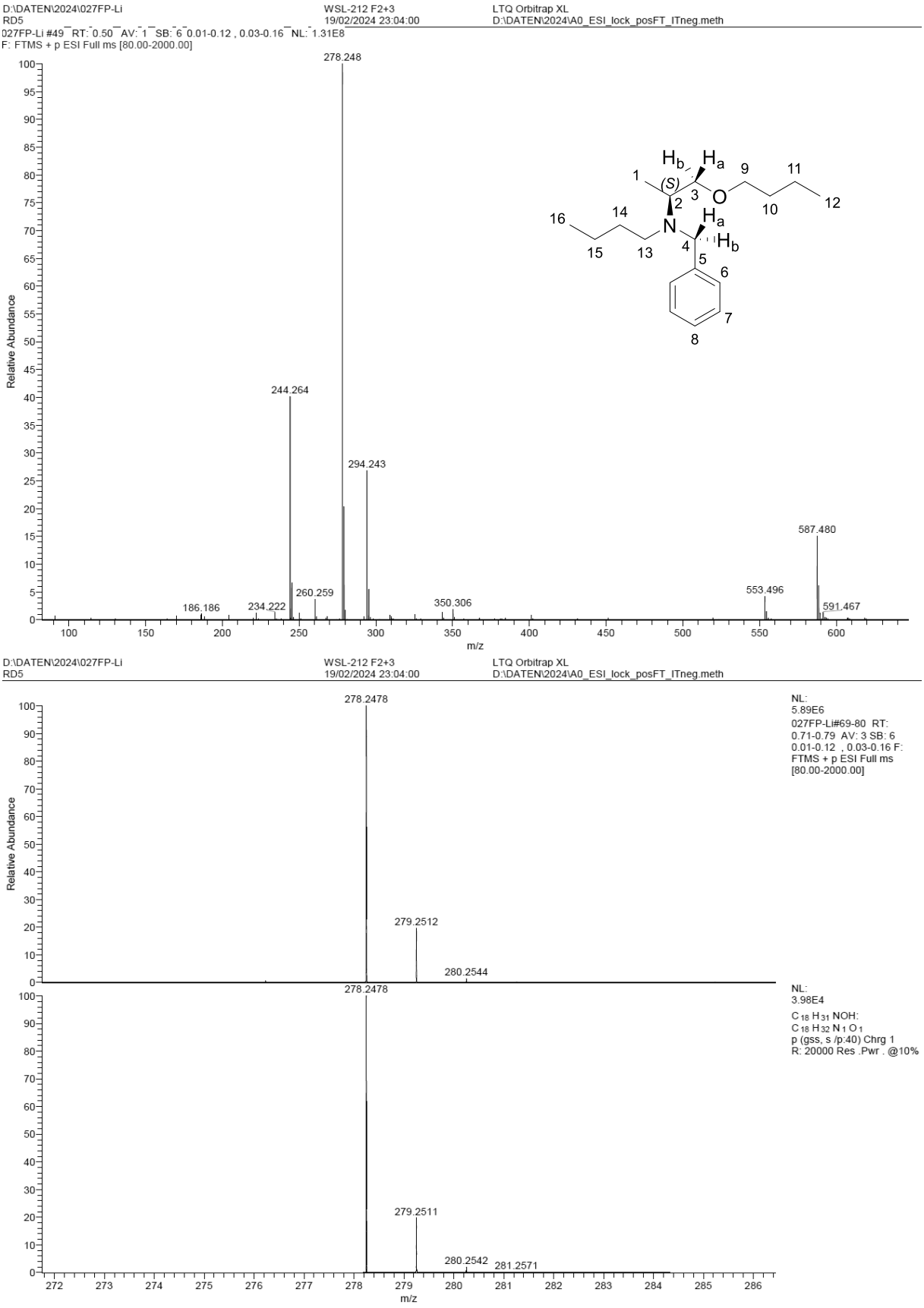

***Figure A77**: ESI(+) Mass spectra of N-benzyl-N-butyl-L-alaninyl butyl ether (**39c**).*

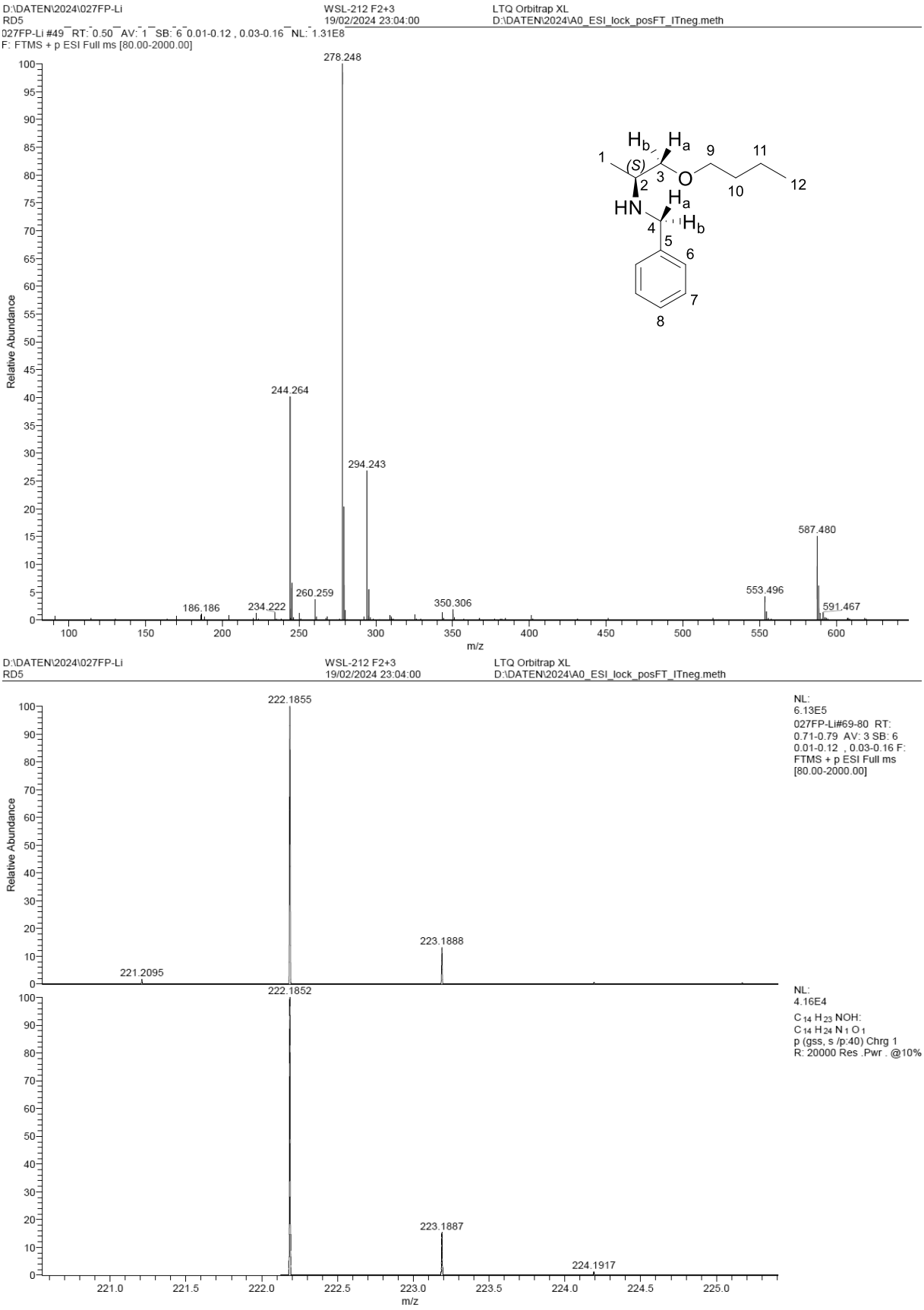

***Figure A78**: ESI(+) Mass spectra of N-benzyl-L-alaninyl butyl ether (**47c**).*

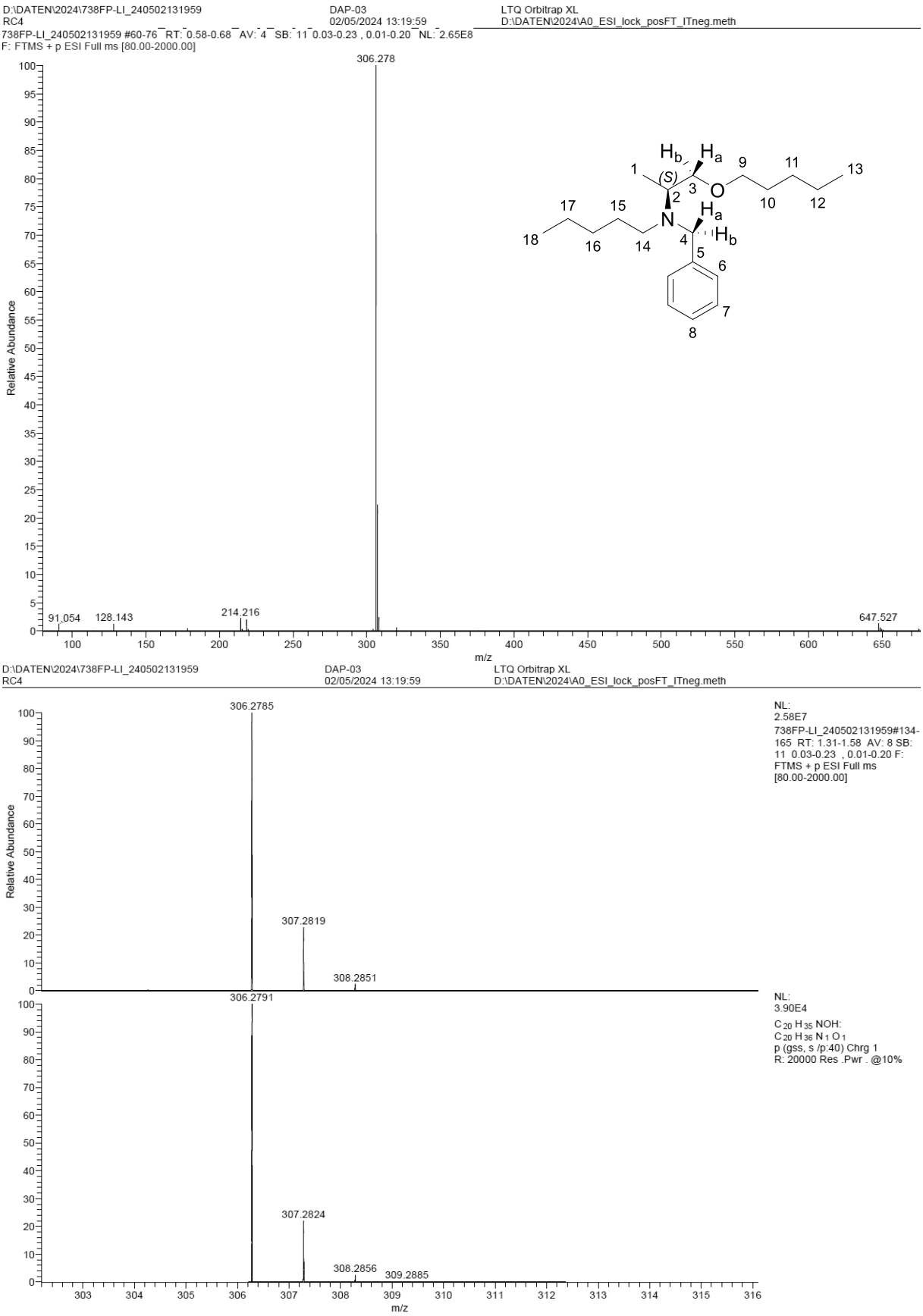

***Figure A79**: ESI(+) Mass spectra of N-benzyl-N-pentyl-L-alaninyl pentyl ether (**39d**).*

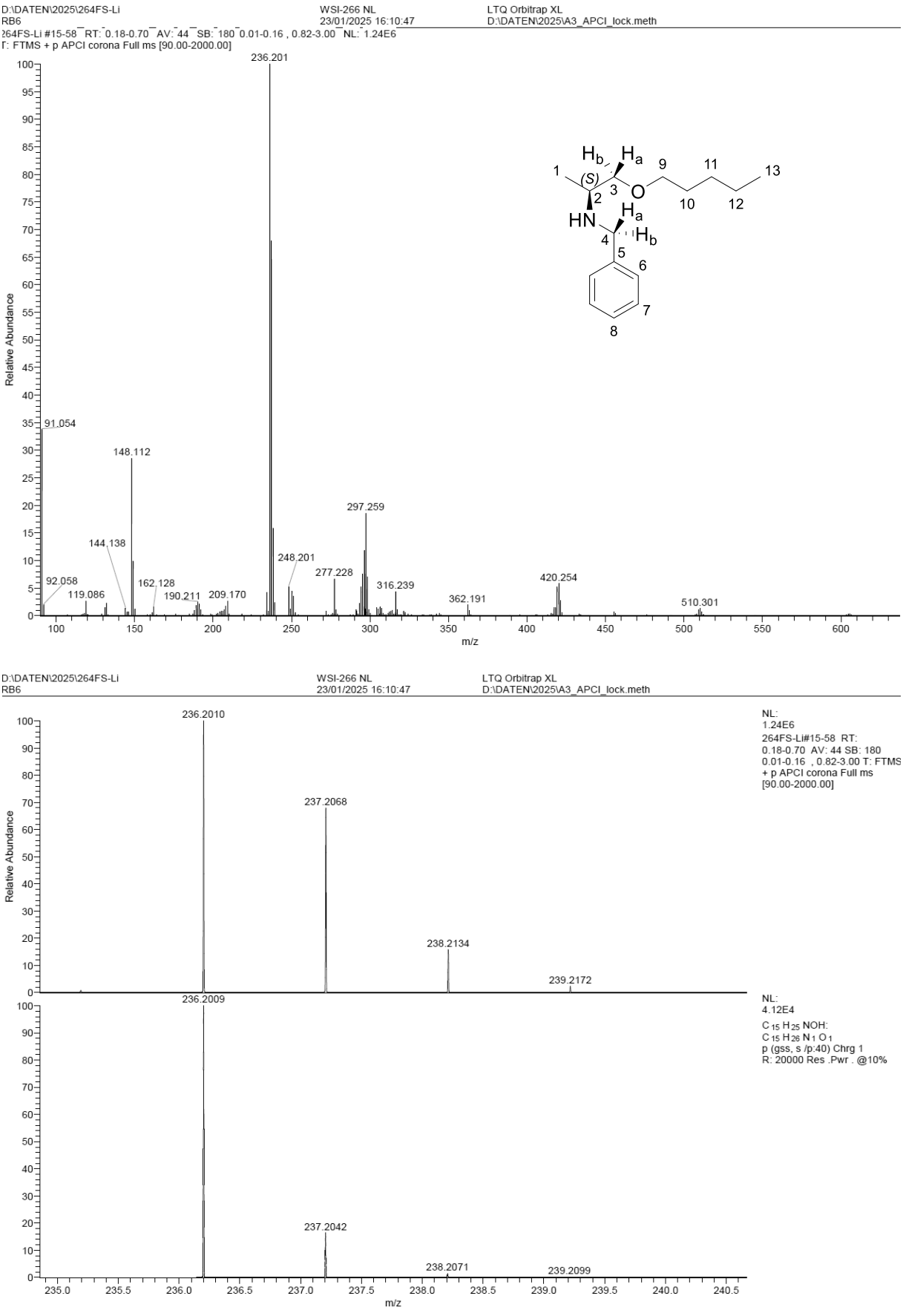

***Figure A80**: ESI(+) Mass spectra of N-benzyl -L-alaninyl pentyl ether (**47d**).*

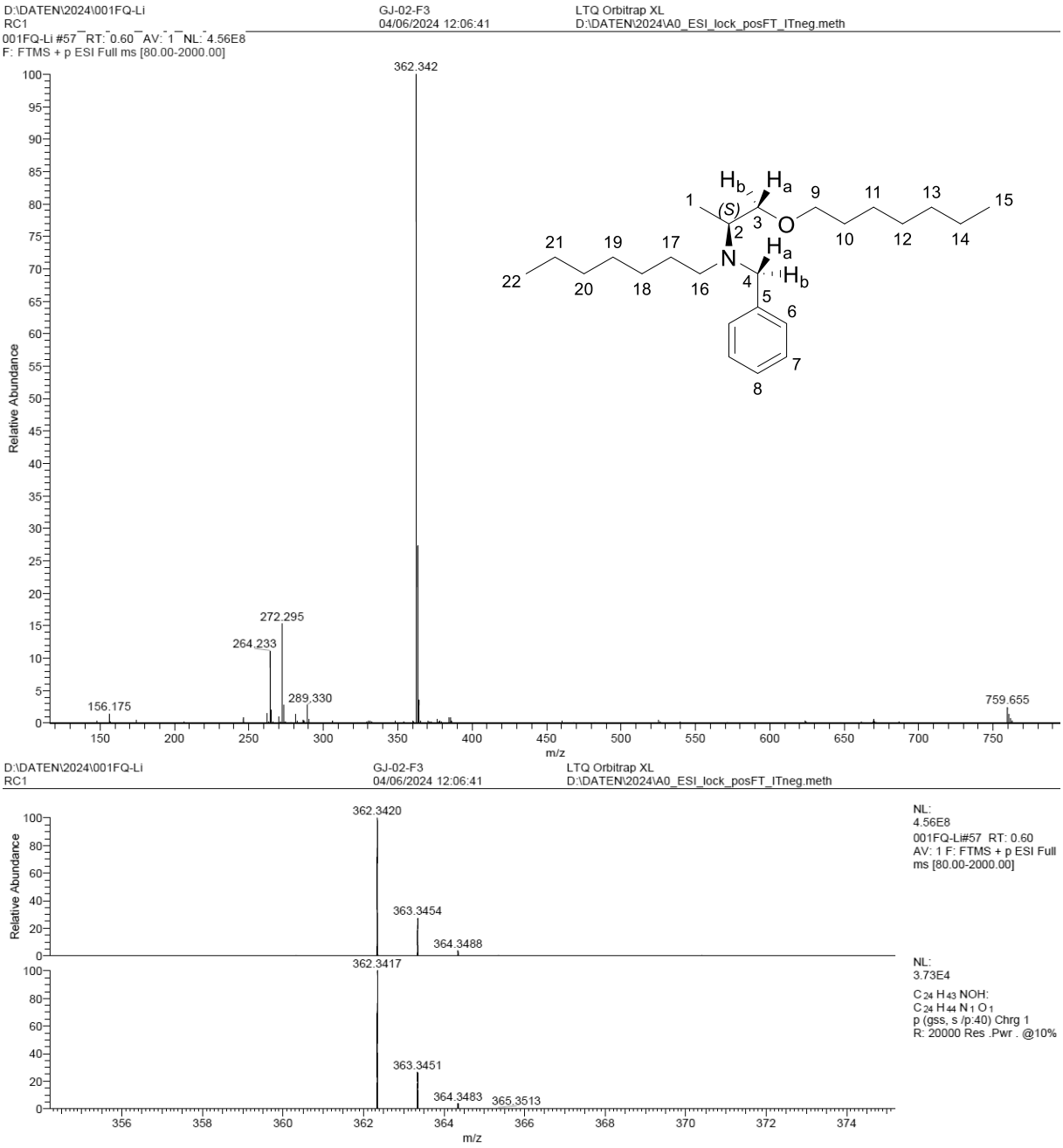

***Figure A81**: ESI(+) Mass spectra of N-benzyl-N-heptyl-L-alaninyl heptyl ether (**39e**).*

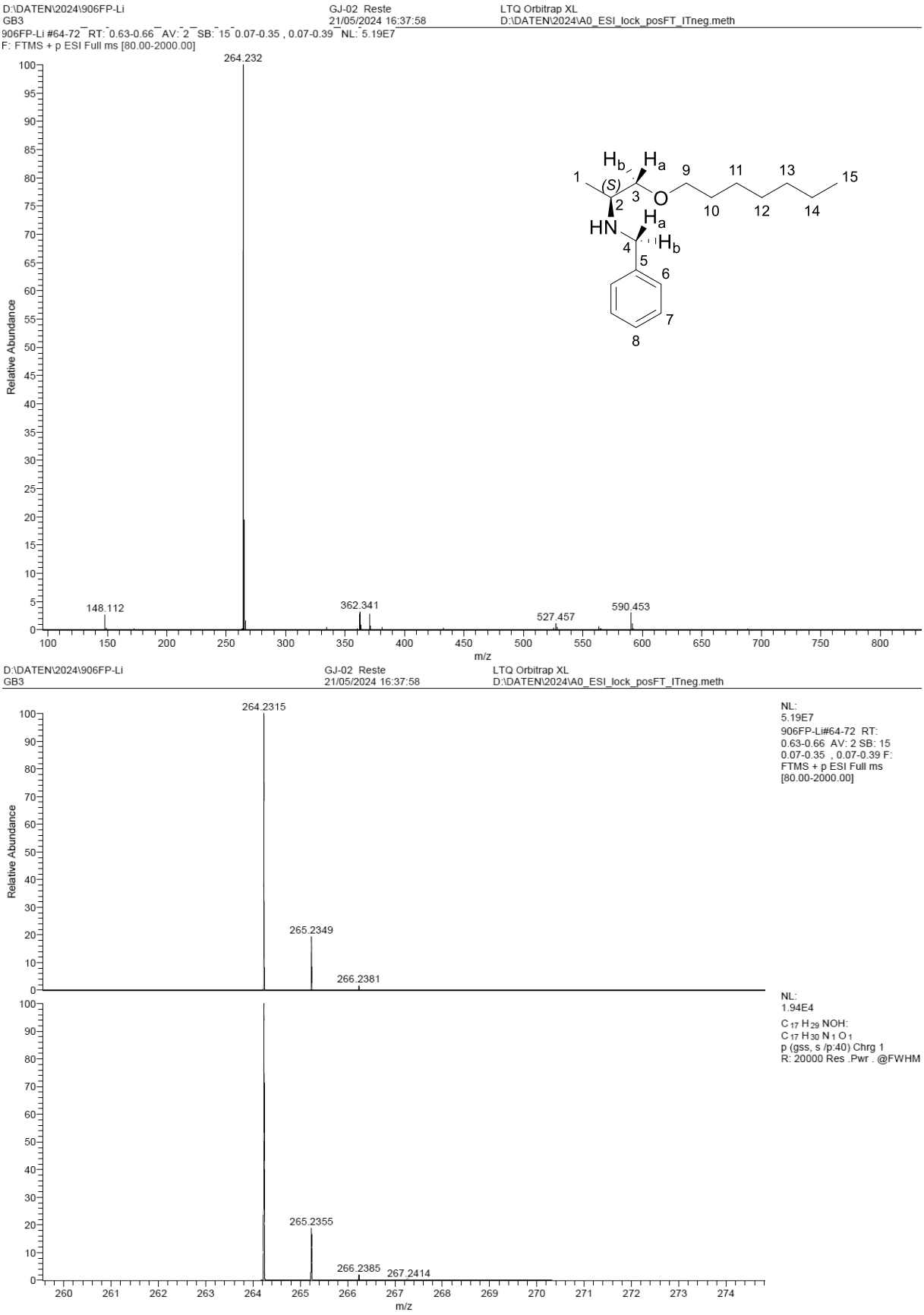

***Figure A82**: ESI(+) Mass spectra of N-benzyl -L-alaninyl heptyl ether (**47e**).*

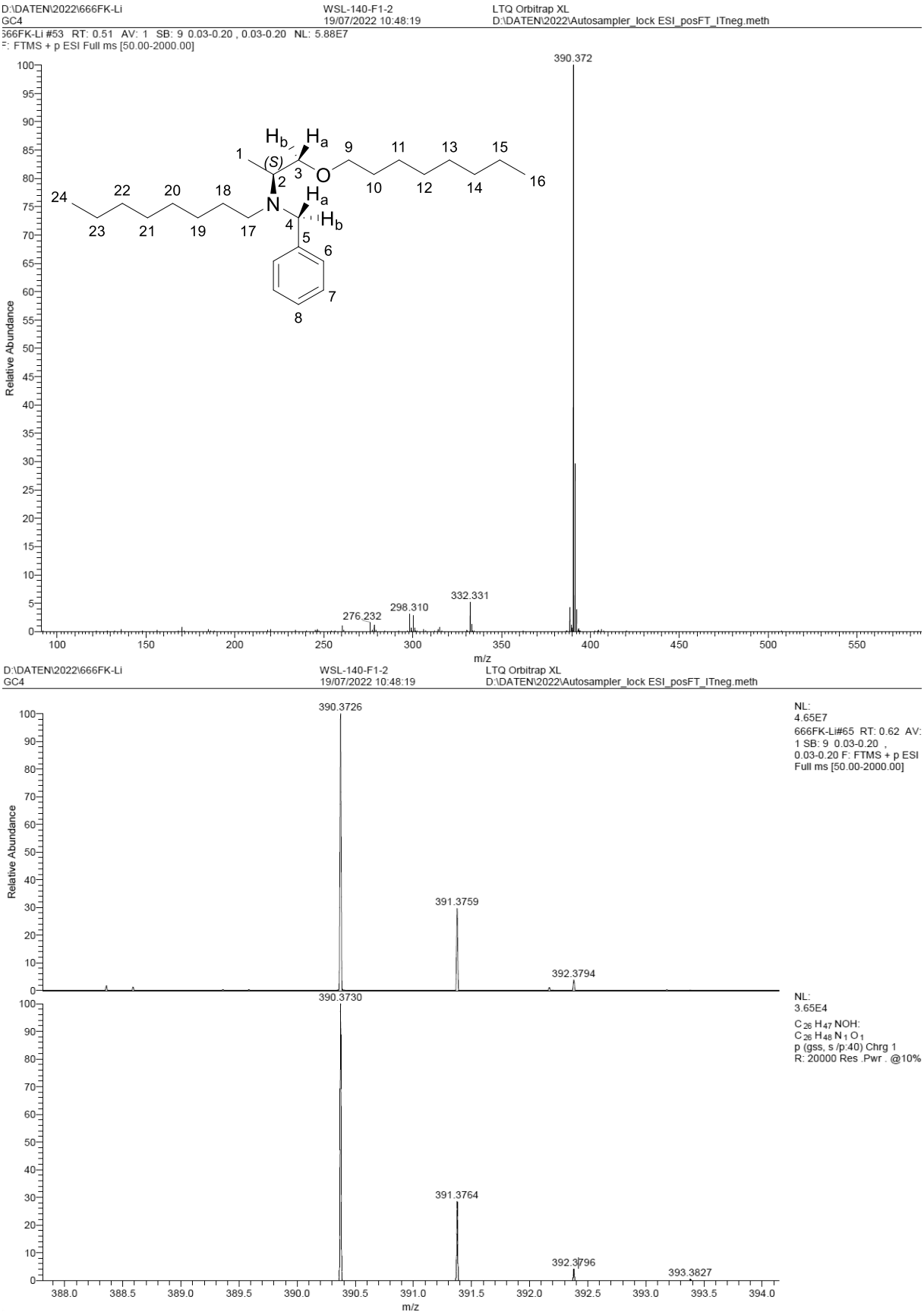

***Figure A83**: ESI(+) Mass spectra of N-benzyl-N-octyl-L-alaninyl octyl ether (**39f**).*

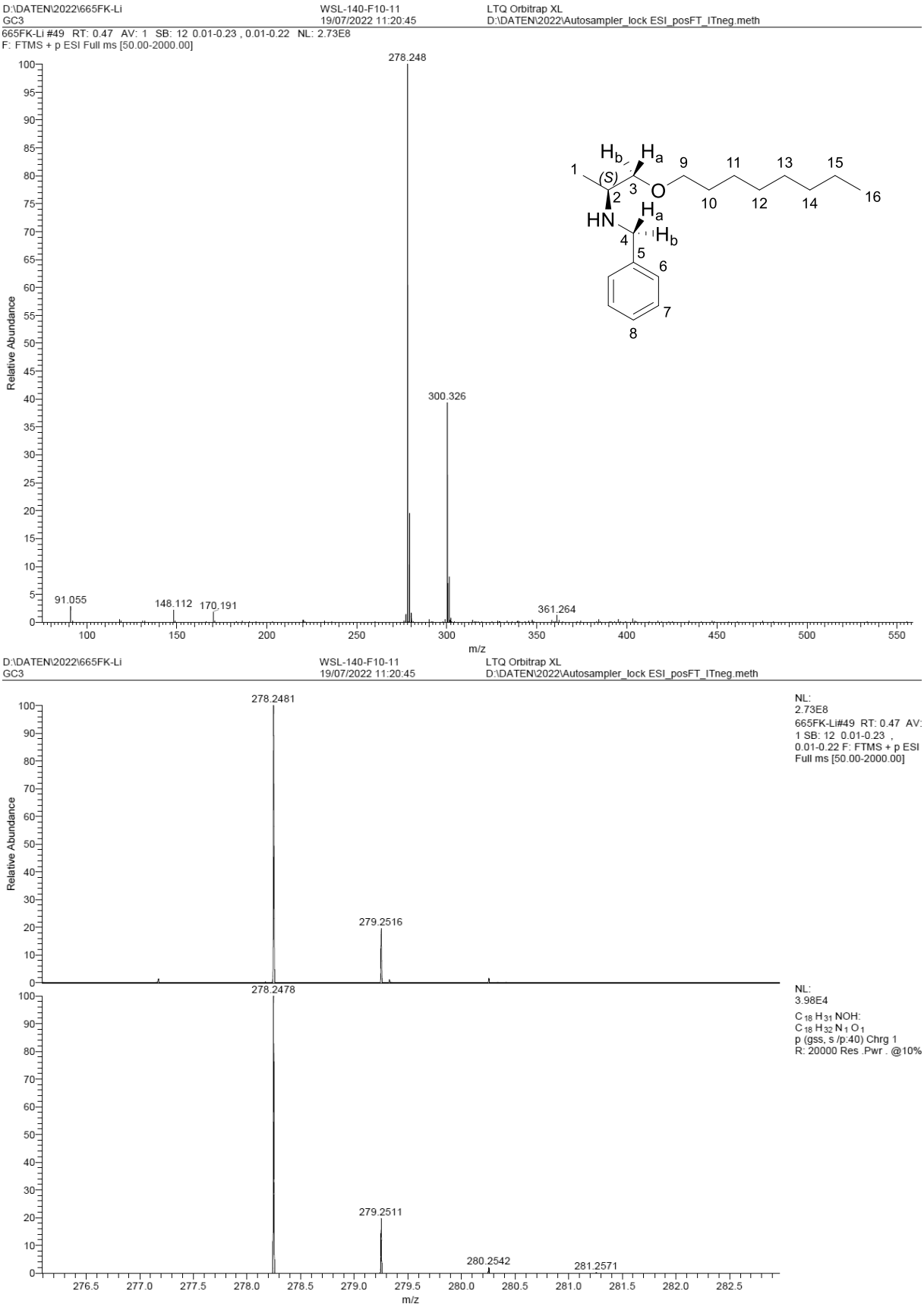

***Figure A84**: ESI(+) Mass spectra* of *N-benzyl -L-alaninyl octyl ether (**47f**).*

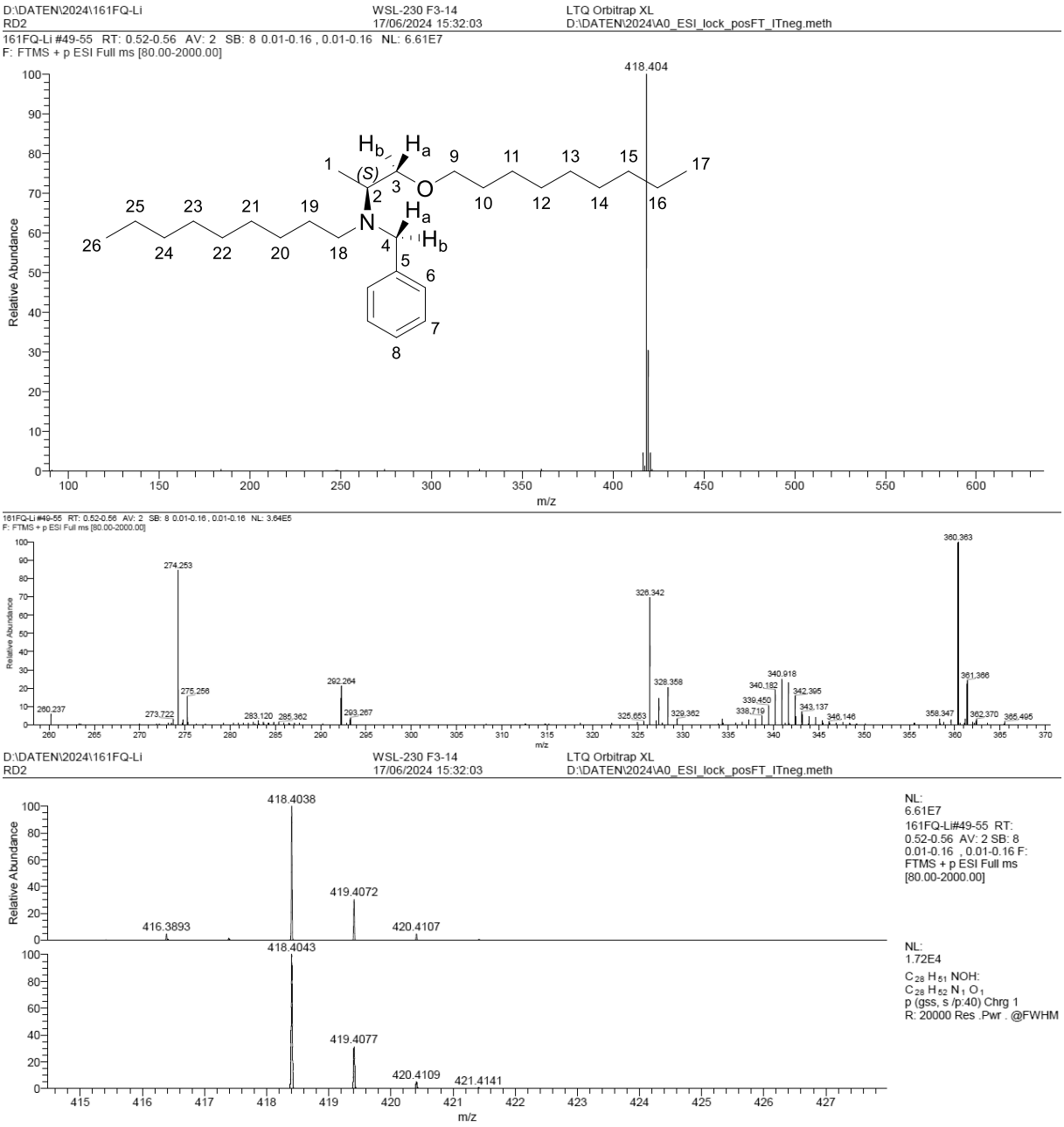

***Figure A85**: ESI(+) Mass spectra of N-benzyl-N-nonyl-L-alaninyl nonyl ether (**39g**).*

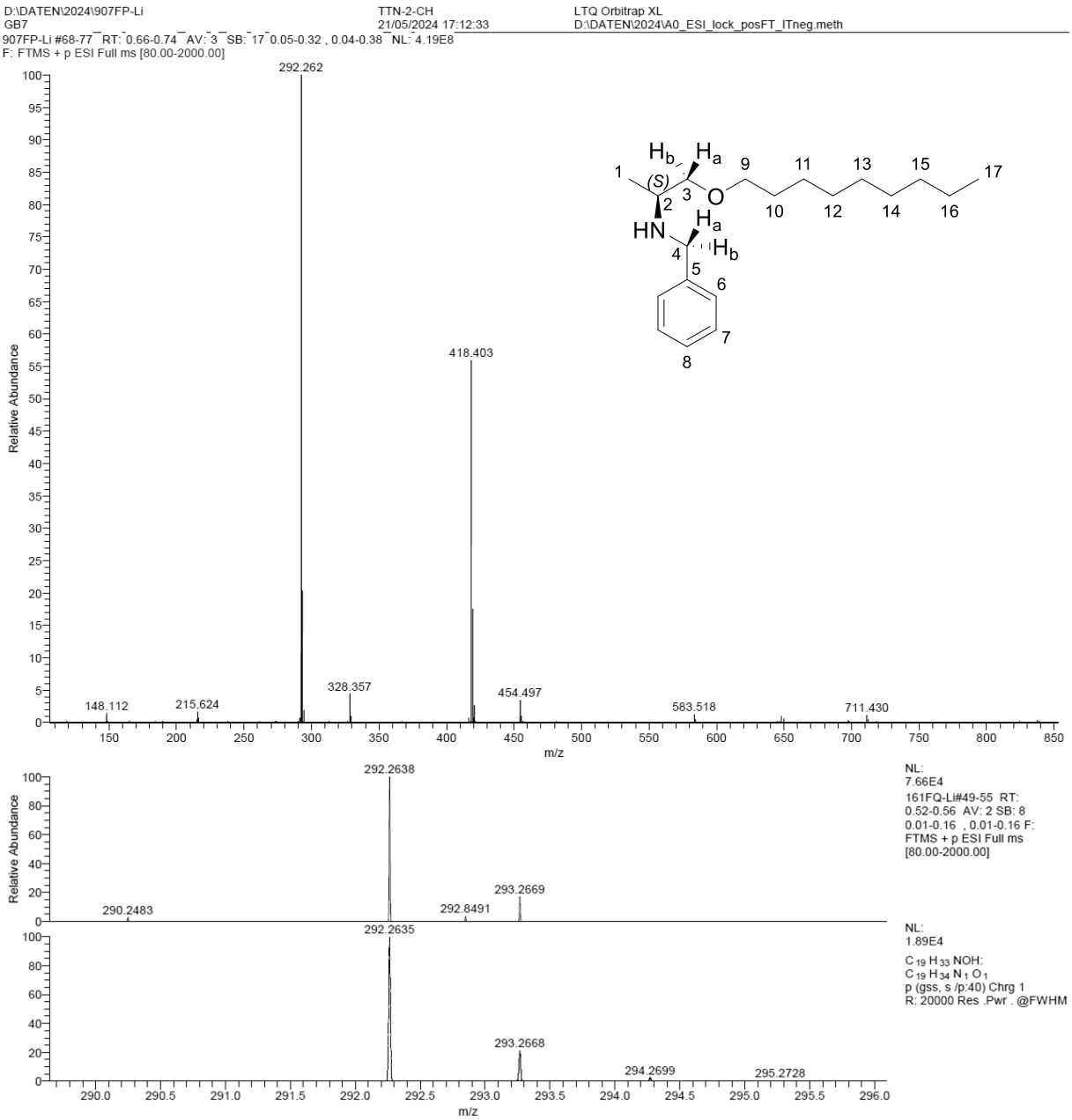

***Figure A86**: ESI(+) Mass spectra of N-benzyl -L-alaninyl nonyl ether (**47g**).*

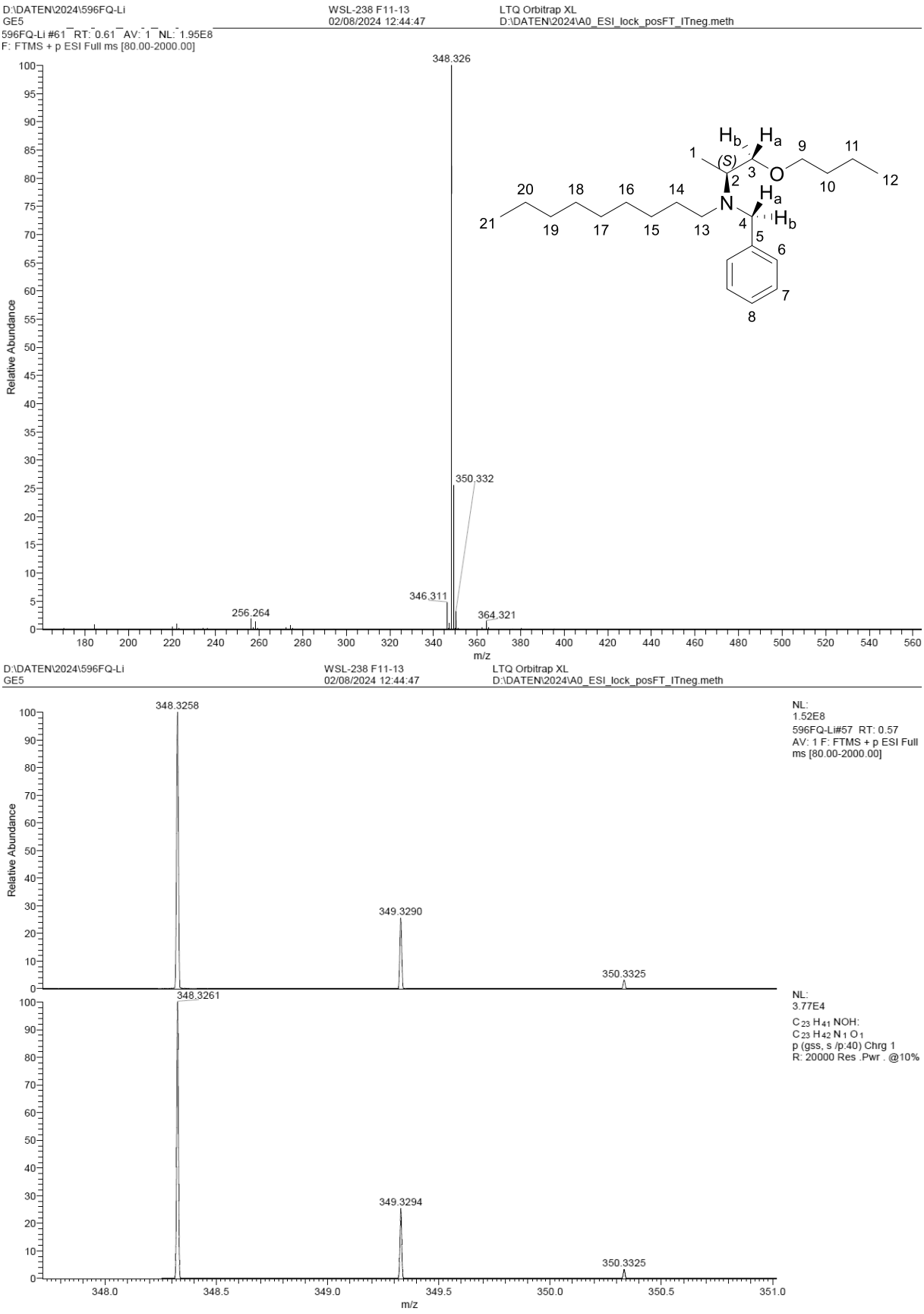

***Figure A87**: ESI(+) Mass spectra of N-benzyl-N-nonyl-L-alaninyl butyl ether (**39h**).*

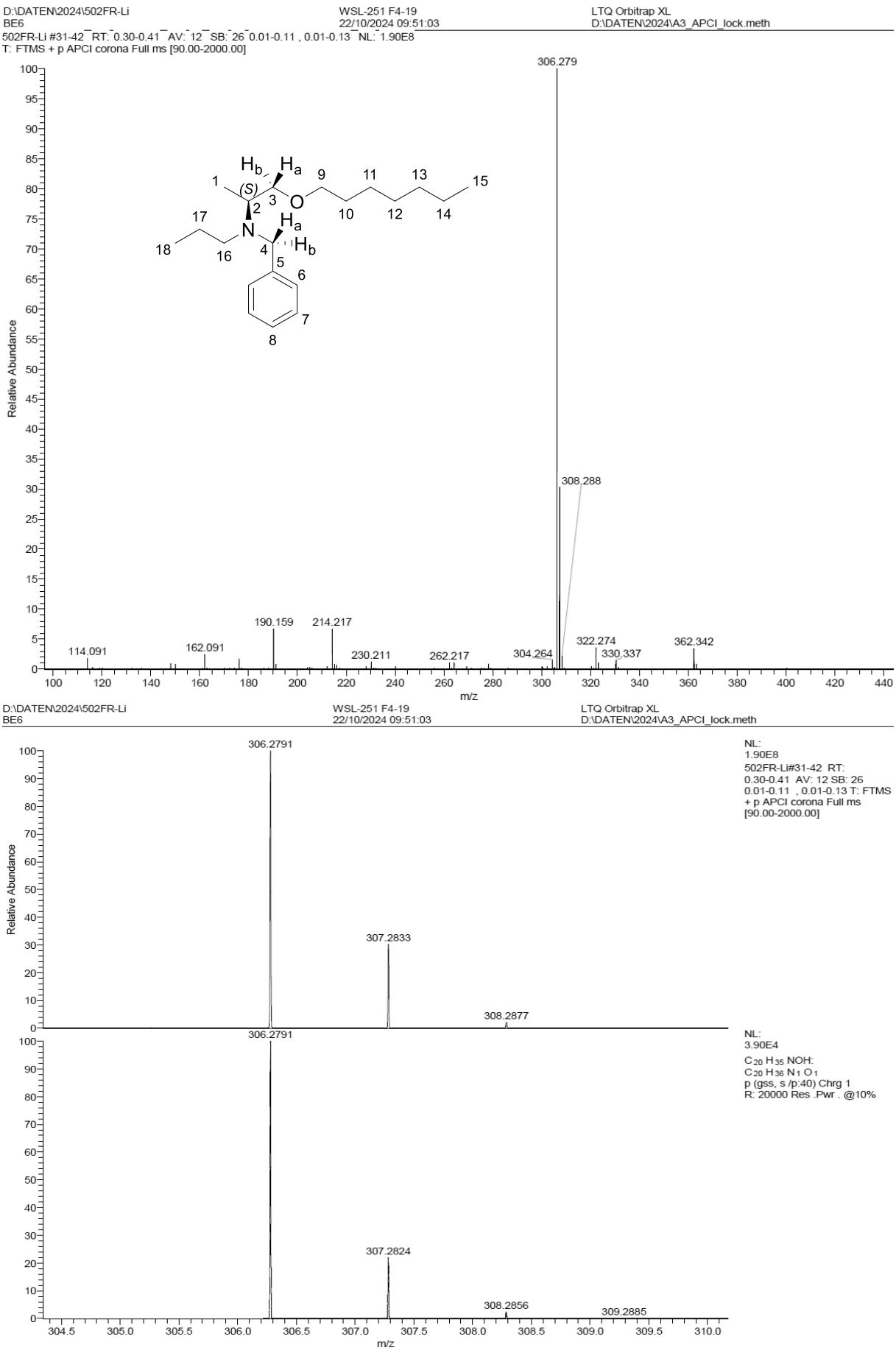

***Figure A88**: APCI Mass spectra of N-benzyl-N-propyl-L-alaninyl heptyl ether (**39i**).*

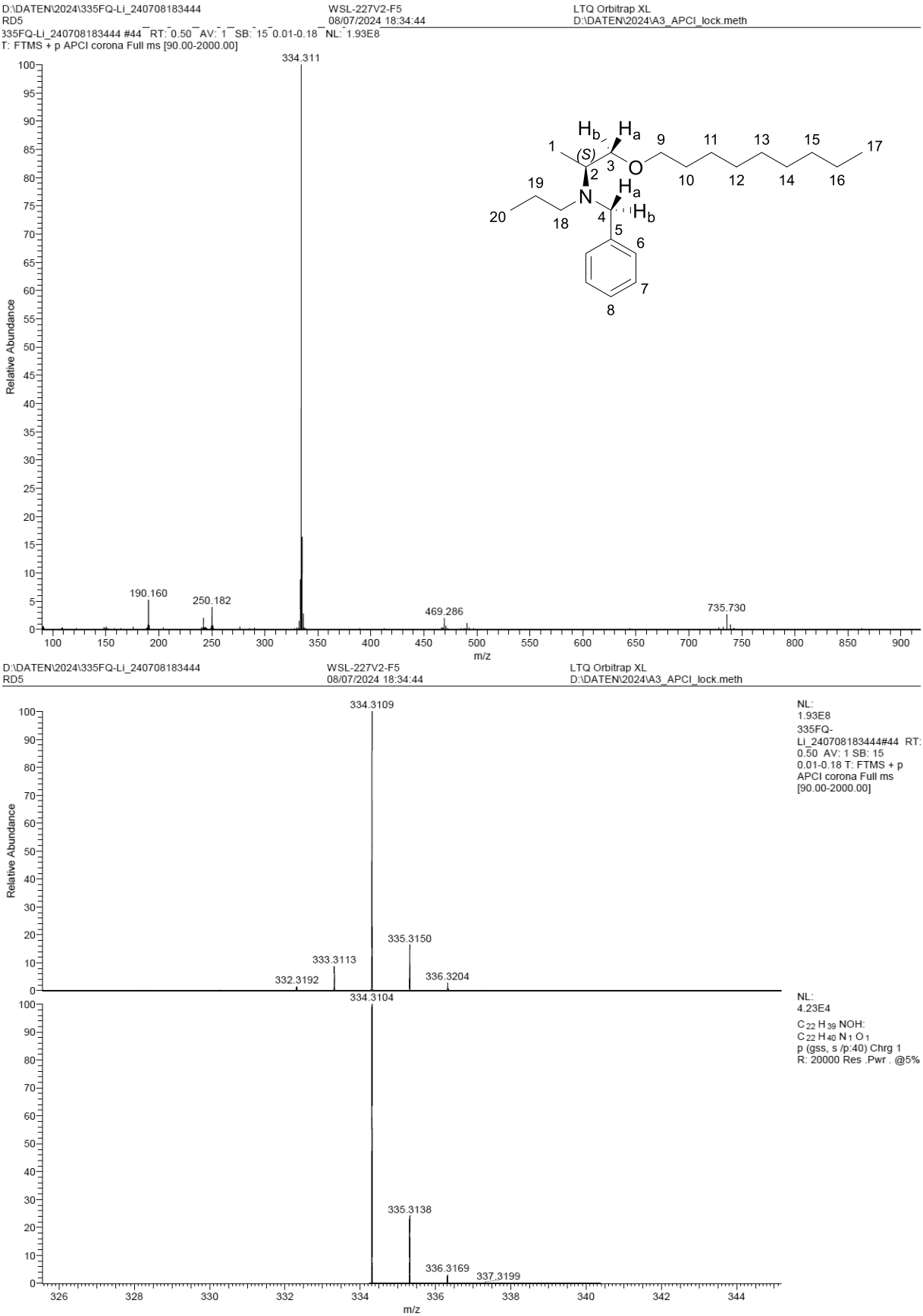

***Figure A89**: APCI Mass spectra of N-benzyl-N-propyl-L-alaninyl nonyl ether (**39j**).*

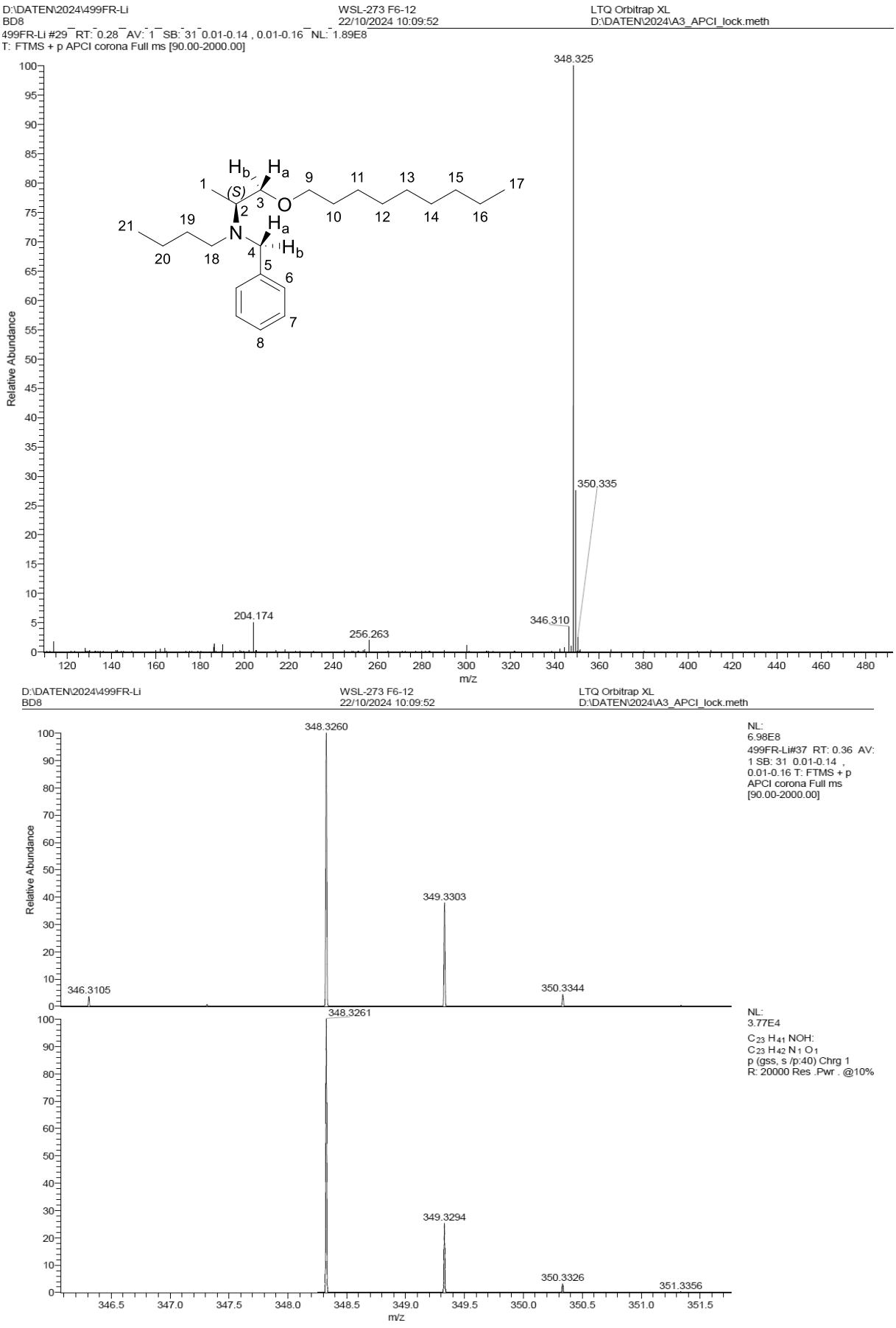

***Figure A90**: APCI Mass spectra of N-benzyl-N-butyl-L-alaninyl nonyl ether (**39k**).*

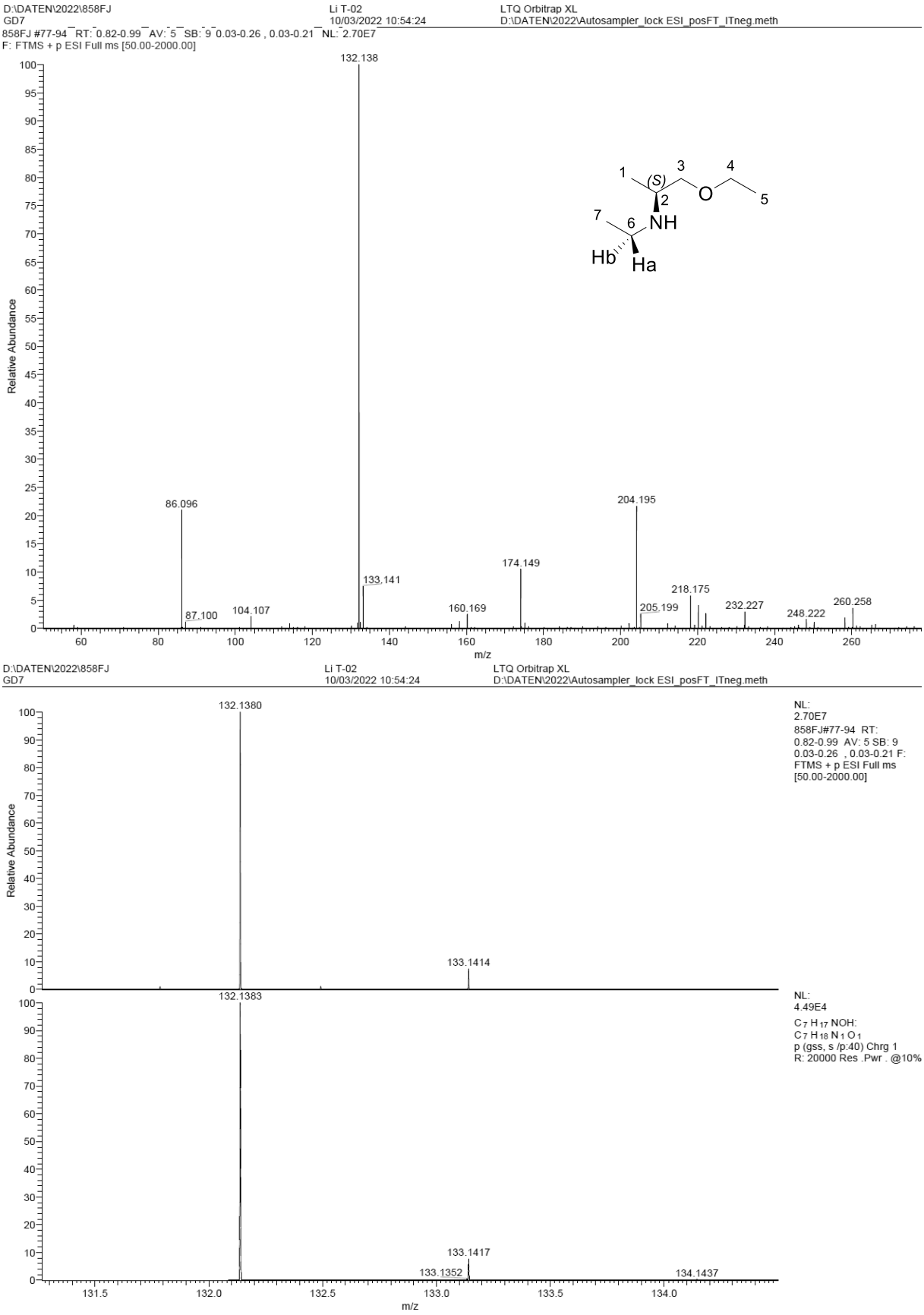

***Figure A91**: ESI(+) Mass spectra of O-ethyl-L-alaninyl N-ethyl amine (**22a**).*

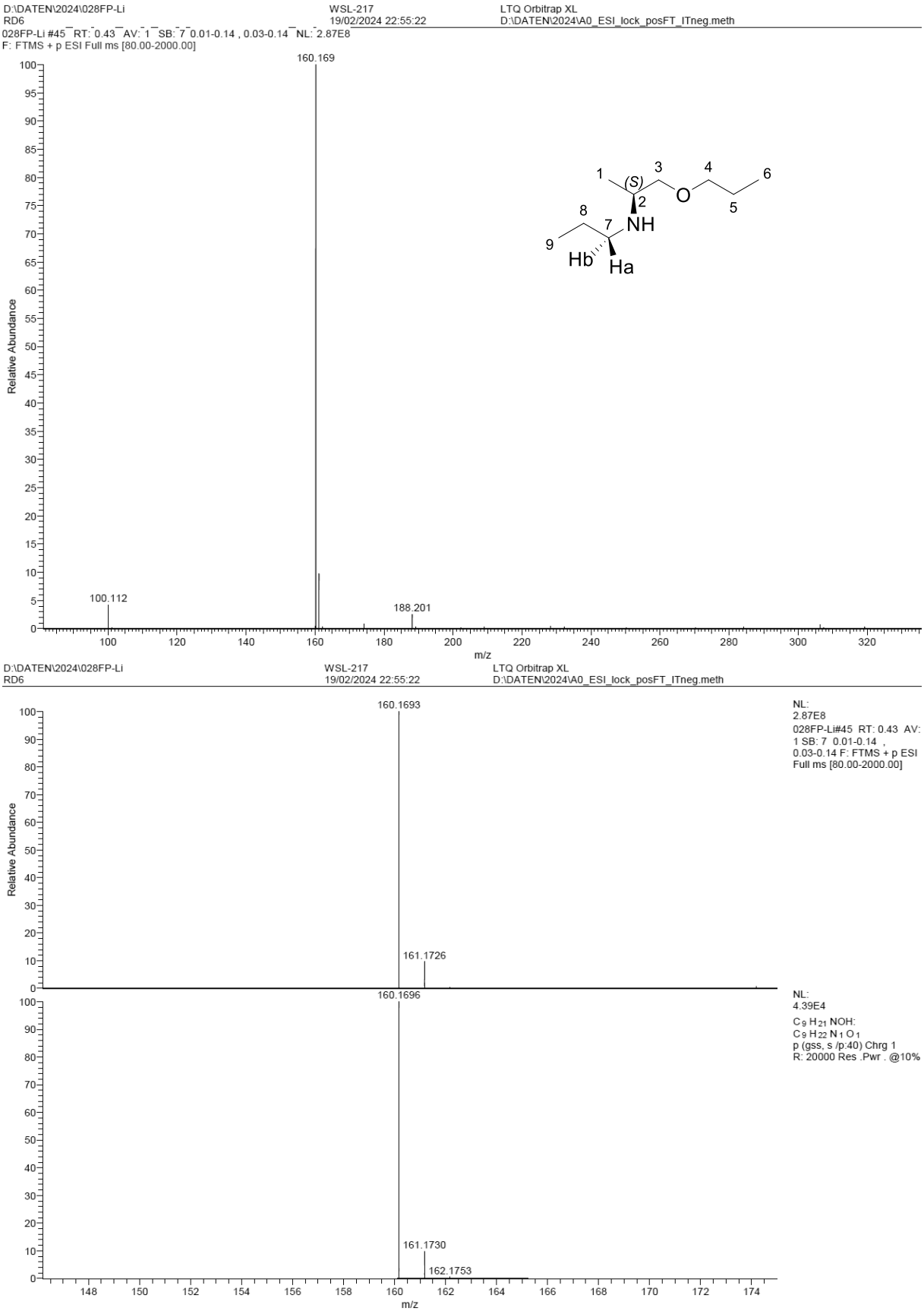

***Figure A92**: ESI (+) Mass spectra of O-propyl-L-alaninyl N-propyl amine (**22b**).*

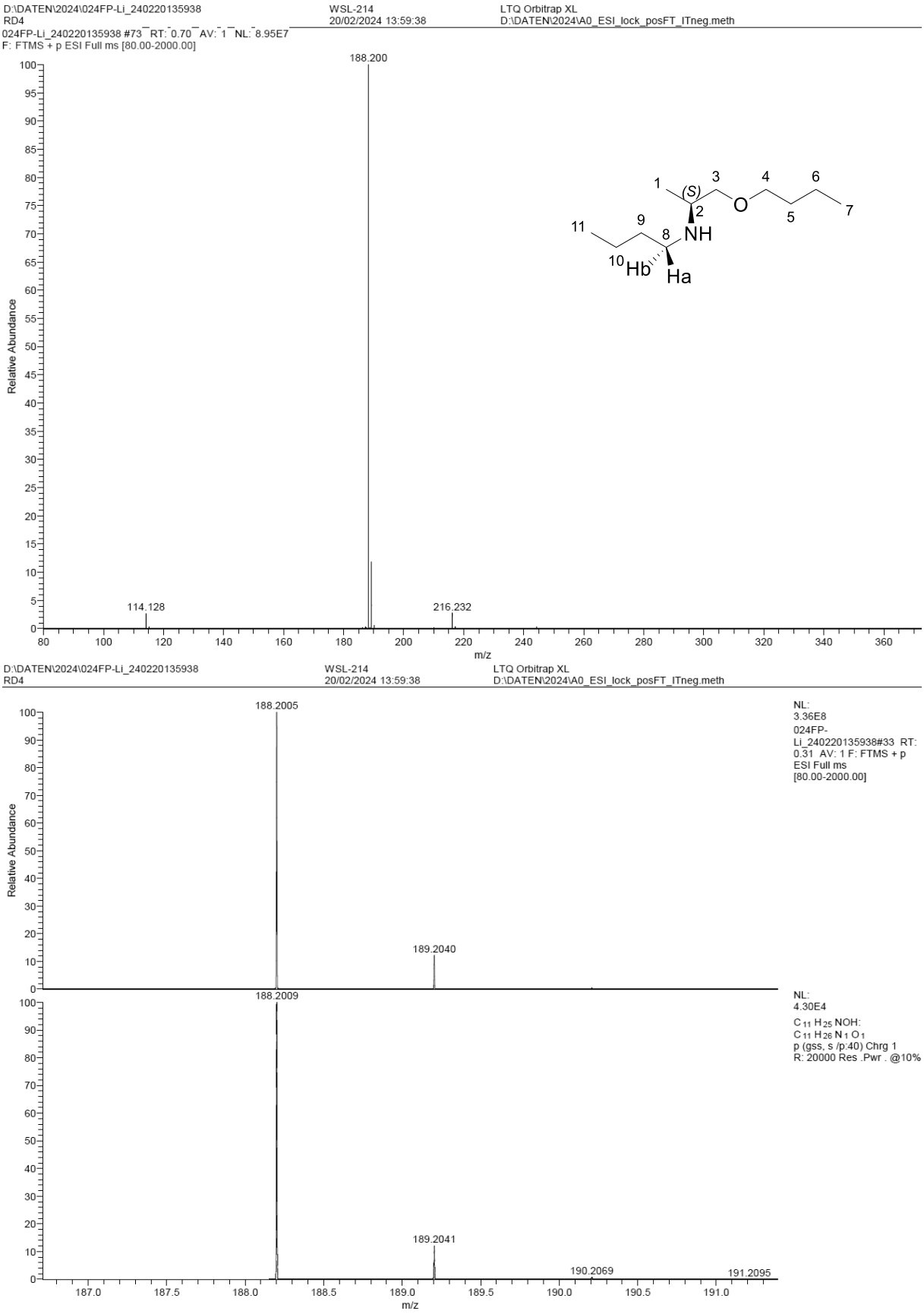

***Figure A93**: ESI (+) Mass spectra of O-butyl-L-alaninyl N-butyl amine (**22c**).*

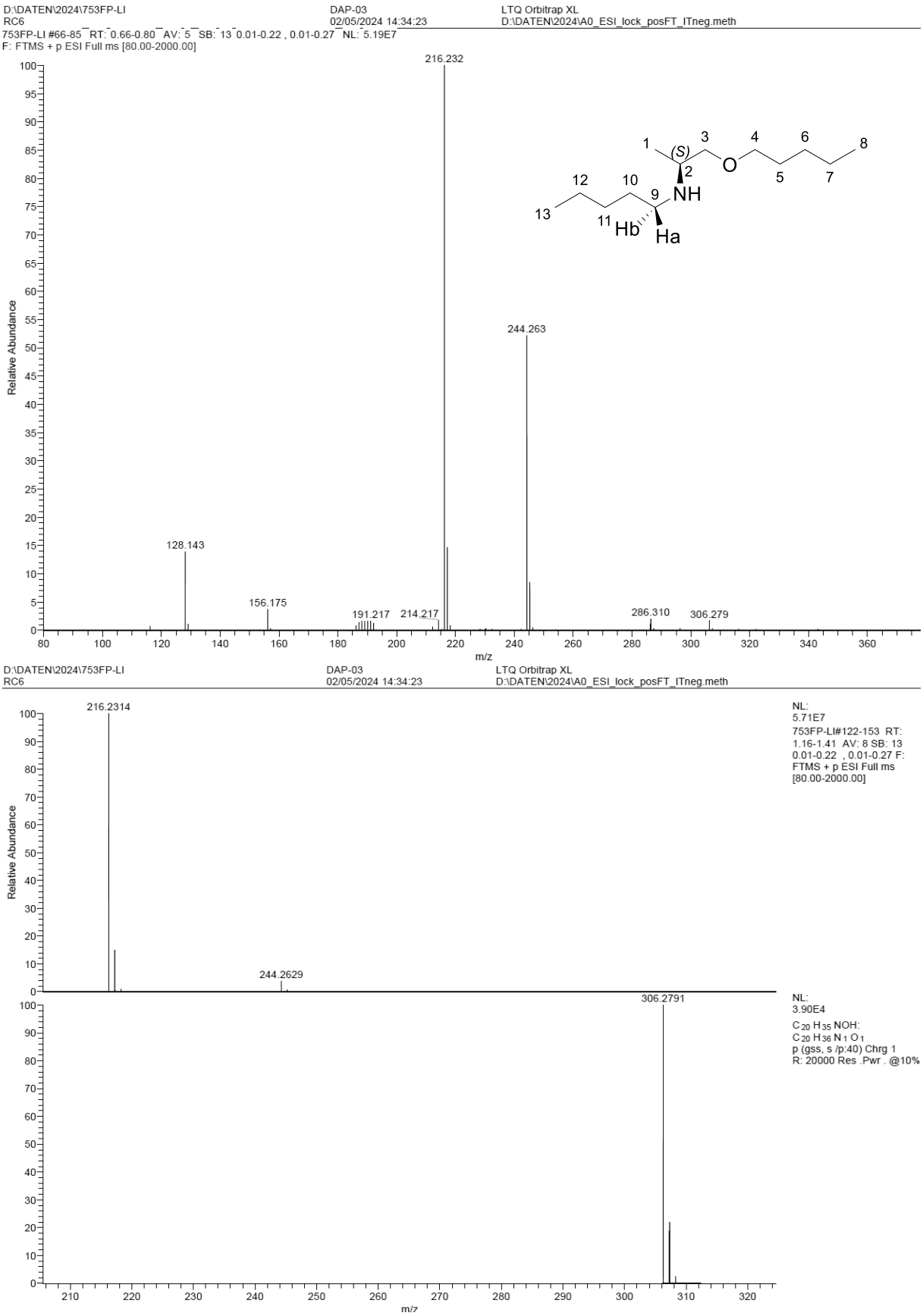

***Figure A94**: ESI (+) Mass spectra of O-pentyl-L-alaninyl N-pentyl amine (**22d**).*

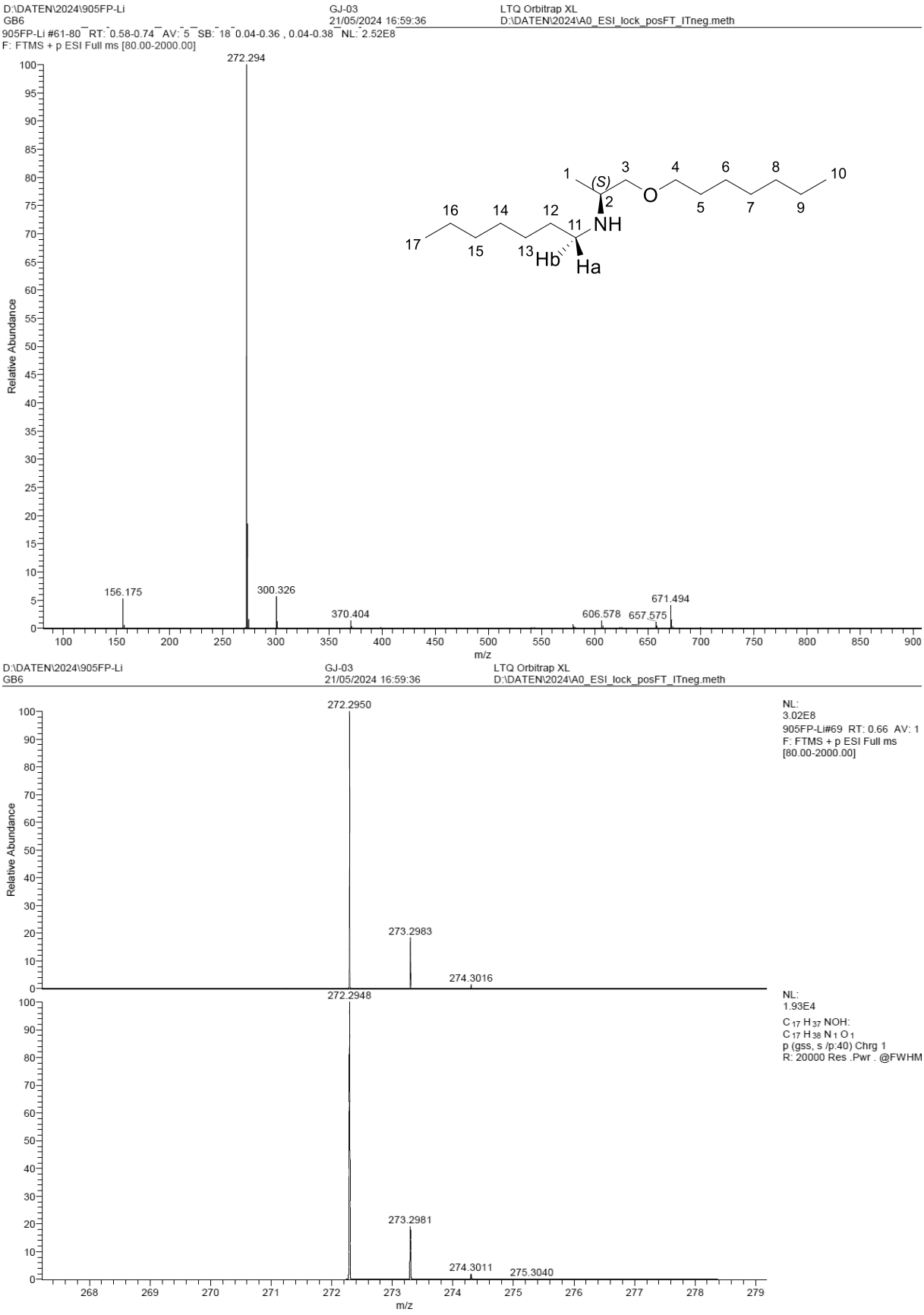

***Figure A95**: ESI (+) Mass spectra of O-heptyl-L-alaninyl N-heptyl amine (**22e**).*

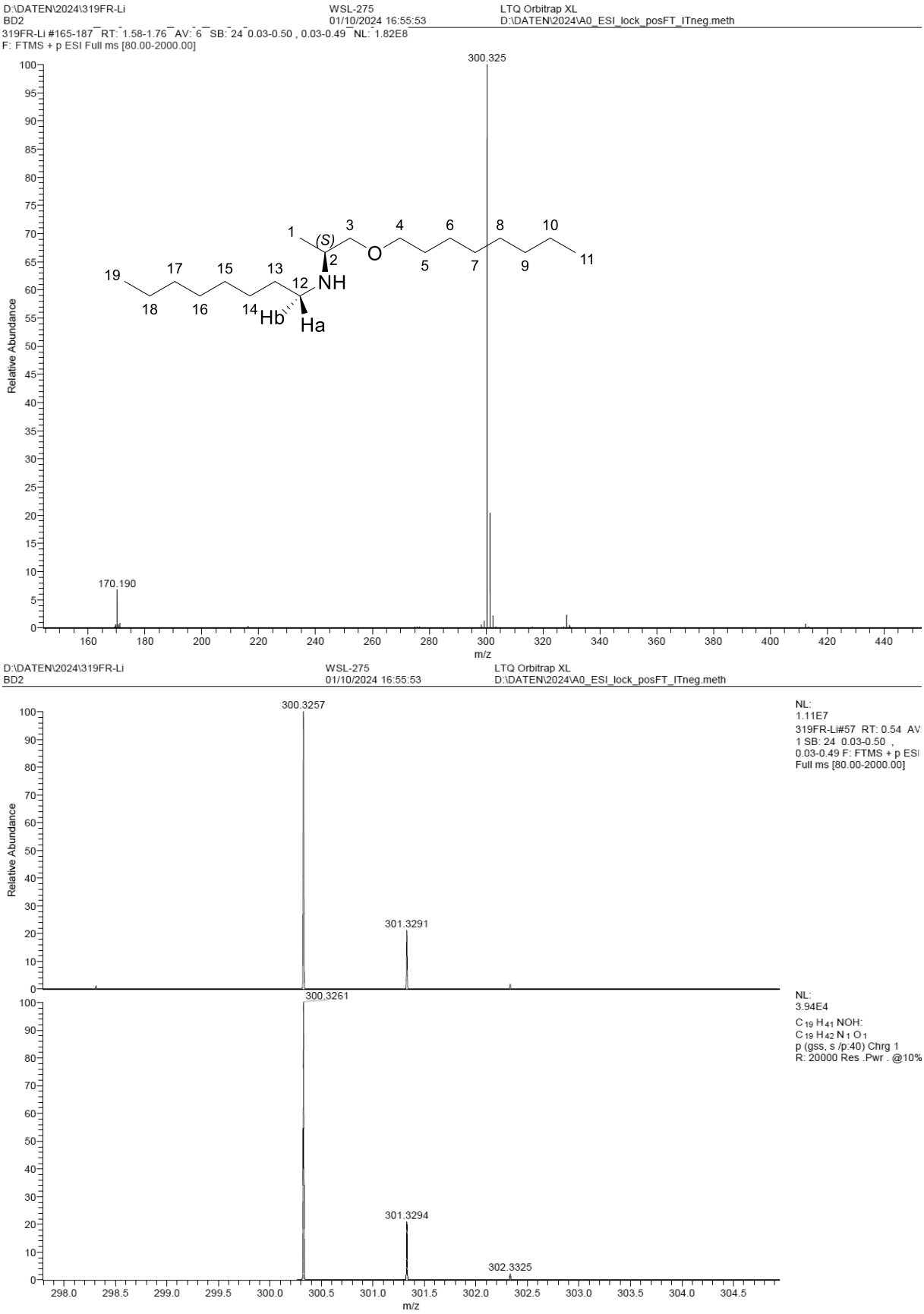

***Figure A96**: ESI (+) Mass spectra of O-octyl-L-alaninyl N-octyl amine (**22f**).*

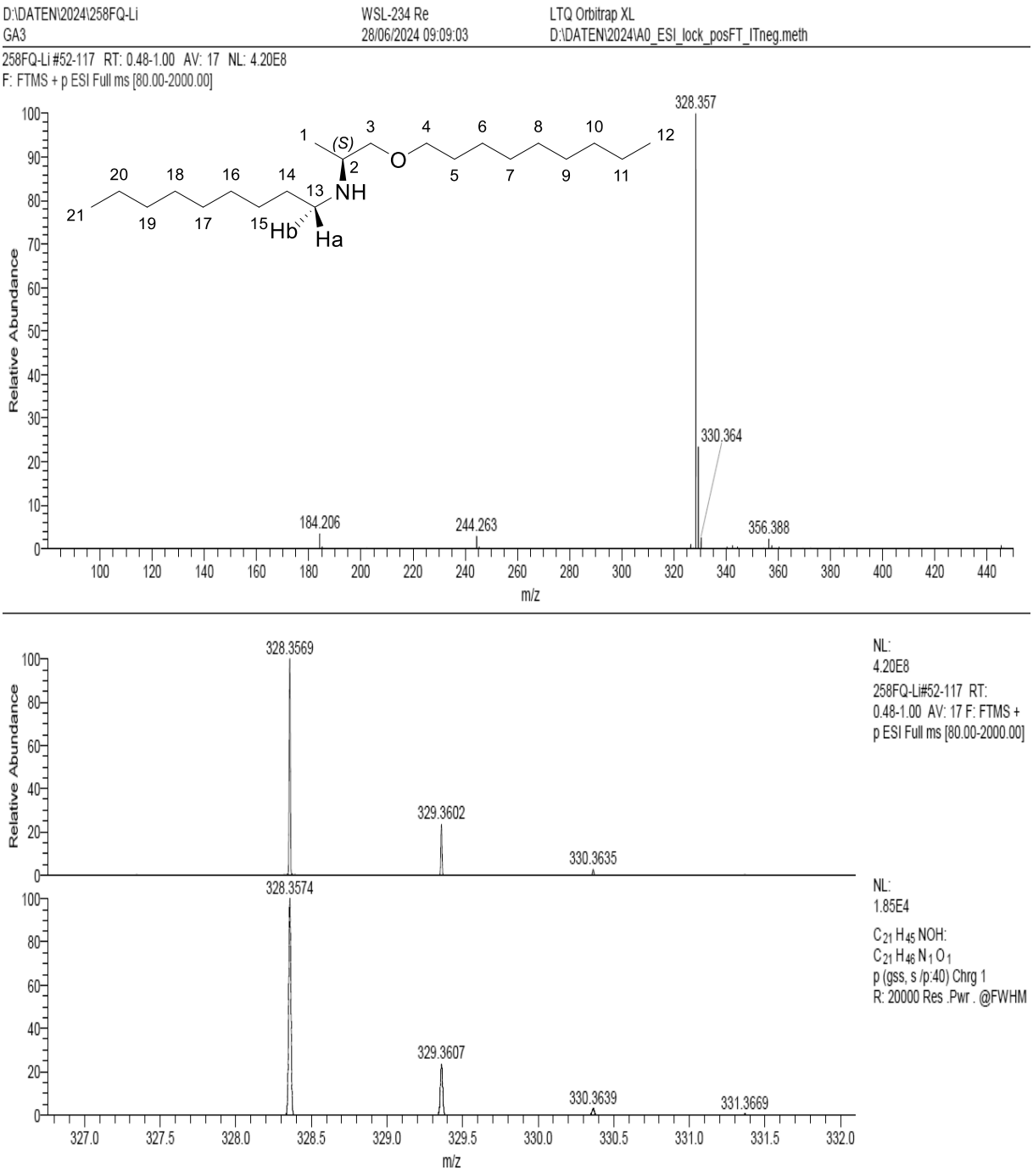

***Figure A97**: ESI (+) Mass spectra of O-nonyl-L-alaninyl N-nonyl amine (**22g**).*

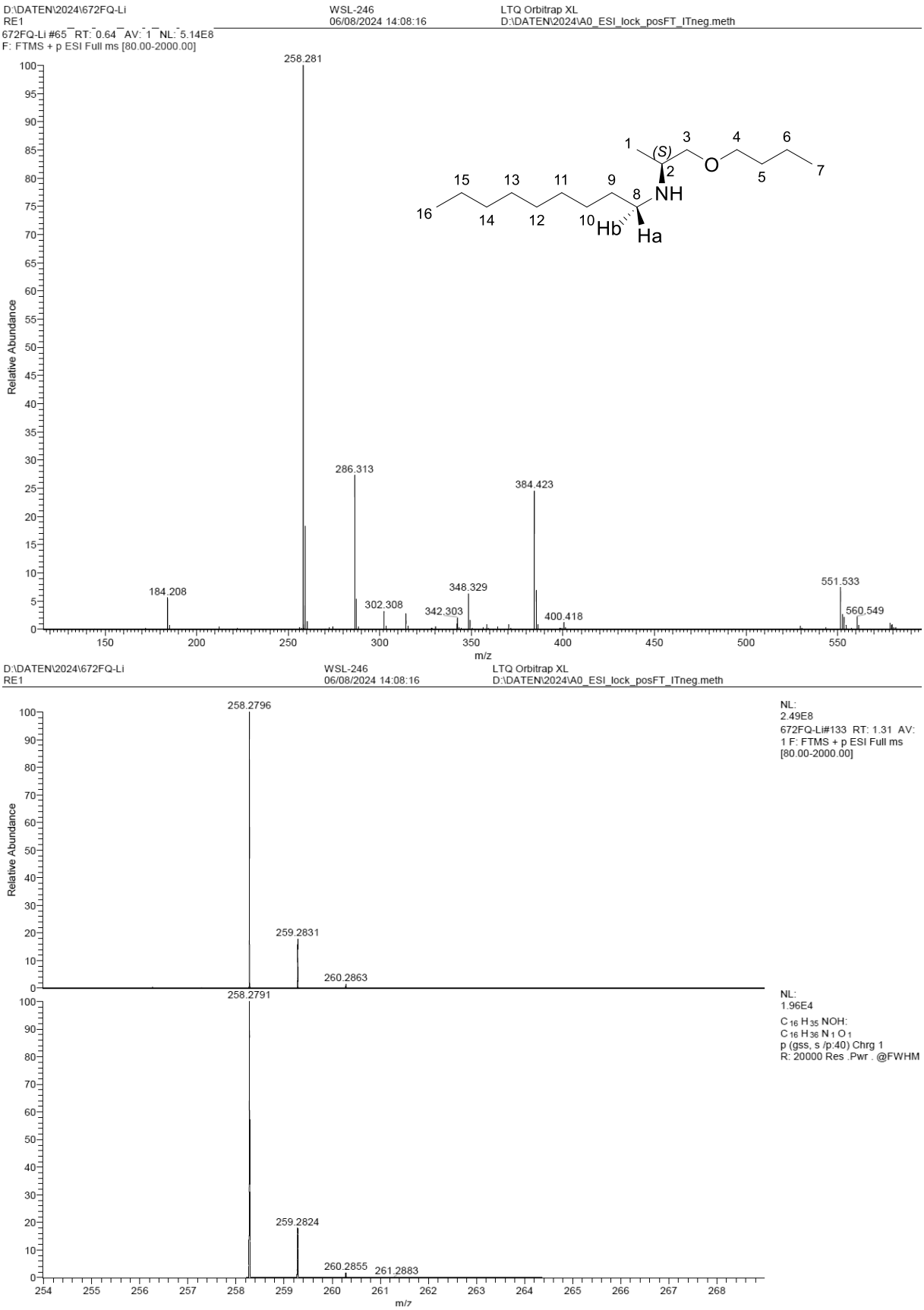

***Figure A98**: ESI (+) Mass spectra of O-butyl-L-alaninyl N-nonyl amine (**22h**).*

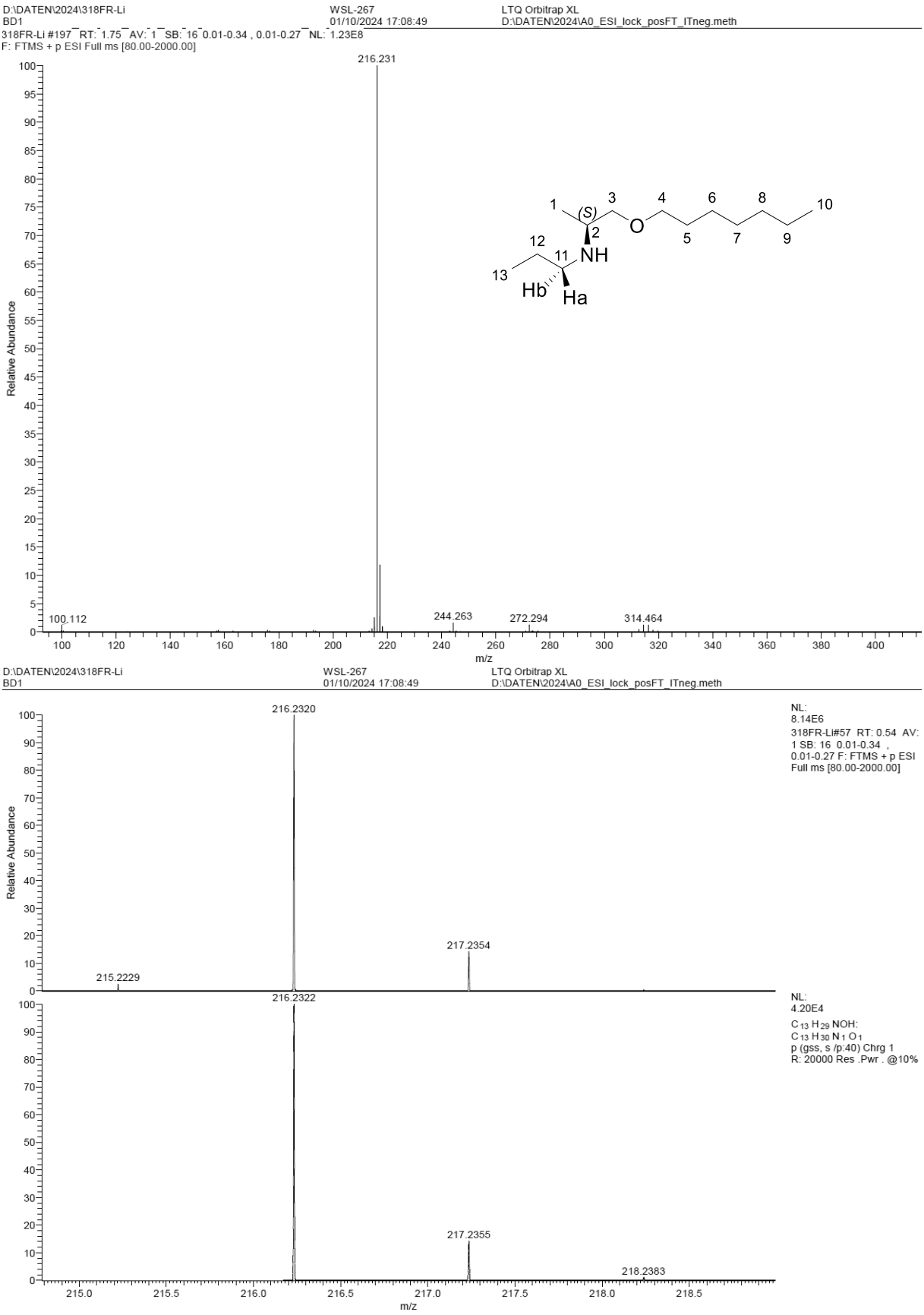

***Figure A99**: ESI (+) Mass spectra of O-heptyl-L-alaninyl N-propyl amine (**22i**).*

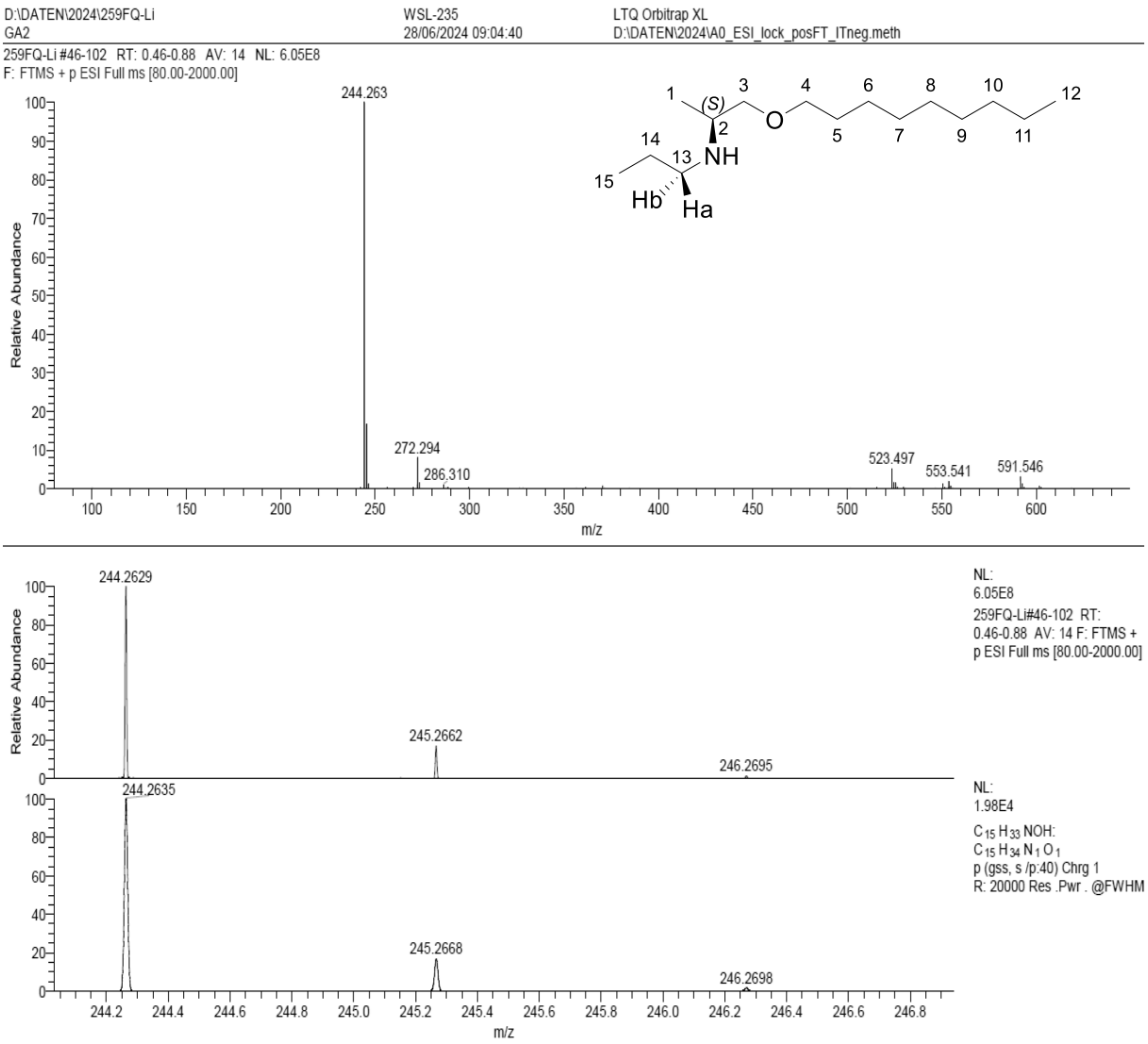

***Figure A100**: ESI (+) Mass spectra of O-nonyl-L-alaninyl N-propyl amine (**22j**).*

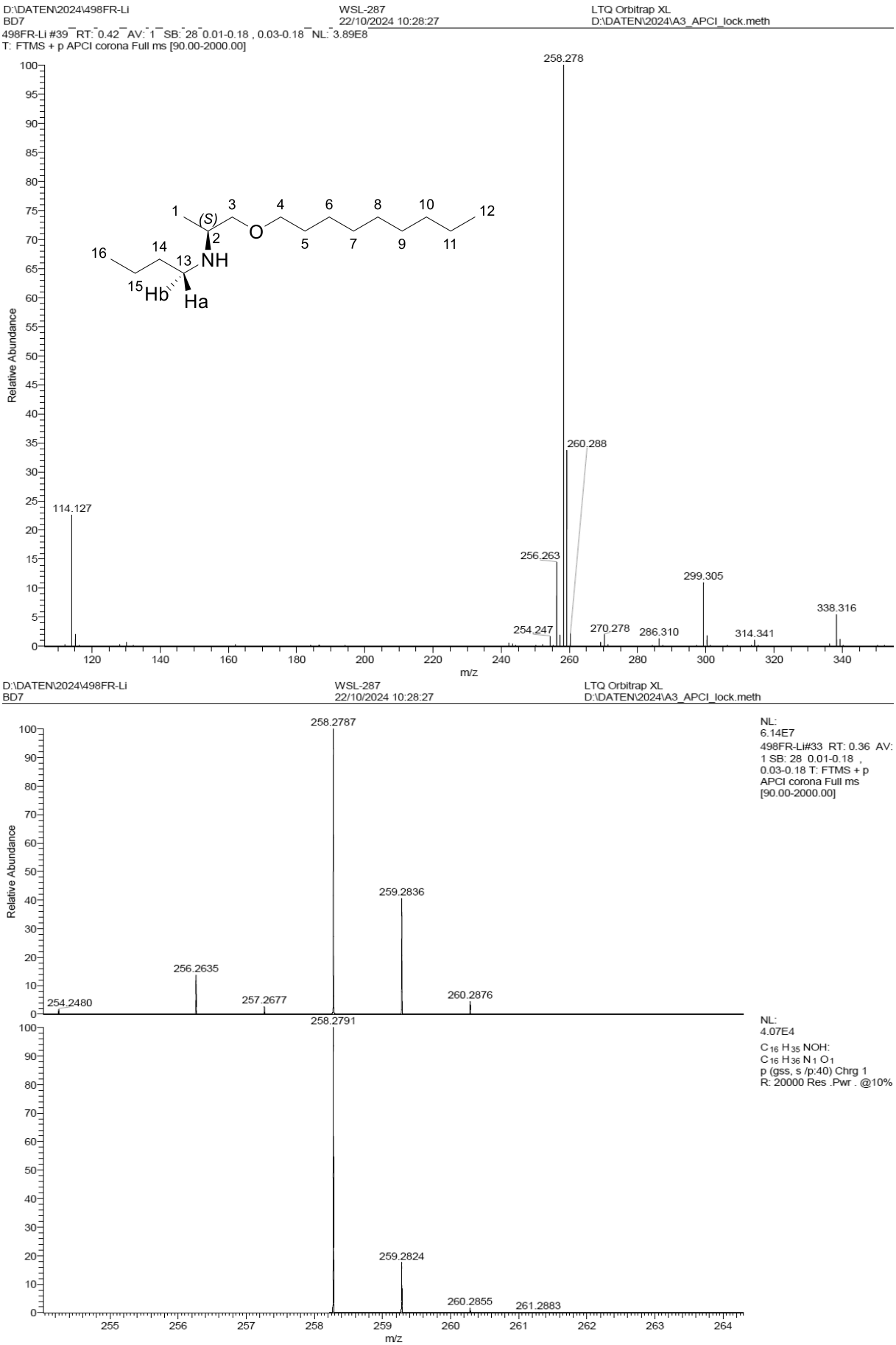

***Figure A101**: APCI Mass spectra of O-nonyl-L-alaninyl N-butyl amine (**22k**).*

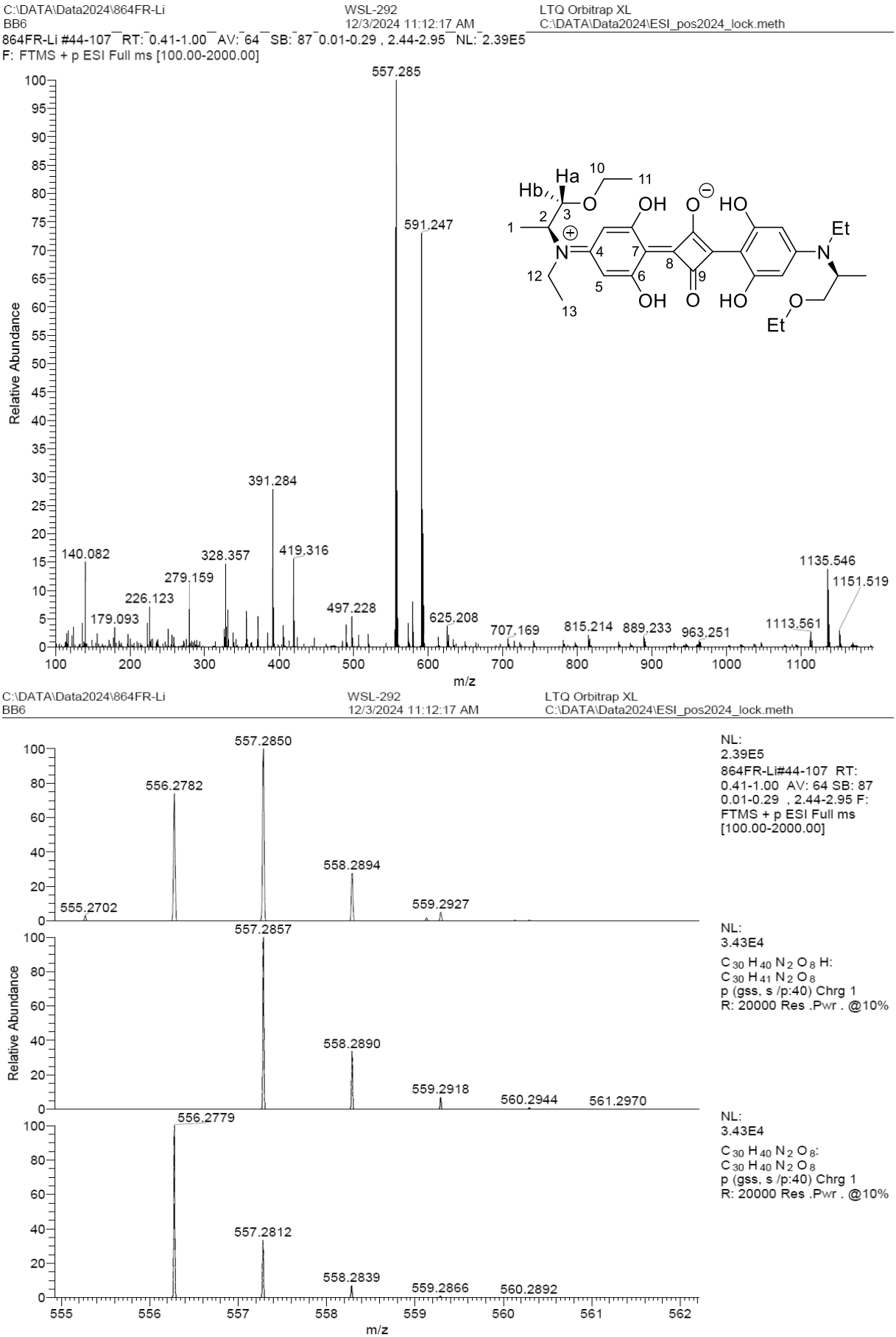

***Figure A102**: ESI (+) Mass spectra of **(S,S)-N-C2,O-C2-AlaSQ (23a)**.*

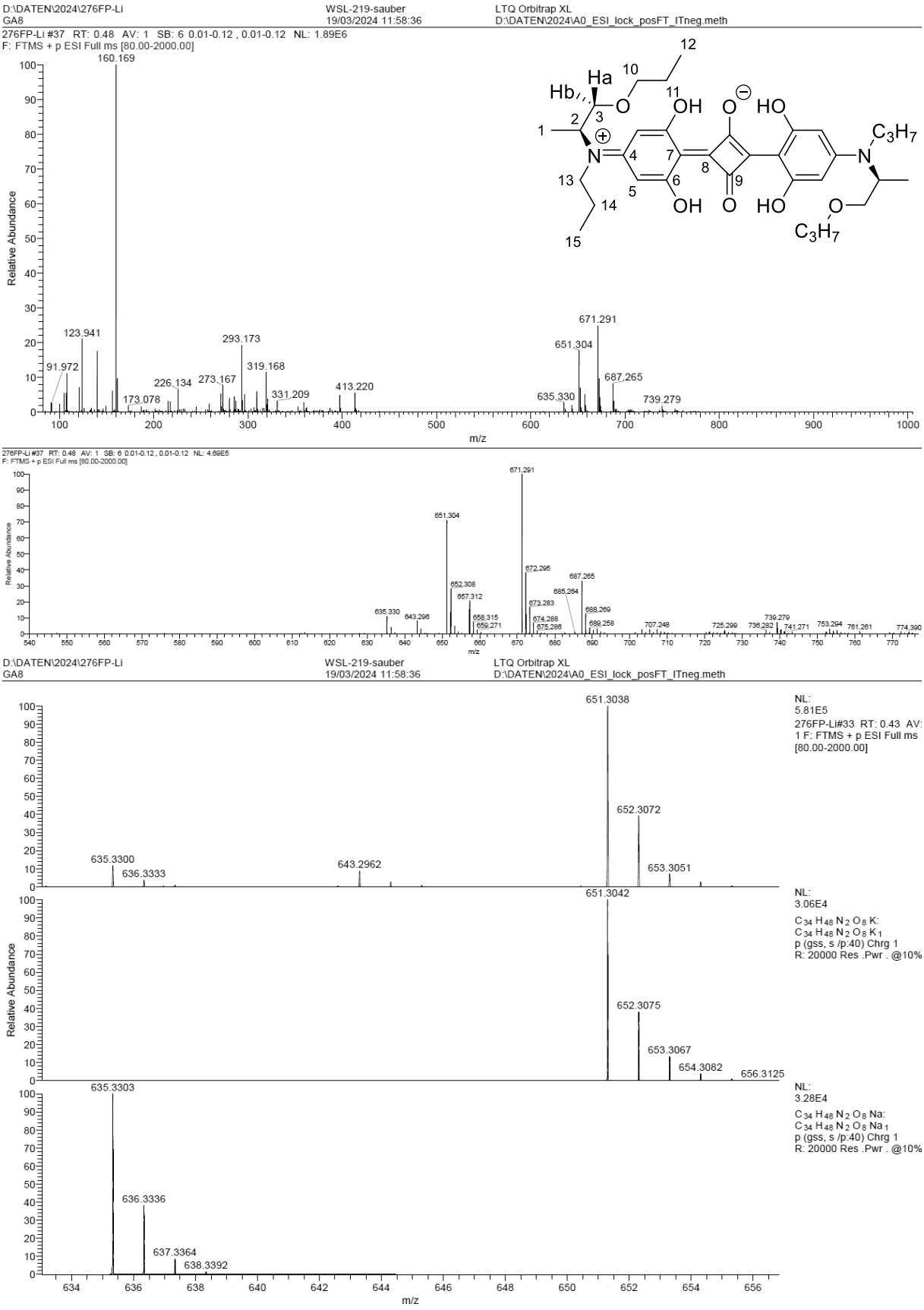

***Figure A103**: ESI (+) Mass spectra of **(S,S)-N-C3,O-C3-AlaSQ (23b)**.*

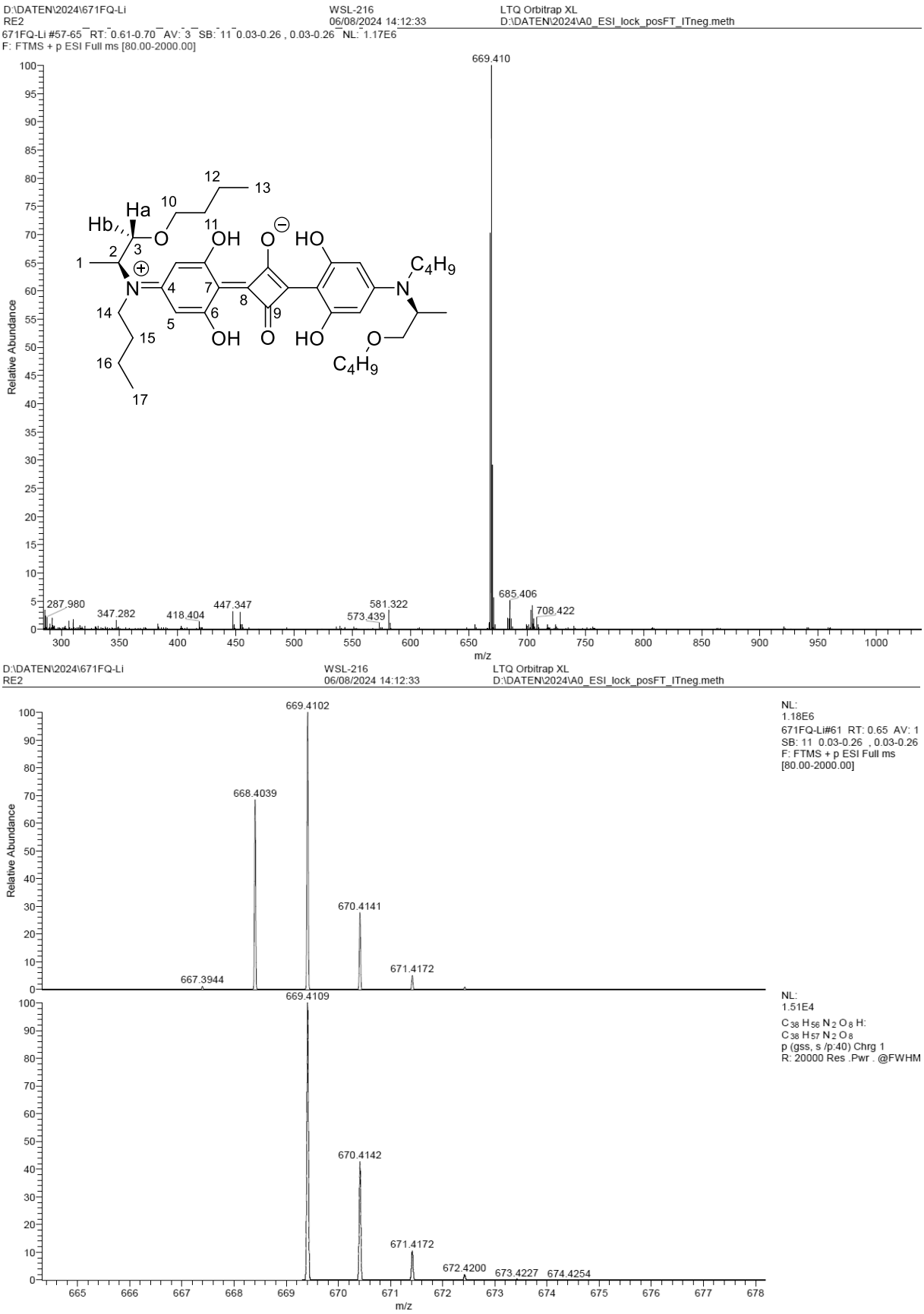

***Figure A104**: ESI (+) Mass spectra of **(S,S)-N-C4,O-C4-AlaSQ** (**23c**).*

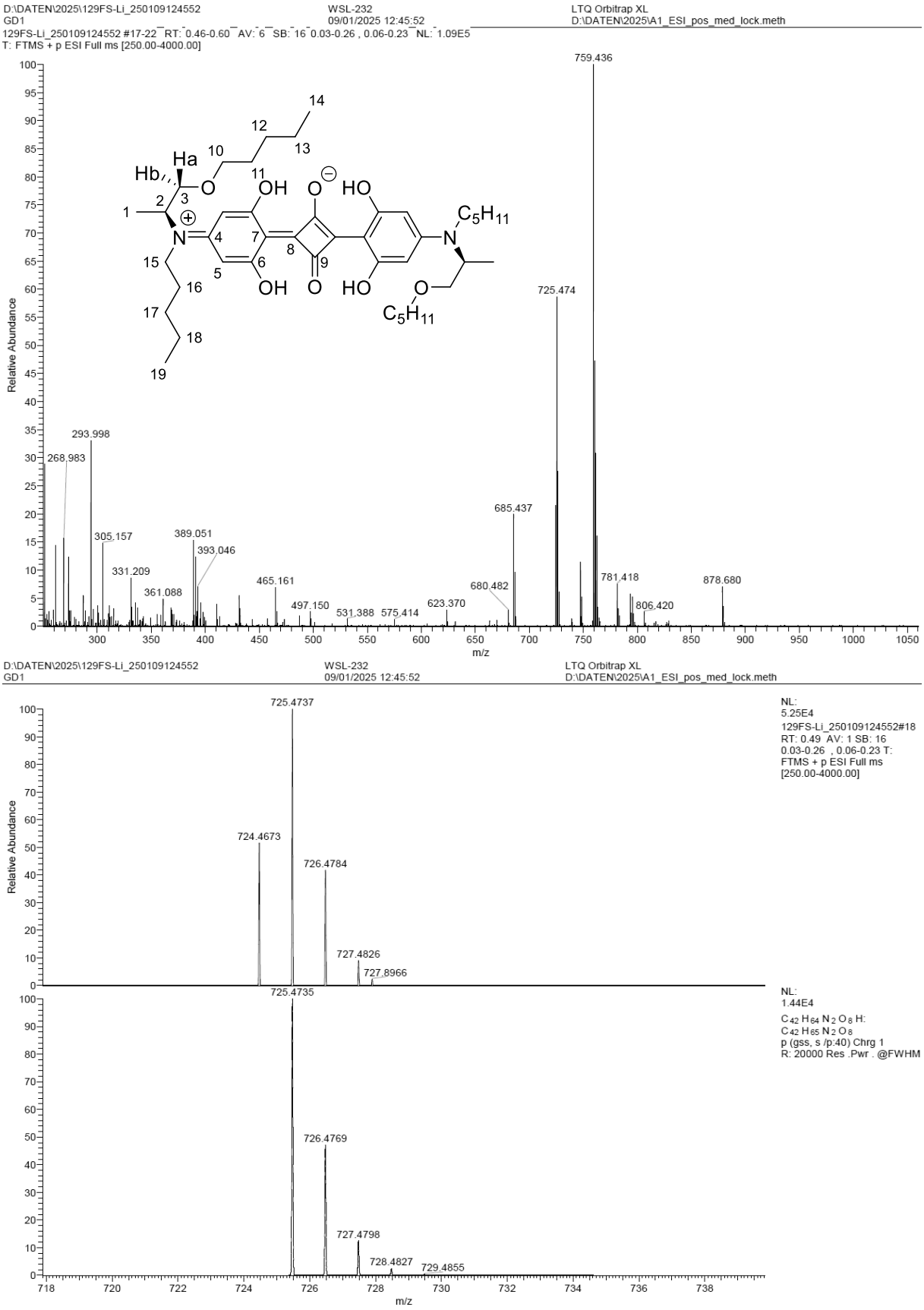

***Figure A105**: ESI (+) Mass spectra of **(S,S)-N-C5,O-C5-AlaSQ** (**23d**).*

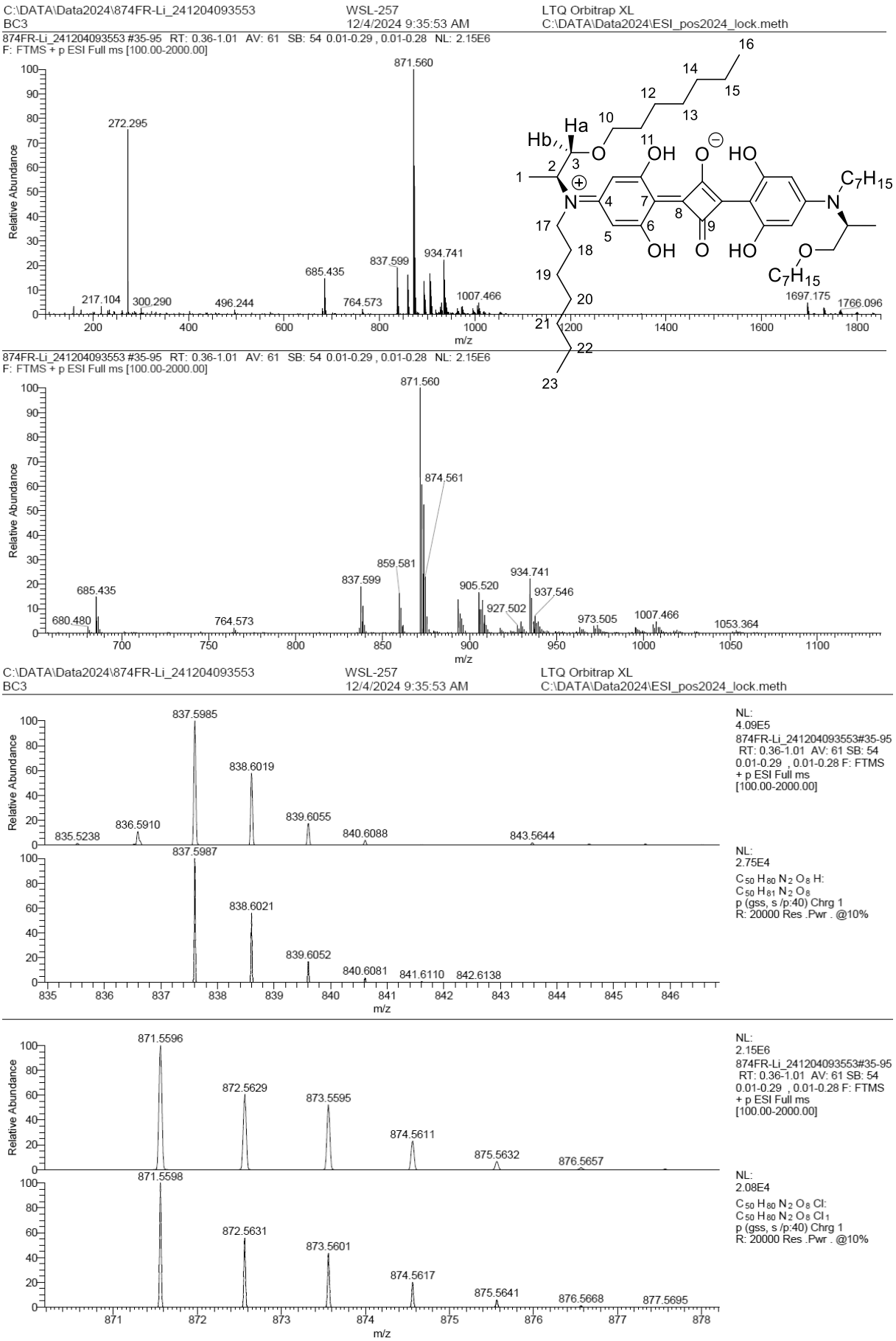

***Figure A106**: ESI (+) Mass spectra of **(S,S)-N-C7,O-C7-AlaSQ (23e)**.*

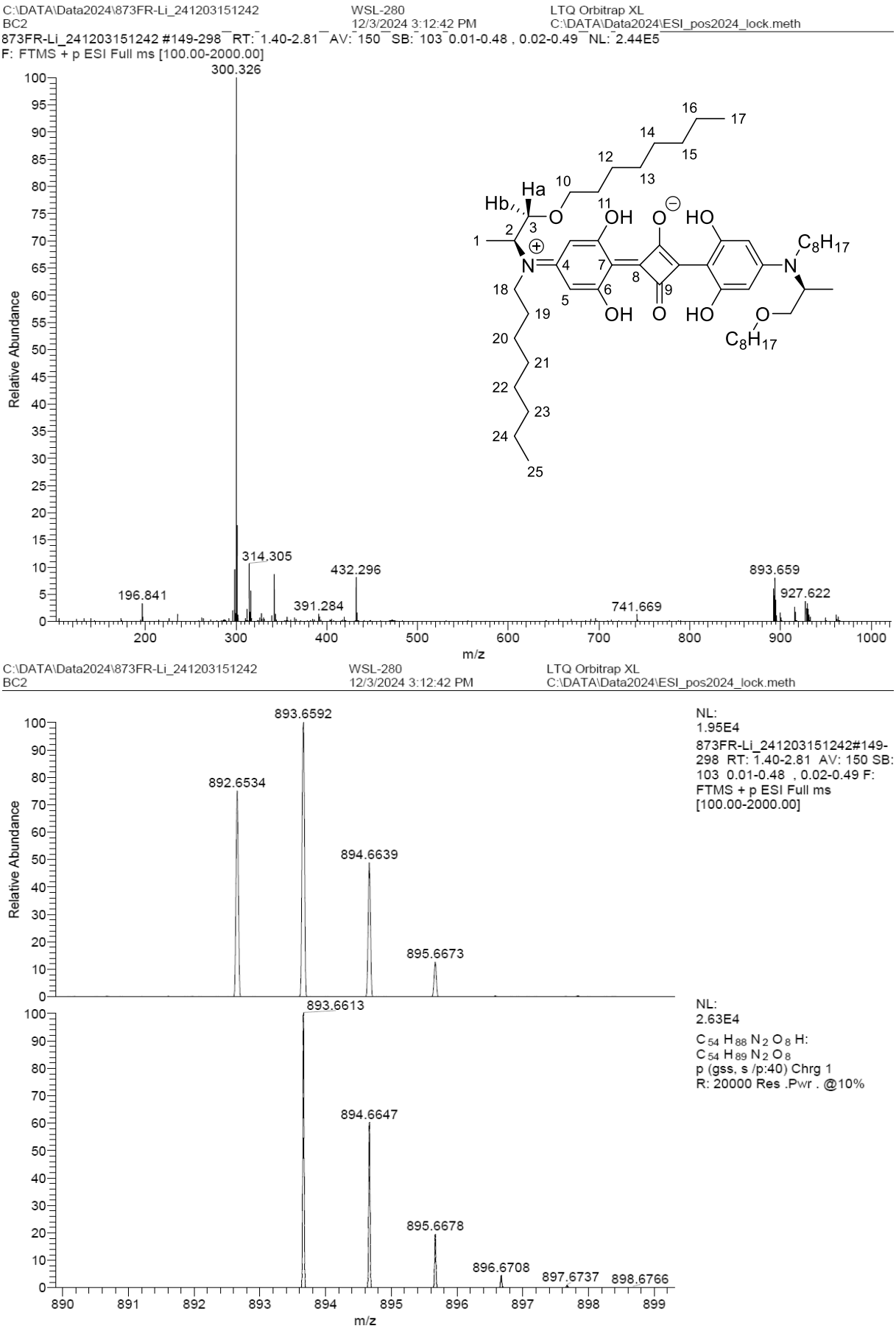

***Figure A107**: ESI (+) Mass spectra of **(S,S)-N-C8,O-C8-AlaSQ (23f)**.*

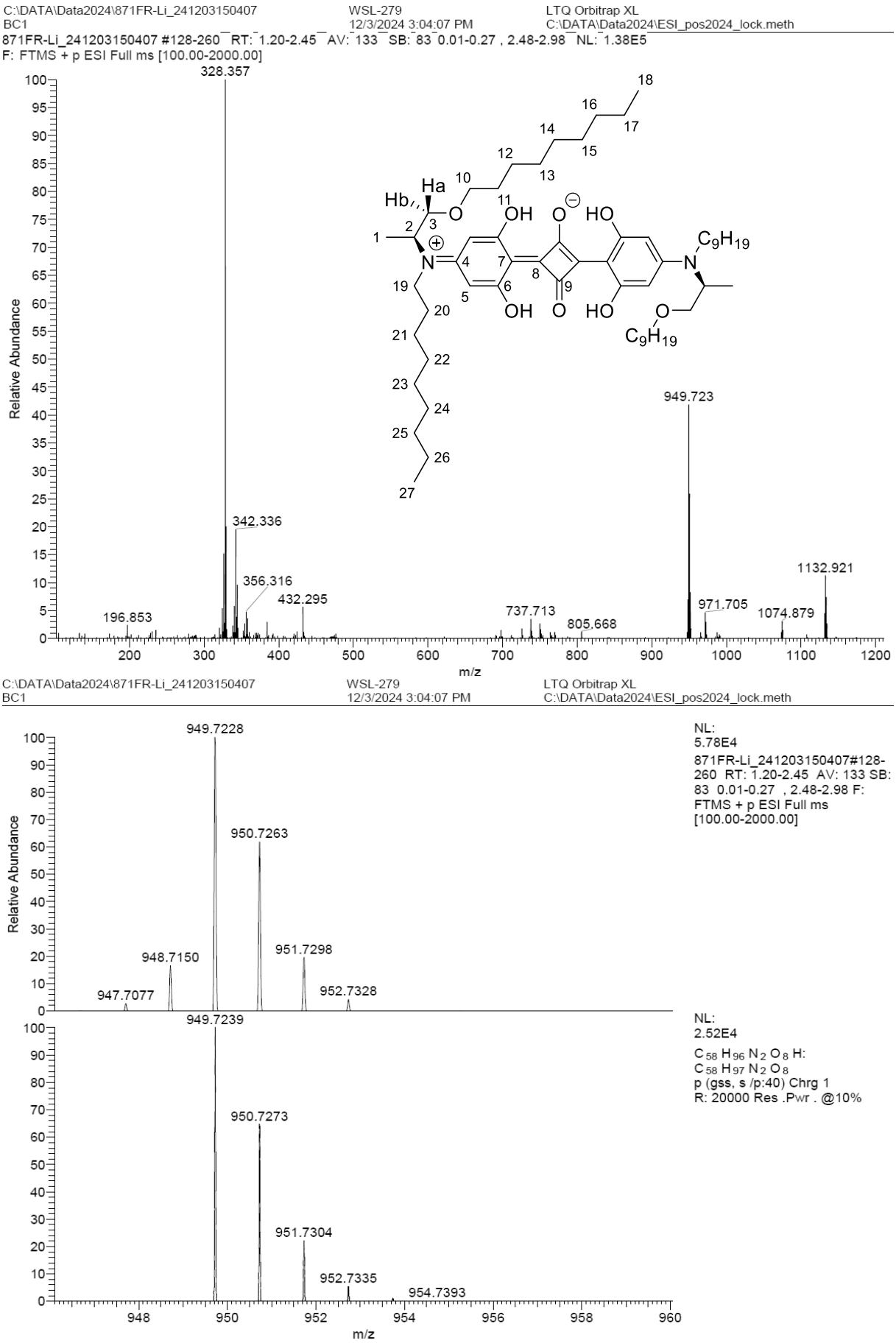

***Figure A108**: ESI (+) Mass spectra of **(S,S)-N-C9,O-C9-AlaSQ (23g)**.*

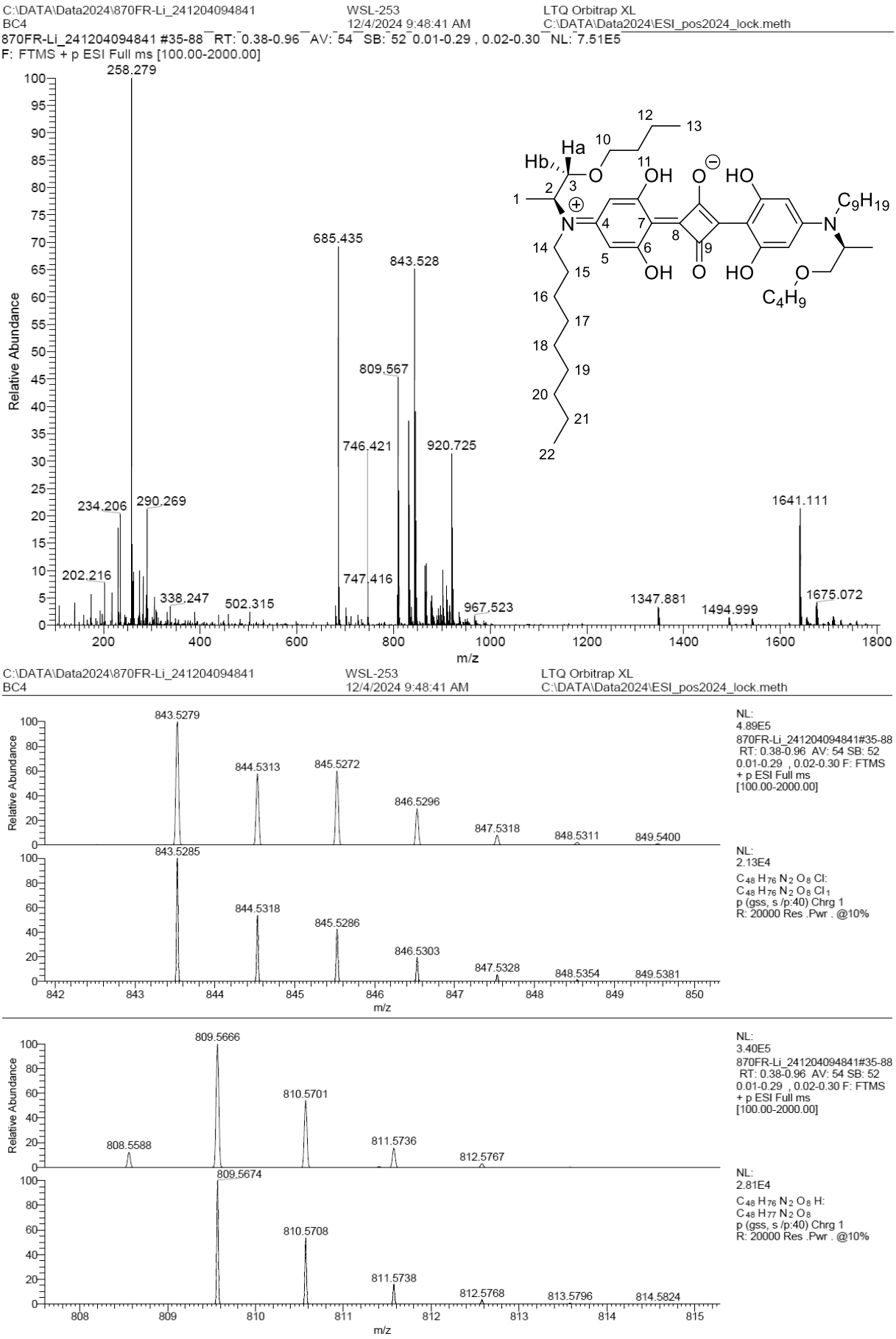

***Figure A109**: ESI (+) Mass spectra of **(S,S)-N-C9,O-C4-AlaSQ (23h)**.*

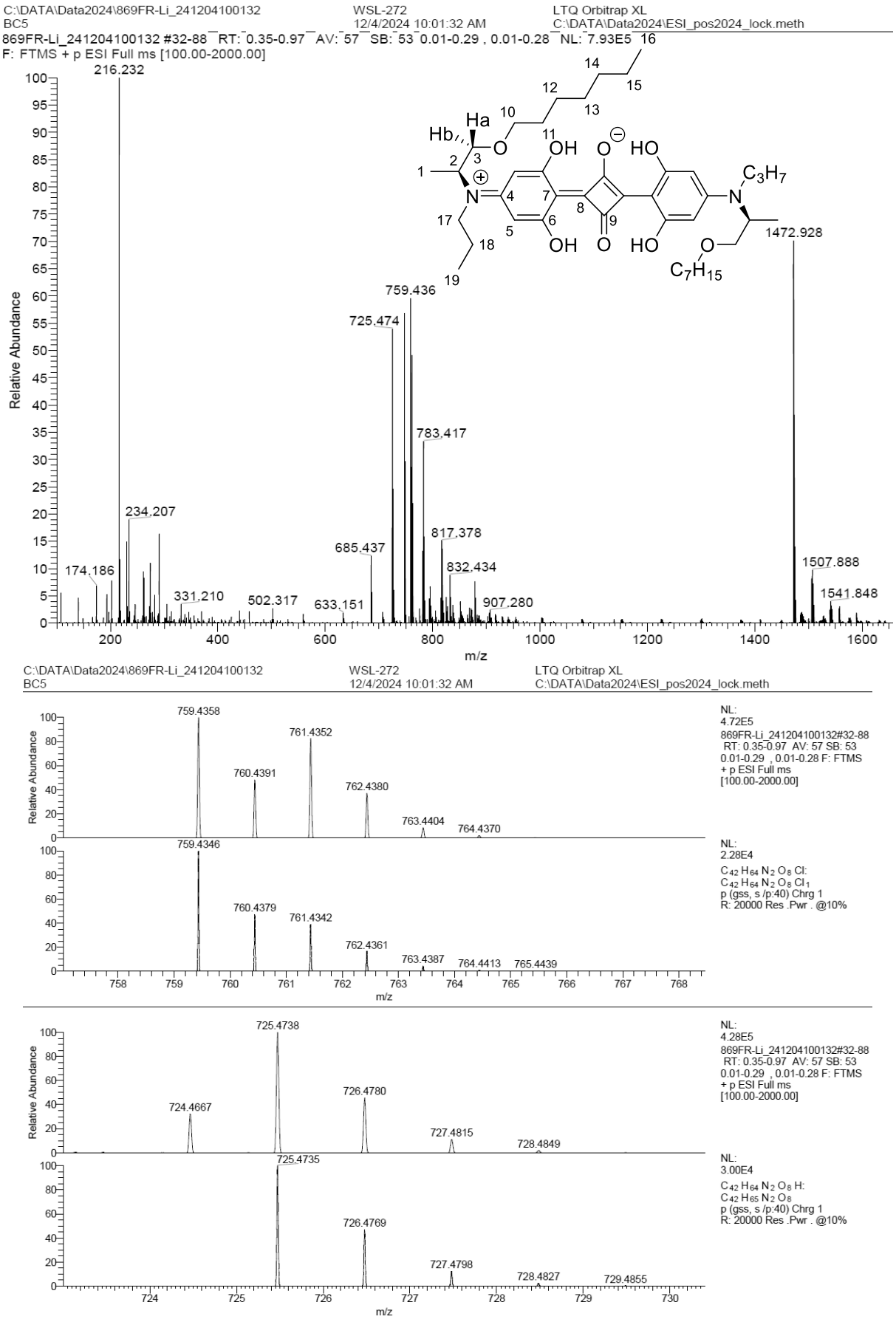

***Figure A110**: ESI (+) Mass spectra of **(S,S)-N-C3,O-C7-AlaSQ (23i)**.*

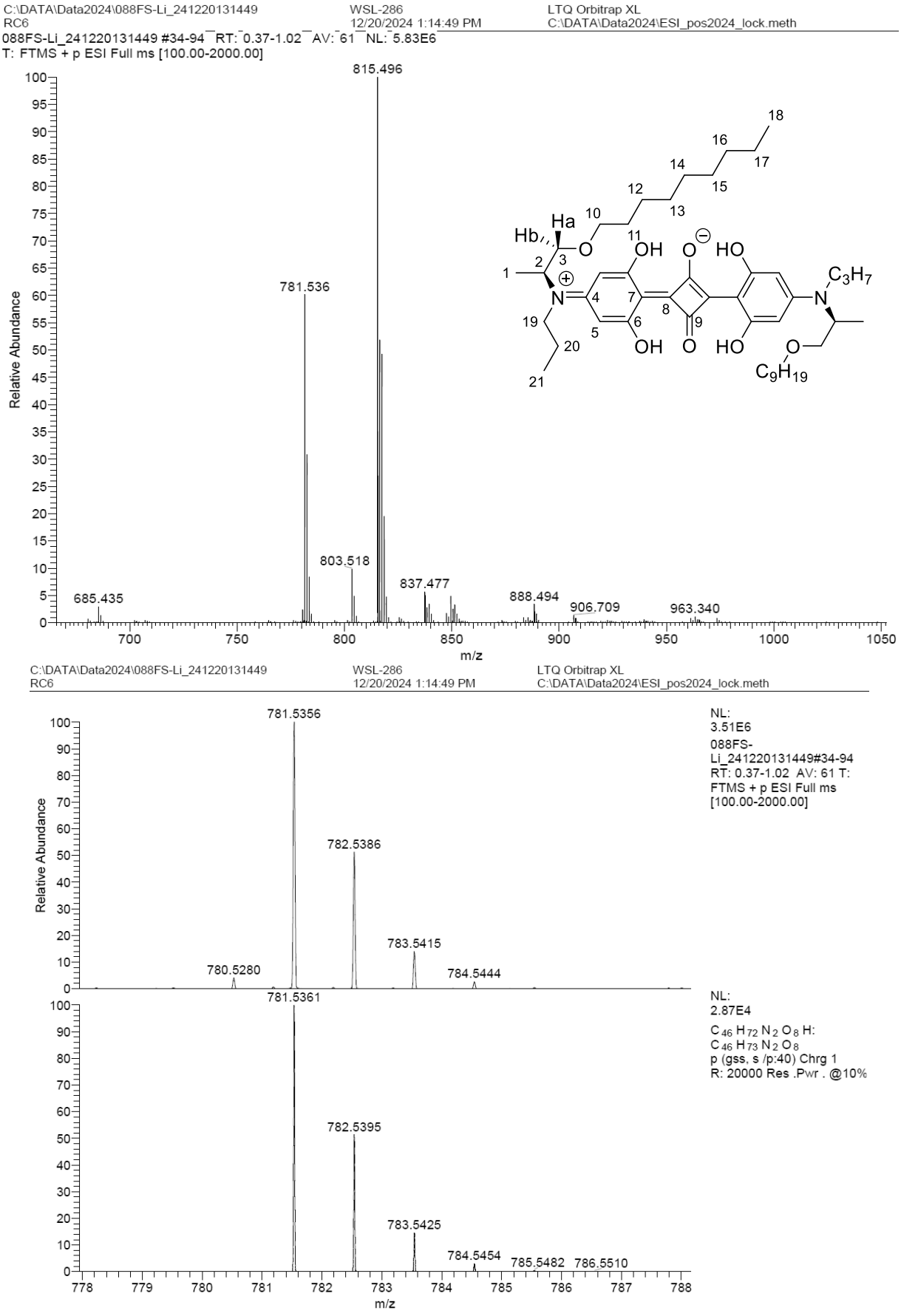

***Figure A111**: ESI (+) Mass spectra of **(S,S)-N-C3,O-C9-AlaSQ (23j)**.*

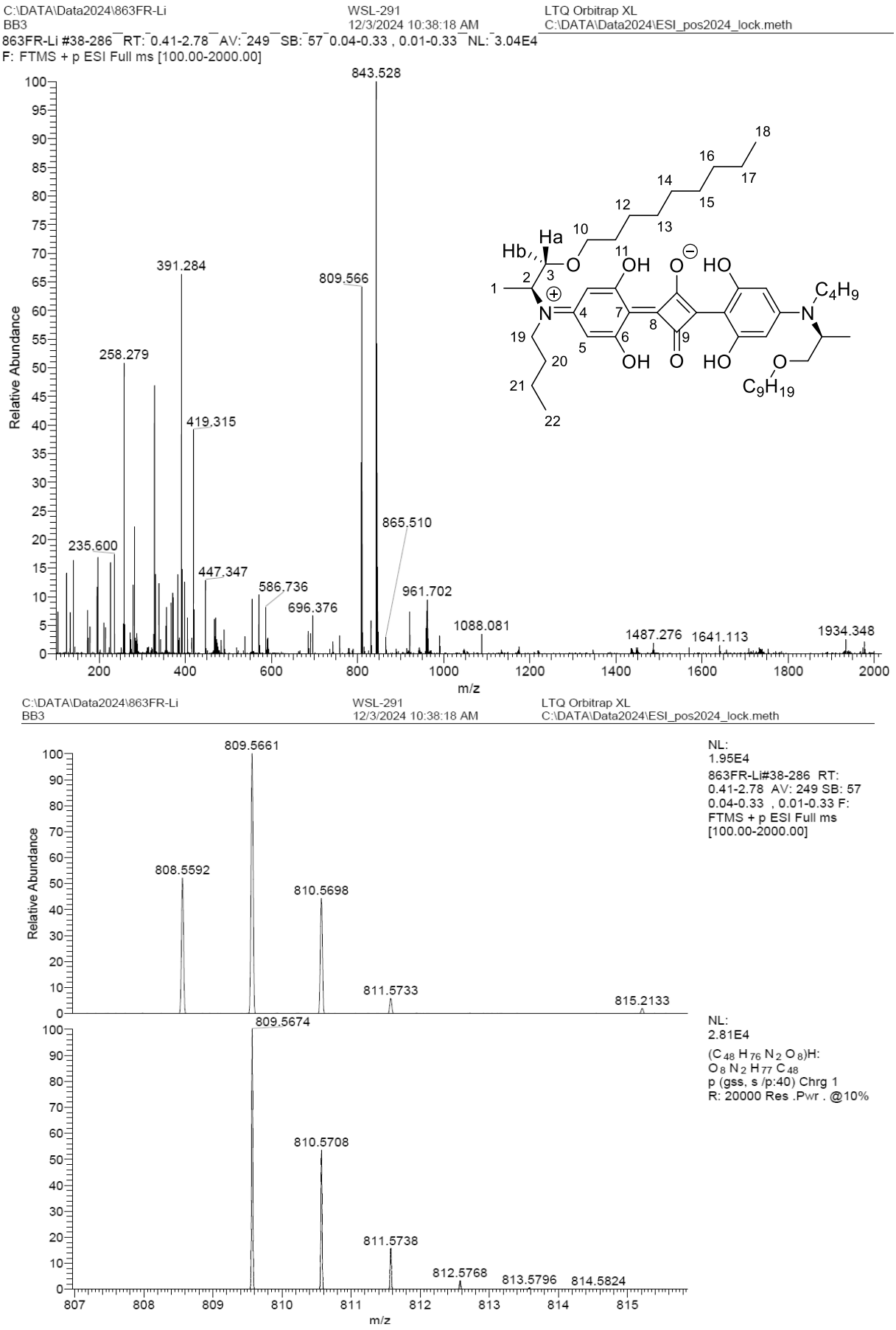

***Figure A112**: ESI (+) Mass spectra of **(S,S)-N-C4,O-C9-AlaSQ (23k)**.*

ADDITIONAL VISUALIZATION OF THE CRYSTAL STRUCTURES

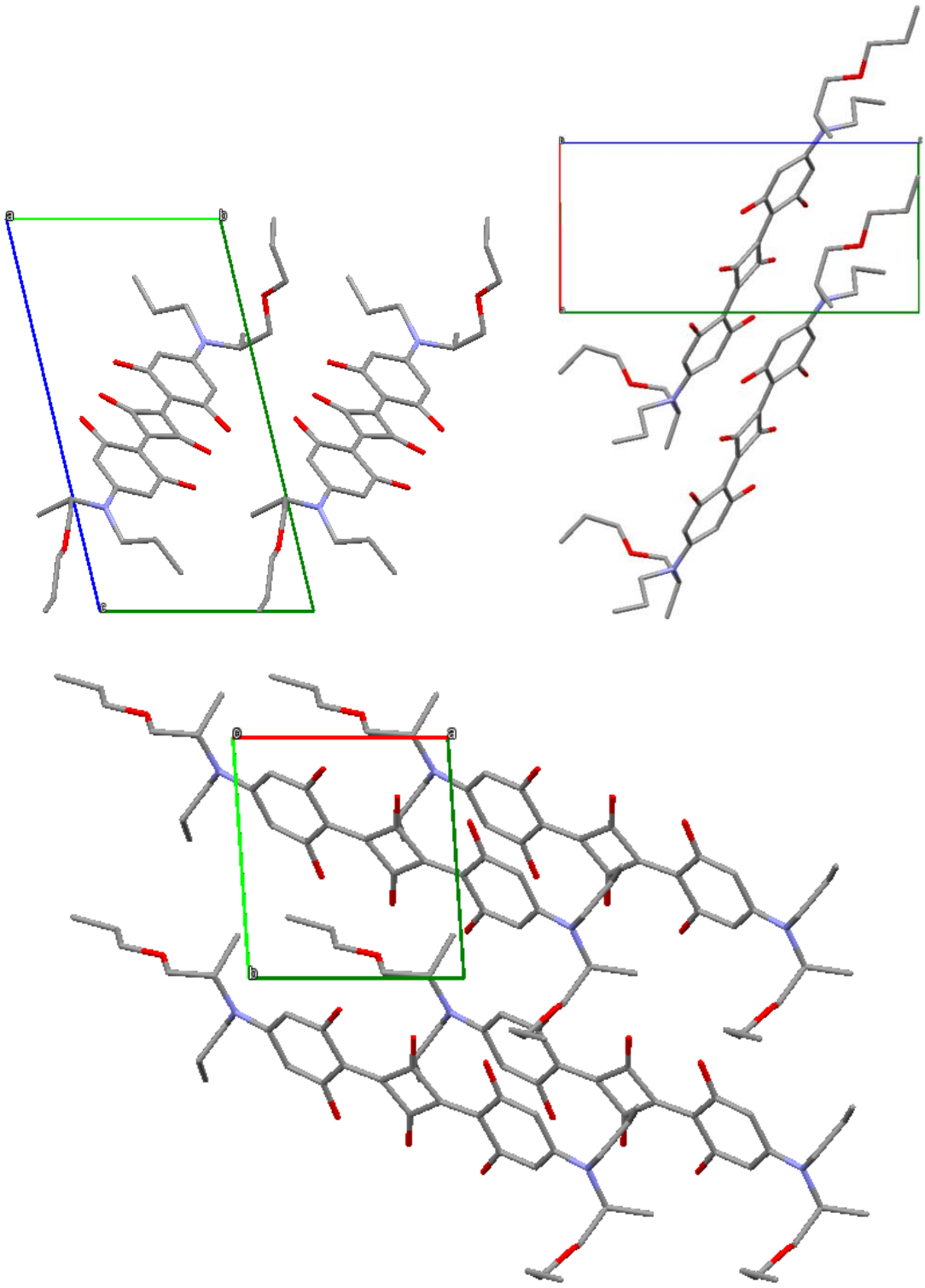

***Figure A113**: Visualization of the molecular packing of (**S,S**)-**N-C3,O-C3-AlaSQ** (**23b**) in its triclinic unit cell viewing along the unit cell axis a (top left), b (top middle) and c (top right) respectively (hydrogen atoms were omitted for clarity; color code: blue: c-axis, nitrogen atoms, dark green: expansion of the unit cell, green: b-axis, grey: carbon atoms, red: a-axis, oxygen atoms).*

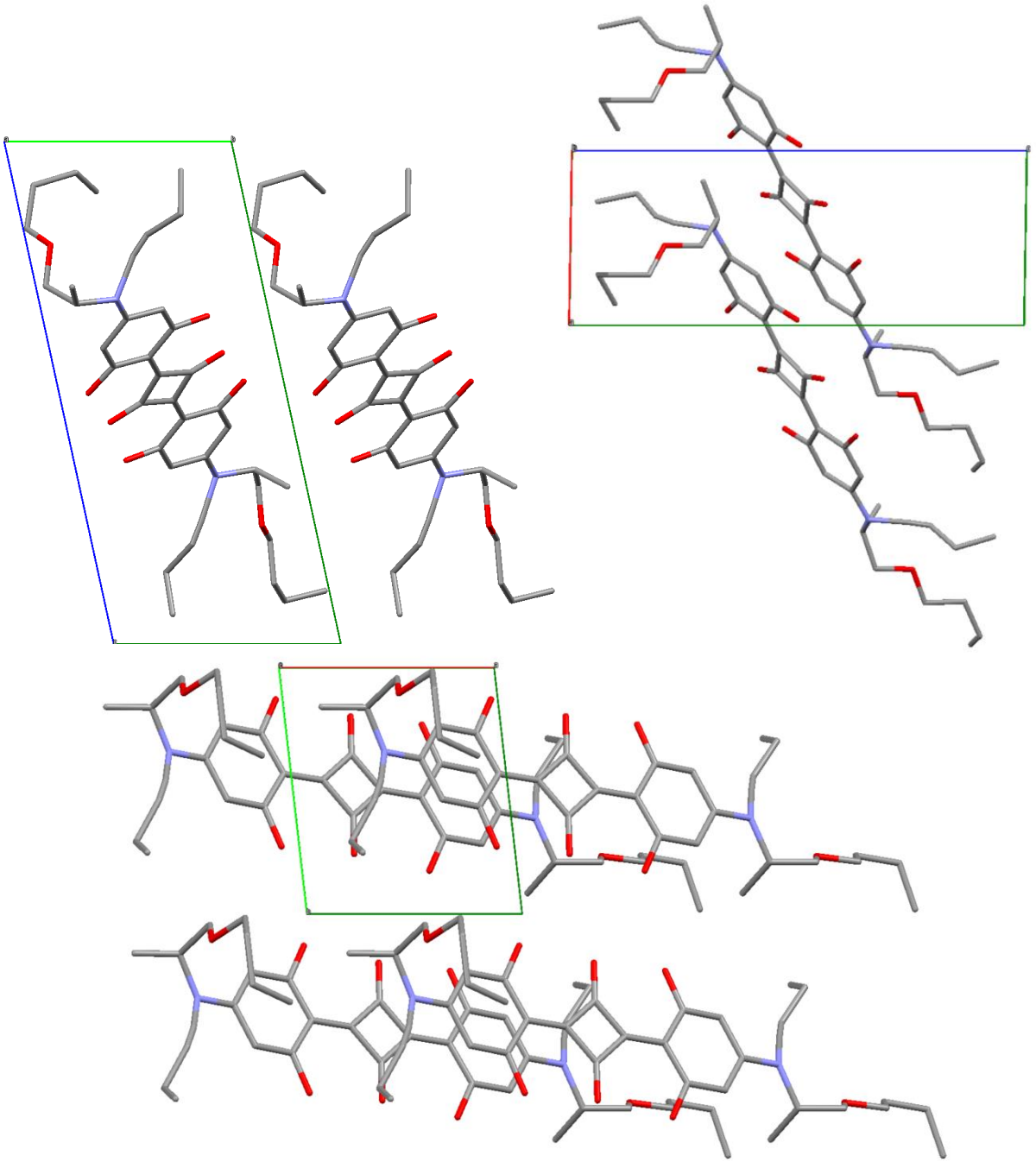

***Figure A114**: Visualization of the molecular packing of **(S,S)-N-C4,O-C4-AlaSQ** (**23c**) in its triclinic unit cell viewing along the unit cell axis a (top left), b (top middle) and c (top right) respectively (hydrogen atoms were omitted for clarity; color code: blue: c-axis, nitrogen atoms, dark green: expansion of the unit cell, green: b-axis, grey: carbon atoms, red: a-axis, oxygen atoms).*

UV-VIS SPECTRA

UV-Vis Experiments in Different Solvents

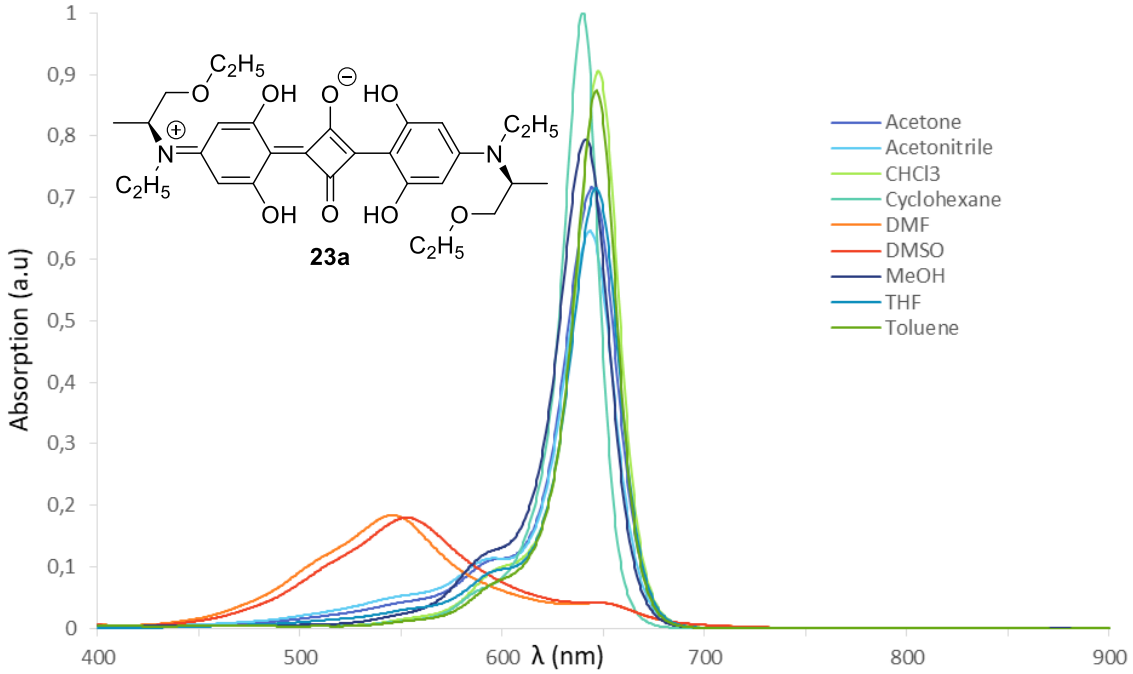

***Figure A115**: UV-Vis absorption spectra of **N-C2,O-C2-AlaSQ** (**23a**) in various solvents.*

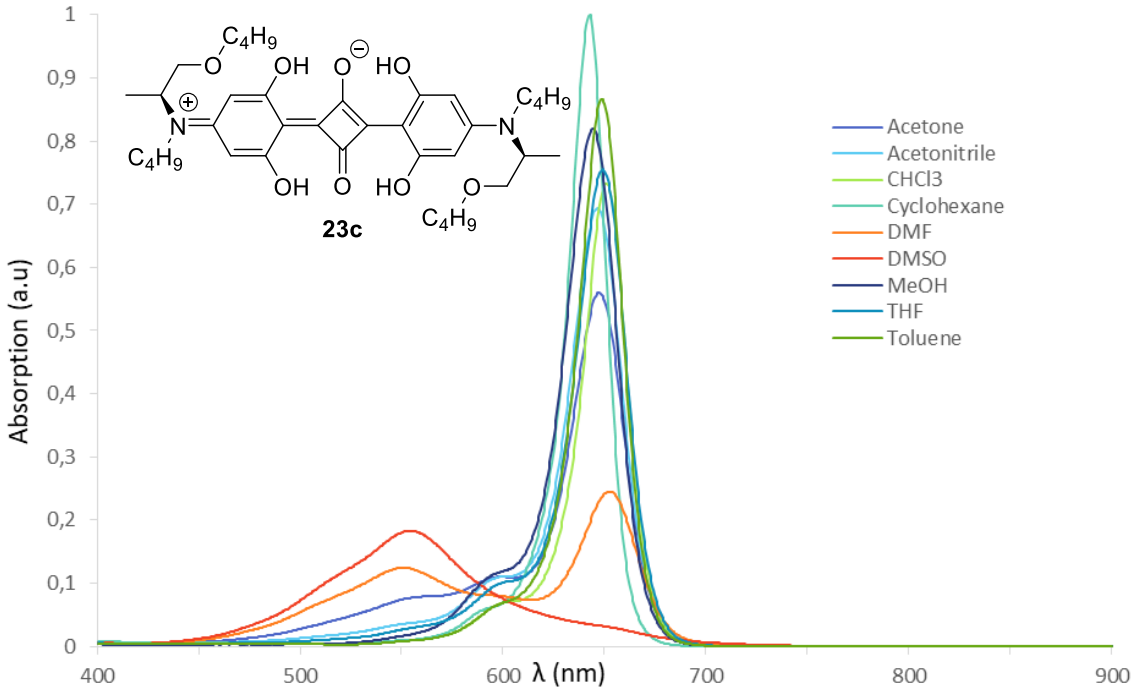

***Figure A116**: UV-Vis absorption spectra of **N-C4,O-C4-AlaSQ** (**23c**) in various solvents.*

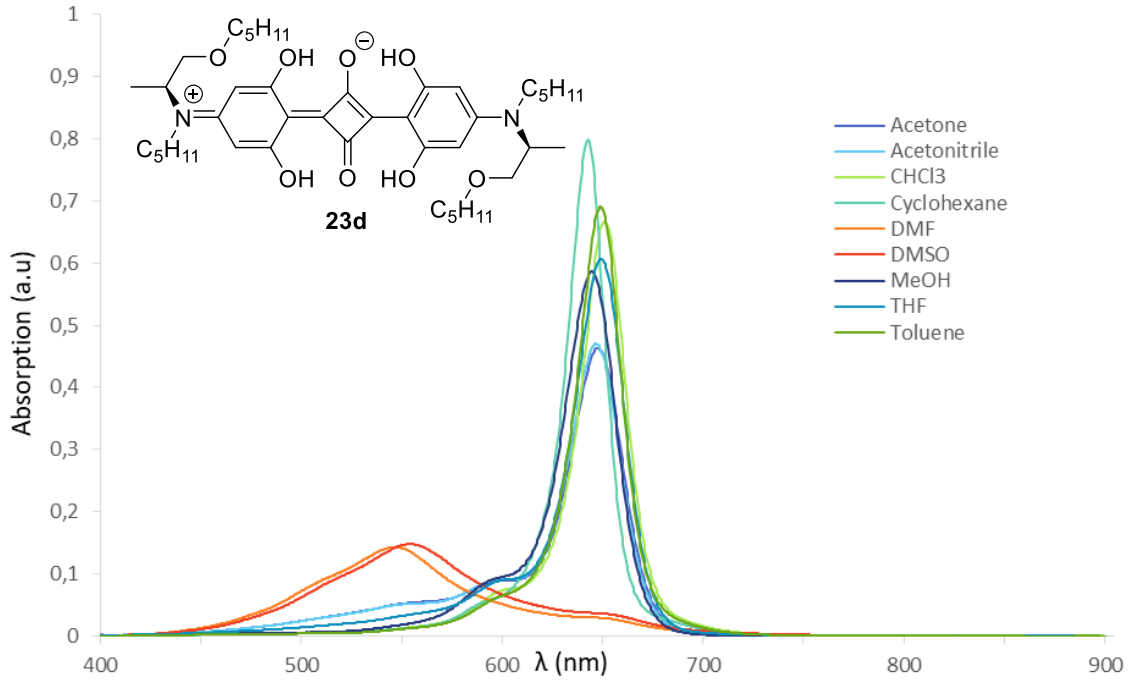

***Figure A117**: UV-Vis absorption spectra of **N-C5,O-C5-AlaSQ** (**23d**) in various solvents.*

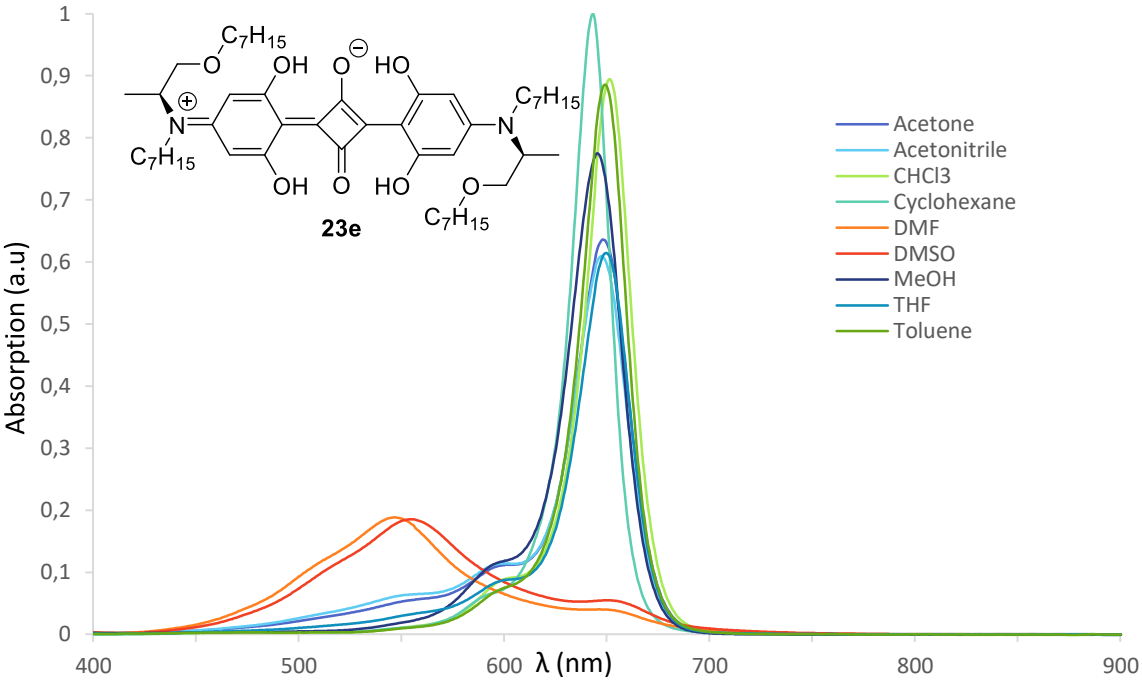

***Figure A118**: UV-Vis absorption spectra of **N-C7,O-C7-AlaSQ** (**23e**) in various solvents.*

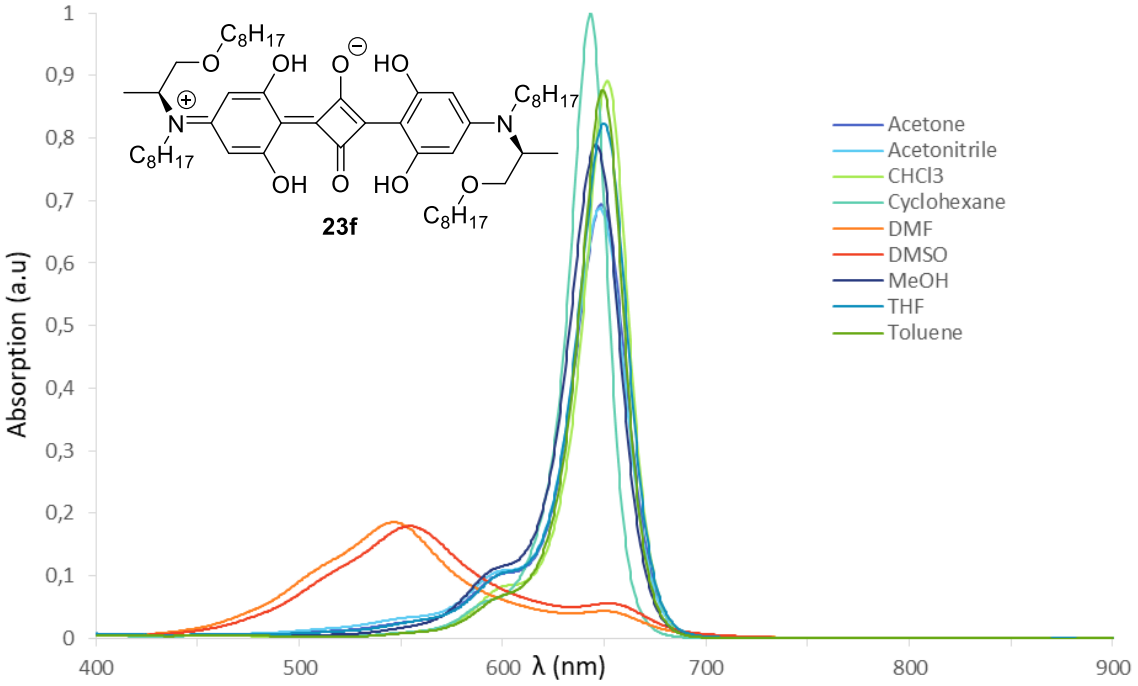

***Figure A119**: UV-Vis absorption spectra of **N-C8,O-C8-AlaSQ** (**23f**) in various solvents.*

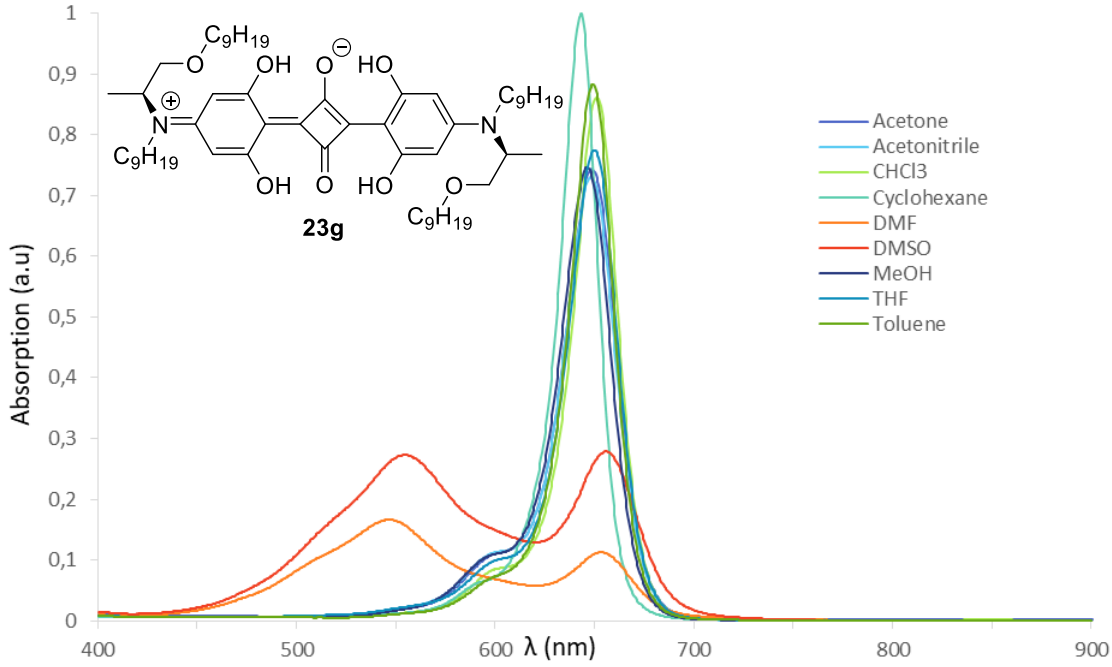

***Figure A120**: UV-Vis absorption spectra of **N-C9,O-C9-AlaSQ** (**23g**) in various solvents.*

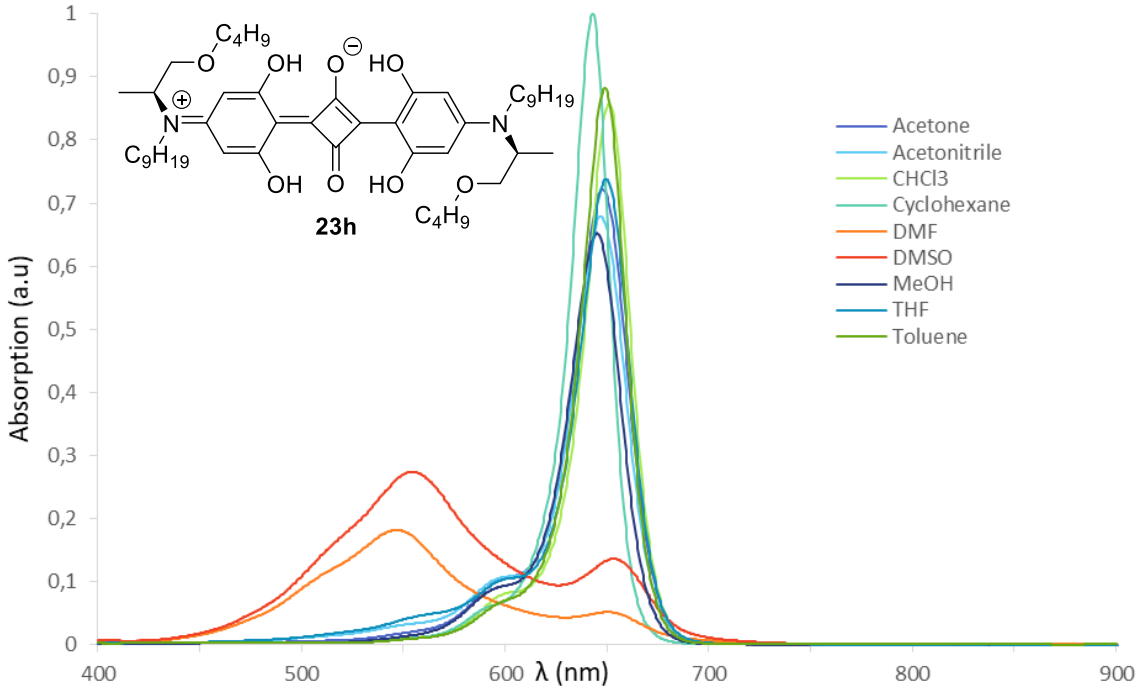

***Figure A121**: UV-Vis absorption spectra of **N-C9,O-C4-AlaSQ** (**23h**) in various solvents.*

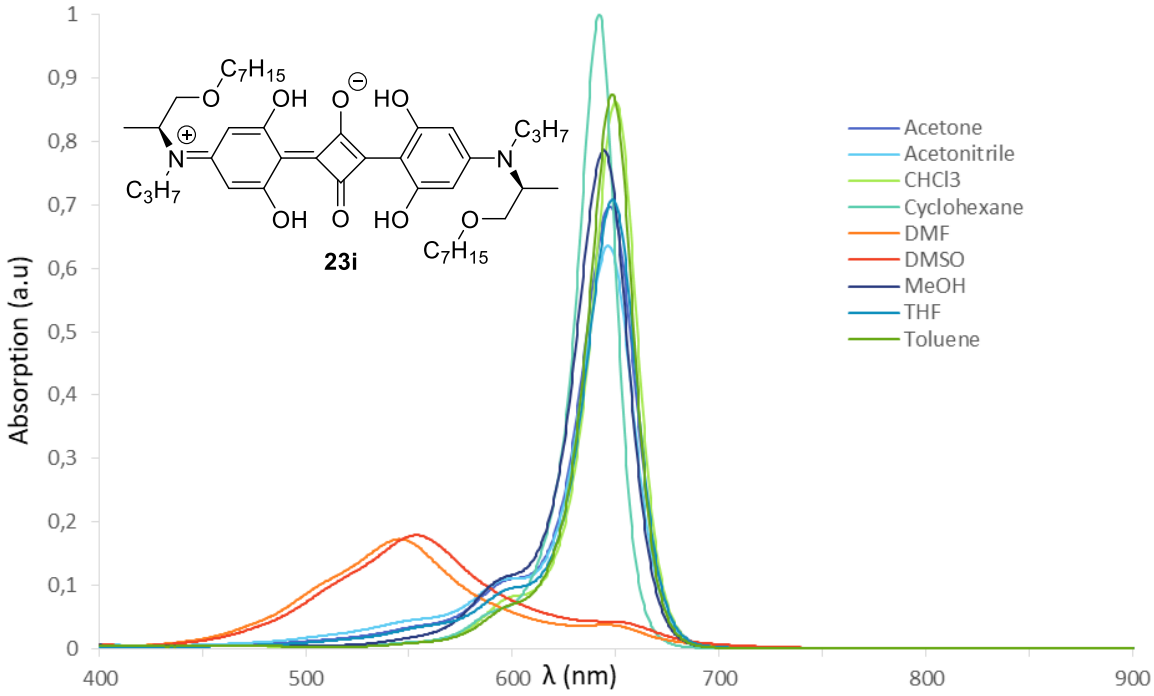

***Figure A122**: UV-Vis absorption spectra of **N-C3,O-C7-AlaSQ** (**23i**) in various solvents.*

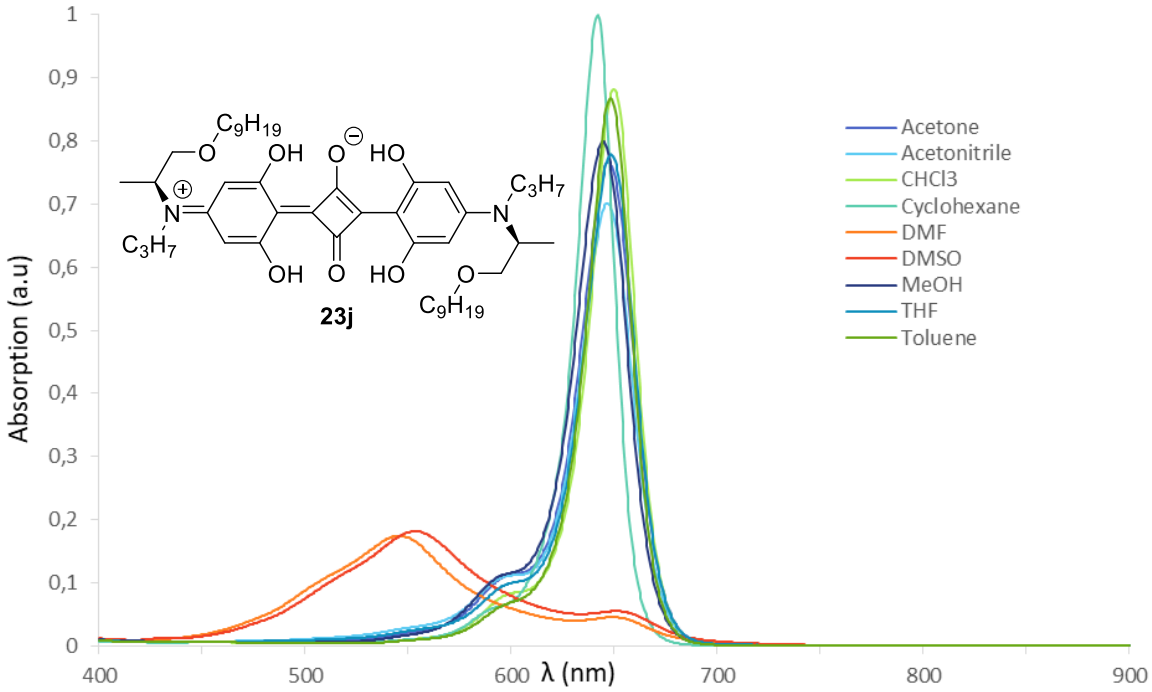

***Figure A123**: UV-Vis absorption spectra of **N-C3,O-C9-AlaSQ** (**23j**) in various solvents.*

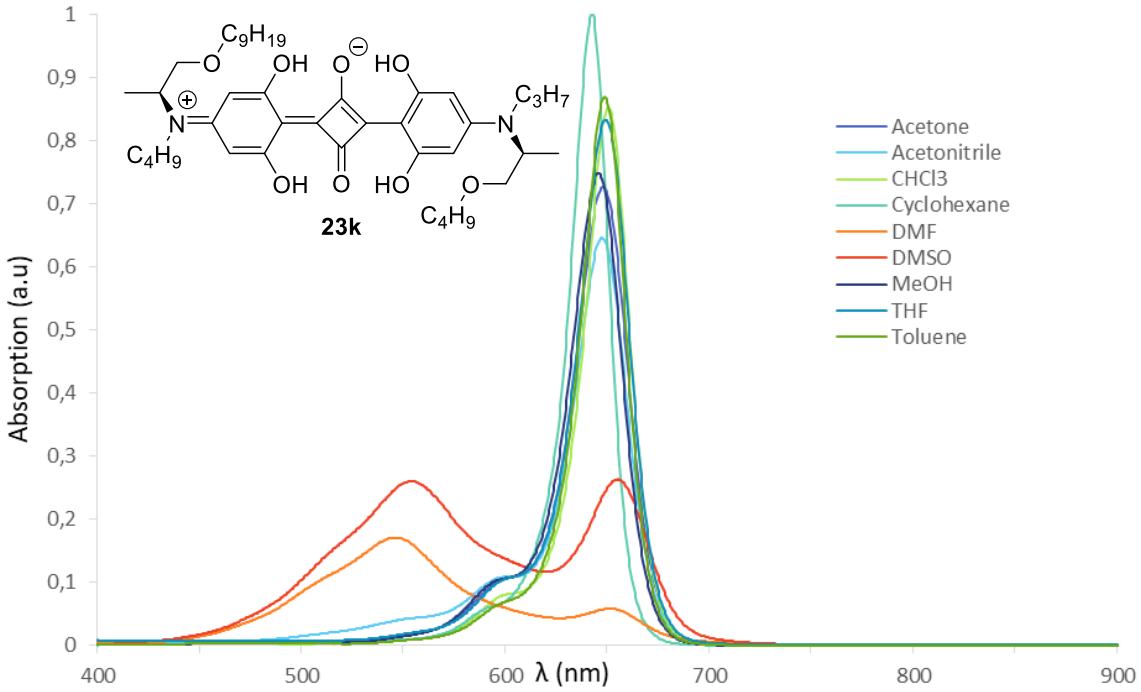

***Figure A124**: UV-Vis absorption spectra of **N-C4,O-C9-AlaSQ** (**23k**) in various solvents.*

UV-Vis Measurements for the Poor-Solvent Experiments

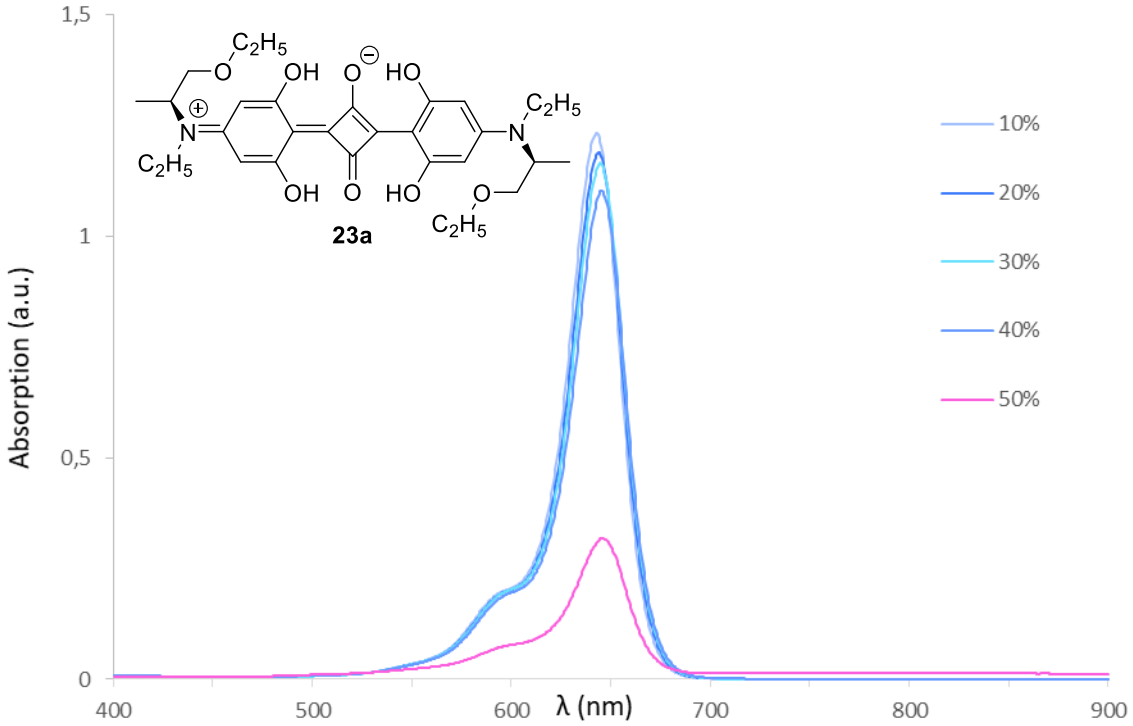

***Figure A125**: UV-vis Absorption spectra of **23a** in mixtures of MeOH/H_2O with varying content of water.*

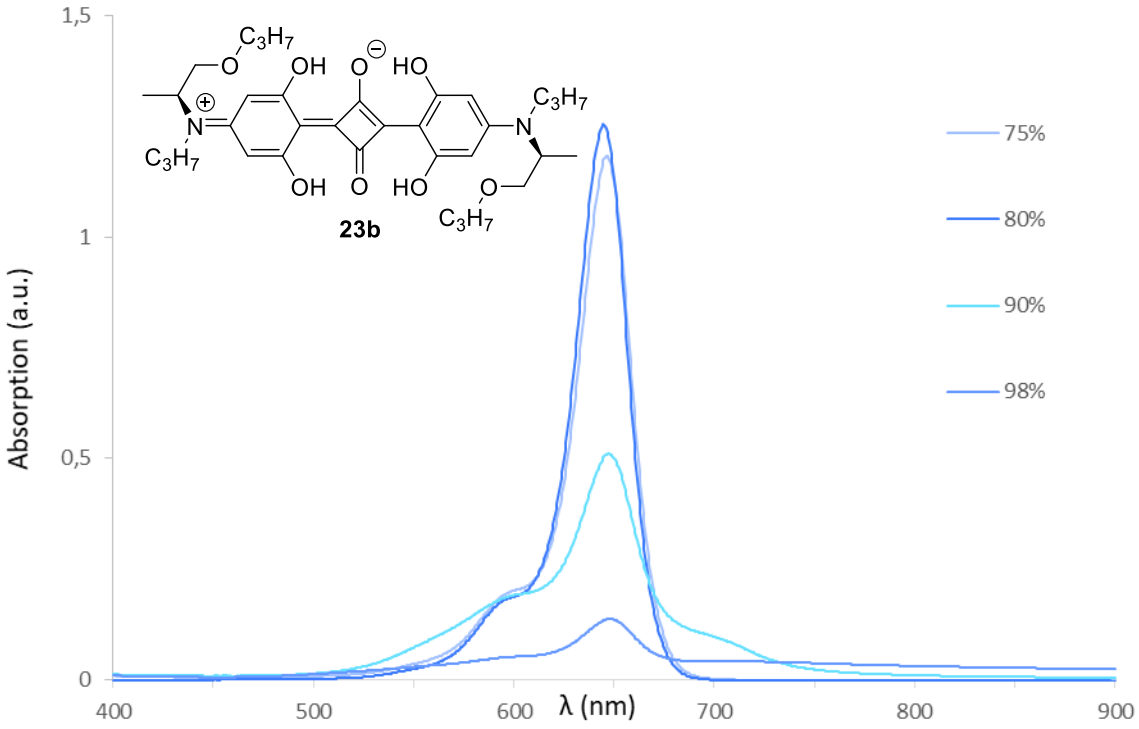

***Figure A126**: UV-vis Absorption spectra of **23b** in mixtures of MeOH/H_2O with varying content of water.*

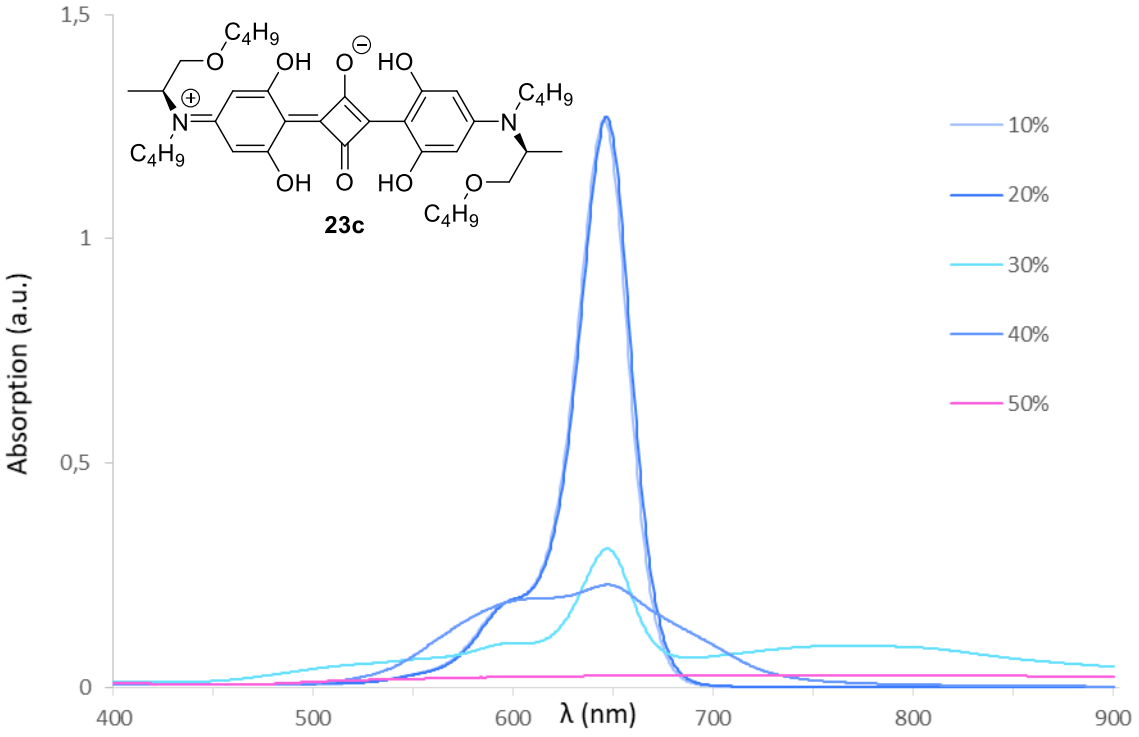

***Figure A127**: UV-vis Absorption spectra of **23c** in mixtures of MeOH/H_2O with varying content of water.*

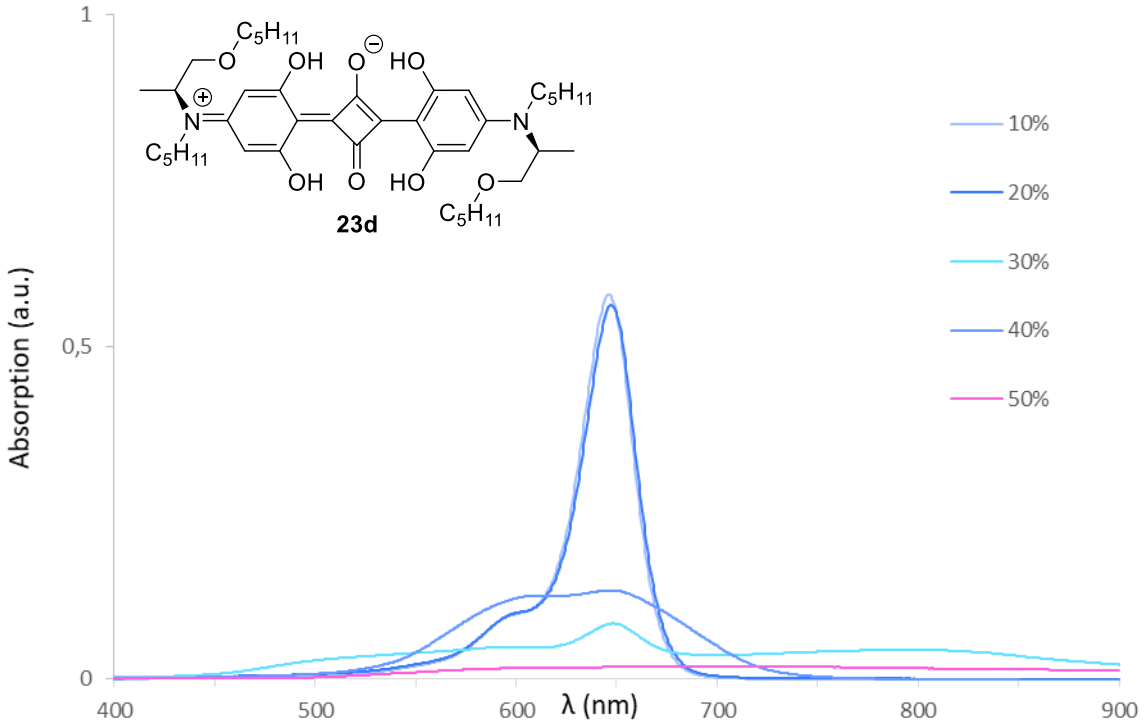

***Figure A128**: UV-vis Absorption spectra of **23d** in mixtures of MeOH/H_2O with varying content of water.*

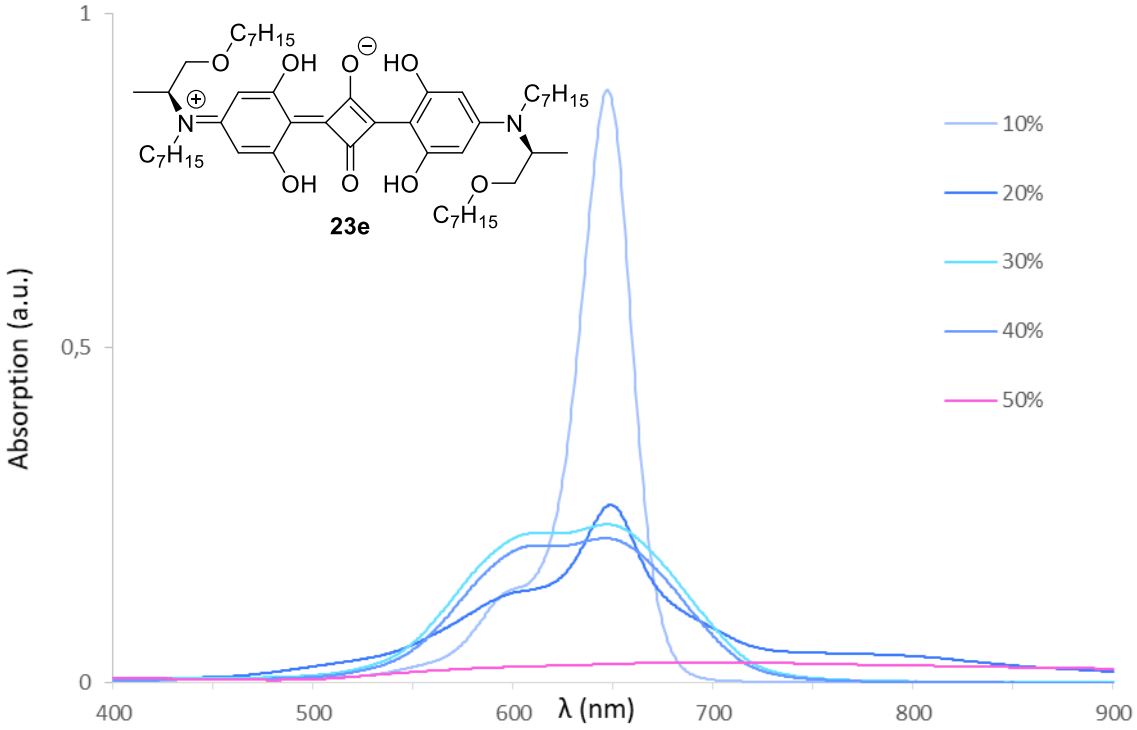

***Figure A129**: UV-vis Absorption spectra of **23e** in mixtures of MeOH/H_2O with varying content of water.*

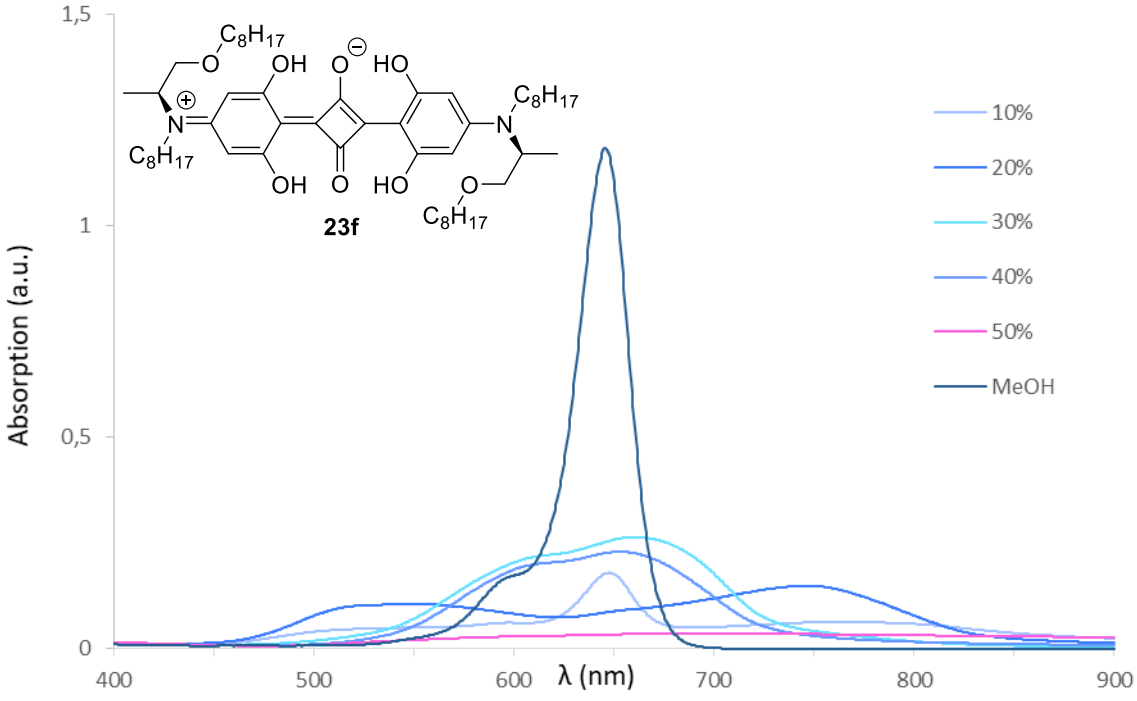

***Figure A130**: UV-vis Absorption spectra of **23f** in mixtures of MeOH/H_2O with varying content of water including pure MeOH to show the drastic decrease of absorption.*

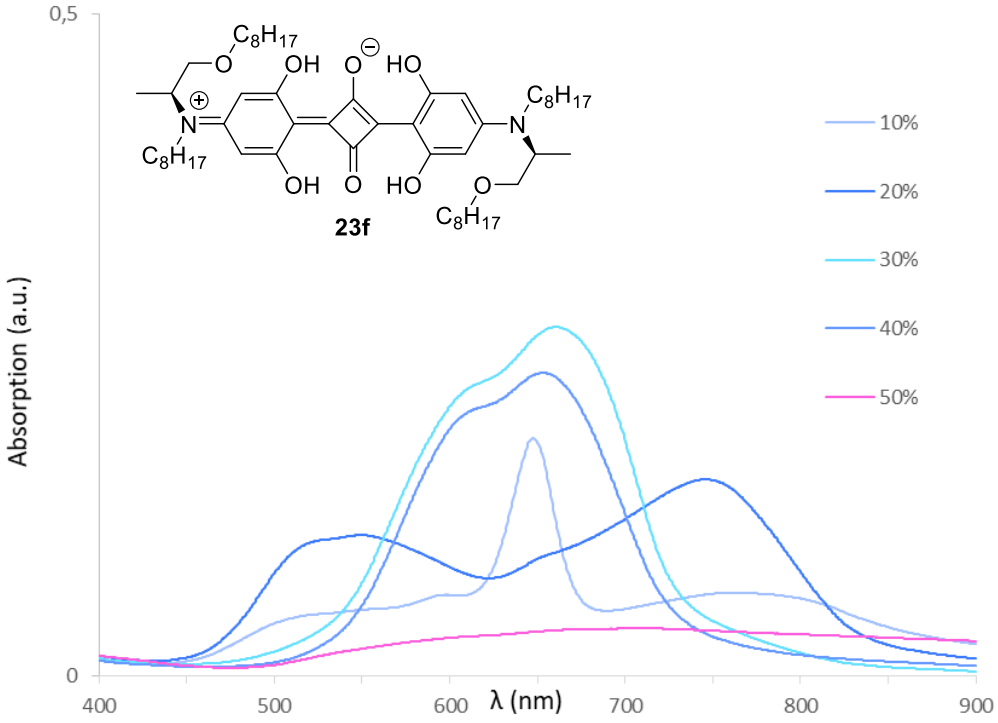

***Figure A131**: Magnified UV-vis absorption spectra of **23f** in mixtures of MeOH/H_2O with varying content of water to highlight the change of absorption region.*

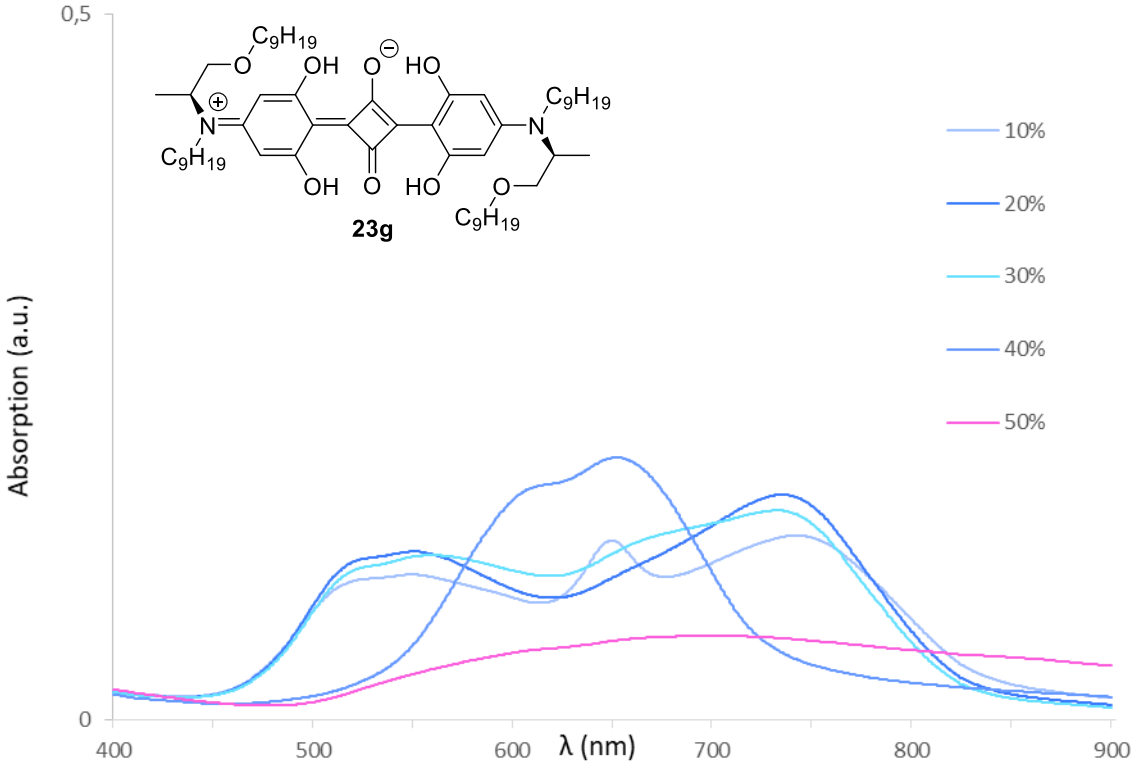

***Figure A132**: Magnified UV-vis absorption spectra of **23g** in mixtures of MeOH/H_2O with varying content of water to highlight the change of absorption region.*

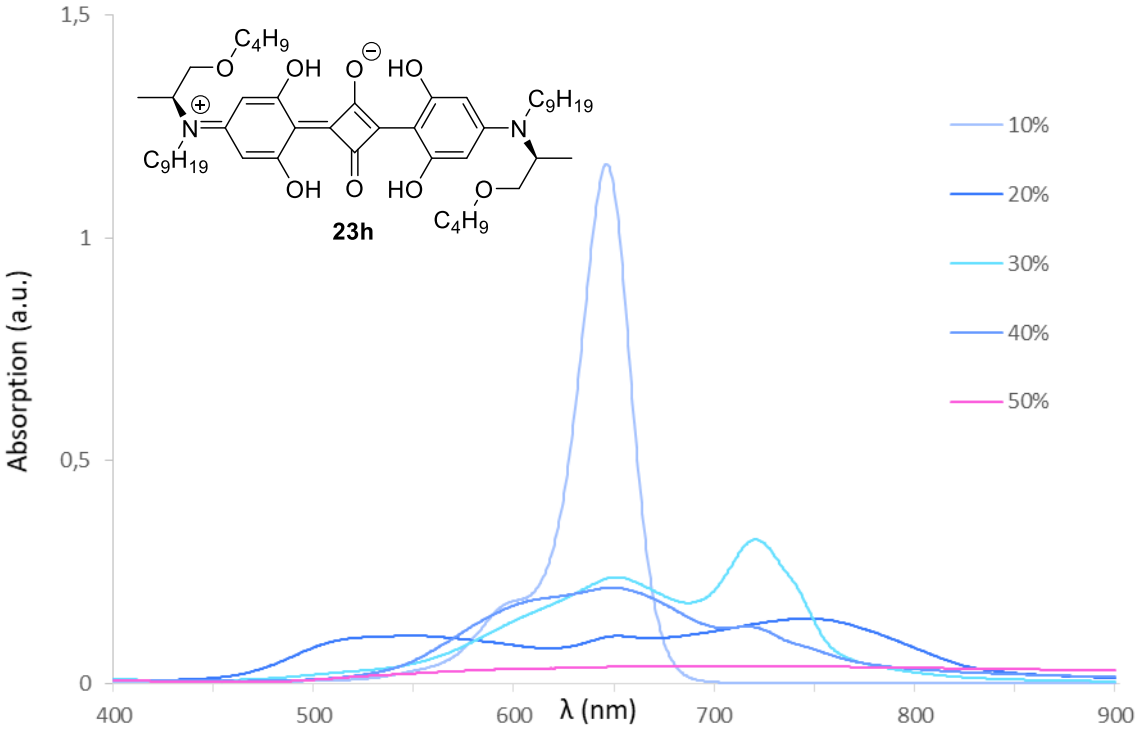

***Figure A133**: UV-vis Absorption spectra of **23h** in mixtures of MeOH/H_2O with varying content of water.*

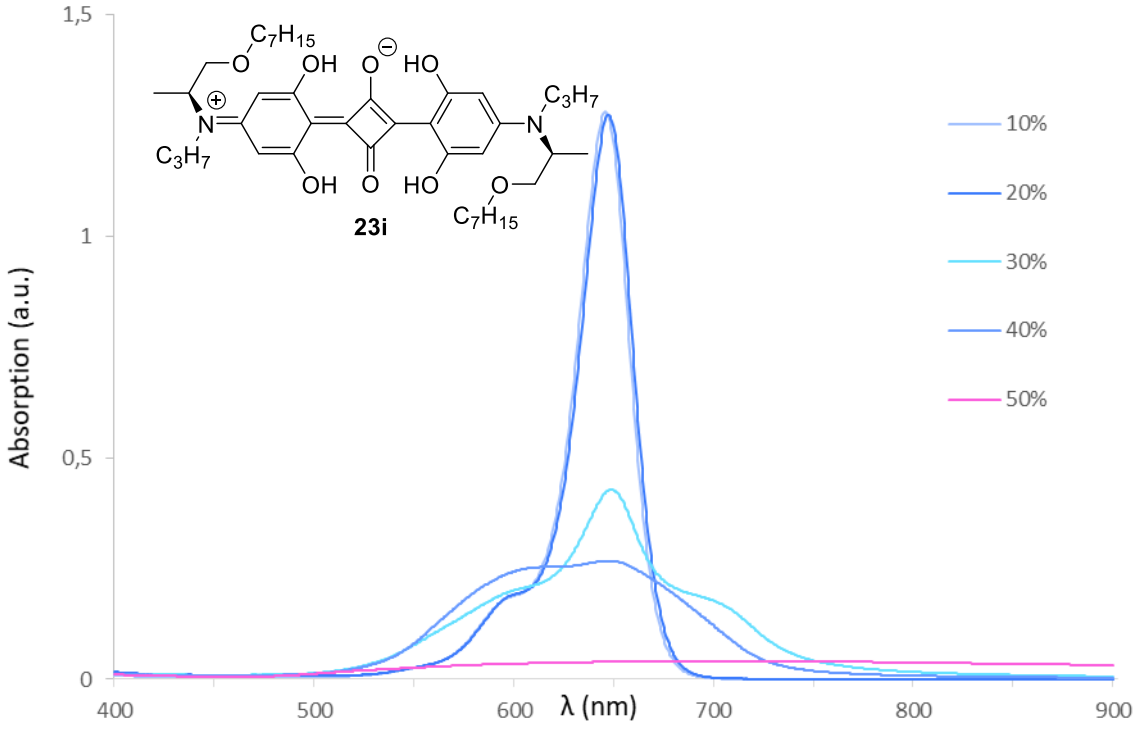

***Figure A134**: UV-vis Absorption spectra of **23i** in mixtures of MeOH/H_2O with varying content of water.*

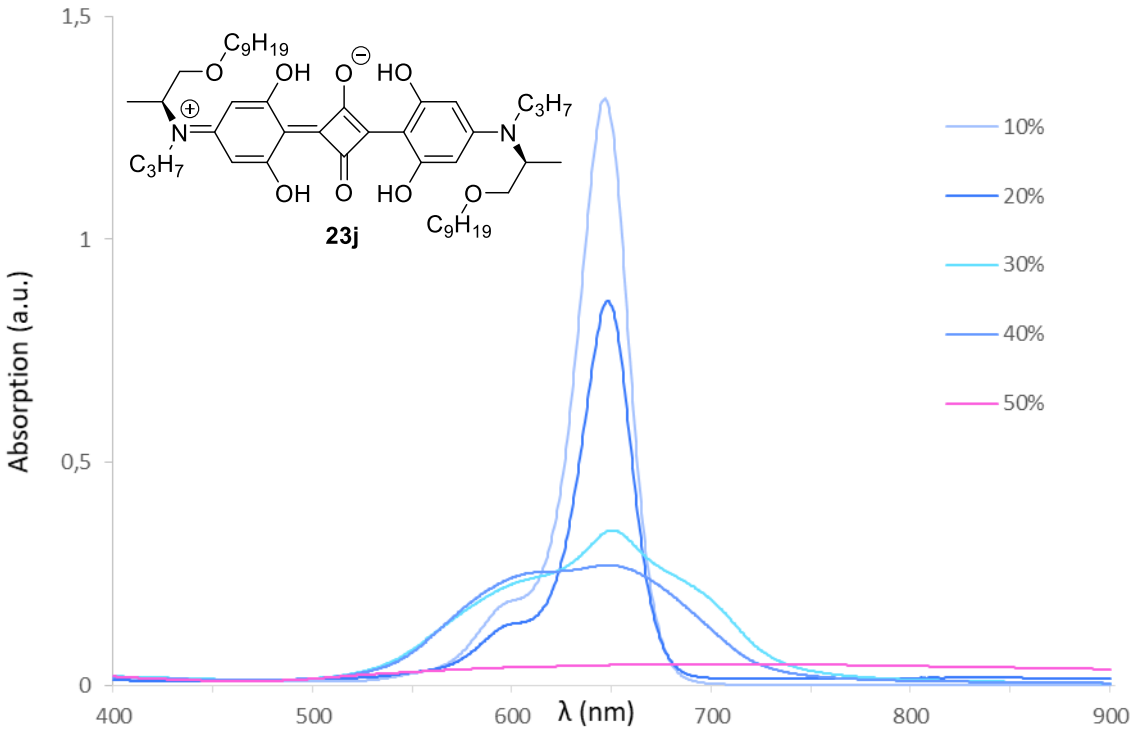

***Figure A135**: UV-vis Absorption spectra of **23j** in mixtures of MeOH/H_2O with varying content of water.*

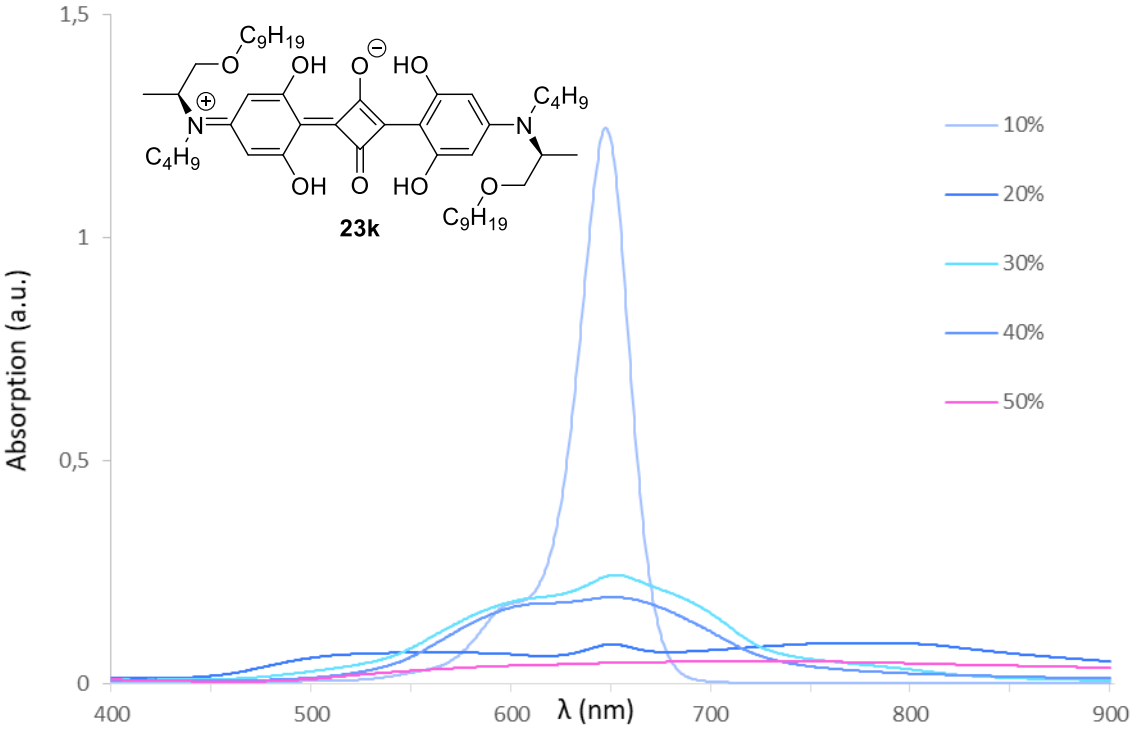

***Figure A136**: UV-vis Absorption spectra of **23k** in mixtures of MeOH/H_2O with varying content of water.*